COSMIC INFLATION AND EVOLUTION IN $f(R)$ AND $f(R,T)$ THEORIES

By

Iqra Nawazish

A THESIS
SUBMITTED IN PARTIAL FULFILLMENT OF THE
REQUIREMENTS FOR THE DEGREE OF
DOCTOR OF PHILOSOPHY
IN
MATHEMATICS

Supervised By

Prof. Dr. Muhammad Sharif

DEPARTMENT OF MATHEMATICS
UNIVERSITY OF THE PUNJAB
LAHORE-PAKISTAN

JULY, 2017

CERTIFICATE

I certify that the research work presented in this thesis is the original work of **Miss Iqra Nawazish** D/O **Rana Nawazish Ali** and is carried out under my supervision. I endorse its evaluation for the award of **Ph.D.** degree through the official procedure of **University of the Punjab**.

Prof. Dr. Muhammad Sharif
(**Supervisor**)

DECLARATION

I, **Miss Iqra Nawazish** D/O **Rana Nawazish Ali**, hereby declare that the matter printed in this thesis is my original work. This thesis does not contain any material that has been submitted for the award of any other degree in any university and to the best of my knowledge, neither does this thesis contain any material published or written previously by any other person, except due reference is made in the text of this thesis. Most of the contents have been appeared as my research papers.

Iqra Nawazish

DEDICATED

To

My Loving Parents

Table of Contents

List of Figures

Acknowledgements

All praises to **Allah Almighty** Who is the most gracious and merciful. I pay my deep gratitude to **Him** Who blessed me with ability, opportunity and knowledge to undertake this research task and enabling me to its completion. After **Allah**, all respects and regards to the **Holy Prophet Hazrat Muhammad (Peace Be Upon Him)** who is the great source of inspiration for all knowledge seekers.

I feel extremely oblige to my supervisor **Prof. Dr. Muhammad Sharif** for his valuable guidance, constructive comments and continuous check and balance throughout the research work despite his busy schedules. I consider it as a great opportunity to do my PhD under his guidance and to learn from his research expertise. I take pride to acknowledge Department of Mathematics and its faculty for providing excellent learning environment. I also place on record my sense of gratitude to M.Phil/Ph.D research fellows for creating a good learning atmosphere. *I would also like to thank Pakistan Academy of Science for his financial support.*

I pay my greatest appreciation to my friend **Saima** for being there whenever I needed and research fellows **Kanwal** and **Saadia** for stimulating discussions, sharing the exhausted situation before the deadlines and all the fun we had together particularly at lunch time. During the most difficult times when writing this thesis, they gave me the moral support and the freedom I needed to move on. Lastly, I wish to acknowledge a friendship that began at Center for Undergraduate Studies and became ripe through nine years. Thank you **Ayesha Ikram** for your continual support, cooperative behavior and unforgettable memories of my precious nine years. I feel proud to have such friends without whom my life would be different.

My words are bound and this acknowledgement would be limited without mentioning the most basic source of my life, my family. I owe a lot to my parents who encouraged and helped me at every stage of my personal and academic life and longed to see this achievement come true. Thank you so much **Abu g** and **Maa** for doing so much for me. I am very much indebted to my brothers **Bilal** and **Umer** who have cherished with me every great moment and supported me whenever I needed it. Many special thanks are due to my sisters **Uzma** and **Ayesha**, **Faiza** bhabhi, nieces and nephews who have been a source of love and energy ever since.

Lahore **Iqra Nawazish**
July, 2017

Abstract

In this thesis, we study inflationary dynamics, cosmic evolution and structure of hypothetical geometries. Firstly, we investigate the behavior of warm intermediate and logamediate inflationary models for flat isotropic and homogeneous universe in Einstein frame representation of $f(R)$ gravity. In this scenario, we study the dynamics of strong and weak constant as well as generalized dissipative regimes. In both regimes, we discuss inflaton solution, slow-roll parameters, scalar and tensor power spectra, corresponding spectral indices as well as tensor-scalar ratio for Starobinsky inflationary model and determine their compatibility with Planck 2015 constraints.

Secondly, we study the existence of Noether symmetry and associated conserved quantity of some isotropic as well as anisotropic universe models in $f(R,T)$ gravity. The cyclic variable is introduced to construct exact solution of Bianchi I model. We also consider a generalized spacetime which corresponds to different anisotropic homogeneous universe models and scalar field model (quintessence and phantom) admitting minimal coupling with $f(R,T)$ models. For these models, we formulate exact solutions without introducing cyclic variable. We investigate the behavior of some cosmological parameters using exact solutions through graphical analysis.

Finally, we discuss wormhole solutions of static spherically symmetric spacetime via Noether symmetry approach in $f(R)$ and $f(R,T)$ theories. We formulate symmetry generators, associated conserved quantities and wormhole solutions for constant as well as variable red-shift functions. For perfect fluid, we evaluate an explicit form of generic function $f(R)$ and also evaluate exact solution for $f(R)$ power-law model. In $f(R,T)$ gravity, we consider two $f(R,T)$ models appreciating indirect curvature-matter coupling and formulate solutions for both dust as well as perfect fluids. We study the behavior of null/weak energy conditions with respect to ordinary matter and effective energy-momentum tensor for physically acceptable of wormhole solutions.

Abbreviations

In this thesis, the signatures of the spacetimes will be $(-,+,+,+)$. Also, we shall use the following list of abbreviations.

BI:	Bianchi Type I
BIII:	Bianchi Type III
CDM:	Cold Dark Matter
CMBR:	Cosmic Microwave Background Radiations
DE:	Dark Energy
EoS:	Equation of State
FRW:	Friedmann-Robertson-Walker
KS:	Kantowski-Sachs
LRS:	Locally Rotationally Symmetric
NEC:	Null Energy Condition
WEC:	Weak Energy Condition
WH:	Wormhole
WMAP:	Wilkinson Microwave Anisotropy Probe

Introduction

The standard model of the universe provides cosmological view of the early universe (radiation or matter dominated phase) leading to decelerated expansion. This expansion introduces some critical issues like horizon (why current universe seems to be isotropically homogeneous?) and flatness (why total density of the universe is getting closer to critical density?). To resolve these long standing issues, the inflationary scenario proposed the most conclusive solution without disturbing the achievements of cosmological model. Guth [1] introduced an epoch of rapid exponential expansion before decelerated expanding universe, called "inflation". This revolutionary approach explains the origin of CMBR as well as distribution of large scale structure. Inflationary scenario is referred as an intrinsic constituent of the standard model.

The inflationary paradigm follows a straightforward mechanism in which scalar field acts as a source of rapid expansion known as "inflaton". This field releases potential energy when it moves from false to true vacuum. The released energy acts as a repulsive force and hence inflates the early universe [2]. The existence of inflaton field incorporating kinetic as well as potential energy leads to split inflation into two distinct regimes, i.e., slow-roll and reheating. In slow-roll regime, the inflaton field is found to be non-interacting which assures the existence of dominant potential energy [3]. In reheating phase, the inflaton field appreciates strong interactions in true vacuum as both kinetic and potential energies are approximately equivalent. This defines an oscillatory motion of inflaton leading to dissipate into radiations around origin of potential energy and consequently, introduces ending stage of inflation [4].

The inflationary paradigm triggered researchers to establish a smooth joining between infant and late-time universe. Berera [5] resolved this issue by introducing the idea of warm inflation. In this scenario, inflaton appreciates interactions with background field that releases vacuum energy in slow-roll regime. When vacuum energy completely dissipates into radiation energy, the inflating universe possesses enough temperature to allow a graceful exit into radiation dominated era without admitting any separate reheating phase. In warm inflation, the existence of thermal fluctuations generates strong dissipation effects leading to create relativistic particles. The dissipation coefficient determines the effect of dissipation by characterizing two important regions, i.e., weak and strong dissipative regimes. In the region of weak dissipation, the dissipation coefficient identifies a slow rate of decaying inflaton due to weak interactions. However, strong interactions of inflaton with any other field yield enough amount of dissipation that effectively increases the decay rate of inflaton in strong dissipative regime.

The exact solutions of scale factor provide an optimistic approach to categorize different inflationary models. The cold inflationary model corresponds to scale factor that measures de Sitter expansion (exponential expansion) while a scale factor with quasi-de Sitter expansion leads to chaotic inflationary model. For intermediate inflationary model, the scale factor incorporates expansion rate slower than that of exponential expansion but faster than power-law expansion [6]. Herrera et al. [7] studied intermediate as well as logamediate warm inflationary models and discussed the behavior of these inflationary models through generalized dissipation coefficient in both weak as well as strong dissipative regimes. Setare and Kamali [8] investigated the dynamical role of warm vector isotropic inflation for same inflationary models and observed the consistency of inflationary parameters with WMAP7 constraints. Sharif and Saleem [9] considered BI universe model to evaluate compatibility criteria of these models in the context of warm vector inflation. After inflationary stage, the cosmic journey represents radiation as well as matter dominated eras and eventually demonstrates current stage of the universe.

Recent observations indicate late-time cosmic accelerated expansion showing the presence of some mysterious force comprising repulsive gravitational effects, referred as DE. There are two main proposals to explain its nature. In the first approach, matter part while in the second approach geometric part of the Einstein-Hilbert action is modified. The second proposal leads to modified theories of gravity like $f(R)$ (R represents Ricci scalar) theory which is obtained by replacing R with an arbitrary function. This theory appreciates minimal coupling with matter part yielding some interesting results in cosmology [10].

Felice and Tsujikawa [11] investigated the dynamics of non-warm inflation with Starobinsky model in both Einstein as well as Jordan frames of $f(R)$ gravity. Bamba et al. [12] reconstructed some $f(R)$ models via non-warm inflationary constraints and identified that observational parameters relative to power-law model yield the most compatible results. Artymowski and Lalak [13] extended Starobinsky inflationary model in the context of non-warm inflation and obtained observational parameters compatible with Planck and BICEP2 in both frames. Sharif and Ikram [14] investigated dynamics of warm inflation via intermediate and logamediate inflationary models in Jordan frame representation of $f(\mathcal{G})$ gravity ($\mathcal{G}$ represents Gauss-Bonnet term). The same authors [15] studied non-warm inflationary dynamics through scalar field and fluid cosmology in this gravity.

The non-minimal coupling provides a fresh insight among researchers as it helps to study various cosmological scenarios. Bertolami et al. [16] merged this concept between gravity and matter such that arbitrary function of R appreciates non-minimal coupling with matter Lagrangian density ($\mathcal{L}_m$). Harko et al. [17] developed an extension of $f(R)$ gravity known as $f(R,T)$ gravity (T identifies trace of the energy-momentum tensor) incorporating non-minimal curvature-matter coupling. Sharif and Zubair [18] explored cosmic evolution through reconstruction of some DE models with energy conditions, exact anisotropic solutions, stability criteria and thermodynamical picture in the this gravity.

The existence of continuous symmetry reduces complexity and yields connection between differentiable symmetry and conserved quantity of the dynamical system. The continuous symmetries relative to Lagrangian are characterized as Noether symmetries. Capozziello et al. [19] used this approach to determine a generalized exact static spherically symmetric solution of $f(R)$ power-law model. The same authors [20] extended this work to non-static spherically symmetric solution as well as axially symmetric model. Hussain et al. [21] found Noether symmetries relative to $f(R)$ power-law model for isotropic universe model and identified that the corresponding boundary term turns out to be zero while Shamir et al. [22] determined some extra symmetries with non-zero boundary term. Kucukakca and Camci [23] analyzed the existence of Noether symmetry for the same universe model via Palatini $f(R)$ formalism. Momeni et al. [24] explored Noether symmetry in mimetic $f(R)$ and $f(R,T)$

theories and analyzed stability of solutions in the presence of normal matter.

Sharif and Fatima [25] explored the existence of conserved quantities relative to Noether symmetries in both vacuum as well as non-vacuum regions in $f(\mathcal{G})$ gravity. Shamir and Ahmad [26] obtained exact solutions through this approach in non-minimally coupled $f(\mathcal{G},T)$ gravity. Sanyal [27] found exact anisotropic solutions for KS universe in modified gravity non-minimally coupled with scalar field. Camci and Kucukakca [28] generalized this work to obtain explicit forms of scalar field for BI and BIII universe models. Kucukakca et al. [29] investigated the presence of continuous symmetry and formulated anisotropic solutions in the same gravity. Subsequently, Camci et al. [30] extended this work for BI, BIII and KS universe models. Zhang et al. [31] studied multiple scalar field scenario and found corresponding potential functions that established a relation between quintessence and phantom models. Jamil et al. [32] explored $f(R)$ tachyon model and obtained explicit forms of potential as well as $f(R)$ functions.

The structure of WH geometry comprises a hypothetical tunnel or bridge through which a smooth passing is possible in different regions of spacetime. Lobo and Oliveira [33] discussed WH geometry for different fluids with constant red-shift function in $f(R)$ gravity. Bahamonde et al. [34] constructed non-static cosmological WH supported by perfect fluid in the same gravity. Mazharimousavi and Halilsoy [35] considered $f(R)$ model admitting polynomial expansion and obtained a sufficient condition leading to a near-throat WH solution for both vacuum as well as non-vacuum cases. Sharif and Fatima [36] found physically acceptable static and non-static WH solutions for galactic halo region and conformal symmetry in modified Gauss-Bonnet gravity, respectively. Zubair et al. [37] discussed static WH solution and explored realistic nature for isotropic, barotropic and anisotropic fluids in $f(R,T)$ gravity. Bahamonde et al. [38] used Noether symmetry technique to obtain exact solutions of red-shift and shape functions. They also discussed geometry of WH solutions to determine their realistic fate in scalar-tensor theory non-minimally coupled with torsion scalar.

This thesis is devoted to study cosmic inflation through warm inflationary universe model and evolution of the universe for isotropic as well as anisotropic universe models using Noether symmetry approach in $f(R)$ and $f(R,T)$ theories of gravity. We also use this approach to investigate the existence of realistic and traversable static WH solutions. This thesis is arranged as follows.

- Chapter **One** provides basic concepts and definitions related to this thesis.

- Chapter **Two** explores the dynamics of warm inflation via intermediate and logamediate inflationary models in Einstein representation of $f(R)$ gravity.

- Chapter **Three** investigates exact solutions of some isotropic and anisotropic universe models via Noether symmetry approach for non-minimal curvature-matter coupling appreciating minimal coupling with matter and scalar fields.

- In chapter **Four**, we discuss the existence of static spherically symmetric WH solutions for both constant as well as variable forms of red-shift function.

- Chapter **Five** presents summary of all results and also specifies some issues for future research.

Chapter 1

Basic Review

This chapter is dedicated to understand some basic aspects of modern cosmology corresponding to this thesis.

1.1 Cosmic Inflation

The revolutionary idea of cosmic inflation was proposed to explain evolution in very early phase of the universe (just after the Planck epoch but prior to radiation era). This notable proposal is not a replacement of standard cosmological model as it supports the standard achievements as well as successfully overcomes some critical shortcomings of the model. Alan Guth defined this cosmological inflation as *an epoch in which the scale factor grows exponentially and* $\ddot{a} > 0$ *leading to accelerated expansion in early universe.* For the existence of inflationary epoch, the necessary condition is

$$\frac{d}{dt}\left(\frac{1}{aH}\right) < 0,$$

where $(aH)^{-1}$ defines comoving Hubble length (an approximate distance that light covers during Hubble time H^{-1}) decreasing with time. The extent of inflation is measured by number of e-folds given by

$$N = \ln[\frac{a_f}{a_i}] = \int_{t_i}^{t_f} H(t)dt,$$

where t_i and t_f represent initial and end times of inflation. We study how inflationary era solves long standing problems, i.e., horizon and flatness problems. The isotropic temperature of CMBR leads to state horizon problem as "why photons of the CMBR coming from opposite directions today have the same temperature to high precision while the size of causally connected regions at the last scattering is at most one degree?" The flatness problem is "if the curvature of the universe is not very large at present scale, then it must have been extremely small at early times".

During inflation, the exponential expansion ($H = H_0$, where H_0 is constant) tremendously increases size of the universe while dramatic reduction of comoving Hubble length indicates that current observable universe originates from a tiny region. This region establishes thermal equilibrium in past and therefore admits causal contact between these regions. Thus, the temperature of CMBR seems to be isotropic in opposite regions of sky because the particles were able to communicate in past. Hence, the horizon problem remains no more a mystery. To resolve the flatness problem, the density parameter not only needs to close to one, in fact it must drives so close to one that even all subsequent expansion from inflation to current cosmic eras is entirely insufficient to move it away again. The exponential expansion with decreasing comoving Hubble length (aH increases with time) drives density parameter extremely close to one implying flat geometry at very early times. Thus, the necessity of fine-tuned initial conditions is completely avoided and flatness problem is successfully resolved.

1.1.1 Inflationary Dynamics

The inflationary scenario offers an admissible explanation for cosmologist to resolve long standing issues but the question arises *what factor is responsible to inflate early universe?* The satisfactory answer demands the presence of some ingredient possessing large negative pressure. Our universe experiences a dramatic phase transition (extensive change in cosmic properties) in early times. On relativistic grounds, this early transition can be explained by scalar field (the only component of cosmic fluid) with large negative pressure. In this regard, the homogeneous scalar field is referred as perfect candidate to study dynamics of inflation.

In inflationary cosmology, the scalar field with potential energy (at each point) is increasing very slowly as the universe expands and since, it is dynamical so kinetic energy also appears. The Lagrangian density relative to scalar field is [39]

$$\mathcal{L}_{\phi}=-\frac{1}{2}g^{\mu\nu}\partial_{\mu}\phi\partial_{\nu}\phi-V(\phi), \tag{1.1.1}$$

where the first term identifies kinetic energy $\frac{\dot{\phi}}{2}$ while the second term denotes potential energy. Due to incredible equivalence of scalar field with perfect fluid (along zero momentum density and isotropic stress), the corresponding energy density and pressure are defined as

$$\rho_{\phi}=\frac{\dot{\phi}^2}{2}+V(\phi),\quad p_{\phi}=\frac{\dot{\phi}^2}{2}-V(\phi), \tag{1.1.2}$$

where dot defines time derivative. The corresponding continuity equation leads to scalar wave equation as

$$\ddot{\phi}+3H\dot{\phi}+V_{,_{\phi}}=0,$$

where subscript of V denotes derivative with respect to ϕ. When the scalar field ϕ rests at its minimum position (vacuum state), both energy density as well as pressure turn out to be zero implying $\frac{\dot{\phi}^2}{2} \approx |V(\phi)|$. In inflationary paradigm, there are two vacuum states, i.e., false and true vacuum. The former stage is defined when $\phi = 0$ but the space is not empty while later stage appears when potential gets minimum with $\phi \neq 0$ and $\frac{\dot{\phi}^2}{2} \approx |V(\phi)|$. The cosmic inflation started its journey when inflaton initiates to move out from false vacuum and begins to roll down very slowly demonstrating slow-roll inflation.

In region of slow-roll, the inflaton field remains non-interacting with any other background field. This non-interacting behavior leaves no possibility of radiation production and consequently, vacuum energy density dominates as well as temperature of the universe dramatically drops down as it expands. The necessary conditions of inflation are accelerated expansion and decreasing comoving Hubble length while sufficient condition is slowly varying Hubble parameter that leads to define slow-roll condition as follows

$$\frac{\ddot{a}}{a} = \dot{H} + H^2 > 0.$$

This condition holds for $\dot{H} > 0$ otherwise, we require $-\frac{\dot{H}}{H^2} < 1$. Thus, the slow-roll parameters are

$$\epsilon = \frac{1}{2}\left(\frac{V_{,\phi}^2}{V^2}\right) = -\frac{\dot{H}}{H^2}, \quad \eta = \frac{V_{,\phi\phi}}{V} = -\frac{\ddot{H}}{H\dot{H}}, \tag{1.1.3}$$

where ϵ characterizes accelerated and decelerated expansion for $\epsilon < 1$ and $\epsilon > 1$, respectively. Besides specifying expansion, the qualitative analysis of these parameters indicate that the scalar field should not quickly roll down towards potential origin. For this purpose, the slope of potential should not be too steep. The slow-roll approximation also avoids $\ddot{\phi}$ from scalar wave equation and provides $\frac{\dot{\phi}^2}{2} << V(\phi)$.

After slow-roll, the inflaton must lead to the end of inflation but the supercooled universe needs to attain enough temperature to enter into radiation dominated era.

To achieve this ending phase, a separate reheating phase is introduced in which the inflaton initiates oscillatory motion in true vacuum phase and kinetic energy becomes equivalent to potential energy. This process decays inflaton into radiations and universe becomes hot enough to admit an exit from inflationary epoch to radiation dominated universe. Thus, cosmological inflation ends for $\epsilon \approx 1$.

1.2 Warm Inflation

In cold inflationary era, the universe expands in one region (supercooled slow-roll phase) while decay of inflaton occurs in another region (reheating phase). In contrast to supercooled inflation, the idea of warm inflation significantly unifies these two dynamical regions. In warm inflation, inflaton interacts with background field implying a continuous production of radiations (create relativistic particles) throughout the inflationary phase and dramatic fall of temperature is elegantly avoided. Therefore, the salient characteristic of warm inflation is to connect end stage of inflationary epoch with the current cosmos as it smoothly heats up enough to enter into radiation era. During inflation, the vacuum energy density dominates over radiation density ρ_r as well as kinetic energy. The radiation density evolves as

$$\dot{\rho}_r + 4H\rho_r = \Gamma\dot{\phi}^2,$$

where Γ_i represents dissipation coefficient and $\Gamma\dot{\phi}^2$ acts as a source term that encourages radiation energy while $4H\rho_r$ is referred as sink term which throws them away.

The radiation production (appears due to inflaton decay) is counterbalanced by dissipation effects introduced in the equation of motion of inflaton as

$$\ddot{\phi}+(3H+\Gamma)\dot{\phi}+V(\phi)=0.$$

Here source term appreciates thermal equilibrium during the decaying process of inflaton. If a system does not admit thermal equilibrium then it is not possible to explain the dissipation effect as well as decay of inflaton through source term [40]. In the decay process, the energy released by inflaton converts into heat and consequently, increases radiation density. During inflation, the Hubble parameter, dissipation factor and inflaton possess an extremely small variation leading to a non-zero steady state point of radiation density. Therefore, the radiation production is entirely based on source rather than initial conditions. The dissipation factor can be considered as constant, ϕ-dependent function or in terms of thermal bath temperature T (due to its interaction with T).

In the dynamics of warm inflation, thermal bath temperature plays a significant role to determine the origin of density perturbations. In cold inflation, the quantum fluctuations of inflaton generate initial density perturbations while these perturbations emerge from thermal fluctuations in warm inflation. For the existence of warm inflation, thermal temperature defines necessary condition $\mathrm{T} > H$ which indicates that thermal fluctuations will dominate over the quantum fluctuations. In case of slow-roll approximation, this temperature turns out to be constant and therefore, successfully eliminates the necessity of reheating phase. The inflationary paradigm is categorized in two distinct regimes relative to strength of dissipation. If the effect of dissipation is small then particles belong to weak dissipative regime whereas the intensive dissipation effect leads to strong dissipative regime. The warm inflation experiences a graceful exit when vacuum energy density ρ_ϕ completely dissipates into radiation density.

1.3 Some Constraints on Inflationary Model

We have discussed fundamental features of inflation, just a theoretical phase occurred in very early times but recent observations successfully support this hypothetical era by evaluating some standard constraints. These observational constraints follow the trail of quantum fluctuations relative to density perturbations (scalar perturbations arising from inflaton) and gravitational waves (tensor perturbations appears from metric tensor). The scalar and tensor perturbations leave a strong impact on the spectrum of CMBR while the scalar perturbations only provide seeds for large scale structure. The vacuum energy released by inflaton dominates over energy density of the universe and generates small inhomogeneities defined as source for structure formation. Recent cosmological observations measure the effect of these perturbations leading to constrain the inflationary models.

To analyze variance in fluctuations, some important parameters like scalar power spectrum (Δ_R^2) and tensor power spectrum (Δ_T^2) have been introduced [41]. For quantum fluctuations, the scalar and tensor power spectra are calculated in terms of slow-roll and Hubble parameters as

$$\Delta_R^2 = \left(\frac{H}{\dot{\phi}} < \delta\phi >\right)^2, \quad \Delta_T^2 = \frac{2\kappa^2 H^2}{\pi^2}. \tag{1.3.1}$$

For non-warm and warm inflationary models, $< \delta\phi >$ is given by

$$< \delta\phi >_{quantum} = \frac{H^2}{2\pi}, \quad < \delta\phi >_{thermal} = \left(\frac{\Gamma H \mathrm{T}^2}{(4\pi)^3}\right)^{\frac{1}{4}}.$$

A slight deviation of scalar and tensor power spectra from physical scale length is measured by the corresponding spectral indices given as

$$n_s = 1 - 6\epsilon + 2\eta, \quad n_T = -2\epsilon.$$

Here n_s and n_T denote scalar and tensor spectral indices, respectively. If the spectral index is unity, then the corresponding spectrum is referred as scale invariant. Recent observations of Planck 2015 [42] provide constraints for spectral index and tensor-scalar ratio ($\mathcal{R}$) as $n_s = 0.9603 \pm 0.0062$ (68%CL) and $\mathcal{R} < 0.10$ (95%CL), respectively.

1.4 Modified Theories of Gravity

In the following, we discuss $f(R)$ theory and its extension $f(R,T)$ theory.

1.4.1 $f(R)$ Theory

In Einstein-Hilbert action, the modification induces the replacement of linear scalar curvature with a more generic function appreciating only minimal coupling with matter. Such gravitational modification defines the action as

$$\mathcal{I} = \int d^4x\sqrt{-g}[\frac{f(R)}{2\kappa^2} + \mathcal{L}_m], \tag{1.4.1}$$

where g identifies determinant of the metric tensor $g_{\mu\nu}$, $f(R)$ represents non-linear generic function minimally coupled with Lagrangian density of matter $\mathcal{L}_m$. There are three standard variational approaches that derive $f(R)$ field equations from action (1.4.1). The first approach defines the metric formalism which drives the field equations by metric variation of the action. In this formalism, the basic entity is the dependence of affine connection $\Gamma^{\sigma}_{\mu\nu}$ on $g_{\mu\nu}$ while matter Lagrangian density depends only on $g_{\mu\nu}$. The second approach is referred as Palatini formalism that comprises

$\Gamma^{\sigma}_{\mu\nu}$ and $g_{\mu\nu}$ as independent variables. In third approach, the same process of Palatini formalism continues but here $\mathcal{L}_m$ is considered to be a function of both $\Gamma^{\sigma}_{\mu\nu}$ as well as $g_{\mu\nu}$. Due to these distinct formalisms, the $f(R)$ gravity is characterized as *metric $f(R)$ gravity, Palatini $f(R)$ gravity* and *metric-affine $f(R)$ gravity*. In the following, we discuss basic formalism and standard models of metric $f(R)$ gravity.

The metric variation of action (1.4.1) leads to

$$f_R R_{\mu\nu} - \frac{1}{2} f g_{\mu\nu} - \nabla_\mu \nabla_\nu f_R + g_{\mu\nu} \Box f_R = \kappa^2 T^{(m)}_{\mu\nu}. \tag{1.4.2}$$

Here, f_R shows derivative of generic function f with respect to R, ∇_μ represents covariant derivative, $\Box = \nabla_\mu \nabla^\mu$ and $T^{(m)}_{\mu\nu}$ denotes the energy-momentum tensor. The equivalent form of Eq.(1.4.2) is

$$G_{\mu\nu} = \frac{1}{f_R}(T^{(m)}_{\mu\nu} + T^{(c)}_{\mu\nu}) = T^{eff}_{\mu\nu}, \tag{1.4.3}$$

where $G_{\mu\nu}$, $T^{(c)}_{\mu\nu}$ and $T^{eff}_{\mu\nu}$ identify Einstein, curvature and effective energy-momentum tensors, respectively. The curvature terms relative to generic function define $T^{(c)}_{\mu\nu}$ as

$$T^{(c)}_{\mu\nu} = \frac{f - Rf_R}{2} g_{\mu\nu} + \nabla_\mu \nabla_\nu f_R - \Box f_R g_{\mu\nu}. \tag{1.4.4}$$

The stability analysis is a significant aspect in modified theories as it provides viability criteria of different modifications in the Einstein-Hilbert action. These gravitational theories avoid instabilities such as ghosts degrees of freedom endorsed in Ostrogradski's instability and Dolgov-Kawasaki instability [43]. Ghost is referred as a field which consists of particles moving with negative kinetic energy. In $f(R)$ gravity, the appearance of ghost is avoided for $f_R > 0$ [11]. Dolgov and Kawasaki [44] discussed instability criteria of $R - \frac{\mu^4}{R}$ model which becomes unstable if $f_{RR} < 0$ and sets stability condition for viable $f(R)$ models as $f_{RR} > 0$. Thus, viable $f(R)$ models require to satisfy stability constraints $f_R(R) > 0$, $f_{RR}(R) > 0$, $R > R_0$, where R_0 is the current value of Ricci scalar.

In this thesis, we shall use three viable $f(R)$ models to study early as well as current cosmic expansion. The first $f(R)$ model is Starobinsky inflationary model given as [45]

$$f(R) = R + \mu R^2, \tag{1.4.5}$$

where μ is a positive constant. This model is also known as the first inflationary model found to be consistent with anisotropy observed in CMBR. Thus, it can be considered as a viable alternative to scalar field inflationary models. Besides explaining early expansion, this model also leads to current cosmic expansion due to R^2 term. The second model is $f(R)$ power-law model defined as [46]

$$f(R) = f_0 R^n, \quad n \neq 0, 1, \tag{1.4.6}$$

where n and f_0 represent constants. This model suffers from big-rip singularity for $n < 0$ but for $n > 1$ with $f_0 > 0$, this singularity may be avoided. The third $f(R)$ model represents a generalization of Starobinsky model which includes an R^n extension as follows [47]

$$f(R) = R + \mu R^2 + \nu R^n, \tag{1.4.7}$$

where $\nu \geq 3$ and clearly, this model is free from singularity.

Jordan Frame of $f(R)$ Theory

In Jordan frame, there is a direct interaction between geometrical and matter parts in the action of $f(R)$ gravity. We consider flat FRW metric as

$$ds^2 = -dt^2 + a^2(t)(dx^2 + dy^2 + dz^2), \tag{1.4.8}$$

where a is the scale factor. The energy-momentum tensor for perfect fluid is given by

$$T^{(m)}_{\mu\nu} = (\rho_m + p_m)u_\mu u_\nu + g_{\mu\nu}p_m,$$

where ρ_m and p_m identify energy density and pressure, respectively while u_μ denotes four-velocity of comoving fluid. For action (1.4.1), we obtain the following field equations along with perfect fluid

$$\frac{f - Rf_R}{2} + 3H^2 f_R + 3H\dot{f}_R = \kappa^2\rho_m, \tag{1.4.9}$$

$$\ddot{f}_R + 2\dot{H}f_R - H\dot{f}_R = -\kappa^2(\rho_m + p_m), \tag{1.4.10}$$

In order to evaluate an expression for a and H, we consider Starobinsky model (1.4.5) with $\mu = \frac{1}{6M^2}$, where M is a positive constant having dimension of mass. Inserting this model into (1.4.9) and (1.4.10), we obtain

$$a = a_i \exp\left[H_i(t - t_i) - \frac{M^2(t - t_i)^2}{12}\right], \quad H = H_i - \frac{M^2(t - t_i)}{6}, \tag{1.4.11}$$

where t_i denotes initial cosmic time whereas a_i and H_i represent scale factor and Hubble parameter at $t = t_i$, respectively. In order to discuss inflationary paradigm, we need to consider perfect fluid as equivalent to scalar field implying $\rho_m = \rho_\phi = \frac{\dot{\phi}^2}{2} + V(\phi)$ and $p_m = p_\phi = \frac{\dot{\phi}^2}{2} - V(\phi)$. It is strongly claimed that the equivalence of perfect fluid with scalar field is not viable in Jordan frame representation due to the existence of negative kinetic energy [48]. To get rid of such negative kinetic energy, the fourth order field equations are transformed conformally from Jordan to Einstein frame which contains an additional scalar degree of freedom with positive kinetic term [49].

Einstein Frame of $f(R)$ Theory

In the Einstein frame, the $f(R)$ gravity indicates existence of extra scalar degree of freedom which drives early as well as late-time cosmic acceleration. A conformal transformation over a metric structure allows to scale time, length and mass whereas angles remain unchanged. The action of $f(R)$ gravity can also be written as

$$I = \frac{1}{2\kappa^2}\int d^4x\sqrt{-g}(f_R R - V(\phi)) + \mathcal{L}_m(g_{\mu\nu}, \psi), \tag{1.4.12}$$

where $V(\phi) = f_R R - f$. For a conformal factor $\tilde{g}_{\mu\nu} = \varphi^2 g_{\mu\nu} = f_R g_{\mu\nu}$, this action takes the form

$$I_E = \int d^4x\sqrt{-\tilde{g}}\left(\frac{\tilde{R}}{2\kappa^2} - \frac{1}{2}\tilde{g}^{\mu\nu}\partial_\mu\phi\partial_\nu\phi - U(\phi) + \tilde{\mathcal{L}}_m(f_R^{-1}(\phi)\tilde{g}_{\mu\nu}, \psi)\right). \tag{1.4.13}$$

Here, $U(\phi) = \frac{V(\phi)}{f_R^2}$, the considered conformal factor becomes field dependent as $\varphi^2 = f_R = \exp[\sqrt{\frac{2}{3}}\kappa\phi]$ and the gravitational term of action (1.4.1) takes equivalent form of the Einstein-Hilbert action appreciating minimal coupling between matter Lagrangian density and scalar field. In this frame, the flat FRW model becomes

$$d\tilde{s}^2 = -d\tilde{t}^2 + \tilde{a}^2(\tilde{t})(dx^2 + dy^2 + dz^2), \tag{1.4.14}$$

where

$$d\tilde{s} = \sqrt{f_R}ds, \quad d\tilde{t} = \sqrt{f_R}dt, \quad \tilde{a} = \sqrt{f_R}a. \tag{1.4.15}$$

The energy-momentum tensor corresponding to matter and scalar parts are

$$\tilde{T}^{(m)}_{\mu\nu} = -\frac{2}{\sqrt{-\tilde{g}}}\frac{\partial\tilde{\mathcal{L}}_m}{\partial\tilde{g}^{\mu\nu}}, \quad \tilde{T}^{(\phi)}_{\mu\nu} = -\frac{2}{\sqrt{-\tilde{g}}}\frac{\partial(\partial\sqrt{-\tilde{g}}\tilde{\mathcal{L}}_\phi)}{\partial\tilde{g}^{\mu\nu}}. \tag{1.4.16}$$

where $\tilde{\mathcal{L}}_\phi$ represents Lagrangian density of a scalar field given by

$$\tilde{\mathcal{L}}_\phi = -\frac{1}{2}\tilde{g}^{\mu\nu}\partial_\mu\phi\partial_\nu\phi - U(\phi).$$

For the action (1.4.13), the field equations and continuity equation turn out to be

$$\frac{3\tilde{H}^2}{\kappa^2} = \tilde{\rho}_m, \quad 3\tilde{H}^2 + 2\frac{d\tilde{H}}{d\tilde{t}} = -\kappa^2\tilde{p_m}, \tag{1.4.17}$$

$$\frac{d\tilde{\rho}_m}{d\tilde{t}} + 3\tilde{H}(\tilde{t})(\tilde{\rho}_m + \tilde{p}_m) = 0. \tag{1.4.18}$$

The energy density and pressure are represented by $\tilde{\rho}_m = \frac{\rho_m}{f_R^2}$ and $\tilde{p}_m = \frac{p_m}{f_R^2}$ whereas $\tilde{H}$ denotes Hubble parameter in this frame. In order to formulate expressions of $\tilde{t}$, $\tilde{a}$ and $\tilde{H}$ for (1.4.5) with $\mu = \frac{1}{6M^2}$, we integrate Eq.(1.4.15) yielding

$$\tilde{t} = \frac{2}{M}\left[H_i(t-t_i) - \frac{M^2(t-t_i)^2}{12}\right], \tag{1.4.19}$$

$$\tilde{a}(\tilde{t}) = \frac{2H_i a_i}{M}\left[1 - \frac{M^3\tilde{t}}{12H_i^2}\right]e^{\frac{M\tilde{t}}{2}}, \quad \tilde{H}(\tilde{t}) = \frac{M}{2}\left[1 - \frac{M^2}{6H_i^2}\left(1 - \frac{M^3\tilde{t}}{12H_i^2}\right)^{-2}\right].$$

The conformal transformation allows a smooth transition between these two frames as it only redefines the scales of fundamental quantities that retain physical predictions in both frames [50]. The main difference in both frames is that the Jordan frame defines $f(R)$ gravity on the basis of metric tensor whereas Einstein frame describes the theory with the help of metric tensor along with scalar field interacting with matter sector.

1.4.2 $f(R,T)$ Theory

The modification carried out by a direct coupling between curvature and matter (known as non-minimally coupled gravity) put forward another step on the road of theoretical developments. If such modification is introduced in $f(R)$ gravity then it yields a generalized theory of gravity named as $f(R,T)$ gravity. For this non-minimally coupled gravity, the Einstein-Hilbert action is modified as

$$\mathcal{I} = \int d^4x\sqrt{-g}[\frac{f(R,T)}{2\kappa^2} + \mathcal{L}_m]. \tag{1.4.20}$$

The field equations are obtained through metric variation of this action as

$$R_{\mu\nu}f_R(R,T)-\frac{1}{2}g_{\mu\nu}f(R,T)+(g_{\mu\nu}\nabla^{\mu}\nabla_{\mu}-\nabla_{\mu}\nabla_{\nu})f_R(R,T)+f_T(R,T)$$
$$\times T^{(m)}_{\mu\nu}+\mathcal{A}_{\mu\nu}f_T(R,T)=\kappa^2T^{(m)}_{\mu\nu}, \tag{1.4.21}$$

where subscripts of f define corresponding partial derivatives, and $\mathcal{A}_{\mu\nu}$ denotes

$$\mathcal{A}_{\mu\nu}=\frac{g^{\mu\nu}\delta T^{(m)}_{\mu\nu}}{\delta g^{\mu\nu}}=g_{\mu\nu}\mathcal{L}_m-2T^{(m)}_{\mu\nu}-2g^{\mu\nu}\frac{\partial^2\mathcal{L}_m}{\partial g^{\mu\nu}\partial g^{\mu\nu}}.$$

The curvature terms evolve as follows

$$T^{(c)}_{\mu\nu}=f_TT^{(m)}_{\mu\nu}-f_Tg_{\mu\nu}\mathcal{L}_m+\frac{1}{2}g_{\mu\nu}(f-Rf_R)+(\nabla_{\mu}\nabla_{\nu}-\nabla^{\mu}\nabla_{\mu}g_{\mu\nu})f_R. \tag{1.4.22}$$

In non-minimally coupled $f(R,T)$ gravity, the covariant derivative of energy-momentum tensor yields an extra force which behaves as a source of deviation for massive test particles given by

$$\nabla^{\mu}T^{(m)}_{\mu\nu}=\frac{f_T}{\kappa^2-f_T}\left[(T^{(m)}_{\mu\nu}+\mathcal{A}_{\mu\nu})\nabla^{\mu}\ln f_T+\nabla^{\mu}\mathcal{A}_{\mu\nu}-\frac{g_{\mu\nu}\nabla^{\mu}T}{2}\right].$$

Harko et al. [17] introduced some theoretical models in this gravity by taking different choices of matter contribution as

- $f(R,T)$=$R+2g(T)$,
- $f(R,T)$=$f(R)+g(T)$,
- $f(R,T)$=$f_1(R)+f_2(R)g(T)$.

The viability of these $f(R,T)$ models can be analyzed through Dolgov-Kawasaki instability which requires similar sort of constraints as in $f(R)$ gravity along with an additional constraint, i.e., $1+f_T(R,T)>0$ [51]. The viability criteria for $f(R,T)$ gravity is based on the following conditions

$$f_R(R)>0,\quad f_{RR}(R)>0,\quad 1+f_T(R,T)>0,\quad R>R_0. \tag{1.4.23}$$

1.5 Noether Symmetry Approach

Symmetry defines features of a mathematical/physical system that are preserved under some change. At geometric level, symmetry appears if the system remains invariant in the presence of particular transformations, i.e., rotation, reflection or scaling while mathematically, it specifies a point transformation. The symmetry which appears due to continuous changes in a system are referred as continuous symmetry (spacetime symmetries) and the continuous symmetry corresponding to Lagrangian of a system is called Noether symmetry. The physical features of a dynamical system can be characterized by constructing the associated Lagrangian which describes energy content as well as provides information about possible symmetries of the system. Noether symmetry approach helps to construct new cosmological models and to specify conserved quantities of a system. This is due to remarkable Noether theorem which states that *every symmetry generator yields associated conserved quantity if pointlike Lagrangian remains invariant under a continuous group.* If a system admits translational symmetry in time and position then it undergoes conservation of energy and linear momentum, respectively whereas rotational symmetry leads to conservation law of angular momentum.

Noether symmetry and associated conserved quantity are highly motivated from Lie symmetries. For the sake of simplicity, we consider two-dimensional system in which the point transformation is defined as $\tilde{x} = \tilde{x}(x, y)$, $\tilde{y} = \tilde{y}(x, y)$ that maps the pair (x, y) onto $(\tilde{x}, \tilde{y})$. In order to evaluate symmetry of the system, we define an infinitesimal parameter ε in point transformation as

$$\tilde{x} = \tilde{x}(x, y; \varepsilon), \quad \tilde{y} = \tilde{y}(x, y; \varepsilon).$$

The corresponding infinitesimal generator can be found by Taylor series as follows

$$\begin{aligned}\bar{x}(x,y;\varepsilon) &= x+\varepsilon\bar{\xi}(x,y)+...=x+\varepsilon Kx+...,\\ \bar{y}(x,y;\varepsilon) &= y+\varepsilon\bar{\eta}(x,y)+...=y+\varepsilon Ky+...,\end{aligned}$$

where K identifies the associated infinitesimal symmetry generator given by

$$K=\bar{\xi}(x,y)\frac{\partial}{\partial x}+\bar{\eta}(x,y)\frac{\partial}{\partial y},$$

where $\bar{\xi}(x,y)=\frac{\partial\bar{x}}{\partial\varepsilon}|_{\varepsilon\to 0}$, $\bar{\eta}(x,y)=\frac{\partial\bar{y}}{\partial\varepsilon}|_{\varepsilon\to 0}$. This point transformation may also determine infinitesimal generalized position as $Q^i=Q^i(q^j,\varepsilon)$ that leads to define the vector field for these generalized positions as

$$K = \bar{\xi}(\vartheta,q^i)\frac{\partial}{\partial\vartheta}+\bar{\eta}^j(\vartheta,q^i)\frac{\partial}{\partial q^j}, \tag{1.5.1}$$

where ϑ represents affine parameter.

Noether symmetry requires the invariance condition given as

$$K^{[1]}\mathcal{L}+(D\bar{\xi})\mathcal{L}=DB(\vartheta,q^i), \tag{1.5.2}$$

where B identifies boundary term while the first order prolongation of vector field $K^{[1]}$ and total derivative D are defined as

$$D=\frac{\partial}{\partial\vartheta}+\dot{q}^i\frac{\partial}{\partial q^i},\quad K^{[1]}=K+(\bar{\eta}^j{}_{,\vartheta}+\bar{\eta}^j{}_{,i}\,\dot{q}^i-\bar{\xi}_{,\vartheta}\,\dot{q}^j-\bar{\xi}_{,i}\,\dot{q}^i\dot{q}^j)\frac{\partial}{\partial\dot{q}^j}. \tag{1.5.3}$$

Symmetries from invariance condition leading to conserved quantities as follows

$$I=B-\bar{\xi}\mathcal{L}-(\bar{\eta}^j-\dot{q}^j\bar{\xi})\frac{\partial\mathcal{L}}{\partial\dot{q}^j}. \tag{1.5.4}$$

This quantity also called Noether integral or first integral. If the first order prolongation of vector field and boundary term of the extended symmetry vanish, then vector field (with complete lift), invariance condition and corresponding first integral take the following form

$$K = \bar{\eta}^i(q^i)\frac{\partial}{\partial q^i} + \left[\frac{d}{dt}(\bar{\eta}^i(q^i))\right]\frac{\partial}{\partial \dot{q}^i}, \quad L_K\mathcal{L} = K\mathcal{L} = 0, \quad I = -\bar{\eta}^i\frac{\partial \mathcal{L}}{\partial \dot{q}^i}, \qquad (1.5.5)$$

where L is Lie derivative. For a dynamical system, the Euler-Lagrange equation and the associated energy function are defined as

$$\frac{\partial \mathcal{L}}{\partial q^i} - \frac{d}{dt}\left(\frac{\partial \mathcal{L}}{\partial \dot{q}^i}\right) = 0, \quad \sum_i \dot{q}^i\frac{\partial \mathcal{L}}{\partial \dot{q}^i} - \mathcal{L} = E_{\mathcal{L}}.$$

The existence of Noether symmetry generator assures the presence of a *cyclic variable* which significantly simplifies the complicated structure of the field equations and leads to formulate corresponding exact solutions. Such variable is determined by a point transformation, $\bar{\varphi} : X(x_i) \to Y(y_i)$. This transformation defines an interior product operator of the vector field K as $\bar{\varphi}_K dy_i = 0$ and $\bar{\varphi}_K dy_j = 1$ with $i \neq j$ yielding y_j as cyclic variable. The complexity of the system will be reduced using this transformation but the cyclic variable is not unique in a dynamical system, therefore an appropriate choice of coordinates is quite critical. If the corresponding Lagrangian is free form this variable then exact solution can be obtained successfully.

1.6 Wormholes

A *wormhole* is defined as a theoretical geometry that creates a shortcut across long distances spacetime. If speculative passage joins two distinct patches of the same spacetime then intra-universe WH exists while inter-universe WH establishes for two distinct spacetimes. The existence of exotic matter (matter possesses negative energy density) at the WH throat encourages a smooth passing for an observer in tunnel but its sufficient amount yields a controversial existence of a realistic WH. The first hypothetical structure is the solution of Einstein field equations named as Schwarzschild WH which opposed the two-way traveling (non-traversable WH). The traversable behavior is disturbed due to the existence of strong tidal forces destroying anything that comes closer to WH throat. This destruction appears because of rapid expansion (circumference expands from zero to finite) and subsequent contraction (compresses to zero) of WH throat. Thus, the Schwarzschild WH strongly denies the presence of stable antihorizon. In order to overcome these shortcomings, Morris and Thorne [52] proposed the existence of unrealistic matter that pushes WH walls apart and keeps the throat open for traversable motion. Different approaches like modified theories, non-minimal curvature-matter coupling and scalar field models have been introduced to investigate the existence of traversable as well as realistic WH [53].

A general static spherically symmetric spacetime is given by [19]

$$ds^2 = -e^{\hat{a}(r)}dt^2 + e^{\hat{b}(r)}dr^2 + \hat{M}(r)(d\theta^2 + \sin^2\theta d\phi^2), \tag{1.6.1}$$

where $\hat{a}$, $\hat{b}$ and $\hat{M}$ are radial functions. This static spacetime explains WH geometry for $e^{\hat{b}(r)} = \left(1 - \frac{h(r)}{r}\right)^{-1}$, where $h(r)$ is the shape function and $\hat{a}(r)$ is referred as red-shift function determining gravitational red-shift. In order to identify a WH throat, the radial coordinate admits non-monotonic behavior such that it starts from infinity, decreases upto a minimum value r_0 locating WH throat at $h(r_0) = r_0$ and then starts increasing from minimum value to infinity providing $r > r_0$. The derivative condition $h'(r_0) < 1$ is introduced at throat, where prime denotes radial derivative. The throat is considered to be the minimum radius of WH geometry leading to the flaring-out condition, i.e., $\frac{h(r)-h(r)'r}{h(r)^2} > 0$. Apart from throat, the shape of WH depends on asymptotically flat space implying $\frac{h(r)}{r} \to 0$. To avoid event horizon in traversable WH, the key point is to have a finite red-shift function everywhere introducing negligible tidal forces at throat. If tidal forces are strong (magnitude of these forces is same as forces at horizon) at throat then horizon will appear and consequently, these forces would crush anything that tries to pass through.

The energy conditions provide a significant way to analyze physical existence of cosmological geometries. The presence of physically acceptable traversable WH is possible if the energy conditions are violated. Raychaudhari equations are considered to be the most fundamental ingredients to define such energy bounds

$$\frac{d\Theta}{d\tau} = -\frac{1}{3}\Theta^2 - \sigma_{\mu\nu}\sigma^{\mu\nu} + w_{\mu\nu}w^{\mu\nu} - R_{\mu\nu}l^{\mu}l^{\nu}, \tag{1.6.2}$$

$$\frac{d\Theta}{d\tau} = -\frac{1}{2}\Theta^2 - \sigma_{\mu\nu}\sigma^{\mu\nu} + w_{\mu\nu}w^{\mu\nu} - R_{\mu\nu}k^{\mu}k^{\nu}, \tag{1.6.3}$$

where Θ, l^{μ}, k^{μ}, $\sigma_{\mu\nu}$ and $w_{\mu\nu}$ represent expansion scalar, timelike vector, null vector, shear and rotation tensors. The set of these two equations is defined for timelike and null congruences. The positivity of the last term of both equations demands attractive gravity. For the Einstein-Hilbert action, these conditions split into null (NEC) ($\rho_m + p_m \geq 0$), weak (WEC) ($\rho_m \geq 0$), strong (SEC) ($\rho_m + 3p_m \geq 0$) and dominant (DEC) ($\rho_m \pm p_m \geq 0$) energy conditions [54]. As the Raychaudhari equations are found to be purely geometric implying that $T^{(m)}_{\mu\nu}k^{\mu}k^{\nu} \geq 0$ can be replaced with $T^{eff}_{\mu\nu}k^{\mu}k^{\nu} \geq 0$. Thus, the energy conditions in modified theories of gravity turn out to be [55]

$$\begin{aligned}
\textbf{NEC}: &\quad \rho_{eff} + p_{eff} \geq 0,\\
\textbf{WEC}: &\quad \rho_{eff} \geq 0, \quad \rho_{eff} + p_{eff} \geq 0,\\
\textbf{SEC}: &\quad \rho_{eff} + p_{eff} \geq 0, \quad \rho_{eff} + 3p_{eff} \geq 0,\\
\textbf{DEC}: &\quad \rho_{eff} \geq 0, \quad \rho_{eff} \pm p_{eff} \geq 0.
\end{aligned}$$

Chapter 2

Warm Intermediate and Logamediate Inflation in $f(R)$ Gravity

This chapter investigates the dynamics of warm intermediate and logamediate inflation for flat isotropic and homogeneous universe in Einstein frame representation of $f(R)$ gravity. For both inflationary models, we discuss dissipative effects with weak and strong interactions of inflaton using constant as well as generalized dissipative coefficient. In both dissipative regimes, we find inflaton solutions corresponding to scalar potential and radiation density. Under slow-roll approximation, we also determine observational parameter, i.e., scalar and tensor power spectra, their spectral indices and tensor-scalar ratio for Starobinsky inflationary model. The behavior of these parameters is analyzed graphically which lead to explore their compatibility with Planck 2015 constraints. The chapter is organized as follows. In section **2.1**, we discuss dynamics of warm inflation in Einstein frame. Section **2.2** is devoted to study warm intermediate strong and weak dissipation regimes for constant as well as generalized dissipation coefficient with Starobinsky inflationary model while Section **2.3** evolves the analysis for warm logamediate inflationary model. The results of warm intermediate as well as logamediate models have been published [56, 57].

2.1 Dynamics of Warm Inflation in Einstein Frame

Here we explore the behavior of warm inflation in Einstein frame of $f(R)$ gravity. The interaction of scalar and radiation fields is considered to be the most basic elements of the universe that realizes warm inflationary paradigm for a minimally coupled scalar field subject to potential $U(\phi)$. The energy density ($\tilde{\rho}_\phi$) and pressure ($\tilde{p}_\phi$) of self-interacting scalar field are

$$\tilde{\rho}_\phi = \frac{\dot{\phi}^2}{2f_R} + U(\phi), \quad \tilde{p}_\phi = \frac{\dot{\phi}^2}{2f_R} - U(\phi). \tag{2.1.1}$$

In warm inflation, the total energy density of the universe not only consist of $\tilde{\rho}_\phi$ but also contain radiation density $\tilde{\rho}_r$. For such inflationary scenario, Eqs.(1.4.17) and (1.4.18) yield

$$\frac{3\tilde{H}^2}{\kappa^2} = \tilde{\rho}_\phi + \tilde{\rho}_r, \quad 3\tilde{H}^2 + 2\frac{d\tilde{H}}{d\tilde{t}} = -\kappa^2(\tilde{p}_\phi + \tilde{p}_r), \tag{2.1.2}$$

$$\frac{d\tilde{\rho}_r}{d\tilde{t}} + 4\tilde{H}\tilde{\rho}_r - \Gamma\left(\frac{d\phi}{d\tilde{t}}\right)^2 = 0, \tag{2.1.3}$$

$$\frac{d\tilde{\rho}_\phi}{d\tilde{t}} + 3\tilde{H}(\tilde{\rho}_\phi + \tilde{p}_\phi) + \Gamma\left(\frac{d\phi}{d\tilde{t}}\right)^2 = 0. \tag{2.1.4}$$

During inflation, the radiation density must attain a non-zero steady state point and gets quasi-stable leading to the following conditions

$$\frac{d\tilde{\rho}_r}{d\tilde{t}} \ll 4\tilde{H}\tilde{\rho}_r, \quad \frac{d\tilde{\rho}_r}{d\tilde{t}} \ll \Gamma\left(\frac{d\phi}{d\tilde{t}}\right)^2. \tag{2.1.5}$$

Using the above conditions in Eq.(2.1.2), we obtain

$$\tilde{\rho}_r = \frac{3}{4f_R^2}\tilde{r}\left(\frac{d\phi}{d\tilde{t}}\right)^2 = \chi_r \mathrm{T}^4, \quad \tilde{r} = \frac{\Gamma}{3\tilde{H}}. \tag{2.1.6}$$

Here, $\tilde{r}$ describes the rate of dissipation factor relative to expansion of the universe and $\chi_r = \frac{\pi^2 g_*}{30}$, g_* represents number of relative degrees of freedom.

In warm inflation, thermal fluctuations of inflaton field are considerable as $\mathrm{T} > \tilde{H}$ and $\tilde{\rho}_r$ dissipates into $\tilde{\rho}_\phi$, i.e., $\tilde{\rho}_\phi \gg \tilde{\rho}_r$. Under this condition, the first field equation of (2.1.2) leads to

$$\left(\frac{d\phi}{d\tilde{t}}\right)^2 = -\left[\frac{2}{\kappa^2(1+\tilde{r})}\right]\frac{d\tilde{H}}{d\tilde{t}}. \tag{2.1.7}$$

The thermal bath temperature is evaluated by using Eq.(2.1.7) into (2.1.6) as

$$\mathrm{T} = \left[-\frac{3f_R^2\tilde{r}d\tilde{H}/d\tilde{t}}{2\kappa^2\chi_r(1+\tilde{r})}\right]^{\frac{1}{4}}. \tag{2.1.8}$$

Inserting Eqs.(2.1.6) and (2.1.7) in (2.1.2), we obtain potential corresponding to inflaton as

$$U(\phi) = \frac{3\tilde{H}^2}{\kappa^2} + \frac{d\tilde{H}/d\tilde{t}}{\kappa^2(1+\tilde{r})}\left[1+\frac{3\tilde{r}}{2}\right]. \tag{2.1.9}$$

For Einstein representation of FRW universe model, the observational parameters under slow-roll approximation ($H = \tilde{H}\sqrt{f_R}$) take the following form

$$\Delta_{\mathcal{R}}^2 = -\frac{\tilde{H}^2\kappa^2(1+\tilde{r})\mathrm{T}}{2d\tilde{H}/d\tilde{t}}\left[\frac{\Gamma\tilde{H}f_R^{\frac{1}{2}}}{(4\pi)^3}\right]^{\frac{1}{2}}, \quad n_s = 1 - \frac{d}{d\tilde{N}}(\ln\Delta_{\mathcal{R}}^2), \tag{2.1.10}$$

$$\Delta_T^2 = 8\kappa^2\left[\frac{\tilde{H}f_R^{\frac{1}{2}}}{2\pi}\right]^2, \quad n_T = -2\epsilon, \quad <\delta\phi>_{thermal} = \left[\frac{\Gamma\tilde{H}\mathrm{T}^2 f_R^{\frac{1}{2}}}{(4\pi)^3}\right]^{\frac{1}{4}}, \tag{2.1.11}$$

$$\mathcal{R} = \frac{\Delta_T^2}{\Delta_{\mathcal{R}}^2} = -\frac{4f_R d\tilde{H}/d\tilde{t}}{\pi^2(1+\tilde{r})\tilde{H}^{\frac{1}{2}}\mathrm{T}}\left[\frac{(4\pi)^3}{\Gamma f_R^{\frac{1}{2}}}\right]^{\frac{1}{2}}, \quad \tilde{N} = \int_{\tilde{t}_i}^{\tilde{t}}\tilde{H}(\tilde{t})d\tilde{t}, \tag{2.1.12}$$

where $\tilde{t}_i$ represents cosmic time at the beginning of inflation in Einstein frame.

2.2 Warm Intermediate Inflation

Here, we analyze warm inflation in weak ($\tilde{r} \ll 1$) as well as strong ($\tilde{r} \gg 1$) dissipative regimes for both constant as well as generalized dissipation coefficient corresponding to a scale factor that represents expansion of the universe less than de Sitter but greater than power-law expansion. In this case, the scale factor takes the form [58]

$$a(t) = a_i \exp[\gamma t^{\bar{g}}], \quad \gamma > 0, \quad 0 < \bar{g} < 1. \tag{2.2.1}$$

In Einstein frame, the intermediate scale factor and corresponding Hubble parameter turn out to be

$$\tilde{a}(\tilde{t}) = \tilde{a}_i \left[1 - \frac{M^3 \tilde{t}}{12 H_i^2}\right] \exp\left[\gamma \left(\frac{\tilde{t} M}{2H_i}\right)^{\bar{g}}\right], \quad \tilde{a}_i = \frac{2a_i H_i}{M}, \tag{2.2.2}$$

$$\tilde{H}(\tilde{t}) = \frac{1}{\tilde{a}}\frac{d\tilde{a}}{d\tilde{t}} = \gamma \bar{g} \left[\frac{\tilde{t} M}{2H_i}\right]^{\bar{g}-1}. \tag{2.2.3}$$

In order to measure the extent of inflation, we have

$$\tilde{N} = \gamma \left[\frac{M}{2H_i}\right]^{\bar{g}} (\tilde{t}^{\bar{g}} - \tilde{t}_i^{\bar{g}}). \tag{2.2.4}$$

2.2.1 Constant Dissipative Coefficient

First, we consider constant dissipation coefficient $\Gamma = \Gamma_i$ and analyze how inflaton evolves from weak to strong dissipation regime. In region of weak dissipation, the inflaton field reduces to

$$\phi = \phi_0 + \bar{\alpha}_1 \tilde{t}^{\frac{\bar{g}}{2}}, \quad U(\phi) = \frac{3}{\kappa^2}\left[\gamma \bar{g} \left(\frac{M}{2H_i}\right)^{\bar{g}} \left(\frac{\phi - \phi_0}{\bar{\alpha}_1}\right)^{\frac{2(\bar{g}-1)}{\bar{g}}}\right]^2, \tag{2.2.5}$$

where

$$\bar{\alpha}_1 = \sqrt{\frac{8\gamma(1-\bar{g})}{\kappa^2 \bar{g}} \left(\frac{M}{2H_i}\right)^{\bar{g}}}.$$

In Einstein frame, the dimensionless slow-roll parameters are introduced as

$$\epsilon = -\frac{1}{\tilde{H}^2}\frac{d\tilde{H}}{d\tilde{t}}, \quad \eta = -\left[\tilde{H}\frac{d\tilde{H}}{d\tilde{t}}\right]^{-1}\frac{d^2\tilde{H}}{d\tilde{t}^2}, \tag{2.2.6}$$

where $d\tilde{H}/d\tilde{t}$ must be negative. For slowly varying inflaton field, the slow-roll parameters (2.2.6) and radiation energy density corresponding to (2.2.3) and (2.2.5) take the form

$$\begin{aligned}
\epsilon &= \frac{1-\bar{g}}{\gamma\bar{g}}\left(\frac{2H_i}{M}\right)^{\bar{g}}\left[\frac{\phi-\phi_0}{\bar{\alpha}_1}\right]^{-2}, \quad \eta = \frac{2-\bar{g}}{\gamma\bar{g}}\left(\frac{2H_i}{M}\right)^{\bar{g}}\left[\frac{\phi-\phi_0}{\bar{\alpha}_1}\right]^{-2}, \\
\tilde{\rho}_r &= \frac{\Gamma_i(1-\bar{g})}{2\kappa^2}\left(\frac{\phi-\phi_0}{\bar{\alpha}_1}\right)^{-\frac{2}{\bar{g}}}.
\end{aligned}$$

At the earliest stage of inflationary epoch, the inflaton field at $\tilde{t} = \tilde{t}_i$ becomes

$$\phi_i = \phi_0 + \bar{\alpha}_1\left(\frac{1-\bar{g}}{\gamma\bar{g}}\right)^{\frac{1}{2}}\left(\frac{2H_i}{M}\right)^{\frac{\bar{g}}{2}}.$$

The corresponding number of e-folds and inflaton field are given by

$$\tilde{N} = \gamma\left(\frac{M}{2H_i}\right)^{\bar{g}}\left[\left(\frac{\phi-\phi_0}{\bar{\alpha}_1}\right)^2 - \left(\frac{\phi_i-\phi_0}{\bar{\alpha}_1}\right)^2\right], \tag{2.2.7}$$

$$\phi = \phi_0 + \bar{\alpha}_1\left(\frac{2H_i}{M}\right)^{\frac{\bar{g}}{2}}\left[\frac{\tilde{N}}{\gamma} + \frac{1-\bar{g}}{\gamma\bar{g}}\right]^{\frac{1}{2}}. \tag{2.2.8}$$

In weak dissipative regime, the observational parameters like scalar and tensor power spectra as well as their spectral indices become

$$\begin{aligned}
\Delta_{\mathcal{R}} &= \frac{\kappa^2}{2}\left(\frac{\Gamma_i}{2\kappa^2\chi_r}\right)^{\frac{1}{4}}(\gamma\bar{g})^2(1-\bar{g})^{-\frac{3}{4}}\left(\frac{2H_i}{M}\right)^{-\frac{1}{4}}\left[\frac{\tilde{N}}{\gamma} + \frac{1-\bar{g}}{\gamma\bar{g}}\right]^{\frac{8\bar{g}-5}{4\bar{g}}}, \\
n_s &= 1 - \frac{1}{\gamma\bar{g}}\left(\frac{8\bar{g}-5}{4\bar{g}}\right)\left[\frac{\tilde{N}}{\gamma} + \frac{1-\bar{g}}{\gamma\bar{g}}\right]^{-1}, \\
\Delta_T &= \frac{2\kappa^2\gamma^2\bar{g}^2}{\pi^2}\left(\frac{\tilde{N}}{\gamma} + \frac{1-\bar{g}}{\gamma\bar{g}}\right)^{\frac{2(\bar{g}-1)}{\bar{g}}}, \quad n_T = 2\left(\frac{\bar{g}-1}{\gamma\bar{g}}\right)\left(\frac{\tilde{N}}{\gamma} + \frac{1-\bar{g}}{\gamma\bar{g}}\right)^{-1}.
\end{aligned}$$

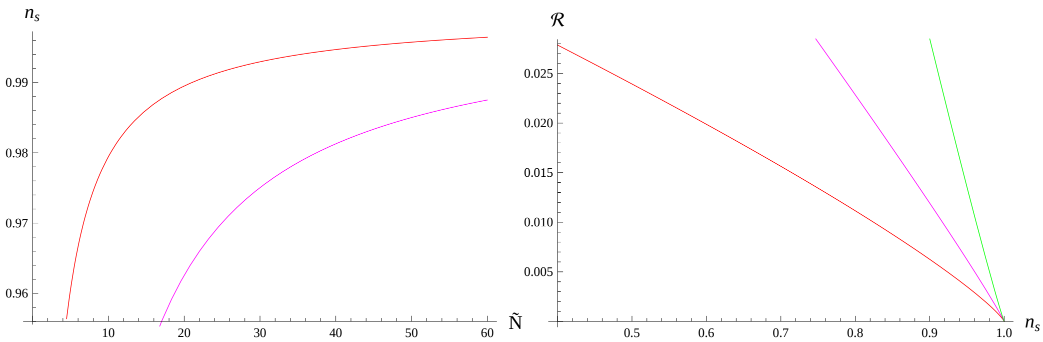

Figure 2.1: n_s versus $\tilde{N}$ (left) for $\bar{g} = 0.7$ (red), 0.999 (magenta) and $\mathcal{R}$ versus n_s (right) for $\bar{g} = 0.7$ (green), 0.8 (magenta), 0.9 (red), $\gamma = 1,\ \Gamma_i \propto \chi_r^{\frac{1}{6}},\ \chi_r = 70$.

The tensor-scalar ratio is

$$\mathcal{R} = \frac{4}{\pi^2}\left[\left(\frac{\Gamma_i}{2\kappa^2\chi_r}\right)^{-1}\left(\frac{2H_i}{M}\right)(1-\bar{g})^3\right]^{\frac{1}{4}}\left(\frac{\tilde{N}}{\gamma}+\frac{1-\bar{g}}{\gamma\bar{g}}\right)^{\frac{-3}{4\bar{g}}}.$$

For weak dissipation regime, the decay rate of inflaton and Hubble parameter in terms of thermal bath temperature turn out to be

$$\tilde{r} = \frac{\Gamma_i}{3\gamma\bar{g}}\left(\frac{2H_i}{M}\right)\left[\frac{8\bar{g}-5}{4\gamma\bar{g}(1-n_s)}\right]^{\frac{1-\bar{g}}{\bar{g}}},$$
$$\tilde{H} = \left[\left(\frac{2\kappa^2\chi_r}{\Gamma_i(1-\bar{g})}\right)^{\frac{1}{4}}\left(\frac{M}{2H_i}\right)^{\frac{3-4\bar{g}}{4(1-\bar{g})}}(\gamma\bar{g})^{\frac{1}{4(1-\bar{g})}}\mathrm{T}\right]^{4(1-\bar{g})}.$$

Figure **2.1** (left plot) represents the graphical behavior of n_s against $\tilde{N}$ in weak dissipative regime which are found in enough abundance to discuss inflationary epoch whereas the right plot indicates compatible $\mathcal{R}$ for the proposed values of $\bar{g}$. Figure **2.2** shows that $\mathrm{T} >> \tilde{H}$ (left panel) and $\tilde{r} << 1$ (right panel) for $0.7 \leq \bar{g} \leq 0.9$ which assures the existence of warm intermediate inflation in weak dissipative regime.

In strong dissipative regime, Eqs.(2.1.7) and (2.1.9) yield the inflaton field and corresponding potential in the following form

$$\phi = \phi_0 + \bar{\alpha}_2\tilde{t}^{\frac{2\bar{g}-1}{2}}, \quad U(\phi) = \frac{3}{\kappa^2}\left[\gamma\bar{g}\left(\frac{M}{2H_i}\right)^{\bar{g}}\left(\frac{\phi-\phi_0}{\bar{\alpha}_2}\right)^{\frac{2(\bar{g}-1)}{2\bar{g}-1}}\right]^2, \tag{2.2.9}$$

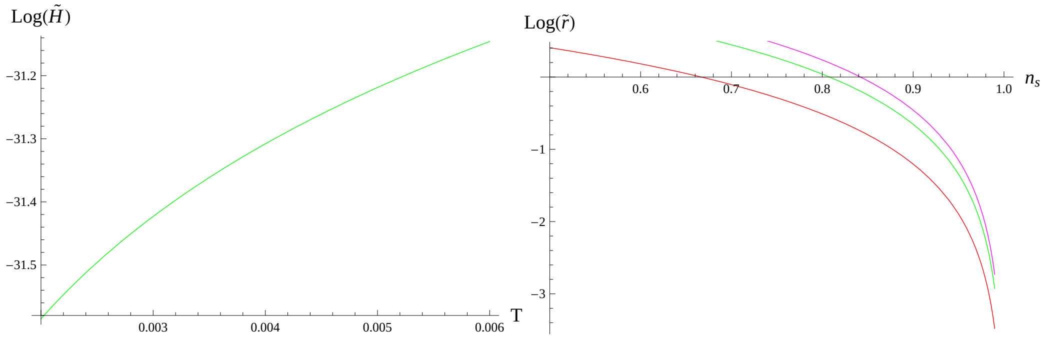

Figure 2.2: Log($\tilde{H}$) versus T (left) for $\bar{g} = 0.9$ (green) and Log($\tilde{r}$) versus n_s (right) for $\bar{g} = 0.7$ (red), 0.8 (green), 0.9 (magenta), $\gamma = 1$, $\Gamma_i \propto \chi_r^{\frac{1}{6}}$, $\chi_r = 70$.

where ϕ_0 is an integration constant and $\bar{\alpha}_2$ is

$$\bar{\alpha}_2 = \sqrt{\frac{24(\gamma\bar{g})^2(1-\bar{g})}{\kappa^2\Gamma_i(2\bar{g}-1)^2}\left(\frac{M}{2H_i}\right)^2}. \tag{2.2.10}$$

Using Eqs.(2.2.3) and (2.2.9), the slow-roll parameters become

$$\epsilon = \frac{1-\bar{g}}{\gamma\bar{g}}\left(\frac{2H_i}{M}\right)^{\bar{g}}\left[\frac{\phi-\phi_0}{\bar{\alpha}_2}\right]^{\frac{2\bar{g}}{1-2\bar{g}}}, \quad \eta = \frac{2-\bar{g}}{\gamma\bar{g}}\left(\frac{2H_i}{M}\right)^{\bar{g}}\left[\frac{\phi-\phi_0}{\bar{\alpha}_2}\right]^{\frac{2\bar{g}}{1-2\bar{g}}}. \tag{2.2.11}$$

For inflaton field (2.2.9), the radiation density and e-folds take the form

$$\tilde{\rho}_r = \frac{3\gamma\bar{g}}{2\kappa^2}(1-\bar{g})\left(\frac{M}{2H_i}\right)^{\bar{g}}\left(\frac{\phi-\phi_0}{\bar{\alpha}_2}\right)^{\frac{2(\bar{g}-2)}{2\bar{g}-1}}, \tag{2.2.12}$$

$$\tilde{N} = \gamma\left(\frac{M}{2H_i}\right)^{\bar{g}}\left[\left(\frac{\phi-\phi_0}{\bar{\alpha}_2}\right)^{\frac{2\bar{g}}{2\bar{g}-1}} - \left(\frac{\phi_i-\phi_0}{\bar{\alpha}_2}\right)^{\frac{2\bar{g}}{2\bar{g}-1}}\right]. \tag{2.2.13}$$

To evaluate an expression for this earliest inflaton field, we take $\epsilon = 1$ at the beginning of inflationary epoch which yields

$$\phi_i = \phi_0 + \bar{\alpha}_2\left[\left(\frac{1-\bar{g}}{\gamma\bar{g}}\right)\left(\frac{M}{2H_i}\right)^{\bar{g}}\right]^{\frac{2\bar{g}-1}{2\bar{g}}}. \tag{2.2.14}$$

Combining Eqs.(2.2.13) and (2.2.14), we obtain inflaton in terms of e-folds as

$$\phi = \phi_0 + \bar{\alpha}_2\left(\frac{2H_i}{M}\right)^{\frac{2\bar{g}-1}{2}}\left[\frac{\tilde{N}}{\gamma} + \frac{1-\bar{g}}{\gamma\bar{g}}\right]^{\frac{2\bar{g}-1}{2\bar{g}}}. \tag{2.2.15}$$

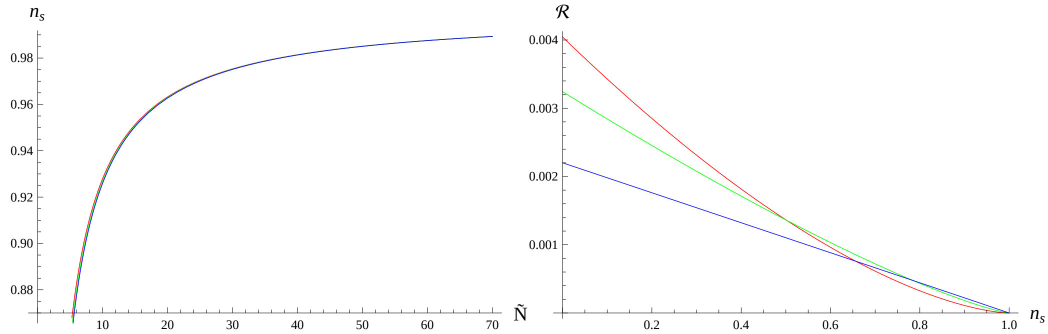

Figure 2.3: n_s versus $\tilde{N}$ (left) and $\mathcal{R}$ versus n_s (right) for $\bar{g} = 0.71$ (red), 0.8 (green), 0.89 (blue), $\gamma = 1,\ \Gamma_i \propto \chi_r^{\frac{1}{6}},\ \chi_r = 70$.

The observational parameters like scalar and tensor power spectra along with their indices as a function of e-folds turn out to be

$$\Delta_{\mathcal{R}} = \sqrt{\frac{\Gamma_i^3 3^{\frac{1}{2}}\kappa^4}{36(4\pi)^3(2\kappa^2\chi_r)^{\frac{1}{2}}}}\left[\left(\frac{\gamma\bar{g}}{1-\bar{g}}\right)^3\left(\frac{2H_i}{M}\right)^2\left(\frac{\tilde{N}}{\gamma}+\frac{1-\bar{g}}{\gamma\bar{g}}\right)^3\right]^{\frac{1}{4}},$$

$$n_s = 1-\frac{3}{4\gamma}\left[\frac{\tilde{N}}{\gamma}+\frac{1-\bar{g}}{\gamma\bar{g}}\right]^{-1},$$

$$\Delta_T = \frac{2\kappa^2\gamma^2\bar{g}^2}{\pi^2}\left(\frac{\tilde{N}}{\gamma}+\frac{1-\bar{g}}{\gamma\bar{g}}\right)^{\frac{2\bar{g}-1}{\bar{g}}}, \quad n_T = 2\left(\frac{\bar{g}-1}{\gamma\bar{g}}\right)\left(\frac{\tilde{N}}{\gamma}+\frac{1-\bar{g}}{\gamma\bar{g}}\right)^{-1}.$$

The ratio of tensor and scalar power spectra yields

$$\mathcal{R} = \left[(\gamma\bar{g})^{\frac{5}{2}}(1-\bar{g})^{\frac{3}{2}}\left(\frac{144(4\pi)^3(2\kappa^2\chi_r)^{\frac{1}{2}}}{\pi^4\Gamma_i^3 3^{\frac{1}{2}}}\right)\right]^{\frac{1}{2}}\left(\frac{M}{2H_i}\right)^{\frac{1}{2}}\left(\frac{\tilde{N}}{\gamma}+\frac{1-\bar{g}}{\gamma\bar{g}}\right)^{\frac{5\bar{g}-8}{4\bar{g}}}.$$

The decay rate of inflaton field is given by

$$\tilde{r} = \frac{\Gamma_i}{3\gamma\bar{g}}\left(\frac{2H_i}{M}\right)\left[\frac{3}{4\gamma(1-n_s)}\right]^{\frac{1-\bar{g}}{\bar{g}}}.$$

In the background of thermal bath radiations, Hubble parameter takes the form

$$\tilde{H} = \left[\left(\frac{2\kappa^2\chi_r}{3}\right)\left(\frac{2H_i}{M}\right)^{\frac{3\bar{g}-2}{1-\bar{g}}}(\gamma\bar{g})^{\frac{1}{1-\bar{g}}}(1-\bar{g})^{-1}\mathrm{T}^4\right]^{\frac{1-\bar{g}}{2-\bar{g}}}.$$

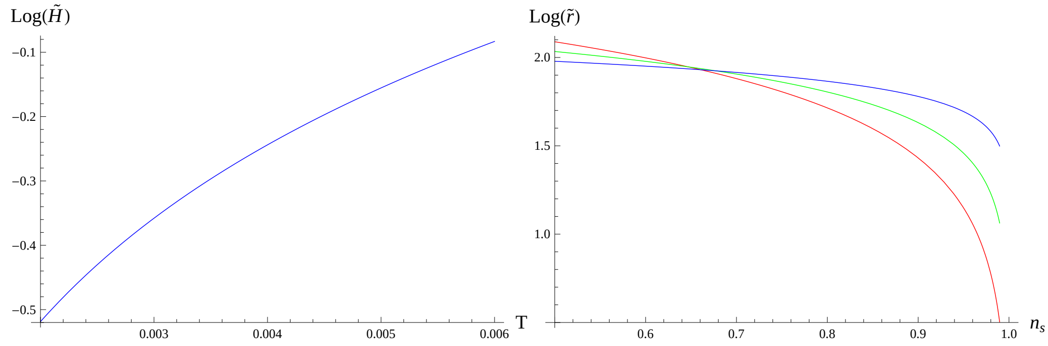

Figure 2.4: Log($\tilde{H}$) versus T (left) for $\bar{g} = 0.89$ (blue) and Log($\tilde{r}$) versus n_s (right) for $\bar{g} = 0.7$ (red), 0.8 (green), 0.89 (blue), $\gamma = 1,\ \Gamma_i \propto \chi_r^{\frac{1}{6}},\ \chi_r = 70$.

Figure **2.3** (left plot) shows the variation of e-folds which are found to be smaller than its standard value, i.e., $\tilde{N} = 19$ at $\bar{g} = 0.71,\ 0.8$ and $\bar{g} = 0.89$. The right panel of Figure **2.3** indicates that $\mathcal{R} < 0.10$ at $n_s = 0.9603$ which implies compatibility of $\mathcal{R}$ in strong dissipation regime. In order to investigate dominant characteristics of warm inflation, we plot $\tilde{H}$ versus T in left panel of Figure **2.4** which yields T $>> \tilde{H}$. The right panel of Figure **2.4** implies that $\tilde{r} >> 1$ which assures the presence of inflaton particles in strong dissipative regime.

2.2.2 Generalized Dissipative Coefficient

The most general form of dissipation factor is given by [59]

$$\Gamma = \Gamma_i \frac{\mathrm{T}^m}{\phi^{m-1}}, \tag{2.2.16}$$

where m represents an integer. For different values of m, dissipation coefficient corresponds to different physical processes, i.e., when $m = 0$, the dissipation coefficient describes an exponential decay propagator in high temperature supersymmetry case. For $m = 1$, it becomes proportional to thermal bath temperature while $m = -1$ deals with non-supersymmetry case [60]. In the present work, we study the behavior of generalized dissipation coefficient in both dissipation regimes.

In weak dissipative regime, the constant as well as proposed generalized dissipative coefficient leave the same effect over inflaton field, number of e-folds and slow-roll parameters whereas radiation density becomes

$$\tilde{\rho}_r = \frac{1}{2\kappa^2}\left(\frac{\Gamma_i}{(2\kappa^2\chi_r)^{\frac{m}{4}}}\right)^{\frac{4}{4-m}}\left(\frac{2H_i}{M}\right)^{\frac{2m-4\bar{g}}{4-m}}(\gamma\bar{g}(1-\bar{g}))^{\frac{4}{4-m}}\bar{\alpha}_1^{\frac{2(2-\bar{g})}{\bar{g}}}\phi^{\frac{2(\bar{g}-2)}{\bar{g}}+\frac{4(1-m)}{4-m}}.$$

The scalar and tensor power spectra, corresponding spectral indices and tensor-scalar ratio are given by

$$\begin{aligned}
\Delta_{\mathcal{R}} &= \frac{\kappa^2}{2}\left[\frac{\Gamma_i\bar{\alpha}_1^{1-m}}{2\kappa^2\chi_r}(\gamma\bar{g})^{2(4-m)}(1-\bar{g})^{m-3}\left(\frac{2H_i}{M}\right)^{\frac{(m-1)(2-\bar{g})}{2}+2(4-m)(\bar{g}-1)}\right.\\
&\times \left.\left(\frac{\tilde{N}}{\gamma}+\frac{1-\bar{g}}{\gamma\bar{g}}\right)^{\frac{2\bar{g}(4-m)+m-5}{\bar{g}}+\frac{1-m}{2}}\right]^{\frac{1}{4-m}},\\
n_s &= 1-\left(\frac{2m-10+\bar{g}(17-5m)}{2(4-m)(1+\bar{g}(\tilde{N}-1))}\right),\\
\Delta_T &= \frac{2\kappa^2\gamma^2\bar{g}^2}{\pi^2}\left(\frac{2m-10+\bar{g}(17-5m)}{\gamma(\bar{g}+2)(4-m)}\right)^{\frac{2(\bar{g}-1)}{\bar{g}}}(1-n_s)^{\frac{2(1-\bar{g})}{\bar{g}}},\\
n_T &= 2\left(\frac{\bar{g}-1}{\gamma\bar{g}}\right)\left(\frac{2m-10+\bar{g}(17-5m)}{\gamma(\bar{g}+2)(4-m)}\right)^{-1}(1-n_s),\\
\mathcal{R} &= \frac{4}{\pi^2}\left[\frac{\Gamma_i\bar{\alpha}_1^{1-m}(1-\bar{g})^{m-3}}{2\kappa^2\chi_r}\left(\frac{2H_i}{M}\right)^{(m-1)(1-\frac{\bar{g}}{2})}\left\{(1-n_s)^{-1}\right.\right.\\
&\times \left.\left.\left(\frac{2m-10+\bar{g}(17-5m)}{\gamma(\bar{g}+2)(4-m)}\right)\right\}^{\frac{3-m}{\bar{g}}+\frac{1-m}{2}}\right]^{\frac{1}{m-4}}.
\end{aligned}$$

The Hubble parameter in the background of thermal radiations and dissipation rate of inflaton field take the form

$$\tilde{H} = \left[\frac{\Gamma_i\bar{\alpha}_1^{m-1}(1-\bar{g})^{-1}}{(2\kappa^2\chi_r)^{m-2}}(\gamma\bar{g})^{\frac{\bar{g}(1-m)-2}{2(\bar{g}-1)}}\left(\frac{2H_i}{M}\right)^{\frac{\bar{g}(1-m)-2}{2(1-\bar{g})}+(m-1)\bar{g}-3}\mathrm{T}^{4-m}\right]^{\frac{2(\bar{g}-1)}{\bar{g}(1-m)-2}}$$

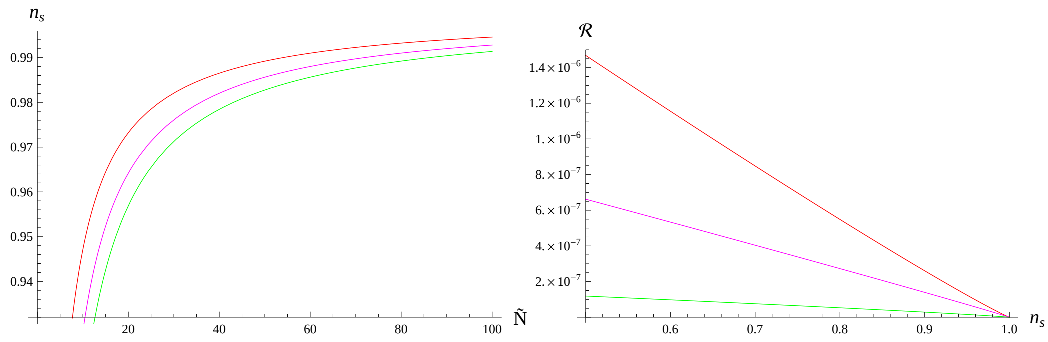

Figure 2.5: n_s versus $\tilde{N}$ (left) and $\mathcal{R}$ versus n_s (right) for $\bar{g} = 0.79$ (red), 0.8 (magenta), 0.99 (green), $\gamma = 1,\ \Gamma_i \propto \chi_r^{\frac{1}{6}},\ \chi_r = 70,\ m = 0$.

$$\begin{aligned}\tilde{r} &= \frac{1}{3}\left(\frac{\Gamma_i}{(2\kappa^2\chi_r)^{\frac{m}{4}}}\right)\bar{\alpha}_1^{\frac{4(1-m)}{4-m}}(1-\bar{g})^{\frac{m}{4-m}}(\gamma\bar{g})^{-1}\left(\frac{2H_i}{M}\right)^{\frac{4+6m+2\bar{g}(1-m)}{4-m}} \\ &\times \left[\left(\frac{2m-10+\bar{g}(17-5m)}{\gamma(\bar{g}+2)(4-m)}\right)(1-n_s)^{-1}\right]^{\frac{4(1-\bar{g})+m(\bar{g}-2)+2\bar{g}(1-m)}{\bar{g}(4-m)}}.\end{aligned}$$

The graphical behavior of n_s against number of e-folds and variation of $\mathcal{R}$ versus n_s for generalized dissipative coefficient is given in Figures **2.5, 2.7** and **2.9** for $m = 0,\ 1$ and $m = -1$, respectively. The e-folds are found to be lesser than standard value, i.e., $\tilde{N} = 60$ while $\mathcal{R}$ remains compatible for all considered values of m. Figures **2.6, 2.8** and **2.10** assure the condition of warm inflation in weak dissipative regime for different values of model parameter $\bar{g}$.

In strong dissipative regime, the inflaton field and corresponding potential yield

$$\phi = \bar{\alpha}_3\tilde{t}^{\frac{4(2\bar{g}-1)+m(2-\bar{g})}{4(3-m)}}, \quad U(\phi) = \frac{3}{\kappa^2}(\gamma\bar{g})^2\left(\frac{M}{2H_i}\right)^{2\bar{g}}\left(\frac{\phi}{\bar{\alpha}_3}\right)^{\frac{8(3-m)(\bar{g}-1)}{4(2\bar{g}-1)+m(2-\bar{g})}}, \qquad (2.2.17)$$

where

$$\begin{aligned}\bar{\alpha}_3 &= \left\{\left(\frac{3-m}{2}\right)\left(\frac{6}{\kappa^2}\right)^{\frac{1}{2}}\left[(\gamma\bar{g})^{8-m}(1-\bar{g})^{4-m}\left(\frac{2H_i}{M}\right)^{\bar{g}(m-8)-4m}\right]^{\frac{1}{8}}\right. \\ &\times \left.\left(\frac{8}{4(2\bar{g}-1)+m(2-\bar{g})}\right)\right\}^{\frac{2}{3-m}}.\end{aligned}$$

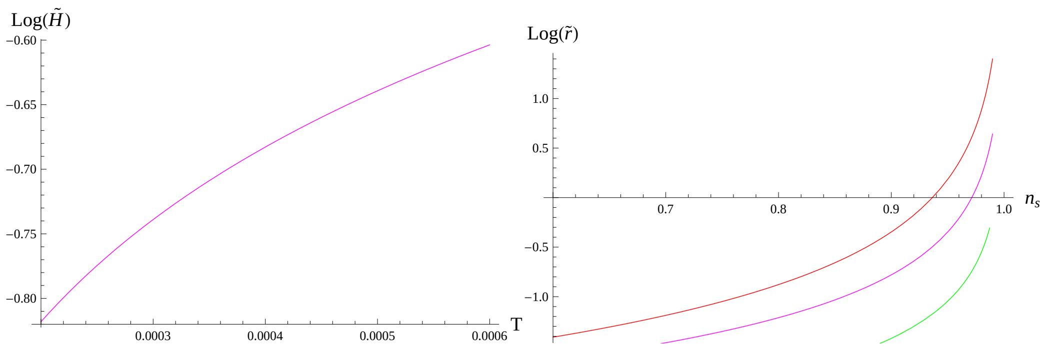

Figure 2.6: Log($\tilde{H}$) versus T (left) for $\bar{g} = 0.975$ (magenta) and Log($\tilde{r}$) versus n_s (right) for $\bar{g} = 0.79$ (red), 0.89 (magenta), 0.96 (green), $\gamma = 1,\ \Gamma_i \propto \chi_r^{\frac{1}{6}},\ \chi_r = 70,\ m = 0$.

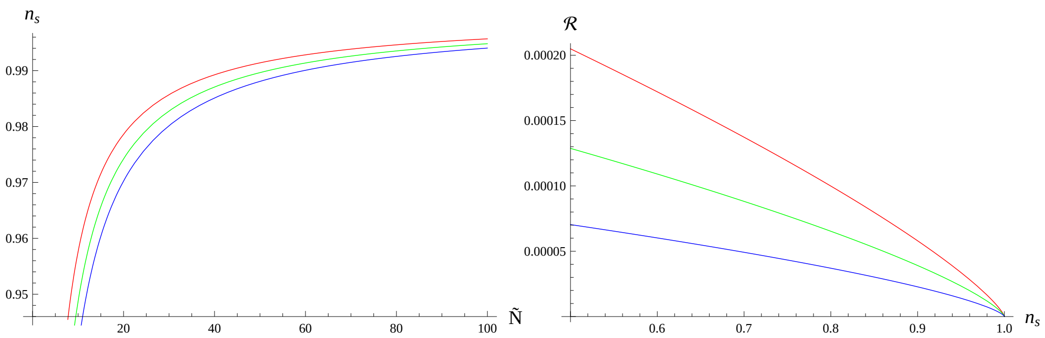

Figure 2.7: n_s versus $\tilde{N}$ (left) and $\mathcal{R}$ versus n_s (right) for $\bar{g} = 0.85$ (red), 0.9 (green), 0.95 (blue), $\gamma = 1,\ \Gamma_i \propto \chi_r^{\frac{1}{6}},\ \chi_r = 70,\ m = 1$.

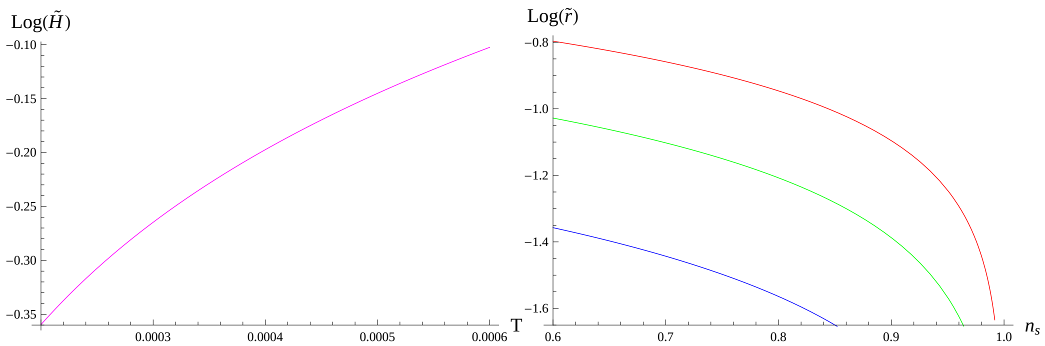

Figure 2.8: Log($\tilde{H}$) versus T (left) for $\bar{g} = 0.922$ (magenta) and Log($\tilde{r}$) versus n_s (right) for $\bar{g} = 0.85$ (red), 0.9 (green), 0.95 (blue), $\gamma = 1,\ \Gamma_i \propto \chi_r^{\frac{1}{6}},\ \chi_r = 70,\ m = 1$.

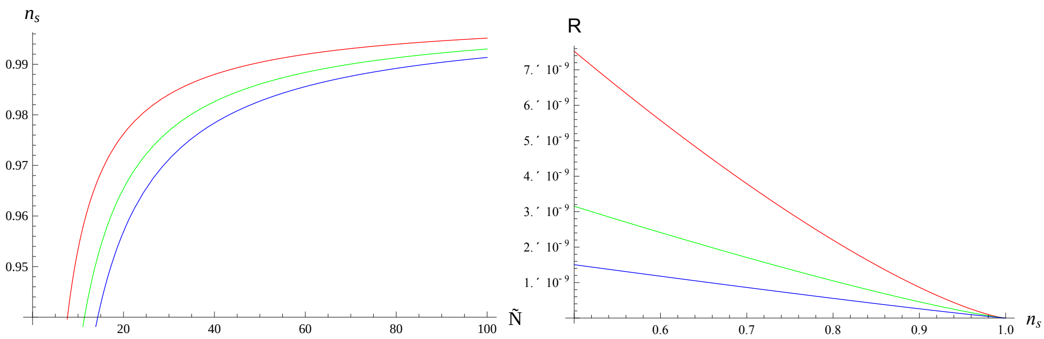

Figure 2.9: n_s versus $\tilde{N}$ (left) and $\mathcal{R}$ versus n_s (right) for $\bar{g} = 0.7$ (red), 0.8 (green), 0.9 (blue), $\gamma = 1,\ \Gamma_i \propto \chi_r^{\frac{1}{6}},\ \chi_r = 70,\ m = -1$.

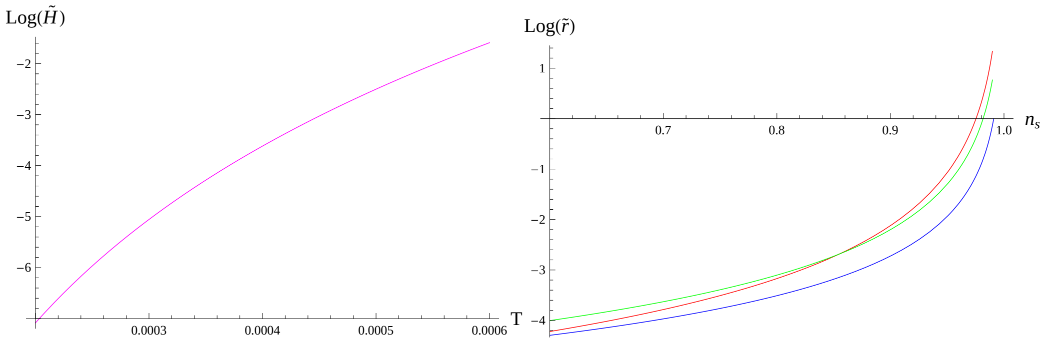

Figure 2.10: Log($\tilde{H}$) versus T (left) for $\bar{g} = 0.9$ (magenta) and Log($\tilde{r}$) versus n_s (right) for $\bar{g} = 0.7$ (red), 0.8 (green), 0.9 (blue), $\gamma = 1,\ \Gamma_i \propto \chi_r^{\frac{1}{6}},\ \chi_r = 70,\ m = -1$.

Under the influence of inflaton field (2.2.17), the corresponding radiation density, Hubble and slow-roll parameters turn out to be

$$\begin{aligned}
\tilde{\rho}_r &= \frac{3}{2\kappa^2}\gamma\bar{g}(1-\bar{g})\left(\frac{M}{2H_i}\right)^{\bar{g}}\left(\frac{\phi}{\bar{\alpha}_3}\right)^{\frac{4(3-m)(\bar{g}-2)}{4(2\bar{g}-1)+m(2-\bar{g})}}, \\
\tilde{H}(\tilde{t}) &= \gamma\bar{g}\left(\frac{M}{2H_i}\right)^{\bar{g}}\left(\frac{\phi}{\bar{\alpha}_3}\right)^{\frac{4(3-m)(\bar{g}-1)}{4(2\bar{g}-1)+m(2-\bar{g})}}, \\
\epsilon &= \frac{(1-\bar{g})}{\gamma\bar{g}}\left(\frac{2H_i}{M}\right)^{\bar{g}}\left(\frac{\phi}{\bar{\alpha}_3}\right)^{\frac{-4(3-m)\bar{g}}{4(2\bar{g}-1)+m(2-\bar{g})}}, \\
\eta &= \left(\frac{2-\bar{g}}{\gamma\bar{g}}\right)\left(\frac{2H_i}{M}\right)^{\bar{g}}\left(\frac{\phi}{\bar{\alpha}_3}\right)^{\frac{-4(3-m)\bar{g}}{4(2\bar{g}-1)+m(2-\bar{g})}}.
\end{aligned} \tag{2.2.18}$$

At the beginning of inflation ($\epsilon = 1$), the initial value of inflaton field leads to

$$\phi = \bar{\alpha}_3\left\{\left(\frac{2H_i}{M}\right)^{\bar{g}}\left(\frac{\tilde{N}}{\gamma}+\frac{1-\bar{g}}{\gamma\bar{g}}\right)\right\}^{\frac{4(2\bar{g}-1)+m(2-\bar{g})}{4(3-m)\bar{g}}}. \tag{2.2.19}$$

The corresponding scalar power spectrum and spectral index are

$$\begin{aligned}
\Delta_R^2 &= \frac{\kappa^2}{6}\left[\left(\frac{3}{2\kappa^2\chi_r}\right)^{\frac{3m+2}{4}}\left(\frac{\Gamma_i}{4\pi}\right)^3(\gamma\bar{g})^{\frac{3}{4}(m+2)}\left(\frac{2H_i}{M}\right)^{\frac{3}{2}+\frac{3}{4}\left\{\frac{(1-m)(4(2\bar{g}-1)-m(2-\bar{g}))}{(3-m)\bar{g}}\right\}}\right. \\
&\times \left.\bar{\alpha}_3^{3(1-m)}\right]^{\frac{1}{2}}\left(\frac{\tilde{N}}{\gamma}+\frac{1-\bar{g}}{\gamma\bar{g}}\right)^{\frac{3}{8}\left[\frac{(3-m)\{\bar{g}(m+2)-2m\}+(1-m)\{4(2\bar{g}-1)+m(2-\bar{g})\}}{(3-m)\bar{g}}\right]}, \\
n_s &= 1-\frac{3\bar{\beta}_0}{8\gamma}\left(\frac{\tilde{N}}{\gamma}+\frac{1-\bar{g}}{\gamma\bar{g}}\right)^{-1},
\end{aligned}$$

where

$$\bar{\beta}_0 = \frac{3}{8}\left[\frac{(3-m)\left\{\bar{g}(m+2)-2m\right\}+(1-m)\left\{4(2\bar{g}-1)+m(2-\bar{g})\right\}}{(3-m)\bar{g}}\right].$$

Similarly, tensor power spectrum and its spectral index become

$$\Delta_T^2 = \frac{2\kappa^2}{\pi^2}(\gamma\bar{g})^2\left(\frac{\tilde{N}}{\gamma}+\frac{1-\bar{g}}{\gamma\bar{g}}\right)^{\frac{2}{\bar{g}}(\bar{g}-1)}, \quad n_T = \frac{2(\bar{g}-1)}{\gamma\bar{g}}\left(\frac{\tilde{N}}{\gamma}+\frac{1-\bar{g}}{\gamma\bar{g}}\right)^{-1}.$$

The above observational parameters generate tensor-scalar ratio as

$$\begin{aligned}\mathcal{R} &= \left[\frac{144}{\pi^4}\left(\frac{2\kappa^2\chi_r}{3}\right)^{\frac{3m+2}{4}}\left(\frac{4\pi}{\Gamma_i}\right)^3(\gamma\bar{g})^{\frac{22-3m}{4}}\left(\frac{2H_i}{M}\right)^{-\frac{3}{2}-\frac{3}{4}\left\{\frac{(1-m)(4(2\bar{g}-1)-\bar{g}(m+2))}{(3-m)\bar{g}}\right\}}\bar{\alpha}_3^{3(m-1)}\right]^{\frac{1}{2}}\\ &\times\ \left((8\gamma(1-n_s))/3\bar{\beta}_0\right)^{\frac{3\bar{\beta}_0}{8}}.\end{aligned}$$

The Hubble parameter in terms of thermal radiations and decay rate of inflaton field take the form

$$\begin{aligned}\tilde{H} &= \left[\left(\frac{2\kappa^2\chi_r}{3}\right)(1-\bar{g})^{-1}(\gamma\bar{g})^{\frac{1}{1-\bar{g}}}\left(\frac{2H_i}{M}\right)^{\frac{5-4\bar{g}}{\bar{g}-1}}\mathrm{T}^4\right]^{\frac{1-\bar{g}}{2-\bar{g}}}\\ \tilde{r} &= \bar{\alpha}_m\bar{\alpha}_3^{1-m}(3\gamma\bar{g})^{\frac{m-4}{4}}(1-\bar{g})^{\frac{m}{4}}\left(\frac{2H_i}{M}\right)^{m+1-\frac{m}{2}+\frac{1-m}{4(3-m)}\{4(2\bar{g}-1)+m(2-\bar{g})\}}\\ &\times\ \left(\frac{8\gamma(1-n_s)}{3\bar{\beta}_0}\right)^{\bar{\zeta}},\end{aligned}$$

where

$$\bar{\zeta}=-\frac{1}{\bar{g}}(1-\bar{g})+\frac{m}{4\bar{g}}(2-\bar{g})+\frac{(m-1)}{4\bar{g}(3-m)}\left\{4(2\bar{g}-1)+m(2-\bar{g})\right\}.$$

The graphical behavior of n_s versus number of e-folds is shown in left plot of Figures **2.11**, **2.13** and **2.16** for $m=0,\ 1$ and $m=-1$, respectively. The right plot of Figure **2.11, 2.13** and **2.16** indicate that $\mathcal{R}$ is constrained at observational value of n_s which leads to the consistent behavior of inflationary model for different values of model parameter $\bar{g}$. Figures **2.12** (left plot), **2.15** and **2.17** (left plot) represent graphical analysis of inflaton particles which satisfy the condition of warm inflation, i.e, $\mathrm{T}>>\tilde{H}$ in strong dissipative regime for $m=0,\ 1,\ -1$. Figures **2.12** (right plot), **2.14** and **2.17** (right plot) show that $\tilde{r}>>1$ which implies that inflaton particles lies in strong dissipative regime.

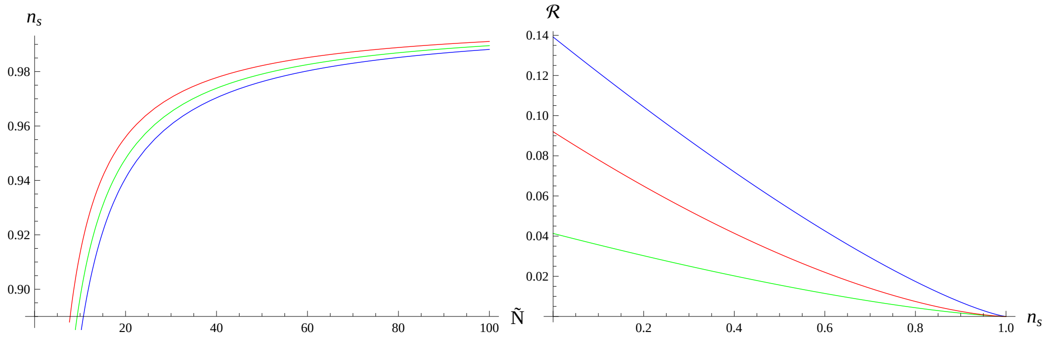

Figure 2.11: n_s versus $\tilde{N}$ (left) and $\mathcal{R}$ versus n_s (right) for $\bar{g} = 0.75$ (red), 0.85 (green), 0.95 (blue), $\gamma = 10^{-15}$, $\Gamma_i \propto \chi_r^{\frac{1}{6}}$, $\chi_r = 70$, $m = 0$.

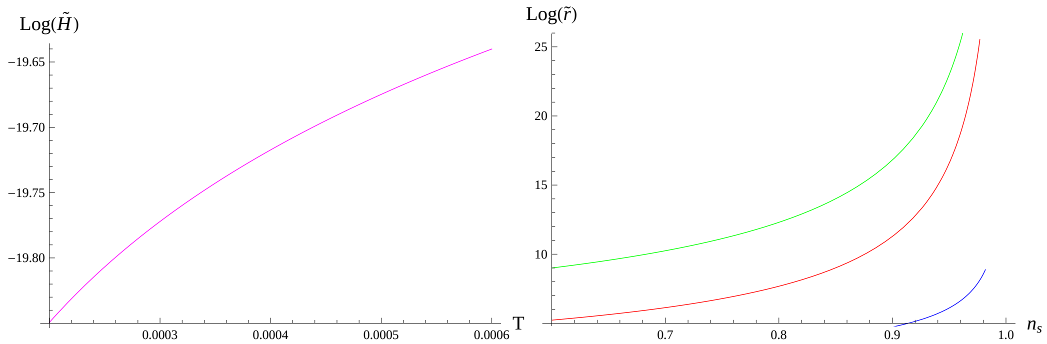

Figure 2.12: Log($\tilde{H}$) versus T (left) for $\bar{g} = 0.95$ (magenta) and Log($\tilde{r}$) versus n_s (right) for $\bar{g} = 0.75$ (red), 0.85 (green), 0.95 (blue), $\gamma = 10^{-15}$, $\Gamma_i \propto \chi_r^{\frac{1}{6}}$, $\chi_r = 70$, $m = 0$.

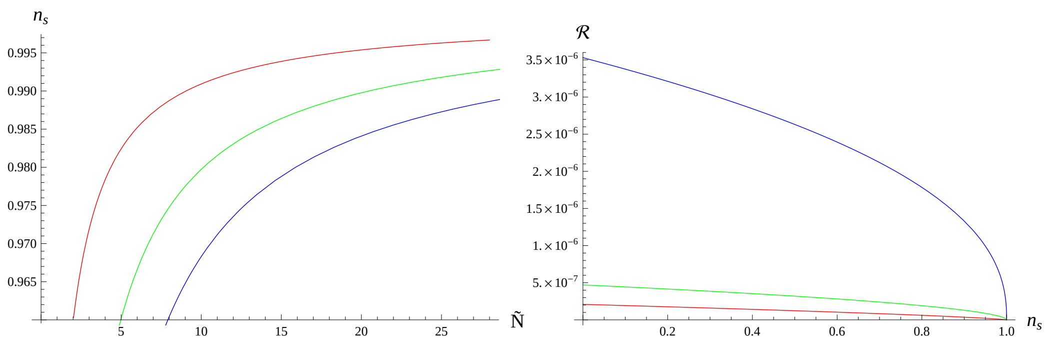

Figure 2.13: n_s versus $\tilde{N}$ (left) and $\mathcal{R}$ versus n_s (right) for $\bar{g} = 0.75$ (red), 0.85 (green), 0.95 (blue), $\gamma = 10^{-18}$, $\Gamma_i \propto \chi_r^{\frac{1}{6}}$, $\chi_r = 70$, $m = 1$.

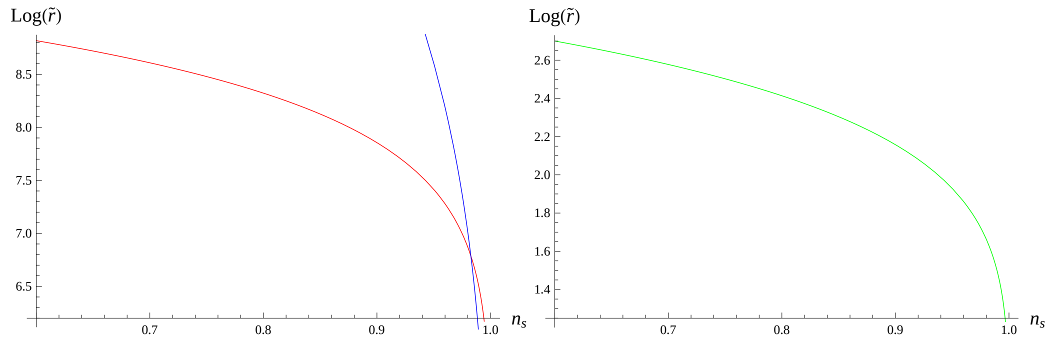

Figure 2.14: Log($\tilde{r}$) versus n_s for $\bar{g} = 0.75$ (red), 0.95 (blue) (left) and 0.85 (green) (right), $\gamma = 10^{-18}$, $\Gamma_i \propto \chi_r^{\frac{1}{6}}$, $\chi_r = 70$, $m = 1$.

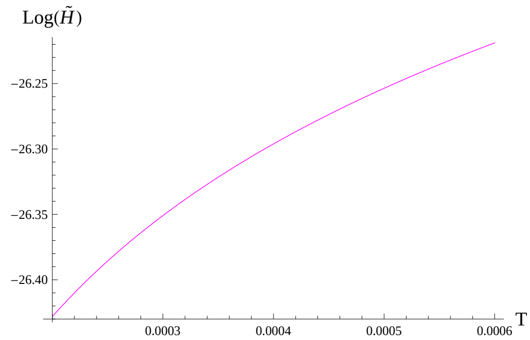

Figure 2.15: Log($\tilde{H}$) versus T for $\bar{g} = 0.95$ (magenta), $\gamma = 10^{-18}$, $\Gamma_i \propto \chi_r^{\frac{1}{6}}$, $\chi_r = 70$, $m = 1$.

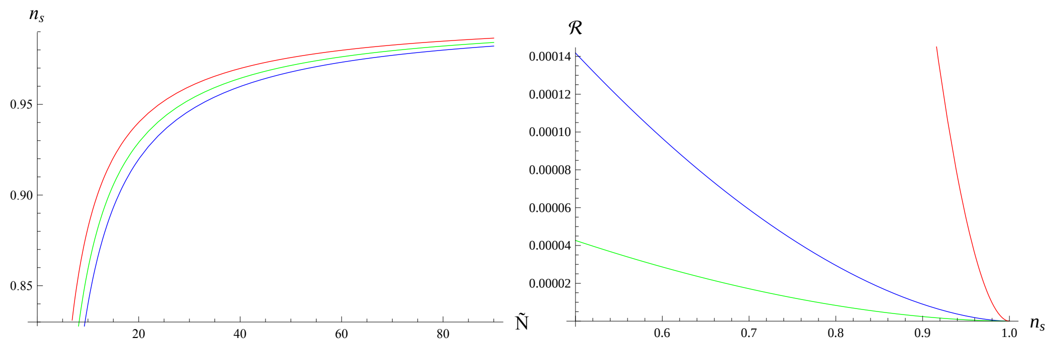

Figure 2.16: n_s versus $\tilde{N}$ (left) and $\mathcal{R}$ versus n_s (right) for $\bar{g} = 0.75$ (red), 0.85 (green), 0.95 (blue), $\gamma = 10^{-18}$, $\Gamma_i \propto \chi_r^{\frac{1}{6}}$, $\chi_r = 70$, $m = -1$.

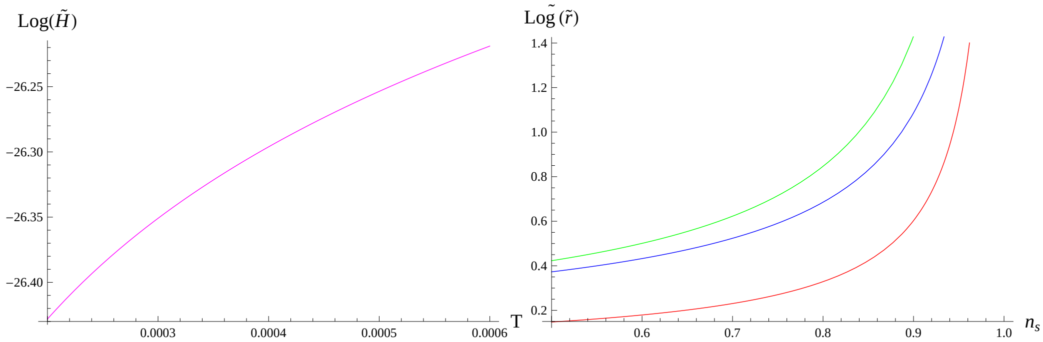

Figure 2.17: Log($\tilde{H}$) versus T (left) for $\bar{g} = 0.95$ (magenta) and Log($\tilde{r}$) versus n_s (right) for $\bar{g} = 0.75$ (red), 0.85 (green), 0.95 (green), $\gamma = 10^{-18}$, $\Gamma_i \propto \chi_r^{\frac{1}{6}}$, $\chi_r = 70$, $m = -1$.

2.3 Warm Logamediate Inflation

Here, we analyze warm inflation in both dissipative regimes for logamediate inflationary model whose scale factor is defined as [58]

$$a(t) = a_i \exp(\hat{g}[\ln t]^{\bar{\beta}}), \quad \hat{g} > 0, \quad \bar{\beta} > 1. \tag{2.3.1}$$

In Einstein frame, the logamediate scale factor and corresponding Hubble parameter turn out to be

$$\tilde{a}(\tilde{t}) = \tilde{a}_i \left[1 - \frac{M^3\tilde{t}}{12H_i^2}\right] \exp\left[\hat{g}\left\{\ln\left(\frac{\tilde{t}M}{2H_i}\right)\right\}^{\bar{\beta}}\right], \quad \tilde{a}_i = \frac{2a_iH_i}{M}, \tag{2.3.2}$$

$$\tilde{H}(\tilde{t}) = \hat{g}\bar{\beta}\tilde{t}^{-1}\left\{\ln\left(\frac{\tilde{t}M}{2H_i}\right)\right\}^{\bar{\beta}-1}. \tag{2.3.3}$$

2.3.1 Constant dissipation Coefficient

In weak dissipative regime, Eqs.(2.1.7) and (2.1.9) yield the inflaton field and corresponding potential in the following form

$$\phi = \phi_0 + \bar{\alpha}_4\left\{\ln\left(\frac{\tilde{t}M}{2H_i}\right)\right\}^{\frac{\bar{\beta}+1}{2}}, \quad \bar{\alpha}_4 = \frac{2}{\bar{\beta}+1}\sqrt{\frac{2\hat{g}\bar{\beta}}{\kappa^2}}, \tag{2.3.4}$$

$$U(\phi) = \frac{3}{\kappa^2}\left[\hat{g}\bar{\beta}\left(\frac{M}{2H_i}\right)\exp\left\{-\left(\frac{\phi}{\bar{\alpha}_4}\right)^{\frac{2}{\bar{\beta}+1}}\right\}\left(\frac{\phi}{\bar{\alpha}_4}\right)^{\frac{2(\bar{\beta}-1)}{\bar{\beta}+1}}\right]^2, \tag{2.3.5}$$

where ϕ_0 is an integration constant. The dimensionless slow-roll parameters for Eqs.(2.3.3) and (2.3.4) become

$$\epsilon = \frac{1}{\bar{\beta}\hat{g}}\left[\frac{\phi}{\bar{\alpha}_4}\right]^{\frac{2(1-\bar{\beta})}{\bar{\beta}+1}}, \quad \eta = \frac{1}{\bar{\beta}\hat{g}}\left[\frac{\phi}{\bar{\alpha}_4}\right]^{\frac{-2\bar{\beta}}{\bar{\beta}+1}}\left(2\left\{\frac{\phi}{\bar{\alpha}_4}\right\}^{\frac{2}{\bar{\beta}+1}} - (\bar{\beta}-1)\right). \tag{2.3.6}$$

For inflaton field (2.3.4), the radiation density and e-folds take the form

$$\tilde{\rho}_r = \frac{\Gamma_i}{2\kappa^2}\left(\frac{M}{2H_i}\right)\exp\left[-\left(\frac{\phi}{\bar{\alpha}_4}\right)^{\frac{2}{\bar{\beta}+1}}\right], \tag{2.3.7}$$

$$\begin{aligned}\tilde{N} &= \bar{\beta}\hat{g}\left[\ln\left(\frac{2H_i}{M}\exp\left[\left(\frac{\phi}{\bar{\alpha}_4}\right)^{\frac{2}{\bar{\beta}+1}}\right]\right)\left(\frac{\phi}{\bar{\alpha}_4}\right)^{\frac{2(\bar{\beta}-1)}{\bar{\beta}+1}}\right.\\ &- \left.\ln\left(\frac{2H_i}{M}\exp\left[\left(\frac{\phi_i}{\bar{\alpha}_4}\right)^{\frac{2}{\bar{\beta}+1}}\right]\right)\left(\frac{\phi_i}{\bar{\alpha}_4}\right)^{\frac{2(\bar{\beta}-1)}{\bar{\beta}+1}}\right].\end{aligned} \tag{2.3.8}$$

For the earliest inflaton field ($\epsilon = 1$), we have

$$\phi_i = \phi_0 + \bar{\alpha}_4(\hat{g}\bar{\beta})^{\frac{\bar{\beta}+1}{2(1-\bar{\beta})}}. \tag{2.3.9}$$

Combining Eqs.(2.3.8) and (2.3.9), we obtain inflaton in terms of e-folds as

$$\phi = \phi_0 + \bar{\alpha}_4\left[\ln\left(\frac{M}{2H_i}\right) + \left\{\frac{\tilde{N}}{\hat{g}\bar{\beta}} + (\hat{g}\bar{\beta})^{\frac{\bar{\beta}}{1-\bar{\beta}}} - \ln\left(\frac{M}{2H_i}\right)^{\frac{1}{\hat{g}\bar{\beta}}}\right\}^{\frac{1}{\bar{\beta}}}\right]^{\frac{\bar{\beta}+1}{2}}. \tag{2.3.10}$$

The corresponding inflationary parameters turn out to be

$$\begin{aligned}\Delta_{\mathcal{R}} &= \frac{\kappa^2}{2}\left(\frac{\Gamma_i}{2\kappa^2\chi_r}\right)^{\frac{1}{4}}\left(\frac{2H_i}{M}\right)^{\frac{3}{4}}(\hat{g}\bar{\beta})^2\exp\left[-\frac{5}{4}\left\{\frac{\tilde{N}}{\hat{g}\bar{\beta}} + (\hat{g}\bar{\beta})^{\frac{\bar{\beta}}{1-\bar{\beta}}}\right.\right.\\ &- \left.\left.\ln\left(\frac{M}{2H_i}\right)^{\frac{1}{\hat{g}\bar{\beta}}}\right\}^{\frac{1}{\bar{\beta}}}\right]\left\{\frac{\tilde{N}}{\hat{g}\bar{\beta}} + (\hat{g}\bar{\beta})^{\frac{\bar{\beta}}{1-\bar{\beta}}} - \ln\left(\frac{M}{2H_i}\right)^{\frac{1}{\hat{g}\bar{\beta}}}\right\}^{\frac{2(\bar{\beta}-1)}{\bar{\beta}}},\end{aligned}$$

$$\begin{aligned}
\Delta_T &= \frac{2\kappa^2\bar{\beta}^2\hat{g}^2}{\pi^2}\exp\left[-2\left\{\frac{\tilde{N}}{\hat{g}\bar{\beta}}+(\hat{g}\bar{\beta})^{\frac{\bar{\beta}}{1-\bar{\beta}}}-\ln\left(\frac{M}{2H_i}\right)^{\frac{1}{\hat{g}\bar{\beta}}}\right\}^{\frac{1}{\bar{\beta}}}\right]\\
&\times \left\{\frac{\tilde{N}}{\hat{g}\bar{\beta}}+(\hat{g}\bar{\beta})^{\frac{\bar{\beta}}{1-\bar{\beta}}}-\ln\left(\frac{M}{2H_i}\right)^{\frac{1}{\hat{g}\bar{\beta}}}\right\}^{\frac{2(\bar{\beta}-1)}{\bar{\beta}}},\\
n_s &= 1-\frac{2(\bar{\beta}-1)}{\hat{g}\bar{\beta}^2}\left\{\frac{\tilde{N}}{\hat{g}\bar{\beta}}+(\hat{g}\bar{\beta})^{\frac{\bar{\beta}}{1-\bar{\beta}}}-\ln\left(\frac{M}{2H_i}\right)^{\frac{1}{\hat{g}\bar{\beta}}}\right\}^{-1},\\
n_T &= -\frac{2}{\hat{g}\bar{\beta}}\left\{\frac{\tilde{N}}{\hat{g}\bar{\beta}}+(\hat{g}\bar{\beta})^{\frac{\bar{\beta}}{1-\bar{\beta}}}-\ln\left(\frac{M}{2H_i}\right)^{\frac{1}{\hat{g}\bar{\beta}}}\right\}^{\frac{1-\bar{\beta}}{\bar{\beta}}}.
\end{aligned}$$

Taking the ratio of tensor and scalar power spectra, it follows that

$$\mathcal{R} = \frac{4}{\pi^2}\left(\frac{2\kappa^2\chi_r}{\Gamma_i}\right)^{\frac{1}{4}}\left(\frac{2H_i}{M}\right)^{-\frac{3}{4}}\exp\left[-\frac{3}{4}\left\{\frac{\tilde{N}}{\hat{g}\bar{\beta}}+(\hat{g}\bar{\beta})^{\frac{\bar{\beta}}{1-\bar{\beta}}}-\ln\left(\frac{M}{2H_i}\right)^{\frac{1}{\hat{g}\bar{\beta}}}\right\}^{\frac{1}{\bar{\beta}}}\right].$$

The temperature of thermal bath radiations and decay rate of inflaton field are

$$\begin{aligned}
\mathrm{T} &= \left(\frac{\Gamma_i}{2\kappa^2\chi_r}\right)^{\frac{1}{4}}\exp\left[-\left\{\frac{\tilde{N}}{\hat{g}\bar{\beta}}+(\hat{g}\bar{\beta})^{\frac{\bar{\beta}}{1-\bar{\beta}}}-\ln\left(\frac{M}{2H_i}\right)^{\frac{1}{\hat{g}\bar{\beta}}}\right\}^{\frac{1}{\bar{\beta}}}\right],\\
\tilde{r} &= \frac{\Gamma_i}{3\bar{\beta}\hat{g}}\left(\frac{2H_i}{M}\right)\exp\left[\left\{\frac{\tilde{N}}{\hat{g}\bar{\beta}}+(\hat{g}\bar{\beta})^{\frac{\bar{\beta}}{1-\bar{\beta}}}-\ln\left(\frac{M}{2H_i}\right)^{\frac{1}{\hat{g}\bar{\beta}}}\right\}^{\frac{1}{\bar{\beta}}}\right]\\
&\times \left\{\frac{\tilde{N}}{\hat{g}\bar{\beta}}+(\hat{g}\bar{\beta})^{\frac{\bar{\beta}}{1-\bar{\beta}}}-\ln\left(\frac{M}{2H_i}\right)^{\frac{1}{\hat{g}\bar{\beta}}}\right\}^{\frac{1-\bar{\beta}}{\bar{\beta}}}.
\end{aligned}$$

Figure **2.18** represents dominant characteristics of warm inflation, i.e., $\mathrm{T} >> \tilde{H}$. Both plots of Figure **2.19** imply that $\tilde{r} << 1$ which represents weak interactions between inflaton and matter fields and assures the presence of inflaton particles in weak dissipative regime. In Figure **2.20** (left plot), the variation of e-folds approaches to its standard value, i.e., $\tilde{N} = 60$ as model parameter of inflationary model increases.

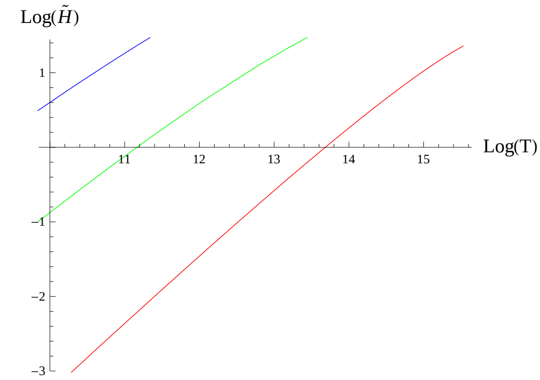

Figure 2.18: Log($\tilde{H}$) versus Log(T) for $\bar{\beta} = 1.5$ (red), 2.5 (green), 3.5 (blue), $\hat{g} = 0.75,\ \Gamma_i \propto \chi_r^{\frac{1}{6}},\ \chi_r = 70$.

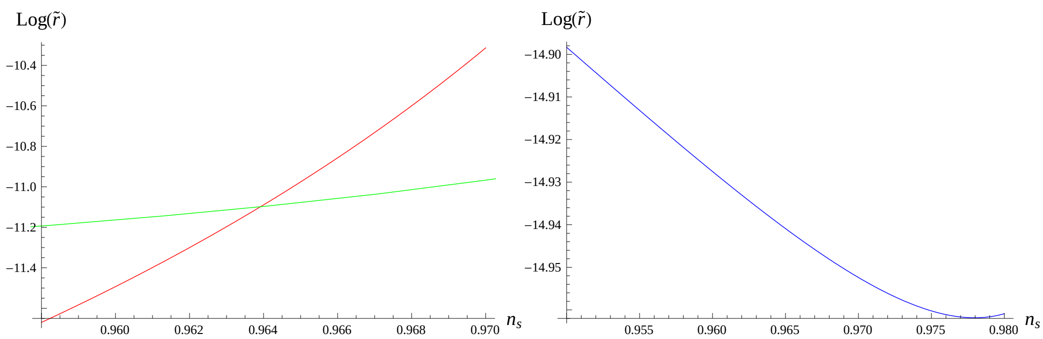

Figure 2.19: Log($\tilde{r}$) versus n_s (left) for $\bar{\beta} = 1.5$ (red), 2.5 (green) and Log($\tilde{r}$) versus n_s (right) for $\bar{\beta} = 3.5$ (blue), $\hat{g} = 0.75,\ \Gamma_i \propto \chi_r^{\frac{1}{6}},\ \chi_r = 70$.

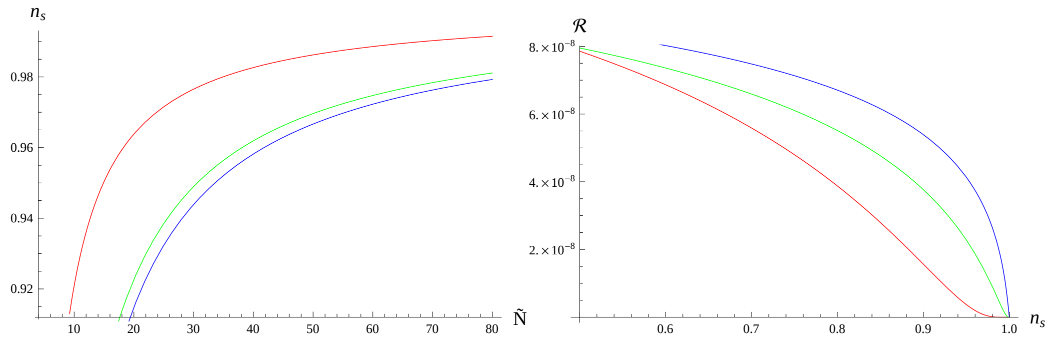

Figure 2.20: n_s versus $\tilde{N}$ (left) and $\mathcal{R}$ versus n_s (right) $\bar{\beta} = 1.5$ (red), 2.5 (green), 3.5 (blue), $\hat{g} = 0.75$, $\Gamma_i \propto \chi_r^{\frac{1}{6}}$, $\chi_r = 70$.

The right panel of Figure **2.20** indicates that $\mathcal{R} < 0.10$ at $n_s = 0.9603$ which implies compatibility of $\mathcal{R}$ in weak dissipation regime.

In case of strong dissipative regime, the inflaton field and potential become

$$\phi = \phi_0 + \bar{\alpha}_5 \Xi(\tilde{t}), \quad U(\phi) = \frac{3(\hat{g}\bar{\beta})^2}{\kappa^2}\left\{\Xi^{-1}\left(\frac{\phi}{\bar{\alpha}_5}\right)\right\}^{-2}\left[\ln\left(\Xi^{-1}\left(\frac{\phi}{\bar{\alpha}_5}\right)\frac{M}{2H_i}\right)\right]^{2(\bar{\beta}-1)}, \tag{2.3.11}$$

where Ξ represents incomplete gamma function given as

$$\Xi(\tilde{t}) = \gamma\left[\bar{\beta}, \frac{1}{2}\ln\left(\frac{\tilde{t}M}{2H_i}\right)\right], \quad \bar{\alpha}_5 = -2^{\bar{\beta}}\hat{g}\bar{\beta}\sqrt{\frac{3M}{H_i\kappa^2\Gamma_i}}.$$

The slow-roll parameters and radiation energy density corresponding to (2.3.11) are given by

$$\begin{aligned}
\epsilon &= \frac{1}{\bar{\beta}\hat{g}}\left[\ln\left(\Xi^{-1}\left(\frac{\phi}{\bar{\alpha}_5}\right)\frac{M}{2H_i}\right)\right]^{(1-\bar{\beta})}, \\
\eta &= \frac{1}{\bar{\beta}\hat{g}}\left[\ln\left(\Xi^{-1}\left(\frac{\phi}{\bar{\alpha}_5}\right)\frac{M}{2H_i}\right)\right]^{-\bar{\beta}}\left(2\ln\left(\Xi^{-1}\left(\frac{\phi}{\bar{\alpha}_5}\right)\frac{M}{2H_i}\right) - (\bar{\beta}-1)\right), \\
\tilde{\rho}_r &= \frac{3\hat{g}\bar{\beta}}{2\kappa^2}\left\{\Xi^{-1}\left(\frac{\phi}{\bar{\alpha}_5}\right)\right\}^{-2}\left[\ln\left(\Xi^{-1}\left(\frac{\phi}{\bar{\alpha}_5}\right)\frac{M}{2H_i}\right)\right]^{(\bar{\beta}-1)}.
\end{aligned}$$

At the initial stage of inflationary epoch, the inflaton at $\tilde{t} = \tilde{t}_i$ gives

$$\phi_i = \phi_0 + \bar{\alpha}_5 \Xi\left(\exp\left[(\hat{g}\bar{\beta})^{\frac{1}{1-\beta}} - \ln\left(\frac{M}{2H_i}\right)\right]\right).$$

The number of e-folds and inflaton field turn out to be

$$\begin{aligned}\tilde{N} &= \hat{g}\bar{\beta}\left\{\ln\left(\Xi^{-1}\left(\frac{\phi}{\bar{\alpha}_5}\right)\right)\left[\ln\left(\Xi^{-1}\left(\frac{\phi}{\bar{\alpha}_5}\right)\frac{M}{2H_i}\right)\right]^{\bar{\beta}-1}\right.\\ &- \left.(\hat{g}\bar{\beta})^{-1}\left((\hat{g}\bar{\beta})^{\frac{1}{1-\beta}} - \ln\left(\frac{M}{2H_i}\right)\right)\right\}, \qquad (2.3.12)\\ \phi &= \phi_0 + \bar{\alpha}_5\Xi\left\{\exp\left(\frac{\tilde{N}}{\hat{g}\bar{\beta}} + (\hat{g}\bar{\beta})^{\frac{\bar{\beta}}{1-\beta}} - \ln\left(\frac{M}{2H_i}\right)^{\frac{1}{\hat{g}\bar{\beta}}}\right)^{\frac{1}{\beta}}\right\}. \qquad (2.3.13)\end{aligned}$$

In this case, the observational parameters take the form

$$\begin{aligned}\Delta_{\mathcal{R}} &= \frac{\kappa^2}{6}\left(\frac{(\hat{g}\bar{\beta})^{\frac{3}{2}}\Gamma_i^3 3^{\frac{1}{2}}}{(2\kappa^2\chi_r)^{\frac{1}{2}}(4\pi)^3}\right)^{\frac{1}{2}}\left(\frac{2H_i}{M}\right)^{\frac{3}{2}}\left(\frac{\tilde{N}}{\hat{g}\bar{\beta}} + (\hat{g}\bar{\beta})^{\frac{\bar{\beta}}{1-\beta}} - \ln\left(\frac{M}{2H_i}\right)^{\frac{1}{\hat{g}\bar{\beta}}}\right)^{\frac{3(\bar{\beta}-1)}{4\bar{\beta}}},\\ \Delta_T &= \frac{2\kappa^2\bar{\beta}^2\hat{g}^2}{\pi^2}\exp\left(-2\left\{\frac{\tilde{N}}{\hat{g}\bar{\beta}} + (\hat{g}\bar{\beta})^{\frac{\bar{\beta}}{1-\beta}} - \ln\left(\frac{M}{2H_i}\right)^{\frac{1}{\hat{g}\bar{\beta}}}\right\}\right)^{\frac{1}{\bar{\beta}}}\left(\frac{2H_i}{M}\right)^2\\ &\times \left[\frac{\tilde{N}}{\hat{g}\bar{\beta}} + (\hat{g}\bar{\beta})^{\frac{\bar{\beta}}{1-\beta}} - \ln\left(\frac{M}{2H_i}\right)^{\frac{1}{\hat{g}\bar{\beta}}}\right]^{\frac{2(\bar{\beta}-1)}{\bar{\beta}}},\\ n_s &= 1 - \frac{3(\bar{\beta}-1)}{4\hat{g}\bar{\beta}^2}\left(\frac{\tilde{N}}{\hat{g}\bar{\beta}} + (\hat{g}\bar{\beta})^{\frac{\bar{\beta}}{1-\beta}} - \ln\left(\frac{M}{2H_i}\right)^{\frac{1}{\hat{g}\bar{\beta}}}\right)^{-1},\\ n_T &= -\frac{2}{\hat{g}\bar{\beta}}\left(\frac{\tilde{N}}{\hat{g}\bar{\beta}} + (\hat{g}\bar{\beta})^{\frac{\bar{\beta}}{1-\beta}} - \ln\left(\frac{M}{2H_i}\right)^{\frac{1}{\hat{g}\bar{\beta}}}\right)^{1-\bar{\beta}}.\end{aligned}$$

The corresponding tensor-scalar ratio yields

$$\begin{aligned}\mathcal{R} &= \left[\left(\frac{144(4\pi)^3(2\kappa^2\chi_r)^{\frac{1}{2}}}{\Gamma_i^3\pi^4 3^{\frac{1}{2}}}\right)\left(\frac{2H_i}{M}\right)(\hat{g}\bar{\beta})^{\frac{5}{2}}\right]^{\frac{1}{2}}\exp\left[-2\left(\frac{\tilde{N}}{\hat{g}\bar{\beta}} + (\hat{g}\bar{\beta})^{\frac{\bar{\beta}}{1-\beta}}\right.\right.\\ &- \left.\left.\ln\left(\frac{M}{2H_i}\right)^{\frac{1}{\hat{g}\bar{\beta}}}\right)^{\frac{1}{\bar{\beta}}}\right]\left(\frac{\tilde{N}}{\hat{g}\bar{\beta}} + (\hat{g}\bar{\beta})^{\frac{\bar{\beta}}{1-\beta}} - \ln\left(\frac{M}{2H_i}\right)^{\frac{1}{\hat{g}\bar{\beta}}}\right)^{\frac{5(\bar{\beta}-1)}{4\bar{\beta}}}.\end{aligned}$$

The decay rate and temperature of thermal bath radiations generates

$$\tilde{r} = \frac{\Gamma_i}{3}\left[\hat{g}\bar{\beta}\exp\left\{\left(\frac{\tilde{N}}{\hat{g}\bar{\beta}} + (\hat{g}\bar{\beta})^{\frac{\bar{\beta}}{1-\beta}} - \ln\left(\frac{M}{2H_i}\right)^{\frac{1}{\hat{g}\bar{\beta}}}\right)^{\frac{1}{\bar{\beta}}}\right\}\left(\frac{\tilde{N}}{\hat{g}\bar{\beta}} + (\hat{g}\bar{\beta})^{\frac{\bar{\beta}}{1-\beta}}\right.\right.$$

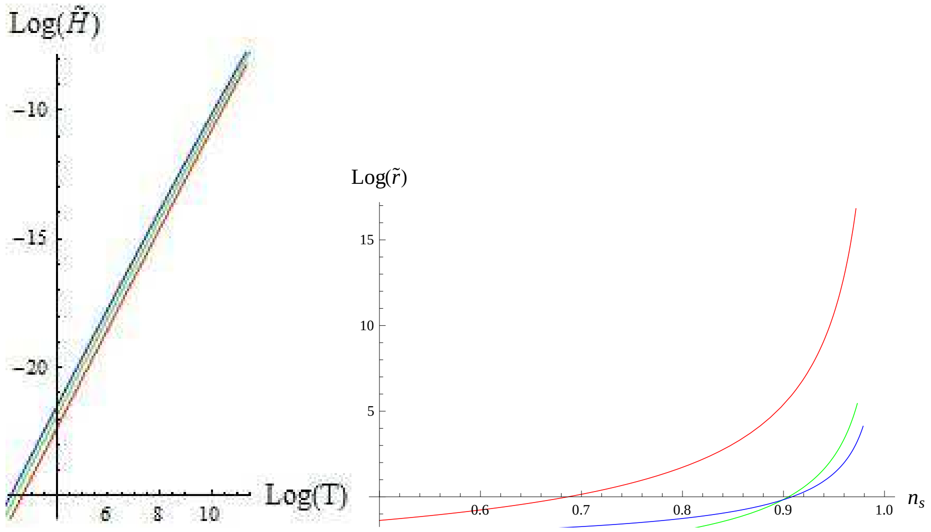

Figure 2.21: Log($\tilde{H}$) versus Log(T) (left) and Log($\tilde{r}$) versus n_s (right) for $\bar{\beta} = 2$ (red), 2.4 (green), 2.7 (blue), $\hat{g} = 0.01$, $\Gamma_i \propto \chi_r^{\frac{1}{6}}$, $\chi_r = 70$.

$$
\begin{aligned}
&- \quad \ln\left(\left(\frac{M}{2H_i}\right)^{\frac{1}{\hat{g}\bar{\beta}}}\right)^{\frac{\bar{\beta}-1}{\beta}}\Bigg]^{-1}, \\
T \quad &= \quad g\bar{\beta}\left(\frac{3}{2\kappa^2\chi_r}\right)^{\frac{1}{4}}\left(\frac{2H_i}{M}\right)\exp\left\{-\frac{1}{2}\left(\frac{\tilde{N}}{\hat{g}\bar{\beta}} + (\hat{g}\bar{\beta})^{\frac{\bar{\beta}}{1-\bar{\beta}}} - \ln\left(\frac{M}{2H_i}\right)^{\frac{1}{\hat{g}\bar{\beta}}}\right)^{\frac{1}{\bar{\beta}}}\right\} \\
&\times \quad \left(\frac{\tilde{N}}{\hat{g}\bar{\beta}} + (\hat{g}\bar{\beta})^{\frac{\bar{\beta}}{1-\bar{\beta}}} - \ln\left(\frac{M}{2H_i}\right)^{\frac{1}{\hat{g}\bar{\beta}}}\right)^{\frac{\bar{\beta}-1}{4\bar{\beta}}}.
\end{aligned}
$$

Figure **2.21** indicates that T >> $\tilde{H}$ (left panel) and $\tilde{r}$ >> 1 (right panel) for $2 \leq \hat{g} \leq 2.7$ which assures the existence of warm inflation for logamediate inflationary model in strong dissipative regime. Figure **2.22** (left plot) represents the graphical behavior of n_s against $\tilde{N}$ which are found in very small ratio due to strong interactions and high dissipation rate whereas the right plot indicates compatible $\mathcal{R}$ for the proposed values of $\hat{g}$ in strong dissipative regime.

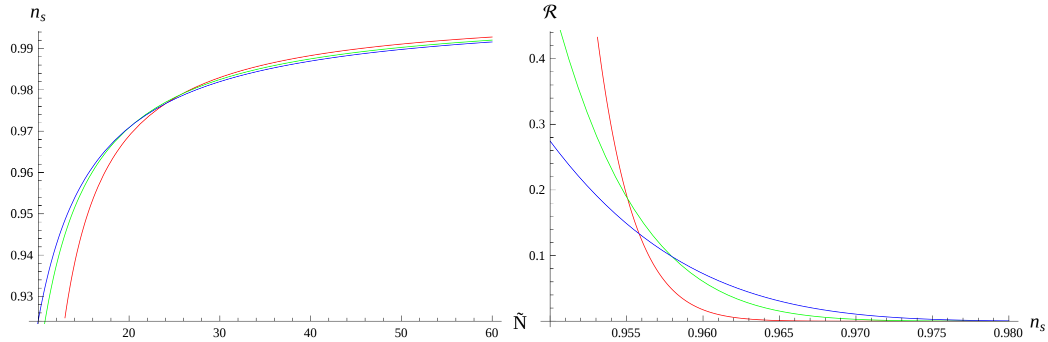

Figure 2.22: n_s versus $\tilde{N}$ (left) for $\hat{g} = 0.1$ and $\mathcal{R}$ versus n_s (right) for $\hat{g} = 0.01$, $\bar{\beta} = 2$ (red), 2.4 (green), 2.7 (blue), $\Gamma_i \propto \chi_r^{\frac{1}{6}}$, $\chi_r = 70$.

2.3.2 Generalized Dissipative Coefficient

Here, the dissipative coefficient (2.2.16) takes the form

$$\Gamma^{\frac{4-m}{4}} = \bar{\alpha}_m \phi^{1-m} \left(\frac{-d\tilde{H}/d\tilde{t}}{\tilde{H}} \right)^{\frac{m}{4}} (1+\tilde{r})^{-\frac{m}{4}} f_R^{\frac{m}{2}},$$

where $\bar{\alpha}_m = \frac{\Gamma_i}{(2\kappa^2\chi_r)^{\frac{m}{4}}}$. For weak and strong regimes, the dissipative coefficient gives

$$\Gamma = (\bar{\alpha}_m \phi^{1-m})^{\frac{4}{4-m}} \left(\frac{d\tilde{H}/d\tilde{t}}{\tilde{H}} \right)^{\frac{m}{4-m}} f_R^{\frac{2m}{4-m}},$$

$$\Gamma = \bar{\alpha}_m \phi^{1-m} \left(-3\frac{d\tilde{H}}{d\tilde{t}} \right)^{\frac{m}{4}} f_R^{\frac{m}{2}}.$$

In weak dissipative regime, the constant as well as generalized dissipative coefficient preserve inflaton field, number of e-folds and slow-roll parameters whereas radiation density for generalized dissipative coefficient becomes

$$\tilde{\rho}_r = \frac{1}{2\kappa^2} \bar{\alpha}_m^{\frac{4}{4-m}} \left(\frac{2H_i}{M} \right)^{\frac{4(m-1)}{4-m}} \exp\left[\left(\frac{4}{m-4} \right) \left(\frac{\phi-\phi_0}{\bar{\alpha}_4} \right)^{\frac{2}{\bar{\beta}+1}} \right] \phi^{\frac{4(1-m)}{4-m}}.$$

The scalar and tensor power spectra along with corresponding spectral indices and tensor-scalar ratio are given by

$$\begin{aligned}
\Delta_{\mathcal{R}} &= \frac{\kappa^2}{2}\left[\left\{\frac{\tilde{N}}{\hat{g}\bar{\beta}}+(\hat{g}\bar{\beta})^{\frac{\bar{\beta}}{1-\bar{\beta}}}+\ln\left(\frac{2H_i}{M}\right)^{\frac{1}{\hat{g}\bar{\beta}}}\right\}^{\frac{1}{\bar{\beta}}}\right]^{\frac{(\bar{\beta}+1)(1-m)}{2(4-m)}+2(\bar{\beta}-1)} \exp\left[\frac{m-5}{4-m}\right. \\
&\times \left.\left\{\left(\frac{\tilde{N}}{\hat{g}\bar{\beta}}+(\hat{g}\bar{\beta})^{\frac{\bar{\beta}}{1-\bar{\beta}}}+\ln\left(\frac{2H_i}{M}\right)^{\frac{1}{\hat{g}\bar{\beta}}}\right)^{\frac{1}{\bar{\beta}}}\right\}\right]\left(\frac{\Gamma_i}{2\kappa^2\chi_r}\right)^{\frac{1}{4-m}}(\hat{g}\bar{\beta})^2 \\
&\times \left\{\left(\frac{2H_i}{M}\right)^{m-1}\bar{\alpha}_4^{1-m}\right\}^{\frac{1}{4-m}}, \\
n_s &= 1-\frac{1}{\hat{g}\bar{\beta}^2}\left\{\frac{\tilde{N}}{\hat{g}\bar{\beta}}+(\hat{g}\bar{\beta})^{\frac{\bar{\beta}}{1-\bar{\beta}}}+\ln\left(\frac{2H_i}{M}\right)^{\frac{1}{\hat{g}\bar{\beta}}}\right\}^{\frac{1}{\bar{\beta}}-1}\left[\left\{\frac{(\bar{\beta}+1)(1-m)}{2(4-m)}\right.\right. \\
&+ \left.2(\bar{\beta}-1)\right\}\left[\left\{\frac{\tilde{N}}{\hat{g}\bar{\beta}}+(\hat{g}\bar{\beta})^{\frac{\bar{\beta}}{1-\bar{\beta}}}+\ln\left(\frac{2H_i}{M}\right)^{\frac{1}{\hat{g}\bar{\beta}}}\right\}^{\frac{1}{\bar{\beta}}}\right]+\left.\left(\frac{m-5}{4-m}\right)\right], \\
\Delta_T &= \frac{2\kappa^2\bar{\beta}^2\hat{g}^2}{\pi^2}\exp\left\{-2\left(\frac{\tilde{N}}{\hat{g}\bar{\beta}}+(\hat{g}\bar{\beta})^{\frac{\bar{\beta}}{1-\bar{\beta}}}+\ln\left(\frac{2H_i}{M}\right)^{\frac{1}{\hat{g}\bar{\beta}}}\right)^{\frac{1}{\bar{\beta}}}\right\} \\
&\times \left(\frac{\tilde{N}}{\hat{g}\bar{\beta}}+(\hat{g}\bar{\beta})^{\frac{\bar{\beta}}{1-\bar{\beta}}}+\ln\left(\frac{2H_i}{M}\right)^{\frac{1}{\hat{g}\bar{\beta}}}\right)^{\frac{2(\bar{\beta}-1)}{\bar{\beta}}}, \\
\mathcal{R} &= \frac{4}{\pi^2}\exp\left[\left(\frac{m-3}{4-m}\right)\left\{\frac{\tilde{N}}{\hat{g}\bar{\beta}}+(\hat{g}\bar{\beta})^{\frac{\bar{\beta}}{1-\bar{\beta}}}+\ln\left(\frac{2H_i}{M}\right)^{\frac{1}{\hat{g}\bar{\beta}}}\right\}^{\frac{1}{\bar{\beta}}}\right]\left(\frac{\Gamma_i}{(2\kappa^2\chi_r)^4}\right)^{\frac{1}{m-4}} \\
&\times \bar{\alpha}_4^{\frac{1-m}{m-4}}\left(\frac{2H_i}{M}\right)^{\frac{3}{m-4}}\left[\left\{\frac{\tilde{N}}{\hat{g}\bar{\beta}}+(\hat{g}\bar{\beta})^{\frac{\bar{\beta}}{1-\bar{\beta}}}+\ln\left(\frac{2H_i}{M}\right)^{\frac{1}{\hat{g}\bar{\beta}}}\right\}^{\frac{1}{\bar{\beta}}}\right]^{\frac{\bar{\beta}+1}{2}\left(\frac{1-m}{m-4}\right)}.
\end{aligned}$$

The dissipation rate of inflaton and temperature of thermal radiations are

$$\begin{aligned}
\tilde{r} &= \frac{1}{3\hat{g}\bar{\beta}}\left(\frac{2H_i}{M}\right)^{\frac{4}{4-m}}\left\{\frac{\tilde{N}}{\hat{g}\bar{\beta}}+(\hat{g}\bar{\beta})^{\frac{\bar{\beta}}{1-\bar{\beta}}}+\ln\left(\frac{2H_i}{M}\right)^{\frac{1}{\hat{g}\bar{\beta}}}\right\}^{\frac{\bar{\beta}+1}{2\bar{\beta}}\left\{\frac{2(1-\bar{\beta})}{(\bar{\beta}+1)}+\frac{4(1-m)}{4-m}\right\}} \\
&\times \left(\frac{\Gamma_i}{(2\kappa^2\chi_r)^{\frac{m}{4}}}\right)\exp\left\{\frac{2m-4}{m-4}\left(\frac{\tilde{N}}{\hat{g}\bar{\beta}}+(\hat{g}\bar{\beta})^{\frac{\bar{\beta}}{1-\bar{\beta}}}+\ln\left(\frac{2H_i}{M}\right)^{\frac{1}{\hat{g}\bar{\beta}}}\right)^{\frac{1}{\bar{\beta}}}\right\},
\end{aligned}$$

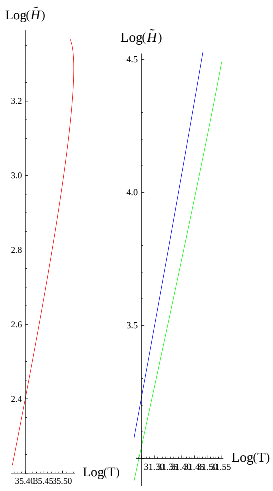

Figure 2.23: Log($\tilde{H}$) versus Log(T) (left) for $\bar{\beta} = 2$ (red) and Log($\tilde{H}$) versus Log(T) (right) for $\bar{\beta} = 3.5$ (green), 4.5 (blue), $\hat{g} = 4,\ \Gamma_i \propto \chi_r^{\frac{1}{6}},\ \chi_r = 70,\ m = 0$.

$$
\begin{aligned}
\mathrm{T} &= \left(\frac{\Gamma_i^2}{(2\kappa^2\chi_r)^{m-2}}\right)^{\frac{1}{2(m-4)}} \left(\frac{\tilde{N}}{\hat{g}\bar{\beta}} + (\hat{g}\bar{\beta})^{\frac{\bar{\beta}}{1-\bar{\beta}}} + \ln\left(\frac{2H_i}{M}\right)^{\frac{1}{\hat{g}\bar{\beta}}}\right)^{\frac{(\bar{\beta}+1)(1-m)}{2\bar{\beta}(4-m)}} \\
&\times \left(\frac{2H_i}{M}\right)^{\frac{3}{4-m}} \bar{\alpha}_3^{\frac{1-m}{4-m}} \exp\left\{\frac{1}{m-4}\left(\frac{\tilde{N}}{\hat{g}\bar{\beta}} + (\hat{g}\bar{\beta})^{\frac{\bar{\beta}}{1-\bar{\beta}}} + \ln\left(\frac{2H_i}{M}\right)^{\frac{1}{\hat{g}\bar{\beta}}}\right)^{\frac{1}{\bar{\beta}}}\right\}.
\end{aligned}
$$

Figures **2.23-2.25** assure the condition of warm inflation for $m = 0,\ 1$ and $m = -1$ in weak dissipative regime for different values of the model parameter $\bar{\beta}$. Figure **2.26** identifies the decay of inflaton particles for $m = 0,\ 1$ but this condition is violated for $m = -1$. The graphical behavior of $\mathcal{R}$ versus n_s and variation of n_s against $\tilde{N}$ for generalized dissipative coefficient is given in Figures **2.27** and **2.28** which lead to compatible results for $m = 0$ and $m = 1$ in weak dissipative regime.

In strong dissipative regime, the inflaton field admitting potential leads to

$$
\phi = \bar{\alpha}_6 \Xi_m(\tilde{t}), \quad U(\phi) = \frac{3(\hat{g}\bar{\beta})^2}{\kappa^2}\left\{\Xi_m^{-1}\left(\frac{\phi}{\bar{\alpha}_4}\right)\right\}^{-2}\left[\ln\left(\Xi_m^{-1}\left(\frac{\phi}{\bar{\alpha}_6}\right)\frac{M}{2H_i}\right)\right]^{2(\bar{\beta}-1)}, \tag{2.3.14}
$$

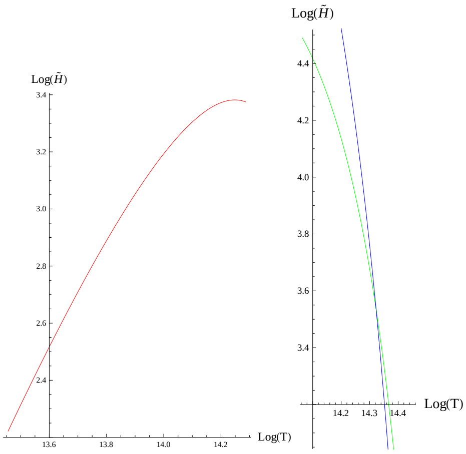

Figure 2.24: Log($\tilde{H}$) versus Log(T) (left) for $\bar{\beta} = 2$ (red) and Log($\tilde{H}$) versus Log(T) (right) for $\bar{\beta} = 3.5$ (green), 4.5 (blue), $\hat{g} = 4,\ \Gamma_i \propto \chi_r^{\frac{1}{6}},\ \chi_r = 70,\ m = 1.$

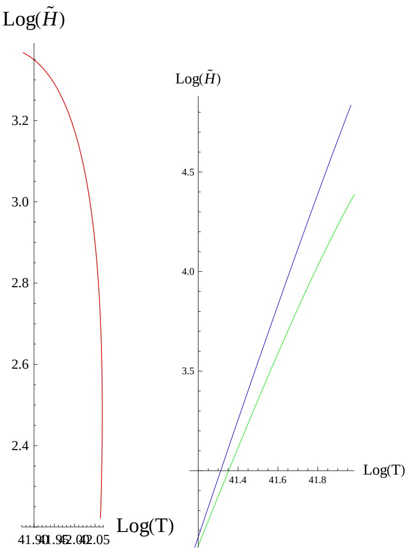

Figure 2.25: Log($\tilde{H}$) versus Log(T) (left) for $\bar{\beta} = 2$ (red) and Log($\tilde{H}$) versus Log(T) (right) for $\bar{\beta} = 3.5$ (green), 4.5 (blue), $\hat{g} = 4,\ \Gamma_i \propto \chi_r^{\frac{1}{6}},\ \chi_r = 70,\ m = -1.$

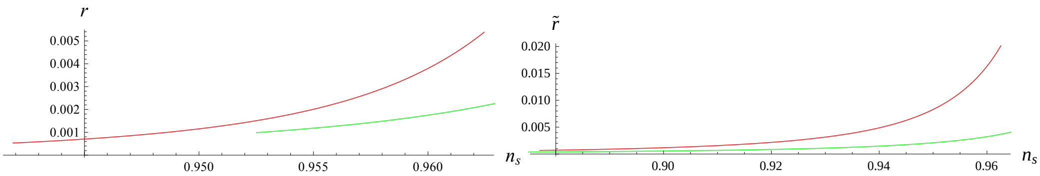

Figure 2.26: $\tilde{r}$ versus n_s (left) for $m = 0$ and $\tilde{r}$ versus n_s (right) for $m = 1$, $\bar{\beta} = 3.5$ (red), 4.5 (green), $\hat{g} = 2$, $\Gamma_i \propto \chi_r^{\frac{1}{6}}$, $\chi_r = 70$.

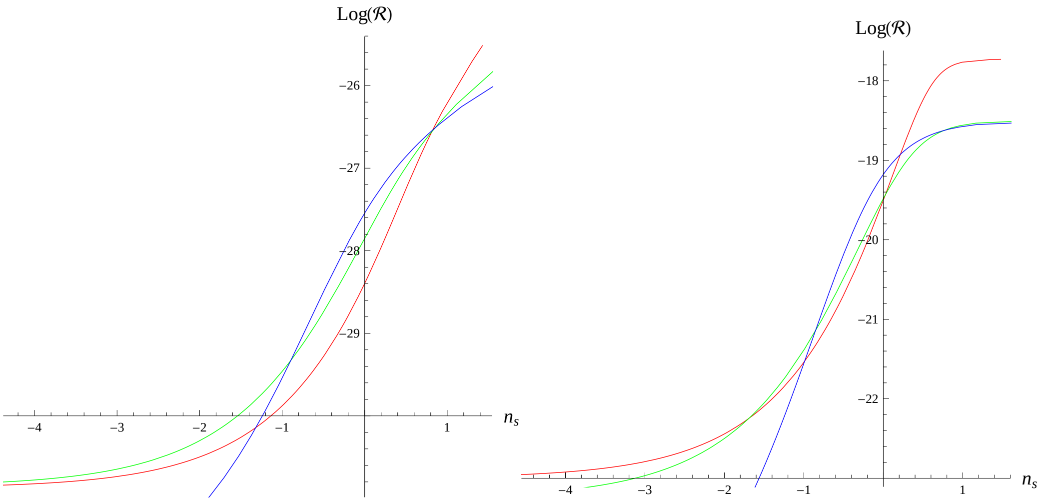

Figure 2.27: Log($\mathcal{R}$) versus n_s (left) for $m = 0$ and Log($\mathcal{R}$) versus n_s (right) for $m = 1$, $\bar{\beta} = 1.25$ (red), 1.45 (green), 1.65 (blue), $\hat{g} = 1$, $\Gamma_i \propto \chi_r^{\frac{1}{6}}$, $\chi_r = 70$.

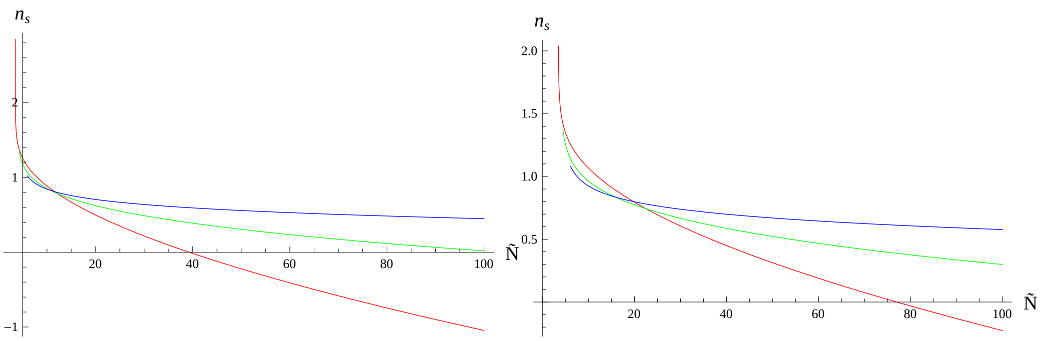

Figure 2.28: n_s versus $\tilde{N}$ (left) for $m = 0$ and n_s versus $\tilde{N}$ (right) for $m = 1$, $\bar{\beta} = 1.25$ (red), 1.45 (green), 1.65 (blue), $\hat{g} = 2$, $\Gamma_i \propto \chi_r^{\frac{1}{6}}$, $\chi_r = 70$.

where

$$\Xi_m(\tilde{t}) = \left(\gamma\left[1+\frac{(8-m)(\bar{\beta}-1)}{8}, \frac{2-m}{4}\ln\left(\frac{\tilde{t}M}{2H_i}\right)\right]\right)^{\frac{2}{3-m}},$$

$$\bar{\alpha}_6 = \left[\left(\frac{3-m}{2}\right)^8 (6\Gamma_i^{\frac{-1}{8}}\kappa^{-2})^4(2\kappa^2\chi_r)^m(\hat{g}\bar{\beta})^{8-m}\left(\frac{M}{2H_i}\right)^{2(m+2)}\right.$$
$$\left.\times \left(\frac{m-2}{4}\right)^{(\bar{\beta}-1)(m-8)-8}\right]^{\frac{1}{4(3-m)}}.$$

The corresponding radiation density, Hubble and slow-roll parameters turn out to be

$$\tilde{\rho}_r = \frac{3\hat{g}\bar{\beta}}{2\kappa^2}\left\{\Xi_m^{-1}\left(\frac{\phi}{\bar{\alpha}_6}\right)\right\}^{-1}\left[\ln\left(\Xi_m^{-1}\left(\frac{\phi}{\bar{\alpha}_6}\right)\frac{M}{2H_i}\right)\right]^{(\bar{\beta}-1)},$$
$$\tilde{H}(\tilde{t}) = \hat{g}\bar{\beta}\left\{\Xi_m^{-1}\left(\frac{\phi}{\bar{\alpha}_6}\right)\right\}^{-1}\left[\ln\left(\Xi_m^{-1}\left(\frac{\phi}{\bar{\alpha}_6}\right)\frac{M}{2H_i}\right)\right]^{(\bar{\beta}-1)}, \tag{2.3.15}$$
$$\epsilon = \frac{1}{\bar{\beta}\hat{g}}\left[\ln\left(\Xi_m^{-1}\left(\frac{\phi}{\bar{\alpha}_6}\right)\frac{M}{2H_i}\right)\right]^{(1-\bar{\beta})},$$
$$\eta = \frac{1}{\bar{\beta}\hat{g}}\left[\ln\left(\Xi_m^{-1}\left(\frac{\phi}{\bar{\alpha}_6}\right)\frac{M}{2H_i}\right)\right]^{-\bar{\beta}}\left(2\ln\left(\Xi_m^{-1}\left(\frac{\phi}{\bar{\alpha}_6}\right)\frac{M}{2H_i}\right)-(\bar{\beta}-1)\right).$$

For $\epsilon = 1$, the initial value of inflaton field leads to ϕ as

$$\phi = \bar{\alpha}_6\Xi_m\left\{\exp\left[\left(\frac{\tilde{N}}{\hat{g}\bar{\beta}}+(\hat{g}\bar{\beta})^{\frac{\bar{\beta}}{1-\bar{\beta}}}-\ln\left(\frac{M}{2H_i}\right)^{\frac{1}{\hat{g}\bar{\beta}}}\right)^{\frac{1}{\bar{\beta}}}\right]\right\}.$$

The corresponding scalar power spectrum and spectral index are

$$\Delta_R^2 = \frac{\kappa^2}{6}\left[(\hat{g}\bar{\beta})^{\frac{3(m+2)}{4}}\left(\frac{M}{2H_i}\right)^{-3(m+1)}\left(\frac{3}{2\kappa^2\chi_r}\right)^{\frac{3m+2}{4}}\left(\frac{\Gamma_i}{4\pi}\right)^3\right]^{\frac{1}{2}}$$
$$\times \exp\left[-\frac{3m}{4}\left(\frac{\tilde{N}}{\hat{g}\bar{\beta}}+(\hat{g}\bar{\beta})^{\frac{\bar{\beta}}{1-\bar{\beta}}}+\ln\left(\frac{2H_i}{M}\right)^{\frac{1}{\hat{g}\bar{\beta}}}\right)^{\frac{1}{\bar{\beta}}}\right]\left(\frac{\tilde{N}}{\hat{g}\bar{\beta}}+(\hat{g}\bar{\beta})^{\frac{\bar{\beta}}{1-\bar{\beta}}}\right.$$
$$\left.+ \ln\left(\frac{2H_i}{M}\right)^{\frac{1}{\hat{g}\bar{\beta}}}\right)^{\frac{3(m+2)(\bar{\beta}-1)}{8\bar{\beta}}}\left\{\bar{\alpha}_6\Xi_m\left(\exp\left[\left(\frac{\tilde{N}}{\hat{g}\bar{\beta}}+(\hat{g}\bar{\beta})^{\frac{\bar{\beta}}{1-\bar{\beta}}}\right.\right.\right.\right.$$

$$
\begin{aligned}
&- \quad \ln\left(\frac{M}{2H_i}\right)^{\frac{1}{\hat{g}\bar{\beta}}}\Bigg)^{\frac{1}{\bar{\beta}}}\Bigg]\Bigg)\Bigg\}^{\frac{3(1-m)}{2}}, \\
n_s &= 1 - \frac{3(m+2)(\bar{\beta}-1)}{8}\left(\frac{\tilde{N}}{\hat{g}\bar{\beta}} + (\hat{g}\bar{\beta})^{\frac{\bar{\beta}}{1-\bar{\beta}}} + \ln\left(\frac{2H_i}{M}\right)^{\frac{1}{\hat{g}\bar{\beta}}}\right)^{\frac{-1}{\bar{\beta}}}.
\end{aligned}
$$

Similarly, tensor power spectrum and its spectral index become

$$
\begin{aligned}
\Delta_T^2 &= \frac{2\kappa^2(\hat{g}\bar{\beta})^2}{\pi^2}\exp\left[-2\left(\frac{\tilde{N}}{\hat{g}\bar{\beta}} + (\hat{g}\bar{\beta})^{\frac{\bar{\beta}}{1-\bar{\beta}}} + \ln\left(\frac{2H_i}{M}\right)^{\frac{1}{\hat{g}\bar{\beta}}}\right)^{\frac{1}{\bar{\beta}}}\right] \\
&\times \left(\frac{\tilde{N}}{\hat{g}\bar{\beta}} + (\hat{g}\bar{\beta})^{\frac{\bar{\beta}}{1-\bar{\beta}}} + \ln\left(\frac{2H_i}{M}\right)^{\frac{1}{\hat{g}\bar{\beta}}}\right)^{\frac{2(\bar{\beta}-1)}{\bar{\beta}}}, \\
n_T &= -\frac{2}{\hat{g}\bar{\beta}}\left(\frac{\tilde{N}}{\hat{g}\bar{\beta}} + (\hat{g}\bar{\beta})^{\frac{\bar{\beta}}{1-\bar{\beta}}} + \ln\left(\frac{2H_i}{M}\right)^{\frac{1}{\hat{g}\bar{\beta}}}\right)^{\frac{1-\bar{\beta}}{\bar{\beta}}}.
\end{aligned}
$$

The above observational parameters generate tensor-scalar ratio as

$$
\begin{aligned}
\mathcal{R} &= \left[\frac{144(4\pi)^3}{\Gamma_i^3\pi^4}\left(\frac{2\kappa^2\chi_r}{3}\right)^{\frac{3m+2}{4}}(\hat{g}\bar{\beta})^{\frac{10-3m}{4}}\left(\frac{2H_i}{M}\right)^{1-3m}\bar{\alpha}_6^{3(m-1)}\right]^{\frac{1}{2}} \\
&\times \exp\left[\frac{3m-8}{4}\left(\frac{\tilde{N}}{\hat{g}\bar{\beta}} + (\hat{g}\bar{\beta})^{\frac{\bar{\beta}}{1-\bar{\beta}}} + \ln\left(\frac{2H_i}{M}\right)^{\frac{1}{\hat{g}\bar{\beta}}}\right)^{\frac{1}{\bar{\beta}}}\right]\Bigg(\frac{\tilde{N}}{\hat{g}\bar{\beta}} + (\hat{g}\bar{\beta})^{\frac{\bar{\beta}}{1-\bar{\beta}}} \\
&+ \ln\left(\frac{2H_i}{M}\right)^{\frac{1}{\hat{g}\bar{\beta}}}\Bigg)^{\frac{(\bar{\beta}-1)(10-3m)}{8\bar{\beta}}}\Bigg\{\Xi_m\Bigg(\exp\Bigg[\Bigg(\frac{\tilde{N}}{\hat{g}\bar{\beta}} + (\hat{g}\bar{\beta})^{\frac{\bar{\beta}}{1-\bar{\beta}}} \\
&+ \ln\left(\frac{2H_i}{M}\right)^{\frac{1}{\hat{g}\bar{\beta}}}\Bigg)^{\frac{1}{\bar{\beta}}}\Bigg]\Bigg)\Bigg\}^{\frac{3(m-1)}{2}},
\end{aligned}
$$

The decay rate of inflaton field and thermal radiations take the form

$$
\begin{aligned}
\tilde{r} &= (\Gamma_i(2\kappa^2\chi_r)^{-\frac{m}{4}})(3\hat{g}\bar{\beta})^{\frac{m-4}{4}}\exp\left[\frac{2-m}{2}\left(\frac{\tilde{N}}{\hat{g}\bar{\beta}} + (\hat{g}\bar{\beta})^{\frac{\bar{\beta}}{1-\bar{\beta}}} + \ln\left(\frac{2H_i}{M}\right)^{\frac{1}{\hat{g}\bar{\beta}}}\right)^{\frac{1}{\bar{\beta}}}\right] \\
&\times \left(\frac{2H_i}{M}\right)^m\bar{\alpha}_6^{1-m}\left(\Xi_m\left\{\exp\left[\left(\frac{\tilde{N}}{\hat{g}\bar{\beta}} + (\hat{g}\bar{\beta})^{\frac{\bar{\beta}}{1-\bar{\beta}}} + \ln\left(\frac{2H_i}{M}\right)^{\frac{1}{\hat{g}\bar{\beta}}}\right)^{\frac{1}{\bar{\beta}}}\right]\right\}\right)^{1-m},
\end{aligned}
$$

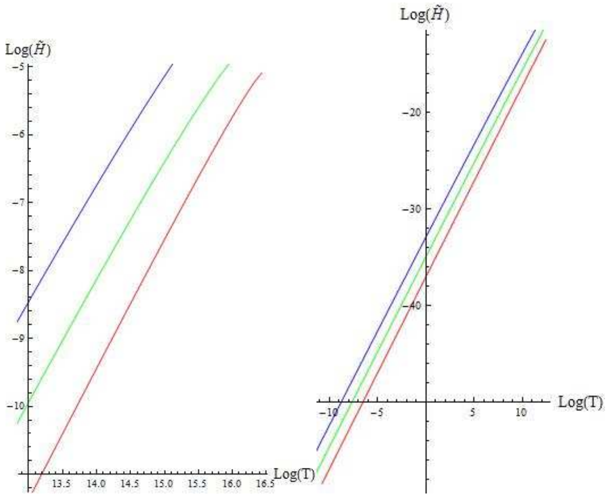

Figure 2.29: Log($\tilde{H}$) versus Log(T) (left) for $m = 0$ and Log($\tilde{H}$) versus Log(T) (right) for $m = 1$, $\bar{\beta} = 1.5$ (red), 2.5 (green), 3.5 (blue), $\hat{g} = 0.01$, $\Gamma_i \propto \chi_r^{\frac{1}{6}}$, $\chi_r = 70$.

$$
\begin{aligned}
\mathrm{T} &= \left(\frac{3\hat{g}\bar{\beta}}{2\kappa^2\chi_r}\right)^{\frac{1}{4}}\left(\frac{2H_i}{M}\right)\exp\left[-\frac{1}{2}\left(\frac{\tilde{N}}{\hat{g}\bar{\beta}}+(\hat{g}\bar{\beta})^{\frac{\bar{\beta}}{1-\bar{\beta}}}+\ln\left(\frac{2H_i}{M}\right)^{\frac{1}{\hat{g}\bar{\beta}}}\right)^{\frac{1}{\bar{\beta}}}\right] \\
&\times \left(\frac{\tilde{N}}{\hat{g}\bar{\beta}}+(\hat{g}\bar{\beta})^{\frac{\bar{\beta}}{1-\bar{\beta}}}+\ln\left(\frac{2H_i}{M}\right)^{\frac{1}{\hat{g}\bar{\beta}}}\right)^{\frac{\bar{\beta}-1}{4\bar{\beta}}}.
\end{aligned}
$$

Figures **2.29-2.31** represent graphical analysis of inflaton particles which satisfy the condition of warm inflation, i.e, T $>>$ $\tilde{H}$ and also show that $\tilde{r} >> 1$. These indications imply that inflaton particles lie in strong dissipative regime for $m = 0, 1$ and $m = -1$. Figures **2.32-2.34** describe the graphical behavior of n_s versus number of e-folds and variation of $\mathcal{R}$ versus n_s for $m = 0,\ 1$ and $m = -1$. These plots indicate that $\mathcal{R}$ is constrained at observational value of n_s which leads to consistent behavior of inflationary model for different values of the model parameter $\hat{g}$.

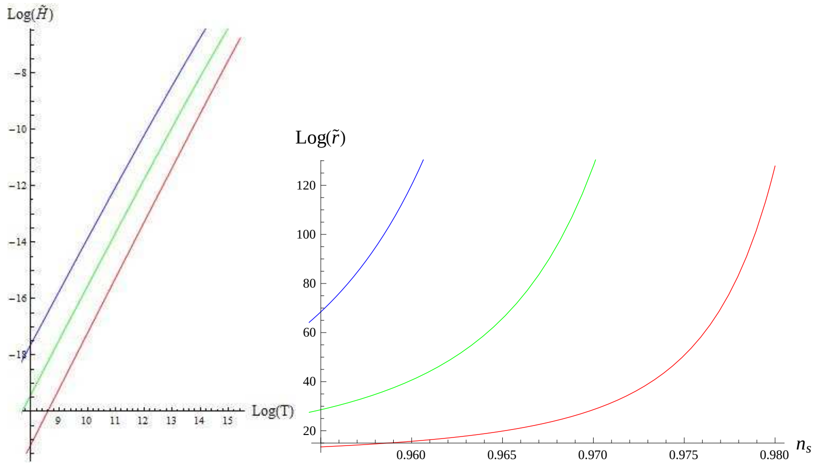

Figure 2.30: Log($\tilde{H}$) versus Log(T) (left) for $\hat{g} = 0.01$, $m = -1$ and Log($\tilde{r}$) versus n_s (right) for $\hat{g} = 0.0027$, $m = 0$,$\bar{\beta} = 1.5$ (red), 2.5 (green), 3.5 (blue), $\Gamma_i \propto \chi_r^{\frac{1}{6}}$, $\chi_r = 70$.

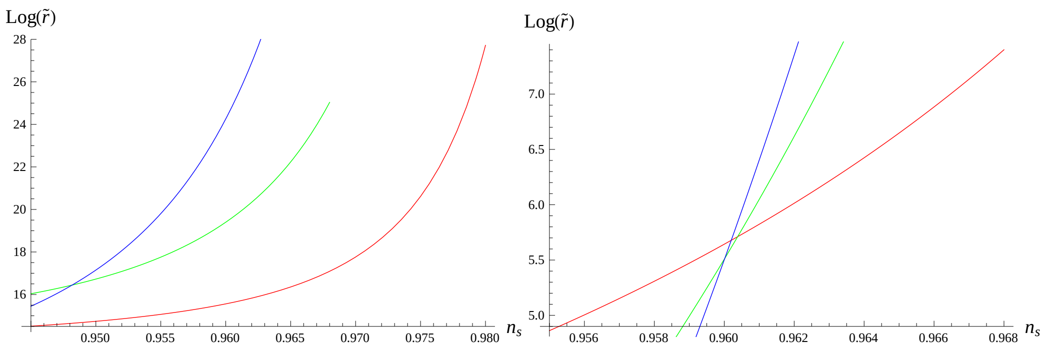

Figure 2.31: Log($\tilde{r}$) versus n_s (left) for $m = -1$ and Log($\tilde{r}$) versus n_s (right) for $m = 1$, $\bar{\beta} = 1.5$ (red), 2.5 (green), 3.5 (blue), $\hat{g} = 0.0027$, $\Gamma_i \propto \chi_r^{\frac{1}{6}}$, $\chi_r = 70$.

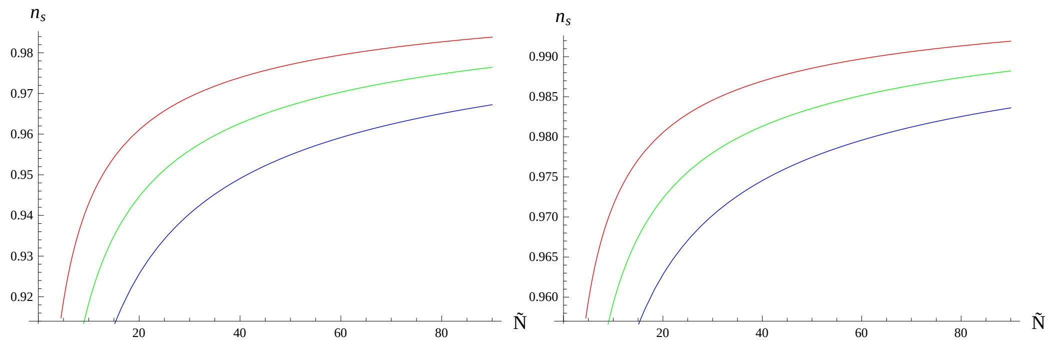

Figure 2.32: n_s versus $\tilde{N}$ (left) for $m = 0$ and n_s versus $\tilde{N}$ (right) for $m = -1$, $\bar{\beta} = 1.65$ (red), 1.75 (green), 1.85 (blue), $\hat{g} = 0.2$, $\Gamma_i \propto \chi_r^{\frac{1}{6}}$, $\chi_r = 70$.

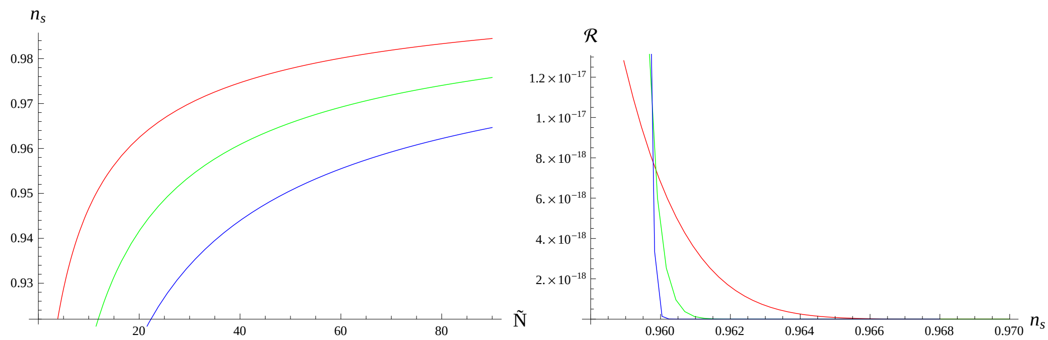

Figure 2.33: n_s versus $\tilde{N}$ (left) for $m = 1$, $\bar{\beta} = 1.65$ (red), 1.75 (green), 1.85 (blue), $\hat{g} = 0.2$, and $\mathcal{R}$ versus n_s (right) for $m = 0$, $\bar{\beta} = 1.1$ (red), 1.15 (green), 1.2 (blue), $\hat{g} = 0.0027$, $\Gamma_i \propto \chi_r^{\frac{1}{6}}$, $\chi_r = 70$.

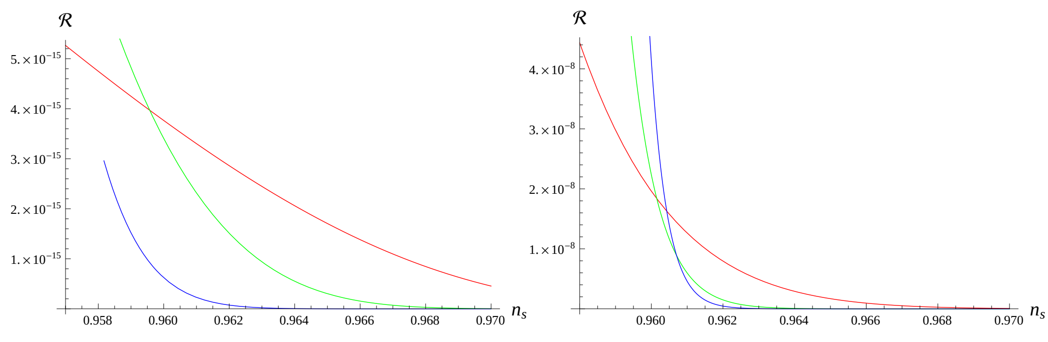

Figure 2.34: $\mathcal{R}$ versus n_s (left) for $m = -1$, $\bar{\beta} = 1.65$ (red), 1.75 (green), 1.85 (blue), and $\mathcal{R}$ versus n_s (right) for $m = 1$, $\bar{\beta} = 1.5$ (red), 2.5 (green), 3.5 (blue), $\hat{g} = 0.0027$, $\Gamma_i \propto \chi_r^{\frac{1}{6}}$, $\chi_r = 70$.

Chapter 3

Some Exact Solutions via Noether Symmetry Approach in $f(R,T)$ Gravity

This chapter investigates the existence of Noether symmetry of some isotropic as well as anisotropic universe models in $f(R,T)$ gravity. Firstly, we evaluate symmetry generators with associated conserved quantities of flat FRW and BI universe models by taking two $f(R,T)$ models admitting indirect curvature-matter coupling while cyclic variable is used to construct exact solution of BI model. Secondly, we consider a generalized spacetime which corresponds to different anisotropic homogeneous universe models in $f(R,T)$ gravity admitting minimal coupling with matter and scalar field models. In this case, $f(R,T)$ models appreciate direct as well as indirect curvature-matter coupling. For these models, we formulate corresponding symmetry generators, conserved quantities and also determine exact solutions without introducing cyclic variable.

The layout of this chapter is as follows. Section **3.1** is devoted to investigate the existence of Noether symmetries of flat FRW and BI universe for both $f(R,T)$ models while the first model leads to evaluate exact solution for perfect fluid. In section **3.2**, we explore all possible Noether symmetries and associated conserved quantities for generalized metric of anisotropic models. We construct exact solutions for both dust as well as perfect fluids. We also construct graphical analysis in both sections to investigate behavior of some cosmological parameters through exact solutions. The results of this chapter have been published in two papers [61, 62].

3.1 Noether Symmetry for BI Universe Model

We apply Noether symmetry approach to deal with non-linear partial differential equation (1.4.21). We consider BI universe model given by

$$ds^2 = -dt^2 + a^2(t)dx^2 + b^2(t)(dy^2 + dz^2), \tag{3.1.1}$$

where scale factors a and b measure expansion of the universe in x and $y,\ z$-directions, respectively. For this purpose, we rewrite the action (1.4.20) as

$$\mathcal{I} = \int \sqrt{-g}[f(R,T) - \lambda(R - \bar{R}) - \chi(T - \bar{T}) + \mathcal{L}_m]dt, \tag{3.1.2}$$

where $\sqrt{-g} = ab^2,\ \bar{R},\ \bar{T}$ represent dynamical constraints while $\lambda,\ \chi$ are Lagrange multipliers given by

$$\begin{aligned}
&\bar{R} = \frac{2}{ab^2}(\ddot{a}b^2 + 2ab\ddot{b} + 2b\dot{a}\dot{b} + a\dot{b}^2), \quad \bar{T} = 3p_m(a,b) - \rho_m(a,b),\\
&\lambda = f_R(R,T), \quad \chi = f_T(R,T).
\end{aligned}$$

The field equation (1.4.21) is not easy to tackle with perfect fluid configuration and also there is no unique definition of matter Lagrangian. Therefore, we consider $\mathcal{L}_m = p_m(a,b)$ [63] and construct Lagrangian as follows

$$\mathcal{L} \;=\; ab^2[f(R,T) - Rf_R(R,T) - Tf_T(R,T) + f_T(R,T)(3p_m(a,b) - \rho_m(a,b))$$

$$
\begin{aligned}
+ &\quad p_m(a,b)] - (4b\dot{a}\dot{b} + 2a\dot{b}^2)f_R(R,T) - (2b^2\dot{a}\dot{R} + 4ab\dot{b}\dot{R})f_{RR}(R,T) - (2b^2\dot{a}\dot{T} \\
+ &\quad 4ab\dot{b}\dot{T})f_{RT}(R,T). \qquad (3.1.3)
\end{aligned}
$$

The corresponding equations of motion and energy function of dynamical system become

$$
\begin{aligned}
&\frac{\dot{b}^2}{b^2} + \frac{2\ddot{b}}{b} = -\frac{1}{2f_R(R,T)}[f(R,T) - Rf_R(R,T) - Tf_T(R,T) + f_T(R,T) \\
&\times(3p_m(a,b) - \rho_m(a,b)) + p_m(a,b) + a\{f_T(3p_{m,a} - \rho_{m,a}) + p_{m,a}\} + 4b^{-1}\dot{b}\dot{R} \\
&\times f_{RR}(R,T) + 2\ddot{R}f_{RR}(R,T) + 2\dot{R}^2 f_{RRR}(R,T) + 4\dot{R}\dot{T}f_{RRT}(R,T) + 2\ddot{T}f_{RT}(R,T) \\
&+2\dot{T}^2 f_{RTT}(R,T) + 4b^{-1}\dot{b}\dot{T}f_{RT}], \qquad (3.1.4) \\
&\frac{\ddot{a}}{a} + \frac{\dot{a}\dot{b}}{ab} + \frac{\ddot{b}}{b} = -\frac{1}{4f_R(R,T)}[2(f(R,T) - Rf_R(R,T) - Tf_T(R,T) \\
&+f_T(R,T)(3p_m(a,b) - \rho_m(a,b)) + p_m(a,b)) + b\{f_T(3p_{m,b} - \rho_{m,b}) + p_{m,b}\}] \\
&+2(a^{-1}\dot{a}\dot{R} + \ddot{R})f_{RR} + 2\dot{R}^2 f_{RRR} + 2(a^{-1}\dot{a}\dot{T} + \ddot{T})f_{RT} + 2(b^{-1}\dot{b}\dot{R} + 2\dot{R}\dot{T} \\
&+\dot{T}^2)f_{RRT} + 2b^{-1}\dot{b}\dot{T}f_{RTT} = 0, \qquad (3.1.5) \\
&\frac{\dot{b}^2}{b^2} + \frac{2\dot{a}\dot{b}}{ab} = -\frac{1}{f_R(R,T)}\left[2\left(\frac{2\dot{b}\dot{R}}{b} + \frac{\dot{a}\dot{R}}{a}\right)f_{RR}(R,T) + 2\left(\frac{2\dot{b}\dot{T}}{b} + \frac{\dot{a}\dot{T}}{a}\right)\right. \\
&\times f_{RT}(R,T) + \frac{1}{2}(f(R,T) - Rf_R(R,T) - Tf_T(R,T) + f_T(R,T)(3p_m(a,b) \\
&\left. -\rho_m(a,b)) + p_m(a,b))\right]. \qquad (3.1.6)
\end{aligned}
$$

The conjugate momenta corresponding to configuration space $(a,\ b,\ R,\ T)$ are

$$
\begin{aligned}
p_a &= \frac{\partial\mathcal{L}}{\partial\dot{a}} = -4b\dot{b}f_R(R,T) - 2b^2(\dot{R}f_{RR}(R,T) + \dot{T}f_{RT}(R,T)), \qquad (3.1.7) \\
p_b &= \frac{\partial\mathcal{L}}{\partial\dot{b}} = -4f_R(R,T)(a\dot{b} + b\dot{a}) - 4ab(\dot{R}f_{RR}(R,T) + \dot{T}f_{RT}(R,T)), \qquad (3.1.8) \\
p_R &= \frac{\partial\mathcal{L}}{\partial\dot{R}} = -(4ab\dot{b} + 2b^2\dot{a})f_{RR}(R,T), \qquad (3.1.9) \\
p_T &= \frac{\partial\mathcal{L}}{\partial\dot{T}} = -(4ab\dot{b} + 2b^2\dot{a})f_{RT}(R,T). \qquad (3.1.10)
\end{aligned}
$$

The vector field with complete lift (1.5.5) takes the following form

$$K = \alpha\frac{\partial}{\partial a} + \beta\frac{\partial}{\partial b} + \gamma\frac{\partial}{\partial R} + \delta\frac{\partial}{\partial T} + \dot{\alpha}\frac{\partial}{\partial \dot{a}} + \dot{\beta}\frac{\partial}{\partial \dot{b}} + \dot{\gamma}\frac{\partial}{\partial \dot{R}} + \dot{\delta}\frac{\partial}{\partial \dot{T}}, \tag{3.1.11}$$

where $\alpha,\ \beta,\ \gamma$ and δ are unknown coefficients of vector field depending on variables $a,\ b,\ R$ and T while the time derivatives of these coefficients are

$$\begin{aligned} \dot{\alpha} &= \dot{a}\frac{\partial \alpha}{\partial a} + \dot{b}\frac{\partial \alpha}{\partial b} + \dot{R}\frac{\partial \alpha}{\partial R} + \dot{T}\frac{\partial \alpha}{\partial T}, \quad \dot{\beta} = \dot{a}\frac{\partial \beta}{\partial a} + \dot{b}\frac{\partial \beta}{\partial b} + \dot{R}\frac{\partial \beta}{\partial R} + \dot{T}\frac{\partial \beta}{\partial T}, \\ \dot{\gamma} &= \dot{a}\frac{\partial \gamma}{\partial a} + \dot{b}\frac{\partial \gamma}{\partial b} + \dot{R}\frac{\partial \gamma}{\partial R} + \dot{T}\frac{\partial \gamma}{\partial T}, \quad \dot{\delta} = \dot{a}\frac{\partial \delta}{\partial a} + \dot{b}\frac{\partial \delta}{\partial b} + \dot{R}\frac{\partial \delta}{\partial R} + \dot{T}\frac{\partial \delta}{\partial T}. \end{aligned}$$

Taking Lie derivative of Lagrangian (3.1.3) with respect to vector field (3.1.11) and inserting time derivative of unknown coefficients, we obtain an over determined system of equations by comparing the coefficients of $\dot{a}^2,\ \dot{b}^2,\ \dot{R}^2,\ \dot{T}^2,\ \dot{a}\dot{b},\ \dot{a}\dot{R},\ \dot{a}\dot{T},\ \dot{b}\dot{R},\ \dot{b}\dot{T}$, $\dot{R}\dot{T}$ and constant coefficient, given in Appendix **A**. We solve this non-linear system of partial differential equations for two $f(R,T)$ models and evaluate possible solutions of symmetry generator coefficients as well as corresponding conserved quantities.

3.1.1 $f(R,T) = R + 2g(T)$

If this model incorporates a trace dependent cosmological constant, then it corresponds to standard ΛCDM model defined as

$$f(R,T) = R + 2\Lambda + g(T). \tag{3.1.12}$$

To find solution of Eqs.(A1)-(A11), we consider power-law form of unknown coefficients of vector field as

$$\alpha = \alpha_0 a^{\alpha_1} b^{\alpha_2} R^{\alpha_3} T^{\alpha_4}, \quad \beta = \beta_0 a^{\beta_1} b^{\beta_2} R^{\beta_3} T^{\beta_4}, \tag{3.1.13}$$

$$\gamma = \gamma_0 a^{\gamma_1} b^{\gamma_2} R^{\gamma_3} T^{\gamma_4}, \quad \delta = \delta_0 a^{\delta_1} b^{\delta_2} R^{\delta_3} T^{\delta_4}, \tag{3.1.14}$$

where powers are unknown constants to be determined. Using these coefficients in Eqs.(A1)-(A9), we obtain

$$\begin{aligned}\alpha_0 &= -\beta_0(\alpha_2+2), \quad \alpha_1=1, \quad \alpha_3=0, \quad \alpha_4=0, \quad \gamma=0,\\ \beta_1 &= 0, \quad \beta_2=\alpha_2+1, \quad \beta_3=0, \quad \beta_4=0.\end{aligned}$$

Inserting these values in Eq.(3.1.13), it follows that

$$\alpha=-\beta_0(\alpha_2+2)ab^{\alpha_2}, \quad \beta=\beta_0 b^{\alpha_2+1}.$$

In order to evaluate α_2, we substitute these solutions in Eq.(A10) which implies that either $\alpha_2=0$ or $\alpha_2=\frac{1}{2}$.

Case I: $\alpha_2=0$

In this case, the generator coefficients turn out to be

$$\alpha=-2\beta_0 a, \quad \beta=\beta_0 b.$$

Insert these values in Eqs.(3.1.4), (3.1.6) and (A11), we have

$$\begin{aligned}g(T) &= l_1T+l_2, \quad \delta=0, \quad p_m=l_3a^{-\frac{1}{5}}b^{-\frac{2}{5}},\\ \rho_m &= -\frac{1}{2l_1}[2\Lambda+l_2+(3l_1-1)l_3a^{-\frac{1}{5}}b^{-\frac{2}{5}}].\end{aligned}$$

Substituting all these solutions in Eqs.(A1)-(A11), we obtain $l_1=-\frac{19}{3}$. Consequently, the coefficients of symmetry generator and $f(R,T)$ model become

$$\alpha=-2\beta_0 a, \quad \beta=\beta_0 b, \quad \gamma=0, \quad \delta=0, \quad f(R,T)=R-\frac{19T}{3},$$

where $g(T)=-\frac{19T}{3}-2\Lambda$ and $T=\frac{87}{19}l_3a^{-\frac{1}{5}}b^{-\frac{2}{5}}$. In this case, the constructed $f(R,T)$ model is found to be viable for $l_3<0$. Using the values of vector field coefficients, we obtain symmetry generator and corresponding conserved quantity as follows

$$K=-2\beta_0 a\frac{\partial}{\partial a}+\beta_0 b\frac{\partial}{\partial b},\quad \Sigma=\beta_0[-4ab\dot{b}+4\dot{a}b^2].$$

The symmetry generator K indicates that scaling symmetry exists in this case.

We solve the field equations by introducing a cyclic variable whose existence is assured by the presence of symmetry generator of Noether symmetry. We consider a point transformation $\bar{\varphi}:(a,b)\rightarrow(v,z)$ which implies that $\bar{\varphi}_K dv=0$ and $\bar{\varphi}_K dz=1$. The second mapping indicates that the Lagrangian must be free from the variable z. Imposing this point transformation, we reduce the complexity of the system as

$$v=\zeta_0 a^{\frac{1}{2}}b,\quad z=\frac{\ln b}{\beta_0}, \tag{3.1.15}$$

where z is cyclic variable and ζ_0 denotes arbitrary constant. The inverse point transformation of variables yields

$$a=\zeta_1 v^{\frac{1}{2}}e^{-2\beta_0 z},\quad b=\zeta_2 e^{\beta_0 z},\quad \rho_m=-\frac{30\zeta_3 v^{-\frac{2}{5}}}{19},\quad p_m=\zeta_3 v^{-\frac{2}{5}}. \tag{3.1.16}$$

Here we redefine arbitrary constants as $\zeta_3=l_3\zeta_1^{-\frac{1}{5}}\zeta_2^{-\frac{2}{5}}$. For the above solutions, the Lagrangian (3.1.3) and the corresponding equations of motion with associated energy function (3.1.4)-(3.1.6) take the form

$$\begin{aligned}
&\mathcal{L}=\zeta_4(4\beta_0 v^{\frac{-1}{2}}\dot{v}\dot{z}+4\beta_0^2 v^{\frac{1}{2}}\dot{z}^2-30v^{\frac{2}{5}}),\\
&2\beta_0 v^{\frac{-1}{2}}\ddot{z}+2\beta_0^2 v^{-\frac{1}{2}}\dot{z}^2-12v^{-\frac{3}{5}}=0,\\
&8\beta_0 v^{\frac{1}{2}}\ddot{z}+v^{-\frac{3}{2}}\dot{v}^2+4\beta_0 v^{-\frac{1}{2}}\dot{z}-2v^{-\frac{1}{2}}\ddot{v}=0,\\
&30v^{\frac{2}{5}}+4\beta_0^2 v^{\frac{1}{2}}\dot{z}^2+\beta_0 v^{-\frac{3}{2}}\dot{v}^2\dot{z}-2\beta_0 v^{-\frac{1}{2}}\dot{v}\ddot{z}=0.
\end{aligned}$$

Solving the above equations, we obtain time dependent solutions of new variables (v,z) as follows

$$v=2(t-\zeta_4)^{\frac{1}{2}}(t^2-2t+\zeta_4^2),\quad z=\frac{1}{12\beta_0}[12\beta_0\zeta_5-2.93-4\ln[(t-\zeta_4)^{\frac{5}{2}}]],$$

where ζ_4 and ζ_5 represent integration constants. Inserting these values into Eq.(3.1.16), we obtain

$$\begin{aligned} a &= \frac{8}{5}\zeta_1 e^{-2\beta_0\zeta_5}(t-\zeta_4)^{\frac{5}{3}}, \quad b = \frac{8}{5}\zeta_2 e^{\beta_0\zeta_5}(t-\zeta_4)^{-\frac{1}{3}}(t^2-2t\zeta_1+\zeta_1^2), \qquad (3.1.17)\\ \rho_m &= -\frac{30\zeta_3}{19}[2(t-\zeta_4)^{\frac{1}{2}}(t^2-2t+\zeta_4^2)]^{-\frac{2}{5}}, \quad p_m = \zeta_3[2(t-\zeta_4)^{\frac{1}{2}}(t^2-2t+\zeta_4^2)]^{-\frac{2}{5}}. \qquad (3.1.18)\end{aligned}$$

Now we study the behavior of some well-known cosmological parameters like Hubble, deceleration and EoS parameters through exact solution of BI universe model. Using Eq.(3.1.17), the Hubble and deceleration parameters turn out to be

$$H=\frac{1}{3}\left(\frac{\dot{a}}{a}+\frac{2\dot{b}}{b}\right)=\frac{5\zeta_6}{3}\left(1+\frac{t}{\zeta_6}\right), \quad q=-\frac{\dot{H}}{H^2}-1=-\frac{3}{5}(\zeta_6+t)^{-2}-1, \quad (3.1.19)$$

where $\zeta_6=-\zeta_4$. Inserting Eqs.(3.1.17) and (3.1.18) in (3.1.4) and (3.1.6), the effective EoS parameter becomes

$$\omega_{eff}=\frac{p_{eff}}{\rho_{eff}}=1-\frac{\zeta_4-t+3(\sqrt{t-\zeta_4}(t^2-2t+\zeta_4^2))^{\frac{2}{5}}}{t-\zeta_4}.$$

The corresponding $r-s$ parameters yield

$$\begin{aligned} r &= q+2q^2-\frac{\dot{q}}{H}=1+\frac{18}{25}\left(2(t-\zeta_4)^{-4}-2(t-\zeta_4)^{-3}+(t-\zeta_4)^{-2}\right),\\ s &= \frac{r-1}{3(q-\frac{1}{2})}=\frac{1}{3}(r-1)\left(-\frac{3(t+\zeta_6)^{-2}}{5}-\frac{3}{2}\right)^{-1}.\end{aligned}$$

Both plots of Figure **3.1** represent graphical analysis of the scale factors a and b which show the increasing behavior in x and y,z-directions, respectively. This increasing nature of scale factors indicates the cosmic accelerated expansion in all directions. The graphical analysis of Hubble and deceleration parameters is shown in Figure **3.2**. Figure **3.2(i)** shows that the Hubble parameter grows continuously representing expanding universe whereas Figure **3.2(ii)** shows negative deceleration parameter

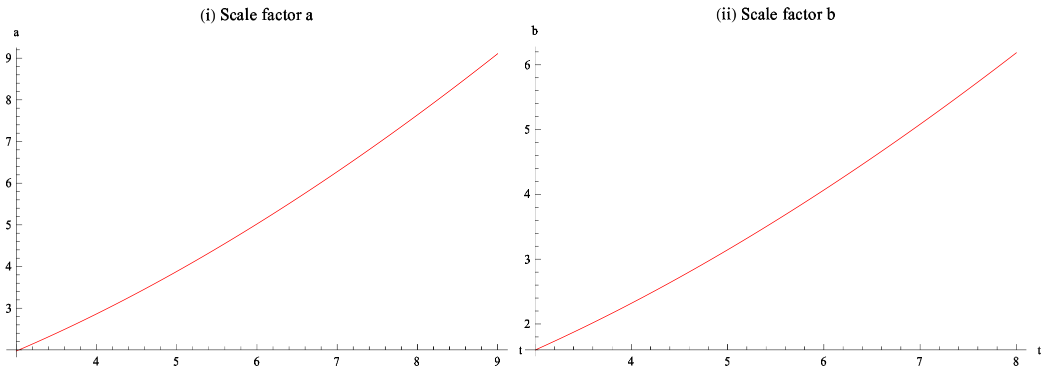

Figure 3.1: Plots of scale factors versus cosmic time t: (i) $a(t)$ versus t; (ii) $b(t)$ versus t for $\zeta_1 = 0.15$, $\zeta_2 = 0.09$, $\zeta_4 = -0.99$, $\zeta_5 = 0.5$, $\beta_0 = 0.1$.

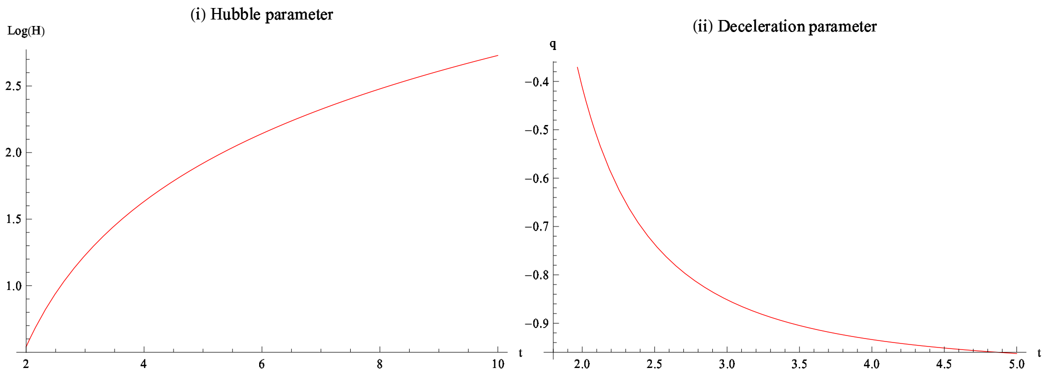

Figure 3.2: Plots of (i) Hubble parameter and (ii) deceleration parameter versus cosmic time t for $\zeta_6 = -0.99$.

which corresponds to accelerated expansion of the universe. In Figure **3.3**, the first plot indicates that the effective EoS parameter describes a smooth transition from radiation dominated era to DE era while the region $-0.3 > \omega_{eff} > -1$ characterizes quintessence phase. Figure **3.3(ii)** represents correspondence of the constructed model with standard ΛCDM universe model as $(r, s) = (1, 0)$. Thus, the analysis of cosmological parameters implies that the universe experiences accelerated expansion for BI universe model.

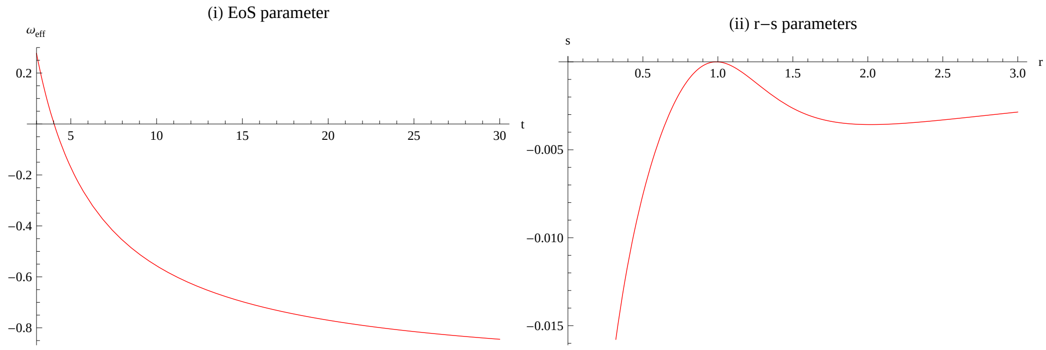

Figure 3.3: Plots of (i) EoS parameter and (ii) r-s parameters versus cosmic time t for $\zeta_6 = -0.99$.

Case II: $\alpha_2 = \frac{1}{2}$

For $\alpha_2 = \frac{1}{2}$, the coefficients of symmetry generator become

$$\alpha = -\frac{5}{2}\beta_0 a b^{\frac{1}{2}}, \quad \beta = \beta_0 b^{\frac{3}{2}},$$

whereas Eq.(A11) yields

$$\begin{aligned}
\delta &= 0, \quad g(T) = -2\Lambda + c_1 T, \quad p_m = m_2 a^{\frac{3m_1^2-3m_1-1}{3m_1-1}} b^{\frac{3(5m_1^2-4m_1-2)}{2(3m_1-1)}}, \\
\rho_m &= \left(\frac{3m_1-1}{m_1-2}\right) m_2 a^{\frac{3m_1^2-3m_1-1}{3m_1-1}} b^{\frac{3(5m_1^2-4m_1-2)}{2(3m_1-1)}},
\end{aligned}$$

where m_1 and m_2 represent arbitrary constants. The above solutions satisfy the system of Eqs.(A1)-(A11) for $m_1 = \frac{3\pm\sqrt{21}}{6}$. Under this condition, the solutions and considered model of $f(R,T)$ gravity take the following form

$$\begin{aligned}
\alpha &= -\frac{5}{2}\beta_0 a b^{\frac{1}{2}}, \quad \beta = \beta_0 b^{\frac{3}{2}}, \quad \gamma, \delta = 0, \quad g(T) = -2\Lambda + \left(\frac{3\pm\sqrt{21}}{6}\right) T, \\
p_m &= m_2 b^{\frac{1}{2}}, \quad \rho_m = \left(\frac{-3\mp\sqrt{21}}{9\mp\sqrt{21}}\right) m_2 b^{\frac{1}{2}}, \quad f(R,T) = R + \left(\frac{3\pm\sqrt{21}}{6}\right) T,
\end{aligned}$$

where $T = \left(\frac{30\mp2\sqrt{21}}{9\mp\sqrt{21}}\right) m_2 b^{\frac{1}{2}}$. Here, the constructed model ignores Dolgov-Kawasaki instability as f_R, f_{RR}, $1 + f_T > 0$. The symmetry generator and its corresponding conserved quantity turn out to be

$$K=-\frac{5}{2}\beta_0 ab^{\frac{1}{2}}\frac{\partial}{\partial a}+\beta_0 b^{\frac{3}{2}}\frac{\partial}{\partial b},\quad \Sigma=\beta_0[6ab^{\frac{3}{2}}\dot{b}-4\dot{a}b^{\frac{5}{2}}].$$

We introduce z as a cyclic variable to evaluate exact solution which yields

$$v=\bar{m}_0 a^{\frac{2}{5}}b,\quad z=-\frac{2b^{-\frac{1}{2}}}{\beta_0},$$

where $\bar{m}_0$ denotes arbitrary constant. The corresponding inverse point transformation leads to

$$\begin{aligned}
a &= \bar{m}_1 v^{\frac{5}{2}}\left(-\frac{\beta_0 z}{2}\right)^5,\quad b=\bar{m}_2\left(-\frac{\beta_0 z}{2}\right)^{-2},\\
p_m &= m_2\bar{m}_2\left(-\frac{\beta_0 z}{2}\right)^{-1},\quad \rho_m=\left(\frac{-3\mp\sqrt{21}}{9\mp\sqrt{21}}\right)m_2\bar{m}_2\left(-\frac{\beta_0 z}{2}\right)^{-1},
\end{aligned}$$

where $\bar{m}_1$ and $\bar{m}_2$ are arbitrary constants. For these solutions, the Lagrangian (3.1.3) becomes

$$\begin{aligned}
\mathcal{L} &= -2\beta_0\bar{m}_1\bar{m}_2^2\left[5v^{\frac{3}{2}}\dot{v}-6\beta_0 v^{\frac{5}{2}}\dot{z}^2\left(-\frac{\beta_0 z}{2}\right)^{-1}\right]+m_2 v^{\frac{5}{2}}\left[4\left(\frac{3\pm\sqrt{21}}{6}\right)\right.\\
&\times\left.\left(\frac{6\mp\sqrt{21}}{9\mp\sqrt{21}}\right)-1\right],
\end{aligned}$$

which depends upon the cyclic variable z. Thus, the resulting symmetry generator for $\alpha_2=0$ yields scaling symmetry providing more significant results as compared to $\alpha_2=\frac{1}{2}$.

3.1.2 $f(R,T)=f(R)+g(T)$

Here we consider $f(R,T)$ model which does not encourage any direct non-minimal coupling of curvature and matter. For vector field K (3.1.11), we substitute this model in Eqs.(A1)-(A7) and (A9) which leads to

$$\begin{aligned}
\alpha &= -\frac{2am_3}{b\sqrt{f_R}} - 2am_4\ln(f_R) - \frac{2m_5}{\sqrt{b}} - 4\ln(b)am_4 - 6\ln(b)m_6a + m_7a,\\
\beta &= \frac{m_3}{\sqrt{f_R}} + (m_8 + \ln(f_R)m_4)b - (m_4+m_6)b\ln(b) + m_6b\ln(a),\\
\gamma &= -\frac{2}{\sqrt{f_R}f_{RR}b}\Big[b((-3m_4-4m_6)\ln(b) + m_4 + m_8 + \frac{m_7}{2}\\
&+ m_6 + m_6\ln(a))(f_R)^{\frac{3}{2}} - m_3f_R\Big].
\end{aligned}$$

Here m_i $(i = 3,4,5,6,7,8)$ are arbitrary constants. Inserting these solutions in Eq.(A8), we obtain two solutions for $f(R)$ as $f(R) = m_9R + m_{10}$ which is similar to the previous case while the second solution increases the complexity of the system. To avoid this situation, we consider $f(R) = f_0R^n$ which yields

$$\begin{aligned}
\alpha &= am_{11}, \quad \beta = bm_{12}, \quad \gamma = \frac{(m_{11}+2m_{12})R}{1-n}, \quad g(T) = \frac{T}{3} + m_{13},\\
p_m &= \frac{1}{12nm_{13}}\left[R^{1-n}b\rho_{m,b} - Rm_{13} - 6R^{1-n}m_{13} + 2R^{1-n}\rho_m + 6nm_{13}R\right],\\
\rho_m &= 3f_0R^n + 3m_{13} - \frac{(m_{11}a\rho_{m,a} + m_{12}b\rho_{m,b})}{(m_{11}+2m_{12})}.
\end{aligned}$$

These solutions satisfy (A1)-(A11) for $n = 2$ which implies that $f(R) = f_0R^2$. Thus, the matter contents and model of $f(R,T)$ gravity turn out to be

$$\begin{aligned}
\rho_m &= 3f_0R^2 + 3m_{13} + \frac{a^{-1+\frac{m_{12}}{m_{11}}}b}{2}, \quad p_m = \frac{1}{24m_{13}}\left[\frac{3a^{-1+\frac{m_{12}}{m_{11}}}bR^{-1}}{2} + 12m_{13}R\right],\\
f(R,T) &= f_0R^2 + \frac{T}{3} + m_{13}, \quad T = 3p_m - \rho_m.
\end{aligned}$$

In this case, the constructed $f(R,T)$ model is found to be viable as it preserves stability conditions. The corresponding symmetry generator takes the form

$$K = am_{11}\frac{\partial}{\partial a} + bm_{12}\frac{\partial}{\partial b} - R(m_{11}+2m_{12})\frac{\partial}{\partial R}.$$

This generator yields scaling symmetry with the following conserved factors

$$\Sigma_1 = 4ab^2\dot{R}f_0 - 4b^2\dot{a}f_0R, \quad \Sigma_2 = -24ab\dot{b}f_0R - 8ab^2\dot{R}f_0,$$

where Σ_1 and Σ_2 are conserved quantities corresponding to m_{11} and m_{12}, respectively. To reduce the complex nature of the system, we consider $\bar{\varphi} : (a, b, R) \rightarrow (u, v, z)$ implying that $\bar{\varphi}_K du = 0$, $\bar{\varphi}_K dv = 0$ and $\bar{\varphi}_K dz = 1$. In this case, we choose z as cyclic variable which gives

$$u = \tilde{A}_0 a^{\frac{m_{11}+2m_{12}}{m_{11}}} R, \quad v = \tilde{A}_1 b^{\frac{m_{11}+2m_{12}}{m_{12}}} R, \quad z = -\frac{1}{m_{11}+2m_{12}} \ln R,$$

where $\tilde{A}_0$ and $\tilde{A}_1$ denote integration constants. The corresponding inverse point transformation yields

$$a = u^{\frac{m_{11}}{m_{11}+2m_{12}}} e^{m_{11}z}, \quad b = v^{\frac{m_{12}}{m_{11}+2m_{12}}} e^{m_{12}z}, \quad R = e^{m_{11}+2m_{12}z}.$$

For these solutions, the Lagrangian (3.1.3) takes the form

$$\begin{aligned}
\mathcal{L} &= \frac{1}{(m_{11}+2m_{12})^2}\Big(24f_0\dot{z}^2 v^{\frac{2m_{12}}{m_{11}+2c_{12}}} m_{11}^3 u^{\frac{m_{11}}{m_{11}+2m_{12}}} m_{12} + 60f_0\dot{z}^2 v^{\frac{2m_{12}}{m_{11}+2m_{12}}} u^{\frac{m_{11}}{m_{11}+2m_{12}}} \\
&\times m_{11}^2 m_{12}^2 + 80f_0\dot{z}^2 v^{\frac{2m_{12}}{m_{11}+2m_{12}}} m_{11} m_{12}^3 u^{\frac{m_{11}}{m_{11}+2m_{12}}} + 16f_0\dot{v}\dot{z} u^{\frac{m_{11}}{m_{11}+2m_{12}}} m_{12}^3 v^{-\frac{m_{11}}{m_{11}+2m_{12}}} \\
&+ 4f_0\dot{u}\dot{z} v^{\frac{2m_{12}}{m_{11}+2m_{12}}} m_{11}^3 u^{-\frac{2m_{12}}{m_{11}+2m_{12}}} - 8f_0\dot{u}\dot{v} m_{12} m_{11} v^{-\frac{m_{11}}{m_{11}+2m_{12}}} u^{-\frac{2m_{12}}{m_{11}+2m_{12}}} + 8f_0\dot{u}\dot{z} \\
&\times v^{\frac{2m_{12}}{m_{11}+2m_{12}}} u^{-\frac{2m_{12}}{m_{11}+2m_{12}}} m_{12} m_{11}^2 + 8f_0\dot{v}\dot{z} u^{\frac{m_{11}}{m_{11}+2m_{12}}} v^{-\frac{m_{11}}{m_{11}+2m_{12}}} m_{12}^2 m_{11} - \Big(u^{\frac{m_{11}}{m_{11}+2m_{12}}} \\
&\times e^{m_{11}z}\Big)^{\frac{m_{12}}{m_{11}}} v^{\frac{3m_{12}}{m_{11}+2m_{12}}} e^{3m_{12}z} m_{11}^2 - 4\left(u^{\frac{m_{11}}{m_{11}+2m_{12}}} e^{m_{11}z}\right)^{\frac{m_{12}}{m_{11}}} v^{\frac{3m_{12}}{m_{11}+2m_{12}}} e^{3m_{12}z} m_{12}^2 \\
&- 4f_0\dot{v}^2 m_{12}^2 u^{\frac{m_{11}}{m_{11}+2m_{12}}} v^{-\frac{2(m_{12}+m_{11})}{m_{11}+2m_{12}}} + 48f_0\dot{z}^2 u^{\frac{m_{11}}{m_{11}+2m_{12}}} v^{\frac{2m_{12}}{m_{11}+2m_{12}}} m_{12}^4 + 4v^{\frac{2m_{12}}{m_{11}+2m_{12}}} \\
&\times u^{\frac{m_{11}}{m_{11}+2m_{12}}} f_0 m_{11}^4 \dot{z}^2 - 4\left(u^{\frac{m_{11}}{m_{11}+2m_{12}}} e^{m_{11}z}\right)^{\frac{m_{12}}{m_{11}}} v^{\frac{3m_{12}}{m_{11}+2m_{12}}} e^{3m_{12}z} m_{11} m_{12}\Big).
\end{aligned}$$

Here, the Lagrangian again depends on the cyclic variable z. Consequently, this approach does not provide a successive way to evaluate exact solution of the anisotropic universe model in this case.

Now we determine Noether symmetry of isotropic as well as anisotropic homogeneous universe models in the presence of first order prolongation and boundary term for $f(R,T)=f_0R^n+g(T)$ model.

Flat FRW Universe Model

For isotropic universe, the Lagrangian depends on configuration space $(a,\ R,\ T)$ with tangent space $(a,\ R,\ T,\ \dot{a},\ \dot{R},\ \dot{T})$. The Lagrange multiplier approach with $\mathcal{L}_m=p_m(a)$ leads to

$$\begin{aligned}\mathcal{L} &= a^3[f(R,T)-Rf_R(R,T)-Tf_T(R,T)+f_T(R,T)(3p_m(a)-\rho_m(a))+p_m(a)]\\ &- 6(a\dot{a}^2f_R(R,T)+a^2\dot{a}\dot{R}f_{RR}(R,T)+a^2\dot{a}\dot{T}f_{RT}(R,T)).\end{aligned}\tag{3.1.20}$$

The vector field with its first order prolongation is defined as

$$\begin{aligned}K &= \tau(t,a,R,T)\frac{\partial}{\partial t}+\alpha(t,a,R,T)\frac{\partial}{\partial a}+\beta(t,a,R,T)\frac{\partial}{\partial R}+\gamma(t,a,R,T)\frac{\partial}{\partial T},\\ K^{[1]} &= \tau\frac{\partial}{\partial t}+\alpha\frac{\partial}{\partial a}+\beta\frac{\partial}{\partial R}+\gamma\frac{\partial}{\partial T}+\dot{\alpha}\frac{\partial}{\partial \dot{a}}+\dot{\beta}\frac{\partial}{\partial \dot{R}}+\dot{\gamma}\frac{\partial}{\partial \dot{T}},\end{aligned}$$

where $\tau,\ \alpha,\ \beta$ and γ are unknown coefficients of vector field to be determined and the time derivatives of these coefficients are

$$\begin{aligned}\dot{\alpha} &= \frac{\partial\alpha}{\partial t}+\dot{a}\frac{\partial\alpha}{\partial a}+\dot{R}\frac{\partial\alpha}{\partial R}+\dot{T}\frac{\partial\alpha}{\partial T}-\dot{a}\left\{\frac{\partial\tau}{\partial t}+\dot{a}\frac{\partial\tau}{\partial a}+\dot{R}\frac{\partial\tau}{\partial R}+\dot{T}\frac{\partial\tau}{\partial T}\right\},\\ \dot{\beta} &= \frac{\partial\beta}{\partial t}+\dot{a}\frac{\partial\beta}{\partial a}+\dot{R}\frac{\partial\beta}{\partial R}+\dot{T}\frac{\partial\beta}{\partial T}-\dot{R}\left\{\frac{\partial\tau}{\partial t}+\dot{a}\frac{\partial\tau}{\partial a}+\dot{R}\frac{\partial\tau}{\partial R}+\dot{T}\frac{\partial\tau}{\partial T}\right\},\\ \dot{\gamma} &= \frac{\partial\gamma}{\partial t}+\dot{a}\frac{\partial\gamma}{\partial a}+\dot{R}\frac{\partial\gamma}{\partial R}+\dot{T}\frac{\partial\gamma}{\partial T}-\dot{T}\left\{\frac{\partial\tau}{\partial t}+\dot{a}\frac{\partial\tau}{\partial a}+\dot{R}\frac{\partial\tau}{\partial R}+\dot{T}\frac{\partial\tau}{\partial T}\right\}.\end{aligned}$$

Substituting the values of vector field, its first order prolongation and corresponding derivatives of coefficients in Eq.(1.5.2), we obtain the system of equations mentioned in Appendix **A**. Solving the system (A12)-(A20), it follows that

$$\begin{aligned}\tau &= \frac{\hat{A}_4 t(3\hat{A}_6\hat{A}_2-\hat{A}_3\hat{A}_5)}{\hat{A}_6}+\hat{A}_8, \quad \alpha=\hat{A}_4(\hat{A}_2 a+\hat{A}_3 a^{-1}),\\ \beta &= \frac{\hat{A}_4\hat{A}_3(\hat{A}_5+\hat{A}_6 a^{-2})R}{\hat{A}_6(1-n)}, \quad B=\frac{\hat{A}_1 t}{2}, \quad \gamma=0, \quad g(T)=\frac{T}{3}+\hat{A}_7,\end{aligned}$$

where $\hat{A}_j$ $(j = 1...8)$ are arbitrary constants. For these coefficients, the symmetry generator becomes

$$\begin{aligned}K &= \left(\frac{\hat{A}_4 t(3\hat{A}_6\hat{A}_2-\hat{A}_3\hat{A}_5)}{\hat{A}_6}+\hat{A}_8\right)\frac{\partial}{\partial t}+\left(\frac{\hat{A}_4\hat{A}_3(\hat{A}_5+\hat{A}_6 a^{-2})R}{\hat{A}_6(1-n)}\right)\frac{\partial}{\partial R}\\ &+ \hat{A}_4(\hat{A}_2 a+\hat{A}_3 a^{-1})\frac{\partial}{\partial a}.\end{aligned}$$

This generator can be split as

$$\begin{aligned}K_1 &= \frac{\partial}{\partial t}, \quad K_2=\left(\frac{t(3\hat{A}_6\hat{A}_2-\hat{A}_3\hat{A}_5)}{\hat{A}_6}\right)\frac{\partial}{\partial t}+\left(\frac{\hat{A}_3(\hat{A}_5+\hat{A}_6 a^{-2})R}{\hat{A}_6(1-n)}\right)\frac{\partial}{\partial R}\\ &+ (\hat{A}_2 a+\hat{A}_3 a^{-1})\frac{\partial}{\partial a},\end{aligned}$$

where the first generator corresponds to energy conservation. The corresponding conserved quantities are

$$\begin{aligned}\Sigma_1 &= -\frac{t(3\hat{A}_6\hat{A}_2-\hat{A}_3\hat{A}_5)}{\hat{A}_6}\Big[a^3(f_0R^n(1-n)+\hat{A}_7-\frac{\rho_m}{3})-6(a\dot{a}^2+(n-1)\\ &\times a^2\dot{a}\dot{R}R^{-1})nf_0R^{n-1}\Big]+6anf_0R^{n-1}(2\dot{a}-(n-1)aR^{-1}\dot{R})\Big[(\hat{A}_2 a+\hat{A}_3 a^{-1})\\ &- \frac{t\dot{a}(3\hat{A}_6\hat{A}_2-\hat{A}_3\hat{A}_5)}{\hat{A}_6}\Big]-6n(n-1)f_0a^2R^{n-2}\dot{a}\left[\frac{\hat{A}_3(\hat{A}_5+\hat{A}_6 a^{-2})R}{\hat{A}_6(1-n)}\right.\\ &+ \left.\frac{t\dot{R}(3\hat{A}_6\hat{A}_2-\hat{A}_3\hat{A}_5)}{\hat{A}_6}\right],\\ \Sigma_2 &= -a^3(f_0R^n(1-n)+\hat{A}_7-\frac{\rho_m}{3})-6(a\dot{a}^2+2(n-1)a^2\dot{a}\dot{R}R^{-1})nf_0R^{n-1}.\end{aligned}$$

BI Universe Model

For $Q = \{t, a, b, R, T\}$, the vector field and corresponding first order prolongation take the form

$$\begin{aligned}
K &= \tau(t,a,b,R,T)\frac{\partial}{\partial t} + \alpha(t,a,b,R,T)\frac{\partial}{\partial a} + \beta(t,a,b,R,T)\frac{\partial}{\partial b}\\
&+ \gamma(t,a,b,R,T)\frac{\partial}{\partial R} + \delta(t,a,b,R,T)\frac{\partial}{\partial T},\\
K^{[1]} &= \tau\frac{\partial}{\partial t} + \alpha\frac{\partial}{\partial a} + \beta\frac{\partial}{\partial b} + \gamma\frac{\partial}{\partial R} + \delta\frac{\partial}{\partial T} + \dot{\alpha}\frac{\partial}{\partial \dot{a}} + \dot{\beta}\frac{\partial}{\partial \dot{b}} + \dot{\gamma}\frac{\partial}{\partial \dot{R}} + \dot{\delta}\frac{\partial}{\partial \dot{T}},
\end{aligned}$$

where

$$\dot{\alpha} = D\alpha - \dot{a}D\tau, \quad \dot{\beta} = D\beta - \dot{b}D\tau, \quad \dot{\gamma} = D\gamma - \dot{R}D\tau, \quad \dot{\delta} = D\delta - \dot{T}D\tau.$$

Using the above vector field, its prolongation and coefficient derivatives in the invariance condition (1.5.2), we formulate the system of equations provided in Appendix **A**. Solving the system of equations (A21)-(A34), it follows that

$$\begin{aligned}
\tau &= \bar{A}_1, \quad B = (\bar{A}_2 t + \bar{A}_3)\bar{A}_4\bar{A}_5, \quad \alpha = \bar{A}_5\bar{A}_6 a, \quad \beta = \bar{A}_5\bar{A}_6 b,\\
\gamma &= \frac{\bar{A}_5\bar{A}_6 R}{2(1-n)}, \quad \delta = 0, \quad \rho_m = -\frac{3\bar{A}_2\bar{A}_4(\bar{A}_7 + \bar{A}_8\ln a)}{ab^2\bar{A}_6\bar{A}_8},\\
p_m &= -\frac{1}{2nf_0}[f_0R^n + R^{1-n}\bar{A}_9 - Rnf_0],\\
f(R,T) &= f_0R^n - \frac{1}{6nf_0}[f_0R^n + R^{1-n}\bar{A}_9 - Rnf_0] - \frac{\bar{A}_2\bar{A}_4(\bar{A}_7 + \bar{A}_8\ln a)}{ab^2\bar{A}_6\bar{A}_8}.
\end{aligned}$$

The solution of these coefficients leads to

$$K = \bar{A}_1\frac{\partial}{\partial t} + \bar{A}_5\bar{A}_6 a\frac{\partial}{\partial a} + \bar{A}_5\bar{A}_6 b\frac{\partial}{\partial b} + \frac{\bar{A}_5\bar{A}_6 R}{2(1-n)}\frac{\partial}{\partial R}.$$

This generator can be split as

$$K_1 = \frac{\partial}{\partial t}, \quad K_2 = a\frac{\partial}{\partial a} + b\frac{\partial}{\partial b} + \frac{R}{2(1-n)}\frac{\partial}{\partial R},$$

where the first generator yields energy conservation whereas the second generator provides scaling symmetry. The corresponding conserved quantities are

$$\begin{aligned}\Sigma_1 &= -ab^2[(f_0R^n(1-n)+\bar{A}_9-\frac{\rho_m}{3})-nf_0R^{n-1}(2a\dot{b}^2+(n-1)R^{-1}(2b^2\dot{a}\dot{R}\\ &+ 4ab\dot{b}\dot{R})+4b\dot{a}\dot{b})],\\ \Sigma_2 &= \bar{A}_2t+\bar{A}_3-4b^2\dot{a}nf_0R^{n-1}.\end{aligned}$$

3.2 Noether Symmetries of Generalized Anisotropic Model

Here we investigate the existence of Noether symmetry in the context of a generalized anisotropic universe model which identifies BI, BIII and KS universe models under certain condition. The action incorporating gravity, matter and scalar field is given as

$$\mathcal{I}=\int d^4x\sqrt{-g}[\mathcal{L}_g+\mathcal{L}_m+\mathcal{L}_\phi]. \tag{3.2.1}$$

We specify the above Lagrangian densities as

$$\mathcal{L}_g=f(R,T),\quad \mathcal{L}_m=p_m(a,b),\quad \mathcal{L}_\phi=\frac{\bar{\epsilon}}{2}g^{\mu\nu}\partial_\mu\phi\partial_\nu\phi-V(\phi), \tag{3.2.2}$$

where $\bar{\epsilon}=1$ and -1 identify scalar field models, i.e., quintessence and phantom models, respectively. Phantom model suffers with number of troubles like violation of dominant energy condition, the entropy of phantom-dominated universe is negative and consequently, black holes disappear. Such a universe ends up with a finite time future singularity dubbed as big-rip singularity [64]. Different ideas are proposed to cure the troubles of this singularity such as considering phantom acceleration as transient phenomenon with different scalar potentials or to modify the gravity, couple DE with dark matter or to use particular forms of EoS for DE taking into account some quantum effects which may delay/stop the singularity occurrence [65]. A generalization of some anisotropic homogeneous universe models is given as [66]

$$ds^2 = -dt^2 + a^2(t)dr^2 + b^2(t)(d\theta^2 + \bar{\zeta}(\theta)d\phi^2), \tag{3.2.3}$$

where $\bar{\zeta}(\theta) = \theta,\ \sin h\theta,\ \sin\theta$ identify BI, BIII and KS models with the following relationship

$$\frac{1}{\bar{\zeta}}\frac{d^2\bar{\zeta}}{d\theta^2} = -\xi.$$

For $\xi = 0, -1, 1$, the spacetime (3.2.3) corresponds to BI, BIII and KS universe models, respectively. Inserting Eq.(3.2.2) into (3.2.1), we obtain

$$\mathcal{I} = \int d^4x\sqrt{-g}[\frac{f(R,T)}{2\kappa^2} + p_m(a,b) + \frac{\bar{\epsilon}}{2}g^{\mu\nu}\partial_\mu\phi\partial_\nu\phi - V(\phi)], \tag{3.2.4}$$

where

$$R = \frac{2}{ab^2}\left(\ddot{a}b^2 + 2ab\ddot{b} + 2b\dot{a}\dot{b} + a\dot{b}^2 + a\xi\right).$$

To evaluate Lagrangian corresponding to the action (3.2.4) for configuration space $\mathcal{Q} = \{a, b, R, T, \phi\}$ and perfect fluid distribution, we use Lagrange multiplier approach which yields

$$\begin{aligned}
\mathcal{L} &= ab^2[f(R,T) - Rf_R(R,T) + f_T(R,T)(3p_m(a,b) - \rho_m(a,b) - T) - \frac{\bar{\epsilon}\dot{\phi}^2}{2} \\
&+ p_m(a,b) - V(\phi)] - (4b\dot{a}\dot{b} + 2a\dot{b}^2 - 2a\xi)f_R(R,T) - (2b^2\dot{a}\dot{R} + 4ab\dot{b}\dot{R}) \\
&\times f_{RR}(R,T) - (2b^2\dot{a}\dot{T} + 4ab\dot{b}\dot{T})f_{RT}(R,T).
\end{aligned} \tag{3.2.5}$$

For Lagrangian (3.2.5), the conjugate momenta take the following form

$$p_a = -4b\dot{b}f_R - 2b^2(\dot{R}f_{RR} + \dot{T}f_{RT}), \quad p_\phi = -ab^2\bar{\epsilon}\dot{\phi},$$

$$\begin{aligned} p_b &= -4f_R(a\dot{b}+b\dot{a})-4ab(\dot{R}f_{RR}+\dot{T}f_{RT}),\\ p_R &= -(4ab\dot{b}+2b^2\dot{a})f_{RR},\quad p_T=-(4ab\dot{b}+2b^2\dot{a})f_{RT}. \end{aligned}$$

The dynamical equations of the system are

$$\begin{aligned} &2f_R(R,T)\left(\frac{\dot{b}^2}{b^2}+\frac{2\ddot{b}}{b}+\frac{2\xi}{b^2}\right)+f-Rf_R+f_T(3p_m(a,b)-\rho_m(a,b)-T)\\ +&\ p_m(a,b)-\frac{\bar{\epsilon}\dot{\phi}^2}{2}-V(\phi)+a\{f_T(3p_{m},_a-\rho_{m},_a)+p_{m},_a\}+4b^{-1}\dot{b}\dot{R}f_{RR}\\ +&\ 4b^{-1}\dot{b}\dot{T}f_{RT}+2\ddot{R}f_{RR}+2\dot{R}^2f_{RRR}+4\dot{R}\dot{T}f_{RRT}+2\ddot{T}f_{RT}+2\dot{T}^2f_{RTT}=0, \end{aligned} \tag{3.2.6}$$

$$\begin{aligned} &2f_R\left(\frac{\ddot{a}}{a}+\frac{\dot{a}\dot{b}}{ab}+\frac{\ddot{b}}{b}\right)+f-Rf_R+f_T(3p_m(a,b)-\rho_m(a,b)-T)+p_m(a,b)\\ -&\ \frac{\bar{\epsilon}\dot{\phi}^2}{2}-V(\phi)+\frac{b}{2}\{f_T(3p_{m},_b-\rho_{m},_b))+p_{m},_b\}+2(a^{-1}\dot{a}\dot{R}+\ddot{R})f_{RR}+2\dot{R}^2\\ \times&\ f_{RRR}+2(a^{-1}\dot{a}\dot{T}+\ddot{T})f_{RT}+2(b^{-1}\dot{b}\dot{R}+2\dot{R}\dot{T}+\dot{T}^2)f_{RRT}+2b^{-1}\dot{b}\dot{T}f_{RTT}=0, \end{aligned} \tag{3.2.7}$$

$$\begin{aligned} &f_{RT}(3p_m(a,b)-\rho_m(a,b)-T)=0,\quad f_{TT}(3p_m(a,b)-\rho_m(a,b)-T)=0,\\ &\bar{\epsilon}\ddot{\phi}+2\bar{\epsilon}b^{-1}\dot{b}\dot{\phi}+\bar{\epsilon}a^{-1}\dot{a}\dot{\phi}-V,_\phi=0. \end{aligned} \tag{3.2.8}$$

We formulate Hamiltonian as

$$\begin{aligned} \mathcal{H} &= 2f_R\left(\frac{\dot{b}^2}{b^2}+\frac{2\dot{a}\dot{b}}{ab}\right)+2\left(\frac{2\dot{b}}{b}+\frac{\dot{a}}{a}\right)\dot{R}f_{RR}+2\left(\frac{2\dot{b}}{b}+\frac{\dot{a}}{a}\right)\dot{T}f_{RT}+f-Rf_R\\ &+ f_T(3p_m(a,b)-\rho_m(a,b)-T)+p_m(a,b)+\frac{\bar{\epsilon}\dot{\phi}^2}{2}-V(\phi)+\frac{2\xi f_R}{b^2}. \end{aligned} \tag{3.2.9}$$

The infinitesimal symmetry generator and corresponding first order prolongation yield

$$\begin{aligned} K &= \tau\frac{\partial}{\partial t}+\alpha\frac{\partial}{\partial a}+\beta\frac{\partial}{\partial b}+\gamma\frac{\partial}{\partial R}+\delta\frac{\partial}{\partial T}+\eta\frac{\partial}{\partial \phi},\quad K^{[1]}=\tau\frac{\partial}{\partial t}+\alpha\frac{\partial}{\partial a}+\beta\frac{\partial}{\partial b}\\ &+ \gamma\frac{\partial}{\partial R}+\delta\frac{\partial}{\partial T}+\eta\frac{\partial}{\partial \phi}+\dot{\alpha}\frac{\partial}{\partial \dot{a}}+\dot{\beta}\frac{\partial}{\partial \dot{b}}+\dot{\gamma}\frac{\partial}{\partial \dot{R}}+\dot{\delta}\frac{\partial}{\partial \dot{T}}+\dot{\eta}\frac{\partial}{\partial \dot{\phi}}, \end{aligned} \tag{3.2.10}$$

where time derivative of unknown coefficients $\tau,\ \alpha,\ \beta,\ \gamma,\ \delta$ and η are

$$\dot{\sigma}_{_l} \;=\; D\sigma_{_l} - \dot{q}^i D\tau, \quad l = 1...5, \tag{3.2.11}$$

Here $\sigma_1,\ \sigma_2,\ \sigma_3,\ \sigma_4$ and σ_5 correspond to $\alpha,\ \beta,\ \gamma,\ \delta$ and η, respectively.

In order to discuss the presence of Noether symmetry generator and relative conserved quantity, we insert Lagrangian (3.2.5) along with (3.2.10) in (1.5.2), it follows a system of equations given in Appendix **A**. From Eq.(A41), we have either $f_R,\ f_{RR},\ f_{RT} = 0$ with $\tau,_a,\ \tau,_b,\ \tau,_R,\ \tau,_T \neq 0$ or vice versa. For non-trivial solution, we consider second possibility $(\tau,_a,\ \tau,_b,\ \tau,_R,\ \tau,_T = 0)$ as the first choice yields trivial solution. We investigate the existence of symmetry generators, relative conserved quantities for two $f(R,T)$ models appreciating direct as well as indirect curvature-matter coupling. We also formulate corresponding exact solutions to analyze cosmological picture of these two models.

3.2.1 $f(R,T) = R + 2g(T)$

To evaluate the coefficients of symmetry generator (3.2.10), we consider separation of variables method which gives

$$\begin{aligned}
\alpha &= \alpha_1(t)\alpha_2(a)\alpha_3(b)\alpha_4(R)\alpha_5(T)\alpha_6(\phi), \quad \delta = \delta_1(t)\delta_2(a)\delta_3(b)\delta_4(R)\delta_5(T)\delta_6(\phi),\\
\gamma &= \gamma_1(t)\gamma_2(a)\gamma_3(b)\gamma_4(R)\gamma_5(T)\gamma_6(\phi), \quad \eta = \eta_1(t)\eta_2(a)\eta_3(b)\eta_4(R)\eta_5(T)\eta_6(\phi),\\
\beta &= \beta_1(t)\beta_2(a)\beta_3(b)\beta_4(R)\beta_5(T)\beta_6(\phi), \quad \tau = \tau_1(t),\\
B &= B_1(t)B_2(a)B_3(b)B_4(R)B_5(T)B_6(\phi).
\end{aligned}$$

For these coefficients, we solve the system (A35)-(A56) yielding

$$\alpha \;=\; -2ac_{_1}, \quad \beta = c_{_1}b, \quad \gamma = 0, \quad \delta = 0, \quad \eta = c_{_4},$$

$$
\begin{aligned}
B &= c_2 t + c_3, \quad \tau = c_5, \quad V(\phi) = c_6\phi + c_7, \\
p_m(a,b) &= -\frac{c_4 c_6 \ln a + 2c_1 a^{\frac{1}{2}} b}{2c_1} - \frac{2\xi}{b^2} - \frac{c_2 \ln a}{2c_1 ab^2}, \qquad (3.2.12) \\
\rho_m(a,b) &= -\frac{3c_4 c_6 \ln a + 2c_1 a^{\frac{1}{2}} b}{2c_1} - \frac{6\xi}{b^2} - \frac{3c_2 \ln a}{2c_1 ab^2}, \qquad (3.2.13)
\end{aligned}
$$

where $c_{\hat{i}}$ ($\hat{i} = 1...7$) denotes arbitrary constants. For these coefficients, we split the symmetry generator and corresponding first integral into the following form

$$
\begin{aligned}
K_1 &= \frac{\partial}{\partial t}, \quad \Sigma_1 = -ab^2\{f - Rf_R + f_T(3p_m - \rho_m - T) + p_m - c_6\phi - c_7\} \\
&+ 2a\xi f_R - 4b\dot{a}\dot{b}f_R - 2a\dot{b}^2 f_R - \frac{\bar{\epsilon}\dot{\phi}^2 ab^2}{2}, \\
K_2 &= -2a\frac{\partial}{\partial a} + b\frac{\partial}{\partial b}, \quad \Sigma_2 = -4ab\dot{b}f_R + 4b^2\dot{a}f_R, \\
K_3 &= \frac{\partial}{\partial \phi}, \quad \Sigma_3 = \bar{\epsilon}ab^2\dot{\phi}.
\end{aligned}
$$

For the considered model, the system (A35)-(A56) yields three symmetry generators and associated conserved quantities. The symmetry generator K_1 leads to energy conservation while K_2 represents scaling symmetry corresponding to conservation of linear momentum.

Next, we explore the presence of Noether symmetry in the absence of first order prolongation and boundary term of extended symmetry which leads to establish corresponding conservation law. In this case, the infinitesimal generator of continuous group for $\mathcal{Q} = \{a, b, R, T, \phi\}$ turns out to be

$$
K = \alpha\frac{\partial}{\partial a} + \beta\frac{\partial}{\partial b} + \gamma\frac{\partial}{\partial R} + \delta\frac{\partial}{\partial T} + \eta\frac{\partial}{\partial \phi} + \dot{\alpha}\frac{\partial}{\partial \dot{a}} + \dot{\beta}\frac{\partial}{\partial \dot{b}} + \dot{\gamma}\frac{\partial}{\partial \dot{R}} + \dot{\delta}\frac{\partial}{\partial \dot{T}} + \dot{\eta}\frac{\partial}{\partial \dot{\phi}}, \quad (3.2.14)
$$

where $\dot{\alpha} = \dot{q}^i\frac{\partial \alpha}{\partial q^i}$, $\dot{\beta} = \dot{q}^i\frac{\partial \beta}{\partial q^i}$, $\dot{\gamma} = \dot{q}^i\frac{\partial \gamma}{\partial q^i}$, $\dot{\delta} = \dot{q}^i\frac{\partial \delta}{\partial q^i}$ and $\dot{\eta} = \dot{q}^i\frac{\partial \eta}{\partial q^i}$. Due to the absence of affine parameter, the separation of variables method yields

$$
\alpha = \alpha_1(a)\alpha_2(b)\alpha_3(R)\alpha_4(T)\alpha_5(\phi), \quad \beta = \beta_1(a)\beta_2(b)\beta_3(R)\beta_4(T)\beta_5(\phi),
$$

$$\begin{aligned}\gamma &= \gamma_1(a)\gamma_2(b)\gamma_3(R)\gamma_5(\phi), \quad \delta = \delta_1(a)\delta_2(b)\delta_3(R)\delta_4(T)\delta_5(\phi),\\ \eta &= \eta_1(a)\eta_2(b)\eta_3(R)\eta_4(T)\eta_5(\phi).\end{aligned}$$

In order to explore the consequences of indirect non-minimal curvature-matter coupling, we evaluate symmetry generators with corresponding conservation laws for non-existing boundary term. We also establish cosmological analysis through exact solutions for both dust and perfect fluid distributions.

Dust Case

We consider $T^{(m)}_{\mu\nu} = \rho_m u_\mu u_\nu$ and solve the system for (3.2.14) via separation of variables which yields

$$\begin{aligned}\alpha &= -2a\hat{c}_1, \quad \beta = \hat{c}_1 b, \quad \gamma = 0, \quad \delta = 0, \quad \eta = 0,\\ \rho_m(a,b) &= \frac{\xi}{b^2\hat{c}_2} + a^{\frac{1}{2}}b, \quad \Lambda(T) = -\frac{g(T)}{2} + \hat{c}_2 T + \hat{c}_3,\end{aligned}$$

where $\hat{c}_1$, $\hat{c}_2$ and $\hat{c}_3$ represent arbitrary constants. The corresponding symmetry generator and associated conserved quantity are

$$K = -2a\hat{c}_1\frac{\partial}{\partial a} + \hat{c}_1 b\frac{\partial}{\partial b}, \quad \Sigma = 4\hat{c}_1 ab\dot{b}f_R - 4\hat{c}_1 b^2\dot{a}f_R.$$

For dust fluid, there exists only scaling symmetry in the absence of affine parameter as well as boundary term of extended symmetry and the considered model reduces to

$$f(R,T) = R + 2\hat{c}_2 T + 2\hat{c}_3. \tag{3.2.15}$$

For exact solution of equations of motion, we insert density of dust fluid and model (3.2.15) in Eqs.(3.2.6) and (3.2.7) yielding

$$a(t) = \frac{(40\hat{c}_2 t + 40\hat{c}_3)^{\frac{4}{5}}}{16}, \quad b(t) = \frac{\hat{c}_1(40\hat{c}_2 t + 40\hat{c}_3)^{\frac{2}{5}}}{4}.$$

To analyze the behavior of this power-law type exact solution, we construct cosmological analysis through some standard parameters such as Hubble, deceleration, $r-s$ and EoS. For generalized anisotropic universe model, the Hubble and deceleration parameters turn out to be

$$H=\frac{64\hat{c}_2(40\hat{c}_2t+40\hat{c}_3)^{-1}}{3},\quad q=\frac{7}{8}.$$

In the present case, we obtain $r=0$ with $s=-\frac{8}{9}$ indicating that the constructed model does not correspond to any standard cosmological model. The corresponding effective EoS parameter is

$$\omega_{eff}=\frac{128\hat{c}_2+(40\hat{c}_2t+40\hat{c}_3)^{\frac{4}{5}}(5\hat{c}_2^2\hat{c}_1t^2+10\hat{c}_1\hat{c}_2\hat{c}_3t+5\hat{c}_1\hat{c}_3^2)}{128\hat{c}_2}$$

The potential and kinetic energies of the scalar field play a dynamical role to study cosmic expansion. For accelerated expansion, the field ϕ evolves negatively and potential dominates over the kinetic energy ($\frac{\dot{\phi}^2}{2}<V(\phi)$) whereas negative potential follows the kinetic energy for decelerated expansion of the universe ($\frac{\dot{\phi}^2}{2}>-V(\phi)$) [67]. Using Eq.(3.2.8), we obtain

$$\begin{aligned}
\phi &= \int\frac{1}{20\bar{\epsilon}(\hat{c}_2t+\hat{c}_3)}\left(\left(-\bar{\epsilon}\hat{c}_2\left(25\hat{c}_2^2(40\hat{c}_2t+40\hat{c}_3)^{\frac{4}{5}}\hat{c}_1t^2+50(40\hat{c}_2t+40\hat{c}_3)^{\frac{4}{5}}\right.\right.\right.\\
&\times\left.\left.\left.\hat{c}_2\hat{c}_1\hat{c}_3t+25(40\hat{c}_2t+40\hat{c}_3)^{\frac{4}{5}}\hat{c}_1\hat{c}_3^2+896\hat{c}_2\right)\right)^{\frac{1}{2}}\right),\\
V(\phi) &= \frac{1}{800\left(\hat{c}_2^2t^2+2\hat{c}_2\hat{c}_3t+\hat{c}_3^2\right)}\left[25\hat{c}_1\left(5\hat{c}_2^3t^2+5\hat{c}_2\hat{c}_3^2+10\hat{c}_2^2\hat{c}_3t\right)(40\hat{c}_2t\right.\\
&+\left.40\hat{c}_3)^{\frac{4}{5}}+8\hat{c}_2\hat{c}_3\left(-200\hat{c}_2t^2+400\hat{c}_3t\right)-8\left(48\hat{c}_2^2+200\hat{c}_3^3\right)\right].
\end{aligned}$$

Figure **3.4** shows graphical analysis of scale factors for the dust case. The scale factor $a(t)$ indicates large cosmic expansion in x-direction but $b(t)$ represents that

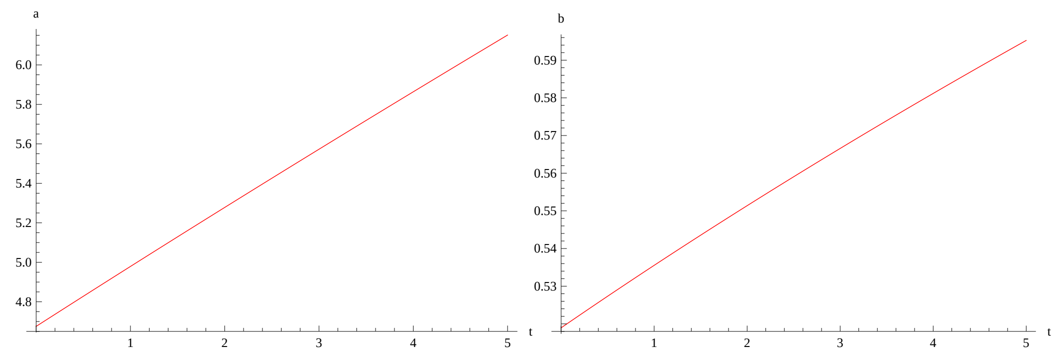

Figure 3.4: Plots of scale factors $a(t)$ (left) and $b(t)$ (right) versus cosmic time t for $\hat{c}_1 = 0.24$, $\hat{c}_2 = 0.45$ and $\hat{c}_3 = 5.5$.

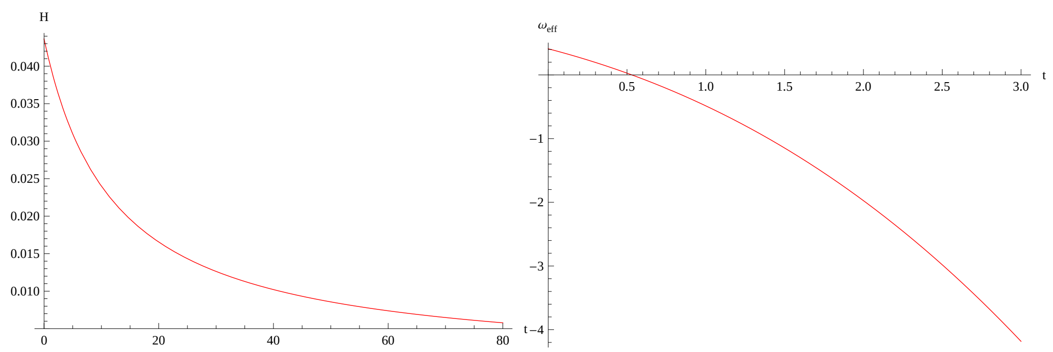

Figure 3.5: Plots of Hubble $H(t)$ (left) and EoS parameters ω_{eff} (right) versus cosmic time t.

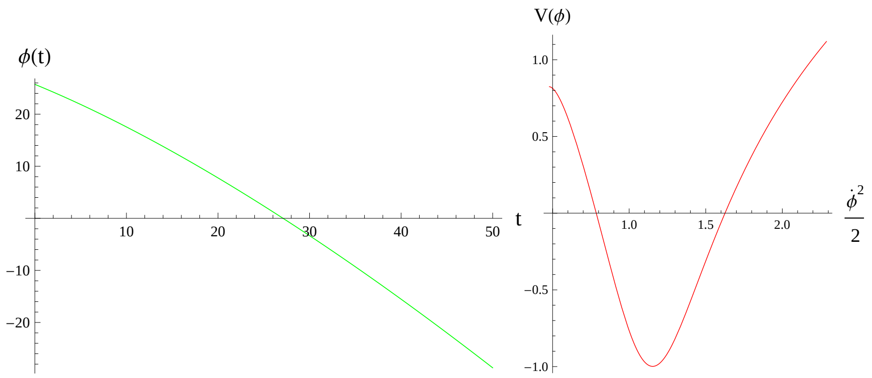

Figure 3.6: Plots of scalar field $\phi(t)$ (left) versus cosmic time t and potential energy $V(\phi)$ versus kinetic energy $\frac{\dot{\phi}^2}{2}$ (right) for $\bar{\epsilon}=-1$.

the universe is expanding very slowly in y and z-directions. Figure **3.5** (left plot) indicates that Hubble parameter is decreasing with the passage of time. In the right plot of Figure **3.5**, the effective EoS parameter identifies that initially, the universe appreciates radiation dominated era and after sometime, it corresponds to DE era by crossing matter dominated phase.

Figures **3.6** and **3.7** analyze the behavior of scalar field and cosmic expansion via phantom and quintessence models. The left plot of Figure **3.6** shows that the scalar field is positive initially yielding decelerated expansion but gradually, it starts increasing negatively which describes accelerated expansion. In case of quintessence model, the scalar field grows from negative to positive indicating decelerated expansion of the universe. The right plots of **3.6** and **3.7** satisfy $\frac{\dot{\phi}^2}{2}<V(\phi)$ and $\frac{\dot{\phi}^2}{2}>-V(\phi)$ implying that phantom model yields accelerated expansion while quintessence model corresponds to decelerated expansion.

To analyze a big-rip free model, the key point is that if EoS parameter rapidly approaches to -1 and Hubble rate tends to be constant (asymptotically de Sitter universe), then it is possible to have a model in which time required for singularity

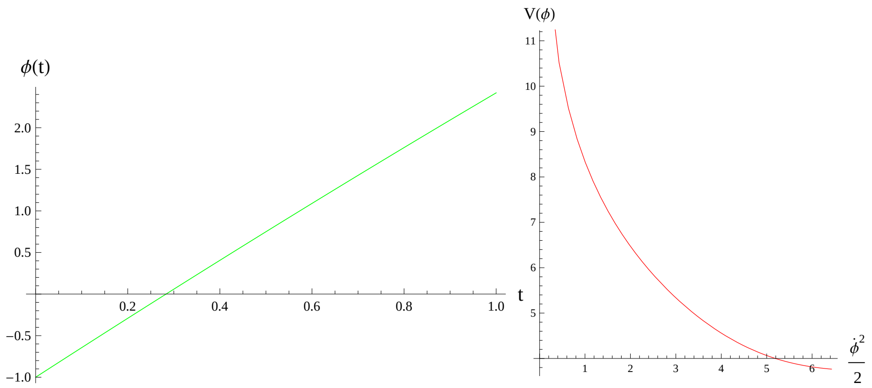

Figure 3.7: Plots of scalar field $\phi(t)$ (left) versus cosmic time t and potential energy $V(\phi)$ versus kinetic energy $\frac{\dot{\phi}^2}{2}$ (right) for $\bar{\epsilon} = 1$.

is infinite, i.e., the singularity effectively does not occur [68]. The occurrence of maximum potential of a phantom scalar field is another fact to avoid this singularity. The graphical behavior of EoS parameter represents that ω_{eff} rapidly approaches to -1 and Hubble rate is decreasing but potential is not maximum. We may avoid the big-rip singularity in the present case if we choose $\hat{c}_2$ to be negatively large that yields asymptotic behavior of Hubble rate.

Non-Dust Case

In the absence of boundary term and affine parameter, the coefficients of symmetry generator (3.2.14) corresponding to a, b, R, T, ϕ remain the same as in the presence of boundary term of extended symmetry. Thus, generator of Noether symmetry and associated first integrals reduce to

$$\begin{aligned} K &= -2ac_1\frac{\partial}{\partial a} + c_1 b\frac{\partial}{\partial b} + c_2\frac{\partial}{\partial \phi}, \\ \Sigma &= -4c_1 ab\dot{b}f_R + 4c_1 b^2\dot{a}f_R + \bar{\epsilon}c_2 ab^2\dot{\phi}. \end{aligned}$$

In order to formulate exact solution of dynamical equations for perfect fluid distribution, we insert Eqs.(3.2.12) and (3.2.13) into (3.2.6) and (3.2.7) yielding

$$\begin{aligned} a(t) &= \frac{\left(\frac{5}{c_9}\right)^{\frac{2}{5}}(c_2\sin(c_{10}t)+c_3\cos(c_{10}t))^{\frac{4}{5}}}{5^{\frac{4}{5}}}, \\ b(t) &= \frac{c_4\left(\frac{5}{c_9}\right)^{\frac{1}{5}}(c_2\sin(c_{10}t)+c_3\cos(c_{10}t))^{\frac{2}{5}}}{5^{\frac{2}{5}}}. \end{aligned}$$

This describes oscillatory solution of $f(R,T)$ model admitting indirect non-minimal curvature-matter coupling. To study the cosmological behavior of this solution, we consider cosmological parameters as follows

$$\begin{aligned} H &= \frac{8c_{10}(c_2\sin(c_{10}t)+c_3\cos(c_{10}t))}{15(c_2\sin(c_{10}t)+c_3\cos(c_{10}t))}, \\ q &= \frac{-8c_2^2\cos^2(c_{10}t)+7c_3^3+8c_3^2\cos^2(c_{10}t)+15c_2^2+16c_2c_3\cos(c_{10}t)\sin(c_{10}t)}{8(c_2\sin(c_{10}t)+c_3\cos(c_{10}t))^2}, \\ r &= \frac{-77c_3^2+32c_3^2\cos^2(c_{10}t)-45c_2^2-32c_2^2\cos^2(c_{10}t)+64c_2\cos(c_{10}t)c_3\sin(c_{10}t)}{32(-c_2^2\cos^2(c_{10}t)+2c_2\cos(c_{10}t)c_3\sin(c_{10}t)-c_3^2+c_3^2\cos^2(c_{10}t))}, \\ s &= (-45((4c_2^4-4c_3^4)\cos^2(c_{10}t)-c_3^4-6c_2^2c_3-5c_2^4-(8c_2^3c_3+8c_2c_3^3) \\ &\times \cos(c_{10}t)\sin(c_{10}t)))/256((c_2^4+c_3^4-6c_2^2c_3^2)\cos^4(c_{10}t)+(6c_2^2c_3^2-2c_3^4) \\ &\times \cos^2(c_{10}t)+(-4c_2^3c_3+4c_2c_3^3)\sin(c_{10}t)\cos^3(c_{10}t)-4c_2c_3^3\cos(c_{10}t) \\ &\times \sin(c_{10}t)+c_3^4), \\ \omega_{eff} &= \frac{\chi(3p_m-\rho_m)+p_m-\frac{\bar{\epsilon}\dot{\phi}^2}{2}-V(\phi)+\frac{2\xi}{b^2}+a(3p_{m},_a-\rho_{m},_a)+p_{m},_a}{\chi(3p_m-\rho_m)+p_m+\frac{\bar{\epsilon}\dot{\phi}^2}{2}-V(\phi)+\frac{2\xi}{b^2}}. \end{aligned}$$

The scalar field as well as corresponding kinetic and potential energies identify the early as well as current cosmic expansion and also characterize decelerated expansion of the universe when kinetic energy dominates negative potential. In this case, Eq.(3.2.8) yields

$$\phi=\int\frac{\bar{\epsilon}c_4-\frac{5c_6c_2^2\cos(2c_{10}t)\ -2\,{}_2F_1\left[\frac{3}{10},\frac{1}{2},\frac{13}{10},\sin\left[\frac{\pi}{4}+c_{10}t\right]^2\right]+\sqrt{2-2\sin[2c_{10}t]}}{16c_{10}\sqrt{\cos\left[\frac{\pi}{4}+c_{10}t\right]^2}(c_2(\cos[c_{10}t]+\sin[c_{10}t]))^{2/5}}dt}{\bar{\epsilon}(c_2\cos[c_{10}t]+c_2\sin[c_{10}t])^{8/5}},$$

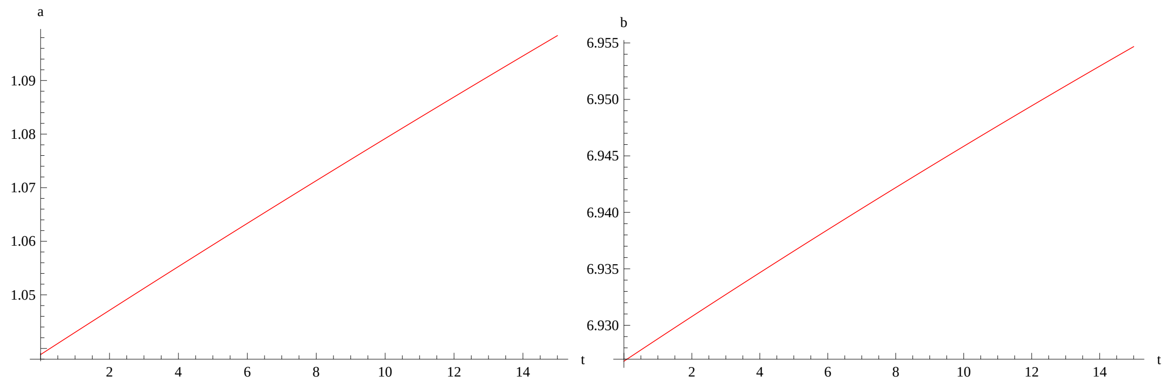

Figure 3.8: Plots of scale factor $a(t)$ (left) and $b(t)$ (right) versus cosmic time t for $c_2 = c_3 = c_9 = 5.5$ and $c_{10} = 0.005$.

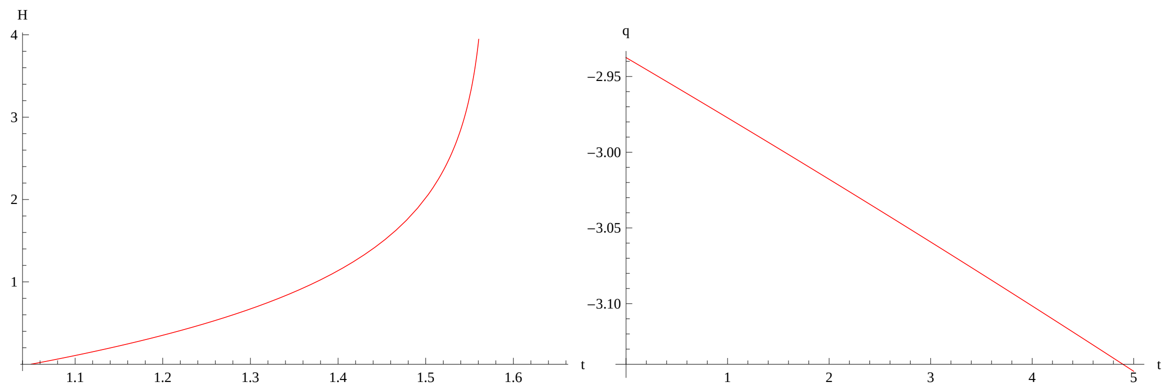

Figure 3.9: Plots of $H(t)$ (left) and $q(t)$ (right) versus cosmic time t.

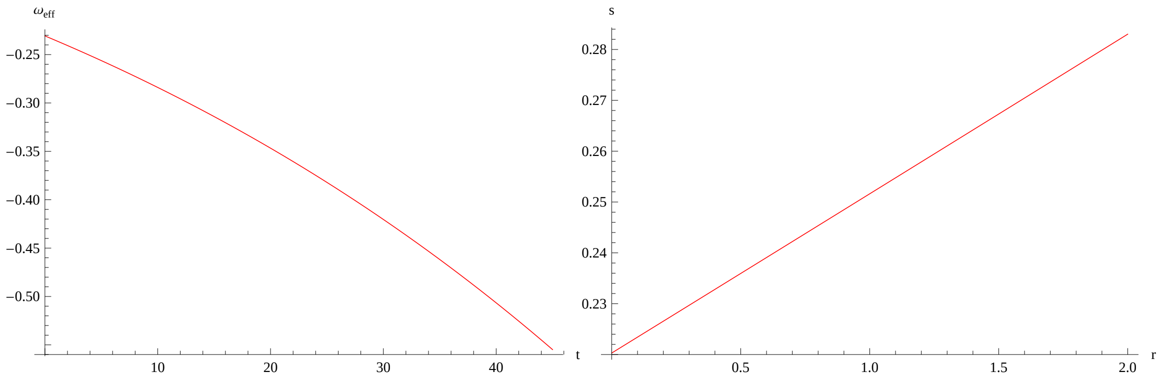

Figure 3.10: Plot of ω_{eff} and $r-s$ parameters versus cosmic time t for $c_2 = c_3 = 5.5$ and $c_{10} = 0.005$.

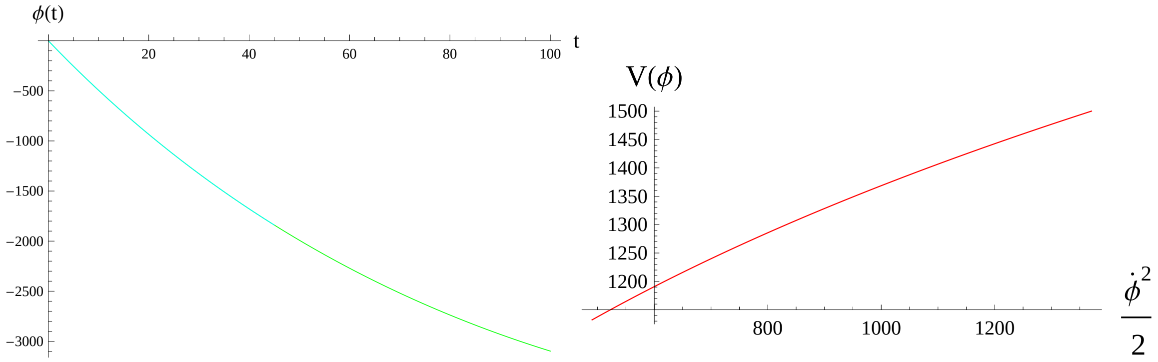

Figure 3.11: Plots of scalar field $\phi(t)$ (left) versus cosmic time t and potential energy $V(\phi)$ versus kinetic energy $\frac{\dot{\phi}^2}{2}$ (right) for $c_2 = 5.5$, $c_4 = -10^3$, $c_6 = 0.5$ and $c_{10} = 0.005$.

where ${}_2F_1$ represents hypergeometric function.

In Figure **3.8**, the right plot shows that the universe experiences immense amount of expansion in y and z-directions whereas the left plot yields comparatively a small amount of expansion in x-direction. Figure **3.9** provides information about increasing rate of expansion through Hubble parameter while negatively increasing deceleration parameter assures accelerated cosmic expansion. The left plot of Figure **3.10** characterizes quintessence phase of DE era while the right plot identifies the $r-s$ parameters trajectories in quintessence and phantom phases as $s > 0$ when $r < 1$. Both plots of Figure **3.11** verify the current cosmic expansion for quintessence as well as phantom models as ϕ continuously increasing negatively and potential energy of the field is dominating over kinetic energy. The graphical interpretation of EoS parameter yields $\omega_{eff} < -1$ which is not a sufficient condition for the existence of singularity as potential turns out to be maximum with the passage of time. Thus, we may avoid big-rip singularity if Hubble rate decreases asymptotically in the presence of minimal coupling of $f(R,T)$ gravity with scalar field.

3.2.2 $f(R,T)=f_1(R)+f_2(R)g(T)$

To analyze the effect of direct non-minimal curvature-matter coupling, we consider this model and evaluate symmetry generators as well as associated conservation laws. Inserting the model in Eqs.(A36)-(A38), (A44), (A45) and (A49) and using separation of variables approach, we obtain

$$\begin{aligned}
\beta &= -\frac{b\alpha}{2a}+\phi Y_1(t,a,b)+Y_2(t,a,b),\\
f_1(R) &= \frac{\bar{\epsilon}}{4d_3}\left(-d_3Y_{12}(R)+d_2Y_9(R)\right)+d_5R+d_6,\\
f_2(R) &= -\frac{\bar{\epsilon}}{4d_3}\left(-d_3Y_9(R),_R+d_1R\right)+d_4,\quad g(T)=d_2+d_3Y_{10}(T),\\
\eta &= \frac{1}{b}\left[Y_1(t,a,b)(Y_{10}(T)(d_1+Y_9(R),_R)-\phi^2+Y_{12}(R),_R)+b\phi\tau,_t-2\phi\right.\\
&\times \left. Y_2(t,a,b)+bY_{14}(t,a,b)\right],
\end{aligned}$$

where d_i denote arbitrary constants. We substitute these values in Eqs.(A35), (A42) and (A43) which yield

$$\begin{aligned}
\tau &= \int -\frac{Y_{23}(t)}{\bar{\epsilon}}dt+d_8t+d_9,\quad B=\frac{1}{6d_4}\left[6ab(Y_{19}(T)d_1+d_4\bar{\epsilon}\phi^2\right.\\
&+ Y_{19}(T)d_4e^{-R})Y_2(t,a,b),_t+6ab\phi(\frac{1}{3}d_4\bar{\epsilon}\phi^2+Y_{19}(T)d_4e^{-R}+Y_{19}(T)
\end{aligned}$$

$$
\begin{aligned}
&\times \quad d_1)Y_{16}(t,b)_{,t} + 3d_4(2Y_{22}(t,a,b) + 2\phi Y_{21}(t,a,b)_{,t} + ab^2\phi^2 Y_{23}(t)_{,t})\big],\\
Y_1(t,a,b) &= Y_{16}(t,b) + Y_{15}(a,b) \quad Y_{10}(T) = -\frac{Y_{19}(T)d_3 + \bar{\epsilon}d_2 d_4}{\bar{\epsilon}d_3 d_4},\\
Y_{12}(R) &= -\frac{d_2 d_4 e^{-R}}{d_3} + d_6 R + d_7, \quad Y_9(R) = -e^{-R}d_4 - 2d_1 R + d_2,\\
Y_{14}(t,a,b) &= -\frac{Y_{21}(t,a,b)}{b^2 a\bar{\epsilon}} - \frac{bad_2\bar{\epsilon}d_1 Y_{16}(t,b) + d_6\bar{\epsilon}bad_3 Y_{16}(t,b)}{\bar{\epsilon}b^2 a d_3} + Y_{24}(b,a).
\end{aligned}
$$

To evaluate remaining unknown functions, we insert the above functions into $\beta,\ \eta,\ f_1,\ g,\ f_2$ and solve Eqs.(A39)-(A41) with (A46)-(A48) and (A50)-(A55) leading to

$$
\begin{aligned}
Y_{21}(t,a,b) &= Y_{26}(a,b), \quad Y_{22}(t,a,b) = d_{10}t, \quad Y_{16}(t,b) = -d_{12}b,\\
Y_{15}(a,b) &= d_{12}b, \quad Y_{24}(b,a) = 0, \quad Y_2(t,a,b) = d_9 b,\\
Y_{23}(t) &= \bar{\epsilon}(-2d_9 + e^{-R}d_4 d_3 d_{11}e^R + d_8), \quad \delta = 0, \quad \gamma = \frac{d_{11}e^R T}{d_1 3}\\
&\times \quad (e^{-R}d_4 T d_{13}d_3 - d_1 d_{13}d_3 T + (2((-2d_5 + \frac{1}{2}\bar{\epsilon}d_6)d_3 + d_1 d_2\bar{\epsilon}))d_4).
\end{aligned}
$$

Using these solutions in Eq.(A56) with d_{11}=0 and $d_6 = \frac{d_2 d_1}{d_3}$, it follows that

$$
\begin{aligned}
\tau &= 3d_9, \quad \alpha = d_{10}a, \quad \beta = b(d_9 - \frac{d_{10}}{2}), \quad \delta = 0, \quad \gamma = 0,\\
B &= d_{10}t, \quad \eta = -\frac{d_1}{\epsilon} + 2d_{12}d_6, \quad f_1(R) = d_6 + d_5 R - \frac{3d_6\bar{\epsilon}R}{4},\\
f_2(R) &= d_4 - \frac{\bar{\epsilon}}{4d_3}(d_4 e^{-R} + d_1 R - 2d_1), \quad g(T) = d_2 - \frac{d_2 d_4\bar{\epsilon} - d_3 d_{13}T}{d_4\bar{\epsilon}}.
\end{aligned}
$$

Inserting $f_1,\ f_2$ and g, the $f(R,T)$ model becomes

$$
f(R,T) = -\frac{3\bar{\epsilon}d_6 R}{4} + d_5 R + d_6 + (d_4 - \frac{\bar{\epsilon}}{4d_3}(d_4 e^{-R} + d_1 R - 2d_1))(\frac{d_3 d_{13}T}{d_4\bar{\epsilon}}).
$$

Thus, the constructed model also experiences a direct coupling between curvature and matter parts. The symmetry generators and associated conserved quantities are

$$
K_1 = 3\frac{\partial}{\partial t} + b\frac{\partial}{\partial b}, \quad \Sigma_1 = \frac{1}{4d_3\bar{\epsilon}}(-4ab^2\bar{\epsilon}^2 d_3\dot{\phi}^2 + 4d_{10}d_3\bar{\epsilon}t + 3tab^2 d_1 RT d_3\bar{\epsilon}
$$

$$
\begin{aligned}
&- && 9tab^2d_1Rp_md_3\bar{\epsilon}+3tab^2d_1R\rho_md_3\bar{\epsilon}-12td_1T\dot{a}\dot{b}bd_3\bar{\epsilon}-4b^2d_4T\\
&\times && \dot{a}e^{-R}d_3\bar{\epsilon}-4b^2a\dot{T}d_4e^{-R}d_3\bar{\epsilon}-9tab^2d_4p_me^{-R}d_3\bar{\epsilon}+3tab^2d_4\rho_m\\
&\times && e^{-R}d_3\bar{\epsilon}+6td_4Ta\dot{b}^2e^{-R}d_3\bar{\epsilon}+6td_4Taqe^{-R}d_3\bar{\epsilon}-4bd_4Ta\dot{b}e^{-R}d_3\bar{\epsilon}\\
&+ && 4b^2a\dot{R}d_4Te^{-R}d_3\bar{\epsilon}+4b^2a\dot{T}d_1d_3\bar{\epsilon}-12tab^2d_2d_1\bar{\epsilon}-12tab^2p_m\\
&\times && d_3\bar{\epsilon}+12tab^2V(\phi)d_3\bar{\epsilon}-24td_5a\dot{b}d_3\bar{\epsilon}-24td_5aqd_3\bar{\epsilon}+16bd_5a\dot{b}\\
&\times && d_3\bar{\epsilon}+36tab^2d_3^2d_4p_m-12tab^2d_3^2d_4\rho_m+18t\bar{\epsilon}^2d_2d_1a\dot{b}^2+18t\bar{\epsilon}^2\\
&\times && d_2d_1aq-12b\bar{\epsilon}^2d_2d_1a\dot{b}+4b^2d_1T\dot{a}d_3\bar{\epsilon}-12b^2\bar{\epsilon}^2d_2d_1\dot{a}+16b^2d_5\\
&\times && \dot{a}d_3\bar{\epsilon}-3tab^2Rd_4Te^{-R}d_3\bar{\epsilon}+12td_4T\dot{a}\dot{b}be^{-R}d_3\bar{\epsilon}+36t\bar{\epsilon}^2d_2d_1\dot{a}\dot{b}b\\
&+ && 4bd_1Ta\dot{b}d_3\bar{\epsilon}+6tab^2e\dot{\phi}^2d_3\bar{\epsilon}+18tab^2d_1p_md_3\bar{\epsilon}-6tab^2d_1\rho_md_3\bar{\epsilon}\\
&- && 48td_5\dot{a}\dot{b}bd_3\bar{\epsilon}-6td_1Ta\dot{b}^2d_3\bar{\epsilon}-6td_1Taqd_3\bar{\epsilon}),\\
K_2 &= && a\frac{\partial}{\partial a}-\frac{b}{2}\frac{\partial}{\partial b},\quad \Sigma_2=-\frac{b}{2d_3}(-a\dot{b}d_1Td_3+3a\dot{b}\bar{\epsilon}d_2d_1+a\dot{b}d_4Te^{-R}d_3\\
&- && 4a\dot{b}d_5d_3+bd_1T\dot{a}d_3+4bd_5\dot{a}d_3-3b\bar{\epsilon}d_2d_1\dot{a}-bd_4T\dot{a}e^{-R}d_3),\\
K_3 &= && -\frac{1}{\bar{\epsilon}}\frac{\partial}{\partial\phi},\quad \Sigma_3=ab^2\dot{\phi},\quad K_4=2d_{12}\frac{\partial}{\partial\phi},\quad \Sigma_4=2d_{12}ab^2\bar{\epsilon}\dot{\phi}.
\end{aligned}
$$

We see that scaling symmetry appears through generator K_2 with the first integral Σ_2 leading to conserved linear momentum.

Now we investigate the existence of Noether symmetry in the absence of affine parameter and boundary term of the extended symmetry and also study the effect of direct curvature-matter coupling on conservation laws. For this purpose, we solve Eqs.(A39), (A40), (A43) and (A46)-(A55) which give

$$
\begin{aligned}
\delta &= && -\frac{a}{2Y_9(T),_T}(\frac{1}{3}Y_4(a,b),_a\phi^3+2Y_4(a,b),_aY_9(T)\phi+2Y_4(a,b),_aY_8(b)\phi\\
&+ && \phi^2Y_5(a,b),_a+2Y_7(a,b),_a\phi)+Y_{12}(a,R,T,b),\quad f_1(R)=k_4R+k_5,\\
\beta &= && -\frac{b}{2a}(Y_{10}(a,R,T,b)+aY_5(a,b)),\quad g(T)=k_1+Y_9(T)k_2
\end{aligned}
$$

$$
\begin{aligned}
\eta &= \frac{1}{2}(\phi^2 + 2Y_9(T) + 2Y_8(b))Y_4(a,b) + Y_5(a,b)\phi + Y_7(b,a), \\
f_2(R) &= \frac{\bar{\epsilon}R}{2(k_2+k_3)}, \quad \gamma = Y_{11}(a,b,R,T), \\
\alpha &= -Y_4(a,b)a\phi + Y_{10}(a,b,R,T),
\end{aligned}
$$

where k_l are arbitrary constants. Inserting these solutions into the remaining equations of the system, we obtain

$$
\begin{aligned}
V(\phi) &= k_{10}\phi + k_{11}, \quad Y_{10}(a,R,T,b) = k_8 a, \quad Y_4(a,b) = 0, \\
Y_{12}(a,R,T,b) &= -\frac{k_8}{2k_2}((\bar{\epsilon}(k_6T + k_7) + 2k_4)k_2 + \bar{\epsilon}k_1), \quad Y_5(a,b) = -\frac{k_6k_8\bar{\epsilon}}{2}, \\
Y_7(b,a) &= k_9, \quad Y_9(T) = k_6T + k_7, \\
p_m &= \frac{2k_9k_{10}}{\bar{\epsilon}k_8k_6} - k_5 + k_{11} + \frac{2k_2k_4k_3}{\epsilon} + a^{-\frac{k_6\bar{\epsilon}}{2}}\bar{\epsilon}k_6ba^{\frac{1}{2}-\frac{\bar{\epsilon}k_6}{4}}, \\
\rho_m &= \frac{k_7}{k_6} + \frac{6k_2k_4k_3}{\bar{\epsilon}} - 3k_5 + 3k_{11} + \frac{2k_4}{k_6\bar{\epsilon}} + \frac{6k_9k_{10}}{k_8k_6\bar{\epsilon}} + \frac{k_1}{k_2k_6} \\
&+ a^{-\frac{k_6\bar{\epsilon}}{2}}\bar{\epsilon}k_6ba^{\frac{1}{2}-\frac{\bar{\epsilon}k_6}{4}}.
\end{aligned}
$$

The corresponding Noether symmetry generator with associated first integral take the form

$$
\begin{aligned}
K_1 &= a\frac{\partial}{\partial a} - \frac{b}{2}\left(1 - \frac{k_6\bar{\epsilon}}{2}\right)\frac{\partial}{\partial b} + R\frac{\partial}{\partial R} - (k_1\bar{\epsilon} + k_2(\bar{\epsilon}(k_6T + k_7) + 2k_4)) \\
&\times \frac{1}{2k_2}\frac{\partial}{\partial T} - \frac{k_6\bar{\epsilon}\phi}{2}\frac{\partial}{\partial \phi}, \quad \Sigma_1 = ab\dot{b}\bar{\epsilon}k_6T - \frac{b^2\bar{\epsilon}k_1\dot{a}}{k_2} - b^2\bar{\epsilon}k_6T\dot{a} - ba\bar{\epsilon}k_6k_4\dot{b} \\
&- \frac{ba\bar{\epsilon}^2k_6^2T\dot{b}}{2} - \frac{ba\bar{\epsilon}^2k_6k_7\dot{b}}{2} + \frac{ab\dot{b}\bar{\epsilon}k_1}{k_2} + ab\dot{b}\bar{\epsilon}k_7 - \frac{ba\bar{\epsilon}^2k_6k_1\dot{b}}{2k_2} - \frac{ab^2\bar{\epsilon}^2\dot{\phi}k_6\phi}{2} \\
&+ 2ab\dot{b}k_4 - 2b^2k_4\dot{a} - b^2\bar{\epsilon}k_7\dot{a} + \frac{b^2a\bar{\epsilon}^2k_6^2\dot{T}}{2}, \\
K_2 &= \frac{\partial}{\partial \phi}, \quad \Sigma_2 = ab^2\bar{\epsilon}\dot{\phi}k_9.
\end{aligned}
$$

Here the symmetry generator K_1 yields scaling symmetry.

Chapter 4

Wormhole Solutions via Noether Symmetry in $f(R)$ and $f(R,T)$ Theories

This chapter investigates WH solutions of spherically symmetric spacetime via Noether symmetry approach in $f(R)$ and $f(R,T)$ theories. We formulate symmetry generators with associated conserved quantities and WH solutions using constant and variable red-shift functions in both theories. For perfect fluid, we determine an explicit form of generic function $f(R)$ and also evaluate exact solution of $f(R)$ power-law model. In $f(R,T)$ gravity, we choose two $f(R,T)$ models appreciating indirect curvature-matter coupling and formulate solutions for both dust as well as perfect fluid. We analyze the behavior of shape function and viability of constructed models graphically. To analyze physical existence of WH solutions, we study the behavior of NEC and WEC with respect to ordinary matter and effective energy-momentum tensor.

The format of this chapter is as follows. In section **4.1**, we determine possible Noether symmetry, corresponding conserved quantity and exact solutions of static WH in the presence of minimal coupling of curvature and matter. Section **4.2** is devoted to determine Noether symmetries as well as viable WH solutions under the influence of non-minimal curvature-matter coupling. The results of this chapter have been submitted in two papers [69, 70].

4.1 Wormhole Solutions in $f(R)$ gravity

We choose $\mathcal{L}_m = p_m(\hat{a})$ and use Eqs.(1.4.2)-(1.4.4) and (1.6.1), it follows that

$$-\frac{1}{4}(2\hat{a}'' + \hat{a}'^2 - \hat{a}'\hat{b}' + \frac{2\hat{a}'\hat{M}'}{\hat{M}}) = \frac{1}{f_R}\left[\frac{e^{\hat{b}}(Rf_R - f)}{2} + f_{RR}\left(R'' + \frac{\hat{M}'R'}{\hat{M}}\right.\right.$$
$$\left.\left.- \frac{\hat{b}'R'}{2}\right) + R'^2 f_{RRR} - e^{\hat{b}}p_m\right], \tag{4.1.1}$$
$$-\frac{1}{4}(2\hat{a}'' + \hat{a}'^2 - \hat{a}'\hat{b}' + \frac{4\hat{M}''}{\hat{M}} - \frac{2\hat{b}'\hat{M}'}{\hat{M}} - \frac{2\hat{M}'^2}{\hat{M}^2}) = \frac{1}{f_R}\left[\frac{(f - Rf_R)}{2}\right.$$
$$\left.- \frac{R'f_{RR}}{e^{\hat{b}}}\left(\frac{\hat{M}'}{\hat{M}} + \frac{\hat{a}'}{2}\right) + p_m\left(1 - \frac{\hat{a}'}{\hat{b}'}\right) - \frac{\hat{a}'\rho_m}{\hat{b}'}\right], \tag{4.1.2}$$
$$-\frac{1}{4}(\hat{a}'\hat{M}' - \hat{b}'\hat{M}' - 4e^{\hat{b}} + 2\hat{M}'') = \frac{1}{f_R}\left[\frac{e^{\hat{b}}(f - Rf_R)}{2} - \frac{\hat{a}'R'f_{RR}}{2} - R''\right.$$
$$\left.\times f_{RR} - R'^2 f_{RRR} - \frac{\hat{b}'R'f_{RR}}{2} + \frac{\hat{M}'R'f_{RR}}{2\hat{M}} + e^{\hat{b}}p_m\right]. \tag{4.1.3}$$

Solving Eqs.(4.1.1) and (4.1.2) simultaneously, we obtain

$$\begin{aligned} p_m &= -\frac{f - Rf_R}{2} + \frac{f_{RR}}{e^{\hat{b}}}\left(R'' + \frac{\hat{M}'R'}{\hat{M}} - \frac{\hat{b}'R'}{2}\right) + \frac{R'^2 f_{RRR}}{e^{\hat{b}}} + \frac{f_R}{4e^{\hat{b}}} \\ &\times (2\hat{a}'' + \hat{a}'^2 - \hat{a}'\hat{b}' + \frac{2\hat{a}'\hat{M}'}{\hat{M}}), \end{aligned} \tag{4.1.4}$$
$$\begin{aligned} \rho_m &= \frac{1}{\hat{a}'}\left[(\hat{b}' - \hat{a}')\left\{-\frac{f - Rf_R}{2} + \frac{f_{RR}}{e^{\hat{b}}}\left(R'' + \frac{\hat{M}'R'}{\hat{M}} - \frac{\hat{b}'R'}{2}\right) + \frac{R'^2 f_{RRR}}{e^{\hat{b}}}\right.\right. \\ &+ \left.\frac{f_R}{4e^{\hat{b}}}(2\hat{a}'' + \hat{a}'^2 - \hat{a}'\hat{b}' + \frac{2\hat{a}'\hat{M}'}{\hat{M}})\right\} - \hat{b}'\left\{-\frac{f_R}{4e^{\hat{b}}}(2\hat{a}'' + \hat{a}'^2 - \hat{a}'\hat{b}' + \frac{4\hat{M}''}{\hat{M}}\right. \\ &- \left.\left.\frac{2\hat{b}'\hat{M}'}{\hat{M}} - \frac{2\hat{M}'^2}{\hat{M}^2}) - \frac{f - Rf_R}{2} + \frac{R'f_{RR}}{e^{\hat{b}}}\left(\frac{\hat{M}'}{\hat{M}} + \frac{\hat{a}'}{2}\right)\right\}\right]. \end{aligned} \tag{4.1.5}$$

The NEC relative to the effective energy-momentum tensor yields

$$\rho_{eff} + p_{eff} = \frac{1}{2e^{\hat{b}}}\left(\frac{\hat{M}'^2}{\hat{M}^2} + \frac{\hat{a}'\hat{M}'}{\hat{M}} + \frac{\hat{b}'\hat{M}'}{\hat{M}} - \frac{2\hat{M}''}{\hat{M}}\right). \tag{4.1.6}$$

4.1.1 Point-like Lagrangian

In this section, we construct point-like Lagrangian corresponding to the action (1.4.1) via Lagrange multiplier approach which gives

$$\mathcal{I} = \int \sqrt{-g}[f(R) - \lambda(R - \bar{R}) + p_m(\hat{a})]dr, \tag{4.1.7}$$

where

$$\sqrt{-g} = e^{\frac{\hat{a}}{2}} e^{\frac{\hat{b}}{2}} \hat{M}, \quad \lambda = f_R, \quad \rho_m = \rho_0 \hat{a}^{-\frac{(1+\omega)}{2\omega}}, \quad p_m = \omega\rho_m = \omega\rho_0\hat{a}^{-\frac{(1+\omega)}{2\omega}},$$
$$\bar{R} = \frac{1}{e^{\hat{b}}}\left(-\frac{\hat{a}'^2}{2} + \frac{\hat{a}'\hat{b}'}{2} - \frac{\hat{a}'\hat{M}'}{\hat{M}} - \frac{2\hat{M}''}{\hat{M}} + \frac{\hat{b}'\hat{M}'}{\hat{M}} + \frac{\hat{M}'^2}{2\hat{M}^2} - \hat{a}'' + \frac{2e^{\hat{b}}}{\hat{M}}\right).$$

Using these values in (4.1.7) and eliminating second order derivatives via integration by parts, we obtain point-like Lagrangian for configuration space $Q = \{\hat{a}, \hat{b}, \hat{M}, R\}$ as

$$\begin{aligned}\mathcal{L} &= e^{\frac{\hat{a}}{2}} e^{\frac{\hat{b}}{2}} \hat{M}\left(f - Rf_R + \omega\rho_0\hat{a}^{-\frac{(1+\omega)}{2\omega}} + \frac{2f_R}{\hat{M}}\right) + \frac{e^{\frac{\hat{a}}{2}}\hat{M}}{e^{\frac{\hat{b}}{2}}}\left\{f_R\left(\frac{\hat{M}'^2}{2\hat{M}^2} + \frac{\hat{a}'\hat{M}'}{\hat{M}}\right)\right. \\ &+ \left. f_{RR}\left(\hat{a}'R' + \frac{2\hat{M}'R'}{M}\right)\right\}. \end{aligned} \tag{4.1.8}$$

The Euler-Lagrange equation and Hamiltonian of the dynamical system or energy function associated with point-like Lagrangian are defined as

$$\frac{\partial\mathcal{L}}{\partial q^i} - \frac{dp_i}{dr} = 0, \quad \mathcal{H} = \sum_i q'^i p_i - \mathcal{L},$$

The variation of Lagrangian with respect to configuration space leads to

$$e^{\hat{b}}\left(f - Rf_R + \omega\rho_0\hat{a}^{-\frac{(1+\omega)}{2\omega}} - (1+\omega)\rho_0\hat{a}^{-\frac{(1+3\omega)}{2\omega}} + \frac{2f_R}{\hat{M}}\right) + \left(\frac{\hat{M}'^2}{2\hat{M}^2} + \frac{\hat{b}'\hat{M}'}{\hat{M}}\right.$$

$$
\begin{aligned}
&- \frac{2\hat{M}''}{\hat{M}}\bigg) f_R + f_{RR}\left(\hat{b}'R' - 2R'' - \frac{2\hat{M}'R'}{\hat{M}}\right) - 2R'^2 f_{RRR} = 0,\\
&e^{\hat{b}}\left(f - Rf_R + \omega\rho_0\hat{a}^{-\frac{(1+\omega)}{2\omega}} + \frac{2f_R}{\hat{M}}\right) - f_R\left(\frac{\hat{M}'^2}{2\hat{M}^2} + \frac{\hat{a}'\hat{M}'}{\hat{M}}\right) - f_{RR}\bigg(\hat{a}'R'\\
&+ \frac{2\hat{M}'R'}{\hat{M}}\bigg) = 0,\\
&e^{\hat{b}}\left(f - Rf_R + \omega\rho_0\hat{a}^{-\frac{(1+\omega)}{2\omega}} + \frac{2f_R}{\hat{M}}\right) + f_R\bigg(-\frac{\hat{a}'^2}{2} + \frac{\hat{a}'\hat{b}'}{2} - \frac{\hat{a}'\hat{M}'}{2\hat{M}} - \frac{\hat{M}''}{\hat{M}} - \hat{a}''\\
&+ \frac{\hat{b}'\hat{M}'}{2\hat{M}} + \frac{\hat{M}'^2}{2\hat{M}^2}\bigg) + f_{RR}\left(\hat{b}'R' - \hat{a}'R' - 2R'' - \frac{\hat{M}'R'}{\hat{M}}\right) - 2R'^2 f_{RRR} = 0,\\
&\left[e^{\hat{b}}\left(\frac{2}{\hat{M}} - R\right) - \frac{\hat{a}'^2}{2} + \frac{\hat{a}'\hat{b}'}{2} - \frac{\hat{a}'\hat{M}'}{\hat{M}} - \frac{2\hat{M}''}{\hat{M}} + \frac{\hat{b}'\hat{M}'}{\hat{M}} + \frac{\hat{M}'^2}{2\hat{M}^2} - \hat{a}''\right] f_{RR} = 0.
\end{aligned}
$$

The energy function and variation of Lagrangian relative to shape function yield

$$
e^{\hat{b}} = \frac{\frac{f_R\hat{M}'}{\hat{M}}\left(\frac{\hat{M}'}{2\hat{M}^2} + \hat{a}'\hat{M}'\right) + R'f_{RR}(\hat{a}'\hat{M} + 2\hat{M}')}{f - Rf_R + \omega\rho_0\hat{a}^{-\frac{(1+\omega)}{2\omega}} + \frac{2f_R}{\hat{M}}}. \tag{4.1.9}
$$

4.1.2 Noether Symmetry Approach

We consider a vector field

$$
K = \tau(r, q^i)\frac{\partial}{\partial r} + \mathcal{U}^i(r, q^i)\frac{\partial}{\partial q^i}, \tag{4.1.10}
$$

where r behaves as an affine parameter while τ and $\mathcal{U}^i$ are unknown coefficients of the vector field. In this case, the invariance condition (1.5.2) is defined as

$$
K^{[1]}\mathcal{L} + (D\tau)\mathcal{L} = DB(r, q^i). \tag{4.1.11}
$$

The first order prolongation and total derivative are given by

$$
K^{[1]} = K + (D\mathcal{U}^i - q'^i D\tau)\frac{\partial}{\partial q'^i}, \quad D = \frac{\partial}{\partial r} + q'^i\frac{\partial}{\partial q^i}. \tag{4.1.12}
$$

For invariance condition (4.1.11), the first integral is defined as

$$\Sigma = B - \tau\mathcal{L} - (\mathcal{U}^i - q'^i\tau)\frac{\partial\mathcal{L}}{\partial q'^i}. \tag{4.1.13}$$

The vector field and first order prolongation for configuration space $Q = \{\hat{a}, \hat{b}, \hat{M}, R\}$ take the following form

$$\begin{aligned} K &= \tau\frac{\partial}{\partial r} + \alpha\frac{\partial}{\partial\hat{a}} + \beta\frac{\partial}{\partial\hat{b}} + \gamma\frac{\partial}{\partial\hat{M}} + \delta\frac{\partial}{\partial R}, \quad K^{[1]} = \tau\frac{\partial}{\partial r} + \alpha\frac{\partial}{\partial\hat{a}} + \beta\frac{\partial}{\partial\hat{b}} \\ &+ \gamma\frac{\partial}{\partial\hat{M}} + \delta\frac{\partial}{\partial R} + \alpha'\frac{\partial}{\partial\hat{a}'} + \beta'\frac{\partial}{\partial\hat{b}'} + \gamma'\frac{\partial}{\partial\hat{M}'} + \delta'\frac{\partial}{\partial R'}, \end{aligned} \tag{4.1.14}$$

where the radial derivative of unknown coefficients of vector field are defined as

$$\sigma'_{\hat{j}} = D\sigma_{\hat{j}} - q'^i D\tau, \quad \hat{j} = 1...4. \tag{4.1.15}$$

Here σ_1, σ_2, σ_3 and σ_4 correspond to α, β, γ and δ, respectively. Inserting Eqs.(4.1.8), (4.1.14) and (4.1.15) in (4.1.11) and comparing the coefficients of $\hat{a}'^2$, $\hat{a}'\hat{b}'\hat{M}'$, $\hat{a}'\hat{M}'^2$ and $\hat{a}'R'^2$, we obtain

$$\tau,_{\hat{a}} f_R = 0, \quad \tau,_{\hat{b}} f_R = 0, \quad \tau,_{\hat{M}} f_R = 0, \quad \tau,_R f_{RR} = 0. \tag{4.1.16}$$

This implies that either $f_R = 0$ or vice verse. The first choice leads to trivial solution. Therefore, we consider $f_R \neq 0$ and compare the remaining coefficients which yield an over determined system of equations given in Appendix **B**.

The geodesic deviation equation determines that $\hat{M}(r) = r^2, \ \sin r, \ \sinh r$ for $\mathcal{K} = 0, 1, -1$ ($\mathcal{K}$ denotes curvature parameter) under the limiting behavior $\hat{M}(r) \to 0$ as $r \to 0$, respectively [67]. In order to solve this system, we consider $\hat{M}(r) = r^2$ and taking $B,_{\hat{a}}$, $B,_{\hat{M}}$, $B,_R = 0$, Eqs.(B1)-(B9) give

$$\alpha = Y_2(\hat{a}, r), \quad \gamma = Y_1(r), \quad \delta = Y_3(r, R).$$

Inserting these values in Eqs.(B10)-(B13), we obtain

$$Y_1(r) = 0, \quad Y_2(\hat{a}, r) = c_2, \quad Y_3(r, R) = \frac{c_1 f_R}{f_{RR}}, \quad \beta = 2c_1 + c_2 - 2\tau,_{r}.$$

where c_1 and c_2 are arbitrary constants. For these solutions, the coefficients of symmetry generator turn out to be

$$\alpha = c_2, \quad \beta = 2c_1 + c_2, \quad \gamma = 0, \quad \delta = \frac{c_1 f_R}{f_{RR}}, \quad \tau = c_0. \tag{4.1.17}$$

Substituting these coefficients in Eq.(B14), we formulate boundary term and explicit form of $f(R)$ as follows

$$\begin{aligned} f(R) &= -\frac{1}{2(c_1 + c_2)}\left[-(1+\omega)\rho_0 \hat{a}^{-\frac{(1+3\omega)}{2\omega}} + 2\omega(c_1 + c_2)\rho_0 \hat{a}^{-\frac{(1+\omega)}{2\omega}} - 6c_4 e^{\frac{-\hat{a}-\hat{b}}{2}}\right], \\ B &= c_3 + c_4 r^3. \end{aligned}$$

The coefficients of symmetry generator, boundary term and solution of $f(R)$ satisfy the system of Eqs.(B1)-(B13) for $c_1 = 0$. Thus, the symmetry generator and the corresponding first integral take the form

$$\begin{aligned} K &= c_0 \frac{\partial}{\partial r} + c_2 \frac{\partial}{\partial \hat{a}} + c_2 \frac{\partial}{\partial \hat{b}}, \\ \Sigma &= c_3 + c_4 r^3 - c_0 \left[e^{\frac{\hat{a}}{2}} e^{\frac{\hat{b}}{2}} r^2 (f - R f_R + \omega \rho_0 \hat{a}^{-\frac{(1+\omega)}{2\omega}} + 2 f_R r^{-2}) \right. \\ &+ \left. \frac{e^{\frac{\hat{a}}{2}} r^2}{e^{\frac{\hat{b}}{2}}} \{ f_R (2r^{-2} + 2a' r^{-1}) + f_{RR} (\hat{a}' R' + 4R' r^{-1}) \} \right] \\ &- c_2 e^{\frac{\hat{a}-\hat{b}}{2}} (R' r^2 f_{RR} + 2r f_R). \end{aligned}$$

The verification of Eq.(B14) yields

$$\hat{b}(r) = \int \frac{8c_6 r^2 + \hat{a}'' r^2 + 4\hat{a}' r' + \hat{a}'^2 r^2 - 4c_7}{r(4 + \hat{a}' r)} dr + c_5, \tag{4.1.18}$$

where c_i are arbitrary constants and this solution satisfies Eq.(B14) for $\omega = 1, 1/3, -1/3, -1$. To discuss physical features and geometry of WH via shape function, we take red-shift function, $\hat{a}(r)=k$ and $\hat{a}(r)=-\frac{k}{r},\ k>0$, where k denotes constant [71]. In the following, we solve integral for both choices of red-shift function.

Case I: $\hat{a}(r)=k$

We first consider red-shift function to be constant and evaluate $\hat{b}(r)$ such as

$$\hat{b}(r)=c_6r^2-c_7\ln r+c_5. \tag{4.1.19}$$

Consequently, the shape function turns out to be

$$h(r)=r(1-e^{-\hat{b}(r)})=r(1-c_7re^{-c_6r^2-c_5}). \tag{4.1.20}$$

In this case, the explicit form of $f(R)$ reduces to

$$f(R)=-\frac{1}{2c_2}\left[-(1+\omega)\rho_0k^{-\frac{(1+3\omega)}{2\omega}}+2\omega c_2\rho_0k^{-\frac{(1+\omega)}{2\omega}}-6c_4\sqrt{c_7r}e^{\frac{-c_6r^2-c_5-k}{2}}\right]. \tag{4.1.21}$$

We investigate viability of the constructed $f(R)$ model and study WH geometry graphically. In Figure **4.1**, both plots indicate that the constructed $f(R)$ model (4.1.21) preserves stability conditions. Figure **4.2** shows graphical analysis of the shape function. The upper left plot represents positive behavior of $h(r)$ while the upper right indicates that the shape function admits asymptotic behavior. The lower left plot locates the WH throat at $r_0=4.4$ and the corresponding right plot identifies that $\frac{dh(r_0)}{dr}=0.9427<1$. To discuss physical existence of WH, we insert constant red-shift function and Eq.(4.1.19) in (4.1.6) yielding

$$\rho_{eff}+p_{eff}=\frac{rh'(r)-h(r)}{r^3}<0,$$

which satisfies the flaring-out condition. Consequently, NEC violates, $\rho_{eff}+p_{eff}<0$ which assures the presence of repulsive gravity leading to traversable WH.

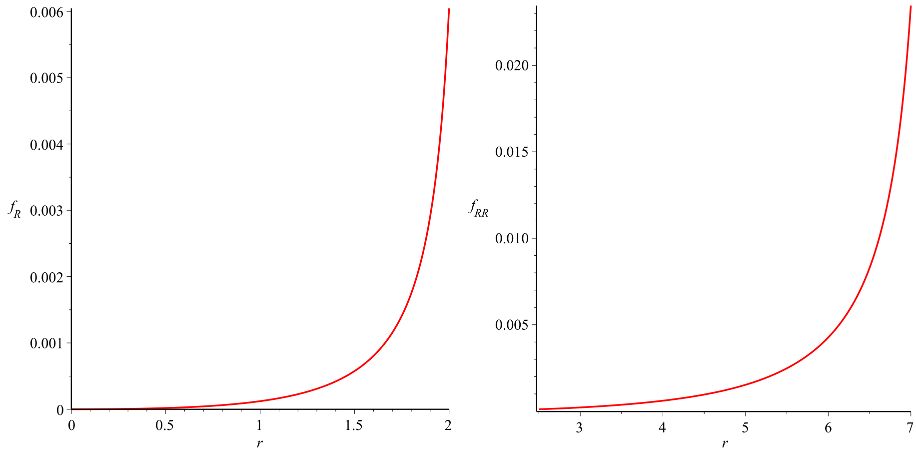

Figure 4.1: Plots of stability conditions of $f(R)$ model versus r for $c_2 = 5$, $c_4 = 0.01$, $c_5 = -0.35$, $c_6 = 0.1$, $c_7 = -0.25$ and $k = 0.5$.

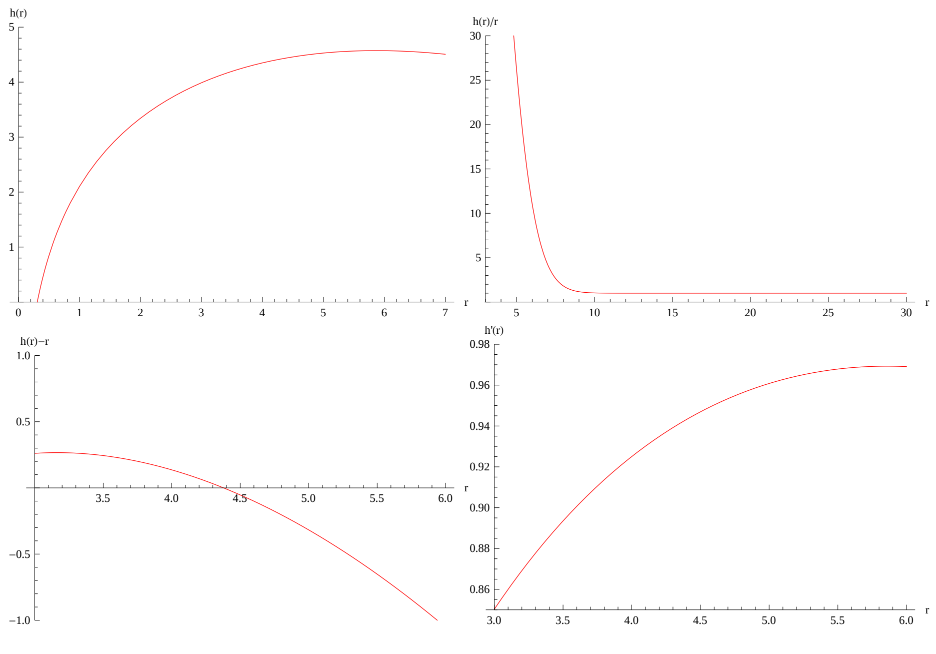

Figure 4.2: Plots of $h(r)$, $\frac{h(r)}{r}$, $h(r) - r$ and $\frac{dh(r)}{dr}$ versus r for $c_5 = -0.35$, $c_6 = 0.1$ and $c_7 = -0.25$.

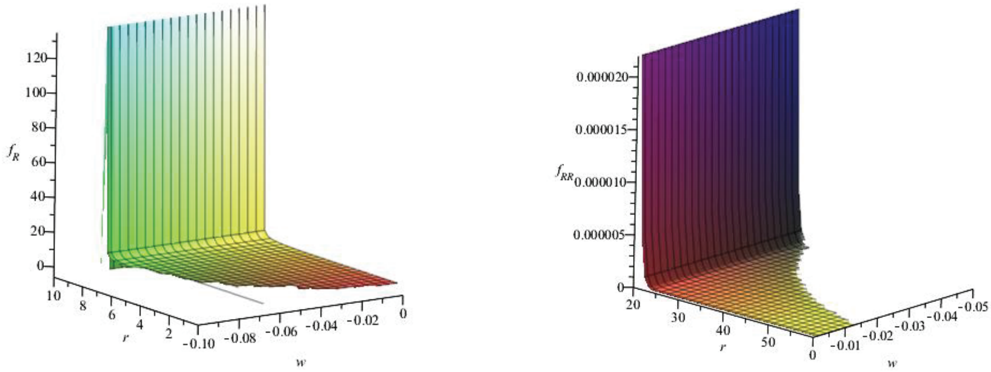

Figure 4.3: Stability conditions of $f(R)$ versus r for $c_2 = 5$, $c_4 = -0.5$, $c_5 = -0.35$, $c_6 = 0.1$, $c_7 = -0.25$ and $k = 0.5$.

Case II: $\hat{a}(r) = -k/r$

In this case, we choose red-shift function in terms of r leading to

$$\begin{aligned}\hat{b}(r) &= \frac{1}{8r}(8c_6r^3 - 4c_6kr^2 - 32c_8r\ln r + 32r\ln(4r+k) - 8c_7r\ln(4r+k) \\ &+ c_6kr^2\ln(4r+k) - 8k/c_8) + c_5, \quad k > 0. \qquad (4.1.22)\end{aligned}$$

The corresponding $f(R)$ and shape function become

$$\begin{aligned}f(R) &= -\frac{1}{2c_2}\left[-(1+\omega)\rho_0\left(-\frac{k}{r}\right)^{-\frac{(1+3\omega)}{2\omega}} + 2\omega c_2\rho_0\left(-\frac{k}{r}\right)^{-\frac{(1+\omega)}{2\omega}} - 6c_4\right. \\ &\times \left.\sqrt{c_8r^4(4r+k)^{-4+c_7-\frac{k^2c_6}{8}}e^{\frac{-(c_6r^2-\frac{c_6kr}{2}-\frac{k}{c_8r})-c_5+k}{2}}}\right], \qquad (4.1.23)\\ h(r) &= r(1 - c_8r^4(4r+k)^{-4+c_7-\frac{k^2c_6}{8}}e^{-(c_6r^2-\frac{c_6kr}{2}-\frac{k}{c_8r})-c_5}). \qquad (4.1.24)\end{aligned}$$

Figure **4.3** shows that the model (4.1.23) follows the stability condition for $0 < \omega < -0.1$, whereas Figure **4.4** represents the graphical behavior of the shape function. In upper face, the left plot preserves the positivity of $h(r)$ while the right plot ensures asymptotic flat geometry of WH. In lower face, the left plot detects WH throat at

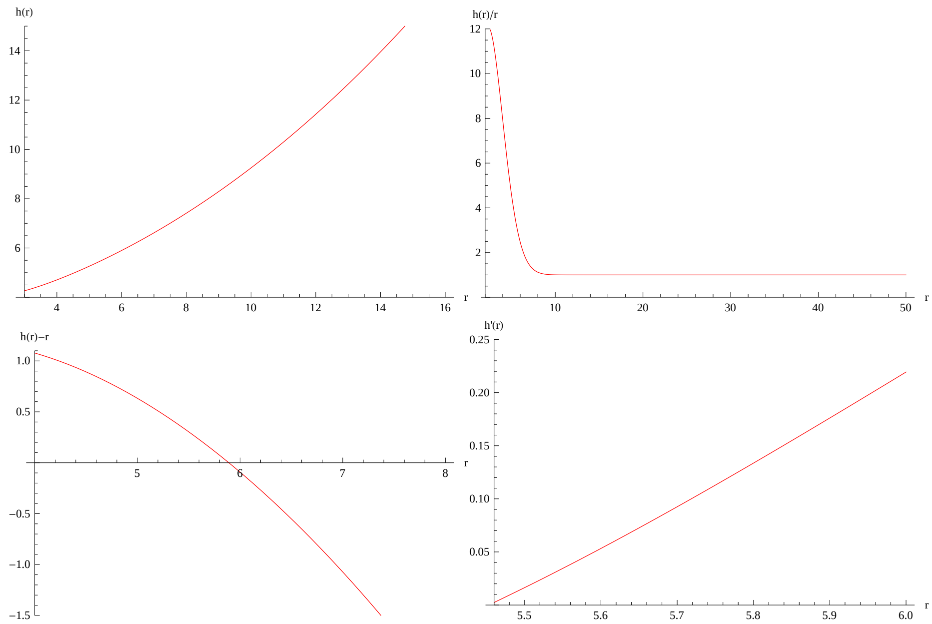

Figure 4.4: Plots of $h(r)$, $\frac{h(r)}{r}$, $h(r)-r$ and $\frac{dh(r)}{dr}$ versus r for $c_5=-4$, $c_6=0.1$, $c_8=-1$ and $k=0.25$.

$r_0=5.878$ whereas the right plot indicates that $\frac{dh(r_0)}{dr}=0.1673<1$. For Eqs.(4.1.6) and (4.1.22), we obtain

$$\rho_{eff}+p_{eff}=\frac{k}{r^2(r-h(r))}+\frac{rh'(r)-h(r)}{r^3}.$$

Figures **4.5-4.7** indicate that $\rho_m+p_m\geq 0$, $\rho_m\geq 0$ and $\rho_{eff}+p_{eff}<0$ for $1<\omega<-1$. Thus, the physical existence of WH is assured in this case.

Power-law $f(R)$ Model

Here, we construct a WH solution with symmetry generator and corresponding conserved quantity for $f(R)$ power-law model. We solve Eqs.(B1)-(B9) leading to

$$\alpha=Y_3(\hat{a},r),\quad \gamma=Y_1(r),\quad \delta=Y_2(r,R).$$

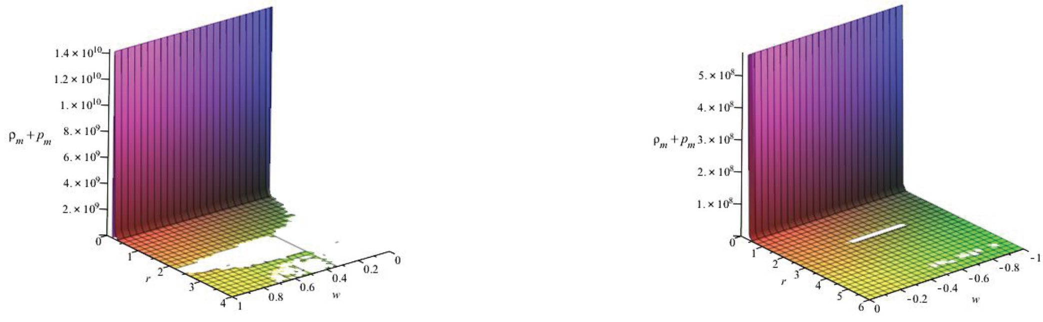

Figure 4.5: Plots of $\rho_m + p_m$ versus r for $\rho_0 = 1$, $c_2 = 5$ and $c_4 = -0.5$.

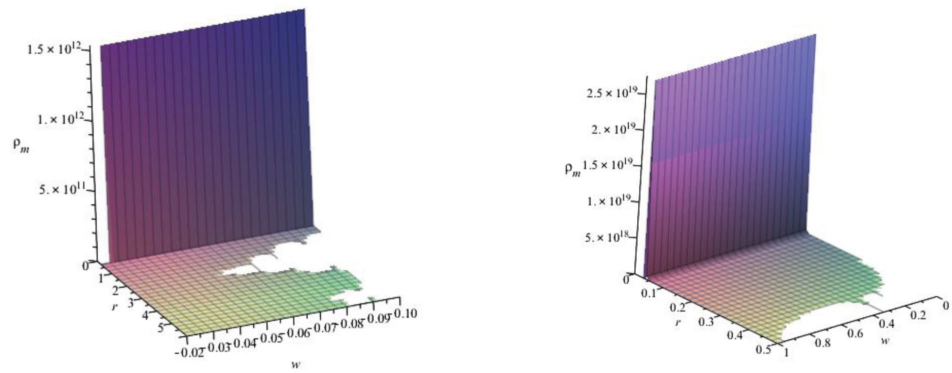

Figure 4.6: Plots of ρ_m versus r for $\rho_0 = 1$, $c_2 = 5$ and $c_4 = -0.5$.

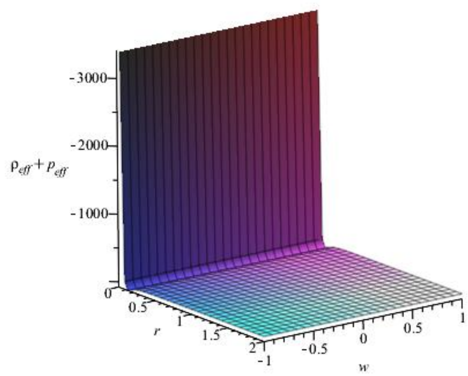

Figure 4.7: Plots of $\rho_{eff} + p_{eff}$, versus r for $\rho_0 = 1$, $c_2 = 5$ and $c_4 = -0.5$.

Inserting this solution into Eqs.(B10)-(B13), we obtain

$$Y_1(r)=0,\quad Y_3(\hat{a},r)=d_2,\quad Y_2(r,R)=d_1R,\quad \beta=2(n-1)d_1+d_2-2\tau_{,r}\,,$$

where d_1 and d_2 represent arbitrary constants. For these values, the coefficients of symmetry generator turn out to be

$$\alpha=d_2,\quad \beta=2(n-1)d_1+d_2-2\tau_{,r}\,,\quad \gamma=0,\quad \delta=d_1R. \tag{4.1.25}$$

Substituting these coefficients in Eq.(B14) and assuming $B=d_0$ and $\tau=\tau_0$, we have

$$\begin{aligned}\hat{b}(r) &= \int\frac{8d_3r^2+2\hat{a}''r^2+4\hat{a}'r'+\hat{a}'^2r^2-4d_4}{r(4+\hat{a}'r)}dr\\ &- \ln\left[-d_1+4\int\frac{e^{\int\frac{8r^2+2\hat{a}''r^2+4\hat{a}'r'+\hat{a}'^2r^2-4}{r(4+\hat{a}'r)}dr}}{r(4+\hat{a}'r)}dr\right].\end{aligned} \tag{4.1.26}$$

The resulting coefficients of symmetry generator verifies the system (B1)-(B13) for $d_2=-2(n-1)d_1$. The symmetry generator and associated first integral give

$$\begin{aligned}K &= \tau_0\frac{\partial}{\partial r}-2(n-1)d_1\frac{\partial}{\partial\hat{a}}+d_1\frac{\partial}{\partial R},\\ \Sigma &= d_0-\tau_0\left[e^{\frac{\hat{a}}{2}}e^{\frac{\hat{b}}{2}}r^2(f-Rf_R+\omega\rho_0\hat{a}^{-\frac{(1+\omega)}{2\omega}}+2f_Rr^{-2})+\frac{e^{\frac{\hat{a}}{2}}r^2}{e^{\frac{\hat{b}}{2}}}\right.\\ &\times \left.\{f_R(2r^{-2}+2\hat{a}'r^{-1})+f_{RR}(\hat{a}'R'+4R'r^{-1})\}\right]-2d_1(1-n)e^{\frac{\hat{a}-\hat{b}}{2}}(R'r^2\\ &\times f_{RR}+2rf_R)-d_1Rf_{RR}e^{\frac{\hat{a}-\hat{b}}{2}}(\hat{a}'r^2+4r).\end{aligned}$$

Now, we solve the integral (4.1.26) for constant and variable forms of red-shift function and study WH geometry via shape function.

Case I: $\hat{a}(r)=k$

For constant red-shift function, the integral (4.1.26) reduces to

$$\hat{b}(r)=d_3r^2-d_4\ln r-\ln\left(\frac{-d_1r+e^{r^2}}{r}\right). \tag{4.1.27}$$

This satisfies Eq.(B14) for $\omega = 1, \frac{1}{3}, -\frac{1}{3}, -1$ and

$$\rho_0 = -\frac{f_o e^{\frac{3\omega \ln d_1 + 4n\omega \ln 2 + \ln d_1}{2\omega}}}{\omega d_1 - (1+\omega)}, \quad \omega \neq 0. \tag{4.1.28}$$

In this case, the shape function yields

$$h(r) = r\left[1 - d_4 r\left(\frac{-d_1 r + e^{r^2}}{r}\right)e^{-d_3 r^2}\right]. \tag{4.1.29}$$

We analyze WH geometry via shape function for $n = \frac{1}{2}, 2$ and $n = 4$. In upper face, the left and right plots of Figure **4.8** show that $h(r)$ remains positive and asymptotic flat for $n = \frac{1}{2}$. The lower left plot identifies WH throat at $r_0 = 5.101$ and right plot satisfies the condition, i.e., $h'(r_0) = 0.17 < 1$. In Figures **4.9** and **4.10**, the shape function preserves its positivity condition and also admits asymptotic flat geometry for both $n = 2$ and $n = 4$. The WH throat is located at $r_0 = 0.23$ and $r_0 = 2.052$ for $n = 2$ and $n = 4$, respectively. The derivative condition is also satisfied at throat, i.e., $h'(r_0) = 0.89 < 1$ and $h'(r_0) = -0.49 < 1$. The NEC relative to effective energy-momentum tensor verifies $\rho_{eff} + p_{eff} < 0$ ensuring the presence of exotic matter at throat.

Case II: $\hat{a}(r) = -k/r$

In this case, the integral (4.1.26) implies that

$$\begin{aligned}
\hat{b}(r) &= r^2 - \frac{rd_1(1-n)}{2} + \frac{d_1^2(1-n)^2\ln(d_1(1-n)+4r)}{8} + (d_1(1-n))^2 \\
&\times \left\{-\frac{1}{rd_1(1-n)} + \frac{4\ln(d_1(1-n)+4r)}{(d_1(1-n))^2} - \frac{4\ln r}{(d_1(1-n))^2}\right\} - \ln((1-n) \\
&\times d_1 + 4r) - \ln\left[4\int\frac{1}{4r+d_1(1-n)}\left(r^{-4}(d_1(1-n)+4r)^{3+\frac{d_1^2(1-n)^2}{8}}\right.\right. \\
&\times \left.\left. e^{r^2 - \frac{rd_1(1-n)}{2} + \frac{d_1(1-n)}{r}}\right)dr - d_1\right],
\end{aligned}$$

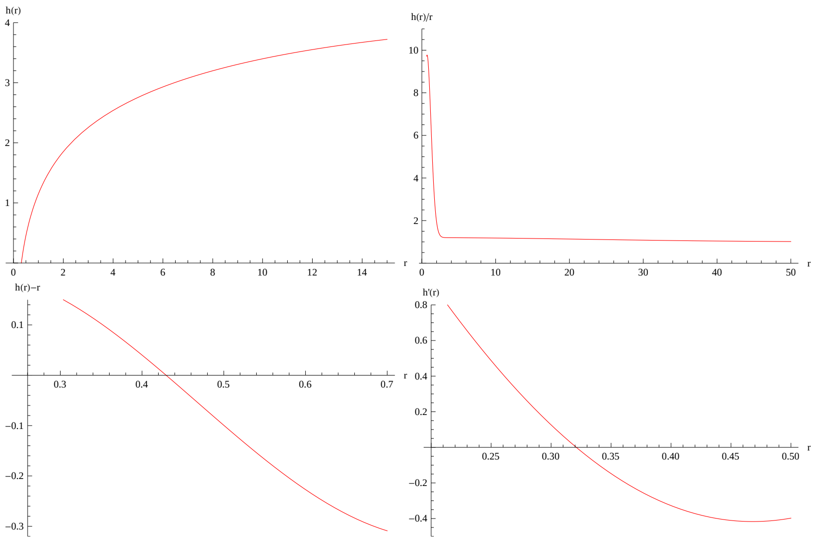

Figure 4.8: Plots of $h(r)$, $\frac{h(r)}{r}$, $h(r)-r$ and $\frac{dh(r)}{dr}$ versus r for $d_2 = 2.8$, $d_3 = 1.001$, $d_4 = -2.2$ and $n = \frac{1}{2}$.

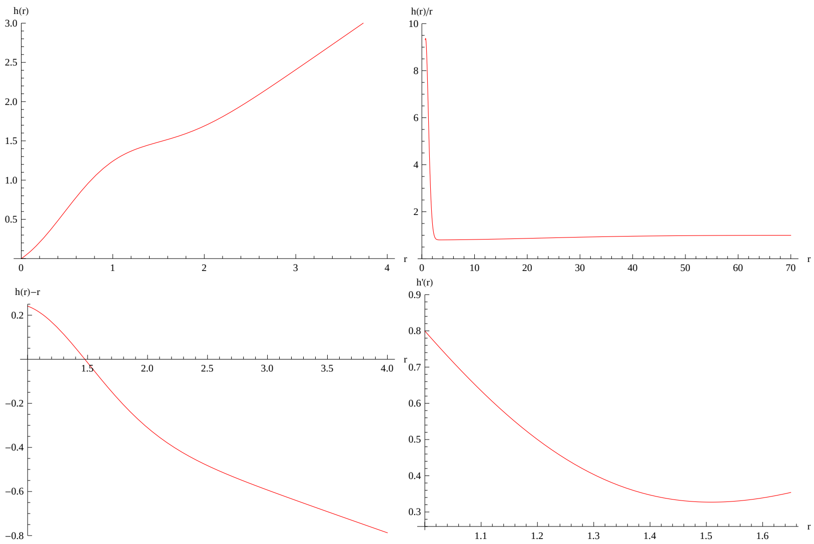

Figure 4.9: Plots of $h(r)$, $\frac{h(r)}{r}$, $h(r)-r$ and $\frac{dh(r)}{dr}$ versus r for $d_2 = -12$, $d_3 = 1.001$, $d_4 = 0.2$ and $n = 2$.

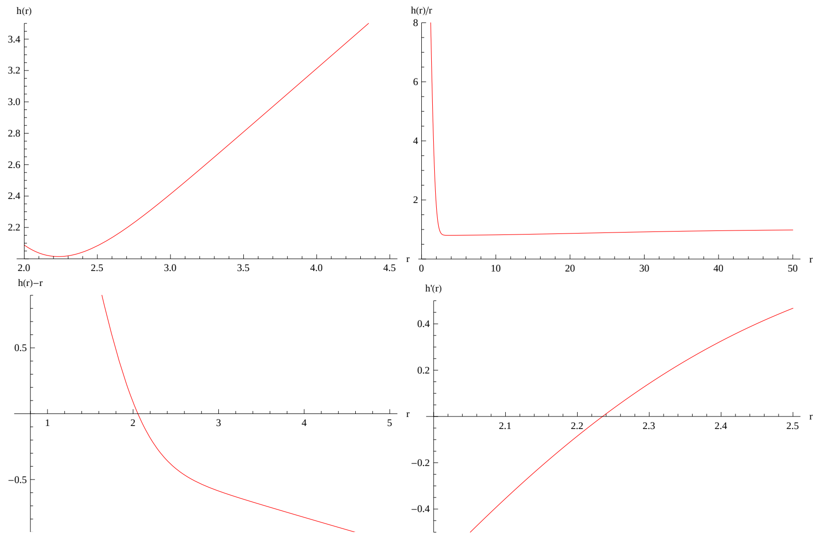

Figure 4.10: Plots of $h(r)$, $\frac{h(r)}{r}$, $h(r)-r$ and $\frac{dh(r)}{dr}$ versus r for $d_2=-200$, $d_3=1.001$, $d_4=0.2$ and $n=4$.

which satisfies Eq.(B14) for $\omega=-1$. The shape function of WH takes the form

$$\frac{h(r)}{r}=\left(1-r^4(d_1(1-n)+4r)^{-3-\frac{d_1^2(1-n)^2}{8}}e^{-r^2+\frac{rd_1(1-n)}{2}-\frac{d_1(1-n)}{r}}\left[\int\{4r+d_1\right.\right.$$
$$\left.\left.\times\ (1-n)\}^{-1}\left(r^{-4}(d_1(1-n)+4r)^{3+\frac{d_1^2(1-n)^2}{8}}e^{r^2-\frac{rd_1(1-n)}{2}+\frac{d_1(1-n)}{r}}\right)dr-d_1\right]\right).$$

When red-shift function is not constant ($\hat{a}'(r)\neq 0$), then the geometry of WH cannot be analyzed for $f(R)$ power-law model due to the complicated forms of $\hat{b}(r)$ and $h(r)$.

4.2 Wormhole Solutions in $f(R,T)$ Gravity

Now we formulate Lagrangian corresponding to the action (1.4.20) by using Lagrange multiplier approach with $\mathcal{L}_m=p_m(\hat{a},\hat{b},\hat{M})$ as follows

$$\mathcal{I}=\int\sqrt{-g}[f(R,T)-\lambda(R-\bar{R})-\chi(T-\bar{T})+p_m(\hat{a},\hat{b},\hat{M})]dr. \tag{4.2.1}$$

Here

$$\begin{aligned}\sqrt{-g} &= e^{\frac{\hat{a}}{2}}e^{\frac{\hat{b}}{2}}\hat{M}, \quad \lambda = f_R, \quad \chi = f_T, \quad T = 3p_m - \rho_m,\\ R &= \frac{1}{e^{\hat{b}}}\left(-\frac{\hat{a}'^2}{2} + \frac{\hat{a}'\hat{b}'}{2} - \frac{\hat{a}'\hat{M}'}{\hat{M}} - \frac{2\hat{M}''}{\hat{M}} + \frac{\hat{b}'\hat{M}'}{\hat{M}} + \frac{\hat{M}'^2}{2\hat{M}^2} - \hat{a}'' + \frac{2e^{\hat{b}}}{\hat{M}}\right).\end{aligned} \tag{4.2.2}$$

Using these values in Eq.(4.2.1) and eliminating second order derivative trough integration by parts, it follows that

$$\begin{aligned}\mathcal{L} &= e^{\frac{\hat{a}}{2}}e^{\frac{\hat{b}}{2}}\hat{M}\left(f - Rf_R - Tf_T(R,T) + f_T(R,T)(3p_m - \rho_m) + p_m + \frac{2f_R}{\hat{M}}\right)\\ &+ \frac{e^{\frac{\hat{a}}{2}}\hat{M}}{e^{\frac{\hat{b}}{2}}}\left\{f_R\left(\frac{\hat{M}'^2}{2\hat{M}^2} + \frac{\hat{a}'\hat{M}'}{\hat{M}}\right)f_{RR}\left(\hat{a}'R' + \frac{2\hat{M}'R'}{\hat{M}}\right) + f_{RT}\left(\hat{a}'T' + \frac{2\hat{M}'T'}{\hat{M}}\right)\right\}.\end{aligned} \tag{4.2.3}$$

The variation of Lagrangian with respect to configuration space $Q = \{\hat{a}, \hat{b}, \hat{M}, R, T\}$ leads to

$$\begin{aligned}&f - Rf_R - Tf_T + f_T(3p_m - \rho_m) + p_m + 2\{f_T(3p_{m,_{\hat{a}}} - \rho_{m,_{\hat{a}}}) + p_{m,_{\hat{a}}}\}\\ &+\frac{1}{e^{\hat{b}}}\left\{f_{RR}\left(\hat{b}'R' - 2R'' - \frac{2\hat{M}'R'}{\hat{M}}\right) + f_{RT}\left(\hat{b}'T' - \frac{2\hat{M}'T'}{\hat{M}}\right) - 2R'^2 f_{RRR}\right.\\ &\left. - 4R'T'f_{RRT} - 2T'^2 f_{RTT}\right\} = \frac{f_R}{e^{\hat{b}}}\left(\frac{\hat{M}'^2}{2\hat{M}^2} + \frac{\hat{b}'\hat{M}'}{\hat{M}} - \frac{2\hat{M}''}{\hat{M}} + \frac{2e^{\hat{b}}}{\hat{M}}\right),\end{aligned} \tag{4.2.4}$$

$$\begin{aligned}&f - Rf_R - Tf_T + f_T(3p_m - \rho_m) + p_m + 2\{f_T(3p_{m,_{\hat{b}}} - \rho_{m,_{\hat{b}}}) + p_{m,_{\hat{b}}}\}\\ &-\frac{1}{e^{\hat{b}}}\left\{f_{RR}\left(\hat{a}'R' + \frac{2\hat{M}'R'}{\hat{M}}\right) - f_{RT}\left(\hat{a}'T' + \frac{2\hat{M}'T'}{\hat{M}}\right)\right\} = \frac{f_R}{e^{\hat{b}}}\left(\frac{\hat{M}'^2}{2\hat{M}^2}\right.\\ &\left. + \frac{\hat{a}'\hat{M}'}{\hat{M}} - \frac{2e^{\hat{b}}}{\hat{M}}\right),\end{aligned} \tag{4.2.5}$$

$$\begin{aligned}&f - Rf_R - Tf_T + f_T(3p_m - \rho_m) + p_m + 2\{f_T(3p_{m,_{\hat{M}}} - \rho_{m,_{\hat{M}}}) + p_{m,_{\hat{M}}}\}\\ &+\frac{1}{e^{\hat{b}}}\left\{f_{RR}\left(\hat{b}'R' - \hat{a}'R' - 2R'' - \frac{\hat{M}'R'}{\hat{M}}\right) - 4R'T'f_{RRT} - 2T'^2 f_{RTT} - 2R'^2\right.\end{aligned}$$

$$\times f_{RRR} + f_{RT}\left(\hat{b}'T' - \hat{a}'T' - 2T'' - \frac{\hat{M}'T'}{\hat{M}}\right)\Bigg\} = -\frac{f_R}{e^{\hat{b}}}\left(-\hat{a}'' + \frac{\hat{M}'^2}{2\hat{M}^2} - \frac{\hat{a}'^2}{2}\right.$$
$$\left. - \frac{\hat{a}'\hat{M}'}{2\hat{M}} + \frac{\hat{a}'\hat{b}'}{2} + \frac{\hat{b}'\hat{M}'}{2\hat{M}} - \frac{\hat{M}''}{\hat{M}}\right),$$
$$e^{\hat{b}}(f_{RT}(3p_m - \rho_m - T) + f_{RR}(2\hat{M}^{-1}R - R)) + f_{RR}\left(-\hat{a}'' + \frac{\hat{M}'^2}{2\hat{M}^2} - \frac{\hat{a}'^2}{2}\right.$$
$$\left. - \frac{\hat{a}'\hat{M}'}{2\hat{M}} + \frac{\hat{a}'\hat{b}'}{2} + \frac{\hat{b}'\hat{M}'}{2\hat{M}} - \frac{\hat{M}''}{\hat{M}}\right) = 0,$$
$$e^{\hat{b}}(f_{TT}(3p_m - \rho_m - T) + f_{RT}(2\hat{M}^{-1}R - R)) + f_{RT}\left(-\hat{a}'' + \frac{\hat{M}'^2}{2\hat{M}^2} - \frac{\hat{a}'^2}{2}\right.$$
$$\left. - \frac{\hat{a}'\hat{M}'}{2\hat{M}} + \frac{\hat{a}'\hat{b}'}{2} + \frac{\hat{b}'\hat{M}'}{2\hat{M}} - \frac{\hat{M}''}{\hat{M}}\right) = 0.$$

For Lagrangian (4.2.3), the variation of energy function leads to

$$e^{\hat{b}(r)} = \left(1 - \frac{h(r)}{r}\right)^{-1} = \frac{f_R\left(\frac{\hat{M}'^2}{2\hat{M}^2} + \frac{\hat{a}'\hat{M}'}{\hat{M}}\right) + (R'f_{RR} + T'f_{RT})\left(\hat{a}' + \frac{2\hat{M}'}{\hat{M}}\right)}{f - Rf_R - Tf_T + f_T(3p_m - \rho_m) + p_m + 2\hat{M}^{-1}f_R}. \quad (4.2.6)$$

The vector field and corresponding first order prolongation turn out to be

$$\begin{aligned} K &= \tau\frac{\partial}{\partial r} + \alpha\frac{\partial}{\partial \hat{a}} + \beta\frac{\partial}{\partial \hat{b}} + \gamma\frac{\partial}{\partial \hat{M}} + \delta\frac{\partial}{\partial R} + \eta\frac{\partial}{\partial T}, \\ K^{[1]} &= \tau\frac{\partial}{\partial r} + \alpha\frac{\partial}{\partial \hat{a}} + \beta\frac{\partial}{\partial \hat{b}} + \gamma\frac{\partial}{\partial \hat{M}} + \delta\frac{\partial}{\partial R} + \eta\frac{\partial}{\partial T} + \alpha'\frac{\partial}{\partial \hat{a}'} + \beta'\frac{\partial}{\partial \hat{b}'} \\ &+ \gamma'\frac{\partial}{\partial \hat{M}'} + \delta'\frac{\partial}{\partial R'} + \eta'\frac{\partial}{\partial T'}. \end{aligned} \quad (4.2.7)$$

The derivative of unknown coefficients of vector field with respect to r are defined as

$$\zeta_\iota' = D\zeta_\iota - q'^i D\tau, \quad (4.2.8)$$

where ζ_1, ζ_2, ζ_3, ζ_4 and ζ_5 correspond to α, β, γ, δ and η, respectively. Inserting Eqs.(4.2.3), (4.2.7) and (4.2.8) in (4.1.11) and comparing the coefficients of $\hat{a}'^2\hat{M}'$, $\hat{a}'\hat{b}'\hat{M}'$, $\hat{a}'\hat{M}'^2$, $\hat{a}'R'^2$ and $\hat{a}'T'^2$, we obtain

$$\tau,_{\hat{a}} f_R = 0, \quad \tau,_{\hat{b}} f_R = 0, \quad \tau,_{\hat{M}} f_R = 0, \quad \tau,_R f_{RR} = 0, \quad \tau,_T f_{RT} = 0. \quad (4.2.9)$$

This implies that either $f_R,\ f_{RR},\ f_{RT}=0$ or vice verse. The first choice yields trivial solution. Thus, we choose $f_R\neq 0$ and equate the remaining coefficients leading to system of equations (B15)-(B34) mentioned in Appendix **B**.

To solve over-determined system, we choose $\hat{M}(r)=r^2$ and study possible existence of symmetry generators, associated conserved quantities lead to analyze WH geometry for two $f(R,T)$ models. We also construct corresponding exact solutions to explore cosmological picture of these models. The models are given as

- $f(R,T)$=$R+2g(T)$,
- $f(R,T)$=$f(R)+g(T)$.

4.2.1 $f(R,T)=R+2g(T)$

We formulate symmetry generators and conserved quantities by solving the system (B15)-(B33) which yields

$$\alpha = 0,\quad \beta=-\frac{2c_2B_{,r}}{r^2},\quad \gamma=0,\quad \delta=0,\quad \eta=0,\quad \tau=c_1+\int\frac{c_2B_{,r}}{r^2}dr. \tag{4.2.10}$$

In the following, we explore the existence of realistic and traversable WH for dust as well as non-dust distribution.

Dust Case

In order to evaluate matter component, we use Eq.(4.2.10) into (B34) which yields

$$\rho_m=-\frac{e^{\frac{-\hat{a}-\hat{b}}{2}}}{2c_2c_3},\quad \Lambda(T)=-\frac{g(T)}{2}+c_3T+c_4, \tag{4.2.11}$$

where c_3 and c_4 represent arbitrary constants. Assuming $B_{,r} = c_5$, the non-zero coefficients of symmetry generator and $f(R,T)$ model take the form

$$B = c_5 r, \quad \tau = c_1 - \frac{c_2 c_5}{r}, \quad \beta = -\frac{2c_2 c_5}{r^2}, \quad f(R,T) = R + 2c_3 T + c_4.$$

The symmetry generators and the corresponding first integral become

$$\begin{aligned}
K_1 &= \frac{\partial}{\partial r}, \quad K_2 = -\frac{c_2}{r}\frac{\partial}{\partial r} - \frac{2c_2}{r^2}\frac{\partial}{\partial \hat{b}}, \\
\Sigma_1 &= -e^{\frac{\hat{a}-\hat{b}}{2}} r^2 \left[e^{\hat{b}} \left(2c_4 + \frac{2}{r^2} + \frac{e^{\frac{-\hat{a}-\hat{b}}{2}}}{c_2} \right) + \frac{2 + 2\hat{a}' r}{r^2} \right], \\
\Sigma_2 &= r + c_2 e^{\frac{\hat{a}-\hat{b}}{2}} r \left[e^{\hat{b}} \left(2c_4 + \frac{2}{r^2} + \frac{e^{\frac{-\hat{a}-\hat{b}}{2}}}{c_2} \right) + \frac{2 + 2\hat{a}' r}{r^2} \right].
\end{aligned}$$

To determine WH solution, we insert Eq.(4.2.11) in (4.2.6) leading to

$$e^{\hat{b}(r)} = \frac{\frac{2}{r^2} + \frac{2\hat{a}'}{r}}{2c_4 + \frac{2}{r^2} + \frac{e^{\frac{-\hat{a}-\hat{b}}{2}}}{c_2}}. \tag{4.2.12}$$

In the following, we solve Eq.(4.2.12) for $\hat{a}(r) = k$ and $\hat{a}(r) = -\frac{k}{r}$, $k > 0$.

Case I: $\hat{a}(r) = k$

In this case, Eq.(4.2.12) yields

$$\hat{b}(r) = 2\ln\left[-\frac{e^{-\frac{k}{2}} r^2 + \sqrt{e^{-k} r^4 + 16 c_4 r^2 c_2^2 + 16 c_2^2}}{4c_2 (c_4 r^2 + 1)} \right], \tag{4.2.13}$$

which leads to shape function as

$$\begin{aligned}
h(r) &= [2r^3 (e^{-k} r^2 + ((e^{-\frac{k}{2}} \sqrt{e^{-k} r^4 + 16 c_4 r^2 c_2^2 + 16 c_2^2} - 8c_2^2 c_4) - 8c_2^2 c_4^2 r^2))] \\
&\times \{(e^{-\frac{k}{2}} r^2 + \sqrt{e^{-k} r^4 + 16 c_4 r^2 c_2^2 + 16 c_2^2})^2\}^{-1}.
\end{aligned}$$

The energy density of dust fluid becomes

$$\rho_m = -\frac{e^{-\frac{k}{2} - \ln\left[\frac{-e^{-\frac{k}{2}} r^2 + \sqrt{\left(e^{-\frac{k}{2}}\right)^2 r^4 + 16 r^2 c_2^2 c_4 + 16 c_2^2}}{4(c_2 (c_4 r^2 + 1))} \right]}}{2c_2 c_3}.$$

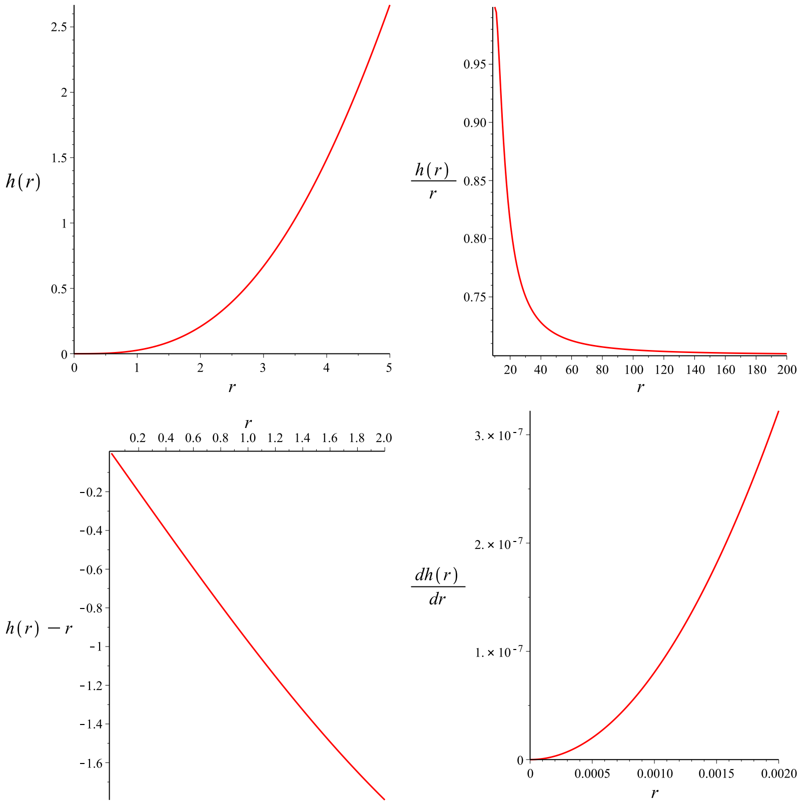

Figure 4.11: Plots of $h(r)$, $\frac{h(r)}{r}$, $h(r)-r$ and $\frac{dh(r)}{dr}$ versus r for $c_2 = 30$, $c_3 = -0.5$, $c_4 = -0.0095$ and $k = -0.08$.

Figure **4.11** shows graphical behavior of the shape function. In upper panel, the left plot shows positively increasing shape function satisfying $h(r) < r_0$ while the right plot represents asymptotic flat behavior as $\frac{h(r)}{r} \to 0$ with $r \to \infty$. In the lower face, the left plot identifies WH throat at $r_0 = 0.001$ and the right plot yields $\frac{dh(r_0)}{dr} < 1$. Figure **4.12** exhibits energy density as positively increasing. For the existence of realistic WH, we substitute constant red-shift function and $\hat{b}(r)$ from Eq.(4.2.13) in (4.1.6), it follows that

$$\rho_{eff} + p_{eff} = \frac{rh'(r) - h(r)}{r^3}.$$

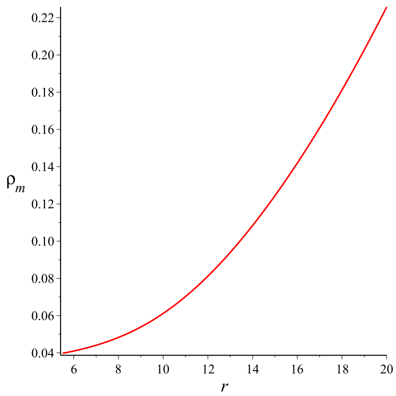

Figure 4.12: Evolution of ρ_m versus r.

Using flaring-out condition, this implies that $\rho_{eff} + p_{eff} < 0$, i.e., NEC is violated for effective stress-energy tensor. This indicates the presence of repulsive gravity and consequently, assures the existence of physically viable traversable WH.

Case II: $\hat{a}(r) = -k/r$

Here, Eq.(4.2.12) gives

$$\begin{aligned} \hat{b}(r) &= 2\ln[(e^{\frac{k}{2r}}r^3 + \{e^{\frac{k}{r}}r^6 + 16r^4c_4c_2^2 + 16r^3c_4c_2^2k + 16c_2^2r^2 + 16c_2^2rk\}^{\frac{1}{2}}) \\ &\times (4\left(c_2r\left(c_4r^2+1\right)\right))^{-1}]. \end{aligned} \tag{4.2.14}$$

The corresponding shape function turns out to be

$$\begin{aligned} h(r) &= (2r^2(e^{k/r}r^5 + (e^{\frac{k}{2r}}r^2\{r(e^{k/r}r^5 + 16c_4c_2^2r^3 + 16c_4c_2^2kr^2 + 16c_2^2r \\ &+ 16kc_2^2)\}^{\frac{1}{2}} - 8c_4c_2^2r^3) + 8c_4c_2^2kr^2 + (8kc_2^2 - 8c_2^2r^5c_4^2)))/(e^{\frac{k}{2r}}r^3 \\ &+ \sqrt{r(e^{k/r}r^5 + 16c_4c_2^2r^3 + 16c_4c_2^2kr^2 + 16c_2^2r + 16kc_2^2)})^2. \end{aligned}$$

Figure **4.13** implies that $h(r)$ preserves its positivity with $h(r) < r$ while far from throat, the shape of WH is found to be asymptotic flat in the upper face. The left

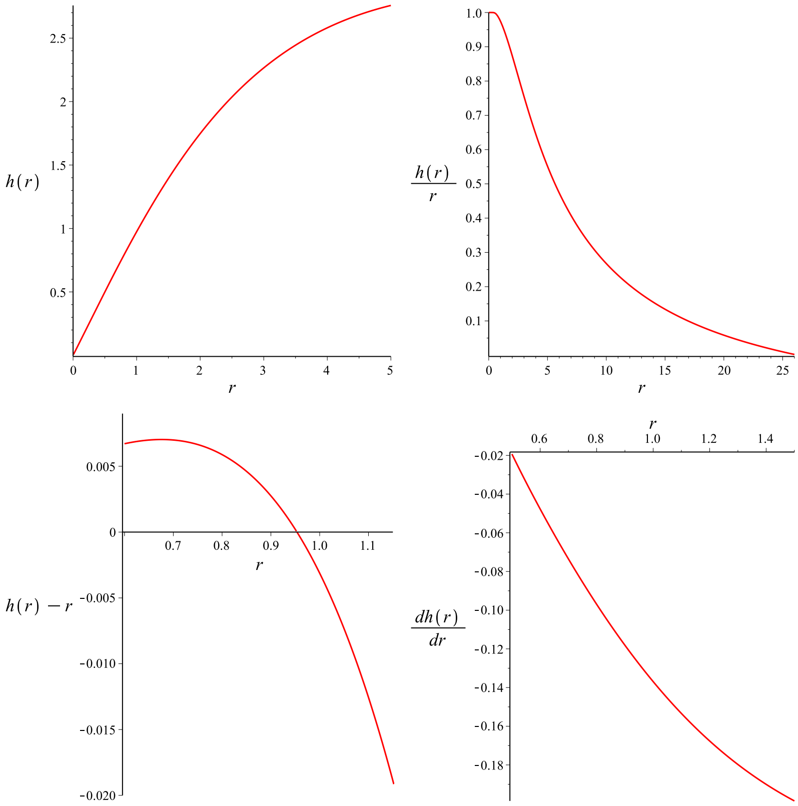

Figure 4.13: Plots of $h(r)$, $\frac{h(r)}{r}$, $h(r)-r$ and $\frac{dh(r)}{dr}$ versus r for $c_2=0.5$, $c_3=0.5$, $c_4=1.1$ and $k=5$.

plot of the lower face locates WH throat at $r_0=0.95$ and the corresponding right plot indicates that $\frac{dh(r_0)}{dr}<1$. To investigate the presence of traversable WH, we insert Eq.(4.2.14) in (4.1.6) yielding

$$\begin{aligned}
\rho_{eff}+p_{eff} &= (64(((e^{\frac{k}{2r}}r^{\frac{7}{2}}(e^{k/r}r^5+16c_4c_2^2r^3+16c_4c_2^2kr^2+16c_2^2r+16kc_2^2)^{\frac{1}{2}}\\
&- 8c_4^2c_2^2r^6)-8c_4c_2^2r^3k)+4c_4^2k^2r^4c_2^2+(8c_4k^2r^2c_2^2-8c_4^2c_2^2kr^5)\\
&+ (e^{k/r}r^6-8r^4c_4c_2^2)+4k^2c_2^2)(c_4r^2+1)c_2^2)/((e^{\frac{k}{2r}}r^3+(r(e^{k/r}r^5\\
&+ 16c_4c_2^2r^3+16c_4c_2^2kr^2+16c_2^2r+16kc_2^2)^{\frac{1}{2}}))^3(r(e^{k/r}r^5+16c_4c_2^2\\
&\times r^3+16c_4c_2^2kr^2+16c_2^2r+16kc_2^2))^{\frac{1}{2}}).
\end{aligned}$$

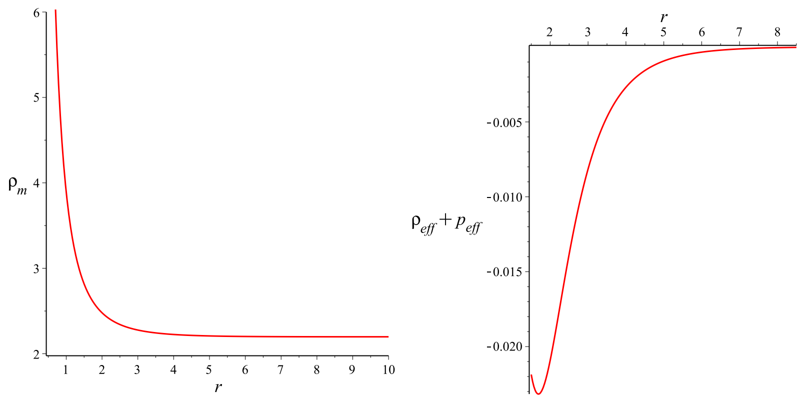

Figure 4.14: Plots of ρ_m and $\rho_{eff}+p_{eff}$ versus r.

Figure **4.14** shows that density is positively decreasing while the effective energy density and pressure are negatively increasing such that $\rho_m \geq 0$ and $\rho_{eff}+p_{eff} \leq 0$. This indicates the violation of NEC by effective energy-momentum tensor leading to realistic traversable WH.

Non-Dust Case

In this case, we consider a particular relation between density and pressure such that $p_m(\hat{a},\hat{b},\hat{M}) = \omega\rho_m(\hat{a},\hat{b},\hat{M})$ and solve Eq.(B34) which yields

$$\rho_m = -\frac{e^{\frac{-\hat{a}-\hat{b}}{2}}}{2c_2(6\omega c_6+\omega-2c_6))}, \quad \Lambda(T) = -\frac{g(T)}{2}+c_3T+c_4, \tag{4.2.15}$$

where c_6 denotes arbitrary constant. Here, symmetry generators remain the same as for dust case but the corresponding conserved integral gives

$$\begin{aligned}
\Sigma_1 &= -e^{\frac{\hat{a}-\hat{b}}{2}}r^2\left[e^{\hat{b}}\left(2c_4+\frac{2}{r^2}+\frac{e^{\frac{-\hat{a}-\hat{b}}{2}}(2c_3(3\omega-1)+1)}{2c_2(6\omega c_6+\omega-2c_6)}\right)+\frac{2+2\hat{a}'r}{r^2}\right],\\
\Sigma_2 &= r+c_2e^{\frac{\hat{a}-\hat{b}}{2}}r\left[e^{\hat{b}}\left(2c_4+\frac{2}{r^2}+\frac{e^{\frac{-\hat{a}-\hat{b}}{2}}(2c_3(3\omega-1)+1)}{2c_2(6\omega c_6+\omega-2c_6)}\right)+\frac{2+2\hat{a}'r}{r^2}\right].
\end{aligned}$$

Inserting Eq.(4.2.15) in (4.2.6), we obtain

$$e^{\hat{b}(r)}=\frac{2(1+\hat{a}'r)c_{2}}{2c_{4}r^{2}c_{2}+2c_{2}+e^{-\frac{\hat{a}(r)}{2}-\frac{\hat{b}(r)}{2}}r^{2}}. \tag{4.2.16}$$

Case I: $\hat{a}(r)=k$

For this case, Eq.(4.2.16) yields

$$\hat{b}(r)=2\ln\left[\frac{-e^{-\frac{k}{2}}r^{2}+\sqrt{e^{-k}r^{4}+16c_{4}r^{2}c_{2}^{2}+16c_{2}^{2}}}{4c_{2}(c_{4}r^{2}+1)}\right]. \tag{4.2.17}$$

The associated shape function takes the form

$$\begin{aligned} h(r) &= -[2r^{3}(-e^{-k}r^{2}+e^{-\frac{k}{2}}\sqrt{e^{-k}r^{4}+16c_{4}r^{2}c_{2}^{2}+16c_{2}^{2}}+8c_{2}^{2}c_{4}+8c_{2}^{2}c_{4}^{2}r^{2})] \\ &\times (e^{-\frac{k}{2}}r^{2}-\sqrt{e^{-k}r^{4}+16c_{4}r^{2}c_{2}^{2}+16c_{2}^{2}})^{-2}. \end{aligned}$$

Inserting Eq.(4.2.17) in (4.2.15), we obtain

$$\rho_{m}=\frac{e^{-\frac{k}{2}-\ln\left[\frac{-e^{-\frac{k}{2}}r^{2}+\sqrt{e^{-k}r^{4}+16c_{4}r^{2}c_{2}^{2}+16c_{2}^{2}}}{4c_{2}(c_{4}r^{2}+1)}\right]}}{c_{2}(6\omega c_{6}+\omega-2c_{6})}. \tag{4.2.18}$$

The upper plane of Figure **4.15** indicates that $h(r)$ remains positive but it does not preserve asymptotic flat shape. In lower face, the left plot identifies WH throat at $r_{0}\approx 0.001$ and the right plot satisfies $h'(r_{0})<1$. Figure **4.16** shows that ρ_{m} and $\rho_{m}+p_{m}$ are positively increasing for $1\leq\omega\leq 0.3$ while $\rho_{eff}+p_{eff}<0$ in this case. Therefore, a realistic traversable WH solution exists.

Case II: $\hat{a}(r)=-k/r$

For variable red-shift function, Eq.(4.2.16) leads to

$$\hat{b}(r) = \ln[(e^{k/r}r^{5}+8c_{2}^{2}k+8c_{2}^{2}r^{3}c_{4}+e^{\frac{k}{2r}}r^{5/2}(e^{k/r}r^{5}+16kc_{2}^{2}+16c_{2}^{2}r$$

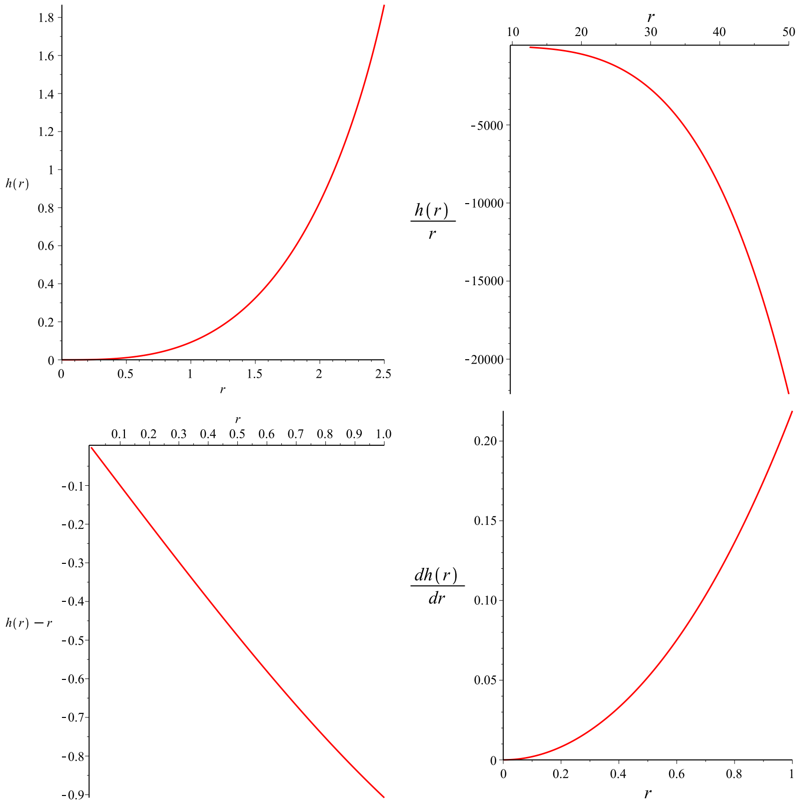

Figure 4.15: Plots of $h(r)$, $\frac{h(r)}{r}$, $h(r) - r$ and $\frac{dh(r)}{dr}$ versus r for $c_2 = 5$, $c_4 = -0.15$, $c_6 = 0.5$ and $k = 1$.

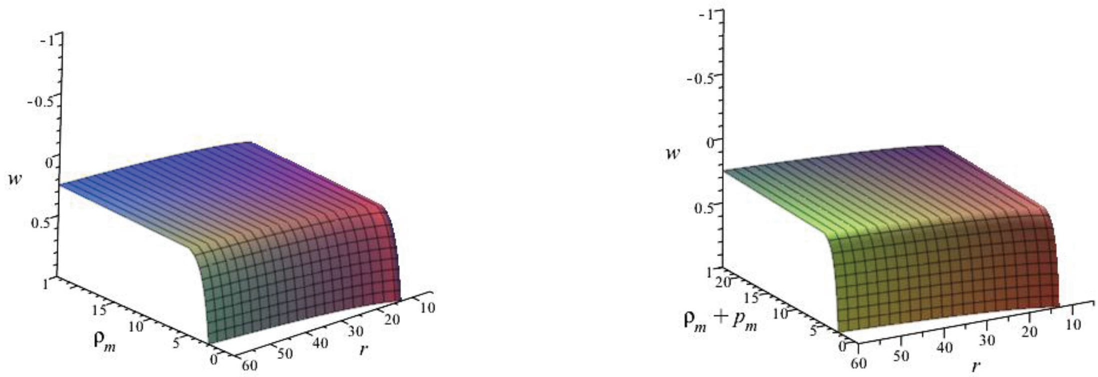

Figure 4.16: Plots of ρ_m and $\rho_m + p_m$ versus r.

$$+ \quad 16c_2^2kr^2c_4 + 16c_2^2r^3c_4)^{\frac{1}{2}})\{8rc_2^2(1+2r^2c_4+r^4r^2c_4+r^4c_4^2)\}^{-1}]. \tag{4.2.19}$$

The corresponding shape function is

$$\begin{aligned} h(r) &= [(e^{k/r}r^5 + 8c_2^2k + (8c_2^2kr^2c_4 - 8c_2^2r^3c_4) + (e^{\frac{k}{2r}}r^{5/2}\{e^{k/r}r^5 + 16c_2^2k \\ &+ 16c_2^2r + 16c_2^2kr^2c_4 + 16c_2^2r^3c_4\}^{\frac{1}{2}} - 8c_2^2r^5c_4^2))r]/(e^{k/r}r^5 + 8c_2^2k + 8c_2^2r \\ &+ 8c_2^2kr^2c_4 + 8c_2^2r^3c_4 + e^{\frac{k}{2r}}r^{5/2}\{e^{k/r}r^5 + 16c_2^2k + 16c_2^2r + 16c_2^2kr^2c_4 \\ &+ 16c_2^2r^3c_4\}^{\frac{1}{2}}). \end{aligned}$$

Figure **4.17** indicates that $h(r) < r$, $\frac{h(r)}{r} \to 0$ as $r \to \infty$, the minimum radius of throat is located at $r_0 = 1$ with $h'(r_0) < 1$. We insert Eq.(4.2.19) in (4.1.6) and (4.2.15) which leads to graphical interpretation of energy density and pressure with respect to perfect fluid and effective energy-momentum tensor. Figure **4.18** shows that $\rho_m \geq 0$ and $\rho_m + p_m \geq$ for $1 \leq \omega \leq 0.3$ while $\rho_{eff} + p_{eff} < 0$ for $1 \leq \omega \leq -1$. Thus, a realistic traversable WH exists for variable red-shift function in non-dust distribution.

4.2.2 $f(R,T) = f(R) + g(T)$

Now we consider a general $f(R,T)$ model appreciating indirect non-minimal curvature-matter coupling. We specify $f(R)$ as follows

$$f(R,T) = R + \mu R^2 + \nu R^n + g(T), \quad n \geq 3, \tag{4.2.20}$$

where μ and ν are arbitrary constants. We solve the system (B15)-(B33) for both dust as well as non-dust distributions and discuss WH geometry for constant and variable red-shift function.

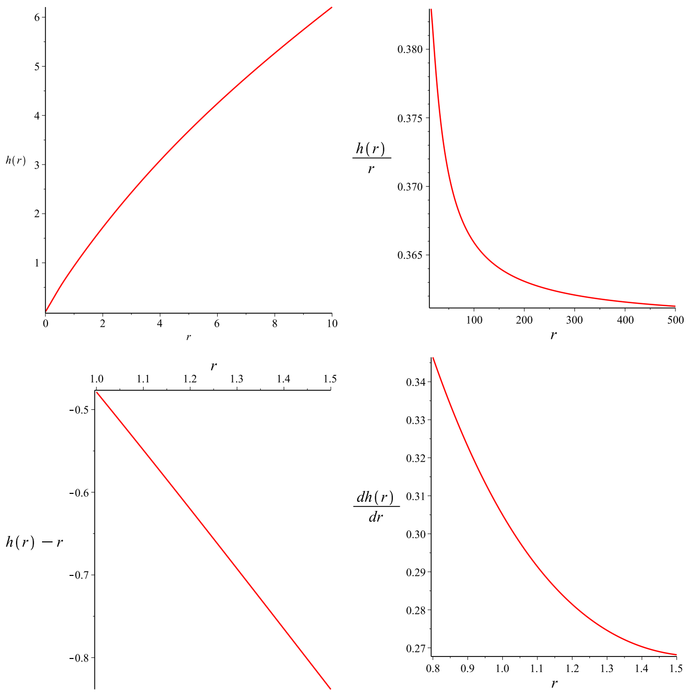

Figure 4.17: Plots of $h(r)$, $\frac{h(r)}{r}$, $h(r)-r$ and $\frac{dh(r)}{dr}$ versus r for $c_2 = 4$, $c_4 = 0.1$, $c_6 = 0.5$, and $k = 1$.

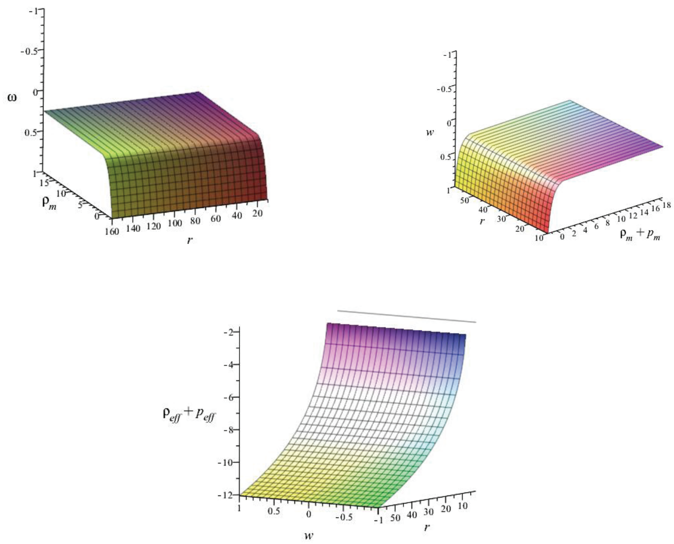

Figure 4.18: Plots of ρ_m, $\rho_m + p_m$ and $\rho_{eff} + p_{eff}$ versus r for $c_2 = 4$, $c_4 = 0.1$, $c_6 = 0.5$ and $k = 1$.

Dust Case

In this case, we solve the system (B15)-(B34) and obtain

$$\begin{aligned}
\alpha &= d_1, \quad \beta = d_1 - 2d_4, \quad \gamma = 0, \quad \delta = 0, \quad \eta = 0, \quad \tau = d_4 r, \quad B = d_5,\\
\rho_m &= e^{-\hat{a}} r^2 - \frac{1}{d_2 r^2}[-\nu R^n r^2 + \nu R^n n r^2 - 2\nu R^(- 1 + n)n + \mu r^2 R^2 - 4\mu R\\
&- 2 - r^2 d_3], \quad g(T) = d_2 T + d_3,
\end{aligned} \tag{4.2.21}$$

where d_l represents arbitrary constants. The symmetry generators and corresponding first integrals are found to be

$$\begin{aligned}
K_1 &= \frac{\partial}{\partial \hat{a}} + \frac{\partial}{\partial \hat{b}}, \quad K_2 = r\frac{\partial}{\partial r} - 2\frac{\partial}{\partial \hat{b}},\\
\Sigma_1 &= -e^{\frac{\hat{a}-\hat{b}}{2}} r[2(1 + \mu R + n\nu R^{n-1}) + rR'(2\mu + n(n-1)\nu R^{n-2})],\\
\Sigma_2 &= -e^{\frac{\hat{a}-\hat{b}}{2}} r[2e^{\hat{b}}(n-1)\nu R^{n-1} + 2(1 + \mu R + n\nu R^{n-1}) + 4rR'(2\mu + n\nu\\
&\times (n-1)R^{n-2})].
\end{aligned}$$

For $\hat{b}(r) = \ln\left(\frac{-r}{-r+h(r)}\right)$, Eq.(4.2.6) reduces to

$$-\frac{r}{(-r + h(r))} + \frac{(2(1 + 2\mu R))(1 + \hat{a}' r)e^{\hat{a}}}{r^4 d_2} = 0. \tag{4.2.22}$$

We solve this equation numerically for both $\hat{a}(r) = k$ and $\hat{a}(r) = -\frac{k}{r}$.

Case I: $\hat{a}(r) = k$

For constant red-shift function, we analyze the geometry of WH for both $n = 0$ as well as $n \neq 0$. Inserting Eq.(4.2.2) in (4.2.22) for $n = 0$, it follows that

$$\frac{r}{h(r) - r} - \frac{2e^k}{d_2 r^4}\left[2\mu\left(\left(\frac{2(h(r) - r)^2\left(\frac{r(h'(r) - 1)}{(h(r) - r)^2} - \frac{1}{h(r) - r}\right)}{r^3} - \frac{2(h(r) - r)}{r^3}\right)\right.\right.$$

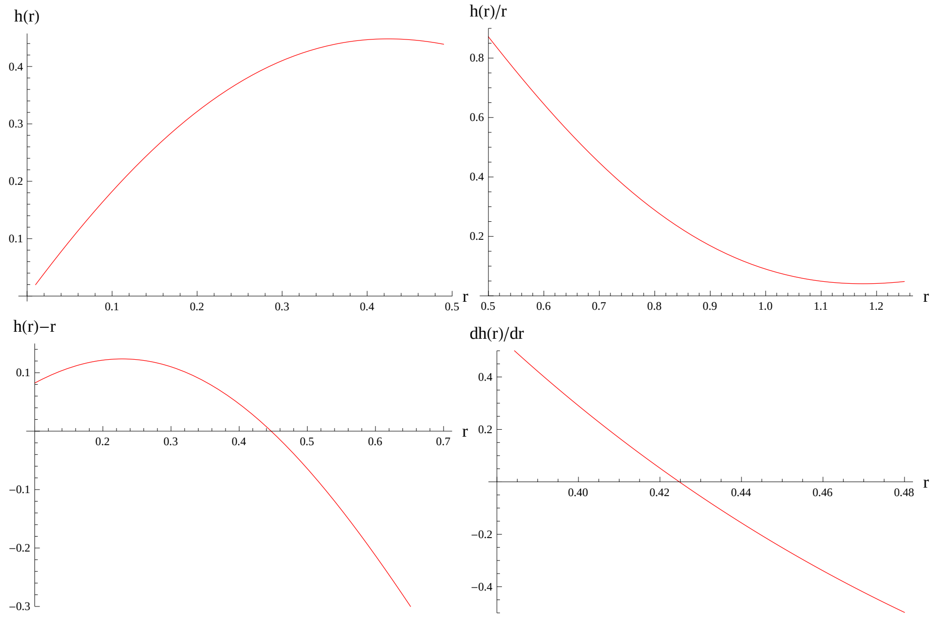

Figure 4.19: Plots of $h(r)$, $\frac{h(r)}{r}$, $h(r)-r$ and $\frac{dh(r)}{dr}$ versus r for $d_2 = 0.0001$, $d_3 = 1$, $\mu = 0.5$, $\nu = 0.1$ and $k = -0.15$.

$$+\frac{4(h(r)-r)}{r}+\frac{2}{r^2}\bigg)+1\bigg]=0. \tag{4.2.23}$$

We solve this equation for $h(r)$ and establish graphical analysis to study its geometrical properties. Figure **4.19** identifies that all WH conditions are satisfied as $h(r) < r$, $\frac{h(r)}{r} \to 0$, the minimum radius is $r_0 = 0.45$ with $h'(r_0) < 1$. Hence, $\rho_{eff} + p_{eff} < 0$ holds trivially while Figure **4.20** indicates that energy density remains positive.

For $n \neq 0$, Eq.(4.2.22) reduces to

$$\frac{r}{-r+h(r)}-\frac{2e^k}{r^4 d_2}\Bigg(2\mu\bigg(\frac{4(-r+h(r))}{r}+\bigg(\frac{2(-r+h(r))^2}{r^3}\bigg(-\frac{1}{-r+h(r)} + \frac{r(-1+h'(r))}{(-r+h(r))^2}\bigg)-2(-r+h(r))\bigg)+\frac{2}{r^2}\bigg)+n\nu\bigg(\frac{4(-r+h(r))}{r}+\frac{2}{r^2} + \bigg(\frac{2\left(-\frac{1}{-r+h(r)}+\frac{r(-1+h'(r))}{(-r+h(r))^2}\right)(-r+h(r))^2}{r^3}-\frac{2(-r+h(r))}{r^3}\bigg)\bigg)^{-1+n}\Bigg)$$

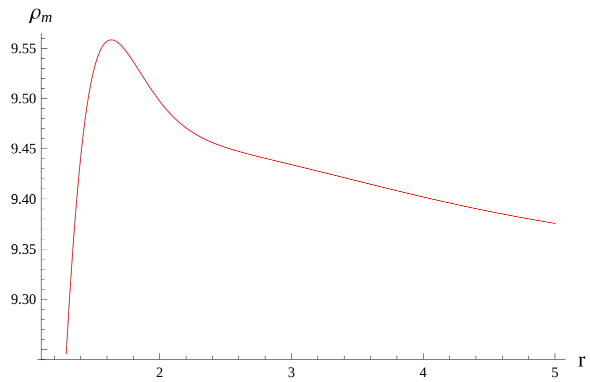

Figure 4.20: Evolution of ρ_m versus r.

$$-\frac{2e^k}{r^4 d_2} = 0. \tag{4.2.24}$$

The numerical solution of $h(r)$ provides two roots for $n = 3$ as shown in Figure **4.21**. The left plot of upper face represents that both roots remain positive with $h(r) < r$ while the right plot identifies asymptotic flat shape of WH. The lower plot locates the corresponding throat at $r_0 = 0.424$ (red) and $r_0 = 0.36$ (blue).

Case II: $\hat{a}(r) = -k/r$

For $n = 0$, Eq.(4.2.22) gives

$$\begin{aligned}
&\frac{r}{h(r)-r} + \frac{(r+k)e^{-\frac{k}{r}}}{r^5 d_2}\left(1 + 2\mu\left(\frac{k^2(-r+h(r))}{2r^5} + \frac{4(-r+h(r))}{r} + \frac{2}{r^2}\right.\right.\\
&+ \frac{k\left(-\frac{1}{-r+h(r)} + \frac{r(-1+h'(r))}{(-r+h(r))^2}\right)(-r+h(r))^2}{2r^4} + \frac{2}{r^3}\left(\left(-\frac{1}{-r+h(r)}\right.\right.\\
&\left.\left.\left.\left.+ \frac{r(-1+h'(r))}{(-r+h(r))^2}\right)(-r+h(r))^2 - (-r+h(r))\right)\right)\right) = 0.
\end{aligned} \tag{4.2.25}$$

The numerical solution of this equation is shown in Figure **4.22** which shows that all geometrical conditions of WH are preserved as $h(r) < r$, $\frac{h(r)}{r} \to 0$, WH throat is located at $r_0 = 0.45$ with $h'(r_0) < 1$. Figure **4.23** shows that $\rho_m > 0$ and $\rho_{eff} +$

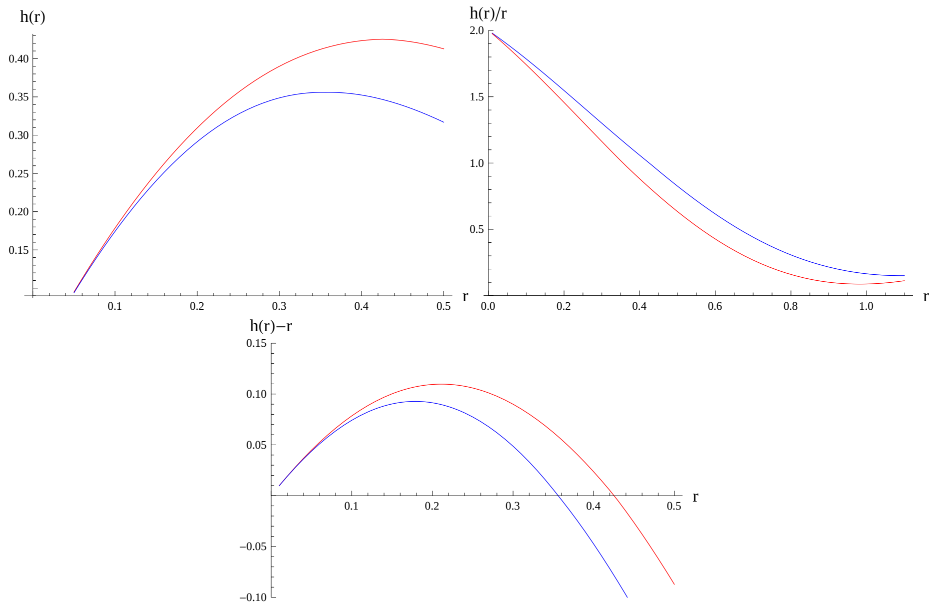

Figure 4.21: Plots of $h(r)$, $\frac{h(r)}{r}$ and $h(r) - r$ versus r for $d_2 = -0.0001$, $d_3 = 1$, $\mu = 0.08$, $\nu = -3.5$, $k = 0.5$ and $n = 3$.

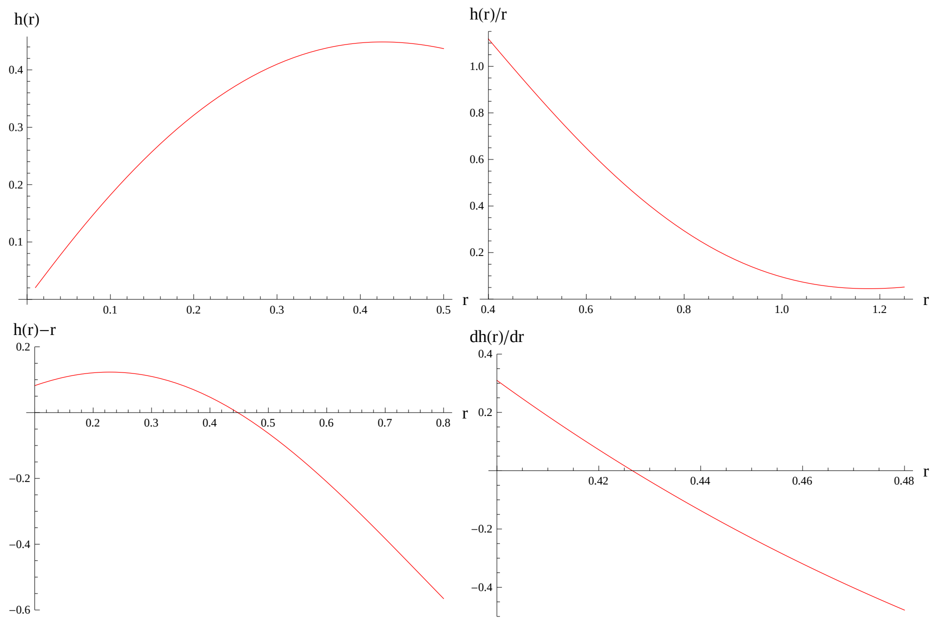

Figure 4.22: Plots of $h(r)$, $\frac{h(r)}{r}$, $h(r) - r$ and $\frac{dh(r)}{dr}$ versus r for $d_2 = 0.0001$, $d_3 = 1$, $\mu = 0.5$, $\nu = 0.1$ and $k = 0.01$.

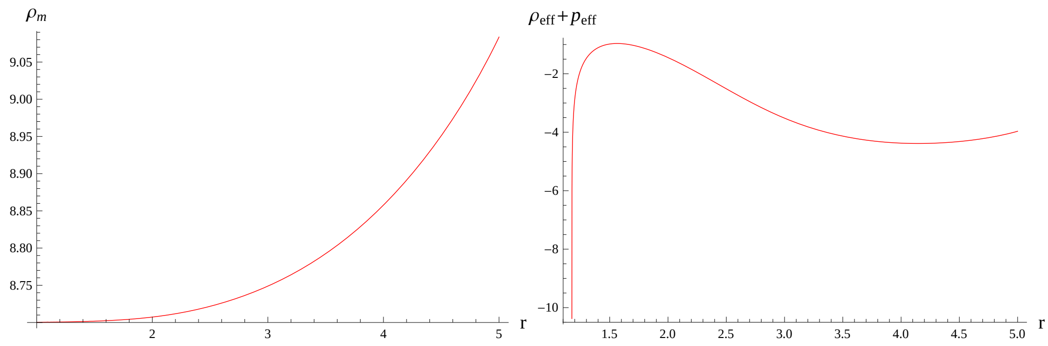

Figure 4.23: Evolution of ρ_m and $\rho_{eff} + p_{eff}$ versus r.

$p_{eff} < 0$ ensuring the violation of NEC for effective energy-momentum tensor yielding physically acceptable traversable WH.

When $n \neq 0$, Eq.(4.2.22) takes the following form

$$\frac{r}{-r+h(r)} - \frac{2(r+k)e^{-\frac{k}{r}}}{r^5 d_2}\left(1+2\mu\left(\frac{k^2(-r+h(r))}{2r^5}+\frac{4(-r+h(r))}{r}+\frac{2}{r^2}\right.\right.$$
$$+\frac{k\left(-\frac{1}{-r+h(r)}+\frac{r(-1+h'(r))}{(-r+h(r))^2}\right)(-r+h(r))^2}{2r^4}+\frac{2(-r+h(r))}{r^3}\left((-r+h(r))\right.$$
$$\left.\left.\times\left(-\frac{1}{-r+h(r)}+\frac{r(-1+h'(r))}{(-r+h(r))^2}\right)-1\right)\right)+n\nu\left(\frac{k^2(-r+h(r))}{2r^5}+\frac{2}{r^2}\right.$$
$$+\frac{k\left(-\frac{1}{-r+h(r)}+\frac{r(-1+h'(r))}{(-r+h(r))^2}\right)(-r+h(r))^2}{2r^4}+\frac{4(-r+h(r))}{r}+\frac{2(-r+h(r))}{r^3}$$
$$\left.\times\left(\left(-\frac{1}{-r+h(r)}+\frac{r(-1+h'(r))}{(-r+h(r))^2}\right)(-r+h(r))-1\right)\right)^{-1+n}\Bigg)=0.$$

This yields two solutions of the shape function whose graphical analysis is established for $n = 3$. In Figure **4.24**, the upper left plot shows that both solutions of $h(r)$ preserve positive behavior with $h(r) < r$ while the corresponding right plot determines asymptotic flat shape of WH. The lower plot identifies minimum radius of WH at $r_0 = 0.35$ (red) and $r_0 = 0.25$ (blue).

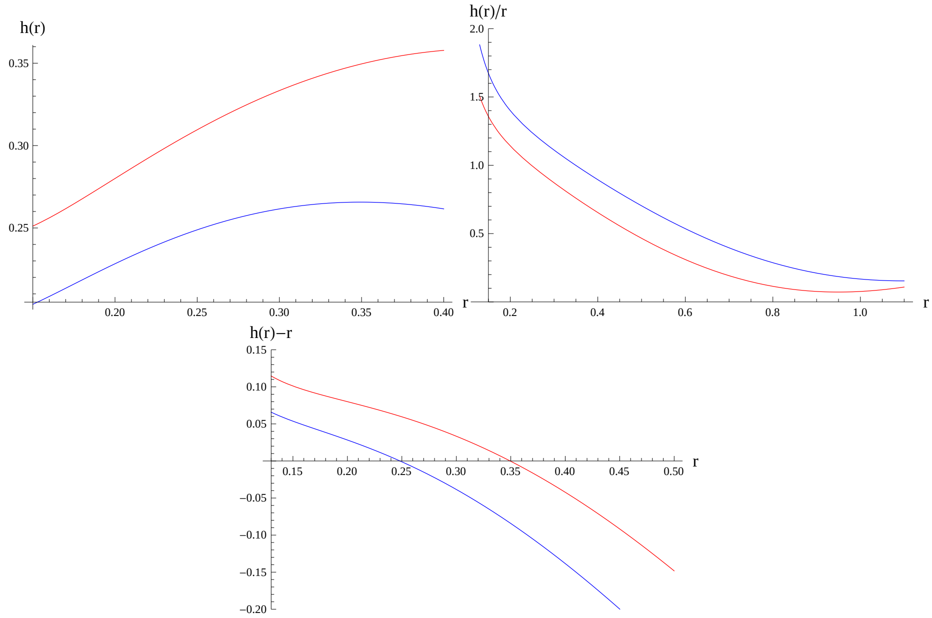

Figure 4.24: Plots of $h(r)$, $\frac{h(r)}{r}$ and $h(r)-r$ versus r for $d_2=-0.0001$, $d_3=1$, $\mu=0.08$, $\nu=-2$, $k=0.5$ and $n=3$.

Non-Dust Case

For perfect fluid, we consider $p_m=\omega\rho_m$ to evaluate symmetry generators and associated conserved quantities. Solving Eqs.(B15)-(B34), we obtain

$$\begin{aligned}\tau &= d_4, \quad B=d_5r, \quad \rho_m=\frac{1}{R((3d_2\omega-d_2)+\omega)r^2d_1}\Big[d_5e^{-\frac{\hat{a}(r)}{2}-\frac{\hat{b}(r)}{2}}\hat{a}(r)R\\ &+ \big(\big(\big(\big(R^3\mu r^2d_1-R\nu r^2d_1\big)-d_3(Rr)^2d_1\big)-2Rd_1\big)-4\mu R^2d_1\big)\Big]. \qquad (4.2.26)\end{aligned}$$

These coefficients lead to the following symmetry generators and conserved integral

$$\begin{aligned}K_1 &= \frac{\partial}{\partial\hat{a}}+\frac{\partial}{\partial\hat{b}}, \quad K_2=\frac{\partial}{\partial r}-2\frac{\partial}{\partial\hat{b}},\\ \Sigma_1 &= -e^{\frac{\hat{a}-\hat{b}}{2}}r[2(1+\mu R+n\nu R^{n-1})+rR'(2\mu+n(n-1)\nu R^{n-2})],\\ \Sigma_2 &= -e^{\frac{\hat{a}-\hat{b}}{2}}r^2[R+\mu R^2+\nu R^n+d_3+(2/r^2-R)(1+2\mu R+n\nu R^{n-1})\\ &- \frac{d_2}{R((3d_2\omega-d_2)+\omega)r^2d_1}\Big[\{(3\omega-1)+\omega\}(d_5e^{-\frac{\hat{a}(r)}{2}-\frac{\hat{b}(r)}{2}}\hat{a}(r)R\end{aligned}$$

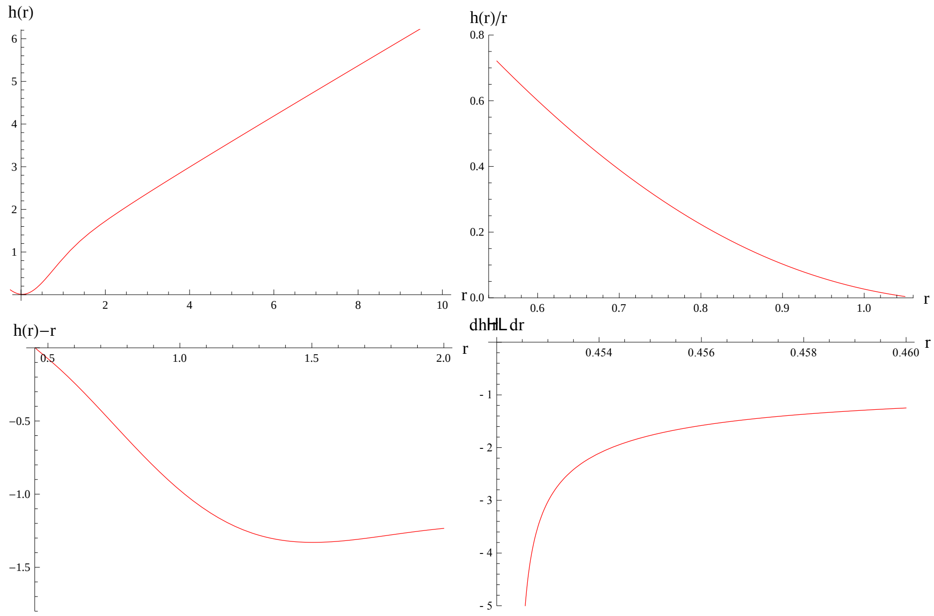

Figure 4.25: Plots of $h(r)$, $\frac{h(r)}{r}$, $h(r)-r$ and $\frac{dh(r)}{dr}$ versus r for $d_2=-1.5$, $d_3=1$, $d_5=-0.84$, $\mu=2.5$, $\nu=-1.1$, $k=0.01$ and $n=0$.

$$\begin{aligned} &+ \quad (((R^3\mu r^2 d_1 - R\nu r^2 d_1) - d_3(Rr)^2 d_1) - 2Rd_1) - 4\mu R^2 d_1)\big] + 2 \\ &\times \quad (1+\mu R + n\nu R^{n-1}) + 4rR'(2\mu + n\nu(n-1)R^{n-2})]. \end{aligned}$$

Substituting $\hat{b}(r) = \ln\left(\frac{-r}{-r+h(r)}\right)$ in Eqs.(4.2.6) and (4.2.22), we obtain Eq.(B35) provided in Appendix **B**. We solve this equation numerically for both forms of red-shift function.

Case I: $\hat{a}(r) = k$

The numerical solution of Eq.(B35) for $n=0$ leads to analyze WH conditions graphically. In Figure **4.25**, the upper left plot shows that $h(r)$ is positively increasing with $h(r) < r$ while the right plot assures asymptotic flat shape of WH. The lower left plot determines throat at the minimum radius, i.e., $r_0 = 0.456$ whereas the right plot preserves the derivative condition at throat as $h'(r_0) < 1$. We examine the behavior of

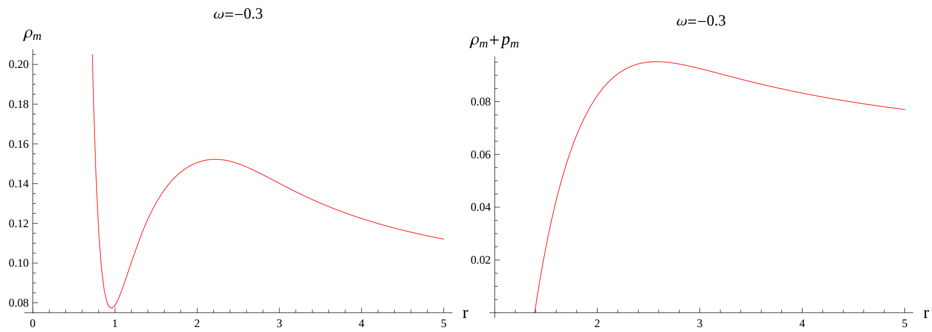

Figure 4.26: Plots of ρ_m and $\rho_m + p_m$ versus r.

energy density and pressure of perfect fluid for $\omega = -0.3$ in Figure **4.26**. Both plots indicate that NEC and WEC are preserved while NEC is trivially violated for the effective energy-momentum tensor. Consequently, there exists a realistic traversable WH for non-dust distribution.

Case II: $\hat{a}(r) = -k/r$

In Figure **4.27**, the left plot of upper panel represent positively increasing behavior of $h(r)$. The upper right plot indicates that WH appreciates asymptotic flat shape. The lower left plot identifies the minimum radius at WH throat, i.e., $r_0 = 0.35$ while the right plot shows that derivative condition is satisfied at throat $h'(r_0) < 1$. Both upper plots of Figure **4.28** represent that NEC and WEC are recovered. For variable red-shift function, the violation of NEC relative to effective energy-momentum tensor is analyzed in lower plot. Thus, the existence of a realistic traversable WH is possible for non-dust distribution with $n = 0$.

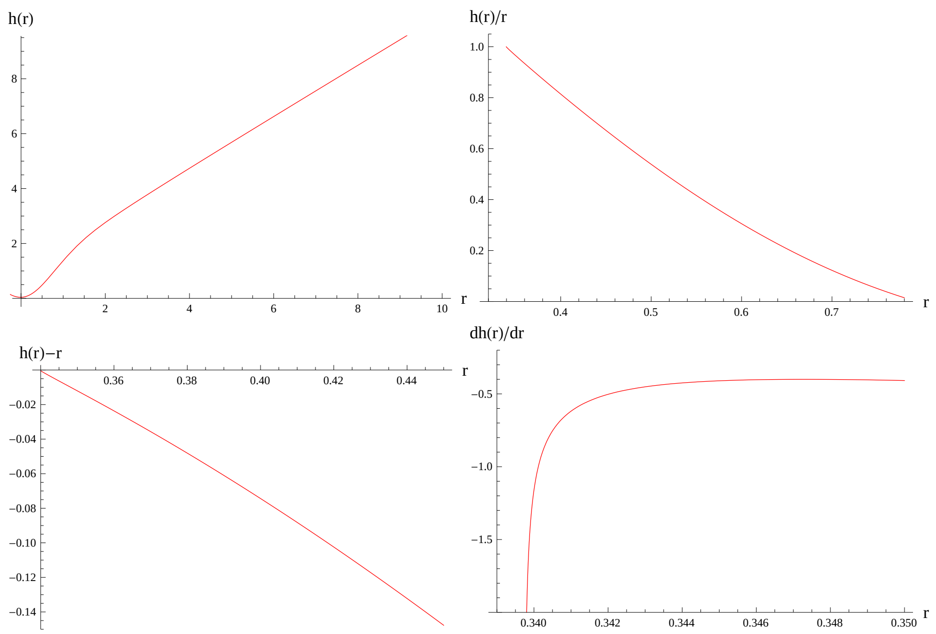

Figure 4.27: Plots of $h(r)$, $\frac{h(r)}{r}$, $h(r)-r$ and $\frac{dh(r)}{dr}$ versus r for $d_2=-1.5$, $d_3=1$, $d_5=-0.84$, $d_6=-0.01$, $\mu=2.5$, $\nu=-1.1$, $k=0.01$ and $n=0$.

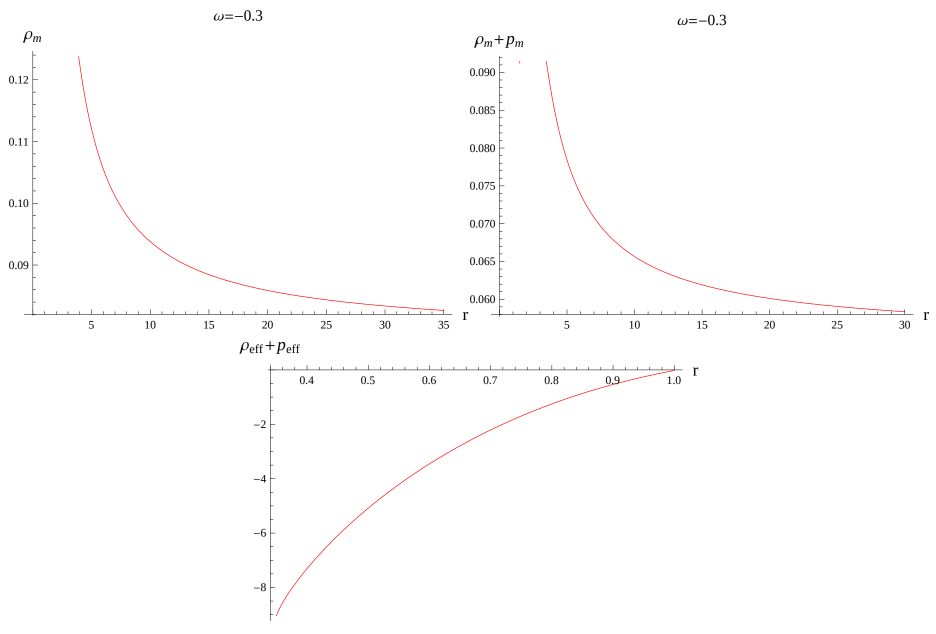

Figure 4.28: Evolution of ρ_m, ρ_m+p_m and $\rho_{eff}+p_{eff}$ versus r.

Chapter 5

Final Results

In this chapter, we summarize all the results obtained and finally provide some future lines of action.

Chapter 2 is devoted to investigate the dynamics of warm inflation for flat FRW universe model in $f(R)$ gravity. We have analyzed warm intermediate as well as logamediate inflationary model in weak and strong regimes for both constant and generalized dissipative coefficients. The results of warm intermediate inflationary model are summarized as follows.

- For weak constant dissipative regime, viable e-folds are obtained only when $0.626 \leq \bar{g} \leq 0.999$ whereas the corresponding tensor-scalar ratio is found to be compatible at the constrained value of scalar spectral index. For $\bar{g} = 0.9$, we have found $\mathrm{T} \gg \tilde{H}$ and $\tilde{r} \ll 1$ that verify the presence of inflaton in weak dissipative regime and inflationary model is found to be consistent with observational data.

- For strong constant dissipative regime, the number of e-folds remains less than 20 for $0.71 \leq \bar{g} \leq 0.89$ while the corresponding graphical behavior of $\mathcal{R} - n_s$ leads to compatible range of $\mathcal{R}$, i.e., $\mathcal{R} < 0.10$. At $\bar{g} = 0.89$, the temperature of thermal bath radiations is found to be greater than Hubble parameter which leads to the existence of warm inflation and $\tilde{r} \gg 1$ indicates that inflaton particles lie in strong dissipative regime.

- In case of weak dissipative regime, inflationary model is compatible for $m = 0,\ 1,\ -1$ when $0.59 < \bar{g} < 1,\ 0.67 < \bar{g} < 1,\ 0.55 < \bar{g} < 1$ ranges, respectively. For generalized dissipative coefficient in strong dissipative regime, the inflationary model yields consistent results with Planck constraints when $m = 0,\ 1,\ -1$ with $0.5 < \bar{g} < 1,\ 0.67 < \bar{g} < 1,\ 0.88 < \bar{g} < 1$ ranges, respectively.

It is worth mentioning here that for $m = 3$, the condition of model parameter is violated, i.e., $0 < \bar{g} < 1$ leading to inconsistent behavior of inflationary model in weak and strong dissipation regimes.

The summary of results for different values of logamediate model parameter $\bar{\beta}$ is given as follows.

- For weak constant dissipative regime, the e-folds are found in abundance to resolve flatness and horizon issues whereas the corresponding tensor-scalar ratio is compatible at the constrained value of scalar spectral index . For $1.5 \leq \bar{\beta} \leq 3.5$, we have found T $\gg \tilde{H}$ and $\tilde{r} \ll 1$ which verify the necessary condition of warm inflation and also describe the existence of inflaton particles in weak dissipative regime. This analysis implies that logamediate inflationary model is found to be consistent with observational data.

- For strong constant dissipative regime, the number of e-folds remains less than 20 for $2 \leq \bar{\beta} \leq 2.7$ while the corresponding graphical behavior of $\mathcal{R} - n_s$ leads to compatible range of $\mathcal{R}$, i.e., $\mathcal{R} < 0.10$ in the same range. The temperature of thermal bath radiations is found to be greater than Hubble parameter which leads to the existence of warm inflation and $\tilde{r} \gg 1$ indicates that inflaton particles lie in strong dissipative regime for the proposed range of $\bar{\beta}$.

- For generalized dissipative coefficient in weak dissipative regime, the inflationary model yields consistent results with Planck constraints for $m = 0,\ 1$ with $1.1 \leq \bar{\beta} \leq 4.5$. For $m = -1$, the existence of warm inflation is verified in this range but $\tilde{r}$ is not found to be constrained at $n_s = 0.9603$ which violates the condition of weak dissipative regime. In case of strong dissipative regime, inflationary model yields compatible results for $m = 0,\ 1,\ -1$ with $1.1 \leq \bar{\beta} \leq 3.5$ but $\tilde{r} \gg 1$ in $1.1 \leq \bar{\beta} \leq 1.9$.

In **Chapter 3**, we have analyzed the presence of Noether symmetry of flat FRW and BI universe models for two $f(R,T)$ models. We have formulated Noether symmetry generators, corresponding conserved quantities, matter contents $(p_m,\ \rho_m)$ as well as particular forms of $g(T)$ for $R+2g(T)$ and $f_0R^n+g(T)$ models. Both models explore symmetries of BI model in the absence of boundary term while the second model provides symmetries and conserved quantities of both isotropic and anisotropic models with non-zero boundary term. The graphical behavior of scale factors indicate that the universe undergoes an expansion while cosmological parameters, i.e., Hubble and deceleration parameters correspond to accelerated cosmic expansion whereas EoS parameter identifies quintessence phase. The trajectory of r and s parameters indicates that the constructed $f(R,T)$ model corresponds to standard ΛCDM model.

We have also formulated Noether symmetry of generalized anisotropic homogeneous model in this gravity admitting minimal interactions with scalar field model. We have considered $f(R,T)$ models admitting direct and indirect curvature-matter coupling and formulated exact solutions for dust and perfect fluid distributions. The indirect curvature-matter coupling yields three symmetry generators with non-zero boundary term. The first generator defines translational symmetry in time yielding energy conservation whereas the second generates scaling symmetry. For the second model, we have found four conserved quantities relative to symmetry generators but only one generator provides scaling symmetry. In the absence of boundary term, the symmetry generator of first model assures the existence of scaling symmetry for dust as well as perfect fluid while we have found two symmetry generators for the second model.

We have also evaluated exact solutions for dust and perfect fluid with vanishing boundary term in the background of indirect curvature-matter interactions. For dust fluid, we have found power-law solution whose graphical analysis leads to decelerating phase of the universe. The positively increasing scalar field and dominant kinetic energy ensure the decelerating behavior of cosmos for quintessence model. For phantom model, the scalar field rolls down positively and tends to increase negatively while kinetic energy dominates over potential energy. The graphical behavior of effective EoS parameter identifies a transition from radiation to DE era. For perfect fluid, we have found an oscillatory solution with increasing rate of Hubble parameter, negative deceleration parameter, $\omega_{eff} < -1$ and $s > 0$ with $r < 1$ indicating phantom phase. In this case, the scalar field increases negatively and potential energy dominates over kinetic energy leading to an epoch of accelerated expansion. Thus, power-law and oscillatory solutions of generalized anisotropic model characterize cosmic evolution from decelerated to current accelerated phase.

Chapter 4 studies static wormhole solutions via Noether symmetry approach in $f(R)$ and $f(R,T)$ theories for constant as well as variable red-shift functions. For constant ($\hat{a}'=0$) and variable red-shift function ($\hat{a}'\neq 0$), we have found that particular form of $f(R)$ satisfies stability conditions while shape function preserves all geometric properties, i.e., $h(r)>0$, $\frac{dh(r)}{dr}<1$ at $r=r_0$ and asymptotic flat geometry. The violation of NEC (using effective energy-momentum tensor) assures the presence of repulsive nature of gravity for both forms of red-shift function whereas the validity of NEC and WEC identifies ordinary matter when $\hat{a}'\neq 0$. These energy bounds confirm the presence of a physically viable WH solution for variable red-shift function. We have also formulated symmetry generator, corresponding first integral and WH solutions for $f(R)$ power-law model. When $\hat{a}'(r)=0$, we have established graphical analysis of traversable WH conditions for $n=1/2$, $n=2$ and $n=4$. In this case, the shape function is found to preserve all conditions and $\rho_{eff}+p_{eff}<0$ assures the violation of NEC identifying the existence of exotic matter at throat. For $\hat{a}'\neq 0$, we have found a complicated form of the shape function.

For the first $f(R,T)$ model (admitting a correspondence with ΛCDM model) with $\hat{a}'=0$, WH solution satisfies all geometric conditions for dust distribution whereas in non-dust case, the asymptotic flatness is not achieved. The energy density corresponding to ordinary matter remains positive for both dust and non-dust cases while the violation of NEC on effective energy-momentum tensor trivially holds. Thus, the repulsive gravitational effects appear at throat leading to traversable WH while the presence of ordinary matter leads to physically viable WH. When $\hat{a}'\neq 0$, we have considered $p_m=\omega\rho_m$ in non-dust case and all WH conditions hold for both fluid distributions. In dust case, we have $\rho_m\geq 0$ while $\rho_m,\ \rho_m+p_m\geq 0$ for non-dust case whereas $\rho_{eff}+p_{eff}\leq 0$ for both fluid distributions. These inequalities indicate that

WH is found to be traversable and physically acceptable.

For the second model, we have evaluated WH solutions for both $n = 0$ and $n = 3$. When $\hat{a}' = 0$ and $n = 0$, we have found that WH conditions are recovered while the validity of NEC and WEC specify ordinary matter for both fluids. When $\hat{a}' \neq 0$ with $n = 0$, we have found viable WH solutions for both dust as well as non-dust cases. The physical existence of WH is verified as $\rho_m \geq 0$ with $\rho_{eff} + p_{eff} \leq 0$ for dust distribution. For non-dust case, we have ρ_m, $\rho_m + p_m \geq 0$ and $\rho_{eff} + p_{eff} \leq 0$ except for $\omega = 1$. When $n \neq 0$ (dust fluid), we have found two solutions of shape function which admit $h(r) < r$, $h(r)/r \to 0$ and $h(r_0) = r_0$ for both constant as well as variable red-shift function. The summary for viable WH solutions corresponding is given in Table **5.1**.

Table 5.1: Viable WH solutions in $f(R,T)$ gravity.

Red-Shift Function	**Model I**	**Model II**
$\hat{a}(r) = k$	dust	dust & Non-dust, $n = 0$
$\hat{a}(r) = -k/r$	dust & Non-dust	dust & Non-dust, $n = 0$

Table **5.1** indicates that Noether symmetry approach leads to viable wormhole solutions in most of the cases.

It would be interesting to extend this work on the following lines.

- To analyze the role of anisotropic warm inflationary model with different fluids and scalar field models in Einstein frame representation of $f(R)$ theory.
- To discuss warm inflationary scenario with/without bulk viscosity in Einstein frame representation of modified theories.
- To investigate the existence of physically viable dynamical as well as non-dynamical WH with anisotropic fluid through Noether symmetry technique in

$f(R)$ and $f(R,T)$ theories.

- To discuss cosmic evolution from exact solutions of higher-dimensional isotropic as well as anisotropic universe models via Noether symmetry approach in more generalized non-minimally coupled modified theories minimally interacting with different DE/matter models.

- To explore the effect of charge in WH geometry with non-commutative geometrical background with/without Noether symmetry approach via different forms of shape and red-shift functions.

Appendix A

For Lagrangian (3.1.3) and vector field (3.1.11), the invariance condition (1.5.5) yields a system of equations as follows

$$(b\alpha,_{R} + 2a\beta,_{R})f_{RR} = 0, \tag{A1}$$

$$(b\alpha,_{T} + 2a\beta,_{T})f_{RT} = 0, \tag{A2}$$

$$2\beta,_{a} f_R + b\gamma,_{a} f_{RR} + b\delta,_{a} f_{RT} = 0, \tag{A3}$$

$$b\alpha,_{R} f_{RT} + b\alpha,_{T} f_{RR} + 2a\beta,_{R} f_{RT} + 2a\beta,_{T} f_{RR} = 0, \tag{A4}$$

$$2\beta f_{RR} + b\gamma f_{RRR} + b\delta f_{RRT} + b\alpha,_{a} f_{RR} + 2a\beta,_{a} f_{RR} + 2\beta,_{R} f_R + b\gamma,_{R} f_{RR} + b\delta,_{R} f_{RT} = 0, \tag{A5}$$

$$2\beta f_{RT} + b\gamma f_{RRT} + b\delta f_{RTT} + b\alpha,_{a} f_{RT} + 2a\beta,_{a} f_{RT} + 2\beta,_{T} f_R + b\gamma,_{T} f_{RR} + b\delta,_{T} f_{RT} = 0, \tag{A6}$$

$$2\beta f_R + 2b\gamma f_{RR} + 2b\delta f_{RT} + 2b\alpha,_{a} f_R + 2a\beta,_{a} f_R + 2b\beta,_{b} f_R + 2ab\gamma,_{a} f_{RR} + b^2\gamma,_{b} f_{RR} + 2ab\delta,_{a} f_{RT} + b^2\delta,_{b} f_{RT} = 0, \tag{A7}$$

$$2b\alpha f_{RR} + 2a\beta f_{RR} + 2ab\gamma f_{RRR} + 2ab\delta f_{RRT} + b^2\alpha,_{b} f_{RR} + 2b\alpha,_{R} f_R + 2ab \times\beta,_{b} f_{RR} + 2a\beta,_{R} f_R + 2ab\gamma,_{R} f_{RR} + 2ab\delta,_{R} f_{RT} = 0, \tag{A8}$$

$$2b\alpha f_{RT} + 2a\beta f_{RT} + 2ab\gamma f_{RRT} + 2ab\delta f_{RTT} + b^2\alpha,_{b} f_{RT} + 2b\alpha,_{T} f_R + 2ab \times\beta,_{b} f_{RT} + 2a\beta,_{T} f_R + 2ab\gamma,_{T} f_{RR} + 2ab\delta,_{T} f_{RT} = 0, \tag{A9}$$

$$\alpha f_R + a\gamma f_{RR} + a\delta f_{RT} + 2b\alpha,_{b} f_R + 2a\beta,_{b} f_R + 2ab\gamma,_{b} f_{RR} + 2ab\delta,_{b} \times f_{RT} = 0, \tag{A10}$$

$$b^2\alpha[f - Rf_R - Tf_T + f_T(3p_m - \rho_m) + p_m + a\{f_T(3p_m,_{a} - \rho_m,_{a}) + p_m,_{a}\}] + \beta[2ab \times(f - Rf_R - Tf_T + f_T(3p_m - \rho_m) + p_m) + ab^2\{f_T(3p_m,_{b} - \rho_m,_{b}) + p_m,_{b}\}] + ab^2 \times\gamma[-(Rf_{RR} + Tf_{RT}) + f_{RT}(3p_m - \rho_m)] + ab^2\delta[-(Rf_{RT} + Tf_{TT}) + f_{TT} \times(3p_m - \rho_m)] = 0. \tag{A11}$$

For invariance condition (1.5.2), the Lagrangian corresponding to flat FRW universe leads to

$$\tau_{,a}=0, \quad \tau_{,R}=0, \quad \tau_{,T}=0, \quad B_{,T}=0, \tag{A12}$$
$$n(n-1)f_0R^{n-2}a^2\alpha_{,R}=0, \tag{A13}$$
$$n(n-1)f_0a^2R^{n-2}\alpha_{,T}=0, \tag{A14}$$
$$2a\alpha_{,T}+(n-1)aR^{-1}\beta_{,T}=0, \tag{A15}$$
$$6n(n-1)f_0a^2R^{n-2}\alpha_{,t}=-B_{,R}, \tag{A16}$$
$$nf_0R^{n-1}[2a\alpha_{,t}+(n-1)a^2R^{-1}\beta_{,t}]=-B_{,a}, \tag{A17}$$
$$\alpha+(n-1)aR^{-1}\beta+2a\alpha_{,a}-a\tau_{,t}+(n-1)a^2R^{-1}\beta_{,a}=0, \tag{A18}$$
$$2(n-1)R^{-1}\alpha+(n-1)(n-2)aR^{-2}\beta+(n-1)aR^{-1}\alpha_{,a}+2\alpha_{,R}-(n-1)$$
$$\times aR^{-1}\tau_{,t}+(n-1)aR^{-1}\beta_{,R}=0, \tag{A19}$$
$$\alpha[3a^2\{f_0R^n(1-n)+g(T)-Tg(T)_{,T}+g(T)_{,T}(3p-\rho_m)+p_m\}+a^3\{g(T)_{,T}$$
$$\times(3p_{m,a}-\rho_{m,a})+p_{m,a}\}]-n(n-1)f_0a^3R^{n-1}\beta+a^3\gamma g(T)_{,TT}(3p_m-\rho_m-T)$$
$$+a^3\tau_{,t}\{f_0R^n(1-n)+g(T)-Tg(T)_{,T}+g(T)_{,T}(3p_m-\rho_m)+p_m\}=B_{,t}. \tag{A20}$$

For BI universe model, the invariance condition (1.5.2) yields

$$\tau_{,a}=0, \quad \tau_{,b}=0, \quad \tau_{,R}=0, \quad \tau_{,T}=0, \quad B_{,T}=0, \tag{A21}$$
$$(b\alpha_{,R}+2a\beta_{,R})n(n-1)f_0R^{n-2}=0, \tag{A22}$$
$$(b\alpha_{,T}+2a\beta_{,T})n(n-1)f_0R^{n-2}=0, \tag{A23}$$
$$2\beta_{,a}+(n-1)bR^{-1}\gamma_{,a}=0, \tag{A24}$$
$$2\beta_{,T}+(n-1)bR^{-1}\gamma_{,T}=0, \tag{A25}$$
$$b\alpha_{,T}+a\beta_{,T}+(n-1)abR^{-1}\gamma_{,T}=0, \tag{A26}$$
$$n(n-1)f_0R^{n-2}[2b^2\alpha_{,t}+4ab\beta_{,t}]=-B_{,R}, \tag{A27}$$
$$nf_0R^{n-1}[4b\beta_{,t}+2(n-1)b^2R^{-1}\gamma_{,t}]=-B_{,a}, \tag{A28}$$
$$nf_0R^{n-1}[4b\alpha_{,t}+4a\beta_{,t}+4(n-1)abR^{-1}\gamma_{,t}]=-B_{,b}, \tag{A29}$$
$$\alpha+(n-1)aR^{-1}\gamma+2b\alpha_{,b}+2a\beta_{,b}+2(n-1)abR^{-1}\gamma_{,b}-a\tau_{,t}=0, \tag{A30}$$
$$2\beta+2(n-1)bR^{-1}\gamma+2b\alpha_{,a}+2a\beta_{,a}+2b\beta_{,b}+2(n-1)abR^{-1}\gamma_{,a}$$
$$+(n-1)b^2R^{-1}\gamma_{,b}-2b\tau_{,t}=0, \tag{A31}$$
$$2(n-1)R^{-1}\beta+(n-1)(n-2)bR^{-2}\gamma+(n-1)bR^{-1}\alpha_{,a}+2\beta_{,R}$$
$$+2(n-1)aR^{-1}\beta_{,a}+(n-1)bR^{-1}\gamma_{,R}-(n-1)bR^{-1}\tau_{,t}=0, \tag{A32}$$

$$2(n-1)bR^{-1}\alpha+2(n-1)aR^{-1}\beta+2(n-1)(n-2)abR^{-2}\gamma+2b\alpha,_{R}$$
$$+(n-1)b^2R^{-1}\alpha,_{b}+2(n-1)abR^{-1}\beta,_{b}+2a\beta,_{R}+2(n-1)abR^{-1}\gamma,_{R}$$
$$-2(n-1)abR^{-1}\tau,_{t}=0, \tag{A33}$$
$$b^2\alpha[f_0R^n(1-n)+g(T)-Tg(T),_{T}+g(T),_{T}(3p_m-\rho_m)+p_m+a\{g(T),_{T}$$
$$\times(3p_{m},_{a}-\rho_{m},_{a})+p_{m},_{a}\}]+\beta[2ab(f_0R^n(1-n)+g(T)-Tg(T),_{T}+g(T),_{T}$$
$$\times(3p_m-\rho_m)+p_m)+ab^2\{g(T),_{T}(3p_{m},_{b}-\rho_{m},_{b})+p_{m},_{b}\}]-n(n-1)f_0ab^2R^{n-1}\gamma$$
$$+ab^2\delta g(T),_{TT}(3p_m-\rho_m-T)+ab^2\tau,_{t}\{f_0R^n(1-n)+g(T)-Tg(T),_{T}$$
$$+g(T),_{T}(3p_m-\rho_m)+p_m\}=B,_{t}. \tag{A34}$$

For invariance condition (1.5.2), the system of equations is

$$\epsilon ab^2\eta,_{t}=-B,_{\phi}, \tag{A35}$$
$$b\alpha+2a\beta+2ab\eta,_{\phi}-ab\tau,_{t}=0, \tag{A36}$$
$$2b\alpha,_{\phi}f_RR+4a\beta,_{\phi}f_RR+ab\epsilon\eta,_{R}=0, \tag{A37}$$
$$2b\alpha,_{\phi}f_RT+2a\beta,_{\phi}f_RT+ab\epsilon\eta,_{T}=0, \tag{A38}$$
$$4\beta,_{\phi}f_R+2b\gamma,_{\phi}f_{RR}+2b\delta,_{\phi}f_{RT}+ab\epsilon\eta,_{a}=0, \tag{A39}$$
$$4b\alpha,_{\phi}f_R+4a\beta,_{\phi}f_R+4ab\gamma,_{\phi}f_{RR}+4ab\delta,_{\phi}f_{RT}+ab^2\epsilon\eta,_{b}=0, \tag{A40}$$
$$\tau,_{a}f_R=0,\quad \tau,_{b}f_R=0,\quad \tau,_{R}f_{RR}=0,\quad \tau,_{T}f_{RT}=0,\quad \tau,_{\phi}=0, \tag{A41}$$
$$2b^2\alpha,_{t}f_{RR}+4ab\beta,_{t}f_{RR}=-B,_{R}, \tag{A42}$$
$$2b^2\alpha,_{t}f_{RT}+4ab\beta,_{t}f_{RT}=-B,_{T}, \tag{A43}$$
$$b\alpha,_{R}f_{RR}+2ab\beta,_{R}f_{RR}=0, \tag{A44}$$
$$b\alpha,_{T}f_{RT}+2ab\beta,_{T}f_{RT}=0, \tag{A45}$$
$$2\beta,_{a}f_R+b\gamma,_{a}f_{RR}+b\delta,_{a}f_{RT}=0, \tag{A46}$$
$$4b\beta,_{t}f_R+2b^2\gamma,_{t}f_{RR}+2b^2\delta,_{t}f_{RT}=-B,_{a}, \tag{A47}$$
$$4b\alpha,_{t}f_R+4a\beta,_{t}f_R+4ab\gamma,_{t}f_{RR}+4ab\delta,_{t}f_{RT}=-B,_{b}, \tag{A48}$$
$$b\alpha,_{T}f_{RR}+b\alpha,_{R}f_{RT}+2a\beta,_{T}f_{RR}+2a\beta,_{R}f_{RT}=0, \tag{A49}$$
$$\alpha f_R+a\gamma f_{RR}+a\delta f_{RT}+2b\alpha,_{b}f_R+2a\beta,_{b}f_R+2ab\gamma,_{b}f_{RR}+2ab\delta,_{b}f_{RT}$$
$$-a\tau,_{t}f_R=0, \tag{A50}$$
$$2\beta f_{RR}+b\gamma f_{RRR}+b\delta f_{RRT}+b\alpha,_{a}f_{RR}+2a\beta,_{a}f_{RR}+2\beta,_{R}f_R+b\gamma,_{R}f_{RR}$$
$$+b\delta,_{R}f_{RT}-b\tau,_{t}f_{RR}=0, \tag{A51}$$
$$2\beta f_{RT}+b\gamma f_{RRT}+b\delta f_{RTT}+b\alpha,_{a}f_{RT}+2a\beta,_{a}f_{RT}+2\beta,_{T}f_R+b\gamma,_{T}f_{RR}$$

$$+b\delta,_{T} f_{RT} - b\tau,_{t} f_{RT} = 0, \tag{A52}$$

$$2\beta f_R + 2b\gamma f_{RR} + 2b\delta f_{RT} + 2b\alpha,_{a} f_R + 4a\beta,_{a} f_R + 2b\beta,_{b} f_R + 2ab\gamma,_{a} f_{RR}$$
$$+b^2\gamma,_{b} f_{RR} + 2ab\delta,_{a} f_{RT} + b^2\delta,_{b} f_{RT} - 2b\tau,_{t} f_R = 0, \tag{A53}$$

$$2b\alpha f_{RR} + 2a\beta f_{RR} + 2ab\gamma f_{RRR} + 2ab\delta f_{RRT} + b^2\alpha,_{b} f_{RR} + 2b\alpha,_{R} f_R + 2ab$$
$$\times\beta,_{b} f_{RR} + 2a\beta,_{R} f_R + 2ab\gamma,_{R} f_{RR} + 2ab\delta,_{R} f_{RT} - 2ab\tau,_{t} f_{RR} = 0, \tag{A54}$$

$$2b\alpha f_{RT} + 2a\beta f_{RT} + 2ab\gamma f_{RRT} + 2ab\delta f_{RTT} + b^2\alpha,_{b} f_{RT} + 2b\alpha,_{T} f_R + 2ab$$
$$\times\beta,_{b} f_{RT} + 2a\beta,_{T} f_R + 2ab\gamma,_{T} f_{RR} + 2ab\delta,_{T} f_{RT} - 2ab\tau,_{t} f_{RT} = 0, \tag{A55}$$

$$b^2\alpha[f - Rf_R + f_T(3p_m - \rho_m - T) + p_m - V(\phi) + a\{f_T(3p_{m},_{a} - \rho_{m},_{a})$$
$$+p_{m},_{a}\} + 2\xi f_R] + \beta[2ab(f - Rf_R + f_T(3p_m - \rho_m - T) + p_m - V(\phi))$$
$$+ab^2\{f_T(3p_{m},_{b} - \rho_{m},_{b}) + p_{m},_{b}\}] + \gamma[-ab^2Rf_{RR} + 2a\xi f_{RR}] + \delta[-ab^2Rf_{RT}$$
$$+2a\xi f_{RT}] - ab^2V,_{\phi}\,\eta + \tau,_{t}[ab^2(f - Rf_R + f_T(3p_m - \rho_m - T) + p_m$$
$$-V(\phi)) + 2a\xi f_R] = B,_{t}\,. \tag{A56}$$

Appendix B

In $f(R)$ gravity, the invariance condition (1.5.2) and Lagrangian (4.1.8) yield

$$B,_{\hat{b}}=0,\quad \tau,_{\hat{a}}=0,\quad \tau,_{\hat{b}}=0,\quad \tau,_{\hat{M}}=0,\quad \tau,_{R}=0, \tag{B1}$$

$$e^{\frac{\hat{a}}{2}}(\gamma,_r f_R+\hat{M}\delta,_r f_{RR})=e^{\frac{\hat{b}}{2}}B,_{\hat{a}}, \tag{B2}$$

$$e^{\frac{\hat{a}}{2}}(\alpha,_r \hat{M}+2\gamma,_r)f_{RR}=e^{\frac{\hat{b}}{2}}B,_{R}, \tag{B3}$$

$$e^{\frac{\hat{a}}{2}}(\alpha,_r f_R+\gamma,_r \hat{M}^{-1}f_R+2\delta,_r f_{RR})=e^{\frac{\hat{b}}{2}}B,_{\hat{M}}, \tag{B4}$$

$$\gamma,_{\hat{a}} f_R+\hat{M}\delta,_{\hat{a}} f_{RR}=0, \tag{B5}$$

$$\gamma,_{\hat{b}} f_R+\hat{M}\delta,_{\hat{b}} f_{RR}=0, \tag{B6}$$

$$\alpha,_{\hat{b}} f_R+\gamma,_{\hat{b}} \hat{M}^{-1}f_R+2\delta,_{\hat{b}} f_{RR}=0, \tag{B7}$$

$$\hat{M}\alpha,_{\hat{b}} f_{RR}+2\gamma,_{\hat{b}} f_{RR}=0, \tag{B8}$$

$$\hat{M}\alpha,_{R} f_{RR}+2\gamma,_{R} f_{RR}=0, \tag{B9}$$

$$f_R(\alpha-\beta-2\gamma\hat{M}^{-1}+4\hat{M}\alpha,_{\hat{M}}+4\gamma,_{\hat{M}}-2\tau,_r)+f_{RR}(2\delta+8\hat{M}\delta,_{\hat{M}})=0, \tag{B10}$$

$$f_R(\alpha-\beta+2\alpha,_{\hat{a}}-2\tau,_r+2\gamma,_{\hat{M}}+2\gamma,_{\hat{a}})+f_{RR}(2\delta+2\hat{M}\delta,_{\hat{M}}+4\delta,_{\hat{a}})=0, \tag{B11}$$

$$\begin{aligned}&f_R(\alpha,_R+\gamma,_R \hat{M}^{-1})+f_{RR}(\alpha-\beta+\hat{M}\alpha,_{\hat{M}}+2\gamma,_{\hat{M}}-2\tau,_r+2\delta,_R)+2\delta\\&\times f_{RRR}=0,\end{aligned} \tag{B12}$$

$$\begin{aligned}&2\gamma,_R f_R+f_{RR}(\hat{M}\alpha-\hat{M}\beta+2\gamma+2\hat{M}\alpha,_{\hat{a}}-2\hat{M}\tau,_r+4\gamma,_{\hat{a}}+2\hat{M}\delta,_R)+2\hat{M}\\&\times\delta f_{RRR}=0,\end{aligned} \tag{B13}$$

$$\begin{aligned}&e^{\frac{\hat{a}}{2}}e^{\frac{\hat{b}}{2}}\hat{M}\{\frac{1}{2}(f-Rf_R+\omega\rho_0\hat{a}^{-\frac{(1+\omega)}{2\omega}}+\frac{2f_R}{\hat{M}})(\alpha+\beta+\tau,_r)-\frac{1}{2}\alpha(1+\omega)\rho_0\\&\times\hat{a}^{-\frac{(1+3\omega)}{2\omega}}+\delta\hat{M}(2\hat{M}^{-1}-R)f_{RR}\}+e^{\frac{\hat{a}}{2}}e^{-\frac{\hat{b}}{2}}\gamma(f-Rf_R+\omega\rho_0\hat{a}^{-\frac{(1+\omega)}{2\omega}})\\&=B,_r.\end{aligned} \tag{B14}$$

In $f(R,T)$ gravity, the over determined system of equations is given as follows

$$B,_{\hat{b}}=0,\quad \tau,_{\hat{a}}=0,\quad \tau,_{\hat{b}}=0,\quad \tau,_{\hat{M}}=0,\quad \tau,_{R}=0,\quad \tau,_{T}=0, \tag{B15}$$

$$e^{\frac{\hat{a}}{2}}(\gamma,_r f_R + \hat{M}\delta,_r f_{RR} + \hat{M}\eta,_r f_{RT}) = e^{\frac{\hat{b}}{2}} B,_{\hat{a}}\,, \tag{B16}$$

$$e^{\frac{\hat{a}}{2}}(\alpha,_r \hat{M} + 2\gamma,_r) f_{RR} = e^{\frac{\hat{b}}{2}} B,_R\,, \tag{B17}$$

$$e^{\frac{\hat{a}}{2}}(\alpha,_r \hat{M} + 2\gamma,_r) f_{RT} = e^{\frac{\hat{b}}{2}} B,_T\,, \tag{B18}$$

$$e^{\frac{\hat{a}}{2}}(\alpha,_r f_R + \gamma,_r \hat{M}^{-1} f_R + 2\delta,_r f_{RR} + 2\eta,_r f_{RT}) = e^{\frac{\hat{b}}{2}} B,_{\hat{M}}\,, \tag{B19}$$

$$\gamma,_{\hat{a}} f_R + \hat{M}\delta,_{\hat{a}} f_{RR} + \hat{M}\eta,_{\hat{a}} f_{RT} = 0, \tag{B20}$$

$$\gamma,_{\hat{b}} f_R + \hat{M}\delta,_{\hat{b}} f_{RR} + \hat{M}\eta,_{\hat{b}} f_{RT} = 0, \tag{B21}$$

$$\alpha,_{\hat{b}} f_R + \gamma,_{\hat{b}} \hat{M}^{-1} f_R + 2\delta,_{\hat{b}} f_{RR} + 2\eta,_{\hat{b}} f_{RT} = 0, \tag{B22}$$

$$\hat{M}\alpha,_{\hat{b}} f_{RR} + 2\gamma,_{\hat{b}} f_{RR} = 0, \tag{B23}$$

$$\hat{M}\alpha,_{\hat{b}} f_{RT} + 2\gamma,_{\hat{b}} f_{RT} = 0, \tag{B24}$$

$$\hat{M}\alpha,_R f_{RR} + 2\gamma,_R f_{RR} = 0, \tag{B25}$$

$$\hat{M}\alpha,_T f_{RT} + 2\gamma,_T f_{RT} = 0, \tag{B26}$$

$$\hat{M}\alpha,_T f_{RR} + 2\gamma,_T f_{RR} + \hat{M}\alpha,_R f_{RT} + 2\gamma,_R f_{RT} = 0, \tag{B27}$$

$$\begin{aligned} &f_R(\alpha - \beta - 2\gamma\hat{M}^{-1} + 4\hat{M}\alpha,_{\hat{M}} + 4\gamma,_{\hat{M}} - 2\tau,_r) + f_{RR}(2\delta + 8\hat{M}\delta,_{\hat{M}}) \\ &+ f_{RT}(2\eta + 8\hat{M}\eta,_{\hat{M}}) = 0, \end{aligned} \tag{B28}$$

$$\begin{aligned} &f_R(\alpha - \beta + 2\alpha,_{\hat{a}} - 2\tau,_r + 2\gamma,_{\hat{M}} + 2\gamma,_{\hat{a}} \hat{M}^{-1}) + f_{RR}(2\delta + 2\hat{M}\delta,_{\hat{M}} + 4\delta,_{\hat{a}}) \\ &+ f_{RT}(2\eta + 2\hat{M}\eta,_{\hat{M}} + 4\eta,_{\hat{a}}) = 0, \end{aligned} \tag{B29}$$

$$\begin{aligned} &f_R(\alpha,_R + \gamma,_R \hat{M}^{-1}) + f_{RR}(\alpha - \beta + \hat{M}\alpha,_{\hat{M}} + 2\gamma,_{\hat{M}} - 2\tau,_r + 2\delta,_R) + 2\delta \\ &\times f_{RRR} + 2\eta f_{RRT} + 2\eta,_R f_{RT} = 0, \end{aligned} \tag{B30}$$

$$\begin{aligned} &f_R(\alpha,_T + \gamma,_T \hat{M}^{-1}) + f_{RT}(\alpha - \beta + \hat{M}\alpha,_{\hat{M}} + 2\gamma,_{\hat{M}} - 2\tau,_r + 2\eta,_T) + 2\delta \\ &\times f_{RRT} + 2\eta f_{RTT} + 2\delta,_T f_{RR} = 0, \end{aligned} \tag{B31}$$

$$\begin{aligned} &2\gamma,_R f_R + f_{RR}(\hat{M}\alpha - \hat{M}\beta + 2\gamma + 2\hat{M}\alpha,_{\hat{a}} - 2\hat{M}\tau,_r + 4\gamma,_{\hat{a}} + 2\hat{M}\delta,_R) \\ &+ 2\hat{M}\delta f_{RRR} + 2\hat{M}\eta f_{RRT} + 2\hat{M}\eta,_R f_{RT} = 0, \end{aligned} \tag{B32}$$

$$\begin{aligned} &2\gamma,_T f_R + f_{RT}(\hat{M}\alpha - \hat{M}\beta + 2\gamma + 2\hat{M}\alpha,_{\hat{a}} - 2\hat{M}\tau,_r + 4\gamma,_{\hat{a}} + 2\hat{M}\delta,_R) \\ &+ 2\hat{M}\delta f_{RRT} + 2\hat{M}\eta f_{RTT} + 2\hat{M}\delta,_T f_{RR} = 0, \end{aligned} \tag{B33}$$

$$\begin{aligned} &e^{\frac{\hat{a}}{2}} e^{\frac{\hat{b}}{2}} \hat{M} \left[(f - Rf_R + f_T(3p_m - \rho_m - T) + 2f_R\hat{M}^{-1} + p_m) \left(\frac{\alpha + \beta}{2} + \tau,_r \right) \right. \\ &+ \alpha\{f_T(3p_m,_{\hat{a}} - \rho_m,_{\hat{a}}) + p_m,_{\hat{a}}\} + \beta\{f_T(3p_m,_{\hat{b}} - \rho_m,_{\hat{b}}) + p_m,_{\hat{b}}\} + \gamma\{f_T \\ &\times (3p_m,_{\hat{M}} - \rho_m,_{\hat{M}}) + p_m,_{\hat{M}}\} + \gamma\hat{M}^{-1}(f - Rf_R + f_T(3p_m - \rho_m - T) + p_m) \\ &+ \delta\{f_{RR}(-R + 2\hat{M}^{-1}) + f_{RT}(3p_m - \rho_m - T)\} + \eta\{f_{RT}(-R + 2\hat{M}^{-1}) \\ &\left. + f_{TT}(3p_m - \rho_m - T)\}\right] = B,_r\,. \end{aligned} \tag{B34}$$

For perfect fluid and $f(R,T)$ model (4.2.20), we obtain

$$
\begin{aligned}
&\frac{1}{(-r+h(r))r^3\hat{a}d_5}\left(-8\sqrt{-\frac{r}{-r+h(r)}}e^{\frac{\hat{a}}{2}}d_6\hat{a}'r^4h(r)\mu\hat{a}''+4e^{\frac{\hat{a}}{2}}d_6\hat{a}'r^3\right.\\
&\times h(r)^2\mu\hat{a}''\sqrt{-\frac{r}{-r+h(r)}}-4\sqrt{-\frac{r}{-r+h(r)}}e^{\frac{\hat{a}}{2}}d_6\hat{a}'^3r^4\mu h(r)-18e^{\frac{\hat{a}}{2}}\\
&\times d_6\hat{a}'^2r^3\mu h(r)\sqrt{-\frac{r}{-r+h(r)}}-2\sqrt{-\frac{r}{-r+h(r)}}e^{\frac{\hat{a}}{2}}d_6\hat{a}'^2r^4\mu h'(r)+2e^{\frac{\hat{a}}{2}}d_6\\
&\times \hat{a}'^3r^3h(r)^2\mu\sqrt{-\frac{r}{-r+h(r)}}+8\sqrt{-\frac{r}{-r+h(r)}}e^{\frac{\hat{a}}{2}}d_6\hat{a}'^2r^2h(r)^2\mu-32e^{\frac{\hat{a}}{2}}\\
&\times d_6\hat{a}'r^4h(r)\mu\sqrt{-\frac{r}{-r+h(r)}}+16\sqrt{-\frac{r}{-r+h(r)}}e^{\frac{\hat{a}}{2}}d_6\hat{a}'r^3h(r)^2\mu-10e^{\frac{\hat{a}}{2}}\\
&\times d_6\hat{a}'rh(r)^2\mu\sqrt{-\frac{r}{-r+h(r)}}+18\sqrt{-\frac{r}{-r+h(r)}}e^{\frac{\hat{a}}{2}}d_6\hat{a}'r^2h(r)\mu-10e^{\frac{\hat{a}}{2}}\\
&\times d_6\hat{a}'r^3h'(r)\mu\sqrt{-\frac{r}{-r+h(r)}}+8\sqrt{-\frac{r}{-r+h(r)}}e^{\frac{\hat{a}}{2}}d_6h(r)\mu rh'(r)+4e^{\frac{\hat{a}}{2}}\\
&\times \sqrt{-\frac{r}{-r+h(r)}}d_6\mu\hat{a}''r^4+r^4\hat{a}d_6-16\sqrt{-\frac{r}{-r+h(r)}}e^{\frac{\hat{a}}{2}}d_6\mu r^2+16e^{\frac{\hat{a}}{2}}d_6r^4\\
&\times \sqrt{-\frac{r}{-r+h(r)}}\mu-16\sqrt{-\frac{r}{-r+h(r)}}e^{\frac{\hat{a}}{2}}d_6\mu h(r)^2-2\sqrt{-\frac{r}{-r+h(r)}}e^{\frac{\hat{a}}{2}}d_6\\
&\times \hat{a}'r^5+2\sqrt{-\frac{r}{-r+h(r)}}e^{\frac{\hat{a}}{2}}d_6r^3h(r)-2\sqrt{-\frac{r}{-r+h(r)}}e^{\frac{\hat{a}}{2}}d_6r^4+10e^{\frac{\hat{a}}{2}}d_6\\
&\times \hat{a}'r^2\sqrt{-\frac{r}{-r+h(r)}}h(r)\mu h'(r)+2\sqrt{-\frac{r}{-r+h(r)}}e^{\frac{\hat{a}}{2}}d_6\hat{a}'^2r^3h(r)\mu h'(r)\\
&+2\sqrt{-\frac{r}{-r+h(r)}}e^{\frac{\hat{a}}{2}}d_6\hat{a}'^3r^5\mu+10\sqrt{-\frac{r}{-r+h(r)}}e^{\frac{\hat{a}}{2}}d_6\hat{a}'^2r^4\mu+16e^{\frac{\hat{a}}{2}}d_6\\
&\times \hat{a}'r^5\mu\sqrt{-\frac{r}{-r+h(r)}}-8\sqrt{-\frac{r}{-r+h(r)}}e^{\frac{\hat{a}}{2}}d_6\hat{a}'r^3\mu-32\sqrt{-\frac{r}{-r+h(r)}}\\
&\times e^{\frac{\hat{a}}{2}}d_6r^3\mu h(r)+16\sqrt{-\frac{r}{-r+h(r)}}e^{\frac{\hat{a}}{2}}d_6r^2h(r)^2\mu+32\sqrt{-\frac{r}{-r+h(r)}}e^{\frac{\hat{a}}{2}}h(r)\\
&\times d_6\mu r-8\sqrt{-\frac{r}{-r+h(r)}}e^{\frac{\hat{a}}{2}}d_6r^2h'(r)\mu+2\sqrt{-\frac{r}{-r+h(r)}}e^{\frac{\hat{a}}{2}}d_6\hat{a}'r^4h(r)+4e^{\frac{\hat{a}}{2}}\\
&\times d_6\hat{a}'r^5\mu\sqrt{-\frac{r}{-r+h(r)}}\hat{a}''-8\sqrt{-\frac{r}{-r+h(r)}}e^{\frac{\hat{a}}{2}}d_6h(r)\mu\hat{a}''r^3+4e^{\frac{\hat{a}}{2}}d_6\mu\\
&\left.\times \sqrt{-\frac{r}{-r+h(r)}}\hat{a}''r^2h(r)^2\right)=0. \qquad\qquad (B35)
\end{aligned}
$$

Appendix C

List of Publications

The contents of this thesis are based on the following research papers published in journals of International repute. These papers are also attached herewith.

1. Sharif, M. and **Nawazish, I.**: *Warm Intermediate Inflation in $f(R)$ Gravity*, Astrophys. Space Sci. **362**(2017)30.

2. Sharif, M. and **Nawazish, I.**: *Warm Logamediate Inflation in Starobinsky Inflationary Model*,
Int. J Mod. Phys. **26**(2017)1750191.

3. Sharif, M. and **Nawazish, I.**: *Exact Solutions and Conserved Quantities in $f(R,T)$ Gravity*,
Gen. Relativ. Gravit. **49**(2017)76.

4. Sharif, M., and **Nawazish, I.**: *Cosmological Analysis of Scalar Field Models in $f(R,T)$ Gravity*,
Eur. Phys. J. C **77**(2017)198.

5. Sharif, M., and **Nawazish, I.**: *Wormhole Geometry and Noether Symmetry in $f(R)$ Gravity*,
Ann. Phys. **389**(2018)283.

6. Sharif, M., and **Nawazish, I.**: *Viable Wormhole Solutions and Noether Symmetry in $f(R,T)$ Gravity*,
(Submitted for Publication).

Also, the following papers related to this thesis have been published, accepted or submitted for publication.

1. Sharif, M. and **Nawazish, I.**: *The View of Chaotic Inflationary Universe from $f(R)$ Gravity*,
   Astrophys. Space Sci. **361**(2016)19.

2. Sharif, M. and **Nawazish, I.**: *Chaotic Inflationary Models in $f(R)$ Gravity*,
   (Submitted for Publication).

3. Sharif, M. and **Nawazish, I.**: *Scalar Field Cosmology in $f(R,T)$ Gravity via Noether Symmetry*,
   (Submitted for Publication).

4. Sharif, M. and **Nawazish, I.**: *Noether Symmetries and Anisotropic Universe Models in $f(R,T)$ Gravity*,
   Mod. Phys. Lett. A **32**(2017)1750136.

5. Sharif, M. and **Nawazish, I.**: *Interacting and Non-Interacting Dark Energy Models in $f(R)$ Gravity*,
   (Submitted for Publication).

Bibliography

[1] Guth, A.: *Inflationary Universe: A Possible Solution to the Horizon and Flatness Problems*, Phys. Rev. D **23**(1981)347.

[2] Linde, A.: *Chaotic Inflation*, Phys. Lett. B **129**(1983)177.

[3] Kolb, E.W. and Turner, M.S.: *The Early Universe*, (Addison-Wesley, 1990).

[4] Kofman, L., Linde, A.D. and Starobinsky, A.A.: *Reheating After Inflation*, Phys. Rev. Lett. **73**(1994)3195.

[5] Berera, A.: *Warm Inflation*, Phys. Rev. Lett. **75**(1995)3218; *Interpolating the Stage of Exponential Expansion in the Early Universe: A Possible Alternative with No Reheating*, Phys. Rev. D **55**(1997)3346.

[6] Barrow, J.D.: *Graduated Inflationary Universes*, Phys. Lett. B **235**(1990)40; Barrow, J.D. and Saich, P.: *The Behaviour of Intermediate Inflationary Universes*, Phys. Lett. B **249**(1990)406.

[7] Herrera, R., Olivares, M. and Videla, N.: *General Dissipative Coefficient in Warm Intermediate and Logamediate Inflation*, Phys. Rev. D **88**(2013)063535.

[8] Setare, M.R. and Kamali, V.: *Warm Vector Inflation*, Phys. Lett. B **726**(2013)56.

[9] Sharif, M. and Saleem, R.: *Warm Anisotropic Inflationary Universe Model*, Eur. Phys. J. C **74**(2014)2738.

[10] Starobinsky, A.A.: *Disappearing Cosmological Constant in $f(R)$ Gravity*, J. Exp. Theor. Phys. Lett. **86**(2007)157; Sotiriou, T.P. and Faraoni, V.: *$f(R)$ Theories of Gravity*, Rev. Mod. Phys. **82**(2010)451.

[11] Felice, A.D. and Tsujikawa, S.: *$f(R)$ Theories*, Living Rev. Rel. **13**(2010)3.

[12] Bamba, K., Nojiri, S., Odintsov, S.D. and Sáez-Gómez, D.: *Inflationary Universe from Perfect Fluid and $f(R)$ Gravity and its Comparison with Observational Data*, Phys. Rev. D **90**(2014)124061.

[13] Artymowski, M. and Lalak, Z.: *Inflation and Dark Energy from $f(R)$ Gravity*, J. Cosmo. Astropart. Phys. **09**(2014)036.

[14] Sharif, M. and Ikram, A.: *Warm Inflation in $f(G)$ Theory of Gravity*, J. Exp. Theor. Phys. **123**(2016)40.

[15] Sharif, M. and Ikram, A.: *Inflationary Dynamics in $f(G)$ Gravity*, Int. J. Mod. Phys. D **26**(2017)1750030.

[16] Bertolami, O., Böhmer, C.G., Harko, T. and Lobo, F.S.N.: *Extra Force in $f(R)$ Modified Theories of Gravity*, Phys. Rev. D **75**(2007)104016.

[17] Harko,T., Lobo, F.S.N., Nojiri, S. and Odintsov, S.D.: *$f(R,T)$ Gravity*, Phys. Rev. D **84**(2011)024020.

[18] Sharif, M. and Zubair, M.: *Thermodynamics in $f(R,T)$ Theory of Gravity*, J. Cosmol. Astropart. Phys. **03**(2012)028; *Thermodynamic Behavior of Particular*

$f(R,T)$ Gravity Models, J. Exp. Theor. Phys. **117**(2013)248; *Cosmology of Holographic and New Agegraphic $f(R,T)$ Models*, J. Phys. Soc. Jpn. **82**(2013)064001; *Energy Conditions Constraints and Stability of Power Law Solutions in $f(R,T)$ Gravity*, ibid. **82**(2013)014002; *Cosmological Reconstruction and Stability in $f(R,T)$ Gravity*, Gen. Relativ. Gravit. **46**(2014)1723.

[19] Capozziello, S., Stabile, A. and Troisi, A.: *Spherically Symmetric Solutions in $f(R)$ Gravity via the Noether Symmetry Approach*, Class. Quantum Grav. **24**(2007)2153.

[20] Capozziello, S., Stabile, A. and Troisi, A.: *Spherical Symmetry in $f(R)$ Gravity*, Class. Quantum Grav. **25**(2008)085004; *Axially Symmetry Solutions in $f(R)$ Gravity*, ibid. **27**(2010)165008.

[21] Hussain, I., Jamil, M. and Mahomed, F.M.: *Noether Gauge Symmetry Approach in $f(R)$ Gravity*, Astrophys. Space Sci. **337**(2012)373.

[22] Shamir, M.F., Jhangeer, A. and Bhatti, A.A.: *Conserved Quantities in $f(R)$ Gravity via Noether Symmetry*, Chin. Phys. Lett. **29**(2012)080402.

[23] Kucukakca, Y. and Camci, U.: *Noether Gauge Symmetry for $f(R)$ Gravity in Palatini Formalism*, Astrophys. Space Sci. **338**(2012)211.

[24] Momeni, D., Myrzakulov, R. and Güdekli, E.: *Cosmological Viable Mimetic $f(R)$ and $f(R,T)$ Theories via Noether Symmetry*, Int. J. Geom. Methods Mod. Phys. **12**(2015)1550101.

[25] Sharif, M. and Fatima, H.I.: *Noether Symmetries in $f(\mathcal{G})$ Gravity*, J. Exp. Theor. Phys. **122**(2016)104.

[26] Shamir, M.F. and Ahmad, M.: *Noether Symmetry Approach in $f(\mathcal{G},T)$ Gravity*, Eur. Phys. J. C **77**(2017)55.

[27] Sanyal, A.K.: *Noether and Some Other Dynamical Symmetries in KantowskiSachs Model*, Phys. Lett. B **524**(2002)177.

[28] Camci, U. and Kucukakca, Y.: *Noether Symmetries of Bianchi I, Bianchi III, and Kantowski-Sachs Spacetimes in Scalar-Coupled Gravity Theories*, Phys. Rev. D **76**(2007)084023.

[29] Kucukakca, Y., Camci, U. and Semiz, I.: *LRS Bianchi Type I Universes Exhibiting Noether Symmetry in the ScalarTensor Brans-Dicke Theory*, Gen. Relativ. Gravit. **44**(2012)1893.

[30] Camci, U., Yildirim, A. and Oz, I.B.: *New Exact Solutions of Bianchi I, Bianchi III and KantowskiSachs Spacetimes in Scalar-Coupled Gravity Theories via Noether Gauge Symmetries*, Astropart. Phys. **76**(2016)29.

[31] Zhang, Y., Gong, Y.G., and Zhu, Z.H.: *Noether Symmetry Approach in Multiple Scalar Fields Scenario*, Phys. Lett. B **688**(2010)13.

[32] Jamil, M., Mahomed, F.M. and Momeni, D.: *Noether Symmetry Approach in $f(R)$ Tachyon Model*, Phys. Lett. B **702**(2011)315.

[33] Lobo F.S. and Oliveira M.A.: *Wormhole Geometries in $f(R)$ Modified Theories of Gravity*, Phys. Rev. D **80**(2009)104012.

[34] Bahamonde, S., Jamil, M., Pavlovic, P. and Sossich, M.: *Cosmological Wormholes in $f(R)$ Theories of Gravity*, Phys. Rev. D **94**(2016)044041.

[35] Mazharimousavi, S.H. and Halilsoy, M.: *Necessary Conditions for Having Wormholes in $f(R)$ Gravity*, Mod. Phys. Lett. A **31**(2016)1650203.

[36] Sharif, M. and Fatima, I.: *Conformally Symmetric Traversable Wormholes in $f(\mathcal{G})$ Gravity*, Gen. Relativ. Gravit. **48**(2016)148; *Wormhole Solutions for $f(\mathcal{G})$ Gravity in Galactic Halo Region*, Astrophys. Space Sci. **361**(2016)127.

[37] Zubair, M., Waheed, S. and Ahmed, Y.: *Static Spherically Symmetric Wormholes in $f(R,T)$ Gravity*, Eur. Phys. J. C **76**(2016)444.

[38] Bahamonde, S., Camci, U., Capozziello, S. and Jamil, M.: *Scalar-Tensor Teleparallel Wormholes by Noether Symmetries*, Phys. Rev. D **94**(2016)084042.

[39] Lyth, H.D., and Liddle, A.: *The Primordial Density Perturbation*, (Cambridge University Press, 2009).

[40] Berera, A. and Fang, L.Z.: *Thermally Induced Density Perturbations in the Inflation Era*, Phys. Rev. Lett. **74**(1995)1912.

[41] Linde, A.: *Particle Physics and Inflationary Cosmology*, (Harwood Academic, 1990), Liddle, A.R. and Lyth, D.H.: *Cosmological Inflation and Large Scale Structure*, (Cambridge University Press, 2000).

[42] Ade, P.A.R. et al.: *Planck 2015 Results. XX. Constraints on Inflation*, Astron. Astrophys. **594**(2016)A20.

[43] Clifton, T., Ferreira, P.G., Padilla, A. and Skordis, C.: *Modified Gravity and Cosmology*, Phys. Rep. **513**(2012)1.

[44] Dolgov, A.D. and Kawasaki, M.: *Can Modified Gravity Explain Accelerated Cosmic Expansion?*, Phys. Lett. B **573**(2003)1.

[45] Starobinsky, A.A.: *A New Type of Isotropic Cosmological Models Without Singularity*, Phys. Lett. B **91**(1980)99.

[46] Allemandi, G., Borowiec, A. and Francaviglia, M.: *Accelerated Cosmological Models in First-Order Nonlinear Gravity*, Phys. Rev. D **70**(2004)043524.

[47] Ozkan, M. and Pang, Y.: *R^n Extension of the Starobinsky Model in Old Minimal Supergravity*, Class. Quantum Grav. **31**(2014)205004.

[48] Sokolowski, L.: *Uniqueness of the Metric Line Element in Dimensionally Reduced Theories*, Class. Quantum Grav. **6**(1989)2045.

[49] Magnano, G. and Sokolowski, L.M.: *Physical Equivalence Between Nonlinear Gravity Theories and a General-Relativistic Self-Gravitating Scalar Field*, Phys. Rev. D **50**(1994)5039.

[50] Faraoni, V. and Nadeau, S.: *(Pseudo) Issue of the Conformal Frame Revisited*, Phys. Rev. D **75**(2007)023501.

[51] Haghani, Z., Harko, T., Lobo, F.S.N., Sepangi, H.R. and Shahidi, S.: *Further Matters in Spacetime Gometry: $f(R,T,R_{\mu\nu}T_{\mu\nu})$ Gravity*, Phys. Rev. D **88**(2013)044023; Odintsov, S.D. and Saez-Gomez, D.: *$f(R,T,R_{\mu\nu}T_{\mu\nu})$ Gravity Phenomenology and ΛCDM Universe*, Phys. Lett. B **725**(2013)437.

[52] Morris, M. and Thorne, A.: *Wormholes in Spacetime and Their Use for Interstellar Travel: A Tool for Teaching General Relativity*, Am. J. Phys. **56**(1988)395.

[53] Bertolami, O. and Ferreira, R.Z.: *Traversable Wormholes and Time Machines in Non-Minimally Coupled Curvature-Matter $f(R)$ Theories*, Phys. Rev. D **85**(2012)104050.

[54] Carroll, S.: *Spacetime and Geomety: An Introduction to General Relativity*, (Addison Wesley, 2004).

[55] Santos, J., Alcaniz, J.S., Reboucas, M.J. and Carvalho, F.C.: *Energy Conditions in $f(R)$ Gravity*, Phys. Rev. D **76**(2007)083513.

[56] Sharif, M. and Nawazish, I.: *Warm Intermediate Inflation in $f(R)$ Gravity*, Astrophys. Space Sci. **362**(2017)30.

[57] Sharif, M. and Nawazish, I.: *Warm Logamediate Inflation in Starobinsky Inflationary Model*, Int. J Mod. Phys. **26**(2017)1750191.

[58] Muslimov, A.: *On the Scalar Field Dynamics in a Spatially Flat Friedman Universe*, Class. Quantum Grav. **7**(1990)231.

[59] Zhang, Y: J. *Warm Inflation with a General Form of the Dissipative Coefficient*, Cosmol. Astropart. Phys. **03**(2009)030.

[60] Berera, A., Moss, I.G. and Ramos, R.O.: *Warm Inflation and Its Microphysical Basis*, Rept. Prog. Phys. **72**(2009)026901; Herrera, R., Videla, N. and Olivares, M.: *Warped DGP Model in Warm Intermediate Inflation With A General Dissipative Coefficient in Light of BICEP2 and Planck Results*, Phys. Rev. D **90**(2014)103502.

[61] Sharif, M. and Nawazish, I.: *Exact Solutions and Conserved Quantities in $f(R,T)$ Gravity*, Gen. Relativ. Gravit. **49**(2017)76.

[62] Sharif, M., and Nawazish, I.: *Cosmological Analysis of Scalar Field Models in $f(R,T)$ Gravity*, Eur. Phys. J. C **77**(2017)198.

[63] Schutz, B.F.: *Perfect Fluids in General Relativity: Velocity Potentials and a Variational Principle*, Phys. Rev. D **2**(1970)2762.

[64] Nojiri, S. and Odintsov, S. D.: *Final State and Thermodynamics of a Dark Energy Universe*, Phys. Rev. D **70**(2004)103522.

[65] Elizalde, E., Nojiri, S. and Odintsov, S.D.: *Late-Time Cosmology in a (Phantom) Scalar-Tensor Theory: Dark Energy and the Cosmic Speed-Up*, Phys. Rev. **D** 70(2004)043539.

[66] MacCallum, M.A.H.: *In General Relativity: An Einstein Centenary Survey*, (Cambridge University Press, 1979).

[67] Ellis, G.F.R., Maartens, R. and MacCallum, M.A.H.: *Relativistic Cosmology*, (Cambridge University Press, 2012).

[68] Barrow, J.: *Sudden Future Singularities*, Class. and Quantum Grav. **21**(2004)L79.

[69] Sharif, M., and Nawazish, I.: *Wormhole Geometry and Noether Symmetry in $f(R)$ Gravity*, Ann. Phys. **389**(2018)283.

[70] Sharif, M., and Nawazish, I.: *Viable Wormhole Solutions and Noether Symmetry in $f(R,T)$ Gravity*, (Submitted for Publication).

[71] Kar, S. and Sahdev, D.: *Restricted Class of Traversable Wormholes with Traceless Matter*, Phys. Rev. D **52**(1995)2030.

Astrophys Space Sci (2017) 362:30
DOI 10.1007/s10509-017-3011-5

ORIGINAL ARTICLE

Warm intermediate inflation in $f(R)$ gravity

M. Sharif[1] · Iqra Nawazish[1]

Received: 13 October 2016 / Accepted: 5 January 2017 / Published online: 19 January 2017

Abstract This paper investigates the behavior of warm intermediate inflation for flat isotropic and homogeneous universe in Einstein frame representation of $f(R)$ gravity. In this scenario, we study the dynamics of two distinct regimes, i.e., strong and weak constant as well as generalized dissipative regimes. In both regimes, we find inflaton solution corresponding to scalar potential and then evaluate dimensionless slow-roll parameters. Under slow-roll approximation, we formulate scalar and tensor power spectra, their spectral indices and tensor-scalar ratio for Starobinsky inflationary model and study the graphical analysis of these observational parameters. It is concluded that isotropic intermediate inflationary model with constant as well as generalized dissipation coefficient for $m = 0$, 1 and -1 remains compatible with Planck 2015 constraints in both dissipative regimes. The inflationary model satisfies warm inflation condition in both dissipation regimes but found to be inconsistent for $m = 3$.

Keywords Slow-roll approximation · Warm inflation · $f(R)$ gravity

1 Introduction

The most revolutionary advancement on the grounds of cosmology is the establishment of a cosmological model entitled as big-bang model. This standard model successfully describes some surprising observational facts such as the existence of cosmic microwave background radiations (CMB), presence of primordial light elements and also explain current cosmic expansion (Gamow 1946; Penzias and Wilson 1965; Perlmutter et al. 1999). However, it suffers from some serious and long standing theoretical issues like horizon, flatness, origin of fluctuations and monopole. To get rid of these problems, the standard model demands an epoch of rapid acceleration in the early universe named as "inflation". This epoch is defined as an era of few Planck lengths that suffers an instant exponential expansion due to the presence of some gravitational effects (Lyth and Liddle 2009).

The first idea of an accelerated epoch was given by Guth (1981) and Sato (1981) who proposed that early stage of the universe experiences a rapid expansion because of the existence of false vacuum. They argued that the inflating universe gets filled with bubbles at the end of inflation. These bubbles introduced some shortcomings like inflationary epoch corresponds to de Sitter expansion that yields inhomogeneous universe at the end of inflation. Such serious shortcomings led to another version of inflation dubbed as new inflation or chaotic inflation where a scalar field being a combination of potential and kinetic energies behaves like a source of accelerated expansion (Linde 1983). At the beginning of inflating universe, the potential energy dominates over kinetic energy due to worthless interactions between scalar and other fields and inflaton starts moving very slowly towards the origin of potential (Hawking 1982; Bardeen et al. 1983). After this evolutionary stage, kinetic and potential energies are comparable due to oscillatory motion of inflatons around minimum position of potential energy. Thus, the reheating phase is initiated due to decay of inflatons into radiation and matter (Kofman et al. 1994; Khlebnikov and Tkachev 1996; Bassett et al. 2006).

✉ M. Sharif
msharif.math@pu.edu.pk

I. Nawazish
iqranawazish07@gmail.com

[1] Department of Mathematics, University of the Punjab, Quaid-e-Azam Campus, Lahore 54590, Pakistan

The most attractive feature for researchers is how to join the ending of inflationary epoch with present accelerating universe. In order to study the possible joining mechanism, Berera (1995, 1997) presented a revolutionary idea which is different from cold inflation as a separate reheating phase is avoided at the end of inflation. He proposed warm inflationary scenario that unifies slow-roll and reheating regimes because production of thermal radiations appeared during inflationary paradigm. The existence of thermal radiations of density plays a crucial role in the production of initial fluctuations which are elementary ingredients of large scale structures. When vacuum energy dissipates into radiation energy, the inflating universe allows a graceful exit into radiation dominated era (Berera 2000; Hall et al. 2004). Yokoyama and Linde (1999) investigated possible behavior of warm inflation scenario and claimed that it is very difficult to study the existence of warm inflation for realistic models of elementary particles.

During warm inflation, thermal fluctuations and scalar field interactions lead to its final outcome in the form of strong dissipation effect which directly corresponds to particle production. This dissipation effect appears as a linear friction term whose characteristics are determined by dissipation coefficient. Berera and Ramos (2001) explored warm inflationary dynamics and low temperature regimes for a particular form of dissipation coefficient corresponding to supersymmetric models. In order to discuss decay as well as scattering rates, Bastero-Gil et al. (2011, 2013) studied warm inflation paradigm in quantum field theory. In warm inflation, dissipation effect characterizes two important regimes, i.e., weak ($\Gamma \ll H$, Γ represents dissipation coefficient) and strong ($\Gamma \gg H$) dissipative regimes. In non-warm inflation, the primordial density perturbation spectrum is established on the basis of quantum fluctuations. In weak dissipative regime, these perturbations are determined by thermal fluctuations whereas in strong dissipative regime, the decay rate increases.

To classify various inflationary universe models, the scale factor plays a vital role as its evolution corresponding to cosmic time determines some interesting exact solutions. When a scale factor possesses a de Sitter expansion (exponential expansion), it leads to the inflationary model which describes old inflation but when scale factor follows quasi-de Sitter expansion, it corresponds to new or chaotic inflation (Linde 1986). An intermediate inflationary model is obtained for a scale factor whose expansion growth is faster than power-law but slower than de Sitter expansion (Barrow 1990; Barrow and Saich 1990). Herrera et al. (2013) analyzed the behavior of isotropic warm inflation for intermediate as well as logamediate inflationary models in both strong and weak dissipative regimes via general dissipative coefficient. Setare and Kamali (2013) studied warm vector isotropic inflation in intermediate as well as logamediate inflationary epochs. They discussed strong dissipative regime for constant as well as variable dissipative coefficient and found compatible results for WMAP7. Sharif and Saleem (2014) found that locally rotationally symmetric Bianchi I universe model yields consistent results in the context of warm vector inflation. Sharif and Saleem (2015, 2016) examined warm anisotropic intermediate and logamediate inflation in strong as well as weak dissipative regimes via general dissipative coefficient.

Recent observational evidences indicate that the universe is again experiencing an accelerated expansion whose source is named as "dark energy" (DE). This cosmic accelerated expansion motivates researchers to establish extended gravitational theories. Many modified theories of gravity have been proposed to explain current cosmic expansion like $f(R)$, $f(\mathcal{G})$, $f(R,\mathcal{G})$ etc. It is a well-known fact that ghosts can occur in higher derivative theories of gravity but they are not problematic in $f(R)$ theory as the Ostrogradski instability does not apply to this gravity (Barth and Christensen 1983; Calcagni et al. 2005; Chiba 2005). Unlike the case of $f(R)$ gravity which preserves Einstein–Hilbert action through conformal transformation, the $f(\mathcal{G})$ or $f(R,\mathcal{G})$ theories are not conformally related to general relativity with a scalar field. This conformal correspondence provides a motivation to choose $f(R)$ gravity to study early expansion through inflationary epoch and also investigates the apparent late-time accelerating expansion of the universe.

Bamba et al. (2014) investigated observational parameters of non-warm inflationary models through reconstruction method in this gravity. They studied different $f(R)$ models and concluded that power-law model gives the best fit values compatible with BICEP2 and Planck observations. We have analyzed the behavior of chaotic inflationary paradigm for isotropic and homogeneous flat universe model in the framework of Jordan frame of $f(R)$ gravity (Sharif and Nawazish 2016). Sharif and Ikram (2016) studied dynamics of warm intermediate and logamediate inflation for flat FRW universe model in Jordan frame of $f(\mathcal{G})$ gravity.

Many theoretical efforts have been made to discuss coupling of gravity with other interactions that demand existence of scalar fields in Jordan frame. Some researchers argued that scalar-tensor gravity is unreliable in Jordan frame as it gives rise to the problem of negative kinetic energy (Teyssandier and Tourrenc 1983; Sokolowski 1989; Santiago and Silbergleit 2000). In $f(R)$ gravity, this issue is resolved by introducing a conformal transformation that relates Einstein–Hilbert action and $f(R)$ action, consequently Jordan frame is shifted to Einstein frame under that conformal factor (Allemandi et al. 2006; Capozziello et al. 2006). Inflationary scenario has become a debatable issue in Jordan as well as Einstein frames. de Felice and Tusjikawa (2010) studied inflationary dynamics of Starobinsky inflationary model for both frames in $f(R)$ gravity. Artymowski and Lalak (2014) investigated modified Starobinsky inflationary model in both Einstein and Jordan frames and obtained compatible results for Planck and BICEP2 observations.

In this paper, we study warm intermediate inflation via Einstein frame representation of $f(R)$ gravity for isotropic and homogeneous universe. The format of this paper is as follows. Section 2 describes some basic features of $f(R)$ gravity in Jordan and Einstein frames. In Sect. 3, we examine strong and weak dissipation regimes for constant as well as generalized dissipation coefficient with Starobinsky inflationary model and discuss their effects graphically. Finally, we conclude our results in the last section.

2 Dynamics of $f(R)$ gravity

In this section, we discuss basic formalism of $f(R)$ gravity both in Jordan as well as Einstein frames which lead to investigate warm inflationary dynamics.

2.1 Representation of Jordan frame

In Jordan frame, there is a direct interaction between geometrical and matter parts in the action of $f(R)$ gravity given by Nojiri and Odintsov (2011)

$$I=\frac{1}{2\kappa^2}\int d^4x\sqrt{-g}f(R)+\mathcal{L}_m(g_{\mu\nu},\psi), \tag{1}$$

where $\mathcal{L}_m$ represents matter Lagrangian. Varying the above action corresponding to $g_{\mu\nu}$, we obtain non-linear fourth order partial differential equation as

$$f_R R_{\mu\nu}-\frac{1}{2}fg_{\mu\nu}-\nabla_\mu\nabla_\nu f_R+g_{\mu\nu}\Box f_R=\kappa^2T_{\mu\nu}, \tag{2}$$

where $f_R=\frac{df(R)}{dR}$, ∇_μ describes covariant derivative and $\Box=\nabla_\mu\nabla^\mu$. Equation (2) can be written in the form

$$G_{\mu\nu}=\frac{\kappa^2}{f_R}\left(T_{\mu\nu}+T_{\mu\nu}^{eff}\right),$$

where the effective energy-momentum tensor is

$$T_{\mu\nu}^{eff}=\frac{1}{\kappa^2}\left(\frac{g_{\mu\nu}(f-Rf_R)}{2}+\nabla_\mu\nabla_\nu f_R-\Box f_R g_{\mu\nu}\right).$$

We consider flat FRW metric as

$$ds^2=-dt^2+a^2(t)\left(dx^2+dy^2+dz^2\right), \tag{3}$$

where a is the scale factor. The corresponding field equations (2) for perfect fluid lead to

$$\frac{f-Rf_R}{2}+3H^2f_R+3H\dot{f}_R=\kappa^2\rho, \tag{4}$$

$$\ddot{f}_R+2\dot{H}f_R-H\dot{f}_R=-\kappa^2(\rho+p), \tag{5}$$

where ρ and p represent energy density and pressure of perfect fluid, respectively and dot denotes time derivative. In order to evaluate an expression for a and H, we consider a standard model given by Starobinsky (1980)

$$f(R)=R+\frac{R^2}{6M^2}, \tag{6}$$

where M is a positive constant which has dimension of mass. The first and second derivatives of this model corresponding to R are positive which ensure its viability. Inserting Eq. (6) into (4) and (5), we obtain

$$\begin{aligned} a&=a_i\exp\left[H_i(t-t_i)-\frac{M^2(t-t_i)^2}{12}\right],\\ H&=H_i-\frac{M^2(t-t_i)}{6}, \end{aligned} \tag{7}$$

where t_i denotes initial cosmic time whereas a_i and H_i represent scale factor and Hubble parameter at $t=t_i$, respectively. The $f(R)$ gravity can be modified into scalar-tensor theory by taking into account interactions of the scalar field in Jordan frame but it is strongly claimed that this frame is physically not suitable to discuss such interactions due to existence of negative kinetic energy (Sokolowski 1989). To get rid of such negative kinetic energy, the fourth order field equations are transformed conformally from Jordan to Einstein frame which contains an additional scalar degree of freedom with positive kinetic term (Magnano and Sokolowski 1994).

2.2 Representation of Einstein frame

In the Einstein frame, the $f(R)$ gravity indicates existence of extra scalar degree of freedom which drives early as well as late-time cosmic acceleration. A conformal transformation over a metric structure allows to scale time, length and mass whereas angles remain unchanged. The action of $f(R)$ gravity can also be written as

$$I=\frac{1}{2\kappa^2}\int d^4x\sqrt{-g}\left(f_RR-V(\phi)\right)+\mathcal{L}_m(g_{\mu\nu},\psi), \tag{8}$$

where $V(\phi)=f_RR-f$. For a conformal factor $\tilde{g}_{\mu\nu}=\varphi^2g_{\mu\nu}=f_Rg_{\mu\nu}$, this action takes the form

$$\begin{aligned} I_E=\int d^4x\sqrt{-\tilde{g}}\Bigg(&\frac{\tilde{R}}{2\kappa^2}-\frac{1}{2}\tilde{g}^{\mu\nu}\partial_\mu\phi\partial_\nu\phi-U(\phi)\\ &+\mathcal{L}_m\left(f_R^{-1}(\phi)\tilde{g}_{\mu\nu},\psi\right)\Bigg). \end{aligned} \tag{9}$$

Here, $U(\phi)=\frac{V(\phi)}{f_R^2}$, the considered conformal factor becomes field dependent as $\varphi^2=f_R=\exp[\sqrt{\frac{2}{3}}\kappa\phi]$ and the gravitational term of action (1) takes the form of Einstein–Hilbert action along with a non-minimal coupling between matter Lagrangian density and scalar field. In this frame, the flat FRW model becomes

$$d\tilde{s}^2 = -d\tilde{t}^2 + \tilde{a}^2(\tilde{t})\big(dx^2 + dy^2 + dz^2\big), \tag{10}$$

where

$$d\tilde{s} = \sqrt{f_R}ds, \quad d\tilde{t} = \sqrt{f_R}dt, \quad \tilde{a} = \sqrt{f_R}a. \tag{11}$$

The energy-momentum tensor corresponding to matter and scalar parts are defined as

$$\tilde{T}^{(m)}_{\mu\nu} = -\frac{2}{\sqrt{-\tilde{g}}}\frac{\partial\mathcal{L}_m}{\partial\tilde{g}^{\mu\nu}}, \qquad \tilde{T}^{(\phi)}_{\mu\nu} = -\frac{2}{\sqrt{-\tilde{g}}}\frac{\partial(\partial\sqrt{-\tilde{g}}\mathcal{L}_\phi)}{\partial\tilde{g}^{\mu\nu}}. \tag{12}$$

where $\mathcal{L}_\phi$ represents Lagrangian density of a scalar field given by

$$\mathcal{L}_\phi = -\frac{1}{2}\tilde{g}^{\mu\nu}\partial_\mu\phi\partial_\nu\phi - U(\phi).$$

For the action (9), the field equations and continuity equation turn out to be

$$\frac{3\tilde{H}^2}{\kappa^2} = \tilde{\rho}_m, \qquad 3\tilde{H}^2 + 2\frac{d\tilde{H}}{d\tilde{t}} = -\kappa^2\tilde{p}_m, \tag{13}$$

$$\frac{d\tilde{\rho}_m}{d\tilde{t}} + 3\tilde{H}(\tilde{t})(\tilde{\rho}_m + \tilde{p}_m) = 0. \tag{14}$$

The energy density and pressure are represented by $\tilde{\rho}_m = \frac{\rho}{f_R^2}$ and $\tilde{p}_m = \frac{p}{f_R^2}$ whereas $\tilde{H}$ denotes Hubble parameter in Einstein frame. In order to formulate expressions of $\tilde{t}$, $\tilde{a}$ and $\tilde{H}$ for standard model (6), we integrate Eq. (11) yielding

$$\begin{aligned}\tilde{t} &= \frac{2}{M}\left[H_i(t-t_i) - \frac{M^2(t-t_i)^2}{12}\right],\\ \tilde{a}(\tilde{t}) &= \frac{2H_ia_i}{M}\left[1 - \frac{M^3\tilde{t}}{12H_i^2}\right]e^{\frac{M\tilde{t}}{2}},\\ \tilde{H}(\tilde{t}) &= \frac{M}{2}\left[1 - \frac{M^2}{6H_i^2}\left(1 - \frac{M^3\tilde{t}}{12H_i^2}\right)^{-2}\right].\end{aligned} \tag{15}$$

The conformal transformation allows a smooth transition between these two frames as it only redefines the scales of fundamental quantities that retain physical predictions in both frames (Faraoni and Nadeau 2007). The main difference in both frames is that the Jordan frame defines $f(R)$ gravity on the basis of metric tensor whereas Einstein frame describes the theory with the help of metric tensor along with scalar field interacting with matter sector.

3 Dynamics of warm inflation in Einstein frame

In this section, we explore the behavior of warm inflation in Einstein frame of $f(R)$ gravity. An interaction of scalar and radiation fields is considered to be the most basic element of the universe that realize warm inflationary paradigm for a minimally coupled scalar field subject to potential $U(\phi)$. The energy density ($\tilde{\rho}_\phi$) and pressure ($\tilde{p}_\phi$) of self-interacting scalar field are

$$\tilde{\rho}_\phi = \frac{\dot{\phi}^2}{2f_R} + U(\phi), \qquad \tilde{p}_\phi = \frac{\dot{\phi}^2}{2f_R} - U(\phi). \tag{16}$$

During warm inflation, the total energy density of the universe not only consists of $\tilde{\rho}_\phi$ but also comprises radiation density $\tilde{\rho}_r$. For such inflationary scenario, Eqs. (13) and (14) yield

$$\frac{3\tilde{H}^2}{\kappa^2} = \tilde{\rho}_\phi + \tilde{\rho}_r, \qquad 3\tilde{H}^2 + 2\frac{d\tilde{H}}{d\tilde{t}} = -\kappa^2(\tilde{p}_\phi + \tilde{p}_r), \tag{17}$$

$$\frac{d\tilde{\rho}_r}{d\tilde{t}} + 4\tilde{H}\tilde{\rho}_r - \Gamma\left(\frac{d\phi}{d\tilde{t}}\right)^2 = 0, \tag{18}$$

$$\frac{d\tilde{\rho}_\phi}{d\tilde{t}} + 3\tilde{H}(\tilde{\rho}_\phi + \tilde{p}_\phi) + \Gamma\left(\frac{d\phi}{d\tilde{t}}\right)^2 = 0. \tag{19}$$

In Eq. (18), the last term behaves like a source of radiations whereas the second term responds as a sink term which dissipates these radiations continuously. During inflation, the Hubble parameter, dissipation factor and inflaton field vary very slowly which imply that the radiation density must attain a non-zero steady state point. Therefore, the radiation production becomes independent of initial conditions and gets quasi-stable which leads to the following conditions

$$\frac{d\tilde{\rho}_r}{d\tilde{t}} \ll 4\tilde{H}\tilde{\rho}_r, \qquad \frac{d\tilde{\rho}_r}{d\tilde{t}} \ll \Gamma\left(\frac{d\phi}{d\tilde{t}}\right)^2. \tag{20}$$

Using the above conditions in Eq. (17), we obtain

$$\tilde{\rho}_r = \frac{3}{4}\tilde{r}\left(\frac{d\phi}{d\tilde{t}}\right)^2 = \chi_r T^4, \quad \tilde{r} = \frac{\Gamma}{3\tilde{H}}. \tag{21}$$

Here, $\tilde{r}$ describes the rate of dissipation factor relative to expansion of the universe via Hubble parameter and $\chi_r = \frac{\pi^2 g_*}{30}$, g_* represents number of relative degrees of freedom and T denotes temperature of thermal bath.

In warm inflation, thermal fluctuations of inflaton field are considerable as $T > \tilde{H}$ and $\tilde{\rho}_r$ dissipates into $\tilde{\rho}_\phi$, i.e., $\tilde{\rho}_\phi \gg \tilde{\rho}_r$. Under this condition, Eq. (18) leads to

$$\left(\frac{d\phi}{d\tilde{t}}\right)^2 = -\left[\frac{2}{\kappa^2(1+\tilde{r})}\right]\frac{d\tilde{H}}{d\tilde{t}}. \tag{22}$$

The thermal bath temperature is evaluated by using Eq. (22) into (21) as

$$T=\left[-\frac{3f_R^2\tilde{r}d\tilde{H}/d\tilde{t}}{2\kappa^2\chi_r(1+\tilde{r})}\right]^{\frac{1}{4}}. \tag{23}$$

Inserting Eqs. (21) and (22) in (17), we obtain potential corresponding to inflaton field as

$$U(\phi)=\frac{3\tilde{H}^2}{\kappa^2}+\frac{d\tilde{H}/d\tilde{t}}{\kappa^2(1+\tilde{r})}\left[1+\frac{3\tilde{r}}{2}\right]. \tag{24}$$

For warm inflation, the variance of inflaton field is described by thermal fluctuations whereas in case of non-warm inflationary scenario, this variation is presented by quantum fluctuation. Inflationary paradigm characterizes these fluctuations into scalar and tensor perturbations that leave a strong impact over the CMB anisotropy as well as on the large scales. To evaluate the variance and characteristics of these fluctuations, some important parameters like scalar power spectrum (Δ_R^2), tensor power spectrum (Δ_T^2) and tensor-scalar ratio ($\mathcal{R}$) have been introduced (Linde 1990). For FRW universe model in Einstein frame representation, these parameters under slow-roll approximation ($H=\tilde{H}\sqrt{f_R}$) take the following form

$$\Delta_{\mathcal{R}}^2=-\frac{\tilde{H}^2\kappa^2(1+\tilde{r})T}{d\tilde{H}/d\tilde{t}}\left[\frac{\Gamma\tilde{H}f_R^{\frac{1}{2}}}{(4\pi)^3}\right]^{\frac{1}{2}},$$
$$n_s=1-\frac{d}{d\tilde{N}}(\ln\Delta_{\mathcal{R}}^2), \tag{25}$$

$$\Delta_T^2=8\kappa^2\left[\frac{\tilde{H}f_R^{\frac{1}{2}}}{2\pi}\right]^2,\qquad n_T=-2\epsilon,$$
$$\langle\delta\phi\rangle_{\text{thermal}}=\left[\frac{\Gamma\tilde{H}T^2f_R^{\frac{1}{2}}}{(4\pi)^3}\right]^{\frac{1}{4}}, \tag{26}$$

$$\mathcal{R}=\frac{\Delta_T^2}{\Delta_{\mathcal{R}}^2}=-\frac{4f_Rd\tilde{H}/d\tilde{t}}{\pi^2(1+\tilde{r})\tilde{H}^{\frac{1}{2}}T}\left[\frac{(4\pi)^3}{\Gamma f_R^{\frac{1}{2}}}\right]^{\frac{1}{2}}. \tag{27}$$

Recent observations of Planck 2015 (Ade et al. 2016) constrain spectral index and tensor-scalar ratio as $n_s=0.9603\pm0.0062$ (68 %CL) and $\mathcal{R}<0.10$ (95 %CL), respectively.

3.1 Warm intermediate inflation for $\Gamma=\Gamma_i=$ Constant

Here, we analyze warm inflation in strong ($\tilde{r}\gg1$) as well as weak dissipative regimes ($\tilde{r}\ll1$) corresponding to a scale factor that represents expansion of the universe less than de Sitter but greater than power-law expansion. In this case, the scale factor takes the form (Muslimov 1990)

$$a(t)=a_i\exp[\gamma t^g],\quad \gamma>0,\quad 0<g<1. \tag{28}$$

In Einstein frame, the intermediate scale factor and corresponding Hubble parameter turn out to be

$$\tilde{a}(\tilde{t})=\tilde{a}_i\left[1-\frac{M^3\tilde{t}}{12H_i^2}\right]\exp\left[\gamma\left(\frac{\tilde{t}M}{2H_i}\right)^g\right],\quad \tilde{a}_i=\frac{2a_iH_i}{M}, \tag{29}$$

$$\tilde{H}(\tilde{t})=\frac{1}{\tilde{a}}\frac{d\tilde{a}}{d\tilde{t}}=\gamma g\left[\frac{\tilde{t}M}{2H_i}\right]^{g-1}. \tag{30}$$

In order to measure the extent of inflation, we have

$$\tilde{N}=\int_{\tilde{t}_i}^{\tilde{t}}\tilde{H}(\tilde{t})d\tilde{t}=\gamma\left[\frac{M}{2H_i}\right]^g(\tilde{t}^g-\tilde{t}_i^g), \tag{31}$$

where $\tilde{t}_i$ represents cosmic time at the beginning of inflation in Einstein frame. The approximate extent of inflation is found to be 70 but fluctuation spectrum of CMB reveals that this limit of e-folds should be less than 70.

In strong dissipative regime, Eqs. (22) and (24) yield the inflaton field and corresponding potential in the following form

$$\phi=\phi_0+\alpha_1\tilde{t}^{\frac{2g-1}{2}},$$
$$U(\phi)=\frac{3}{\kappa^2}\left[\gamma g\left(\frac{M}{2H_i}\right)^g\left(\frac{\phi-\phi_0}{\alpha_1}\right)^{\frac{2(g-1)}{2g-1}}\right]^2, \tag{32}$$

where ϕ_0 is an integration constant and α_1 is

$$\alpha_1=\sqrt{\frac{24(\gamma g)^2(1-g)}{\kappa^2\Gamma_i(2g-1)^2}\left(\frac{M}{2H_i}\right)^2}. \tag{33}$$

In order to discuss inflationary paradigm during slow-roll dynamics, an approximation is considered when interactions between inflaton and radiation or matter become meaningless and even potential energy dominates kinetic energy during slowly varying inflaton field (Kolb and Turner 1994). The dimensionless slow-roll parameters are introduced as (Hwang and Noh 2002)

$$\epsilon=-\frac{1}{\tilde{H}^2}\frac{d\tilde{H}}{d\tilde{t}},\qquad \eta=-\left[\tilde{H}\frac{d\tilde{H}}{d\tilde{t}}\right]^{-1}\frac{d^2\tilde{H}}{d\tilde{t}^2}, \tag{34}$$

where $d\tilde{H}/d\tilde{t}$ must be negative. When ϵ takes the value of unity, the inflating universe vanishes which implies that ϵ and so η must be very small but positive for the existence of inflationary epoch. Using Eqs. (30) and (32), these parameters become

$$\epsilon=\frac{1-g}{\gamma g}\left(\frac{2H_i}{M}\right)^g\left[\frac{\phi-\phi_0}{\alpha_1}\right]^{\frac{2g}{1-2g}},$$
$$\eta=\frac{2-g}{\gamma g}\left(\frac{2H_i}{M}\right)^g\left[\frac{\phi-\phi_0}{\alpha_1}\right]^{\frac{2g}{1-2g}}. \tag{35}$$

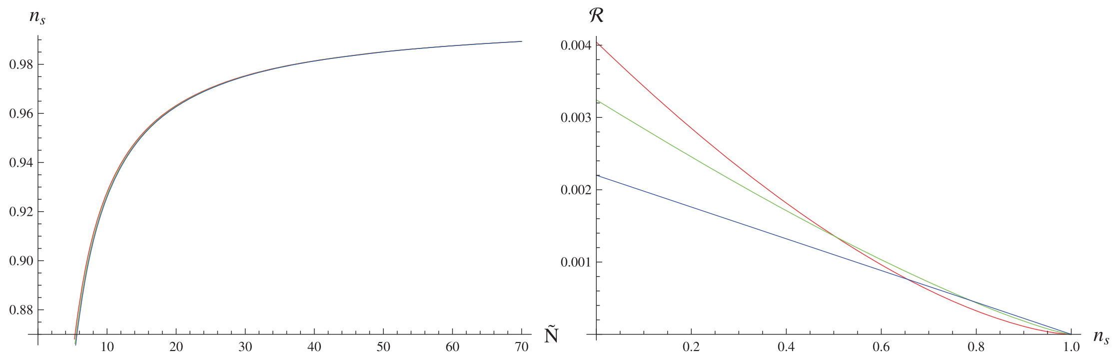

Fig. 1 n_s versus $\tilde{N}$ (*left*) and $\mathcal{R}$ versus n_s (*right*) for $g = 0.71$ (*red*), 0.8 (*green*), 0.89 (*blue*), $\gamma = 1$, $\Gamma_i \propto \chi_r^{\frac{1}{6}}$, $\chi_r = 70$

For inflaton field (32), the radiation density and e-folds take the form

$$\tilde{\rho}_r = \frac{3\gamma g}{2\kappa^2}(1-g)\left(\frac{M}{2H_i}\right)^g\left(\frac{\phi-\phi_0}{\alpha_1}\right)^{\frac{2(g-2)}{2g-1}}, \tag{36}$$

$$\tilde{N} = \gamma\left(\frac{M}{2H_i}\right)^g\left[\left(\frac{\phi-\phi_0}{\alpha_1}\right)^{\frac{2g}{2g-1}} - \left(\frac{\phi_i-\phi_0}{\alpha_1}\right)^{\frac{2g}{2g-1}}\right], \tag{37}$$

where ϕ_i denotes inflaton field at $\tilde{t} = \tilde{t}_i$. To evaluate an expression for this earliest inflaton field, we take $\epsilon = 1$ at the beginning of inflationary epoch which yields

$$\phi_i = \phi_0 + \alpha_1\left[\left(\frac{1-g}{\gamma g}\right)\left(\frac{M}{2H_i}\right)^g\right]^{\frac{2g-1}{2g}}. \tag{38}$$

Combining Eqs. (37) and (38), we obtain inflaton in terms of e-folds as

$$\phi = \phi_0 + \alpha_1\left(\frac{2H_i}{M}\right)^{\frac{2g-1}{2}}\left[\frac{\tilde{N}}{\gamma} + \frac{1-g}{\gamma g}\right]^{\frac{2g-1}{2g}}. \tag{39}$$

The perturbation parameters like scalar and tensor power spectra along with their indices as a function of e-folds turn out to be

$$\Delta_{\mathcal{R}} = \sqrt{\frac{\Gamma_i^3 3^{\frac{1}{2}}\kappa^4}{36(4\pi)^3(2\kappa^2\chi_r)^{\frac{1}{2}}}} \times\left[\left(\frac{\gamma g}{1-g}\right)\left(\frac{2H_i}{M}\right)^2\left(\frac{\tilde{N}}{\gamma} + \frac{1-g}{\gamma g}\right)\right]^{\frac{1}{4}}, \tag{40}$$

$$n_s = 1 + \frac{3}{4\gamma}\left[\frac{\tilde{N}}{\gamma} + \frac{1-g}{\gamma g}\right]^{-1}, \tag{41}$$

$$\Delta_T = \frac{2\kappa^2\gamma^2 g^2}{\pi^2}\left(\frac{\tilde{N}}{\gamma} + \frac{1-g}{\gamma g}\right)^{\frac{2g-1}{g}},$$
$$n_T = 2\left(\frac{g-1}{\gamma g}\right)\left(\frac{\tilde{N}}{\gamma} + \frac{1-g}{\gamma g}\right)^{-1}. \tag{42}$$

The ratio of tensor and scalar power spectra yields

$$\mathcal{R} = \left[(\gamma g)^{\frac{5}{2}}(1-g)^{\frac{3}{2}}\left(\frac{144(4\pi)^3(2\kappa^2\chi_r)^{\frac{1}{2}}}{\pi^4\Gamma_i^3 3^{\frac{1}{2}}}\right)\right]^{\frac{1}{2}} \times\left(\frac{M}{2H_i}\right)^{\frac{1}{2}}\left(\frac{\tilde{N}}{\gamma} + \frac{1-g}{\gamma g}\right)^{\frac{5g-8}{4g}}. \tag{43}$$

The decay rate of inflaton field is given by

$$\tilde{r} = \frac{\Gamma_i}{3\gamma g}\left(\frac{2H_i}{M}\right)\left[\frac{3}{4\gamma(1-n_s)}\right]^{\frac{1-g}{g}}. \tag{44}$$

In the background of thermal bath radiations, Hubble parameter takes the form

$$\tilde{H} = \left[\left(\frac{2\kappa^2\chi_r}{3}\right)\left(\frac{2H_i}{M}\right)^{\frac{3g-2}{1-g}}(\gamma g)^{\frac{1}{1-g}}(1-g)^{-1}T^4\right]^{\frac{1-g}{2-g}}. \tag{45}$$

Fig. 1(left plot) shows the variation of e-folds which are found to be smaller than its standard value, i.e., $\tilde{N} = 19$ at $g = 0.71$, 0.8 and $g = 0.89$. The right panel of Fig. 1 indicates that $\mathcal{R} < 0.10$ at $n_s = 0.9603$ which implies compatibility of $\mathcal{R}$ in strong dissipation regime. In order to investigate dominant characteristics of warm inflation, we plot $\tilde{H}$ versus T in left panel of Fig. 2 which yields $T \gg \tilde{H}$. The right panel of Fig. 2 implies that $\tilde{r} \gg 1$ which assures the presence of inflaton particles in strong dissipative regime.

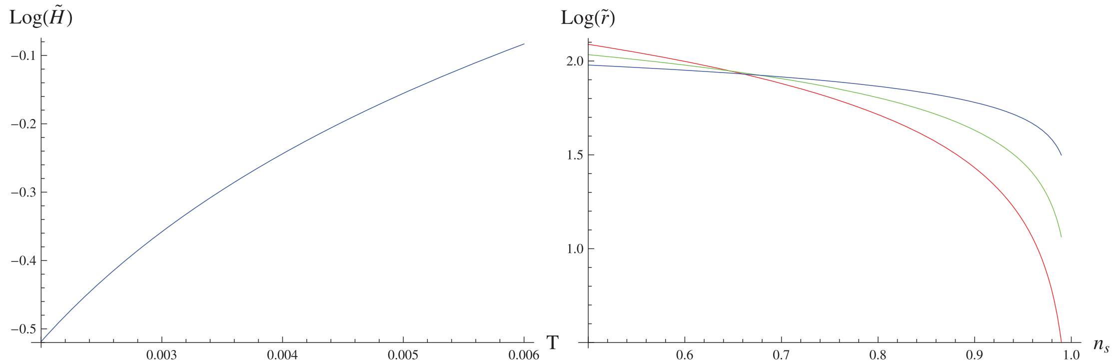

Fig. 2 Log($\tilde{H}$) versus T (*left*) for $g = 0.89$ (*blue*) and Log($\tilde{r}$) versus n_s (*right*) for $g = 0.7$ (*red*), 0.8 (*green*), 0.89 (*blue*), $\gamma = 1$, $\Gamma_i \propto \chi_r^{\frac{1}{6}}$, $\chi_r = 70$

In case of weak dissipative regime ($\tilde{r} \ll 1$), the inflaton field reduces to

$$\phi = \phi_0 + \alpha_2 \tilde{t}^{\frac{g}{2}},$$
$$U(\phi) = \frac{3}{\kappa^2}\left[\gamma g\left(\frac{M}{2H_i}\right)^g \left(\frac{\phi-\phi_0}{\alpha_2}\right)^{\frac{(g-1)}{2g}}\right]^2, \tag{46}$$

where

$$\alpha_2 = \sqrt{\frac{8\gamma(1-g)}{\kappa^2 g}\left(\frac{M}{2H_i}\right)^g}.$$

For slowly varying inflaton field, the slow-roll parameters and radiation energy density corresponding to ϕ take the form

$$\epsilon = \frac{1-g}{\gamma g}\left(\frac{2H_i}{M}\right)^g \left[\frac{\phi-\phi_0}{\alpha_2}\right]^{-2},$$
$$\eta = \frac{2-g}{\gamma g}\left(\frac{2H_i}{M}\right)^g \left[\frac{\phi-\phi_0}{\alpha_2}\right]^{-2},$$
$$\tilde{\rho}_r = \frac{\Gamma_i(1-g)}{2\kappa^2}\left(\frac{\phi-\phi_0}{\alpha_2}\right)^{-\frac{2}{g}}.$$

At the earliest stage of inflationary epoch, the inflaton field at $\tilde{t} = \tilde{t}_i$ becomes

$$\phi_i = \phi_0 + \alpha_2\left(\frac{1-g}{\gamma g}\right)\left(\frac{2H_i}{M}\right)^g.$$

The corresponding number of e-folds and inflaton field are given by

$$\tilde{N} = \gamma\left(\frac{M}{2H_i}\right)^g\left[\left(\frac{\phi-\phi_0}{\alpha_2}\right)^2 - \left(\frac{\phi_i-\phi_0}{\alpha_2}\right)^2\right], \tag{47}$$
$$\phi = \phi_0 + \alpha_2\left(\frac{2H_i}{M}\right)^{\frac{g}{2}}\left[\frac{\tilde{N}}{\gamma} + \frac{1-g}{\gamma g}\right]^{\frac{1}{2}}. \tag{48}$$

The corresponding observational parameters like scalar and tensor power spectra as well as their spectral indices become

$$\Delta_{\mathcal{R}} = \frac{\kappa^2}{2}\left(\frac{\Gamma_i}{2\kappa^2\chi_r}\right)^{\frac{1}{4}}(\gamma g)^2(1-g)^{-\frac{3}{4}}\left(\frac{2H_i}{M}\right)^{-\frac{1}{4}} \times\left[\frac{\tilde{N}}{\gamma} + \frac{1-g}{\gamma g}\right]^{\frac{8g-5}{4g}}, \tag{49}$$
$$n_s = 1 - \frac{1}{\gamma g}\left(\frac{8g-5}{4g}\right)\left[\frac{\tilde{N}}{\gamma} + \frac{1-g}{\gamma g}\right]^{-1}, \tag{50}$$
$$\Delta_T = \frac{2\kappa^2\gamma^2 g^2}{\pi^2}\left(\frac{\tilde{N}}{\gamma} + \frac{1-g}{\gamma g}\right)^{\frac{2(g-1)}{g}},$$
$$n_T = 2\left(\frac{g-1}{\gamma g}\right)\left(\frac{\tilde{N}}{\gamma} + \frac{1-g}{\gamma g}\right)^{-1}. \tag{51}$$

The tensor-scalar ratio is

$$\mathcal{R} = \frac{4}{\pi^2}\left[\left(\frac{\Gamma_i}{2\kappa^2\chi_r}\right)^{-1}\left(\frac{2H_i}{M}\right)(1-g)^3\right]^{\frac{1}{4}}\left(\frac{\tilde{N}}{\gamma} + \frac{1-g}{\gamma g}\right)^{\frac{-3}{4g}}. \tag{52}$$

For weak dissipation regime, the decay rate and Hubble parameter in terms of thermal bath temperature turn out to be

$$\tilde{r} = \frac{\Gamma_i}{3\gamma g}\left(\frac{2H_i}{M}\right)\left[\frac{8g-5}{4\gamma g(1-n_s)}\right]^{\frac{1-g}{g}}, \tag{53}$$
$$\tilde{H} = \left[\left(\frac{2\kappa^2\chi_r}{\Gamma_i(1-g)}\right)^{\frac{1}{4}}\left(\frac{M}{2H_i}\right)^{\frac{3-4g}{4(1-g)}}(\gamma g)^{\frac{1}{4(1-g)}}T\right]^{4(1-g)}. \tag{54}$$

Fig. 3(left plot) represents the graphical behavior of n_s against $\tilde{N}$ in weak dissipative regime which are found in enough abundance to discuss inflationary epoch whereas

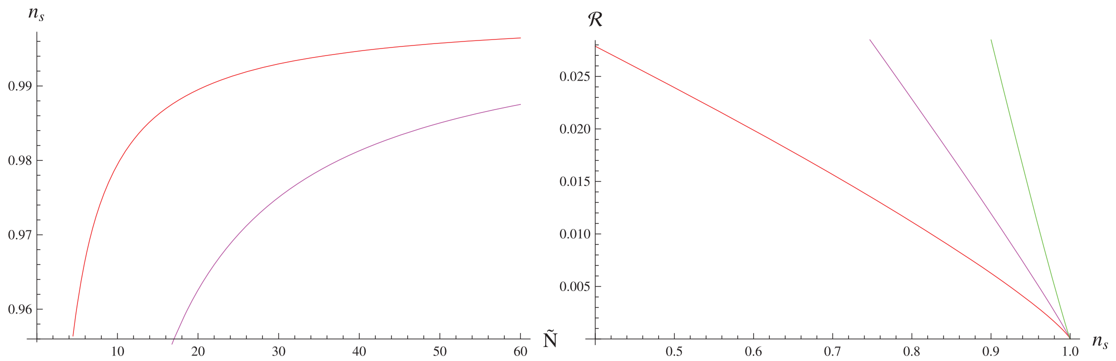

Fig. 3 n_s versus $\tilde{N}$ (*left*) for $g = 0.7$ (*red*), 0.999 (*magenta*) and $\mathcal{R}$ versus n_s (*right*) for $g = 0.7$ (*green*), 0.8 (*magenta*), 0.9 (*red*), $\gamma = 1$, $\Gamma_i \propto \chi_r^{\frac{1}{6}}$, $\chi_r = 70$

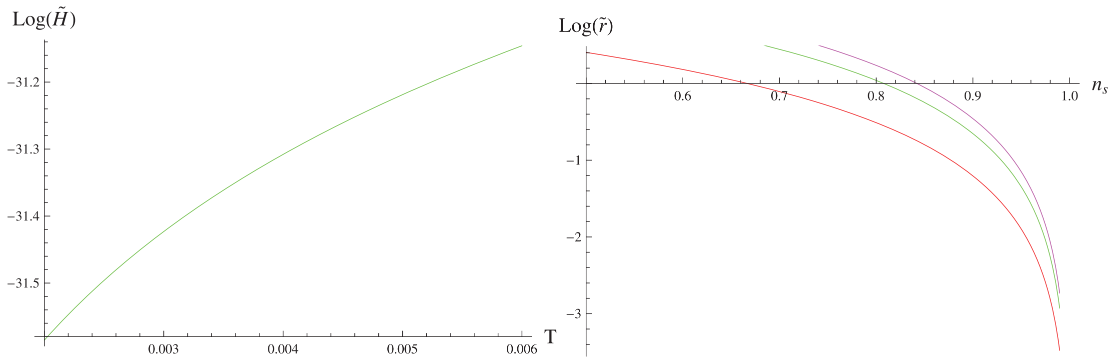

Fig. 4 Log$(\tilde{H})$ versus T (*left*) for $g = 0.9$ (*green*) and Log$(\tilde{r})$ versus n_s (*right*) for $g = 0.7$ (*red*), 0.8 (*green*), 0.9 (*magenta*), $\gamma = 1$, $\Gamma_i \propto \chi_r^{\frac{1}{6}}$, $\chi_r = 70$

the right plot indicates compatible $\mathcal{R}$ for the proposed values of g. Figure 4 shows that $T \gg \tilde{H}$ (left panel) and $\tilde{r} \ll 1$ (right panel) for $0.7 \leq g \leq 0.9$ which assures the existence of warm intermediate inflation in weak dissipative regime.

3.2 Warm intermediate inflation for generalized dissipative coefficient

In warm inflationary scenario, the dissipative coefficient plays a dynamical role as it represents a physical process of dissipation regarding to inflaton field and thermal bath. This coefficient may be a function of inflaton field, or thermal bath, or both. The most general form of dissipation factor is given by Zhang (2009)

$$\Gamma = \Gamma_i \frac{T^m}{\phi^{m-1}},$$

where Γ_i denotes a constant that describes microscopic dynamics of dissipation process and m represents an integer. For different values of m, dissipation coefficient corresponds to different physical processes, i.e., when $m = 0$, the dissipation coefficient describes an exponential decay propagator in high temperature supersymmetry case. For $m = 1$, it becomes proportional to thermal bath temperature while $m = -1$ deals with non-supersymmetry case (Berera et al. 2009; Herrera et al. 2014). In the present work, we study the behavior of generalized dissipation coefficient in strong as well as weak dissipation regimes.

In strong dissipative regime, the inflaton field and corresponding potential take the form

$$\phi = \alpha_3 \tilde{t}^{\frac{4(2g-1)+m(2-g)}{4(3-m)}},$$
$$U(\phi) = \frac{3}{\kappa^2}(\gamma g)^2 \left(\frac{M}{2H_i}\right)^{2g} \left(\frac{\phi}{\alpha_3}\right)^{\frac{8(3-m)(g-1)}{4(2g-1)+m(2-g)}}, \quad (55)$$

where

$$\alpha_3=\left\{\left(\frac{3-m}{2}\right)\left(\frac{6}{\kappa^2}\right)^{\frac{1}{2}}\times\left[(\gamma g)^{8-m}(1-g)^{4-m}\left(\frac{2H_i}{M}\right)^{g(m-8)-4m}\right]^{\frac{1}{8}}\times\left(\frac{8}{4(2g-1)+m(2-g)}\right)\right\}^{\frac{2}{3-m}}.$$

Under the influence of inflaton field (55), the corresponding radiation density, Hubble and slow-roll parameters turn out to be

$$\begin{aligned}\tilde{\rho}_r&=\frac{3}{2\kappa^2}\gamma g(1-g)\left(\frac{M}{2H_i}\right)^g\left(\frac{\phi}{\alpha_3}\right)^{\frac{4(3-m)(g-2)}{4(2g-1)+m(2-g)}},\\ \tilde{H}(\tilde{t})&=\gamma g\left(\frac{M}{2H_i}\right)^g\left(\frac{\phi}{\alpha_3}\right)^{\frac{4(3-m)(g-1)}{4(2g-1)+m(2-g)}},\\ \epsilon&=\frac{(1-g)}{\gamma g}\left(\frac{2H_i}{M}\right)^g\left(\frac{\phi}{\alpha_3}\right)^{\frac{-4(3-m)g}{4(2g-1)+m(2-g)}},\\ \eta&=\left(\frac{2-g}{\gamma g}\right)\left(\frac{2H_i}{M}\right)^g\left(\frac{\phi}{\alpha_3}\right)^{\frac{-4(3-m)g}{4(2g-1)+m(2-g)}}.\end{aligned}\tag{56}$$

At the beginning of inflation ($\epsilon=1$), the initial value of inflaton field leads to express ϕ in the following form

$$\phi=\alpha_3\left\{\left(\frac{2H_i}{M}\right)^g\left(\frac{\tilde{N}}{\gamma}+\frac{1-g}{\gamma g}\right)\right\}^{\frac{4(2g-1)+m(2-g)}{4(3-m)g}}.\tag{57}$$

The corresponding scalar power spectrum and spectral index are

$$\begin{aligned}\Delta_R^2&=\frac{\kappa^2}{6}\left[\left(\frac{3}{2\kappa^2\chi_r}\right)^{\frac{3m+2}{4}}\left(\frac{\Gamma_i}{4\pi}\right)^3(\gamma g)^{\frac{3}{4}(m+2)}\times\left(\frac{2H_i}{M}\right)^{\frac{3}{2}+\frac{3}{4}\{\frac{(1-m)(4(2g-1)-g(m+2))}{(3-m)g}\}}\alpha_3^{3(1-m)}\right]^{\frac{1}{2}}\\&\quad\times\left(\frac{\tilde{N}}{\gamma}+\frac{1-g}{\gamma g}\right)^{\beta_0},\\ n_s&=1-\frac{3\beta_0}{8\gamma}\left(\frac{\tilde{N}}{\gamma}+\frac{1-g}{\gamma g}\right)^{-1},\end{aligned}\tag{58}$$

where

$$\beta_0=\frac{3}{8}\left[\frac{(3-m)\{g(m+2)-2m\}+(1-m)\{4(2g-1)+m(2-g)\}}{(3-m)g}\right].$$

Similarly, tensor power spectrum and its spectral index become

$$\Delta_T^2=\frac{2\kappa^2}{\pi^2}(\gamma g)^2\left(\frac{\tilde{N}}{\gamma}+\frac{1-g}{\gamma g}\right)^{\frac{2}{g}(g-1)},$$

$$n_T=\frac{2(g-1)}{\gamma g}\left(\frac{\tilde{N}}{\gamma}+\frac{1-g}{\gamma g}\right)^{-1}.$$

The above observational parameters generate tensor-scalar ratio as

$$\begin{aligned}\mathcal{R}&=\left[\frac{144}{\pi^4}\left(\frac{2\kappa^2\chi_r}{3}\right)^{\frac{3m+2}{4}}\left(\frac{4\pi}{\Gamma_i}\right)^3(\gamma g)^{\frac{22-3m}{4}}\times\left(\frac{2H_i}{M}\right)^{-\frac{3}{2}-\frac{3}{4}\{\frac{(1-m)(4(2g-1)-g(m+2))}{(3-m)g}\}}\alpha_3^{3(m-1)}\right]^{\frac{1}{2}}\\&\quad\times\Big(\big(8\gamma(1-n_s)(3-m)g\big)\big/\big(3\big[(3-m)\big\{g(m+2)\\&\quad-2m\big\}+(1-m)\big\{4(2g-1)+m(2-g)\big\}\big]\big)\Big)^{\beta_0-\frac{2(g-1)}{g}}.\end{aligned}\tag{59}$$

The Hubble parameter in terms of thermal radiations and decay rate of inflaton field take the form

$$\tilde{H}=\left[\left(\frac{2\kappa^2\chi_r}{3}\right)(1-g)^{-1}(\gamma g)^{\frac{1}{1-g}}\left(\frac{2H_i}{M}\right)^{\frac{5-4g}{g-1}}T^4\right]^{\frac{1-g}{2-g}}\tag{60}$$

$$\begin{aligned}\tilde{r}&=\alpha_m\alpha_3^{1-m}(3\gamma g)^{\frac{m-4}{4}}(1-g)^{\frac{m}{4}}\times\left(\frac{2H_i}{M}\right)^{m+1-\frac{m}{2}+\frac{1-m}{4(3-m)}\{4(2g-1)+m(2-g)\}}\\&\quad\times\left(\frac{8\gamma(1-n_s)(3-m)g}{3[(3-m)\{g(m+2)-2m\}+(1-m)\{4(2g-1)+m(2-g)\}]}\right)^{\zeta},\end{aligned}\tag{61}$$

where

$$\zeta=-\frac{1}{g}(1-g)+\frac{m}{4g}(2-g)+\frac{(m-1)}{4g(3-m)}\big\{4(2g-1)+m(2-g)\big\}.$$

The graphical behavior of n_s versus number of e-folds is shown in left plot of Figs. 5, 6 and 7 for $m=0,\ 1$ and $m=-1$, respectively. The right plot of Fig. 5, 6 and 7 indicate that $\mathcal{R}$ is constrained at observational value of n_s which leads to the consistent behavior of inflationary model for different values of model parameter g. Figures 8 and 9 represent graphical analysis of inflaton particles which satisfy the condition of warm inflation, i.e, $T\gg\tilde{H}$ in strong dissipative regime for $m=0,-1$. Figure 10 shows that $\tilde{r}\gg1$ which implies that inflaton particles lies in strong dissipative regime while Fig. 11 supports the existence of warm inflation for $m=1$.

In weak dissipative regime, the constant as well as proposed generalized dissipative coefficient leave the same effect over inflaton field, number of e-folds and slow-roll parameters whereas radiation density becomes

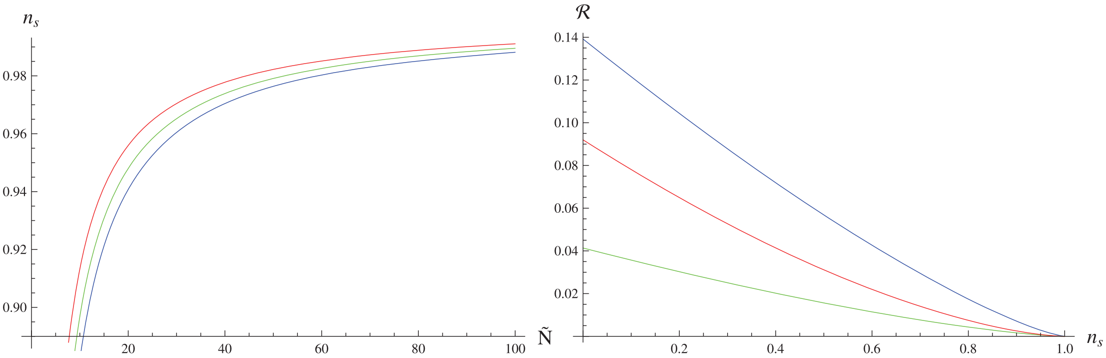

Fig. 5 n_s versus $\tilde{N}$ (*left*) and $\mathcal{R}$ versus n_s (*right*) for $g = 0.75$ (*red*), 0.85 (*green*), 0.95 (*blue*), $\gamma = 10^{-15}$, $\Gamma_i \propto \chi_r^{\frac{1}{6}}$, $\chi_r = 70$, $m = 0$

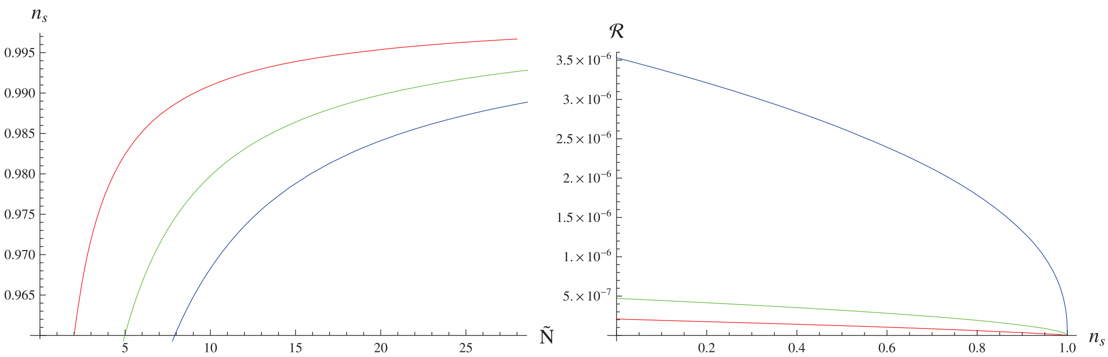

Fig. 6 n_s versus $\tilde{N}$ (*left*) and $\mathcal{R}$ versus n_s (*right*) for $g = 0.75$ (*red*), 0.85 (*green*), 0.95 (*blue*), $\gamma = 10^{-18}$, $\Gamma_i \propto \chi_r^{\frac{1}{6}}$, $\chi_r = 70$, $m = 1$

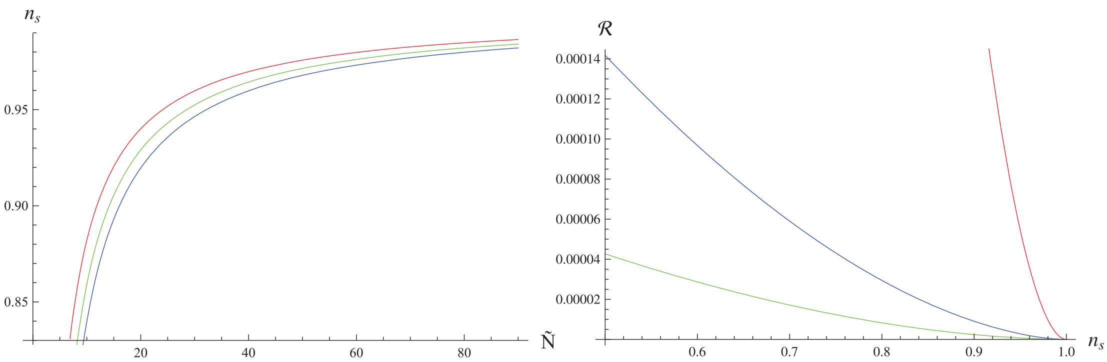

Fig. 7 n_s versus $\tilde{N}$ (*left*) and $\mathcal{R}$ versus n_s (*right*) for $g = 0.75$ (*red*), 0.85 (*green*), 0.95 (*blue*), $\gamma = 10^{-18}$, $\Gamma_i \propto \chi_r^{\frac{1}{6}}$, $\chi_r = 70$, $m = -1$

$$\tilde{\rho}_r = \frac{1}{2\kappa^2}\left(\frac{\Gamma_i}{(2\kappa^2\chi_r)^{\frac{m}{4}}}\right)^{\frac{4}{4-m}}\left(\frac{2H_i}{M}\right)^{\frac{2m-4g}{4-m}} \times \left(\gamma g(1-g)\right)^{\frac{4}{4-m}}\alpha_2^{\frac{2(2-g)}{g}}\phi^{\frac{2(g-2)}{g}+\frac{4(1-m)}{4-m}}.$$

The scalar and tensor power spectra along with corresponding spectral indices and tensor-scalar ratio are given by

$$\Delta_{\mathcal{R}} = \frac{\kappa^2}{2}\left[\frac{\Gamma_i\alpha_2^{1-m}}{2\kappa^2\chi_r}(\gamma g)^{2(4-m)}(1-g)^{m-3}\right.$$

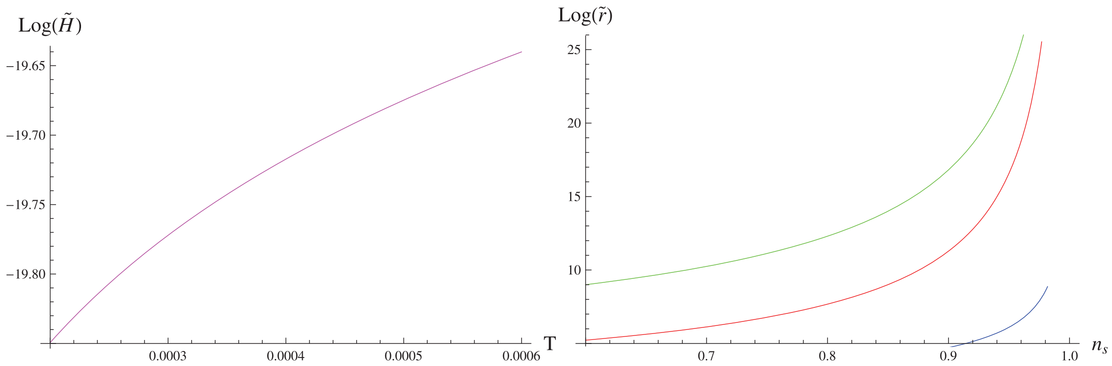

Fig. 8 Log($\tilde{H}$) versus T (*left*) for $g = 0.95$ (*magenta*) and Log($\tilde{r}$) versus n_s (*right*) for $g = 0.75$ (*red*), 0.85 (*green*), 0.95 (*blue*), $\gamma = 10^{-15}$, $\Gamma_i \propto \chi_r^{\frac{1}{6}}$, $\chi_r = 70$, $m = 0$

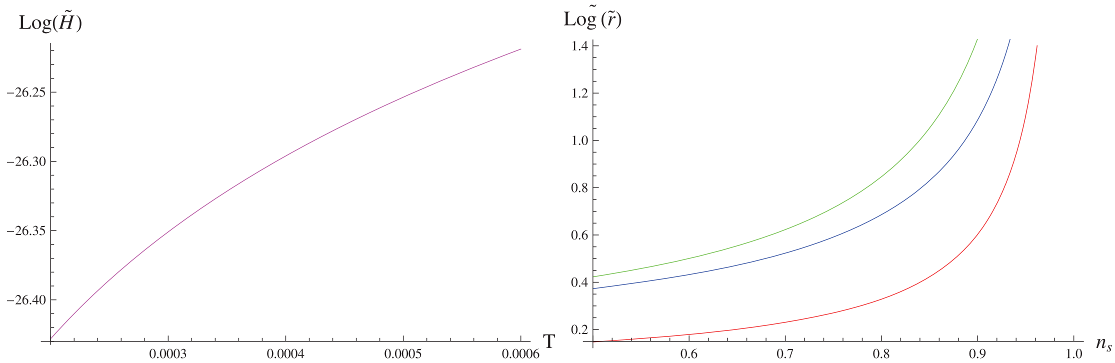

Fig. 9 Log($\tilde{H}$) versus T (*left*) for $g = 0.95$ (*magenta*) and Log($\tilde{r}$) versus n_s (*right*) for $g = 0.75$ (*red*), 0.85 (*green*), 0.95 (*green*), $\gamma = 10^{-18}$, $\Gamma_i \propto \chi_r^{\frac{1}{6}}$, $\chi_r = 70$, $m = -1$

$$\times \left(\frac{2H_i}{M}\right)^{\frac{(m-1)(2-g)}{2}+2(4-m)(g-1)}$$

$$\times \left(\frac{\tilde{N}}{\gamma} + \frac{1-g}{\gamma g}\right)^{\frac{2g(4-m)+m-5}{g}+\frac{1-m}{2}}\Bigg]^{\frac{1}{4-m}}, \tag{62}$$

$$n_s = 1 - \left(\frac{2m-10+g(17-5m)}{2(4-m)(1+g(\tilde{N}-1))}\right), \tag{63}$$

$$\Delta_T = \frac{2\kappa^2\gamma^2 g^2}{\pi^2}\left(\frac{2m-10+g(17-5m)}{\gamma(g+2)(4-m)}\right)^{\frac{2(g-1)}{g}} \times (1-n_s)^{\frac{2(1-g)}{g}}, \tag{64}$$

$$n_T = 2\left(\frac{g-1}{\gamma g}\right)\left(\frac{2m-10+g(17-5m)}{\gamma(g+2)(4-m)}\right)^{-1}(1-n_s), \tag{65}$$

$$\mathcal{R} = \frac{4}{\pi^2}\Bigg[\frac{\Gamma_i \alpha_2^{1-m}(1-g)^{m-3}}{2\kappa^2\chi_r}$$

$$\times \left(\frac{2H_i}{M}\right)^{(m-1)(1-\frac{g}{2})}\Bigg\{(1-n_s)^{-1}$$

$$\times \left(\frac{2m-10+g(17-5m)}{\gamma(g+2)(4-m)}\right)\Bigg\}^{\frac{3-m}{g}+\frac{1-m}{2}}\Bigg]^{\frac{1}{m-4}}. \tag{66}$$

The Hubble parameter in the background of thermal radiations and dissipation rate of inflaton field take the form

$$\tilde{H} = \Bigg[\frac{\Gamma_i \alpha_2^{m-1}(1-g)^{-1}}{(2\kappa^2\chi_r)^{m-2}}(\gamma g)^{\frac{g(1-m)-2}{2(g-1)}} \times \left(\frac{2H_i}{M}\right)^{\frac{g(1-m)-2}{2(1-g)}+(m-1)g-3} T^{4-m}\Bigg]^{\frac{2(g-1)}{g(1-m)-2}} \tag{67}$$

$$\tilde{r} = \frac{1}{3}\left(\frac{\Gamma_i}{(2\kappa^2\chi_r)^{\frac{m}{4}}}\right)\alpha_2^{\frac{4(1-m)}{4-m}}(1-g)^{\frac{m}{4-m}}(\gamma g)^{-1}$$

$$\times \left(\frac{2H_i}{M}\right)^{\frac{4+6m+2g(1-m)}{4-m}}\Bigg[\left(\frac{2m-10+g(17-5m)}{\gamma(g+2)(4-m)}\right)$$

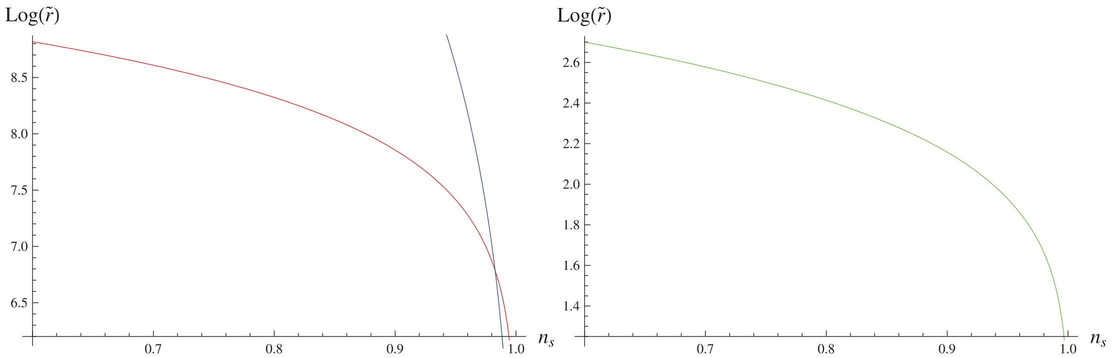

Fig. 10 Log($\tilde{r}$) versus n_s for $g = 0.75$ (*red*), 0.95 (*blue*) (*left*) and 0.85 (*green*) (*right*), $\gamma = 10^{-18}$, $\Gamma_i \propto \chi_r^{\frac{1}{6}}$, $\chi_r = 70$, $m = 1$

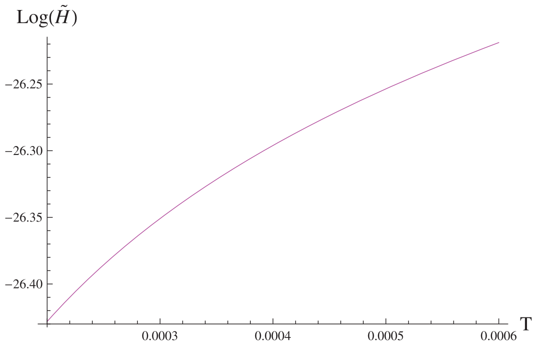

Fig. 11 Log($\tilde{H}$) versus T for $g = 0.95$ (*magenta*), $\gamma = 10^{-18}$, $\Gamma_i \propto \chi_r^{\frac{1}{6}}$, $\chi_r = 70$, $m = 1$

$$\times (1 - n_s)^{-1}\Bigg]^{\frac{4(1-g)g+m(g-2)+2g(1-m)}{g(4-m)}}. \tag{68}$$

The graphical behavior of n_s against number of e-folds and variation of $\mathcal{R}$ versus n_s for generalized dissipative coefficient is given in Figs. 12, 13 and 14 for $m = 0,\ 1$ and $m = -1$, respectively. Figures 15, 16 and 17 assure the condition of warm inflation in weak dissipative regime for different values of model parameter g.

4 Concluding remarks

In this paper, we have investigated the dynamics of warm inflation for flat FRW universe model in Einstein representation of $f(R)$ gravity. In warm inflation, a separate reheating phase is avoided and interactions between inflaton and other fields such as matter or radiations are taken into account. These interactions give rise to friction term in equation of motion of inflaton which provides dissipation effects in strong and weak dissipative regimes. We have analyzed warm intermediate inflationary model in strong and weak regimes for both constant and generalized dissipative coefficients. To avoid negative kinetic energy of inflaton field, we have studied inflationary paradigm for Starobinsky inflationary model in Einstein frame.

We have explored solutions of inflaton field and corresponding potentials and also formulated dimensionless slow-roll parameters in terms of inflaton field. In warm inflation, density perturbations appear due to thermal fluctuations instead of quantum fluctuations and the characteristics of these fluctuations are described by observational parameters such as scalar and tensor power spectra, their corresponding spectral indices and tensor-scalar ratio. We have calculated these parameters under slow-roll approximation and studied their graphical analysis for different values of intermediate model parameter g. The results are summarized as follows.

- For strong constant dissipative regime, the number of e-folds remain less than 20 for $0.71 \leq g \leq 0.89$ while the corresponding graphical behavior of $\mathcal{R} - n_s$ leads to compatible range of $\mathcal{R}$, i.e., $\mathcal{R} < 0.10$. At $g = 0.89$, the temperature of thermal bath radiations is found to be greater than Hubble parameter which leads to the existence of warm inflation and $\tilde{r} \gg 1$ indicates that inflaton particles lie in strong dissipative regime.
- For weak constant dissipative regime, viable e-folds are obtained only when $0.626 \leq g \leq 0.999$ whereas the corresponding tensor-scalar ratio is found to be compatible at the constrained value of scalar spectral index in this interval of g. For $g = 0.9$, we have found $T \gg \tilde{H}$ and $\tilde{r} \ll 1$ which verify the presence of warm inflation in weak dissipative regime and inflationary model is found to be consistent with observational data.
- For generalized dissipative coefficient in strong dissipative regime, the inflationary model yields consistent results with Planck constraints for $m = 0, 1, -1$ with $0.5 < g < 1$, $0.67 < g < 1$, $0.88 < g < 1$, respectively. In case

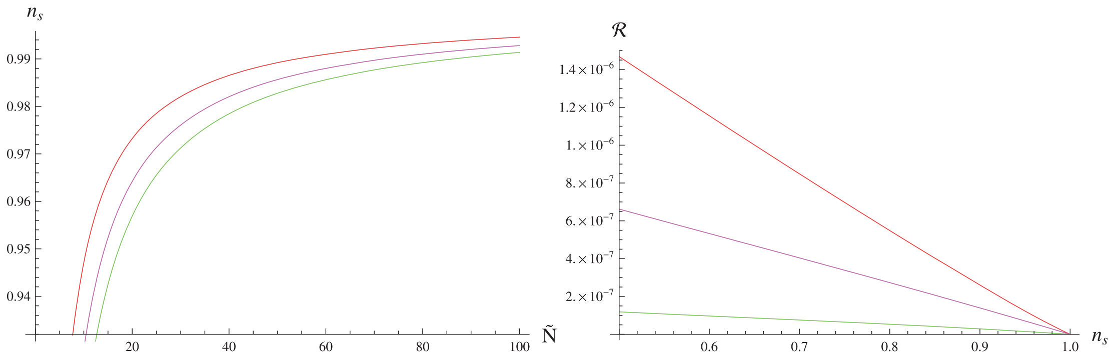

Fig. 12 n_s versus $\tilde{N}$ (*left*) and $\mathcal{R}$ versus n_s (*right*) for $g = 0.79$ (*red*), 0.8 (*magenta*), 0.99 (*green*), $\gamma = 1$, $\Gamma_i \propto \chi_r^{\frac{1}{6}}$, $\chi_r = 70$, $m = 0$

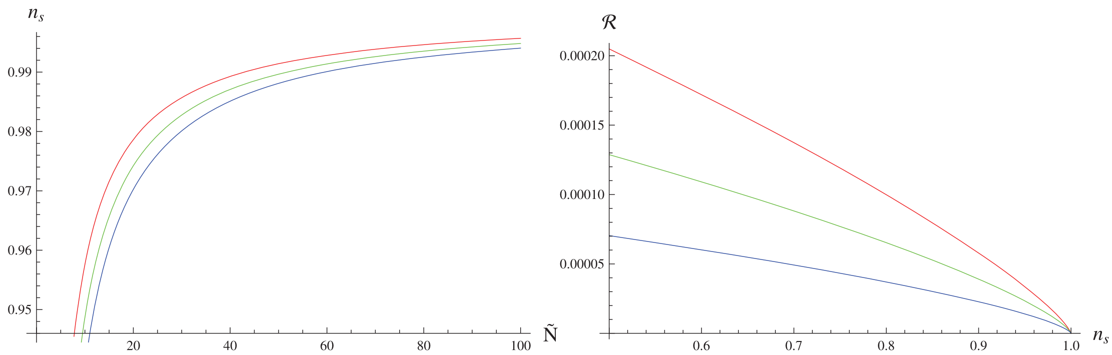

Fig. 13 n_s versus $\tilde{N}$ (*left*) and $\mathcal{R}$ versus n_s (*right*) for $g = 0.85$ (*red*), 0.9 (*green*), 0.95 (*blue*), $\gamma = 1$, $\Gamma_i \propto \chi_r^{\frac{1}{6}}$, $\chi_r = 70$, $m = 1$

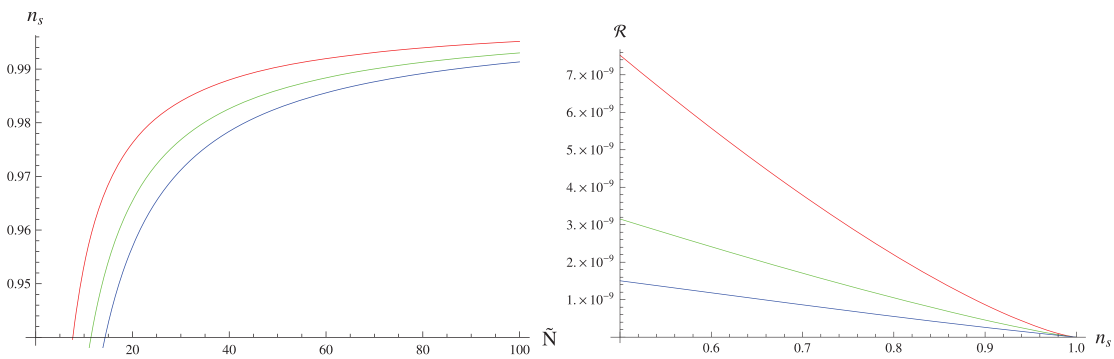

Fig. 14 n_s versus $\tilde{N}$ (*left*) and $\mathcal{R}$ versus n_s (*right*) for $g = 0.7$ (*red*), 0.8 (*green*), 0.9 (*blue*), $\gamma = 1$, $\Gamma_i \propto \chi_r^{\frac{1}{6}}$, $\chi_r = 70$, $m = -1$

of weak dissipative regime, inflationary model is compatible for $m = 0, 1, -1$ with $0.59 < g < 1$, $0.67 < g < 1$, $0.55 < g < 1$, respectively.

Sharif and Ikram (2016) have explored the dynamics of warm intermediate inflation for flat FRW universe model in Jordan frame of $f(\mathcal{G})$ gravity. They have found consistent results for constant dissipation coefficient through e-folds and tensor-scalar ratio whereas for generalized dissipative coefficient with $m = 3$, the observational parameters lead to inconsistent results. We have studied warm intermediate inflationary dynamics in strong as well as weak dissipation

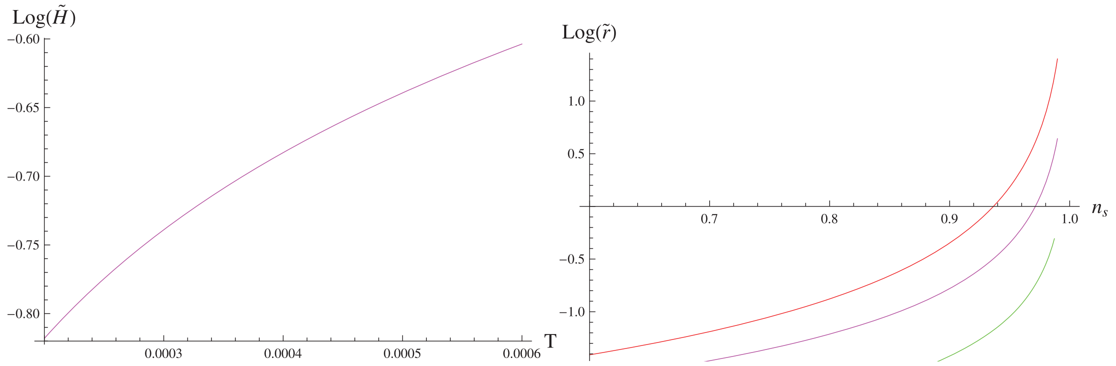

Fig. 15 Log($\tilde{H}$) versus T (*left*) for $g = 0.975$ (*magenta*) and Log($\tilde{r}$) versus n_s (*right*) for $g = 0.79$ (*red*), 0.89 (*magenta*), 0.96 (*green*), $\gamma = 1$, $\Gamma_i \propto \chi_r^{\frac{1}{6}}$, $\chi_r = 70$, $m = 0$

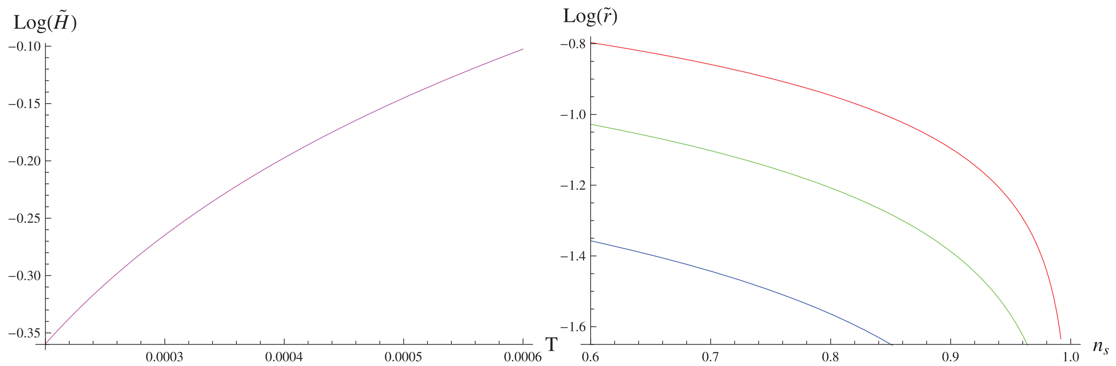

Fig. 16 Log($\tilde{H}$) versus T (*left*) for $g = 0.922$ (*magenta*) and Log($\tilde{r}$) versus n_s (*right*) for $g = 0.85$ (*red*), 0.9 (*green*), 0.95 (*blue*), $\gamma = 1$, $\Gamma_i \propto \chi_r^{\frac{1}{6}}$, $\chi_r = 70$, $m = 1$

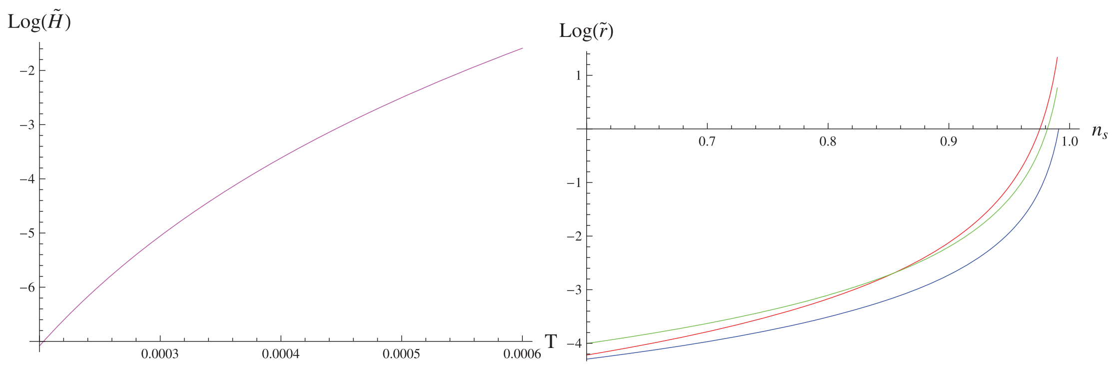

Fig. 17 Log($\tilde{H}$) versus T (*left*) for $g = 0.9$ (*magenta*) and Log($\tilde{r}$) versus n_s (*right*) for $g = 0.7$ (*red*), 0.8 (*green*), 0.9 (*blue*), $\gamma = 1$, $\Gamma_i \propto \chi_r^{\frac{1}{6}}$, $\chi_r = 70$, $m = -1$

regimes. For constant dissipation coefficient, we have found consistent results for both regimes. The graphical analysis ensures the presence of warm inflation ($T \gg \tilde{H}$) as well as existence of inflaton particles in strong ($\tilde{r} \gg 1$) and weak ($\tilde{r} \ll 1$) dissipative regimes. In case of generalized dissipative coefficient, we have obtained compatible results for $m = 0, -1, 1$ which satisfy warm inflation condition but for $m = 3$, the observational parameters yield inconsistent results in both regimes.

Finally, it is concluded that isotropic warm intermediate inflationary universe model remains consistent to Planck 2015 constraints for constant dissipation coefficient as well as generalized dissipation coefficient for $m = 0, 1$ and -1 in weak and strong dissipation regimes. For $m = 3$, the condition for intermediate model parameter is violated, i.e., $0 < g < 1$ which leads to inconsistent behavior of inflationary model in weak and strong dissipation regimes.

Acknowledgements This work has been supported by the *Pakistan Academy of Sciences Project*.

References

Ade, P.A.R., et al.: Astron. Astrophys. **594**, A20 (2016)
Allemandi, G., Capone, M., Capozziello, S., Francaviglia, M.: Gen. Relativ. Gravit. **38**, 33 (2006)
Artymowski, M., Lalak, Z.: J. Cosmol. Astropart. Phys. **9**, 036 (2014)
Bamba, K., Nojiri, S., Odintsov, S.D., Sáez-Gómez, D.: Phys. Rev. D **90**, 124061 (2014)
Bardeen, J.M., Steinhardt, P.J., Turner, M.S.: Phys. Rev. D **28**, 679 (1983)
Barrow, J.D.: Phys. Lett. B **235**, 40 (1990)
Barrow, J.D., Saich, P.: Phys. Lett. B **249**, 406 (1990)
Barth, N.H., Christensen, S.M.: Phys. Rev. D **28**, 1876 (1983)
Bassett, B.A., Tsujikawa, S., Wands, D.: Rev. Mod. Phys. **78**, 537 (2006)
Bastero-Gil, M., Berera, A., Ramos, R.O.: J. Cosmol. Astropart. Phys. **9**, 033 (2011)
Bastero-Gil, M., Berera, A., Ramos, R.O., Rosa, J.G.: J. Cosmol. Astropart. Phys. **1**, 016 (2013)
Berera, A.: Phys. Rev. Lett. **75**, 3218 (1995)
Berera, A.: Phys. Rev. D **55**, 3346 (1997)
Berera, A.: Nucl. Phys. B **585**, 666 (2000)
Berera, A., Ramos, R.O.: Phys. Rev. D **63**, 103509 (2001)
Berera, A., Moss, I.G., Ramos, R.O.: Rep. Prog. Phys. **72**, 026901 (2009)
Calcagni, G., Tsujikawa, S., Sami, M.: Class. Quantum Gravity **22**, 3977 (2005)
Capozziello, S., Nojiri, S., Odintsov, S.D.: Phys. Lett. B **634**, 93 (2006)
Chiba, T.: J. Cosmol. Astropart. Phys. **3**, 8 (2005)
de Felice, A., Tusjikawa, S.: Living Rev. Relativ. **13**, 3 (2010)
Faraoni, V., Nadeau, S.: Phys. Rev. D **75**, 023501 (2007)
Gamow, G.: Phys. Rev. **70**, 572 (1946)
Guth, A.H.: Phys. Rev. D **23**, 347 (1981)
Hall, L.M.H., Moss, I.G., Berera, A.: Phys. Rev. D **69**, 083525 (2004)
Hawking, S.W.: Phys. Lett. B **115**, 295 (1982)
Herrera, R., Olivares, M., Videla, N.: Phys. Rev. D **88**, 063535 (2013)
Herrera, R., Videla, N., Olivares, M.: Phys. Rev. D **90**, 103502 (2014)
Hwang, J.C., Noh, H.: Phys. Rev. D **66**, 084009 (2002)
Khlebnikov, S.Y., Tkachev, I.I.: Phys. Rev. Lett. **77**, 219 (1996)
Kofman, L., Linde, A., Starobinsky, A.A.: Phys. Rev. Lett. **73**, 3195 (1994)
Kolb, E.W., Turner, M.S.: The Early Universe. Westview Press, Boulder (1994)
Linde, A.: Phys. Lett. B **129**, 177 (1983)
Linde, A.: Phys. Lett. B **175**, 395 (1986)
Linde, A.: Particle Physics and Inflationary Cosmology. Harwood Academic, Reading (1990)
Lyth, D.H., Liddle, A.R.: The Primordial Density Perturbation: Cosmology, Inflation and the Origin of Structure. Cambridge University Press, Cambridge (2009)
Magnano, G., Sokolowski, L.M.: Phys. Rev. D **50**, 5039 (1994)
Muslimov, A.: Class. Quantum Gravity **7**, 231 (1990)
Nojiri, S., Odintsov, S.D.: Phys. Rep. **505**, 59 (2011)
Penzias, A.A., Wilson, R.W.: Astrophys. J. **142**, 419 (1965)
Perlmutter, S., et al.: Astrophys. J. **517**, 565 (1999)
Santiago, D.I., Silbergleit, A.S.: Gen. Relativ. Gravit. **32**, 565 (2000)
Sato, K.: Mon. Not. R. Astron. Soc. **195**, 467 (1981)
Setare, M.R., Kamali, V.: Phys. Lett. B **726**, 56 (2013)
Sharif, M., Ikram, A.: J. Exp. Theor. Phys. **123**, 40 (2016)
Sharif, M., Nawazish, I.: Astrophys. Space Sci. **361**, 19 (2016)
Sharif, M., Saleem, R.: Eur. Phys. J. C **74**, 2738 (2014)
Sharif, M., Saleem, R.: Astrophys. Space Sci. **360**, 46 (2015)
Sharif, M., Saleem, R.: Astrophys. Space Sci. **361**, 107 (2016)
Sokolowski, L.: Class. Quantum Gravity **6**, 2045 (1989)
Starobinsky, A.A.: Phys. Lett. B **91**, 99 (1980)
Teyssandier, P., Tourrenc, P.: J. Math. Phys. **24**, 2793 (1983)
Yokoyama, J., Linde, A.: Phys. Rev. D **60**, 083509 (1999)
Zhang, Y.: J. Cosmol. Astropart. Phys. **3**, 030 (2009)

International Journal of Modern Physics D
Vol. 26, No. 14 (2017) 1750191 (25 pages)

DOI: 10.1142/S0218271817501917

Warm logamediate inflation in Starobinsky inflationary model

M. Sharif* and Iqra Nawazish†

Department of Mathematics, University of the Punjab,
Quaid-e-Azam Campus, Lahore 54590, Pakistan
**msharif.math@pu.edu.pk*
†iqranawazish07@gmail.com

Received 24 February 2017
Revised 9 September 2017
Accepted 11 September 2017
Published 25 October 2017

This paper investigates the dynamics of warm logamediate inflation for flat isotropic and homogeneous universe in Einstein frame representation of $f(R)$ gravity. In this scenario, we study dissipative effects for weak and strong interactions of inflaton field via constant and generalized dissipative coefficient. In both interacting regimes, we find inflaton solution corresponding to scalar potential and radiation density of dissipating inflaton. Under slow-roll approximation, we formulate scalar and tensor power spectra, their spectral indices and tensor–scalar ratio for Starobinsky inflationary model and construct graphical analysis of these observational parameters. It is concluded that this model remains compatible with Planck 2015 constraints in weak and strong regimes for constant dissipative coefficient. For generalized dissipative coefficient, the inflationary model yields consistent results for $m = 0, 1$ and -1 in strong regime while condition of warm inflation is violated for $m = -1$ in weak regime.

Keywords: Slow-roll approximation; warm inflation; $f(R)$ gravity.

PACS Number(s): 05.40.+j, 98.80.Cq, 95.36.+x

1. Introduction

The development of a standard model describing observational facts like the existence of cosmic microwave background radiations (CMBR), presence of primordial light elements and current cosmic expansion[1] is considered as the crucial advancement in cosmology. This model explains decelerated expansion at the initial stage of the universe but leads to some issues like horizon, monopole and flatness. The standard model needs an epoch of rapid acceleration in the early universe named as "inflation"[2] to overcome these issues. It was suggested[3] that initial stage of the universe passes through a rapid expansion due to the existence of false vacuum filled with bubbles. The presence of these bubbles leads to de Sitter expansion which yields inhomogeneous universe at the end of inflation. Consequently, another version of inflation dubbed as new or chaotic inflation was proposed.[4] According to this proposal, a scalar field behaves like a source of accelerated expansion. At the beginning of inflating universe, the potential energy dominates over kinetic energy and inflaton starts moving very slowly towards the origin of potential.[5] After this evolutionary stage, kinetic and potential energies are comparable due to oscillatory motion of inflatons around minimum position of potential energy. Thus, the reheating phase is initiated due to decay of inflatons into radiation and matter.[6] Mukhanov and Chibisov[7] explored the existence of primordial curvature perturbations via Starobinsky inflationary model.

Berera[8] presented a revolutionary idea to study possible joining of the early and present universe entitled as warm inflationary scenario that unifies slow-roll and reheating regimes. The existence of thermal radiations of density plays a crucial role in the production of initial fluctuations which are elementary ingredients of large scale structures. When vacuum energy dissipates into radiation energy, the inflating universe allows a graceful exit into radiation dominated era.[9,10] Yokoyama and Linde[11] investigated possible behavior of warm inflation scenario and claimed that it is very difficult to study the existence of warm inflation for realistic models of elementary particles. During warm inflation, thermal fluctuations and scalar field interactions lead to its final outcome in the form of strong dissipation effect which directly corresponds to particle production. This dissipation effect appears as a linear friction term whose characteristics are determined by dissipation coefficient.

Berera and Ramos[12] explored warm inflationary dynamics and low temperature regimes for a particular form of dissipative coefficient corresponding to supersymmetric models. Watanabe and Komatsu[13] studied decay process of inflaton in $f(\phi)R$ gravity and found that such model successfully eliminates the necessity of explicit couplings between ϕ and bosonic or fermionic matter fields. In order to discuss decay as well as scattering rates, Bastero-Gil *et al.*[14] studied warm inflation paradigm in quantum-field theory. Takeda and Watanabe[15] discussed the behavior of decaying inflaton via Einstein frame picture of Starobinsky inflation model. In warm inflation, dissipation effect characterizes two important regimes, i.e. weak ($\Gamma \ll H$) and strong ($\Gamma \gg H$) dissipative regimes. In nonwarm inflation, the primordial density perturbation spectrum is established on the basis of quantum fluctuations. In dissipative regime, these perturbations are determined by thermal fluctuations whereas decay rate determines the fate of inflaton particles.

The scale factor plays a crucial role in the classification of inflationary models as its evolution determines some interesting exact solutions. When a scale factor possesses a de Sitter expansion (exponential expansion), it leads to the inflationary model which describes old inflation but when scale factor follows quasi-de Sitter expansion, it corresponds to new or chaotic inflation.[16] Logamediate inflationary model is obtained by taking weak general conditions on cosmological model which corresponds to power-law inflation for certain conditions.[17] Herrera *et al.*[18] analyzed the behavior of isotropic warm inflation for intermediate as well as logamediate inflationary models in both dissipative regimes via general dissipative coefficient. Setare and Kamali[19] studied warm vector isotropic inflation for intermediate and logamediate models. Sharif and Saleem[20] found that locally rotationally symmetric Bianchi I universe model yields consistent results in the context of warm vector inflation. The same authors[21] examined warm anisotropic intermediate and logamediate inflation in strong as well as weak dissipative regimes via general dissipative coefficient.

The current cosmic accelerated expansion motivates researchers to establish extended gravitational theories. The $f(R)$ theory is one of such modifications where the Ricci scalar (R) is replaced by a generic function $f(R)$. The puzzling nature of DE provides an interesting way to discuss the present inflating universe in the context of modified theories of gravity via inflationary models. Bamba *et al.*[22] investigated observational parameters of nonwarm inflationary models through reconstruction method in this gravity and found compatible results for power-law model. We have analyzed the behavior of chaotic inflationary paradigm for isotropic and homogenous flat universe model in the framework of Jordan frame of $f(R)$ gravity.[23] Sharif and Ikram[24] studied dynamics of warm intermediate and logamediate inflation for flat FRW universe model in Jordan frame of $f(\mathcal{G})$ gravity.

Many theoretical efforts have been made to discuss coupling of gravity with other interactions that demands existence of scalar fields in Jordan frame. Some researchers argued that scalar–tensor gravity is unreliable in Jordan frame as it gives rise to the problem of negative kinetic energy.[25,33] In $f(R)$ gravity, this issue is resolved by introducing a conformal transformation that relates Einstein–Hilbert action and $f(R)$ action,[26] consequently Jordan frame is shifted to Einstein frame under that conformal factor. Inflationary scenario has become a debatable issue in Jordan as well as Einstein frames. Artymowski and Lalak[27] investigated modified Starobinsky inflationary model in both Einstein and Jordan frame and obtained compatible results for Planck and BICEP2 observations. de Felice and Tsujikawa[28] studied inflationary dynamics of Starobinsky inflationary model for both frames in $f(R)$ gravity.

In this paper, we study warm logamediate inflation via Einstein frame representation of $f(R)$ gravity for isotropic and homogeneous universe. The format of this paper is as follows. Section 2 describes inflationary dynamics of $f(R)$ gravity in Jordan and Einstein frames. In Sec. 3, we examine strong and weak dissipation regimes for constant as well as generalized dissipative coefficient with Starobinsky inflationary model and discuss their effects graphically. Finally, we conclude our results in the last section.

2. Inflationary Dynamics of $f(R)$ Gravity

In this section, we discuss basic formalism of $f(R)$ gravity both in Jordan as well as Einstein frame which leads to investigate warm inflationary dynamics.

2.1. *Inflationary dynamics in Jordan frame*

In Jordan frame representation, the geometric part directly interacts with matter part in the action of $f(R)$ gravity given by[29]

$$\mathcal{I}_J = \frac{1}{2\kappa^2}\int d^4x\sqrt{-g}f(R) + \mathcal{L}_m(g_{\mu\nu},\psi), \tag{1}$$

where $\mathcal{L}_m$ represents matter Lagrangian. Varying the above action corresponding to $g_{\mu\nu}$, we obtain nonlinear fourth-order partial differential equation as

$$f_R R_{\mu\nu} - \frac{1}{2}f g_{\mu\nu} - \nabla_\mu\nabla_\nu f_R + g_{\mu\nu}\Box f_R = \kappa^2 T_{\mu\nu}, \tag{2}$$

where $f_R = \frac{df(R)}{dR}$, ∇_μ describes covariant derivative, $\Box = \nabla_\mu\nabla^\mu$ and $\kappa^2 = 8\pi G_N = \frac{8\pi}{M_{Pl}^2}$, $M_{Pl}^2 = 1.2\times 10^{19}$ GeV is the Planck mass. Equation (2) can be written in the form

$$G_{\mu\nu} = \frac{\kappa^2}{f_R}(T_{\mu\nu} + T_{\mu\nu}^{\mathrm{eff}}),$$

where the effective energy–momentum tensor is

$$T_{\mu\nu}^{\mathrm{eff}} = \frac{1}{\kappa^2}\left(\frac{g_{\mu\nu}(f - Rf_R)}{2} + \nabla_\mu\nabla_\nu f_R - \Box f_R g_{\mu\nu}\right).$$

We consider flat FRW metric as

$$ds^2 = -dt^2 + a^2(t)(dx^2 + dy^2 + dz^2), \tag{3}$$

where a is the scale factor. The corresponding field equations (2) for action (1) become

$$\frac{f - Rf_R}{2} + 3H^2 f_R + 3H\dot{f}_R = \kappa^2\rho, \tag{4}$$

$$\ddot{f}_R + 2\dot{H}f_R - H\dot{f}_R = -\kappa^2(\rho + p), \tag{5}$$

where ρ and p represent energy density and pressure of perfect fluid, respectively and dot denotes time derivative. We evaluate a and H for a viable model given by[30]

$$f(R) = R + \frac{R^2}{6M^2}, \tag{6}$$

where M is a positive constant with dimension of mass. Inserting Eq. (6) into (4) and (5), we obtain

$$a = a_i\exp\left[H_i(t - t_i) - \frac{M^2(t - t_i)^2}{12}\right], \quad H = H_i - \frac{M^2(t - t_i)}{6}, \tag{7}$$

where t_i denotes initial cosmic time whereas a_i and H_i represent scale factor and Hubble parameter at $t = t_i$, respectively.

In order to discuss inflationary paradigm, we need to consider perfect fluid as equivalent to scalar field implying $\rho = \frac{\dot{\phi}^2}{2} + V(\phi)$ and $p = \frac{\dot{\phi}^2}{2} - V(\phi)$. During inflation, the interactions between inflaton field and matter or radiations are considered to be meaningless which implies that kinetic energy becomes smaller than potential energy due to slow-roll approximation.[31] This approximation is carried out to investigate inflationary paradigm via slow-roll parameters defined as

$$\epsilon = -\frac{\dot{H}}{H^2}, \quad \eta = -\frac{\ddot{H}}{H\dot{H}}, \tag{8}$$

where $\dot{H}$ must be negative. For the existence of inflating universe, ϵ and η should be very small but positive, while the inflating universe vanishes for $\epsilon = 1 = \eta$.[32] The extent of inflation is measured by number of e-folds given by

$$\mathcal{N} = \int_{t_i}^{t_f} H(t)dt, \tag{9}$$

where t_f represents cosmic time at the ending of inflationary epoch. It is strongly claimed that the equivalence of perfect fluid with scalar field is not viable in Jordan frame representation due to the existence of negative kinetic energy.[33] This issue is resolved by introducing a conformal transformation which connects Jordan frame to Einstein frame with an additional nonlinear scalar field which contains a positive kinetic term.[34]

2.2. *Inflationary dynamics in Einstein frame*

The Einstein frame representation of $f(R)$ gravity contains an extra scalar degree of freedom which analyzes early as well as late-time cosmic acceleration. A conformal transformation provides a relationship between two metrics through a conformal factor which allows to scale time, length and mass whereas angles remain unchanged under this transformation. The action of $f(R)$ gravity with a scalar field can be rewritten as

$$\mathcal{I}_J = \frac{1}{2\kappa^2}\int d^4x\sqrt{-g}(f_R R - V(\phi)) + \mathcal{L}_m(g_{\mu\nu}, \psi), \tag{10}$$

where $V(\phi) = f_R R - f$. For a conformal factor $\tilde{g}_{\mu\nu} = \varphi^2 g_{\mu\nu} = f_R g_{\mu\nu}$, this action reduces to

$$\mathcal{I}_E = \int d^4x\sqrt{-\tilde{g}}\left(\frac{\tilde{R}}{2\kappa^2} - \frac{1}{2}\tilde{g}^{\mu\nu}\partial_\mu\phi\partial_\nu\phi - U(\phi) + \mathcal{L}_m(f_R^{-1}(\phi)\tilde{g}_{\mu\nu}, \psi)\right). \tag{11}$$

Here, $U(\phi) = \frac{V(\phi)}{f_R^2}$, the scalar field directly coupled with matter sector while conformal factor becomes field dependent as $\varphi^2 = f_R = \exp[\sqrt{\frac{2}{3}}\kappa\phi]$.

In Einstein formulation, the gravitational term of action (1) takes the form of Einstein–Hilbert action with a nonminimal coupling between matter Lagrangian density and scalar field. In this frame, the flat FRW model becomes

$$d\tilde{s}^2 = -d\tilde{t}^2 + \tilde{a}^2(\tilde{t})(dx^2 + dy^2 + dz^2), \tag{12}$$

where

$$d\tilde{s} = \sqrt{f_R}ds, \quad d\tilde{t} = \sqrt{f_R}dt, \quad \tilde{a} = \sqrt{f_R}a. \tag{13}$$

For $\tilde{g}^{\mu\nu} = f_R^{-1}g^{\mu\nu}$ and $\sqrt{-\tilde{g}} = f_R^2\sqrt{-g}$, the energy–momentum tensor corresponding to matter and scalar parts take the form

$$\tilde{T}^{(m)}_{\mu\nu} = -\frac{2}{\sqrt{-\tilde{g}}}\frac{\delta(\sqrt{-\tilde{g}}\mathcal{L}_m)}{\delta\tilde{g}^{\mu\nu}}, \quad \tilde{T}^{(\phi)}_{\mu\nu} = -\frac{2}{\sqrt{-\tilde{g}}}\frac{\delta(\sqrt{-\tilde{g}}\mathcal{L}_\phi)}{\delta\tilde{g}^{\mu\nu}}, \tag{14}$$

where $\mathcal{L}_\phi$ represents Lagrangian density of a scalar field given by

$$\mathcal{L}_\phi = -\frac{1}{2}\tilde{g}^{\mu\nu}\partial_\mu\phi\partial_\nu\phi - U(\phi).$$

For the action (11), the field equations and continuity equation yield

$$\frac{3\tilde{H}^2}{\kappa^2} = \tilde{\rho}, \quad 3\tilde{H}^2 + 2\frac{d\tilde{H}}{d\tilde{t}} = -\kappa^2\tilde{p}, \tag{15}$$

$$\frac{d\tilde{\rho}}{d\tilde{t}} + 3\tilde{H}(\tilde{t})(\tilde{\rho} + \tilde{p}) = 0, \tag{16}$$

where $\tilde{H}$ denotes Hubble parameter whereas $\tilde{\rho} = \tilde{\rho}_\phi + \tilde{\rho}_r$ and $\tilde{p} = \tilde{p}_\phi + \tilde{p}_r$ represent total energy density and pressure in Einstein frame given by

$$\tilde{H} = \frac{1}{\tilde{a}}\frac{d\tilde{a}}{d\tilde{t}} = \frac{1}{\sqrt{f_R}}\left(H + \frac{\dot{f}_R}{2f_R}\right),$$

$$\tilde{\rho}_\phi = \frac{\rho_\phi}{f_R^2} = \frac{\dot{\phi}^2}{2f_R} + U(\phi), \quad \tilde{p}_\phi = \frac{p_\phi}{f_R^2} = \frac{\dot{\phi}^2}{2f_R} - U(\phi).$$

In order to formulate $\tilde{t}$, $\tilde{a}$ and $\tilde{H}$ for the standard model (6), we integrate Eq. (13) yielding

$$\begin{aligned} \tilde{t} &= \frac{2}{M}\left[H_i(t - t_i) - \frac{M^2(t - t_i)^2}{12}\right], \\ \tilde{a}(\tilde{t}) &= \frac{2H_ia_i}{M}\left[1 - \frac{M^3\tilde{t}}{12H_i^2}\right]e^{\frac{M\tilde{t}}{2}}, \quad \tilde{H}(\tilde{t}) = \frac{M}{2}\left[1 - \frac{M^2}{6H_i^2}\left(1 - \frac{M^3\tilde{t}}{12H_i^2}\right)^{-2}\right]. \end{aligned} \tag{17}$$

In Einstein frame, the slow-roll parameters and extent of inflation are measured as

$$\epsilon = -\frac{1}{\tilde{H}^2}\frac{d\tilde{H}}{d\tilde{t}}, \quad \eta = -\frac{1}{\tilde{H}}\left(\frac{d\tilde{H}}{d\tilde{t}}\right)^{-1}\frac{d^2\tilde{H}}{d\tilde{t}^2}, \quad \tilde{N} = \int_{\tilde{t}_i}^{\tilde{t}}\tilde{H}(\tilde{t})d\tilde{t}, \tag{18}$$

where $\tilde{t}_i$ represents initial time in Einstein frame. The approximate extent of inflation is found to be 70 but fluctuation spectrum of CMBR reveals that this limit of e-folds should be less than 70. Thus, the conformal transformation allows a smooth transition between these two frames as it only redefines the scales of fundamental quantities that retain physical predictions in both frames.[35] The main difference in both frames is that the Jordan frame defines $f(R)$ gravity on the basis of metric tensor whereas Einstein frame describes the theory with the help of metric tensor along with scalar field interacting with matter sector. The Einstein representation of $f(R)$ gravity admits an equivalence with scalar–tensor theory whose gravitational part incorporates $R\phi$. This equivalence provides a way to explore dissipation effects in nonsupersymmetric background.

3. Warm Inflation in Einstein Frame

In this section, we study the basic mechanism of warm inflation in Einstein representation of $f(R)$ gravity. As opposed to the cold inflation, the most attractive feature of warm inflation is not to have a separate reheating phase at the end of rapid accelerated expansion of the universe. This happened due to the decay of inflaton particles into radiations during slow-roll inflation. Consequently, temperature of the universe drops down smoothly and the universe enters into radiation dominated era. During warm inflation, the total energy density of the universe also comprises radiation density $\tilde{\rho}_r$ while density perturbations arising from thermal fluctuations are larger than those of quantum fluctuations. For such inflationary scenario, Eqs. (15) and (16) yield

$$\frac{3\tilde{H}^2}{\kappa^2} = \tilde{\rho}_\phi + \tilde{\rho}_r, \quad 3\tilde{H}^2 + 2\frac{d\tilde{H}}{d\tilde{t}} = -\kappa^2(\tilde{p}_\phi + \tilde{p}_r), \tag{19}$$

$$\frac{d\tilde{\rho}_r}{d\tilde{t}} + 4\tilde{H}\tilde{\rho}_r - \Gamma\left(\frac{d\phi}{d\tilde{t}}\right)^2 = 0, \tag{20}$$

$$\frac{d\tilde{\rho}_\phi}{d\tilde{t}} + 3\tilde{H}(\tilde{\rho}_\phi + \tilde{p}_\phi) + \Gamma\left(\frac{d\phi}{d\tilde{t}}\right)^2 = 0, \tag{21}$$

where Γ is a dissipation factor which describes the decay of inflaton field into radiations. In Eq. (20), the last term behaves like a source of radiations whereas the second term responds as a sink term which dissipates these radiations continuously. During inflation, the Hubble parameter, dissipation factor and inflaton field vary very slowly which imply that the radiation density must attain a nonzero steady state point. Therefore, the radiation production becomes independent of initial conditions and gets quasi-stable which leads to the following conditions

$$\frac{d\tilde{\rho}_r}{d\tilde{t}} \ll 4\tilde{H}\tilde{\rho}_r, \quad \frac{d\tilde{\rho}_r}{d\tilde{t}} \ll \Gamma\left(\frac{d\phi}{d\tilde{t}}\right)^2. \tag{22}$$

Using the above conditions in Eq. (20), we obtain

$$\tilde{\rho}_r = \frac{3}{4}\tilde{r}\left(\frac{d\phi}{d\tilde{t}}\right)^2 = \chi_r T^4, \quad \tilde{r} = \frac{\Gamma}{3\tilde{H}}. \tag{23}$$

Here, $\tilde{r}$ describes the rate of dissipation factor relative to expansion of the universe via Hubble parameter, $\chi_r = \frac{\pi^2 g_*}{30}$, g_* represents number of relative degrees of freedom and T denotes temperature of thermal bath.

In warm inflation, thermal fluctuations of inflaton field are considerable as $T > \tilde{H}$ and $\tilde{\rho}_r$ dissipates into $\tilde{\rho}_\phi$, i.e. $\tilde{\rho}_\phi \gg \tilde{\rho}_r$. Under this condition, the first field equation of (19) leads to

$$\left(\frac{d\phi}{d\tilde{t}}\right)^2 = -\left[\frac{2}{\kappa^2(1+\tilde{r})}\right]\frac{d\tilde{H}}{d\tilde{t}}. \tag{24}$$

The thermal bath temperature is evaluated by using Eq. (24) in (23) as

$$T = \left[-\frac{\dfrac{3\tilde{r}d\tilde{H}}{d\tilde{t}}}{2\kappa^2\chi_r(1+\tilde{r})}\right]^{\frac{1}{4}}. \tag{25}$$

Inserting Eqs. (23) and (24) in (19), we obtain potential corresponding to inflaton field as

$$U(\phi) = \frac{3\tilde{H}^2}{\kappa^2} + \frac{\dfrac{d\tilde{H}}{d\tilde{t}}}{\kappa^2(1+\tilde{r})}\left[1+\frac{3\tilde{r}}{2}\right]. \tag{26}$$

For warm inflation, the variance of inflaton field is described by thermal fluctuations whereas in case of nonwarm inflationary scenario, this variation is presented by quantum fluctuation. Inflationary paradigm characterizes these fluctuations into scalar and tensor perturbations that leave a strong impact over the CMB anisotropy as well as on the large scales.[5] To evaluate the variance and characteristics of these fluctuations, some important parameters like scalar power spectrum (Δ_R^2), tensor power spectrum (Δ_T^2) and tensor–scalar ratio ($\mathcal{R}$) have been introduced.[36] For FRW universe model in Einstein frame representation, these parameters under slow-roll approximation ($H = \tilde{H}\sqrt{f_R}$) take the following form

$$\Delta_{\mathcal{R}}^2 = -\frac{\tilde{H}^2\kappa^2(1+\tilde{r})T}{\dfrac{2d\tilde{H}}{d\tilde{t}}}\left[\frac{\Gamma\tilde{H}}{(4\pi)^3}\right]^{\frac{1}{2}}, \quad n_s = 1 - \frac{d}{d\tilde{N}}(\ln\Delta_{\mathcal{R}}^2), \tag{27}$$

$$\Delta_T^2 = 8\kappa^2\left[\frac{\tilde{H}}{2\pi}\right]^2, \quad n_T = -2\epsilon, \tag{28}$$

$$\mathcal{R} = \frac{\Delta_T^2}{\Delta_{\mathcal{R}}^2} = -\frac{\dfrac{4d\tilde{H}}{d\tilde{t}}}{\pi^2(1+\tilde{r})\tilde{H}^{\frac{1}{2}}T}\left[\frac{(4\pi)^3}{\Gamma}\right]^{\frac{1}{2}}. \tag{29}$$

Thermal fluctuations for strong and weak dissipative regimes are found to be[9,37]

$$\langle\delta\phi\rangle_{\text{thermal}} = \left[\frac{\Gamma\tilde{H}T^2}{(4\pi)^3}\right]^{\frac{1}{4}}, \quad \langle\delta\phi\rangle_{\text{thermal}} = \sqrt{\tilde{H}T}.$$

Recent observations of Planck 2015[38] constrain spectral index and tensor–scalar ratio as $n_s = 0.9603 \pm 0.0062$ (68%CL) and $\mathcal{R} < 0.10$ (95%CL), respectively.

3.1. *Warm logamediate inflation for* $\mathbf{\Gamma = \Gamma_i}$ = *constant*

For all inflationary models, the exact solutions are expressed in exponential or power-law forms. Here, we analyze warm inflation in weak ($\tilde{r} \ll 1$) as well as strong ($\tilde{r} \gg 1$) dissipative regimes for logamediate inflationary model whose scale factor is defined as[39]

$$a(t) = a_i \exp(g[\ln t]^{\beta}), \quad g > 0, \quad \beta > 1. \tag{30}$$

The logamediate inflationary model is motivated by weak general conditions imposed on the indefinitely expanding cosmological models which corresponds to power-law inflation for $g = p$ and $\beta = 1$.[40] In Einstein frame, the logamediate scale factor and corresponding Hubble parameter turn out to be

$$\tilde{a}(\tilde{t}) = \tilde{a}_i\left[1 - \frac{M^3\tilde{t}}{12H_i^2}\right]\exp\left[g\left\{\ln\left(\frac{\tilde{t}M}{2H_i}\right)\right\}^{\beta}\right], \quad \tilde{a}_i = \frac{2a_iH_i}{M}, \tag{31}$$

$$\tilde{H}(\tilde{t}) = g\beta\tilde{t}^{-1}\left\{\ln\left(\frac{\tilde{t}M}{2H_i}\right)\right\}^{\beta-1}. \tag{32}$$

Interactions of inflaton particles with matter leads to dissipate these particles into thermal bath radiations. If these interactions are weak then dissipation will be small and consequently, inflaton particles belong to weak dissipative regime. In case of strong interactions, the dissipation effect will be large which leads to strong dissipative regime. In weak dissipative regime, Eqs. (24) and (26) yield the inflaton field and corresponding potential in the following form

$$\phi = \phi_0 + \alpha_1\left\{\ln\left(\frac{\tilde{t}M}{2H_i}\right)\right\}^{\frac{\beta+1}{2}}, \quad \alpha_1 = \frac{2}{\beta+1}\sqrt{\frac{2g\beta}{\kappa^2}}, \tag{33}$$

$$U(\phi) = \frac{3}{\kappa^2}\left[g\beta\left(\frac{M}{2H_i}\right)\exp\left\{-\left(\frac{\phi}{\alpha_1}\right)^{\frac{2}{\beta+1}}\right\}\left(\frac{\phi}{\alpha_1}\right)^{\frac{2(\beta-1)}{\beta+1}}\right]^2, \tag{34}$$

where ϕ_0 is an integration constant. In order to discuss inflationary paradigm during slow-roll dynamics, the dimensionless slow-roll parameters for Eqs. (32) and (33) become

$$\epsilon = \frac{1}{\beta g}\left[\frac{\phi}{\alpha_1}\right]^{\frac{2(1-\beta)}{\beta+1}}, \quad \eta = \frac{1}{\beta g}\left[\frac{\phi}{\alpha_1}\right]^{\frac{-2\beta}{\beta+1}}\left(2\left\{\frac{\phi}{\alpha_1}\right\}^{\frac{2}{\beta+1}} - (\beta - 1)\right). \tag{35}$$

For inflaton field (33), the radiation density and e-folds take the form

$$\tilde{\rho}_r = \frac{\Gamma_i}{2\kappa^2}\left(\frac{M}{2H_i}\right)\exp\left[-\left(\frac{\phi}{\alpha_1}\right)^{\frac{2}{\beta+1}}\right], \tag{36}$$

$$\tilde{N} = \beta g\left[\ln\left(\frac{2H_i}{M}\exp\left[\left(\frac{\phi}{\alpha_1}\right)^{\frac{2}{\beta+1}}\right]\right)\left(\frac{\phi}{\alpha_1}\right)^{\frac{2(\beta-1)}{\beta+1}} - \ln\left(\frac{2H_i}{M}\exp\left[\left(\frac{\phi_i}{\alpha_1}\right)^{\frac{2}{\beta+1}}\right]\right)\left(\frac{\phi_i}{\alpha_1}\right)^{\frac{2(\beta-1)}{\beta+1}}\right], \tag{37}$$

where ϕ_i denotes inflaton field at $\tilde{t} = \tilde{t}_i$. To evaluate an expression for this earliest inflaton field, we take $\epsilon = 1$ at the beginning of inflationary epoch which yields

$$\phi_i = \phi_0 + \alpha_1(g\beta)^{\frac{\beta+1}{2(1-\beta)}}. \tag{38}$$

Combining Eqs. (37) and (38), we obtain inflaton in terms of e-folds as

$$\phi = \phi_0 + \alpha_1\left[\ln\left(\frac{M}{2H_i}\right) + \left\{\frac{\tilde{N}}{g\beta} + (g\beta)^{\frac{\beta}{1-\beta}} - \ln\left(\frac{M}{2H_i}\right)^{\frac{1}{g\beta}}\right\}^{\frac{1}{\beta}}\right]^{\frac{\beta+1}{2}}. \tag{39}$$

The perturbation parameters like scalar and tensor power spectra along with their indices as a function of e-folds turn out to be

$$\Delta_{\mathcal{R}} = \frac{\kappa^2}{2}\left(\frac{\Gamma_i}{2\kappa^2\chi_r}\right)^{\frac{1}{4}}\left(\frac{2H_i}{M}\right)^{-\frac{5}{4}}(g\beta)^2\exp\left[-\frac{5}{4}\left\{\frac{\tilde{N}}{g\beta} + (g\beta)^{\frac{\beta}{1-\beta}} - \ln\left(\frac{M}{2H_i}\right)^{\frac{1}{g\beta}}\right\}^{\frac{1}{\beta}}\right]\left\{\frac{\tilde{N}}{g\beta} + (g\beta)^{\frac{\beta}{1-\beta}} - \ln\left(\frac{M}{2H_i}\right)^{\frac{1}{g\beta}}\right\}^{\frac{2(\beta-1)}{\beta}}, \tag{40}$$

$$\Delta_T = \frac{2\kappa^2\beta^2g^2}{\pi^2}\exp\left[-2\left\{\frac{\tilde{N}}{g\beta} + (g\beta)^{\frac{\beta}{1-\beta}} - \ln\left(\frac{M}{2H_i}\right)^{\frac{1}{g\beta}}\right\}^{\frac{1}{\beta}}\right] \times\left\{\frac{\tilde{N}}{g\beta} + (g\beta)^{\frac{\beta}{1-\beta}} - \ln\left(\frac{M}{2H_i}\right)^{\frac{1}{g\beta}}\right\}^{\frac{2(\beta-1)}{\beta}}\left(\frac{M}{2H_i}\right)^2, \tag{41}$$

$$n_s = 1 - \frac{2(\beta-1)}{g\beta^2}\left\{\frac{\tilde{N}}{g\beta} + (g\beta)^{\frac{\beta}{1-\beta}} - \ln\left(\frac{M}{2H_i}\right)^{\frac{1}{g\beta}}\right\}^{-1}, \tag{42}$$

$$n_T = -\frac{2}{g\beta}\left\{\frac{\tilde{N}}{g\beta} + (g\beta)^{\frac{\beta}{1-\beta}} - \ln\left(\frac{M}{2H_i}\right)^{\frac{1}{g\beta}}\right\}^{\frac{1-\beta}{\beta}}. \tag{43}$$

The ratio of tensor and scalar power spectra yields

$$\mathcal{R} = \frac{4}{\pi^2}\left(\frac{2\kappa^2\chi_r}{\Gamma_i}\right)^{\frac{1}{4}}\left(\frac{2H_i}{M}\right)^{-\frac{3}{4}}\exp\left[-\frac{3}{4}\left\{\frac{\tilde{N}}{g\beta} + (g\beta)^{\frac{\beta}{1-\beta}} - \ln\left(\frac{M}{2H_i}\right)^{\frac{1}{g\beta}}\right\}^{\frac{1}{\beta}}\right]. \tag{44}$$

In order to verify the warm inflationary condition and presence of inflaton particles in weak dissipative regime, we evaluate temperature of thermal bath radiations and decay rate of inflaton field as

$$T = \left(\frac{\Gamma_i}{2\kappa^2\chi_r}\right)^{\frac{1}{4}}\left(\frac{M}{2H_i}\right)\exp\left[-\left\{\frac{\tilde{N}}{g\beta}+(g\beta)^{\frac{\beta}{1-\beta}}-\ln\left(\frac{M}{2H_i}\right)^{\frac{1}{g\beta}}\right\}^{\frac{1}{\beta}}\right], \tag{45}$$

$$\tilde{r} = \frac{\Gamma_i}{3\beta g}\left(\frac{2H_i}{M}\right)\exp\left[\left\{\frac{\tilde{N}}{g\beta}+(g\beta)^{\frac{\beta}{1-\beta}}-\ln\left(\frac{M}{2H_i}\right)^{\frac{1}{g\beta}}\right\}^{\frac{1}{\beta}}\right]$$
$$\times\left\{\frac{\tilde{N}}{g\beta}+(g\beta)^{\frac{\beta}{1-\beta}}-\ln\left(\frac{M}{2H_i}\right)^{\frac{1}{g\beta}}\right\}^{\frac{1-\beta}{\beta}}. \tag{46}$$

Figure 1 (left plot) represents dominant characteristics of warm inflation, i.e. $T \gg \tilde{H}$. The right panel of Fig. 1 identifies $\tilde{r} \ll 1$ specifying weak interactions between inflaton and matter fields which assures the presence of inflaton particles in weak dissipative regime. In Fig. 2, the left plot indicates the variation of e-folds approaching to its standard value, i.e. $\tilde{N} = 60$ as model parameter of inflationary model increases. The right plot represents $\mathcal{R} < 0.10$ at $n_s = 0.9603$ which preserves compatibility of $\mathcal{R}$ in weak dissipation regime.

In case of strong dissipative regime ($\tilde{r} \gg 1$), the inflaton field along with its potential take the following form

$$\phi = \phi_0 + \alpha_2\Xi(\tilde{t}),$$
$$U(\phi) = \frac{3(g\beta)^2}{\kappa^2}\left\{\Xi^{-1}\left(\frac{\phi}{\alpha_2}\right)\right\}^{-2}\left[\ln\left(\Xi^{-1}\left(\frac{\phi}{\alpha_2}\right)\frac{M}{2H_i}\right)\right]^{2(\beta-1)}, \tag{47}$$

where Ξ represents incomplete gamma function given as

$$\Xi(\tilde{t}) = \gamma\left[\beta, \frac{1}{2}\ln\left(\frac{\tilde{t}M}{2H_i}\right)\right], \quad \alpha_2 = -2^\beta g\beta\sqrt{\frac{3M}{H_i\kappa^2\Gamma_i}}.$$

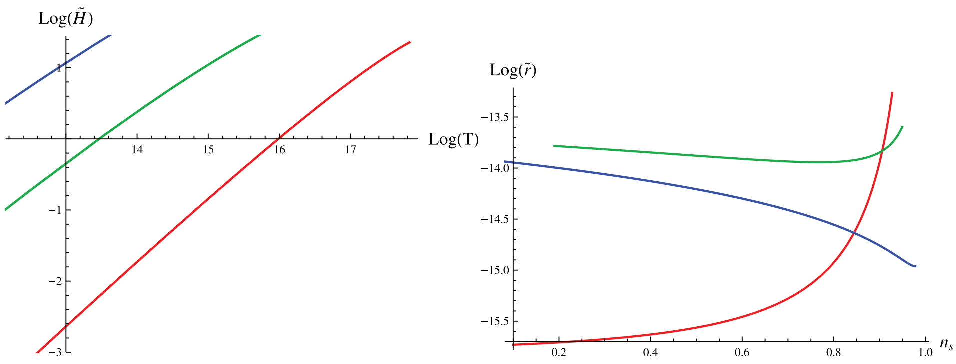

Fig. 1. (Color online) Log($\tilde{H}$) versus Log(T) (left) and Log($\tilde{r}$) versus n_s (right) for $\beta = 1.5$ (red), 2.5 (green), 3.5 (blue), $g = 0.75$, $\Gamma_i \propto \chi_r^{\frac{1}{6}}$, $\chi_r = 70$.

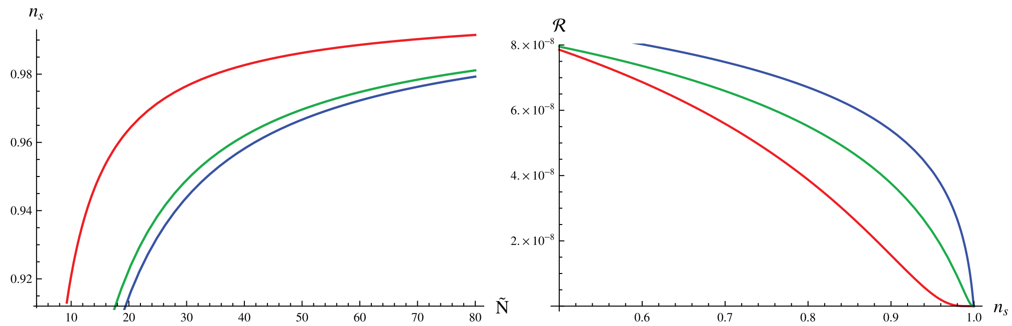

Fig. 2. (Color online) n_s versus $\tilde{N}$ (left) and $\mathcal{R}$ versus n_s (right) for $\beta = 1.5$ (red), 2.5 (green) for $\beta = 3.5$ (blue), $g = 0.75$, $\Gamma_i \propto \chi_r^{\frac{1}{6}}$, $\chi_r = 70$.

For slowly varying inflaton field, the slow-roll parameters and radiation energy density corresponding to ϕ take the form

$$\epsilon = \frac{1}{\beta g}\left[\ln\left(\Xi^{-1}\left(\frac{\phi}{\alpha_2}\right)\frac{M}{2H_i}\right)\right]^{(1-\beta)},$$

$$\eta = \frac{1}{\beta g}\left[\ln\left(\Xi^{-1}\left(\frac{\phi}{\alpha_2}\right)\frac{M}{2H_i}\right)\right]^{-\beta}\left(2\ln\left(\Xi^{-1}\left(\frac{\phi}{\alpha_2}\right)\frac{M}{2H_i}\right) - (\beta-1)\right),$$

$$\tilde{\rho}_r = \frac{3g\beta}{2\kappa^2}\left\{\Xi^{-1}\left(\frac{\phi}{\alpha_2}\right)\right\}^{-2}\left[\ln\left(\Xi^{-1}\left(\frac{\phi}{\alpha_2}\right)\frac{M}{2H_i}\right)\right]^{(\beta-1)}.$$

At the earliest stage of inflationary epoch, the inflaton field at $\tilde{t} = \tilde{t}_i$ becomes

$$\phi_i = \phi_0 + \alpha_2\Xi\left(\exp\left[(g\beta)^{\frac{1}{1-\beta}} - \ln\frac{M}{2H_i}\right]\right).$$

The corresponding number of e-folds and inflaton field are given by

$$\tilde{N} = g\beta\left\{\ln\left(\Xi^{-1}\left(\frac{\phi}{\alpha_2}\right)\right)\left[\ln\left(\Xi^{-1}\left(\frac{\phi}{\alpha_2}\right)\right)\frac{M}{2H_i}\right]^{\beta-1} - (g\beta)^{-1}\left((g\beta)^{\frac{1}{1-\beta}} - \ln\frac{M}{2H_i}\right)\right\}, \tag{48}$$

$$\phi = \phi_0 + \alpha_2\Xi\left\{\exp\left(\frac{\tilde{N}}{g\beta} + (g\beta)^{\frac{\beta}{1-\beta}} - \ln\left(\frac{M}{2H_i}\right)^{\frac{1}{g\beta}}\right)^{\frac{1}{\beta}}\right\}. \tag{49}$$

The corresponding observational parameters become

$$\Delta_{\mathcal{R}} = \frac{\kappa^2}{6}\left(\frac{(g\beta)^{\frac{3}{2}}\Gamma_i^3 3^{\frac{1}{2}}}{(2\kappa^2\chi_r)^{\frac{1}{2}}(4\pi)^3}\right)^{\frac{1}{2}}\left(\frac{\tilde{N}}{g\beta} + (g\beta)^{\frac{\beta}{1-\beta}} - \ln\left(\frac{M}{2H_i}\right)^{\frac{1}{g\beta}}\right)^{\frac{3(\beta-1)}{4\beta}}, \tag{50}$$

$$\Delta_T = \frac{2\kappa^2\beta^2 g^2}{\pi^2}\exp\left(-2\left\{\frac{\tilde{N}}{g\beta} + (g\beta)^{\frac{\beta}{1-\beta}} - \ln\left(\frac{M}{2H_i}\right)^{\frac{1}{g\beta}}\right\}\right)^{\frac{1}{\beta}}$$
$$\times\left[\frac{\tilde{N}}{g\beta} + (g\beta)^{\frac{\beta}{1-\beta}} - \ln\left(\frac{M}{2H_i}\right)^{\frac{1}{g\beta}}\right]^{2(\beta-1)}, \tag{51}$$

$$n_s = 1 - \frac{3(\beta-1)}{4g\beta^2}\left(\frac{\tilde{N}}{g\beta} + (g\beta)^{\frac{\beta}{1-\beta}} - \ln\left(\frac{M}{2H_i}\right)^{\frac{1}{g\beta}}\right)^{-1},$$
$$n_T = -\frac{2}{g\beta}\left(\frac{\tilde{N}}{g\beta} + (g\beta)^{\frac{\beta}{1-\beta}} - \ln\left(\frac{M}{2H_i}\right)^{\frac{1}{g\beta}}\right)^{1-\beta}. \tag{52}$$

The tensor–scalar ratio is found to be

$$\mathcal{R} = \left[\left(\frac{144(4\pi)^3(2\kappa^2\chi_r)^{\frac{1}{2}}}{\Gamma_i^3\pi^4 3^{\frac{1}{2}}}\right)(g\beta)^{\frac{5}{2}}\right]^{\frac{1}{2}}\exp\left[-2\left(\frac{\tilde{N}}{g\beta} + (g\beta)^{\frac{\beta}{1-\beta}} - \ln\left(\frac{M}{2H_i}\right)^{\frac{1}{g\beta}}\right)^{\frac{1}{\beta}}\right]$$
$$\times\left(\frac{\tilde{N}}{g\beta} + (g\beta)^{\frac{\beta}{1-\beta}} - \ln\left(\frac{M}{2H_i}\right)^{\frac{1}{g\beta}}\right)^{\frac{5(\beta-1)}{4\beta}}. \tag{53}$$

The decay rate and temperature of thermal bath radiations turn out to be

$$\tilde{r} = \frac{\Gamma_i}{3}\left[g\beta\exp\left\{\left(\frac{\tilde{N}}{g\beta} + (g\beta)^{\frac{\beta}{1-\beta}} - \ln\left(\frac{M}{2H_i}\right)^{\frac{1}{g\beta}}\right)^{\frac{1}{\beta}}\right\}\right.$$
$$\left.\times\left(\frac{\tilde{N}}{g\beta} + (g\beta)^{\frac{\beta}{1-\beta}} - \ln\left(\frac{M}{2H_i}\right)^{\frac{1}{g\beta}}\right)^{\frac{\beta-1}{\beta}}\right]^{-1}, \tag{54}$$

$$T = g\beta\left(\frac{3}{2\kappa^2\chi_r}\right)^{\frac{1}{4}}\exp\left\{-\frac{1}{2}\left(\frac{\tilde{N}}{g\beta} + (g\beta)^{\frac{\beta}{1-\beta}} - \ln\left(\frac{M}{2H_i}\right)^{\frac{1}{g\beta}}\right)^{\frac{1}{\beta}}\right\}$$
$$\times\left(\frac{\tilde{N}}{g\beta} + (g\beta)^{\frac{\beta}{1-\beta}} - \ln\left(\frac{M}{2H_i}\right)^{\frac{1}{g\beta}}\right)^{\frac{\beta-1}{4\beta}}. \tag{55}$$

Figure 3 indicates that $T \gg \tilde{H}$ (left panel) and $\tilde{r} \gg 1$ (right panel) for $2 \leq g \leq 2.7$ which assures the existence of warm inflation for logamediate inflationary model in strong dissipative regime. Figure 4 (left plot) represents the graphical behavior of n_s against $\tilde{N}$ which are found in very small ratio due to strong interactions and high dissipation rate whereas the right plot indicates compatible $\mathcal{R}$ for the proposed values of g in strong dissipative regime.

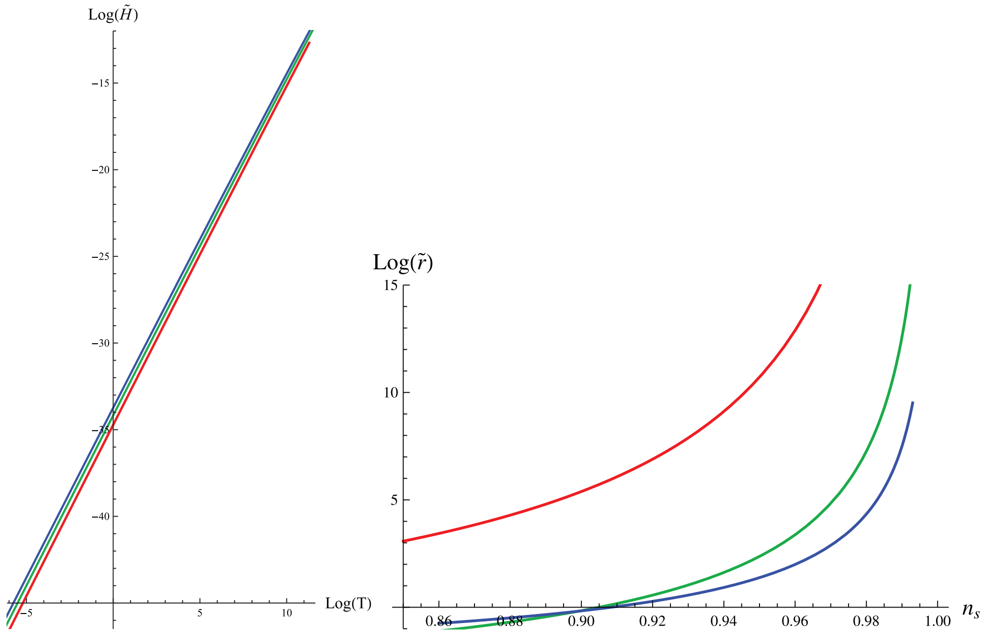

Fig. 3. (Color online) Log($\tilde{H}$) versus Log(T) (left) and Log($\tilde{r}$) versus n_s (right) for $\beta = 2$ (red), 2.4 (green), 2.7 (blue), $g = 0.01$, $\Gamma_i \propto \chi_r^{\frac{1}{6}}$, $\chi_r = 70$.

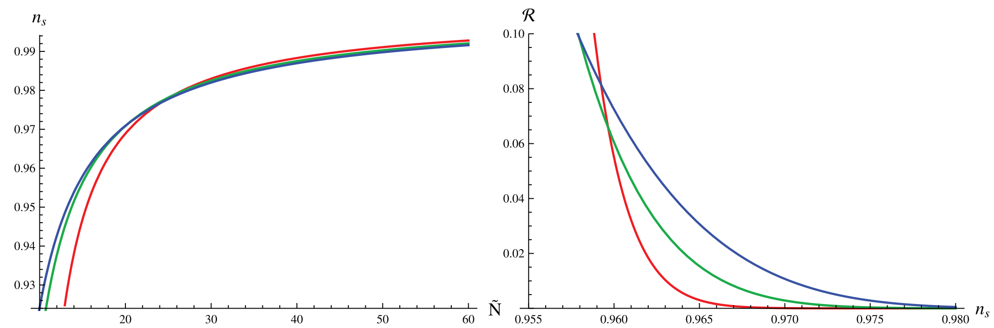

Fig. 4. (Color online) n_s versus $\tilde{N}$ (left) for $g = 0.1$ and $\mathcal{R}$ versus n_s (right) for $g = 0.01$, $\beta = 2$ (red), 2.4 (green), 2.7 (blue), $\Gamma_i \propto \chi_r^{\frac{1}{6}}$, $\chi_r = 70$.

3.2. *Warm logamediate inflation for generalized dissipative coefficient*

In warm inflationary scenario, the dissipative coefficient plays a dynamical role as it represents a physical process of dissipation regarding to interacting inflaton field. The dissipating effects appear from friction term which characterizes the process of scalar field dissipating into thermal bath radiations via its interaction with other fields. Due to such dissipative effects, radiations produced instantly during rapid accelerated expansion of the universe and hence the universe smoothly entered into radiation dominated era. This dissipative coefficient may be expressed as a function of inflaton field, or thermal bath, or both. The most general form of dissipation factor is given by[41]

$$\Gamma = \Gamma_i \frac{T^m}{\phi^{m-1}},$$

where Γ_i denotes a constant that describes microscopic dynamics of dissipation process and m represents an integer. In the background of thermal bath radiations, this dissipative coefficient takes the form

$$\Gamma^{\frac{4-m}{4}} = \alpha_m \phi^{1-m} \left(\frac{-\frac{d\tilde{H}}{d\tilde{t}}}{\tilde{H}} \right)^{\frac{m}{4}} (1+\tilde{r})^{-\frac{m}{4}},$$

where $\alpha_m = \frac{C_\phi}{(2\kappa^2 \chi_r)^{\frac{m}{4}}}$. For different values of m, dissipation coefficient corresponds to different physical processes, i.e. when $m = 0$, the dissipation coefficient describes an exponential decay propagator in high temperature supersymmetry case. For $m = 1$, it becomes proportional to thermal bath temperature while $m = -1$ deals with nonsupersymmetry case.[42] For weak and strong regimes, the dissipative coefficient turns out to be

$$\Gamma = (\alpha_m \phi^{1-m})^{\frac{4}{4-m}} \left(\frac{\frac{d\tilde{H}}{d\tilde{t}}}{\tilde{H}} \right)^{\frac{m}{4-m}}, \quad \Gamma = \alpha_m \phi^{1-m} \left(-3\frac{d\tilde{H}}{d\tilde{t}} \right)^{\frac{m}{4}}.$$

In the present work, we study the behavior of generalized dissipation coefficient both in weak as well as strong dissipation regimes.

In weak dissipative regime, the constant as well as proposed generalized dissipative coefficient leave the same effect over inflaton field, number of e-folds and slow-roll parameters whereas radiation density becomes

$$\tilde{\rho}_r = \frac{1}{2\kappa^2} \alpha_m^{\frac{4}{4-m}} \left(\frac{2H_i}{M} \right)^{\frac{4}{m-4}} \exp\left[\left(\frac{4}{m-4} \right) \left(\frac{\phi - \phi_0}{\alpha_2} \right)^{\frac{2}{\beta+1}} \right] \phi^{\frac{4(1-m)}{4-m}}.$$

The scalar and tensor power spectra along with corresponding spectral indices and tensor–scalar ratio are given by

$$\begin{aligned}
\Delta_{\mathcal{R}} = \frac{\kappa^2}{2} & \left[\left\{ \frac{\tilde{N}}{g\beta} + (g\beta)^{\frac{\beta}{1-\beta}} + \ln\left(\frac{2H_i}{M} \right)^{\frac{1}{g\beta}} \right\}^{\frac{1}{\beta}} \right]^{\frac{(\beta+1)(1-m)}{2(4-m)} + 2(\beta-1)} \\
& \times \exp\left[\frac{m-5}{4-m} \left\{ \left(\frac{\tilde{N}}{g\beta} + (g\beta)^{\frac{\beta}{1-\beta}} + \ln\left(\frac{2H_i}{M} \right)^{\frac{1}{g\beta}} \right)^{\frac{1}{\beta}} \right\} \right] \left(\frac{\Gamma_i}{2\kappa^2 \chi_r} \right)^{\frac{1}{4-m}} (g\beta)^2 \\
& \times \left\{ \left(\frac{2H_i}{M} \right)^{(m-5)(4-m)} \alpha_3^{1-m} \right\}^{\frac{1}{4-m}},
\end{aligned} \tag{56}$$

$$n_s = 1 - \frac{1}{g\beta^2}\left\{\frac{\tilde{N}}{g\beta} + (g\beta)^{\frac{\beta}{1-\beta}} + \ln\left(\frac{2H_i}{M}\right)^{\frac{1}{g\beta}}\right\}^{\frac{1}{\beta}-1}$$
$$\times\left[\left\{\frac{(\beta+1)(1-m)}{2(4-m)} + 2(\beta-1)\right\}\right.$$
$$\left.\times\left[\left\{\frac{\tilde{N}}{g\beta} + (g\beta)^{\frac{\beta}{1-\beta}} + \ln\left(\frac{2H_i}{M}\right)^{\frac{1}{g\beta}}\right\}^{\frac{1}{\beta}}\right] + \left(\frac{m-5}{4-m}\right)\right], \tag{57}$$

$$\Delta_T = \frac{2\kappa^2\beta^2 g^2}{\pi^2}\exp\left\{-2\left(\frac{\tilde{N}}{g\beta} + (g\beta)^{\frac{\beta}{1-\beta}} + \ln\left(\frac{2H_i}{M}\right)^{\frac{1}{g\beta}}\right)^{\frac{1}{\beta}}\right\}$$
$$\times\left(\frac{\tilde{N}}{g\beta} + (g\beta)^{\frac{\beta}{1-\beta}} + \ln\left(\frac{2H_i}{M}\right)^{\frac{1}{g\beta}}\right)^{\frac{2(\beta-1)}{\beta}}, \tag{58}$$

$$\mathcal{R} = \frac{4}{\pi^2}\exp\left[\left(\frac{m-3}{4-m}\right)\left\{\frac{\tilde{N}}{g\beta} + (g\beta)^{\frac{\beta}{1-\beta}} + \ln\left(\frac{2H_i}{M}\right)^{\frac{1}{g\beta}}\right\}^{\frac{1}{\beta}}\right]\left(\frac{\Gamma_i}{(2\kappa^2\chi_r)^4}\right)^{\frac{1}{m-4}}$$
$$\times\alpha_3^{\frac{1-m}{m-4}}\left(\frac{2H_i}{M}\right)^{\frac{3-m}{m-4}}\left[\left\{\frac{\tilde{N}}{g\beta} + (g\beta)^{\frac{\beta}{1-\beta}} + \ln\left(\frac{2H_i}{M}\right)^{\frac{1}{g\beta}}\right\}^{\frac{1}{\beta}}\right]^{\left(\frac{\beta+1}{2}\right)\left(\frac{1-m}{m-4}\right)}. \tag{59}$$

The dissipation rate of inflaton field and temperature of thermal radiations are found to be

$$\tilde{r} = \frac{1}{3g\beta}\left(\frac{2H_i}{M}\right)^{\frac{2m-4}{4-m}}\left\{\frac{\tilde{N}}{g\beta} + (g\beta)^{\frac{\beta}{1-\beta}} + \ln\left(\frac{2H_i}{M}\right)^{\frac{1}{g\beta}}\right\}^{\left(\frac{\beta+1}{2\beta}\right)\left\{\frac{2(1-\beta)}{(\beta+1)} + \frac{4(1-m)}{4-m}\right\}}$$
$$\times\left(\frac{\Gamma_i}{(2\kappa^2\chi_r)^{\frac{m}{4}}}\right)\exp\left\{\frac{2m-4}{m-4}\left(\frac{\tilde{N}}{g\beta} + (g\beta)^{\frac{\beta}{1-\beta}} + \ln\left(\frac{2H_i}{M}\right)^{\frac{1}{g\beta}}\right)^{\frac{1}{\beta}}\right\}, \tag{60}$$

$$T = \left(\frac{\Gamma_i^2}{(2\kappa^2\chi_r)^{m-2}}\right)^{\frac{1}{2(m-4)}}\left(\frac{\tilde{N}}{g\beta} + (g\beta)^{\frac{\beta}{1-\beta}} + \ln\left(\frac{2H_i}{M}\right)^{\frac{1}{g\beta}}\right)^{\frac{(\beta+1)(1-m)}{2\beta(4-m)}}$$
$$\times\left(\frac{2H_i}{M}\right)^{\frac{1}{m-4}}\alpha_3^{\frac{1-m}{4-m}}\exp\left\{\frac{1}{m-4}\left(\frac{\tilde{N}}{g\beta} + (g\beta)^{\frac{\beta}{1-\beta}} + \ln\left(\frac{2H_i}{M}\right)^{\frac{1}{g\beta}}\right)^{\frac{1}{\beta}}\right\}. \tag{61}$$

Figure 5 assures the condition of warm inflation for $m = 0,\ 1$ and $m = -1$ in weak dissipative regime for different values of the model parameter β. Figure 6

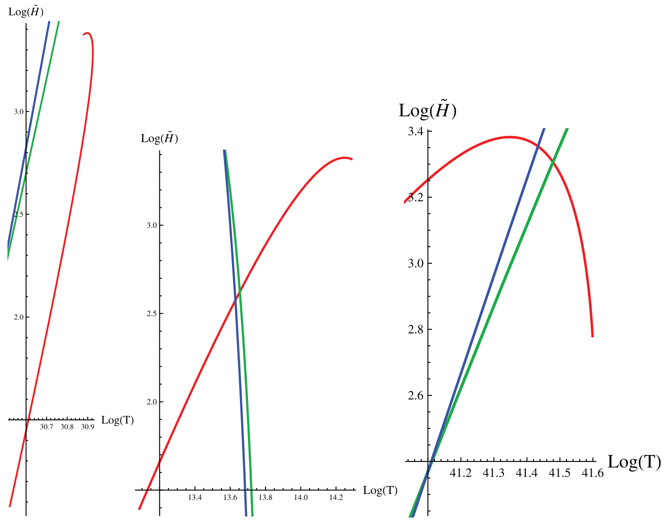

Fig. 5. (Color online) $\mathrm{Log}(\tilde{H})$ versus $\mathrm{Log}(T)$ for $\beta = 2$ (red), $\beta = 3.5$ (green), 4.5 (blue), $g = 4$, $\Gamma_i \propto \chi_r^{\frac{1}{6}}$, $\chi_r = 70$, $m = 0$, $m = 1$ and $m = -1$.

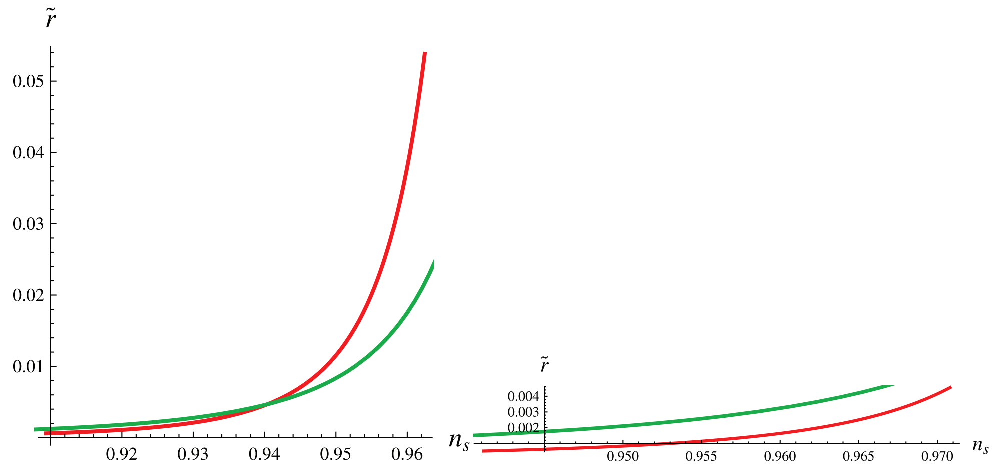

Fig. 6. (Color online) $\tilde{r}$ versus n_s (left) for $m = 0$ and $\tilde{r}$ versus n_s (right) for $m = 1$, $\beta = 3.5$ (red), 4.5 (green), $g = 2$, $\Gamma_i \propto \chi_r^{\frac{1}{6}}$, $\chi_r = 70$.

identifies the inflaton particles for $m = 0,\ 1$ but this condition is violated for $m = -1$. The graphical behavior of $\mathcal{R}$ versus n_s and variation of n_s against $\tilde{N}$ for generalized dissipative coefficient is given in Figs. 7 and 8 which lead to compatible results for $m = 0$ and $m = 1$ in weak dissipative regime.

In strong dissipative regime, the inflaton field and corresponding potential take the form

$$\phi = \alpha_4 \Xi_m(\tilde{t}), \quad U(\phi) = \frac{3(g\beta)^2}{\kappa^2}\left\{\Xi_m^{-1}\left(\frac{\phi}{\alpha_4}\right)\right\}^{-2}\left[\ln\left(\Xi_m^{-1}\left(\frac{\phi}{\alpha_4}\right)\frac{M}{2H_i}\right)\right]^{2(\beta-1)}, \tag{62}$$

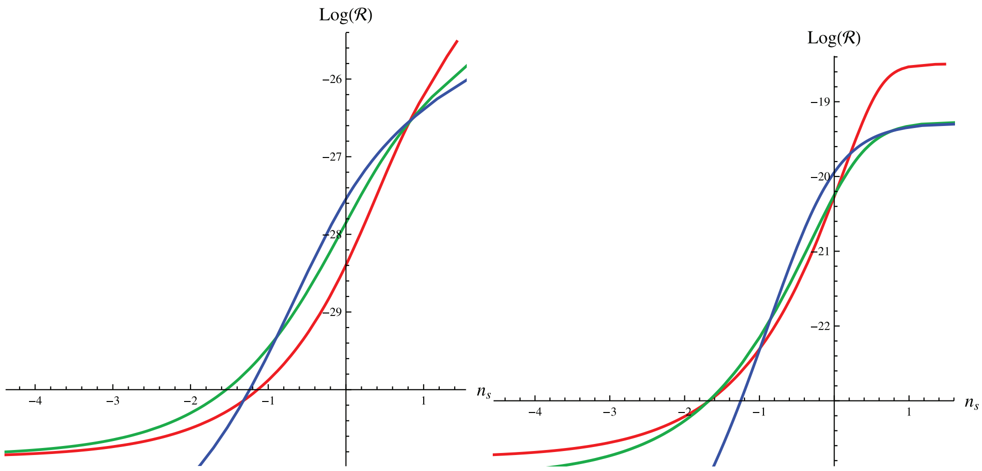

Fig. 7. (Color online) Log($\mathcal{R}$) versus n_s (left) for $m = 0$ and Log($\mathcal{R}$) versus n_s (right) for $m = 1$, $\beta = 1.25$ (red), 1.45 (green), 1.65 (blue), $g = 1$, $\Gamma_i \propto \chi_r^{\frac{1}{6}}$, $\chi_r = 70$.

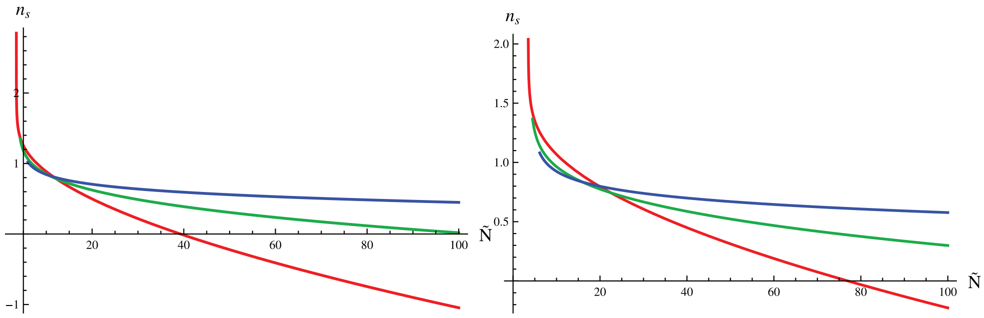

Fig. 8. (Color online) n_s versus $\tilde{N}$ (left) for $m = 0$ and n_s versus $\tilde{N}$ (right) for $m = 1$, $\beta = 1.25$ (red), 1.45 (green), 1.65 (blue), $g = 2$, $\Gamma_i \propto \chi_r^{\frac{1}{6}}$, $\chi_r = 70$.

where

$$\Xi_m(\tilde{t}) = \left(\gamma\left[1 + \frac{(8-m)(\beta-1)}{8}, \frac{2-m}{4}\ln\left(\frac{\tilde{t}M}{2H_i}\right)\right]\right)^{\frac{2}{3-m}},$$

$$\alpha_4 = \left[\left(\frac{3-m}{2}\right)^8 (6\Gamma_i^{-1}\kappa^{-2})^4(2\kappa^2\chi_r)^m(g\beta)^{8-m}\left(\frac{M}{2H_i}\right)^{2-m} \times\left(\frac{m-2}{4}\right)^{(\beta-1)(m-8)-8}\right]^{\frac{1}{4(3-m)}}.$$

Under the influence of inflaton field (62), the corresponding radiation density, Hubble and slow-roll parameters turn out to be

$$\tilde{\rho}_r = \frac{3g\beta}{2\kappa^2}\left\{\Xi_m^{-1}\left(\frac{\phi}{\alpha_4}\right)\right\}^{-1}\left[\ln\left(\Xi_m^{-1}\left(\frac{\phi}{\alpha_4}\right)\frac{M}{2H_i}\right)\right]^{(\beta-1)},$$

$$\tilde{H}(\tilde{t}) = g\beta\left\{\Xi_m^{-1}\left(\frac{\phi}{\alpha_4}\right)\right\}^{-1}\left[\ln\left(\Xi_m^{-1}\left(\frac{\phi}{\alpha_4}\right)\frac{M}{2H_i}\right)\right]^{(\beta-1)},$$
$$\epsilon = \frac{1}{\beta g}\left[\ln\left(\Xi_m^{-1}\left(\frac{\phi}{\alpha_4}\right)\frac{M}{2H_i}\right)\right]^{(1-\beta)},$$
$$\eta = \frac{1}{\beta g}\left[\ln\left(\Xi_m^{-1}\left(\frac{\phi}{\alpha_4}\right)\frac{M}{2H_i}\right)\right]^{-\beta}\left(2\ln\left(\Xi_m^{-1}\left(\frac{\phi}{\alpha_4}\right)\frac{M}{2H_i}\right)-(\beta-1)\right). \tag{63}$$

For $\epsilon = 1$, the initial value of inflaton field leads to ϕ as

$$\phi = \alpha_4\Xi_m\left\{\exp\left[\left(\frac{\tilde{N}}{g\beta}+(g\beta)^{\frac{\beta}{1-\beta}}-\ln\left(\frac{M}{2H_i}\right)^{\frac{1}{g\beta}}\right)^{\frac{1}{\beta}}\right]\right\}.$$

The corresponding scalar power spectrum and spectral index are

$$\begin{aligned}\Delta_R^2 = {} & \frac{\kappa^2}{6}\left[(g\beta)^{\frac{3(m+2)}{4}}\left(\frac{3}{2\kappa^2\chi_r}\right)^{\frac{3m+2}{4}}\left(\frac{\Gamma_i}{4\pi}\right)^3\right]^{\frac{1}{2}} \\ & \times\exp\left[-\frac{3m}{4}\left(\frac{\tilde{N}}{g\beta}+(g\beta)^{\frac{\beta}{1-\beta}}+\ln\left(\frac{2H_i}{M}\right)^{\frac{1}{g\beta}}\right)^{\frac{1}{\beta}}\right] \\ & \times\left(\frac{\tilde{N}}{g\beta}+(g\beta)^{\frac{\beta}{1-\beta}}+\ln\left(\frac{2H_i}{M}\right)^{\frac{1}{g\beta}}\right)^{\frac{3(m+2)(\beta-1)}{8\beta}} \\ & \times\left\{\alpha_4\Xi_m\left(\exp\left[\left(\frac{\tilde{N}}{g\beta}+(g\beta)^{\frac{\beta}{1-\beta}}-\ln\left(\frac{M}{2H_i}\right)^{\frac{1}{g\beta}}\right)^{\frac{1}{\beta}}\right]\right)\right\}^{\frac{3(1-m)}{2}},\end{aligned} \tag{64}$$

$$n_s = 1-\frac{3(m+2)(\beta-1)}{8}\left(\frac{\tilde{N}}{g\beta}+(g\beta)^{\frac{\beta}{1-\beta}}+\ln\left(\frac{2H_i}{M}\right)^{\frac{1}{g\beta}}\right)^{-1}.$$

Similarly, tensor power spectrum and its spectral index become

$$\begin{aligned}\Delta_T^2 = {} & \frac{2\kappa^2(g\beta)^2}{\pi^2}\exp\left[-2\left(\frac{\tilde{N}}{g\beta}+(g\beta)^{\frac{\beta}{1-\beta}}+\ln\left(\frac{2H_i}{M}\right)^{\frac{1}{g\beta}}\right)^{\frac{1}{\beta}}\right] \\ & \times\left(\frac{\tilde{N}}{g\beta}+(g\beta)^{\frac{\beta}{1-\beta}}+\ln\left(\frac{2H_i}{M}\right)^{\frac{1}{g\beta}}\right)^{\frac{2(\beta-1)}{\beta}},\end{aligned}$$

$$n_T = -\frac{2}{g\beta}\left(\frac{\tilde{N}}{g\beta}+(g\beta)^{\frac{\beta}{1-\beta}}+\ln\left(\frac{2H_i}{M}\right)^{\frac{1}{g\beta}}\right)^{\frac{1-\beta}{\beta}}.$$

The above observational parameters generate tensor–scalar ratio as

$$\mathcal{R} = \left[\frac{144(4\pi)^3}{\Gamma_i^3\pi^4}\left(\frac{2\kappa^2\chi_r}{3}\right)^{\frac{3m+2}{4}}(g\beta)^{\frac{10-3m}{4}}\alpha_4^{3(m-1)}\right]^{\frac{1}{2}}$$
$$\times\exp\left[\frac{3m-8}{4}\left(\frac{\tilde{N}}{g\beta}+(g\beta)^{\frac{\beta}{1-\beta}}+\ln\left(\frac{2H_i}{M}\right)^{\frac{1}{g\beta}}\right)^{\frac{1}{\beta}}\right]$$
$$\times\left(\frac{\tilde{N}}{g\beta}+(g\beta)^{\frac{\beta}{1-\beta}}+\ln\left(\frac{2H_i}{M}\right)^{\frac{1}{g\beta}}\right)^{\frac{(\beta-1)(10-3m)}{8\beta}}$$
$$\times\left\{\Xi_m\left(\exp\left[\left(\frac{\tilde{N}}{g\beta}+(g\beta)^{\frac{\beta}{1-\beta}}+\ln\left(\frac{2H_i}{M}\right)^{\frac{1}{g\beta}}\right)^{\frac{1}{\beta}}\right]\right)\right\}^{\frac{3(m-1)}{2}}.$$

The decay rate of inflaton field and thermal radiations take the form

$$\tilde{r} = (\Gamma_i(2\kappa^2\chi_r)^{-\frac{m}{4}})(3g\beta)^{\frac{m-4}{4}}\exp\left[\frac{2-m}{2}\left(\frac{\tilde{N}}{g\beta}+(g\beta)^{\frac{\beta}{1-\beta}}+\ln\left(\frac{2H_i}{M}\right)^{\frac{1}{g\beta}}\right)^{\frac{1}{\beta}}\right]$$
$$\times\alpha_4^{1-m}\left(\Xi_m\left\{\exp\left[\left(\frac{\tilde{N}}{g\beta}+(g\beta)^{\frac{\beta}{1-\beta}}+\ln\left(\frac{2H_i}{M}\right)^{\frac{1}{g\beta}}\right)^{\frac{1}{\beta}}\right]\right\}\right)^{1-m}, \tag{65}$$

$$T = \left(\frac{3}{2\kappa^2\chi_r}\right)^{\frac{1}{4}}\exp\left[-\frac{1}{2}\left(\frac{\tilde{N}}{g\beta}+(g\beta)^{\frac{\beta}{1-\beta}}+\ln\left(\frac{2H_i}{M}\right)^{\frac{1}{g\beta}}\right)^{\frac{1}{\beta}}\right]$$
$$\times\left(\frac{\tilde{N}}{g\beta}+(g\beta)^{\frac{\beta}{1-\beta}}+\ln\left(\frac{2H_i}{M}\right)^{\frac{1}{g\beta}}\right)^{\frac{\beta-1}{4\beta}}. \tag{66}$$

Figures 9–11 represent graphical analysis of inflaton particles which satisfy the condition of warm inflation, i.e. $T \gg \tilde{H}$ and also show that $\tilde{r} \gg 1$. These indications imply that inflaton particles lie in strong dissipative regime for $m = 0, 1$ and $m = -1$. Figures 12–14 describe the graphical behavior of n_s versus number of e-folds and variation of $\mathcal{R}$ versus n_s for $m = 0, 1$ and $m = -1$. These plots indicate that $\mathcal{R}$ is constrained at observational value of n_s which leads to consistent behavior of inflationary model for different values of the model parameter g.

4. Concluding Remarks

In this paper, we have investigated the dynamics of warm inflation for flat FRW universe model in Einstein representation of $f(R)$ gravity. In warm inflation, interactions between inflaton and other fields like matter or radiations avoid a separate

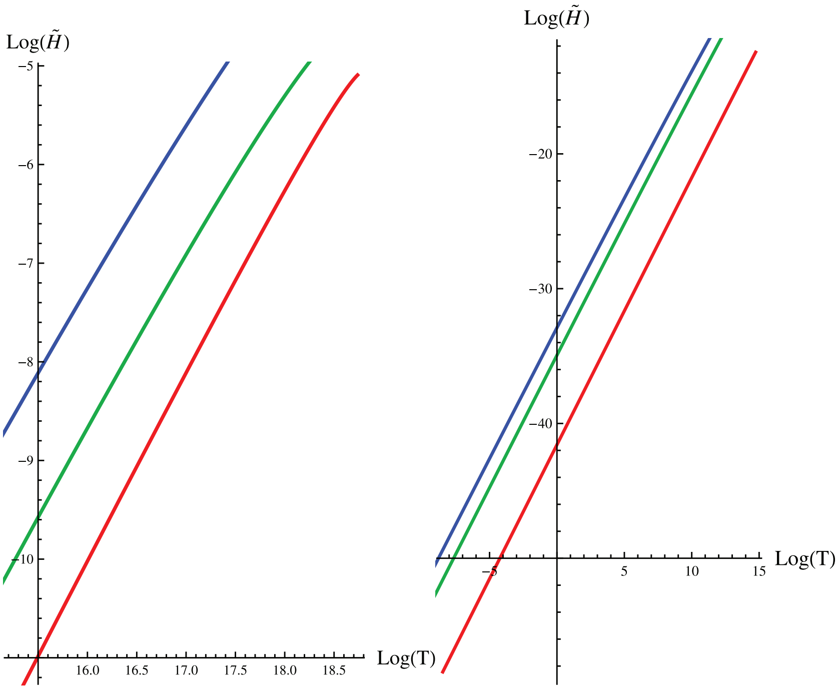

Fig. 9. (Color online) Log($\tilde{H}$) versus Log(T) (left) for $m = 0$ and Log($\tilde{H}$) versus Log(T) (right) for $m = 1$, $\beta = 1.5$ (red), 2.5 (green), 3.5 (blue), $g = 0.01$, $\Gamma_i \propto \chi_r^{\frac{1}{6}}$, $\chi_r = 70$.

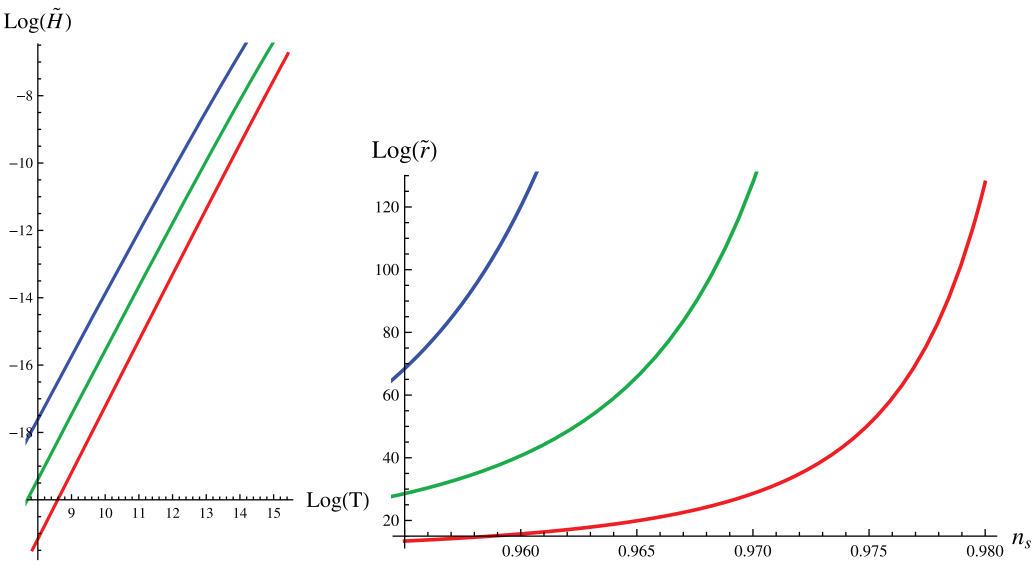

Fig. 10. (Color online) Log($\tilde{H}$) versus Log(T) (left) for $g = 0.01$, $m = -1$ and Log($\tilde{r}$) versus n_s (right) for $g = 0.0027$, $m = 0$, $\beta = 1.5$ (red), 2.5 (green), 3.5 (blue), $\Gamma_i \propto \chi_r^{\frac{1}{6}}$, $\chi_r = 70$.

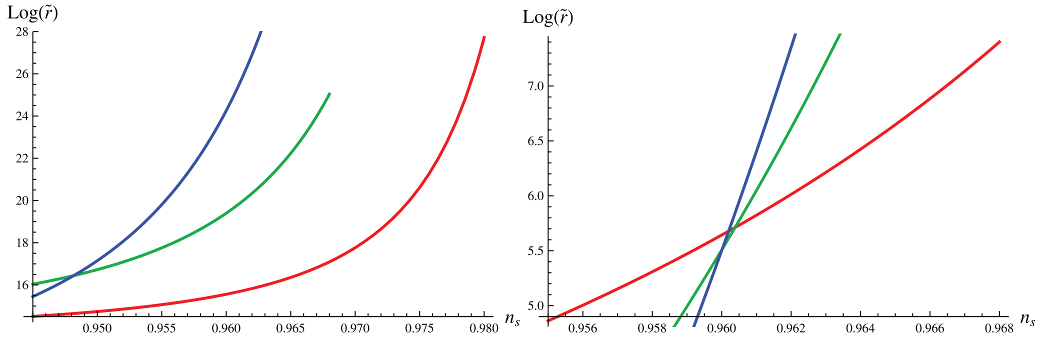

Fig. 11. (Color online) Log($\tilde{r}$) versus n_s (left) for $m = -1$ and Log($\tilde{r}$) versus n_s (right) for $m = 1$, $\beta = 1.5$ (red), 2.5 (green), 3.5 (blue), $g = 0.0027$, $\Gamma_i \propto \chi_r^{\frac{1}{6}}$, $\chi_r = 70$.

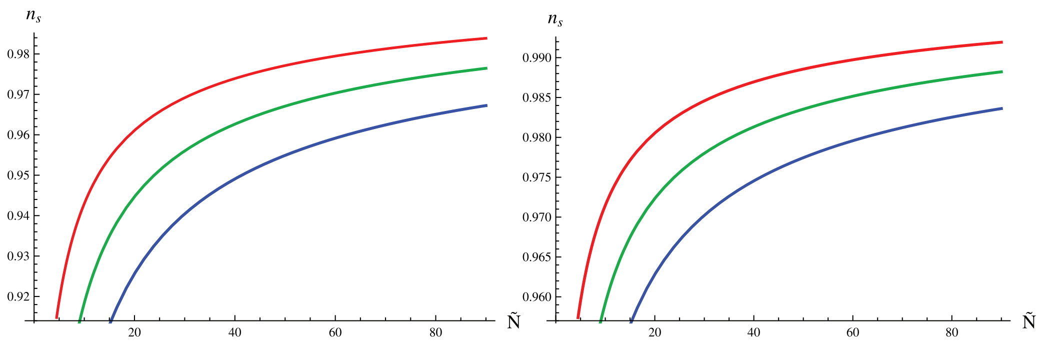

Fig. 12. (Color online) n_s versus $\tilde{N}$ (left) for $m = 0$ and n_s versus $\tilde{N}$ (right) for $m = -1$, $\beta = 1.65$ (red), 1.75 (green), 1.85 (blue), $g = 0.2$, $\Gamma_i \propto \chi_r^{\frac{1}{6}}$, $\chi_r = 70$.

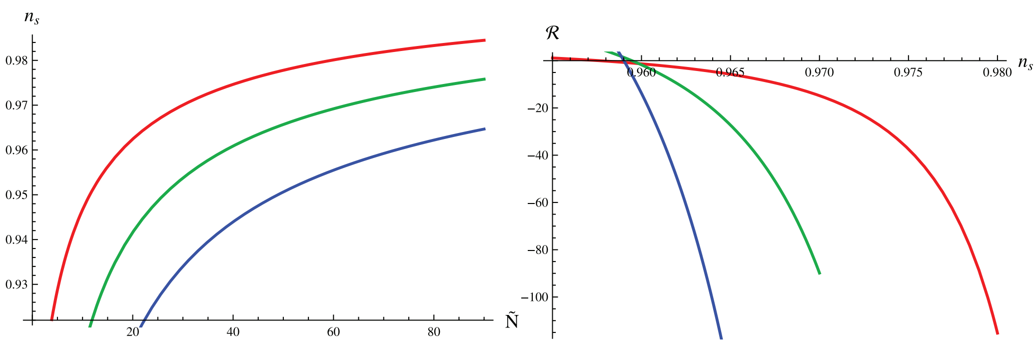

Fig. 13. (Color online) n_s versus $\tilde{N}$ (left) for $m = 1$, $\beta = 1.65$ (red), 1.75 (green), 1.85 (blue), $g = 0.2$, and $\mathcal{R}$ versus n_s (right) for $m = 0$, $\beta = 1.1$ (red), 1.15 (green), 1.2 (blue), $g = 0.0027$, $\Gamma_i \propto \chi_r^{\frac{1}{6}}$, $\chi_r = 70$.

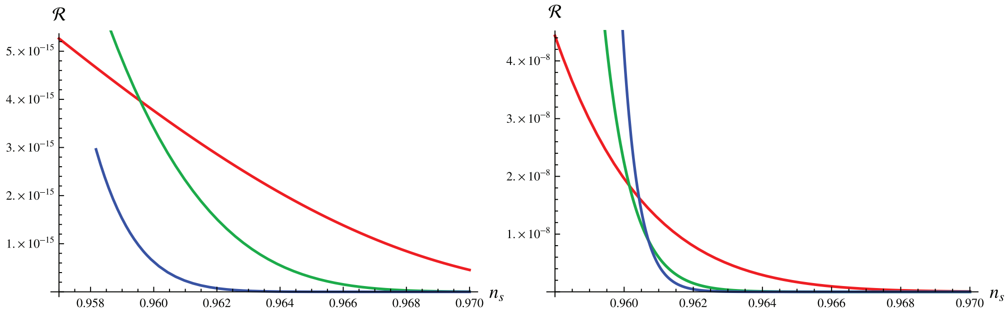

Fig. 14. (Color online) $\mathcal{R}$ versus n_s (left) for $m = -1$, $\beta = 1.65$ (red), 1.75 (green), 1.85 (blue), and $\mathcal{R}$ versus n_s (right) for $m = 1$, $\beta = 1.5$ (red), 2.5 (green), 3.5 (blue), $g = 0.0027$, $\Gamma_i \propto \chi_r^{\frac{1}{6}}$, $\chi_r = 70$.

reheating phase in the inflationary universe. These interactions give rise to friction term in the equation of motion of inflaton which yield dissipation effects in strong and weak dissipative regimes. The strong dissipative effects lead to strong dissipative regime whereas weak dissipation regime is supported by small dissipation and weak interactions. We have analyzed warm logamediate inflationary model in both regimes for constant and generalized dissipative coefficients. To avoid negative kinetic energy of inflaton field, we have studied inflationary paradigm for Starobinsky inflationary model in Einstein frame.

We have explored solutions of inflaton field along with corresponding potentials and also formulated dimensionless slow-roll parameters in terms of inflaton field. In warm inflation, density perturbations appear due to thermal fluctuations instead of quantum fluctuations and characteristics of these fluctuations are described by observational parameters such as scalar and tensor power spectra, their corresponding spectral indices and tensor–scalar ratio. We have calculated these parameters under slow-roll approximation and studied their graphical analysis for different values of logamediate model parameter β. The results are summarized as follows:

- For weak constant dissipative regime, the e-folds are found in abundance to resolve flatness and horizon issues whereas the corresponding tensor–scalar ratio is compatible at the constrained value of scalar spectral index. For $1.5 \leq \beta \leq 3.5$, we have found $T \gg \tilde{H}$ and $\tilde{r} \ll 1$ which verify the presence of warm inflation and also describe the existence of inflaton particles in weak dissipative regime. This analysis implies that logamediate inflationary model is found to be consistent with observational data.
- For strong constant dissipative regime, the number of e-folds remains less than 20 for $2 \leq \beta \leq 2.7$ while the corresponding graphical behavior of $\mathcal{R} - n_s$ leads to compatible range of $\mathcal{R}$, i.e. $\mathcal{R} < 0.10$ in the same range. The temperature of thermal bath radiations is found to be greater than Hubble parameter which leads to the existence of warm inflation and $\tilde{r} \gg 1$ indicates that inflaton particles lie in strong dissipative regime for the proposed range of β.

- For generalized dissipative coefficient in weak dissipative regime, the inflationary model yields consistent results with Planck constraints for $m = 0,\ 1$ with $1.1 \leq \beta \leq 4.5$. For $m = -1$, the existence of warm inflation is verified in this range but $\tilde{r}$ is not found to be constrained at $n_s = 0.9603$ which violates the condition of weak dissipative regime. In case of strong dissipative regime, inflationary model yields compatible results for $m = 0, 1, -1$ with $1.1 \leq \beta \leq 3.5$ but $\tilde{r} \gg 1$ in $1.1 \leq \beta \leq 1.9$.

Finally, it is concluded that isotropic warm logamediate inflationary universe model remains consistent with Planck 2015 constraints for both constant as well as generalized dissipation coefficient for $m = 0,\ 1$ and -1 in strong dissipation regime. In case of weak dissipation regime, the inflationary model yields compatible results with constant and generalized dissipative coefficients for $m = 0, 1$ but for $m = -1$, the behavior of model is found to be inconsistent.

References

1. G. Gamow, *Phys. Rev.* **70** (1946) 572; A. A. Penzias and R. W. Wilson, *Astrophys. J.* **142** (1965) 419; S. Perlmutter *et al.*, *Astrophys. J.* **517** (1999) 565.
2. D. H. Lyth and A. R. Liddle, *The Primordial Density Perturbation: Cosmology, Inflation and the Origin of Structure* (Cambridge University Press, 2009).
3. A. H. Guth, *Phys. Rev. D* **23** (1981) 347; K. Sato, *Mon. Not. R. Astron. Soc.* **195** (1981) 467.
4. A. Linde, *Phys. Lett. B* **129** (1983) 177.
5. S. W. Hawking, *Phys. Lett. B* **115** (1982) 295; J. M. Bardeen, P. J. Steinhardt and M. S. Turner, *Phys. Rev. D* **28** (1983) 679.
6. L. Kofman, A. D. Linde and A. A. Starobinsky, *Phys. Rev. Lett.* **73** (1994) 3195; S. Y. Khlebnikov and I. I. Tkachev, *Phys. Rev. Lett.* **77** (1996) 219; B. A. Bassett, S. Tsujikawa and D. Wands, *Rev. Mod. Phys.* **78** (2006) 537.
7. V. F. Mukhanov and G. V. Chibisov, *J. Exp. Theor. Phys. Lett.* **33** (1981) 532.
8. A. Berera, *Phys. Rev. Lett.* **75** (1995) 3218; *Phys. Rev. D* **55** (1997) 3346.
9. A. Berera, *Nucl. Phys. B* **585** (2000) 666.
10. L. M. H. Hall, I. G. Moss and A. Berera, *Phys. Rev. D* **69** (2004) 083525.
11. J. Yokoyama and A. Linde, *Phys. Rev. D* **60** (1999) 083509.
12. A. Berera and R. O. Ramos, *Phys. Rev. D* **63** (2001) 103509.
13. Y. Watanabe and E. Komatsu, *Phys. Rev. D* **75** (2007) 061301.
14. M. Bastero-Gil, A. Berera and R. O. Ramos, *J. Cosmol. Astropart. Phys.* **09** (2011) 033; M. Bastero-Gil, A. Berera, R. O. Ramos and J. G. Rosa, *J. Cosmol. Astropart. Phys.* **01** (2013) 016.
15. N. Takeda and Y. Watanabe, *Phys. Rev. D* **90** (2014) 023519.
16. A. Linde, *Phys. Lett. B* **175** (1986) 395.
17. J. D. Barrow, *Phys. Lett. B* **235** (1990) 40; J. D. Barrow and P. Saich, *Phys. Lett. B* **249** (1990) 406.
18. R. Herrera, M. Olivares and N. Videla, *Phys. Rev. D* **88** (2013) 063535.
19. M. R. Setare and V. Kamali, *Phys. Lett. B* **726** (2013) 56.
20. M. Sharif and R. Saleem, *Eur. Phys. J. C* **74** (2014) 2738.
21. M. Sharif and R. Saleem, *Astrophys. Space Sci.* **360** (2015) 46; *Astrophys. Space Sci.* **361** (2016) 107.

22. K. Bamba, S. Nojiri, S. D. Odintsov and D. Sáez-Gómez, *Phys. Rev. D* **90** (2014) 124061.
23. M. Sharif and I. Nawazish, *Astrophys. Space Sci.* **361** (2016) 19.
24. M. Sharif and A. Ikram, *J. Exp. Theor. Phys.* **123** (2016) 40, arXiv:1507.00905.
25. P. Teyssandier and P. Tourrenc, *J. Math. Phys.* **24** (1983) 2793; D. I. Santiago and A. S. Silbergleit, *Gen. Relativ. Gravit.* **32** (2000) 565.
26. G. Allemandi, M. Capone, S. Capozziello and M. Francaviglia, *Gen. Relativ. Gravit.* **38** (2006) 33; S. Capozziello, S. Nojiri and S. D. Odintsov, *Phys. Lett. B* **634** (2006) 93.
27. M. Artymowski and Z. Lalak, *J. Cosmol. Astropart. Phys.* **09** (2014) 036.
28. A. de Felice and S. Tusjikawa, *Living Rev. Rel.* **13** (2010) 3.
29. S. Nojiri and S. D. Odintsov, *Phys. Rep.* **505** (2011) 59.
30. A. A. Starobinsky, *Phys. Lett. B* **91** (1980) 99.
31. E. W. Kolb and M. S. Turner, *The Early Universe* (Westview Press, 1994).
32. J. C. Hwang and H. Noh, *Phys. Rev. D* **66** (2002) 084009.
33. L. Sokolowski, *Class. Quantum Grav.* **6** (1989) 2045.
34. G. Magnano and L. M. Sokolowski, *Phys. Rev. D* **50** (1994) 5039.
35. V. Faraoni and S. Nadeau, *Phys. Rev. D* **75** (2007) 023501.
36. A. Linde, *Particle Physics and Inflationary Cosmology* (Harwood Academic, 1990).
37. I. G. Moss, *Phys. Lett. B* **154** (1985) 120; A. Berera and L. Z. Fang, *Phys. Rev. Lett.* **74** (1995) 1912.
38. P. A. R. Ade *et al.*, *Astron. Astrophys.* **594** (2016) A20, arXiv:1502.02114.
39. A. Muslimov, *Class. Quantum Grav.* **7** (1990) 231.
40. F. Lucchin and S. Matarrese, *Phys. Rev. D* **32** (1985) 1316.
41. Y. Zhang, *J. Cosmol. Astropart. Phys.* **03** (2009) 030.
42. A. Berera, I. G. Moss and R. O. Ramos, *Rept. Prog. Phys.* **72** (2009) 026901; R. Herrera, N. Videla and M. Olivares, *Phys. Rev. D* **90** (2014) 103502.

Gen Relativ Gravit (2017) 49:76
DOI 10.1007/s10714-017-2240-9

RESEARCH ARTICLE

Exact solutions and conserved quantities in $f(R,T)$ Gravity

M. Sharif[1] · **Iqra Nawazish**[1]

Received: 12 January 2017 / Accepted: 4 May 2017

Abstract This paper explores Noether and Noether gauge symmetries of anisotropic universe model in $f(R,T)$ gravity. We consider two particular models of this gravity and evaluate their symmetry generators as well as associated conserved quantities. We also find exact solution by using cyclic variable and investigate its behavior via cosmological parameters. The behavior of cosmological parameters turns out to be consistent with recent observations which indicates accelerated expansion of the universe. Next we study Noether gauge symmetry and corresponding conserved quantities for both isotropic and anisotropic universe models. We conclude that symmetry generators and the associated conserved quantities appear in all cases.

Keywords Noether symmetry · Conserved quantity · $f(R,T)$ gravity

1 Introduction

In the last century, the crucial observational discoveries established revolutionary advancements in modern cosmology that introduced a new vision of the current accelerated expanding universe. The accelerated epoch of the universe known as "dark energy" (DE) possesses a huge amount of negative pressure. At theoretical level, the conclusive evidences about accelerated expansion of the universe and enigmatic behavior of DE lead to introduce modified theories of gravity. The $f(R)$ gravity is

✉ M. Sharif
msharif.math@pu.edu.pk

Iqra Nawazish
iqranawazish07@gmail.com

[1] Department of Mathematics, University of the Punjab, Quaid-e-Azam Campus, Lahore 54590, Pakistan

Published online: 16 May 2017

the simplest proposal (R represents Ricci scalar) developed by replacing R with a generic function independent of any non-minimal curvature and matter coupling in the Einstein–Hilbert action.

Different researchers established basic review of $f(R)$ gravity [1–3] and also discussed stability of its different models [4]. The idea of coupling between curvature and matter was initially presented by Nojiri and Odintsov [5] who explored explicit and implicit couplings in $f(R)$ gravity. Harko et al. [6] developed a gravitational theory involving both curvature as well as matter components known as $f(R, T)$ gravity (T denotes trace of the energy-momentum tensor). Sharif and Zubair [7–12] discussed universe evolution via energy conditions along with stability criteria, reconstructed different DE models, exact solutions of anisotropic universe and thermodynamical picture in $f(R, T)$ gravity.

The discovery of CMBR reveals that the early universe was spatially homogeneous but largely anisotropic while this anisotropy still exists in terms of CMB temperature in the present universe. We consider Bianchi type models which measure the effect of anisotropy in the early universe through current observations [13]. The anisotropic universe model indicates that the initial anisotropy determines the fate of rapid expansion of the early universe which will continue for initially large values of anisotropy. If the initial anisotropy is small then the rapid expansion will end leading to a highly isotropic universe [14,15]. Akarsu and Kilinc [16] studied Bianchi type I (BI) model that corresponds to de Sitter universe for different equation of state (EoS) models. Sharif and Zubair [17] formulated exact solutions of BI universe model for power-law and exponential expansions in $f(R, T)$ gravity. Shamir [18] discussed exact solutions of locally rotationally symmetric (LRS) BI universe model and investigated physical behavior of cosmological parameters in this gravity. Kanakavalli and Ananda [19] obtained exact solutions of LRS BI model in the presence of cosmic string source and curvature-matter coupling.

Symmetry approximation plays a crucial role to determine exact solutions or elegantly reduces complexity of a non-linear system of equations. Noether symmetry is a useful approach to evaluate unknown parameters of differential equations. Sharif and Waheed explored Bardeen model [20] as well as stringy charged black holes [21] via approximate symmetry. They also evaluated Noether symmetries of FRW and LRS BI models by including an inverse curvature term in the action of Brans-Dicke theory [22]. Kucukakca et al. [23] established exact solutions of LRS BI universe model through Noether symmetry approach in the same gravity. Jamil et al. [24] discussed Noether symmetry in $f(\mathcal{T})$ gravity ($\mathcal{T}$ denotes torsion) that involves matter as well as scalar field contributions and determined explicit form of $f(\mathcal{T})$ for quintessence and phantom models. Kucukakca [25] found exact solutions of flat FRW universe model via Noether symmetry in scalar–tensor theory incorporating non-minimal coupling with torsion scalar. Sharif and Shafique [26] discussed Noether and Noether gauge symmetries in this gravity. Sharif and Fatima [27] explored Noether symmetry of flat FRW model through vacuum and non-vacuum cases in $f(G)$ gravity.

Capozziello et al. [28] explored Noether symmetry to determine exact solutions of spherically symmetric spacetime in $f(R)$ gravity. Vakili [29] obtained Noether symmetry of flat FRW metric and analyzed the behavior of effective EoS parameter in quintessence phase. Jamil et al. [30] studied Noether symmetry of flat FRW universe using tachyon model in this gravity. Hussain et al. [31] studied Noether gauge symmetry of flat FRW universe model for $f(R)$ power-law model which generates zero gauge term. Shamir et al. [32] analyzed Noether gauge symmetry for the same model as well as for static spherically symmetric spacetime and found non-zero gauge term. Kucukakca and Camci [33] established Noether gauge symmetry of FRW universe model in Palatini formalism of $f(R)$ gravity. Momeni et al. [34] investigated the existence of Noether symmetry and discussed stability of solutions for flat FRW universe model in $f(R,T)$ and mimetic $f(R)$ gravity. They also explored a class of solutions with future singularities.

In this paper, we discuss Noether and Noether gauge symmetries of BI universe model in $f(R,T)$ gravity. We formulate exact solution of the field equations to discuss cosmic evolution via cosmological parameters. The format of this paper is as follows. In Sect. 2, we discuss a basic formalism of $f(R,T)$ gravity, Noether and Noether gauge symmetries. Section 3 explores Noether symmetry of BI model for two theoretical models of $f(R,T)$ gravity and also establish exact solution via cyclic variables. In Sect. 4, we obtain symmetry generator and corresponding conserved quantities through Noether gauge symmetry for flat FRW and BI models. In the last section, we summarize the results.

2 Basic framework

The current cosmic expansion successfully discusses not only from the contribution of the scalar-curvature part but also describes from a non-minimal coupling between curvature and matter components as well. This non-minimal coupling yields non-zero divergence of the energy-momentum tensor due to which an extra force appears that deviates massive test particles from geodesic trajectories. The action of such modified gravity is given by [6]

$$\mathcal{I}=\int d^4x\sqrt{-g}\left[\frac{f(R,T)}{2\kappa^2}+\mathcal{L}_m\right], \tag{1}$$

where f describes a simple coupling of geometry and matter whereas $\mathcal{L}_m$ denotes the matter Lagrangian. The variation of action (1) with respect to $g_{\mu\nu}$ yields non-linear partial differential equation of the following form

$$\begin{aligned} &f_R(R,T)R_{\mu\nu}-\frac{1}{2}f(R,T)g_{\mu\nu}+(g_{\mu\nu}\Box-\nabla_\mu\nabla_\nu)f_R(R,T)+f_T(R,T)T_{\mu\nu}\\ &+f_T(R,T)\Theta_{\mu\nu}=\kappa^2T_{\mu\nu}, \end{aligned} \tag{2}$$

where ∇_μ shows covariant derivative and

$$\begin{aligned} &\Box=\nabla_\mu\nabla^\mu, \quad f_R(R,T)=\frac{\partial f(R,T)}{\partial R}, \quad f_T(R,T)=\frac{\partial f(R,T)}{\partial T},\\ &\Theta_{\mu\nu}=\frac{g^{\alpha\beta}\delta T_{\alpha\beta}}{\delta g^{\mu\nu}}=g_{\mu\nu}\mathcal{L}_m-2T_{\mu\nu}-2g^{\alpha\beta}\frac{\partial^2\mathcal{L}_m}{\partial g^{\alpha\beta}\partial g^{\mu\nu}}. \end{aligned}$$

The trace of Eq. (2) provides a significant relationship between geometric and matter parts as follows

$$Rf_R(R,T)+3\Box f_R(R,T)-2f(R,T)+Tf_T(R,T)+\Theta f_T(R,T)=\kappa^2 T.$$

Harko et al [6] introduced some theoretical models for different choices of matter as

- $f(R,T)=R+2f(T)$,
- $f(R,T)=f_1(R)+f_2(T)$,
- $f(R,T)=f_1(R)+f_2(R)f_3(T)$.

Noether symmetry is the most significant approach to deal with non-linear partial differential equations. The existence of Noether symmetry is possible only if Lie derivative of Lagrangian vanishes, i.e., the vector field is unique on the tangent space. In such situation, the vector field behaves as a symmetry generator which further generates conserved quantity. Noether gauge symmetry being generaliztion of Noether symmetry preserves some extra symmetries along a non-vanishing gauge term. The vector field and its first order prolongation are defined as

$$K=\xi\left(t,q^i\right)\frac{\partial}{\partial t}+\eta^j\left(t,q^i\right)\frac{\partial}{\partial q^j},$$
$$K^{[1]}=K+\left(\eta^j{}_{,t}+\eta^j{}_{,i}\dot{q}^i-\xi_{,t}\dot{q}^j-\xi_{,i}\dot{q}^i\dot{q}^j\right)\frac{\partial}{\partial\dot{q}^i},$$

where t identifies as affine parameter, $\xi,\ \eta$ are symmetry generator coefficients, q^i represents n generalized positions and dot denotes time derivative. The vector field K generates Noether gauge symmetry if Lagrangian preserves the following condition

$$K^{[1]}\mathcal{L}+(D\xi)\mathcal{L}=DG(t,q^i).$$

Here $G(t,q^i)$ represents the gauge term and D denotes the total derivative operator defined as

$$D=\frac{\partial}{\partial t}+\dot{q}^i\frac{\partial}{\partial q^i}.$$

According to Noether theorem, there exists a conserved quantity corresponding to each symmetry of a system. In case of Noether gauge symmetry, the conserved quantity for vector field K takes the form

$$\Sigma=G-\xi\mathcal{L}-\left(\eta^j-\dot{q}^j\xi\right)\frac{\partial\mathcal{L}}{\partial\dot{q}^j}.$$

For the existence of Noether symmetry, the following condition must holds

$$L_K\mathcal{L}=K\mathcal{L}=0,$$

where L represents Lie derivative while the vector field K and conserved quantity corresponding to symmetry generator turn out to be

$$K=\beta^i\left(q^i\right)\frac{\partial}{\partial q^i}+\left[\frac{d}{dt}\left(\beta^i\left(q^i\right)\right)\right]\frac{\partial}{\partial \dot{q}^i},\quad \Sigma=-\eta^j\frac{\partial\mathcal{L}}{\partial\dot{q}^j}. \tag{3}$$

The equation of motion and associated Hamiltonian equation of a dynamical system are defined as

$$\frac{\partial\mathcal{L}}{\partial q^i}-\frac{d}{dt}\left(\frac{\partial\mathcal{L}}{\partial\dot{q}^i}\right)=0,\quad \Sigma_i\dot{q}^i p_i-\mathcal{L}=\mathcal{H},\quad p_i=\frac{\partial\mathcal{L}}{\partial q^i},$$

where p_i represents conjugate momenta of configuration space.

3 Noether symmetry for BI universe model

Here we apply Noether symmetry approach to deal with non-linear partial differential Eq. (2) and evaluate symmetry generators as well as corresponding conserved quantities of BI universe model given by

$$ds^2=-dt^2+a^2(t)dx^2+b^2(t)(dy^2+dz^2), \tag{4}$$

where t denotes cosmic time, scale factors a and b measure expansion of the universe in x and $y,\ z$-directions, respectively. We consider the perfect fluid distribution given by

$$T_{\mu\nu}=(\rho+p)u_\mu u_\nu+pg_{\mu\nu},$$

where $p,\ \rho$ and u_μ represent pressure, energy density and four-velocity of the fluid, respectively. To evaluate the Lagrangian, we rewrite the action (1) as

$$\mathcal{I}=\int\sqrt{-g}[f(R,T)-\lambda(R-\bar{R})-\chi(T-\bar{T})+\mathcal{L}_m]dt, \tag{5}$$

where $\sqrt{-g}=ab^2$, $\bar{R},\ \bar{T}$ are dynamical constraints while $\lambda,\ \chi$ are Lagrange multipliers given by

$$\bar{R}=\frac{2}{ab^2}(\ddot{a}b^2+2ab\ddot{b}+2b\dot{a}\dot{b}+a\dot{b}^2),\quad \bar{T}=3p(a,b)-\rho(a,b),$$
$$\lambda=f_R(R,T),\quad \chi=f_T(R,T).$$

The field Eq. (2) is not easy to tackle with perfect fluid configuration and also there is no unique definition of matter Lagrangian. In order to construct Lagrangian, we consider $\mathcal{L}_m=p(a,b)$ which yields

$$\begin{aligned}\mathcal{L}(a,b,R,T,\dot{a},\dot{b},\dot{R},\dot{T})&=ab^2[f(R,T)-Rf_R(R,T)-Tf_T(R,T)\\&+f_T(R,T)(3p(a,b)-\rho(a,b))+p(a,b)]-(4b\dot{a}\dot{b}+2a\dot{b}^2)f_R(R,T)\\&-(2b^2\dot{a}\dot{R}+4ab\dot{b}\dot{R})f_{RR}(R,T)-(2b^2\dot{a}\dot{T}+4ab\dot{b}\dot{T})f_{RT}(R,T).\end{aligned} \tag{6}$$

The corresponding equations of motion and energy function of dynamical system become

$$\begin{aligned}
\frac{\dot{b}^2}{b^2}+\frac{2\ddot{b}}{b}=&-\frac{1}{2f_R(R,T)}\Big[f(R,T)-Rf_R(R,T)-Tf_T(R,T)+f_T(R,T)\\
&\times(3p(a,b)-\rho(a,b))+p(a,b)+a\left\{f_T(3p,_a-\rho,_a)+p,_a\right\}\\
&+\frac{4\dot{b}\dot{R}f_{RR}(R,T)}{b}\\
&+2\ddot{R}f_{RR}(R,T)+2\dot{R}^2f_{RRR}(R,T)\\
&+4\dot{R}\dot{T}f_{RRT}(R,T)+2\ddot{T}f_{RT}(R,T)\\
&+2\dot{T}^2f_{RTT}(R,T)\Big], \qquad (7)
\end{aligned}$$

$$\begin{aligned}
\frac{\ddot{a}}{a}+\frac{\dot{a}\dot{b}}{ab}+\frac{\ddot{b}}{b}=&-\frac{1}{4f_R(R,T)}[2(f(R,T)-Rf_R(R,T)-Tf_T(R,T)\\
&+f_T(R,T)(3p(a,b)-\rho(a,b))+p(a,b))\\
&+b\left\{f_T(3p,_b-\rho,_b)+p,_b\right\}]\\
&+2(a^{-1}\dot{a}\dot{R}+\ddot{R})f_{RR}+2\dot{R}^2f_{RRR}+2(a^{-1}\dot{a}\dot{T}+\ddot{T})f_{RT}\\
&+2(b^{-1}\dot{b}\dot{R}+2\dot{R}\dot{T}+\dot{T}^2)f_{RRT}+2b^{-1}\dot{b}\dot{T}f_{RTT}, \qquad (8)
\end{aligned}$$

$$\begin{aligned}
\frac{\dot{b}^2}{b^2}+\frac{2\dot{a}\dot{b}}{ab}=&-\frac{1}{f_R(R,T)}\left[\left(\frac{2\dot{b}\dot{R}}{b}+\frac{\dot{a}\dot{R}}{a}\right)f_{RR}(R,T)+\left(\frac{2\dot{b}\dot{T}}{b}+\frac{\dot{a}\dot{T}}{a}\right)\right.\\
&\times f_{RT}(R,T)+\frac{1}{2}(f(R,T)-Rf_R(R,T)\\
&-Tf_T(R,T)+f_T(R,T)(3p(a,b)\\
&\left.-\rho(a,b))+p(a,b))\right]. \qquad (9)
\end{aligned}$$

The conjugate momenta corresponding to configuration space $(a,\ b,\ R,\ T)$ are

$$p_a=\frac{\partial\mathcal{L}}{\partial\dot{a}}=-4b\dot{b}f_R(R,T)-2b^2(\dot{R}f_{RR}(R,T)+\dot{T}f_{RT}(R,T)), \qquad (10)$$

$$p_b=\frac{\partial\mathcal{L}}{\partial\dot{b}}=-4f_R(R,T)(a\dot{b}+b\dot{a}-4ab(\dot{R}f_{RR}(R,T)+\dot{T}f_{RT}(R,T)), \qquad (11)$$

$$p_R=\frac{\partial\mathcal{L}}{\partial\dot{R}}=-(4ab\dot{b}+2b^2\dot{a})f_{RR}(R,T), \qquad (12)$$

$$p_T=\frac{\partial\mathcal{L}}{\partial\dot{T}}=-(4ab\dot{b}+2b^2\dot{a})f_{RT}(R,T). \qquad (13)$$

For Noether symmetry, the vector field (3) takes the following form

$$K=\alpha\frac{\partial}{\partial a}+\beta\frac{\partial}{\partial b}+\gamma\frac{\partial}{\partial R}+\delta\frac{\partial}{\partial T}+\dot{\alpha}\frac{\partial}{\partial\dot{a}}+\dot{\beta}\frac{\partial}{\partial\dot{b}}+\dot{\gamma}\frac{\partial}{\partial\dot{R}}+\dot{\delta}\frac{\partial}{\partial\dot{T}}, \qquad (14)$$

where $\alpha,\ \beta,\ \gamma$ and δ are unknown coefficients of generator which depend on variables $a,\ b,\ R$ and T while the time derivatives of these coefficients are

$$\dot{\alpha}=\dot{a}\frac{\partial\alpha}{\partial a}+\dot{b}\frac{\partial\alpha}{\partial b}+\dot{R}\frac{\partial\alpha}{\partial R}+\dot{T}\frac{\partial\alpha}{\partial T},\quad \dot{\beta}=\dot{a}\frac{\partial\beta}{\partial a}+\dot{b}\frac{\partial\beta}{\partial b}+\dot{R}\frac{\partial\beta}{\partial R}+\dot{T}\frac{\partial\beta}{\partial T},\tag{15}$$

$$\dot{\gamma}=\dot{a}\frac{\partial\gamma}{\partial a}+\dot{b}\frac{\partial\gamma}{\partial b}+\dot{R}\frac{\partial\gamma}{\partial R}+\dot{T}\frac{\partial\gamma}{\partial T},\quad \dot{\delta}=\dot{a}\frac{\partial\delta}{\partial a}+\dot{b}\frac{\partial\delta}{\partial b}+\dot{R}\frac{\partial\delta}{\partial R}+\dot{T}\frac{\partial\delta}{\partial T}.\tag{16}$$

Taking Lie derivative of Lagrangian (6) for vector field (14) and inserting Eqs. (15) and (16), we obtain the following over determined system of equations by comparing the coefficients of $\dot{a}^2,\ \dot{b}^2,\ \dot{R}^2,\ \dot{T}^2,\ \dot{a}\dot{b},\ \dot{a}\dot{R},\ \dot{a}\dot{T},\ \dot{b}\dot{R},\ \dot{b}\dot{T}$ and $\dot{R}\dot{T}$ as

$$(b\alpha,_R+2a\beta,_R)f_{RR}=0,\tag{17}$$

$$(b\alpha,_T+2a\beta,_T)f_{RT}=0,\tag{18}$$

$$2\beta,_a f_R+b\gamma,_a f_{RR}+b\delta,_a f_{RT}=0,\tag{19}$$

$$b\alpha,_R f_{RT}+b\alpha,_T f_{RR}+2a\beta,_R f_{RT}+2a\beta,_T f_{RR}=0,\tag{20}$$

$$\begin{aligned}&2\beta f_{RR}+b\gamma f_{RRR}+b\delta f_{RRT}+b\alpha,_a f_{RR}+2a\beta,_a f_{RR}+2\beta,_R f_R+b\gamma,_R f_{RR}\\&\quad+b\delta,_R f_{RT}=0,\end{aligned}\tag{21}$$

$$\begin{aligned}&2\beta f_{RT}+b\gamma f_{RRT}+b\delta f_{RTT}+b\alpha,_a f_{RT}+2a\beta,_a f_{RT}+2\beta,_T f_R+b\gamma,_T f_{RR}\\&\quad+b\delta,_T f_{RT}=0,\end{aligned}\tag{22}$$

$$\begin{aligned}&2\beta f_R+2b\gamma f_{RR}+2b\delta f_{RT}+2b\alpha,_a f_R+2a\beta,_a f_R+2b\beta,_b f_R+2ab\gamma,_a f_{RR}\\&\quad+b^2\gamma,_b f_{RR}+2ab\delta,_a f_{RT}+b^2\delta,_b f_{RT}=0,\end{aligned}\tag{23}$$

$$\begin{aligned}&2b\alpha f_{RR}+2a\beta f_{RR}+2ab\gamma f_{RRR}+2ab\delta f_{RRT}+b^2\alpha,_b f_{RR}+2b\alpha,_R f_R+2ab\\&\quad\times\beta,_b f_{RR}+2a\beta,_R f_R+2ab\gamma,_R f_{RR}+2ab\delta,_R f_{RT}=0,\end{aligned}\tag{24}$$

$$\begin{aligned}&2b\alpha f_{RT}+2a\beta f_{RT}+2ab\gamma f_{RRT}+2ab\delta f_{RTT}+b^2\alpha,_b f_{RT}+2b\alpha,_T f_R+2ab\\&\quad\times\beta,_b f_{RT}+2a\beta,_T f_R+2ab\gamma,_T f_{RR}+2ab\delta,_T f_{RT}=0,\end{aligned}\tag{25}$$

$$\begin{aligned}&\alpha f_R+a\gamma f_{RR}+a\delta f_{RT}+2b\alpha,_b f_R+2a\beta,_b f_R+2ab\gamma,_b f_{RR}+2ab\delta,_b\\&\quad\times f_{RT}=0,\end{aligned}\tag{26}$$

$$\begin{aligned}&b^2\alpha[f-Rf_R-Tf_T+f_T(3p-\rho)+p+a\{f_T(3p,_a-\rho,_a)+p,_a\}]+\beta[2ab\\&\quad\times(f-Rf_R-Tf_T+f_T(3p-\rho)+p)+ab^2\{f_T(3p,_b-\rho,_b)+p,_b\}]+ab^2\\&\quad\times\gamma[-(Rf_{RR}+Tf_{RT})+f_{RT}(3p-\rho)]+ab^2\delta[-(Rf_{RT}+Tf_{TT})+f_{TT}\\&\quad\times(3p-\rho)]=0.\end{aligned}\tag{27}$$

We solve this non-linear system of partial differential equations for two models of $f(R,T)$ gravity and evaluate possible solutions of symmetry generator coefficients as well as corresponding conserved quantities.

3.1 $f(R,T)=R+2f(T)$

Here we discuss a solution for a simple model that explores Einstein gravity with matter components such as $f(R,T)=R+2f(T)$, where the curvature term behaves as a leading term of the model. This model corresponds to ΛCDM model when matter part comprises cosmological constant as a function of trace T. Consequently, this model reduces to

$$f(R,T) = R + 2\Lambda + h(T). \tag{28}$$

To find the solution of Eqs. (17)–(27), we consider power-law form of unknown coefficients of vector field as

$$\alpha = \alpha_0 a^{\alpha_1} b^{\alpha_2} R^{\alpha_3} T^{\alpha_4}, \quad \beta = \beta_0 a^{\beta_1} b^{\beta_2} R^{\beta_3} T^{\beta_4}, \tag{29}$$
$$\gamma = \gamma_0 a^{\gamma_1} b^{\gamma_2} R^{\gamma_3} T^{\gamma_4}, \quad \delta = \delta_0 a^{\delta_1} b^{\delta_2} R^{\delta_3} T^{\delta_4}, \tag{30}$$

where the powers are unknown constants to be determined. Using these coefficients in Eqs. (17)–(25), we obtain

$$\alpha_0 = -\beta_0(\alpha_2 + 2), \quad \alpha_1 = 1, \quad \alpha_3 = 0, \quad \alpha_4 = 0, \quad \gamma = 0,$$
$$\beta_1 = 0, \quad \beta_2 = \alpha_2 + 1, \quad \beta_3 = 0, \quad \beta_4 = 0.$$

Inserting these values in Eq. (29), it follows that

$$\alpha = -\beta_0(\alpha_2 + 2) a b^{\alpha_2}, \quad \beta = \beta_0 b^{\alpha_2 + 1}.$$

In order to evaluate α_2, we substitute these solutions in Eq. (26) which implies that either $\alpha_2 = 0$ or $\alpha_2 = \frac{1}{2}$.

Case I: $\alpha_2 = 0$

In this case, the generator coefficients turn out to be

$$\alpha = -2\beta_0 a, \quad \beta = \beta_0 b.$$

In order to evaluate the remaining coefficients, we insert these values in Eqs. (7), (9) and (27) which give

$$h(T) = l_1 T + l_2, \quad \delta = 0, \quad p = l_3 a^{-\frac{1}{5}} b^{-\frac{2}{5}},$$
$$\rho = -\frac{1}{2l_1}\left[2\Lambda + l_2 + (3l_1 - 1) l_3 a^{-\frac{1}{5}} b^{-\frac{2}{5}}\right].$$

Substituting all these solutions in Eqs. (17)–(25), we obtain $l_1 = -\frac{19}{3}$. Consequently, the coefficients of symmetry generator and $f(R,T)$ model become

$$\alpha = -2\beta_0 a, \quad \beta = \beta_0 b, \quad \gamma = 0, \quad \delta = 0, \quad f(R,T) = R - \frac{19T}{3},$$

where $h(T) = -\frac{19T}{3} - 2\Lambda$ and $T = \frac{87}{19} l_3 a^{-\frac{1}{5}} b^{-\frac{2}{5}}$. To avoid Dolgov–Kawasaki instability, the $f(R,T)$ model preserves the following conditions [35,36]

$$f_R(R) > 0, \quad f_{RR}(R) > 0, \quad 1 + f_T(R,T) > 0, \quad R > R_0. \tag{31}$$

In this case, the constructed $f(R, T)$ model is found to be viable for $l_3 < 0$. Using the values of symmetry generator coefficients, we obtain symmetry generator which yields scaling symmetry and its conserved quantity as

$$K = -2\beta_0 a\frac{\partial}{\partial a} + \beta_0 b\frac{\partial}{\partial b}, \quad \Sigma = \beta_0\left[-4ab\dot{b} + 4\dot{a}b^2\right].$$

Now we solve the field equations using cyclic variable whose existence is assured by the presence of symmetry generator of Noether symmetry. We consider a point transformation which reduces complex nature of the system to $\phi : (a, b) \rightarrow (v, z)$ implying that $\phi_K dv = 0$ and $\phi_K dz = 1$. The second mapping indicates that the Lagrangian must be free from the variable z. Imposing this point transformation, we reduce the complexity of the system as

$$v = \zeta_0 a^{\frac{1}{2}} b, \quad z = \frac{\ln b}{\beta_0}, \tag{32}$$

where z is cyclic variable and ζ_0 denotes arbitrary constant. The inverse point transformation of variables yields

$$a = \zeta_1 v^{\frac{1}{2}} e^{-2\beta_0 z}, \quad b = \zeta_2 e^{\beta_0 z}, \quad \rho = -\frac{30\zeta_3 v^{-\frac{2}{5}}}{19}, \quad p = \zeta_3 v^{-\frac{2}{5}}. \tag{33}$$

Here we redefine arbitrary constants as $\zeta_3 = l_3\zeta_1^{-\frac{1}{5}}\zeta_2^{-\frac{2}{5}}$. For the above solutions, the Lagrangian (6) and the corresponding equations of motion with associated energy function (7)–(9) take the form

$$\begin{aligned}
&\mathcal{L} = \zeta_4\left(4\beta_0 v^{\frac{-1}{2}}\dot{v}\dot{z} + 4\beta_0^2 v^{\frac{1}{2}}\dot{z}^2 - 30v^{\frac{2}{5}}\right),\\
&2\beta_0 v^{\frac{-1}{2}}\ddot{z} + 2\beta_0^2 v^{-\frac{1}{2}}\dot{z}^2 - 12v^{-\frac{3}{5}} = 0,\\
&8\beta_0 v^{\frac{1}{2}}\ddot{z} + v^{-\frac{3}{2}}\dot{v}^2 + 4\beta_0 v^{-\frac{1}{2}}\dot{z} - 2v^{-\frac{1}{2}}\ddot{v} = 0,\\
&30v^{\frac{2}{5}} + 4\beta_0^2 v^{\frac{1}{2}}\dot{z}^2 + \beta_0 v^{-\frac{3}{2}}\dot{v}^2\dot{z} - 2\beta_0 v^{-\frac{1}{2}}\dot{v}\ddot{z} = 0.
\end{aligned}$$

We solve the above equations to evaluate the time dependent solutions of new variables $(v,\ z)$

$$v = 2(t-\zeta_4)^{\frac{1}{2}}\left(t^2 - 2t + \zeta_4^2\right), \quad z = \frac{1}{12\beta_0}\left[12\beta_0\zeta_5 - 2.93 - 4\ln\left[(t-\zeta_4)^{\frac{5}{2}}\right]\right],$$

where ζ_4 and ζ_5 represent integration constants. Inserting these values into Eq. (33), we obtain

$$a = \frac{8}{5}\zeta_1 e^{-2\beta_0\zeta_5}(t-\zeta_4)^{\frac{5}{3}}, \quad b = \frac{8}{5}\zeta_2 e^{\beta_0\zeta_5}(t-\zeta_4)^{-\frac{1}{3}}(t^2 - 2t\zeta_1 + \zeta_1^2), \tag{34}$$

$$\rho = -\frac{30\zeta_3}{19}[2(t-\zeta_4)^{\frac{1}{2}}(t^2 - 2t + \zeta_4^2)]^{-\frac{2}{5}},$$

$$p = \zeta_3[2(t-\zeta_4)^{\frac{1}{2}}(t^2-2t+\zeta_4^2)]^{-\frac{2}{5}}. \tag{35}$$

We study the behavior of some well-known cosmological parameters like Hubble, deceleration and EoS parameters using scale factors and matter contents. These parameters play significant role to discuss cosmic expansion as Hubble parameter (H) measures the rate of cosmic expansion while deceleration parameter (q) determines that either expansion is accelerated ($q < 0$) or decelerated ($q > 0$) or constant expansion ($q = 0$). The EoS parameter ($\omega = \frac{p}{\rho}$) evaluates different eras of the universe and also differentiates DE era into different phases like quintessence ($-1 < \omega \leq -1/3$) or phantom ($\omega < -1$). In case of BI universe model, the Hubble and deceleration parameters are

$$H = \frac{1}{3}\left(\frac{\dot{a}}{a}+\frac{2\dot{b}}{b}\right), \quad q = -\frac{\dot{H}}{H^2}-1.$$

Using Eq. (34), the Hubble and deceleration parameters turn out to be

$$H = \frac{5\zeta_6}{3}\left(1+\frac{t}{\zeta_6}\right), \quad q = -\frac{3}{5}(\zeta_6+t)^{-2}-1, \tag{36}$$

where $\zeta_6 = -\zeta_4$. Inserting Eqs. (34) and (35) in (7) and (9), the effective EoS parameter becomes

$$\omega_{eff} = \frac{p_{eff}}{\rho_{eff}} = 1 - \frac{\zeta_4 - t + 3(\sqrt{t-\zeta_4}(t^2-2t+\zeta_4^2))^{\frac{2}{5}}}{t-\zeta_4}.$$

The crucial pair of (r, s) parameters study the correspondence between constructed and standard universe models such as for $(r, s) = (1, 0)$, the constructed model corresponds to standard constant cosmological constant cold dark matter (ΛCDM) model. In terms of Hubble and deceleration parameters, these are defined as

$$r = q + 2q^2 - \frac{\dot{q}}{H}, \quad s = \frac{r-1}{3(q-\frac{1}{2})}.$$

Using Eq. (36), these parameters take the form

$$r = 1 + \frac{18}{25}\left(2(t-\zeta_4)^{-4} - 2(t-\zeta_4)^{-3} + (t-\zeta_4)^{-2}\right),$$
$$s = \frac{1}{3}(r-1)\left(-\frac{3(t+\zeta_6)^{-2}}{5} - \frac{3}{2}\right)^{-1}.$$

Both plots of Fig. 1 represent graphical analysis of the scale factors a and b which show the increasing behavior of both scale factors in x and y, z-directions, respectively. This increasing nature of scale factors indicates the cosmic accelerated expansion in all directions. The graphical analysis of Hubble and deceleration parameters is shown in Fig. 2. Figure 2i shows that the Hubble parameter grows continuously representing expanding universe whereas Fig. 2ii shows negative deceleration parameter which corresponds to accelerated expansion of the universe. In Fig. 3, the first plot indicates that the effective EoS parameter corresponds to quintessence phase while

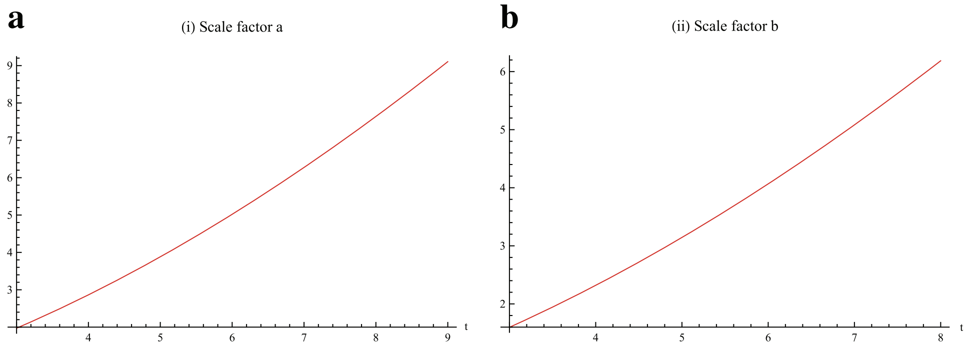

Fig. 1 Plots of scale factors versus cosmic time t: **i** $a(t)$ versus t; **ii** $b(t)$ versus t for $\zeta_1 = 0.15$, $\zeta_2 = 0.09$, $\zeta_4 = -0.99$, $\zeta_5 = 0.5$, $\beta_0 = 0.1$

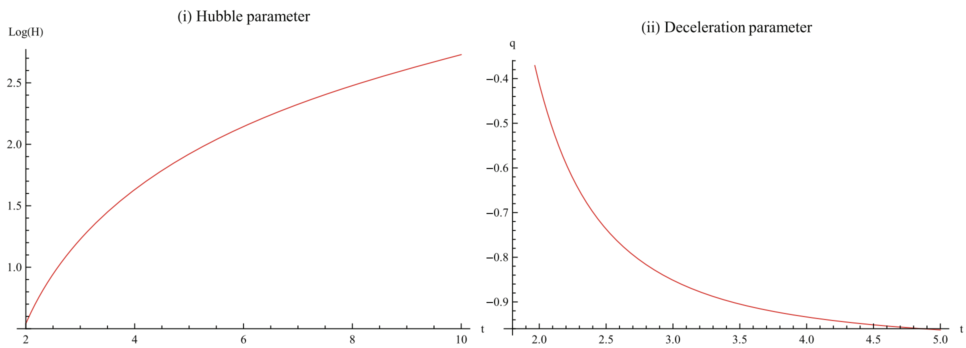

Fig. 2 Plots of **i** Hubble parameter and **ii** deceleration parameter versus cosmic time t for $\zeta_6 = -0.99$

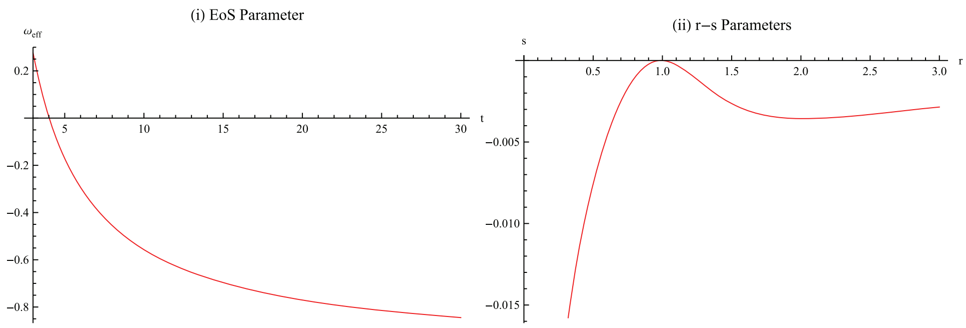

Fig. 3 Plots of **i** EoS Parameter and **ii** r-s parameters versus cosmic time t for $\zeta_6 = -0.99$

Fig. 3ii represents correspondence of the constructed model with standard ΛCDM universe model. Thus, the analysis of cosmological parameters implies that the universe experiences accelerated expansion for BI universe model in the context of $f(R, T)$ gravity.

Case II: $\alpha_2 = \frac{1}{2}$

For $\alpha_2 = \frac{1}{2}$, the solutions become

$$\alpha=-\frac{5}{2}\beta_0 ab^{\frac{1}{2}},\quad \beta=\beta_0 b^{\frac{3}{2}},$$

whereas Eq. (27) yields

$$\delta=0,\quad h(T)=-2\Lambda+c_1T,\quad p=c_2a^{\frac{3c_1^2-3c_1-1}{3c_1-1}}b^{\frac{3(5c_1^2-4c_1-2)}{2(3c_1-1)}},$$
$$\rho=\left(\frac{3c_1-1}{c_1-2}\right)c_2a^{\frac{3c_1^2-3c_1-1}{3c_1-1}}b^{\frac{3(5c_1^2-4c_1-2)}{2(3c_1-1)}}.$$

The above solutions satisfy the system of Eqs. (17)–(25) for $c_1=\frac{3\pm\sqrt{21}}{6}$. Under this condition, the solutions and considered model of $f(R,T)$ gravity take the following form

$$\alpha=-\frac{5}{2}\beta_0 ab^{\frac{1}{2}},\quad \beta=\beta_0 b^{\frac{3}{2}},\quad \gamma,\delta=0,\quad h(T)=-2\Lambda+\left(\frac{3\pm\sqrt{21}}{6}\right)T,$$
$$p=c_2b^{\frac{1}{2}},\quad \rho=\left(\frac{-3\mp\sqrt{21}}{9\mp\sqrt{21}}\right)c_2b^{\frac{1}{2}},\quad f(R,T)=R+\left(\frac{3\pm\sqrt{21}}{6}\right)T,$$

where $T=\left(\frac{30\mp2\sqrt{21}}{9\mp\sqrt{21}}\right)c_2b^{\frac{1}{2}}$. Here, the constructed model ignores Dolgov–Kawasaki instability as $f_R,\ f_{RR},\ 1+f_T>0$. The symmetry generator and its corresponding conserved quantity turn out to be

$$K=-\frac{5}{2}\beta_0 ab^{\frac{1}{2}}\frac{\partial}{\partial a}+\beta_0 b^{\frac{3}{2}}\frac{\partial}{\partial b},\quad \Sigma=\beta_0\left[6ab^{\frac{3}{2}}\dot{b}-4\dot{a}b^{\frac{5}{2}}\right].$$

We consider z to be a cyclic variable which yields

$$v=\chi_0a^{\frac{2}{5}}b,\quad z=-\frac{2b^{-\frac{1}{2}}}{\beta_0},$$

where χ_0 denotes arbitrary constant. The corresponding inverse point transformation leads to

$$a=\chi_1v^{\frac{5}{2}}\left(-\frac{\beta_0z}{2}\right)^5,\quad b=\chi_2\left(-\frac{\beta_0z}{2}\right)^{-2},$$
$$p=c_2\chi_2\left(-\frac{\beta_0z}{2}\right)^{-1}\quad \rho=\left(\frac{-3\mp\sqrt{21}}{9\mp\sqrt{21}}\right)c_2\chi_2\left(-\frac{\beta_0z}{2}\right)^{-1},$$

where χ_1,χ_2 are arbitrary constants. For these solutions, the Lagrangian (6) becomes

$$\mathcal{L} = -2\beta_0\chi_1\chi_2^2\left[5v^{\frac{3}{2}}\dot{v} - 6\beta_0 v^{\frac{5}{2}}\dot{z}^2\left(-\frac{\beta_0 z}{2}\right)^{-1}\right] + c_2 v^{\frac{5}{2}}\left[4\left(\frac{3\pm\sqrt{21}}{6}\right)\right.$$
$$\left.\times\left(\frac{6\mp\sqrt{21}}{9\mp\sqrt{21}}\right) - 1\right],$$

which depends upon the cyclic variable z. Thus, the resulting symmetry generator for $\alpha_2 = 0$ yields scaling symmetry providing more significant results as compared to $\alpha_2 = \frac{1}{2}$.

3.2 $f(R, T) = f_1(R) + f_2(T)$

Here we consider $f(R, T)$ model which does not encourage any absolute non-minimal coupling of curvature and matter. For vector field K (14), we substitute this model in Eqs. (17)–(23) and (25) yielding the coefficients of symmetry generator in the form

$$\alpha = -\frac{2ac_3}{b\sqrt{f_1'(R)}} - 2ac_4\ln(f_1'(R)) - \frac{2c_5}{\sqrt{b}} - 4\ln(b)ac_4 - 6\ln(b)c_6 a + c_7 a,$$
$$\beta = \frac{c_3}{\sqrt{f_1'(R)}} + (c_8 + \ln(f_1'(R))c_4)b - (c_4 + c_6)b\ln(b) + c_6 b\ln(a),$$
$$\gamma = -\frac{2}{\sqrt{f_1'(R)f_1''(R)b}}\left[b((-3c_4 - 4c_6)\ln(b) + c_4 + c_8 + \frac{c_7}{2}\right.$$
$$\left. + c_6 + c_6\ln(a))(f_1'(R))^{\frac{3}{2}} - c_3 f_1'(R)\right],$$

where prime denotes derivative with respect to R and c_i $(i = 3, 4, 5, 6, 7, 8)$ are arbitrary constants. Inserting these solutions in Eq. (24), we obtain two solutions for $f_1(R)$ as $f_1(R) = c_9 R + c_{10}$ which is similar to the previous case while the second solution increases the complexity of the system. To avoid this situation, we consider $f_1(R) = f_0 R^n$, $(n \neq 0,\ 1)$ which yields

$$\alpha = ac_{11},\quad \beta = bc_{12},\quad \gamma = \frac{(c_{11} + 2c_{12})R}{1-n},\quad f_2(T) = \frac{T}{3} + c_{13},$$
$$p = \frac{1}{12nc_{13}}\left[R^{1-n}b\rho_{,b} - Rc_{13} - 6R^{1-n}c_{13} + 2R^{1-n}\rho + 6nc_{13}R\right],$$
$$\rho = 3f_0R^n + 3c_{13} - \frac{(c_{11}a\rho_{,a} + c_{12}b\rho_{,b})}{(c_{11} + 2c_{12})}.$$

These solutions satisfy (17)–(27) for $n = 2$ which implies that $f_1(R) = f_0R^2$ and hence this quadratic curvature term describes an indirect non-minimal coupling of the matter components with geometry. Thus the matter contents and model of $f(R, T)$ gravity turn out to be

$$\rho = 3f_0R^2 + 3c_{13} + \frac{a^{-1+\frac{c_{12}}{c_{11}}}b}{2}, \quad p = \frac{1}{24c_{13}}\left[\frac{3a^{-1+\frac{c_{12}}{c_{11}}}bR^{-1}}{2} + 12c_{13}R\right],$$

$$f(R,T) = f_0R^2 + \frac{T}{3} + c_{13}, \quad T = 3p - \rho.$$

In this case, the constructed $f(R,T)$ model is found to be viable as it preserves stability conditions (31). The corresponding symmetry generator takes the form

$$K = ac_{11}\frac{\partial}{\partial a} + bc_{12}\frac{\partial}{\partial b} - R(c_{11}+2c_{12})\frac{\partial}{\partial R}.$$

This generator yields scaling symmetry with the following conserved factors

$$\Sigma_1 = 4ab^2\dot{R}f_0 - 4b^2\dot{a}f_0R, \quad \Sigma_2 = -24ab\dot{b}f_0R - 8ab^2\dot{R}f_0,$$

where Σ_1 and Σ_2 are conserved quantities corresponding to c_{11} and c_{12}, respectively.

To reduce the complex nature of the system, we consider $\phi : (a, b, R) \rightarrow (u, v, z)$ implying that $\phi_K du = 0$, $\phi_K dv = 0$ and $\phi_K dz = 1$. In this case, we choose z as cyclic variable which gives

$$u = A_0a^{\frac{c_{11}+2c_{12}}{c_{11}}}R, \quad v = A_1b^{\frac{c_{11}+2c_{12}}{c_{12}}}R, \quad z = -\frac{1}{c_{11}+2c_{12}}\ln R,$$

where A_0 and A_1 denote integration constants. The corresponding inverse point transformation yields

$$a = u^{\frac{c_{11}}{c_{11}+2c_{12}}}e^{c_{11}z}, \quad b = v^{\frac{c_{12}}{c_{11}+2c_{12}}}e^{c_{12}z}, \quad R = e^{c_{11}+2c_{12}z}.$$

For these solutions, the Lagrangian (6) takes the form

$$\begin{aligned}
\mathcal{L} = \frac{1}{(c_{11}+2c_{12})^2}\Bigg(&24f_0\dot{z}^2v^{\frac{2c_{12}}{c_{11}+2c_{12}}}c_{11}^3u^{\frac{c_{11}}{c_{11}+2c_{12}}}c_{12} + 60f_0\dot{z}^2v^{\frac{2c_{12}}{c_{11}+2c_{12}}}u^{\frac{c_{11}}{c_{11}+2c_{12}}}\\
&\times c_{11}^2c_{12}^2 + 80f_0\dot{z}^2v^{\frac{2c_{12}}{c_{11}+2c_{12}}}c_{11}c_{12}^3u^{\frac{c_{11}}{c_{11}+2c_{12}}} + 16f_0\dot{v}\dot{z}u^{\frac{c_{11}}{c_{11}+2c_{12}}}c_{12}^3v^{-\frac{c_{11}}{c_{11}+2c_{12}}}\\
&+ 4f_0\dot{u}\dot{z}v^{\frac{2c_{12}}{c_{11}+2c_{12}}}c_{11}^3u^{-\frac{2c_{12}}{c_{11}+2c_{12}}} - 8f_0\dot{u}\dot{v}c_{12}c_{11}v^{-\frac{c_{11}}{c_{11}+2c_{12}}}u^{-\frac{2c_{12}}{c_{11}+2c_{12}}} + 8f_0\dot{u}\dot{z}\\
&\times v^{\frac{2c_{12}}{c_{11}+2c_{12}}}u^{-\frac{2c_{12}}{c_{11}+2c_{12}}}c_{12}c_{11}^2 + 8f_0\dot{v}\dot{z}u^{\frac{c_{11}}{c_{11}+2c_{12}}}v^{-\frac{c_{11}}{c_{11}+2c_{12}}}c_{12}^2c_{11} - \left(u^{\frac{c_{11}}{c_{11}+2c_{12}}}e^{c_{11}z}\right)^{\frac{c_{12}}{c_{11}}}\\
&\times v^{\frac{3c_{12}}{c_{11}+2c_{12}}}e^{3c_{12}z}c_{11}^2 - 4\left(u^{\frac{c_{11}}{c_{11}+2c_{12}}}e^{c_{11}z}\right)^{\frac{c_{12}}{c_{11}}}v^{\frac{3c_{12}}{c_{11}+2c_{12}}}e^{3c_{12}z}c_{12}^2 - 4f_0\dot{v}^2c_{12}^2\\
&\times u^{\frac{c_{11}}{c_{11}+2c_{12}}}v^{-\frac{2(c_{12}+c_{11})}{c_{11}+2c_{12}}} + 48f_0\dot{z}^2u^{\frac{c_{11}}{c_{11}+2c_{12}}}v^{\frac{2c_{12}}{c_{11}+2c_{12}}}c_{12}^4 + 4v^{\frac{2c_{12}}{c_{11}+2c_{12}}}u^{\frac{c_{11}}{c_{11}+2c_{12}}}\\
&\times f_0c_{11}^4\dot{z}^2 - 4\left(u^{\frac{c_{11}}{c_{11}+2c_{12}}}e^{c_{11}z}\right)^{\frac{c_{12}}{c_{11}}}v^{\frac{3c_{12}}{c_{11}+2c_{12}}}e^{3c_{12}z}c_{11}c_{12}\Bigg).
\end{aligned}$$

Here, the Lagrangian again depends on the cyclic variable z. Consequently, this approach does not provide a successive way to evaluate exact solution of the anisotropic universe model in this case.

4 Noether gauge symmetry

In this section, we determine Noether gauge symmetry of homogeneous and isotropic as well as anisotropic universe for $f(R,T) = f_0 R^n + h(T)$ model.

4.1 Flat FRW universe model

We first consider flat FRW metric given by

$$ds^2 = -dt^2 + a^2(t)(dx^2 + dy^2 + dz^2), \tag{37}$$

where the scale factor a describes expansion in $x,\ y$ and z-directions. For isotropic universe, the Lagrangian depends on configuration space $(a,\ R,\ T)$ with tangent space $(a,\ R,\ T,\ \dot{a},\ \dot{R},\ \dot{T})$. The metric variation of action (1) with $\mathcal{L}_m = p(a)$ leads to

$$\begin{aligned}\mathcal{L}(a,R,T,\dot{a},\dot{R},\dot{T}) &= a^3[f(R,T) - Rf_R(R,T) - Tf_T(R,T) + f_T(R,T)\\&\quad\times(3p(a) - \rho(a)) + p(a)] - 6(a\dot{a}^2 f_R(R,T) + a^2\dot{a}\dot{R}f_{RR}(R,T)\\&\quad+ a^2\dot{a}\dot{T}f_{RT}(R,T)).\end{aligned} \tag{38}$$

For Noether gauge symmetry, the vector field K with its first order prolongation is defined as

$$K = \tau(t,a,R,T)\frac{\partial}{\partial t} + \alpha(t,a,R,T)\frac{\partial}{\partial a} + \beta(t,a,R,T)\frac{\partial}{\partial R} + \gamma(t,a,R,T)\frac{\partial}{\partial T},$$
$$K^{[1]} = \tau\frac{\partial}{\partial t} + \alpha\frac{\partial}{\partial a} + \beta\frac{\partial}{\partial R} + \gamma\frac{\partial}{\partial T} + \dot{\alpha}\frac{\partial}{\partial \dot{a}} + \dot{\beta}\frac{\partial}{\partial \dot{R}} + \dot{\gamma}\frac{\partial}{\partial \dot{T}},$$

where $\tau,\ \alpha,\ \beta$ and γ are unknown coefficients of vector field to be determined and the time derivatives of these coefficients are

$$\dot{\alpha} = \frac{\partial\alpha}{\partial t} + \dot{a}\frac{\partial\alpha}{\partial a} + \dot{R}\frac{\partial\alpha}{\partial R} + \dot{T}\frac{\partial\alpha}{\partial T} - \dot{a}\left\{\frac{\partial\tau}{\partial t} + \dot{a}\frac{\partial\tau}{\partial a} + \dot{R}\frac{\partial\tau}{\partial R} + \dot{T}\frac{\partial\tau}{\partial T}\right\},$$
$$\dot{\beta} = \frac{\partial\beta}{\partial t} + \dot{a}\frac{\partial\beta}{\partial a} + \dot{R}\frac{\partial\beta}{\partial R} + \dot{T}\frac{\partial\beta}{\partial T} - \dot{R}\left\{\frac{\partial\tau}{\partial t} + \dot{a}\frac{\partial\tau}{\partial a} + \dot{R}\frac{\partial\tau}{\partial R} + \dot{T}\frac{\partial\tau}{\partial T}\right\},$$
$$\dot{\gamma} = \frac{\partial\gamma}{\partial t} + \dot{a}\frac{\partial\gamma}{\partial a} + \dot{R}\frac{\partial\gamma}{\partial R} + \dot{T}\frac{\partial\gamma}{\partial T} - \dot{T}\left\{\frac{\partial\tau}{\partial t} + \dot{a}\frac{\partial\tau}{\partial a} + \dot{R}\frac{\partial\tau}{\partial R} + \dot{T}\frac{\partial\tau}{\partial T}\right\}.$$

The existence of Noether gauge symmetry demands

$$K^{[1]}\mathcal{L} + (D\tau)\mathcal{L} = DG(t,a,R,T), \tag{39}$$

where G represents gauge function and $D = \partial_t + \dot{a}\partial_a + \dot{R}\partial_R + \dot{T}\partial_T$. Substituting the values of vector field, its first order prolongation and corresponding derivatives of coefficients in Eq. (39), we obtain the following system of equations

$$\tau,_a = 0, \quad \tau,_R = 0, \quad \tau,_T = 0, \quad G,_T = 0, \tag{40}$$

$$n(n-1) f_0 R^{n-2} a^2 \alpha,_R = 0, \tag{41}$$

$$n(n-1) f_0 a^2 R^{n-2} \alpha,_T = 0, \tag{42}$$

$$2a\alpha,_T + (n-1) a R^{-1} \beta,_T = 0, \tag{43}$$

$$6n(n-1) f_0 a^2 R^{n-2} \alpha,_t = -G,_R\,, \tag{44}$$

$$n f_0 R^{n-1} [2a\alpha,_t + (n-1) a^2 R^{-1} \beta,_t] = -G,_a\,, \tag{45}$$

$$\alpha + (n-1) a R^{-1} \beta + 2a\alpha,_a - a\tau,_t + (n-1) a^2 R^{-1} \beta,_a = 0, \tag{46}$$

$$\begin{aligned} &2(n-1) R^{-1} \alpha + (n-1)(n-2) a R^{-2} \beta + (n-1) a R^{-1} \alpha,_a + 2\alpha,_R - (n-1) \\ &\quad \times a R^{-1} \tau,_t + (n-1) a R^{-1} \beta,_R = 0, \end{aligned} \tag{47}$$

$$\begin{aligned} &\alpha[3a^2\{f_0 R^n (1-n) + h(T) - T h(T),_T + h(T),_T (3p - \rho) + p\} + a^3 \{h(T),_T \\ &\quad \times (3p,_a - \rho,_a) + p,_a\}] - n(n-1) f_0 a^3 R^{n-1} \beta + a^3 \gamma h(T),_{TT} (3p - \rho - T) \\ &\quad + a^3 \tau,_t \{f_0 R^n (1-n) + h(T) - T h(T),_T + h(T),_T (3p - \rho) + p\} = G,_t\,. \end{aligned} \tag{48}$$

Solving the above system, it follows that

$$\tau = \frac{\xi_4 t (3\xi_{11}\xi_2 - \xi_3\xi_{10})}{\xi_{11}} + \xi_{13}, \quad \alpha = \xi_4(\xi_2 a + \xi_3 a^{-1}),$$

$$\beta = \frac{\xi_4\xi_3\,(\xi_{10} + \xi_{11} a^{-2}) R}{\xi_{11}(1-n)}, \quad G = \frac{\xi_1 t}{2}, \quad \gamma = 0,$$

where ξ_i are arbitrary constants. For these coefficients, the symmetry generator becomes

$$\begin{aligned} K = &\left(\frac{\xi_4 t (3\xi_{11}\xi_2 - \xi_3\xi_{10})}{\xi_{11}} + \xi_{13}\right)\frac{\partial}{\partial t} + \left(\frac{\xi_4\xi_3(\xi_{10} + \xi_{11} a^{-2}) R}{\xi_{11}(1-n)}\right)\frac{\partial}{\partial R} \\ &+ \xi_4(\xi_2 a + \xi_3 a^{-1})\frac{\partial}{\partial a}. \end{aligned}$$

This generator can be split as

$$\begin{aligned} K_1 = \frac{\partial}{\partial t}, \quad K_2 = &\left(\frac{t(3\xi_{11}\xi_2 - \xi_3\xi_{10})}{\xi_{11}}\right)\frac{\partial}{\partial t} + \left(\frac{\xi_3(\xi_{10} + \xi_{11} a^{-2}) R}{\xi_{11}(1-n)}\right)\frac{\partial}{\partial R} \\ &+ (\xi_2 a + \xi_3 a^{-1})\frac{\partial}{\partial a}, \end{aligned}$$

where the first generator corresponds to energy conservation. The corresponding conserved quantities are

$$\Sigma_1 = -\frac{t(3\xi_{11}\xi_2 - \xi_3\xi_{10})}{\xi_{11}}\Big[a^3\left(f_0 R^n (1-n) + \epsilon_0 - \frac{\rho}{3}\right) - 6(a\dot{a}^2 + (n-1)$$

$$\times\ a^2\dot{a}\dot{R}R^{-1})nf_0R^{n-1}\Big] + 6anf_0R^{n-1}(2\dot{a} - (n-1)aR^{-1}\dot{R})\Big[\Big(\xi_2 a + \xi_3 a^{-1}\Big)$$
$$- \frac{t\dot{a}(3\xi_{11}\xi_2 - \xi_3\xi_{10})}{\xi_{11}}\Big] - 6n(n-1)f_0a^2R^{n-2}\dot{a}\Big[\frac{\xi_3(\xi_{10} + \xi_{11}a^{-2})R}{\xi_{11}(1-n)}$$
$$+ \frac{t\dot{R}(3\xi_{11}\xi_2 - \xi_3\xi_{10})}{\xi_{11}}\Big],$$
$$\Sigma_2 = -a^3\left(f_0R^n(1-n) + \epsilon_0 - \frac{\rho}{3}\right) - 6(a\dot{a}^2 + 2(n-1)a^2\dot{a}\dot{R}R^{-1})nf_0R^{n-1}.$$

4.2 Bianchi I universe model

Here we investigate Noether gauge symmetry for BI universe model. In this case, the vector field and corresponding first order prolongation take the form

$$K = \tau(t, a, b, R, T)\frac{\partial}{\partial t} + \alpha(t, a, b, R, T)\frac{\partial}{\partial a} + \beta(t, a, b, R, T)\frac{\partial}{\partial b}$$
$$+ \gamma(t, a, b, R, T)\frac{\partial}{\partial R} + \delta(t, a, b, R, T)\frac{\partial}{\partial T},$$
$$K^{[1]} = \tau\frac{\partial}{\partial t} + \alpha\frac{\partial}{\partial a} + \beta\frac{\partial}{\partial b} + \gamma\frac{\partial}{\partial R} + \delta\frac{\partial}{\partial T} + \dot{\alpha}\frac{\partial}{\partial \dot{a}} + \dot{\beta}\frac{\partial}{\partial \dot{b}} + \dot{\gamma}\frac{\partial}{\partial \dot{R}} + \dot{\delta}\frac{\partial}{\partial \dot{T}},$$

where

$$\dot{\alpha} = D\alpha - \dot{a}D\tau, \quad \dot{\beta} = D\beta - \dot{b}D\tau, \quad \dot{\gamma} = D\gamma - \dot{R}D\tau, \quad \dot{\delta} = D\delta - \dot{T}D\tau.$$

Using the above vector field, its prolongation and coefficients derivatives in the condition of the existence of Noether gauge symmetry, we formulate the following system of nonlinear partial differential equations as

$$\tau,_a = 0, \quad \tau,_b = 0, \quad \tau,_R = 0, \quad \tau,_T = 0, \quad G,_T = 0, \tag{49}$$
$$b\alpha,_R + 2a\beta,_R = 0, \tag{50}$$
$$b\alpha,_T + 2a\beta,_T = 0, \tag{51}$$
$$2\beta,_a + (n-1)bR^{-1}\gamma,_a = 0, \tag{52}$$
$$2\beta,_T + (n-1)bR^{-1}\gamma,_T = 0, \tag{53}$$
$$b\alpha,_T + a\beta,_T + (n-1)abR^{-1}\gamma,_T = 0, \tag{54}$$
$$n(n-1)f_0R^{n-2}[2b^2\alpha,_t + 4ab\beta,_t] = -G,_R, \tag{55}$$
$$nf_0R^{n-1}[4b\beta,_t + 2(n-1)b^2R^{-1}\gamma,_t] = -G,_a, \tag{56}$$
$$nf_0R^{n-1}[4b\alpha,_t + 4a\beta,_t + 4(n-1)abR^{-1}\gamma,_t] = -G,_b, \tag{57}$$
$$\alpha + (n-1)aR^{-1}\gamma + 2b\alpha,_b + 2a\beta,_b + 2(n-1)abR^{-1}\gamma,_b + a\tau,_t = 0, \tag{58}$$
$$2\beta + 2(n-1)bR^{-1}\gamma + 2b\alpha,_a + 2a\beta,_a + 2b\beta,_b + 2(n-1)abR^{-1}\gamma,_a$$
$$+ (n-1)b^2R^{-1}\gamma,_b - 2b\tau,_t = 0, \tag{59}$$
$$2(n-1)R^{-1}\beta + (n-1)(n-2)bR^{-2}\gamma + (n-1)bR^{-1}\alpha,_a + 2\beta,_R$$

$$+2(n-1)aR^{-1}\beta,_a+(n-1)bR^{-1}\gamma,_R-(n-1)bR^{-1}\tau,_t=0, \tag{60}$$

$$\begin{aligned}&2(n-1)bR^{-1}\alpha+2(n-1)aR^{-1}\beta+2(n-1)(n-2)abR^{-2}\gamma+2b\alpha,_R\\&\quad+(n-1)b^2R^{-1}\alpha,_b+2(n-1)abR^{-1}\beta,_b+2a\beta,_R+2(n-1)abR^{-1}\gamma,_R\\&\quad-2(n-1)abR^{-1}\tau,_t=0,\end{aligned} \tag{61}$$

$$\begin{aligned}&b^2\alpha[f_0R^n(1-n)+h(T)-Th(T),_T+h(T),_T(3p-\rho)+p+a\{h(T),_T\\&\quad\times(3p,_a-\rho,_a)+p,_a\}]+\beta[2ab(f_0R^n(1-n)+h(T)-Th(T),_T+h(T),_T\\&\quad\times(3p-\rho)+p)+ab^2\{h(T),_T(3p,_b-\rho,_b)+p,_b\}]-n(n-1)f_0ab^2R^{n-1}\gamma\\&\quad+ab^2\delta h(T),_{TT}(3p-\rho-T)+ab^2\tau,_t\{f_0R^n(1-n)+h(T)-Th(T),_T\\&\quad+h(T),_T(3p-\rho)+p\}=G,_t.\end{aligned} \tag{62}$$

We solve this system of equations

$$\begin{aligned}&\tau=\eta_1,\quad G=(\eta_2t+\eta_3)\eta_4\eta_5,\quad \alpha=\eta_5\eta_6a,\quad \beta=\eta_5\eta_6b,\\&\gamma=\frac{\eta_5\eta_6R}{2(1-n)},\quad \delta=0,\quad \rho=-\frac{3\eta_2\eta_4(\eta_7+\eta_8\ln a)}{ab^2\eta_6\eta_8},\\&p=-\frac{1}{2nf_0}[f_0R^n+R^{1-n}\eta_9-Rnf_0],\\f(R,T)=\;&f_0R^n-\frac{1}{6nf_0}[f_0R^n+R^{1-n}\eta_9-Rnf_0]-\frac{\eta_2\eta_4(\eta_7+\eta_8\ln a)}{ab^2\eta_6\eta_8},\end{aligned}$$

where the constants η_i are redefined. The solution of these coefficients lead to

$$K=\eta_1\frac{\partial}{\partial t}+\eta_5\eta_6a\frac{\partial}{\partial a}+\eta_5\eta_6b\frac{\partial}{\partial b}+\frac{\eta_5\eta_6R}{2(1-n)}\frac{\partial}{\partial R}.$$

This generator can be split as

$$K_1=\frac{\partial}{\partial t},\quad K_2=a\frac{\partial}{\partial a}+b\frac{\partial}{\partial b}+\frac{R}{2(1-n)}\frac{\partial}{\partial R},$$

where the first generator yields energy conservation whereas the second generator provides scaling symmetry. The corresponding conserved quantities are

$$\begin{aligned}\Sigma_1=&-ab^2\Big[\Big(f_0R^n(1-n)+\epsilon_1-\frac{\rho}{3}\Big)-nf_0R^{n-1}(2a\dot{b}^2+(n-1)R^{-1}(2b^2\dot{a}\dot{R}\\&+4ab\dot{b}\dot{R})+4b\dot{a}\dot{b})\Big],\\\Sigma_2=&\;\eta_2t+\eta_3-4b^2\dot{a}nf_0R^{n-1}.\end{aligned}$$

5 Final remarks

In this paper, we have discussed Noether and Noether gauge symmetries of BI universe model in $f(R,T)$ gravity. We have formulated Noether symmetry generators, corresponding conserved quantities, matter contents $(p,\ \rho)$ as well as explicit forms of generic function $f(R,T)$ for BI model via two theoretical models of $f(R,T)$ gravity, i.e., $R+2\Lambda+h(T)$ and $f_0R^n+h(T)$. We have also evaluated Noether gauge symmetries and conserved quantities of homogeneous isotropic as well as anisotropic universe models for $f_0R^n+h(T)$ model.

For BI universe model, we have found two Noether symmetry generators for the first model in which the first generator gives scaling symmetry. We have solved the system by introducing cyclic variable which lead to exact solution of the scale factors and $f(R,T)$ model. The graphical behavior of scale factors indicate that the universe undergoes an expansion in x, y and z-directions. To evaluate exact solution of the anisotropic universe model for the second symmetry generator, we have constructed Lagrangian in terms of cyclic variable. The Lagrangian violates the mapping $\phi_K dz = 1$ as it is not independent of cyclic variable z. Thus, the symmetry generator with scaling symmetry yields exact solution of the anisotropic universe model. We have investigated graphical behavior of the cosmological parameters, i.e., Hubble and deceleration parameters for this solution. This indicates an accelerated expansion of the universe while EoS parameter corresponds to quintessence phase. The trajectory of r and s parameters indicates that the constructed $f(R,T)$ model corresponds to standard ΛCDM model. For the second model ($f(R,T)=f_1(R)+f_2(T)$) when $f_1(R)=f_0R^n$, the symmetry generator provides scaling symmetry for $n=2$. This implies that the scaling symmetry induces an indirect non-minimal quadratic curvature matter coupling in this gravity.

Finally, we have discussed Noether gauge symmetry and associated conserved quantities of flat FRW and BI universe models. The time coefficient of symmetry generator is found to be t dependent for FRW universe but becomes constant for BI model while gauge function is non-zero in both cases. The symmetry generator provides energy conservation for isotropic universe whereas for anisotropic universe, we have energy conservation along with scaling symmetry. In the previous work [37], we have formulated exact solution through Noether symmetry approach for LRS BI universe using $f(R)$ power-law model. The cosmological parameters correspond to accelerated expanding universe while the EoS parameter describes phantom divide line from quintessence to phantom phase. The Noether symmetry generator provides scaling symmetry whereas Noether gauge symmetry yields energy conservation with constant time coefficient of symmetry generator and gauge term. Here, we have discussed exact solution via Noether symmetry for BI model. The cosmological parameters yield consistent results but EoS parameter corresponds to phantom era. In case of Noether gauge symmetry, we have found time dependent gauge term and time coefficient of symmetry generator for flat FRW model but this time coefficient remains constant for BI model. Thus, the Noether and Noether gauge symmetries yield more symmetries for non-minimal curvature matter coupling in $f(R,T)$ gravity as compared to $f(R)$ gravity.

Acknowledgements This work has been supported by the *Pakistan Academy of Sciences Project.*

References

1. Felice, A.D., Tsujikawa, S.: Living Rev. Rel. **13**, 3 (2010)
2. Nojiri, S., Odintsov, S.D.: Phys. Rep. **505**, 59 (2011)
3. Bamba, K., Capozziello, S., Nojiri, S., Odintsov, S.D.: Astrophys. Space Sci. **342**, 155 (2012)
4. Starobinsky, A.A.: J. Exp. Theor. Phys. Lett. **86**, 157 (2007)
5. Nojiri, S., Odintsov, S.D.: Phys. Lett. B **599**, 137 (2004)
6. Harko, T., Lobo, F.S.N., Nojiri, S., Odintsov, S.D.: Phys. Rev. D **84**, 024020 (2011)
7. Sharif, M., Zubair, M.: J. Cosmol. Astropart. Phys. **03**, 028 (2012)
8. Sharif, M., Zubair, M.: J. Exp. Theor. Phys. **117**, 248 (2013)
9. Sharif, M., Zubair, M.: J. Phys. Soc. Jpn. **82**, 064001 (2013)
10. Sharif, M., Zubair, M.: ibid. **82**(2013)014002
11. Sharif, M., Zubair, M.: Astrophys. Space Sci. **349**, 52 (2014)
12. Sharif, M., Zubair, M.: Gen. Rel. Grav. **46**, 1723 (2014)
13. Ellis, G.F.R., Maartens, R., MacCallum, M.A.H.: Relativistic Cosmology. Cambridge University Press, Cambridge (2012)
14. Barrow, J.D., Turner, M.S.: Nature **292**, 35 (1982)
15. Demianski, M.: Nature **307**, 140 (1984)
16. Akarsu, Ö., Kilinc, C.B.: Astrophys. Space Sci. **326**, 315 (2010)
17. Sharif, M., Zubair, M.: Astrophys. Space Sci. **349**, 457 (2014)
18. Shamir, M.F.: Eur. Phys. J. C **75**, 8 (2015)
19. Kanakavalli, T., Ananda, R.G.: Astrophys. Space Sci. **361**, 206 (2016)
20. Sharif, M., Waheed, S.: Can. J. Phys. **88**, 833 (2010)
21. Sharif, M., Waheed, S.: Phys. Scr. **83**, 015014 (2011)
22. Sharif, M., Waheed, S.: J. Cosmol. Astropart. Phys. **02**, 043 (2013)
23. Kucukakca, Y., Camci, U., Semiz, İ.: Gen. Rel. Grav. **44**, 1893 (2012)
24. Jamil, M., Momeni, D., Myrzakulov, R.: Eur. Phys. J. C **72**, 2137 (2012)
25. Kucukakca, Y.: Eur. Phys. J. C **73**, 2327 (2013)
26. Sharif, M., Shafique, I.: Phys. Rev. D **90**, 084033 (2014)
27. Sharif, M., Fatima, I.: J. Exp. Theor. Phys. **122**, 104 (2016)
28. Capozziello, S., Stabile, A., Troisi, A.: Class. Quantum Grav. **24**, 2153 (2007)
29. Vakili, B.: Phys. Lett. B **16**, 664 (2008)
30. Jamil, M., Mahomed, F.M., Momeni, D.: Phys. Lett. B **702**, 315 (2011)
31. Hussain, I., Jamil, M., Mahomed, F.M.: Astrophys. Space Sci. **337**, 373 (2012)
32. Shamir, M.F., Jhangeer, A., Bhatti, A.A.: Chin. Phys. Lett. A **29**, 080402 (2012)
33. Kucukakca, Y., Camci, U.: Astrophys. Space Sci. **338**, 211 (2012)
34. Momeni, D., Myrzakulov, R., Gdekli, E.: Int. J. Geom. Methods Mod. Phys. **12**, 1550101 (2015)
35. Haghani, Z., Harko, T., Lobo, F.S.N., Sepangi, H.R., Shahidi, S.: Phys. Rev. D **88**, 044023 (2013)
36. Odintsov, S.D., Saez-Gomez, D.: Phys. Lett. B **725**, 437 (2013)
37. Sharif, M., Nawazish, I.: J. Exp. Theor. Phys. **120**, 49 (2014)

Eur. Phys. J. C (2017) 77:198
DOI 10.1140/epjc/s10052-017-4773-1

THE EUROPEAN PHYSICAL JOURNAL C

Regular Article - Theoretical Physics

Cosmological analysis of scalar field models in $f(R, T)$ gravity

M. Sharif[a], **Iqra Nawazish**[b]

Department of Mathematics, University of the Punjab, Quaid-e-Azam Campus, Lahore 54590, Pakistan

Received: 1 February 2017 / Accepted: 15 March 2017 / Published online: 28 March 2017

Abstract This paper determines the existence of Noether symmetry in non-minimally coupled $f(R, T)$ gravity admitting minimal coupling with scalar field models. We consider a generalized spacetime which corresponds to different anisotropic and homogeneous universe models. We formulate symmetry generators along with conserved quantities through Noether symmetry technique for direct and indirect curvature–matter coupling. For dust and perfect fluids, we evaluate exact solutions and construct their cosmological analysis through some cosmological parameters. We conclude that decelerated expansion is obtained for the quintessence model with a dust distribution, while a perfect fluid with dominating potential energy over kinetic energy leads to the current cosmic expansion for both phantom as well as quintessence models.

1 Introduction

The generic function in $f(R)$ gravity is a coupling-free function which helps to resolve many cosmological issues. Nojiri and Odintsov [1] proposed the concept of a non-minimal curvature–matter coupling, which led to fresh insight among researchers. This coupling successfully incorporates clusters of galaxies or dark matter in galaxies, yielding natural preheating conditions corresponding to inflationary models and thus one introduced the idea of traversable wormholes in the absence of any exotic matter [2–5]. Harko et al. [6] proposed a new version of modified theory whose generic function incorporates curvature as well as matter, known as $f(R, T)$ gravity (T is the trace of the energy-momentum tensor). This function induces strong interactions of gravity and matter, which play a dynamical role in analyzing the current cosmic expansion [7]. Sharif and Zubair [8–13] investigated some cosmic issues like energy conditions, thermodynamics, anisotropic exact solutions, reconstruction of some dark energy models, and also they studied the stability issue in this theory of gravity.

The interest in exact solutions of higher order non-linear differential equations keeps researchers motivated as these are extensively used to investigate different cosmic aspects. Harko and Lake [14] discussed exact solutions of the cylindrical spacetime in the presence of non-minimal coupling between R and matter Lagrangian density ($\mathcal{L}_m$). The higher order non-linear differential equations of $f(R, T)$ gravity attract many researchers as they perform cosmological analysis via exact solutions of the field equations. Sharif and Zubair [15] considered exponential and power-law expansions to evaluate some exact solutions and kinematical quantities of the Bianchi type I (BI) model in this gravity. Shamir and Raza [16] formulated exact solutions corresponding to cosmic strings as well as a non-null electromagnetic field. Shamir [17] found exact solutions of a locally rotationally symmetric BI model and studied the physical behavior through cosmological parameters.

In mathematical physics and theoretical cosmology, continuous symmetry reduces the complexity of non-linear systems, which successfully yields exact solutions. In a dynamical system, Noether symmetry points to a correspondence between infinitesimal symmetry generator and conserved quantity. Capozziello et al. [18] used this approach to find exact solutions of spherically symmetric spacetime in $f(R)$ gravity. Hussain et al. [19] investigated the existence of Noether symmetry of a power-law $f(R)$ model and found the boundary term to vanish for the flat FRW universe model but Shamir et al. [20] obtained a non-zero boundary term of the same model. Momeni et al. [21] explored a Noether point symmetry of the isotropic universe in mimetic $f(R)$ and $f(R, T)$ gravity theories. Shamir and Ahmad [22] constructed exact solutions in $f(\mathcal{G}, T)$ gravity ($\mathcal{G}$ denotes the Gauss–Bonnet term).

Sanyal [23] determined exact solutions of the Kantowski–Sachs (KS) universe model through the Noether symmetry

[a] e-mail: msharif.math@pu.edu.pk
[b] e-mail: iqranawazish07@gmail.com

technique in non-minimally coupled gravity with a scalar field. Camci and Kucukakca [24] extended this work by adding BI as well as BIII universe models and formulated explicit forms of the scalar field. Kucukakca et al. [25] discussed the presence of Noether symmetry to formulate exact solutions of a locally rotationally symmetric BI universe. Camci et al. [26] generalized this work for anisotropic universe models such as BI, BIII and KS. We have obtained exact solutions of a $f(R)$ power-law model [27] as well as of a $f(R,T)$ model admitting indirect non-minimal curvature–matter coupling [28].

In non-minimally coupled gravitational theory, the Noether symmetry approach is extensively used to study different cosmological models and the dynamical role of various scalar field models [29]. Vakili [30] identified the existence of Noether point symmetry along with a conserved quantity for the flat FRW universe and studied the behavior of effective equation of state (EoS) parameter for the quintessence model in $f(R)$ gravity. Zhang et al. [31] explored a multiple scalar field scenario and formulated a relationship of the potential function with quintessence and phantom models. Jamil et al. [32] ensured the presence of Noether symmetry with conservation law for the $f(R)$ tachyon model. Sharif and Shafique [33] obtained exact solutions of isotropic and anisotropic universe models in scalar–tensor theory non-minimally coupled with the torsion scalar.

In this paper, we discuss the existence of Noether symmetries of non-minimally coupled $f(R,T)$ gravity interacting with generalized scalar field model. The format of the paper is as follows. Section 2 introduces some basic aspects of this gravity. In Sect. 3, we discuss all possible Noether symmetries with associated conserved quantities for two particular models of this theory. We also formulate exact solutions for dust as well as perfect fluid distribution and study their physical behavior through some cosmological parameters. In the last section, we present final remarks.

2 Some basics of $f(R,T)$ gravity

We consider the action incorporating gravity, matter and scalar field:

$$\mathcal{I}=\int d^4x\sqrt{-g}[\mathcal{L}_g+\mathcal{L}_{\rm m}+\mathcal{L}_\phi], \tag{1}$$

where g denotes the determinant of the metric tensor, $\mathcal{L}_g$ and $\mathcal{L}_\phi$ represent gravity and scalar field Lagrangian densities. For non-minimal coupling, the gravitational Lagrangian is considered to be a generic function $f(R,T)$ admitting minimal coupling only with $\mathcal{L}_{\rm m}$ and $\mathcal{L}_\phi$ [6]. In this case, the metric variation of $\mathcal{L}_g$ and $\mathcal{L}_{\rm m}$ yields

$$\begin{aligned}&f_R(R,T)R_{\mu\nu}-\frac{1}{2}f(R,T)g_{\mu\nu}\\&+(g_{\mu\nu}\nabla_\mu\nabla^\mu-\nabla_\mu\nabla_\nu)f_R(R,T)+f_T(R,T)T_{\mu\nu}\\&+f_T(R,T)\left(g_{\mu\nu}\mathcal{L}_{\rm m}-2T_{\mu\nu}-2g^{\alpha\beta}\frac{\partial^2\mathcal{L}_{\rm m}}{\partial g^{\alpha\beta}\partial g^{\mu\nu}}\right)=\kappa^2T_{\mu\nu},\end{aligned}$$

where the subscripts R and T describe corresponding partial derivatives of f, ∇_μ indicates the covariant derivative and $T_{\mu\nu}$ represents the energy-momentum tensor. The divergence of the energy-momentum tensor leads to

$$\nabla^\mu T_{\mu\nu}=\frac{f_T}{\kappa^2-f_T}\Big[(T_{\mu\nu}+\Theta_{\mu\nu})\nabla^\mu\ln f_T+\nabla^\mu\Theta_{\mu\nu}-\frac{g_{\mu\nu}\nabla^\mu T}{2}\Big].$$

In non-minimally coupled modified gravity, the energy-momentum tensor no more remains conserved. This non-zero divergence introduces an extra force in the equation of motion which is responsible for a deviation of massive test particles from the geodesic trajectories.

A generalization of some anisotropic and homogeneous universe models is given as [34]

$$ds^2=-dt^2+a^2(t)dr^2+b^2(t)(d\theta^2+\zeta(\theta)d\phi^2), \tag{2}$$

where a and b are scale factors and $\zeta(\theta)=\theta,\ \sin h\theta,\ \sin\theta$ identify BI, BIII and KS models with the following relationship:

$$\frac{1}{\zeta}\frac{d^2\zeta}{d\theta^2}=-\xi.$$

For $\xi=0,-1,1$, the spacetime (2) corresponds to the BI, BIII and KS universe models, respectively. For a perfect fluid, the energy-momentum tensor is

$$T_{\mu\nu}=(\rho_{\rm m}+p_{\rm m})u_\mu u_\nu+p_m g_{\mu\nu},$$

where $p_{\rm m}$ and $\rho_{\rm m}$ define pressure and energy density, respectively whereas u represents the four-velocity of the fluid. For the action (1), the Lagrangian density of matter and scalar fields are defined as [35,36]

$$\mathcal{L}_{\rm m}=p_{\rm m}(a,b),\quad \mathcal{L}_\phi=\frac{\epsilon}{2}g^{\mu\nu}\partial_\mu\phi\partial_\nu\phi-V(\phi), \tag{3}$$

where $V(\phi)$ denotes the potential energy of the scalar field and $\epsilon=1,-1$ indicate scalar field models, i.e., quintessence and phantom models.

Phantom model suffers with number of troubles like violation of dominant energy condition, the entropy of phantom-dominated universe is negative and consequently, black holes disappear. Such a universe ends up with a finite time future singularity dubbed a big-rip singularity [37]. Different ideas are proposed to cure the troubles of this singularity such as considering phantom acceleration as transient phenomenon with different scalar potentials or to modify the gravity, couple dark energy with dark matter or to use particular forms of EoS for dark energy taking into account some quantum effects (giving rise to the second quantum gravity era) which may delay/stop the singularity occurrence [38–42]. Inserting Eq. (3) into (1), we obtain

$$\mathcal{I} = \int \mathrm{d}^4x\sqrt{-g}\Big[\frac{f(R,T)}{2\kappa^2} + p_{\mathrm{m}}(a,b) + \frac{\epsilon}{2}g^{\mu\nu}\partial_\mu\phi\partial_\nu\phi - V(\phi)\Big], \quad (4)$$

where

$$R = \frac{2}{ab^2}(\ddot{a}b^2 + 2ab\ddot{b} + 2b\dot{a}\dot{b} + a\dot{b}^2 + a\xi),$$
$$T = 3p_{\mathrm{m}}(a,b) - \rho_{\mathrm{m}}(a,b).$$

To evaluate Lagrangian corresponding to the action (4) for configuration space $\mathcal{Q} = \{a, b, R, T, \phi\}$, we use the Lagrange multiplier approach which yields

$$\begin{aligned}\mathcal{L} = ab^2\Big[&f(R,T) - Rf_R(R,T) + f_T(R,T)(3p_{\mathrm{m}}(a,b) \\ &-\rho_{\mathrm{m}}(a,b) - T) - \frac{\epsilon\dot{\phi}^2}{2} + p_{\mathrm{m}}(a,b) - V(\phi)\Big] \\ &-(4b\dot{a}\dot{b} + 2a\dot{b}^2 - 2a\xi)f_R(R,T) \\ &-(2b^2\dot{a}\dot{R} + 4ab\dot{b}\dot{R}) \\ &\times f_{RR}(R,T) - (2b^2\dot{a}\dot{T} + 4ab\dot{b}\dot{T})f_{RT}(R,T).\end{aligned} \quad (5)$$

In a dynamical system, the Euler–Lagrange equation, the Hamiltonian ($\mathcal{H}$) and conjugate momenta (p_i) play a significant role to determine basic features of the system, defined as

$$\frac{\partial\mathcal{L}}{\partial q^i} - \frac{\mathrm{d}p_i}{\mathrm{d}t} = 0, \quad \mathcal{H} = \sum_i \dot{q}^i p_i - \mathcal{L}, \quad p_i = \frac{\partial\mathcal{L}}{\partial\dot{q}^i},$$

where q^i refers to n coordinates of the system. For the Lagrangian (5), the conjugate momenta take the following form:

$$p_a = -4b\dot{b}f_R - 2b^2(\dot{R}f_{RR} + \dot{T}f_{RT}), \quad p_\phi = -ab^2\epsilon\dot{\phi},$$
$$p_b = -4f_R(a\dot{b} + b\dot{a}) - 4ab(\dot{R}f_{RR} + \dot{T}f_{RT}),$$
$$p_R = -(4ab\dot{b} + 2b^2\dot{a})f_{RR}, \quad p_T = -(4ab\dot{b} + 2b^2\dot{a})f_{RT}.$$

The dynamical equations of the system are

$$\begin{aligned}&2f_R(R,T)\left(\frac{\dot{b}^2}{b^2} + \frac{2\ddot{b}}{b} + \frac{2\xi}{b^2}\right) + f - Rf_R \\ &+f_T(3p_{\mathrm{m}}(a,b) - \rho_{\mathrm{m}}(a,b) - T) \\ &+p_{\mathrm{m}}(a,b) - \frac{\epsilon\dot{\phi}^2}{2} - V(\phi) \\ &+a\{f_T(3p_{\mathrm{m}},_a - \rho_{\mathrm{m}},_a) + p_{\mathrm{m}},_a\} + 4b^{-1}\dot{b}\dot{R}f_{RR} \\ &+4b^{-1}\dot{b}\dot{T}f_{RT} + 2\ddot{R}f_{RR} + 2\dot{R}^2f_{RRR} + 4\dot{R}\dot{T}f_{RRT} \\ &+2\ddot{T}f_{RT} + 2\dot{T}^2f_{RTT} = 0,\end{aligned} \quad (6)$$

$$\begin{aligned}&2f_R\left(\frac{\ddot{a}}{a} + \frac{\dot{a}\dot{b}}{ab} + \frac{\ddot{b}}{b}\right) \\ &+f - Rf_R + f_T(3p_{\mathrm{m}}(a,b) - \rho_{\mathrm{m}}(a,b) - T) \\ &+p_{\mathrm{m}}(a,b) - \frac{\epsilon\dot{\phi}^2}{2} - V(\phi) + \frac{b}{2}\{f_T(3p_{\mathrm{m}},_b - \rho_{\mathrm{m}},_b)) \\ &+p_{\mathrm{m}},_b\} + 2(a^{-1}\dot{a}\dot{R} + \ddot{R})f_{RR} + 2\dot{R}^2 \\ &\times f_{RRR} + 2(a^{-1}\dot{a}\dot{T} + \ddot{T})f_{RT} + 2(b^{-1}\dot{b}\dot{R} \\ &+2\dot{R}\dot{T} + \dot{T}^2)f_{RRT} + 2b^{-1}\dot{b}\dot{T}f_{RTT} = 0,\end{aligned} \quad (7)$$

$$f_{RT}(3p_{\mathrm{m}}(a,b) - \rho_{\mathrm{m}}(a,b) - T) = 0,$$
$$f_{TT}(3p_{\mathrm{m}}(a,b) - \rho_{\mathrm{m}}(a,b) - T) = 0,$$
$$\epsilon\ddot{\phi} + 2\epsilon b^{-1}\dot{b}\dot{\phi} + \epsilon a^{-1}\dot{a}\dot{\phi} - V'(\phi) = 0. \quad (8)$$

In order to evaluate the total energy of the dynamical system, we formulate the Hamiltonian as

$$\begin{aligned}\mathcal{H} = &2f_R\left(\frac{\dot{b}^2}{b^2} + \frac{2\dot{a}\dot{b}}{ab}\right) + 2\left(\frac{2\dot{b}}{b} + \frac{\dot{a}}{a}\right)\dot{R}f_{RR} \\ &+2\left(\frac{2\dot{b}}{b} + \frac{\dot{a}}{a}\right)\dot{T}f_{RT} + f - Rf_R \\ &+f_T(3p_{\mathrm{m}}(a,b) - \rho_{\mathrm{m}}(a,b) - T) + p_{\mathrm{m}}(a,b) \\ &+\frac{\epsilon\dot{\phi}^2}{2} - V(\phi) + \frac{2\xi f_R}{b^2}.\end{aligned} \quad (9)$$

The Hamiltonian constraint $\mathcal{H} = 0$ yields the total pressure of the dynamical system.

3 Noether symmetry and conserved quantities

The Noether symmetry approach helps to solve complicated non-linear system of partial differential equations yielding exact solutions at theoretical grounds of physics and cosmology. Noether theorem states that if Lagrangian of a dynamical system remains invariant under a continuous group then group generator leads to the associated conserved quantity. The conservation of energy and linear momentum appears for translational invariant Lagrangian in time and position, respectively whereas the angular momentum is conserved for rotationally symmetric Lagrangian [43]. In gravitational theories, the presence of conserved quantities also enhances physical interpretation of theory but if it does not appreciate the existence of any conserved quantity, then the theory will be abandoned due to its non-physical features.

To investigate the existence of Noether symmetry and associated conserved quantity in non-minimally coupled gravitational theory, we consider the first order prolongation $K^{[1]}$ of continuous group defined as

$$K^{[1]} = K + (\varphi^j,_t + \varphi^j,_i\dot{q}^i - \vartheta,_t\dot{q}^j - \vartheta,_i\dot{q}^i\dot{q}^j)\frac{\partial}{\partial\dot{q}^j}, \quad (10)$$

where the cosmic time t is considered to be an affine parameter and K represents the symmetry generator given by

$$K = \vartheta(t, q^i)\frac{\partial}{\partial t} + \varphi^j(t, q^i)\frac{\partial}{\partial q^j}. \quad (11)$$

Here ϑ and φ^j are unknown coefficients of the generator. The existence of Noether symmetry is ensured when K follows the invariance condition,

$$K^{[1]}\mathcal{L} + (D\vartheta)\mathcal{L} = DB(t, q^i), \quad D = \frac{\partial}{\partial t} + \dot{q}^i\frac{\partial}{\partial q^i}, \quad (12)$$

where D is the total derivative, while B represents a boundary term of K. When the symmetry generator becomes independent of the affine parameter then boundary term along with first order prolongation vanishes yielding

$$K = \varrho^i(q^i)\frac{\partial}{\partial q^i} + \left[\frac{\mathrm{d}}{\mathrm{d}t}(\varrho^i(q^i))\right]\frac{\partial}{\partial \dot{q}^i}, \quad L_K\mathcal{L} = 0, \quad (13)$$

where L identifies Lie derivative. The symmetries coming from symmetry generators (11) and (13) lead to corresponding conservation law through the first integral defined as

$$\Sigma = B - \vartheta\mathcal{L} - (\varphi^j - \dot{q}^j\vartheta)\frac{\partial\mathcal{L}}{\partial\dot{q}^j}, \quad \Sigma = -\eta^j\frac{\partial\mathcal{L}}{\partial\dot{q}^j}. \quad (14)$$

For $Q = \{t, a, b, R, T, \phi\}$, the infinitesimal symmetry generator and corresponding first order prolongation take the form

$$K = \tau\frac{\partial}{\partial t} + \alpha\frac{\partial}{\partial a} + \beta\frac{\partial}{\partial b} + \gamma\frac{\partial}{\partial R} + \delta\frac{\partial}{\partial T} + \eta\frac{\partial}{\partial \phi},$$
$$K^{[1]} = \tau\frac{\partial}{\partial t} + \alpha\frac{\partial}{\partial a} + \beta\frac{\partial}{\partial b} + \gamma\frac{\partial}{\partial R} + \delta\frac{\partial}{\partial T} + \dot{\alpha}\frac{\partial}{\partial \dot{a}} + \dot{\beta}\frac{\partial}{\partial \dot{b}} + \dot{\gamma}\frac{\partial}{\partial \dot{R}} + \dot{\delta}\frac{\partial}{\partial \dot{T}} + \dot{\eta}\frac{\partial}{\partial \dot{\phi}}, \quad (15)$$

where the time derivative of the unknown coefficients $\tau,\ \alpha,\ \beta,\ \gamma,\ \delta$ and η are

$$\dot{\sigma}_l = D\sigma_l - \dot{q}^i D\tau, \quad l = 1, \ldots, 5, \quad (16)$$

Here $\sigma_1,\ \sigma_2,\ \sigma_3,\ \sigma_4$ and σ_5 correspond to $\alpha,\ \beta,\ \gamma,\ \delta$ and η, respectively.

In order to discuss the presence of Noether symmetry generator and relative conserved quantity of the model (2), we insert the first order prolongation (10) along with (11) in (12), it obeys a system of equations given in Appendix **A**. From Eq. (A7), we have either $f_R,\ f_{RR},\ f_{RT} = 0$ with $\tau,_a,\ \tau,_b,\ \tau,_R,\ \tau,_T \neq 0$ or vice versa. For non-trivial solution, we consider second possibility ($\tau,_a,\ \tau,_b,\ \tau,_R,\ \tau,_T = 0$) as the first choice yields trivial solution. We investigate the existence of symmetry generators, relative conserved quantities for the following two models [6]:

- $f(R, T) = R + 2g(T)$,
- $f(R, T) = F(R) + h(R)g(T)$.

We also formulate corresponding exact solutions to analyze cosmological picture of these two models.

3.1 $f(R, T) = R + 2g(T)$

This model incorporates an indirect non-minimal curvature–matter coupling and also admits a correspondence with standard cosmological constant cold dark matter (ΛCDM) model if it comprises a trace dependent cosmological constant defined as

$$f(R, T) = R + 2\Lambda(T) + g(T). \quad (17)$$

To evaluate the coefficients of symmetry generator (11), we solve the system (A1)–(A22) via separation of variables method which gives

$$\begin{aligned}
\alpha &= \alpha_1(t)\alpha_2(a)\alpha_3(b)\alpha_4(R)\alpha_5(T)\alpha_6(\phi),\\
\delta &= \delta_1(t)\delta_2(a)\delta_3(b)\delta_4(R)\delta_5(T)\delta_6(\phi),\\
\gamma &= \gamma_1(t)\gamma_2(a)\gamma_3(b)\gamma_4(R)\gamma_5(T)\gamma_6(\phi),\\
\eta &= \eta_1(t)\eta_2(a)\eta_3(b)\eta_4(R)\eta_5(T)\eta_6(\phi),\\
\beta &= \beta_1(t)\beta_2(a)\beta_3(b)\beta_4(R)\beta_5(T)\beta_6(\phi),\\
\tau &= \tau_1(t),\\
B &= B_1(t)B_2(a)B_3(b)B_4(R)B_5(T)B_6(\phi).
\end{aligned} \quad (18)$$

For these coefficients, the system (A1)–(A22) yields

$$\alpha = -2ac_1, \quad \beta = c_1 b, \quad \gamma = 0, \quad \delta = 0, \quad \eta = c_4,$$
$$B = c_2 t + c_3, \quad \tau = c_5, \quad V(\phi) = c_6\phi + c_7,$$

$$p_{\mathrm{m}}(a, b) = -\frac{c_4 c_6 \ln a + 2c_1 a^{\frac{1}{2}} b}{2c_1} - \frac{2\xi}{b^2} - \frac{c_2 \ln a}{2c_1 ab^2}, \quad (19)$$

$$\rho_{\mathrm{m}}(a, b) = -\frac{3c_4 c_6 \ln a + 2c_1 a^{\frac{1}{2}} b}{2c_1} - \frac{6\xi}{b^2} - \frac{3c_2 \ln a}{2c_1 ab^2}, \quad (20)$$

where the c_i $(i = 1, \ldots, 7)$ denotes arbitrary constants. For these coefficients, we split the symmetry generator and corresponding first integral into the following form:

$$K_1 = \frac{\partial}{\partial t}, \quad \Sigma_1 = -ab^2\{f - Rf_R + f_T(3p_{\mathrm{m}} - \rho_{\mathrm{m}} - T) + p_{\mathrm{m}} - c_6\phi - c_7\} + 2a\xi f_R - 4b\dot{a}\dot{b}f_R - 2a\dot{b}^2 f_R - \frac{\epsilon\dot{\phi}^2 ab^2}{2},$$

$$K_2 = -2a\frac{\partial}{\partial a} + b\frac{\partial}{\partial b}, \quad \Sigma_2 = -4ab\dot{b}f_R + 4b^2\dot{a}f_R,$$

$$K_3 = \frac{\partial}{\partial \phi}, \quad \Sigma_3 = \epsilon ab^2\dot{\phi}.$$

For the model (17), the system (A1)–(A22) yields three symmetry generators and associated conserved quantities. In this case, the symmetry generator K_1 leads to energy conservation while K_2 represents the scaling symmetry corresponding to conservation of linear momentum.

Next, we explore the presence of Noether symmetry in the absence of affine parameter and boundary term of extended symmetry which leads to establish corresponding conservation law. In this case, the infinitesimal generator of continuous group for $\mathcal{Q} = \{a, b, R, T, \phi\}$ turns out to be

$$K = \alpha\frac{\partial}{\partial a} + \beta\frac{\partial}{\partial b} + \gamma\frac{\partial}{\partial R} + \delta\frac{\partial}{\partial T} + \eta\frac{\partial}{\partial \phi} + \dot{\alpha}\frac{\partial}{\partial \dot{a}} + \dot{\beta}\frac{\partial}{\partial \dot{b}} + \dot{\gamma}\frac{\partial}{\partial \dot{R}} + \dot{\delta}\frac{\partial}{\partial \dot{T}} + \dot{\eta}\frac{\partial}{\partial \dot{\phi}}, \tag{21}$$

where $\dot{\alpha} = \dot{q^i}\frac{\partial\alpha}{\partial q^i}$, $\dot{\beta} = \dot{q^i}\frac{\partial\beta}{\partial q^i}$, $\dot{\gamma} = \dot{q^i}\frac{\partial\gamma}{\partial q^i}$, $\dot{\delta} = \dot{q^i}\frac{\partial\delta}{\partial q^i}$ and $\dot{\eta} = \dot{q^i}\frac{\partial\eta}{\partial q^i}$. Due to the absence of affine parameter, the separation of variables method yields

$$\alpha = \alpha_1(a)\alpha_2(b)\alpha_3(R)\alpha_4(T)\alpha_5(\phi),$$
$$\beta = \beta_1(a)\beta_2(b)\beta_3(R)\beta_4(T)\beta_5(\phi),$$
$$\gamma = \gamma_1(a)\gamma_2(b)\gamma_3(R)\gamma_5(\phi),$$
$$\delta = \delta_1(a)\delta_2(b)\delta_3(R)\delta_4(T)\delta_5(\phi),$$
$$\eta = \eta_1(a)\eta_2(b)\eta_3(R)\eta_4(T)\eta_5(\phi).$$

In order to explore the consequences of indirect non-minimal curvature–matter coupling, we evaluate symmetry generators with corresponding conservation laws for non-existing boundary term. We also establish cosmological analysis through exact solutions for both dust and perfect fluid distributions.

3.1.1 Dust case

Dust fluid investigates matter contents of the universe when the existence of radiations is not so worthy and the formation of massive stars is possible only if dust particles interact with radiations. Here we consider $T_{\mu\nu} = \rho_{\mathrm{m}} u_\mu u_\nu$ and solve the system for (21) via separation of variables which yields

$$\alpha = -2ac_1', \quad \beta = c_1' b, \quad \gamma = 0, \quad \delta = 0, \quad \eta = 0,$$
$$\rho_{\mathrm{m}}(a, b) = \frac{\xi}{b^2 c_2'} + a^{\frac{1}{2}} b, \quad \Lambda(T) = -\frac{g(T)}{2} + c_2' T + c_3',$$

where the c_j' $(j = 1, \ldots, 3)$ represent arbitrary constants. The corresponding symmetry generator and associated conserved quantity are

$$K = -2ac_1'\frac{\partial}{\partial a} + c_1' b\frac{\partial}{\partial b}, \quad \Sigma = 4c_1' ab\dot{b} f_R - 4c_1' b^2 \dot{a} f_R.$$

For dust fluid, there exists only scaling symmetry in the absence of affine parameter as well as boundary term of extended symmetry and the model (17) reduces to

$$f(R, T) = R + 2c_2' T + 2c_3'. \tag{22}$$

For exact solution of equations of motion, we insert density of dust fluid and model (22) in Eqs. (6) and (7) yielding

$$a(t) = \frac{(40c_2' t + 40c_3')^{\frac{4}{5}}}{16}, \quad b(t) = \frac{c_1'(40c_2' t + 40c_3')^{\frac{2}{5}}}{4}.$$

This leads to expansion of the universe whether it is accelerated or decelerated. The power-law scale factor $(a(t) = t^\lambda)$ identifies both expansions as for $\lambda > 1$, it measures accelerated expansion while it corresponds to decelerated expansion for $\lambda < 1$. When $\lambda = \frac{1}{2}$ and $\lambda = \frac{2}{3}$, we have radiation and matter dominated eras of the universe.

To analyze the behavior of power-law type exact solution, we construct cosmological analysis through some cosmological parameters such as Hubble, deceleration, r–s and EoS. These parameters are useful to study current expansion as well as different eras of the universe. The Hubble parameter (H) determines the rate of expansion, while the deceleration parameter (q) evaluates the nature of cosmic expansion, telling whether we have the decelerated $(q > 0)$, accelerated $(q < 0)$ or constant $(q = 0)$ case, respectively. In the case of anisotropic universe models, these parameters turn out to be

$$H = \frac{64c_2'(40c_2' t + 40c_3')^{-1}}{3}, \quad q = \frac{7}{8}.$$

The relevant pair of r–s parameters explores the characteristics of dark energy candidates by establishing a correspondence between constructed and standard cosmic models. When the pair lies in the $(r, s) = (1, 0)$ region, this corresponds to standard ΛCDM model while the trajectories with $s > 0$ and $r < 1$ correspond to quintessence and phantom phases of dark energy. In the present case, we obtain $r = 0$ with $s = -\frac{8}{9}$ indicating that the constructed model does not correspond to any standard dark energy universe model. The EoS parameter (ω) investigates different cosmic eras such as it identifies radiation and matter dominated eras for $\omega = \frac{1}{3}$ and $\omega = 0$, respectively. This parameter specifies dark energy era $(\omega = -1)$ into quintessence and phantom phases when $-1 < \omega \leq -1/3$ and $\omega < -1$, respectively. The corresponding effective EoS parameter is

$$\omega_{\mathrm{eff}} = \frac{128c_2' + (40c_2' t + 40c_3')^{\frac{4}{5}}(5c_2'^2 c_1' t^2 + 10c_1' c_2' c_3' t + 5c_1' c_3'^2)}{128c_2'}$$

The potential and kinetic energies of the scalar field play a dynamical role to study cosmic expansion. For accelerated expansion, the field ϕ evolves negatively and potential dominates over the kinetic energy $(\frac{\dot{\phi}^2}{2} < V(\phi))$ whereas negative potential follows the kinetic energy for decelerated expansion of the universe $(\frac{\dot{\phi}^2}{2} > -V(\phi))$. Using Eq. (8), we obtain

$$\phi = \int \frac{1}{20\epsilon(c_2' t + c_3')}((-\epsilon c_2'(25c_2'^2(40c_2' t + 40c_3')^{\frac{4}{5}} c_1' t^2 + 50(40c_2' t + 40c_3')^{\frac{4}{5}} \times c_2' c_1' c_3' t + 25(40c_2' t + 40c_3')^{\frac{4}{5}} c_1' c_3'^2 + 896c_2'))^{\frac{1}{2}}),$$

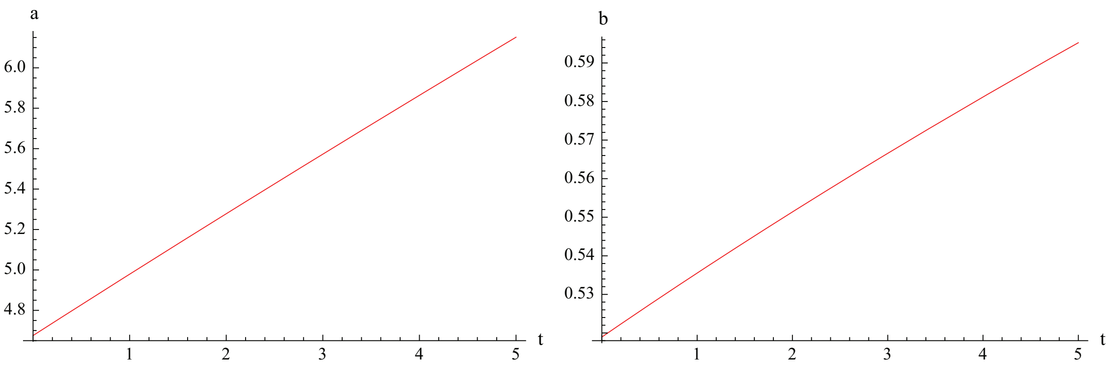

Fig. 1 Plots of scale factors $a(t)$ (*left*) and $b(t)$ (*right*) versus cosmic time t for $c_1' = 0.24$, $c_2' = 0.45$ and $c_3' = 5.5$

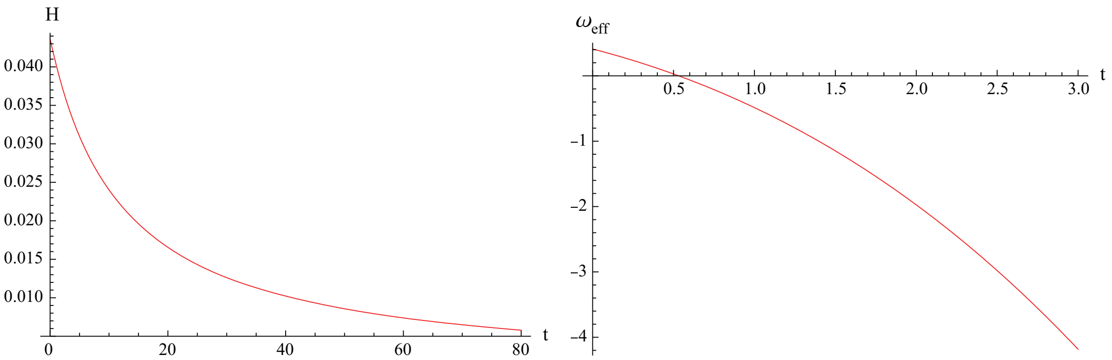

Fig. 2 Plots of Hubble $H(t)$ (*left*) and EoS parameters ω_{eff} (*right*) versus cosmic time t

$$\begin{aligned} V(\phi) = & \frac{1}{800(c_2'^2 t^2 + 2c_2'c_3't + c_3'^2)}[25c_1'(5c_2'^3 t^2 \\ & +5c_2'c_3'^2 + 10c_2'^2 c_3' t)(40c_2' t \\ & +40c_3')^{\frac{4}{5}} + 8c_2'c_3'(-200c_2't^2 + 400c_3't) \\ & -8(48c_2'^2 + 200c_3'^3)]. \end{aligned}$$

Figure 1 shows the graphical analysis of the scale factors for the dust case. The scale factor $a(t)$ indicates large cosmic expansion in the x-direction but $b(t)$ represents that the universe is expanding very slowly in the y- and z-directions. Figure 2 (left plot) indicates that the Hubble parameter is decreasing with the passage of time. In the right plot of Fig. 2, the effective EoS parameter identifies that, initially, the universe associates with a radiation dominated era and, after some time, it corresponds to a dark energy era by crossing the matter dominated phase.

Figures 3 and 4 analyze the behavior of scalar field and cosmic expansion via phantom and quintessence models. The left plot of Fig. 3 shows that the scalar field is positive initially yielding decelerated expansion but gradually, it starts increasing negatively which describes accelerated expansion. In case of quintessence model, the scalar field grows from negative to positive indicating decelerated expansion of the universe. The right plots of **3** and **4** satisfy $\frac{\dot{\phi}^2}{2} < V(\phi)$ and $\frac{\dot{\phi}^2}{2} > -V(\phi)$, implying that the phantom model yields accelerated expansion, while the quintessence model corresponds to decelerated expansion.

To analyze a big-rip free model, the key point is that if the EoS parameter rapidly approaches -1 and the Hubble rate tends to be constant (asymptotically de Sitter universe), then it is possible to have a model in which the time required for a singularity is infinite, i.e., the singularity effectively does not occur [44]. The occurrence of a maximum potential of a phantom scalar field is another evident issue as regards avoiding this singularity [45]. The graphical behavior of the EoS parameter represents that ω_{eff} rapidly approaches -1 and the Hubble rate is decreasing but the potential is not maximum. We may avoid the big-rip singularity in the present case if we choose c_2' to be negatively large, which yields an asymptotic behavior of the Hubble rate.

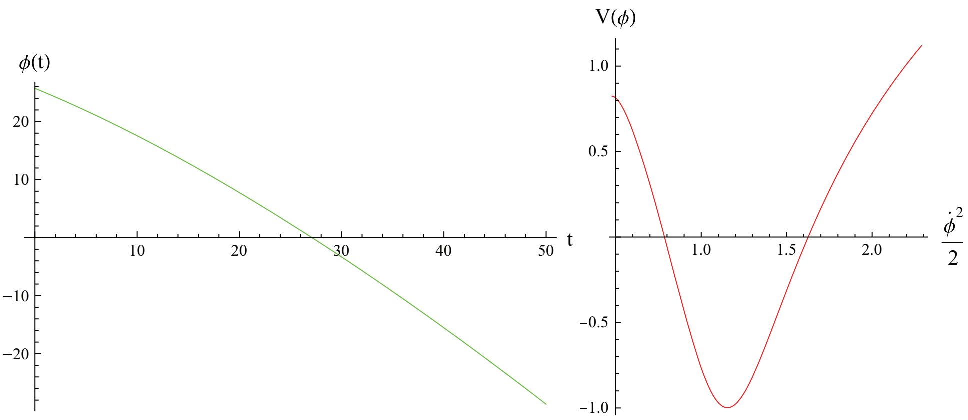

Fig. 3 Plots of scalar field $\phi(t)$ (*left*) versus cosmic time t and potential energy $V(\phi)$ versus kinetic energy $\frac{\dot{\phi}^2}{2}$ (*right*) for $\epsilon = -1$

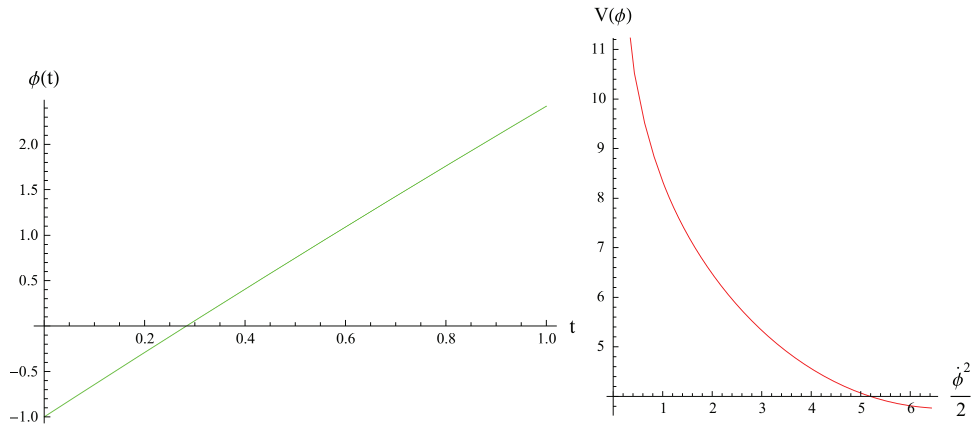

Fig. 4 Plots of scalar field $\phi(t)$ (*left*) versus cosmic time t and potential energy $V(\phi)$ versus kinetic energy $\frac{\dot{\phi}^2}{2}$ (*right*) for $\epsilon = 1$

3.1.2 Non-dust case

At large scales, the perfect fluid successfully illustrates a cosmic matter distribution in the presence of radiation. In the absence of a boundary term and an affine parameter, the coefficients of the symmetry generator (21) corresponding to a, b, R, T, ϕ remain the same as in the presence of a boundary term of extended symmetry. Thus, the generator of the Noether symmetry and the associated first integrals reduce to

$$K = -2ac_1\frac{\partial}{\partial a} + c_1 b\frac{\partial}{\partial b} + c_2\frac{\partial}{\partial \phi},$$
$$\Sigma = -4c_1 ab\dot{b}f_R + 4c_1 b^2\dot{a}f_R + \epsilon c_2 ab^2\dot{\phi}.$$

In order to formulate an exact solution of the dynamical equations for a perfect fluid distribution, we insert Eqs. (19) and (20) into (6) and (7), yielding

$$a(t) = \frac{\left(\frac{5}{c_9}\right)^{\frac{2}{5}}(c_2\sin(c_{10}t) + c_3\cos(c_{10}t))^{\frac{4}{5}}}{5^{\frac{4}{5}}},$$
$$b(t) = \frac{c_4\left(\frac{5}{c_9}\right)^{\frac{1}{5}}(c_2\sin(c_{10}t) + c_3\cos(c_{10}t))^{\frac{2}{5}}}{5^{\frac{2}{5}}}.$$

This describes an oscillatory solution of the $f(R, T)$ model admitting an indirect non-minimal curvature–matter coupling. To study the cosmological behavior of this solution, we consider the cosmological parameters as follows:

$$H = \frac{8c_{10}(c_2\sin(c_{10}t) + c_3\cos(c_{10}t))}{15(c_2\sin(c_{10}t) + c_3\cos(c_{10}t))},$$
$$q = \frac{-8c_2^2\cos^2(c_{10}t) + 7c_3^3 + 8c_3^2\cos^2(c_{10}t) + 15c_2^2 + 16c_2c_3\cos(c_{10}t)\sin(c_{10}t)}{8(c_2\sin(c_{10}t) + c_3\cos(c_{10}t))^2},$$
$$s = (-45((4c_2^4 - 4c_3^4)\cos^2(c_{10}t) - c_3^4 - 6c_2^2c_3 - 5c_2^4 - (8c_2^3c_3 + 8c_2c_3^3)$$

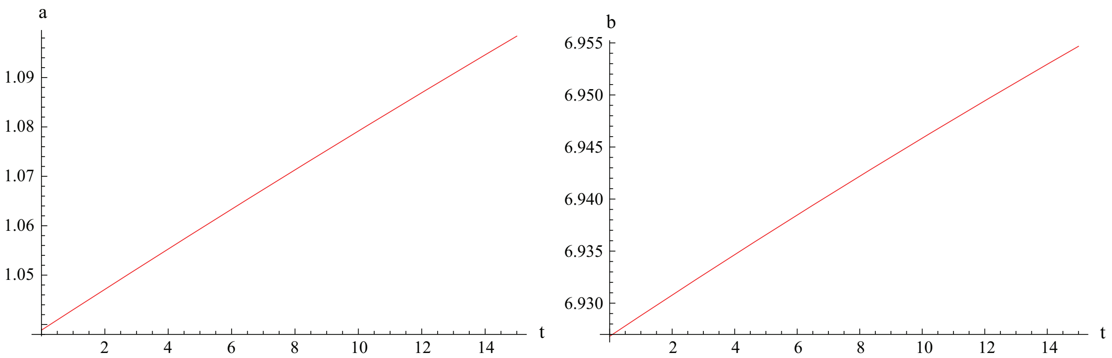

Fig. 5 Plots of scale factor $a(t)$ (*left*) and $b(t)$ (*right*) versus cosmic time t for $c_2 = c_3 = c_9 = 5.5$ and $c_{10} = 0.005$

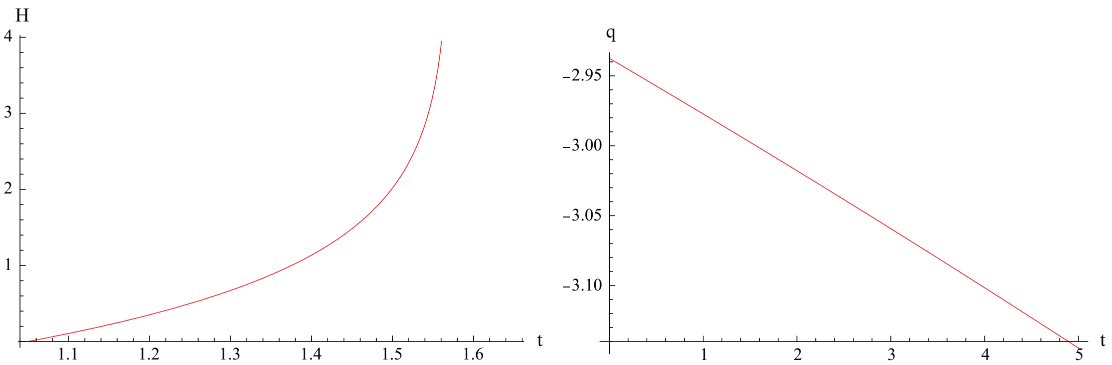

Fig. 6 Plots of $H(t)$ (*left*) and $q(t)$ (*right*) versus cosmic time t

$$\times \cos(c_{10}t)\sin(c_{10}t)))/256((c_2^4 + c_3^4 - 6c_2^2c_3^2)\cos^4(c_{10}t) + (6c_2^2c_3^2 - 2c_3^4)$$
$$\times \cos^2(c_{10}t) + (-4c_2^3c_3 + 4c_2c_3^3)\sin(c_{10}t)\cos^3(c_{10}t) - 4c_2c_3^3\cos(c_{10}t)$$
$$\times \sin(c_{10}t) + c_3^4),$$
$$\omega_{\rm eff} = \frac{\chi(3p_{\rm m} - \rho_{\rm m}) + p_{\rm m} - \frac{\epsilon\dot{\phi}^2}{2} - V(\phi) + \frac{2\xi}{b^2} + a(3p_{{\rm m},a} - \rho_{{\rm m},a}) + p_{{\rm m},a}}{\chi(3p_{\rm m} - \rho_{\rm m}) + p_{\rm m} + \frac{\epsilon\dot{\phi}^2}{2} - V(\phi) + \frac{2\xi}{b^2}}.$$

The scalar field and the corresponding kinetic and potential energies identify the early as well as the current cosmic expansion and also characterize the decelerated expansion of the universe when the kinetic energy dominates the negative potential. In this case, Eq. (8) yields

$$\phi = \int \frac{\epsilon c_4 - \frac{5c_6c_2^2\cos(2c_{10}t)\left(-2\,{}_2F_1\left[\frac{3}{10},\frac{1}{2},\frac{13}{10},\sin[\frac{\pi}{4}+c_{10}t]^2\right]+\sqrt{2-2\sin[2c_{10}t]}\right)}{16c_{10}\sqrt{\cos[\frac{\pi}{4}+c_{10}t]^2}(c_2(\cos[c_{10}t]+\sin[c_{10}t]))^{2/5}}}{\epsilon(c_2\cos[c_{10}t] + c_2\sin[c_{10}t])^{8/5}}\,\mathrm{d}t,$$

where ${}_2F_1$ represents the hypergeometric function.

In Fig. 5, the right plot shows that the universe experiences an immense amount of expansion in the y- and z-directions, whereas the left plot shows a small amount of expansion in the x-direction. Figure 6 provides information as regards an increasing rate of expansion through the Hubble parameter, while the negatively increasing deceleration parameter ensures accelerated cosmic expansion. The left plot of Fig. 7 characterizes the quintessence phase of the dark energy era, while the right plot identifies the r–s parameter trajectories in the quintessence and phantom phases as $s > 0$ when $r < 1$. Both plots of Fig. 8 verify the current cosmic expansion for quintessence as well as phantom models as ϕ is continuously increasing negatively, and the potential energy of the field is dominating over the kinetic energy. The graphical interpretation of the EoS parameter yields $\omega_{\rm eff} < -1$, which is not a sufficient condition for the existence of a singularity as the potential turns out to be maximum with the passage of time. Thus, we may avoid a big-rip singularity if the Hubble rate decreases asymptotically in the presence of minimal coupling of $f(R, T)$ gravity with scalar field.

3.2 $f(R, T) = F(R) + h(R)g(T)$

To analyze the effect of a direct non-minimal curvature–matter coupling, we consider this model and evaluate the symmetry generators as well as the associated conservation laws. Inserting the model in Eqs. (A2)–(A4), (A10), (A11)

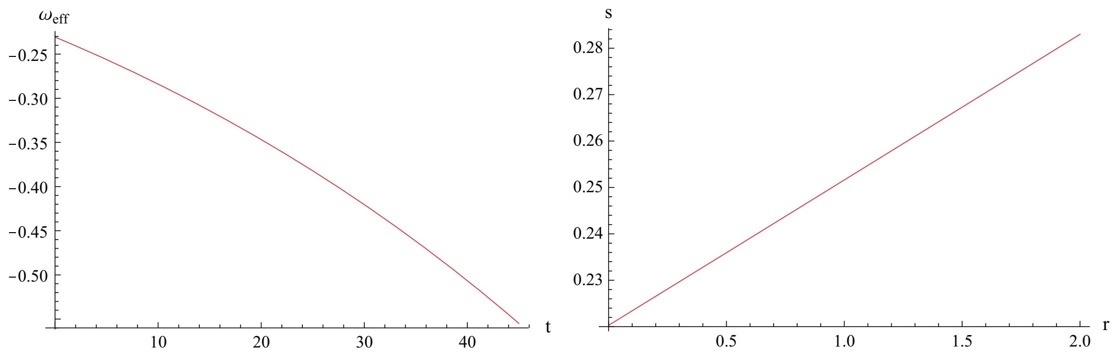

Fig. 7 Plot of ω_{eff} and r–s parameters versus cosmic time t for $c_2 = c_3 = 5.5$ and $c_{10} = 0.005$

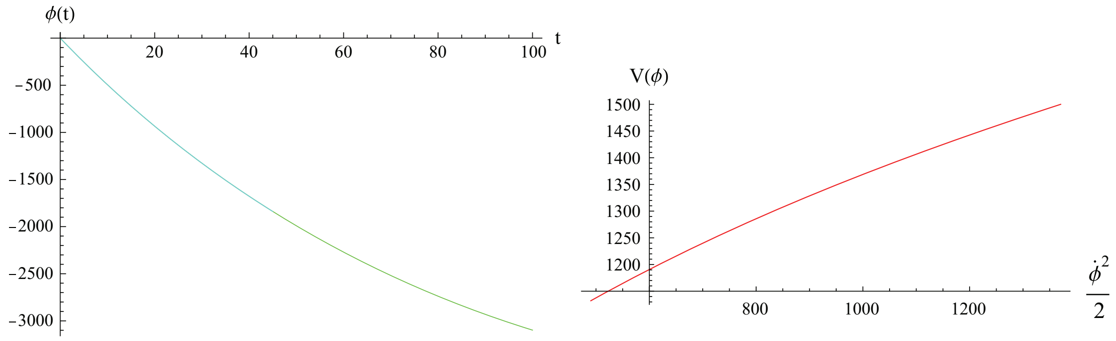

Fig. 8 Plots of scalar field $\phi(t)$ (*left*) versus cosmic time t and potential energy $V(\phi)$ versus kinetic energy $\frac{\dot{\phi}^2}{2}$ (*right*) for $c_2 = 5.5$, $c_4 = -10^3$, $c_6 = 0.5$ and $c_{10} = 0.005$

and (A15) and using separation of variables approach, we obtain

$$\beta = -\frac{b\alpha}{2a} + \phi Y_1(t,a,b) + Y_2(t,a,b),$$
$$F(R) = \frac{\epsilon}{4d_3}\left(-d_3Y_{12}(R) + d_2Y_9(R)\right) + d_5R + d_6,$$
$$h(R) = -\frac{\epsilon}{4d_3}\left(-d_3Y_9(R)_{,R} + d_1R\right) + d_4,$$
$$g(T) = d_2 + d_3Y_{10}(T),$$
$$\eta = \frac{1}{b}[Y_1(t,a,b)(Y_{10}(T)(d_1 + Y_9(R)_{,R}) - \phi^2 + Y_{12}(R)_{,R}) + b\phi\tau_{,t} - 2\phi \times Y_2(t,a,b) + bY_{14}(t,a,b)],$$

where the d_i $(i = 1,\ldots,7)$ denote constants. We substitute these values in Eqs. (A1), (A8) and (A9) which yield

$$\tau = \int -\frac{Y_{23}(t)}{\epsilon}\mathrm{d}t + d_8t + d_9,$$
$$B = \frac{1}{6d_4}\Big[6ab(Y_{19}(T)d_1 + d_4\epsilon\phi^2 + Y_{19}(T)d_4e^{-R})Y_2(t,a,b)_{,t} + 6ab\phi(\frac{1}{3}d_4\epsilon\phi^2 + Y_{19}(T)d_4e^{-R} + Y_{19}(T) \times d_1)Y_{16}(t,b)_{,t} + 3d_4(2Y_{22}(t,a,b) + 2\phi Y_{21}(t,a,b)_{,t} + ab^2\phi^2Y_{23}(t)_{,t})\Big],$$
$$Y_1(t,a,b) = Y_{16}(t,b) + Y_{15}(a,b),$$
$$Y_{10}(T) = -\frac{Y_{19}(T)d_3 + \epsilon d_2d_4}{\epsilon d_3d_4},$$
$$Y_{12}(R) = -\frac{d_2d_4e^{-R}}{d_3} + d_6R + d_7,$$
$$Y_9(R) = -e^{-R}d_4 - 2d_1R + d_2,$$
$$Y_{14}(t,a,b) = -\frac{Y_{21}(t,a,b)}{b^2a\epsilon} - \frac{bad_2\epsilon d_1Y_{16}(t,b) + d_6\epsilon bad_3Y_{16}(t,b)}{\epsilon b^2ad_3} + Y_{24}(b,a).$$

To evaluate remaining unknown functions, we insert the above functions into β, η, F, g, h and solve Eqs. (A5)–(A7) with (A12)–(A14) and (A16)–(A21), leading to

$$Y_{21}(t,a,b) = Y_{26}(a,b), \quad Y_{22}(t,a,b) = d_{10}t,$$
$$Y_{16}(t,b) = -d_{12}b,$$

$$Y_{15}(a,b)=d_{12}b,\quad Y_{24}(b,a)=0,\quad Y_2(t,a,b)=d_9b,$$
$$Y_{23}(t)=\epsilon(-2d_9+e^{-R}d_4d_3d_{11}e^R+d_8),\quad \delta=0,$$
$$\gamma=\frac{d_{11}e^RT}{d_13}\times(e^{-R}d_4Td_{13}d_3-d_1d_{13}d_3T+(2((-2d_5+\frac{1}{2}\epsilon d_6)d_3+d_1d_2\epsilon))d_4).$$

Using these solutions in Eq. (A22) with $d_{11}=0$ and $d_6=\frac{d_2d_1}{d_3}$, it follows that

$$\tau=3d_9,\quad \alpha=d_{10}a,\quad \beta=b(d_9-\frac{d_{10}}{2}),\quad \delta=0,\quad \gamma=0,$$
$$B=d_{10}t,\quad \eta=-\frac{d_1}{\epsilon}+2d_{12}d_6,$$
$$F(R)=d_6+d_5R-\frac{3d_6\epsilon R}{4},$$
$$h(R)=d_4-\frac{\epsilon}{4d_3}(d_4e^{-R}+d_1R-2d_1),$$
$$g(T)=d_2-\frac{d_2d_4\epsilon-d_3d_{13}T}{d_4\epsilon}.$$

Inserting F, h and g, the $f(R,T)$ model becomes

$$f(R,T)=-\frac{3\epsilon d_6R}{4}+d_5R+d_6+(d_4-\frac{\epsilon}{4d_3}(d_4e^{-R}+d_1R-2d_1))\left(\frac{d_3d_{13}T}{d_4\epsilon}\right).$$

Thus, the constructed model also experiences a direct coupling between curvature and matter parts. In this case, the symmetry generators and associated conserved quantities are

$$K_1=3\frac{\partial}{\partial t}+b\frac{\partial}{\partial b},\quad \Sigma_1=\frac{1}{4d_3\epsilon}(-4ab^2\epsilon^2d_3\dot{\phi}^2+4d_{10}d_3\epsilon t+3\mathrm{tab}^2d_1RTd_3\epsilon-9\mathrm{tab}^2d_1Rp_{\mathrm{m}}d_3\epsilon+3\mathrm{tab}^2d_1R\rho_{\mathrm{m}}d_3\epsilon-12td_1T\dot{a}\dot{b}bd_3\epsilon-4b^2d_4T\times\dot{a}e^{-R}d_3\epsilon-4b^2a\dot{T}d_4e^{-R}d_3\epsilon-9\mathrm{tab}^2d_4p_{\mathrm{m}}e^{-R}d_3\epsilon+3\mathrm{tab}^2d_4\rho_{\mathrm{m}}\times e^{-R}d_3\epsilon+6td_4Ta\dot{b}^2e^{-R}d_3\epsilon+6td_4\mathrm{Taq}e^{-R}d_3\epsilon-4bd_4Ta\dot{b}e^{-R}d_3\epsilon+4b^2a\dot{R}d_4Te^{-R}d_3\epsilon+4b^2a\dot{T}d_1d_3\epsilon-12\mathrm{tab}^2d_2d_1\epsilon-12\mathrm{tab}^2p_{\mathrm{m}}\times d_3\epsilon+12\mathrm{tab}^2V(\phi)d_3\epsilon-24td_5a\dot{b}d_3\epsilon-24td_5aqd_3\epsilon+16bd_5a\dot{b}\times d_3\epsilon+36\mathrm{tab}^2d_3^2d_4p_{\mathrm{m}}-12\mathrm{tab}^2d_3^2d_4\rho_{\mathrm{m}}+18t\epsilon^2d_2d_1a\dot{b}^2+18t\epsilon^2\times d_2d_1aq-12b\epsilon^2d_2d_1a\dot{b}+4b^2d_1T\dot{a}d_3\epsilon-12b^2\epsilon^2d_2d_1\dot{a}+16b^2d_5\times\dot{a}d_3\epsilon-3\mathrm{tab}^2Rd_4Te^{-R}d_3\epsilon+12td_4T\dot{a}\dot{b}be^{-R}d_3\epsilon+36t\epsilon^2d_2d_1\dot{a}\dot{b}b+4bd_1Ta\dot{b}d_3\epsilon+6\mathrm{tab}^2\epsilon\dot{\phi}^2d_3\epsilon+18\mathrm{tab}^2d_1p_{\mathrm{m}}d_3\epsilon-6\mathrm{tab}^2d_1\rho_{\mathrm{m}}d_3\epsilon-48td_5\dot{a}\dot{b}bd_3\epsilon-6td_1Ta\dot{b}^2d_3\epsilon-6td_1\mathrm{Taq}d_3\epsilon),$$
$$K_2=a\frac{\partial}{\partial a}-\frac{b}{2}\frac{\partial}{\partial b},\quad \Sigma_2=-\frac{b}{2d_3}(-a\dot{b}d_1Td_3+3a\dot{b}\epsilon d_2d_1+a\dot{b}d_4Te^{-R}d_3-4a\dot{b}d_5d_3+bd_1T\dot{a}d_3+4bd_5\dot{a}d_3-3b\epsilon d_2d_1\dot{a}-bd_4T\dot{a}e^{-R}d_3),$$
$$K_3=-\frac{1}{\epsilon}\frac{\partial}{\partial\phi},\quad \Sigma_3=ab^2\dot{\phi},\quad K_4=2d_{12}\frac{\partial}{\partial\phi},\quad \Sigma_4=2d_{12}ab^2\epsilon\dot{\phi}.$$

We see that scaling symmetry appears through generator K_2 with the first integral Σ_2 leading to conserved linear momentum.

Now we investigate the existence of Noether symmetry in the absence of affine parameter and boundary term of the extended symmetry and also study the effect of direct curvature–matter coupling on conservation laws. For this purpose, we solve Eqs. (A5), (A6), (A9) and (A12)–(A21), which gives

$$\delta=-\frac{a}{2Y_9(T)_{,T}}\left(\frac{1}{3}Y_4(a,b)_{,a}\phi^3+2Y_4(a,b)_{,a}Y_9(T)\phi+2Y_4(a,b)_{,a}Y_8(b)\phi+\phi^2Y_5(a,b)_{,a}+2Y_7(a,b)_{,a}\phi\right)+Y_{12}(a,R,T,b),\quad F(R)=k_4R+k_5,$$
$$\beta=-\frac{b}{2a}(Y_{10}(a,R,T,b)+aY_5(a,b)),\quad g(T)=k_1+Y_9(T)k_2,$$
$$\eta=\frac{1}{2}(\phi^2+2Y_9(T)+2Y_8(b))Y_4(a,b)+Y_5(a,b)\phi+Y_7(b,a),$$
$$h(R)=\frac{\epsilon R}{2(k_2+k_3)},\quad \gamma=Y_{11}(a,b,R,T),$$
$$\alpha=-Y_4(a,b)a\phi+Y_{10}(a,b,R,T),$$

where the k_l $(l=1,\ldots,5)$ are arbitrary constants. Inserting these solutions into the remaining equations of the system, we obtain

$$V(\phi)=k_{10}\phi+k_{11},\quad Y_{10}(a,R,T,b)=k_8a,\quad Y_4(a,b)=0,$$
$$Y_{12}(a,R,T,b)=-\frac{k_8}{2k_2}((\epsilon(k_6T+k_7)+2k_4)k_2+\epsilon k_1),$$
$$Y_5(a,b)=-\frac{k_6k_8\epsilon}{2},$$
$$Y_7(b,a)=k_9,\quad Y_9(T)=k_6T+k_7,$$
$$p_{\mathrm{m}}=\frac{2k_9k_{10}}{\epsilon k_8k_6}-k_5+k_{11}+\frac{2k_2k_4k_3}{\epsilon}$$

$$
\begin{aligned}
&+a^{-\frac{k_6\epsilon}{2}}\epsilon k_6 b a^{\frac{1}{2}-\frac{\epsilon k_6}{4}},\\
\rho_{\mathrm{m}} &= \frac{k_7}{k_6}+\frac{6k_2k_4k_3}{\epsilon}-3k_5+3k_{11}+\frac{2k_4}{k_6\epsilon}+\frac{6k_9k_{10}}{k_8k_6\epsilon}+\frac{k_1}{k_2k_6}\\
&+a^{-\frac{k_6\epsilon}{2}}\epsilon k_6 b a^{\frac{1}{2}-\frac{\epsilon k_6}{4}}.
\end{aligned}
$$

The corresponding Noether symmetry generator with the associated first integral take the form

$$
\begin{aligned}
K_1 &= a\frac{\partial}{\partial a}-\frac{b}{2}\left(1-\frac{k_6\epsilon}{2}\right)\frac{\partial}{\partial b}\\
&\quad +R\frac{\partial}{\partial R}-(k_1\epsilon+k_2(\epsilon(k_6T+k_7)+2k_4))\\
&\quad \times\frac{1}{2k_2}\frac{\partial}{\partial T}-\frac{k_6\epsilon\phi}{2}\frac{\partial}{\partial\phi},\quad \Sigma_1=ab\dot{b}\epsilon k_6T\\
&\quad -\frac{b^2\epsilon k_1\dot{a}}{k_2}-b^2\epsilon k_6T\dot{a}-ba\epsilon k_6k_4\dot{b}\\
&\quad -\frac{ba\epsilon^2k_6^2T\dot{b}}{2}-\frac{ba\epsilon^2k_6k_7\dot{b}}{2}+\frac{ab\dot{b}\epsilon k_1}{k_2}\\
&\quad +ab\dot{b}\epsilon k_7-\frac{ba\epsilon^2k_6k_1\dot{b}}{2k_2}-\frac{ab^2\epsilon^2\dot{\phi}k_6\phi}{2}\\
&\quad +2ab\dot{b}k_4-2b^2k_4\dot{a}-b^2\epsilon k_7\dot{a}+\frac{b^2a\epsilon^2k_6^2\dot{T}}{2},\\
K_2 &= \frac{\partial}{\partial\phi},\quad \Sigma_2=ab^2\epsilon\dot{\phi}k_9.
\end{aligned}
$$

Here the symmetry generator K_1 yields the scaling symmetry.

4 Final remarks

In this paper, we have analyzed the existence of Noether symmetry in a non-minimally coupled $f(R,T)$ gravity interacting with scalar field model for anisotropic homogeneous universe models like BI, BIII and KS models. Using Noether symmetry approach, we have found conserved quantities associated with symmetry generators and studied the contribution of direct as well as indirect curvature–matter coupling through two $f(R,T)$ models. We have also formulated exact solutions for dust and perfect fluid distributions whose cosmological analysis is discussed through cosmological parameters.

For the $f(R,T)$ model admitting indirect curvature–matter coupling, we have found three symmetry generators in the presence of an affine parameter and a boundary term. The first generator of translational symmetry in time yields the energy conservation law, whereas the second generator generates scaling symmetry. For the second model, we have formulated four conserved quantities associated with symmetry generators but only one generator provides the scaling symmetry leading to the conservation of linear momentum. In the absence of a boundary term of extended symmetry and an affine parameter, the symmetry generator of the first model ensures the existence of scaling symmetry for dust as well as perfect fluid, while we have found two symmetry generators for the second model.

For the first model, we have evaluated exact solutions without considering boundary term. For the dust distribution, we have found a power-law solution. The graphical analysis of scale factors and cosmological parameters leads to a decelerating phase of the universe. The positively increasing scalar field and the kinetic energy dominating over the potential energy ensure the decelerating behavior of the cosmos for the quintessence model. In the case of the phantom model, the scalar field rolls down positively and tends to increase negatively while the kinetic energy dominates over the potential energy for $t \in [0.8, 1.6]$. The graphical behavior of the effective EoS parameter reveals that the universe experiences a phase transition from a radiation dominated era to a dark energy era by crossing the matter dominated phase. For a perfect fluid, we have determined an oscillatory solution with increasing rate of the Hubble parameter, a negative deceleration parameter and $\omega_{\mathrm{eff}} < -1$. The trajectories of the r–s parameters identify quintessence and phantom phases as $s > 0$ when $r < 1$. For the quintessence and phantom models, with the scalar field continuously increasing negatively, the potential energy of the field is dominating over the kinetic energy. This analysis indicates that an epoch of accelerated expansion is achieved for a non-dust distribution.

Shamir [17] investigated the exact solution of the BI model without using Noether symmetry approach in $f(R,T)$ gravity. For indirect curvature–matter coupling, the exact solution is determined using a relationship between expansion and shear scalars. The study of corresponding cosmological parameters yields a positive deceleration parameter, $\omega_{\mathrm{eff}} = 1$, the volume and average scale factor turn out to be zero at $t = 0$. Thus, the analysis of this exact solution yields a decelerating epoch for the $R + 2f(T)$ model. For the $f_1(R) + f_2(T)$ model, a power-law form of $f_1(R)$ is considered that gives exponential and power-law solutions for different choices of $f_2(T)$. For the exponential solution, the average Hubble parameter becomes zero, leading to the Einstein universe. Camci et al. [26] formulated exact solutions of these anisotropic models via the Noether symmetry approach in non-minimally scalar coupled gravity. The scale factors are found to be proportional to the inverse of the scalar field whose explicit form is not determined for any anisotropic model. Consequently, the cosmological analysis of these exact solutions is not established. In the present paper, we have found two exact solutions, power-law and oscillatory solutions, via the Noether symmetry approach, that correspond to decelerating as well as current accelerating universe for dust and non-dust distributions.

We conclude that the constructed $f(R,T)$ models admit direct as well as indirect curvature–matter coupling. The existence of symmetry generators and associated conserved quantities is ensured for both $f(R, T)$ models. It is worthwhile to mention here that we have found maximum symmetry generators along with conserved quantities for the second $f(R, T)$ model in the presence of boundary term. This indicates that the model appreciating a direct curvature–matter coupling leads to more physical results relative to the first model, while the exact solutions describe cosmic evolution.

Acknowledgements This work has been supported by the *Pakistan Academy of Sciences Project*.

Appendix A

For the invariance condition (12), the system of equations is

$$\epsilon ab^2\eta,_t = -B,_\phi, \tag{A1}$$

$$b\alpha + 2a\beta + 2ab\eta,_\phi - ab\tau,_t = 0, \tag{A2}$$

$$2b\alpha,_\phi f_{RR} + 4a\beta,_\phi f_{RR} + ab\epsilon\eta,_R = 0, \tag{A3}$$

$$2b\alpha,_\phi f_{RT} + 2a\beta,_\phi f_{RT} + ab\epsilon\eta,_T = 0, \tag{A4}$$

$$4\beta,_\phi f_R + 2b\gamma,_\phi f_{RR} + 2b\delta,_\phi f_{RT} + ab\epsilon\eta,_a = 0, \tag{A5}$$

$$4b\alpha,_\phi f_R + 4a\beta,_\phi f_R + 4ab\gamma,_\phi f_{RR} + 4ab\delta,_\phi f_{RT} + ab^2\epsilon\eta,_b = 0, \tag{A6}$$

$$\tau,_a f_R = 0,\ \tau,_b f_R = 0,\ \tau,_R f_{RR} = 0,\ \tau,_T f_{RT} = 0,\ \tau,_\phi = 0, \tag{A7}$$

$$2b^2\alpha,_t f_{RR} + 4ab\beta,_t f_{RR} = -B,_R, \tag{A8}$$

$$2b^2\alpha,_t f_{RT} + 4ab\beta,_t f_{RT} = -B,_T, \tag{A9}$$

$$b\alpha,_R f_{RR} + 2ab\beta,_R f_{RR} = 0, \tag{A10}$$

$$b\alpha,_T f_{RT} + 2ab\beta,_T f_{RT} = 0, \tag{A11}$$

$$2\beta,_a f_R + b\gamma,_a f_{RR} + b\delta,_a f_{RT} = 0, \tag{A12}$$

$$4b\beta,_t f_R + 2b^2\gamma,_t f_{RR} + 2b^2\delta,_t f_{RT} = -B,_a, \tag{A13}$$

$$4b\alpha,_t f_R + 4a\beta,_t f_R + 4ab\gamma,_t f_{RR} + 4ab\delta,_t f_{RT} = -B,_b, \tag{A14}$$

$$b\alpha,_T f_{RR} + b\alpha,_R f_{RT} + 2a\beta,_T f_{RR} + 2a\beta,_R f_{RT} = 0, \tag{A15}$$

$$\alpha f_R + a\gamma f_{RR} + a\delta f_{RT} + 2b\alpha,_b f_R + 2a\beta,_b f_R + 2ab\gamma,_b f_{RR} + 2ab\delta,_b f_{RT} - a\tau,_t f_R = 0, \tag{A16}$$

$$2\beta f_{RR} + b\gamma f_{RRR} + b\delta f_{RRT} + b\alpha,_a f_{RR} + 2a\beta,_a f_{RR} + 2\beta,_R f_R + b\gamma,_R f_{RR} + b\delta,_R f_{RT} - b\tau,_t f_{RR} = 0, \tag{A17}$$

$$2\beta f_{RT} + b\gamma f_{RRT} + b\delta f_{RTT} + b\alpha,_a f_{RT} + 2a\beta,_a f_{RT} + 2\beta,_T f_R + b\gamma,_T f_{RR} + b\delta,_T f_{RT} - b\tau,_t f_{RT} = 0, \tag{A18}$$

$$2\beta f_R + 2b\gamma f_{RR} + 2b\delta f_{RT} + 2b\alpha,_a f_R + 4a\beta,_a f_R + 2b\beta,_b f_R + 2ab\gamma,_a f_{RR} + b^2\gamma,_b f_{RR} + 2ab\delta,_a f_{RT} + b^2\delta,_b f_{RT} - 2b\tau,_t f_R = 0, \tag{A19}$$

$$2b\alpha f_{RR} + 2a\beta f_{RR} + 2ab\gamma f_{RRR} + 2ab\delta f_{RRT} + b^2\alpha,_b f_{RR} + 2b\alpha,_R f_R + 2ab \times\beta,_b f_{RR} + 2a\beta,_R f_R + 2ab\gamma,_R f_{RR} + 2ab\delta,_R f_{RT} - 2ab\tau,_t f_{RR} = 0, \tag{A20}$$

$$2b\alpha f_{RT} + 2a\beta f_{RT} + 2ab\gamma f_{RRT} + 2ab\delta f_{RTT} + b^2\alpha,_b f_{RT} + 2b\alpha,_T f_R + 2ab \times\beta,_b f_{RT} + 2a\beta,_T f_R + 2ab\gamma,_T f_{RR} + 2ab\delta,_T f_{RT} - 2ab\tau,_t f_{RT} = 0, \tag{A21}$$

$$\begin{aligned} &b^2\alpha[f - Rf_R + f_T(3p_m - \rho_m - T) + p_m - V(\phi) \\ &+a\{f_T(3p_m,_a - \rho_m,_a) + p_m,_a\} + 2\xi f_R] \\ &+\beta[2ab(f - Rf_R + f_T(3p_m - \rho_m - T) + p_m - V(\phi)) \\ &+ab^2\{f_T(3p_m,_b - \rho_m,_b) + p_m,_b\}] \\ &+\gamma[-ab^2Rf_{RR} + 2a\xi f_{RR}] + \delta[-ab^2Rf_{RT} \\ &+2a\xi f_{RT}] - ab^2V'(\phi)\eta \\ &+\tau,_t[ab^2(f - Rf_R + f_T(3p_m - \rho_m - T) + p_m \\ &-V(\phi)) + 2a\xi f_R] = B,_t. \end{aligned} \tag{A22}$$

References

1. S. Nojiri, S.D. Odintsov, Phys. Lett. B **599**, 137 (2004)
2. O. Bertolami, M.C. Sequeira, Phys. Rev. D **79**, 104010 (2009)
3. O. Bertolami, J. Pramos, J. Cosmol. Astropart. Phys. **03**, 009(2010)
4. O. Bertolami, P. Frazao, J. Paramos, Phys. Rev. D **81**, 104046 (2010)
5. O. Bertolami, Frazao, P., Paramos, J., Phys. Rev. D **83**, 044010 (2011)
6. T. Harko, F.S.N. Lobo, S. Nojiri, S.D. Odintsov, Phys. Rev. D **84**, 024020 (2011)
7. T. Harko, F.S.N. Lobo, Galaxies **2**, 410 (2014)
8. M. Sharif, M. Zubair, J. Cosmol. Astropart. Phys. **03**, 028 (2012)
9. M. Sharif, M. Zubair, J. Exp. Theor. Phys. **117**, 248 (2013)
10. M. Sharif, M. Zubair, J. Phys. Soc. Jpn. **82**, 064001 (2013)
11. M. Sharif, M. Zubair, J. Phys. Soc. Jpn. **82**, 014002 (2013)
12. M. Sharif, M. Zubair, Astrophys. Space Sci. **349**, 52 (2014)
13. M. Sharif, M. Zubair, Gen. Relativ. Gravit. **46**, 1723 (2014)

14. T. Harko, M.J. Lake, Eur. Phys. J. C **75**, 60 (2015)
15. M. Sharif, M. Zubair, Astrophys. Space Sci. **349**, 457 (2014)
16. M.F. Shamir, Z. Raza, Astrophys. Space Sci. **356**, 111 (2015)
17. M.F. Shamir, Eur. Phys. J. C **75**, 354 (2015)
18. S. Capozziello, A. Stabile, A. Troisi, Class. Quantum Grav. **24**, 2153 (2007)
19. I. Hussain, M. Jamil, F.M. Mahomed, Astrophys. Space Sci. **337**, 373 (2012)
20. M.F. Shamir, A. Jhangeer, A.A. Bhatti, Chin. Phys. Lett. A **29**, 080402 (2012)
21. D. Momeni, R. Myrzakulov, E. Güdekli, Int. J. Geom. Methods Mod. Phys. **12**, 1550101 (2015)
22. M.F. Shamir, M. Ahmad, Eur. Phys. J. C **77**, 55 (2017)
23. A.K. Sanyal, Phys. Lett. B **524**, 177 (2002)
24. U. Camci, Y. Kucukakca, Phys. Rev. D **76**, 084023 (2007)
25. Y. Kucukakca, U. Camci, I. Semiz, Gen. Relativ. Gravit. **44**, 1893 (2012)
26. U. Camci, A. Yildirim, I. Basaran Oz, Astropart. Phys. **76**, 29 (2016)
27. M. Sharif, I. Nawazish, J. Exp. Theor. Phys. **120**, 49 (2014)
28. M. Sharif, I. Nawazish, arXiv:1609.02430
29. S. Capozziello, R. de Ritis, Class. Quant. Grav. **11**, 107 (1994)
30. B. Vakili, Phys. Lett. B **16**, 664 (2008)
31. Y. Zhang, Y.G. Gong, Z.H. Zhu, Phys. Lett. B **688**, 13 (2010)
32. M. Jamil, F.M. Mahomed, D. Momeni, Phys. Lett. B **702**, 315 (2011)
33. M. Sharif, I. Shafique, Phys. Rev. D **90**, 084033 (2014)
34. M.A.H. MacCallum, *In General Relativity : An Einstein Centenary Survey*. (Cambridge University Press, Cambridge, 1979)
35. B.F. Schutz, Phys. Rev. D **2**, 2762 (1970)
36. J.D. Brown, Class. Quantum Grav. **10**, 1579 (1993)
37. S. Nojiri, S.D. Odintsov, Phys. Rev. D **70**, 103522 (2004)
38. E. Elizalde, S. Nojiri, S.D. Odintsov, Phys. Rev. D **70**, 043539 (2004)
39. S. Nojiri, S.D. Odintsov, Phys. Lett. B **595**, 1 (2004)
40. K. Bamba, S. Nojiri, S.D. Odintsov, J. Cosmol. Astropart. Phys. **0810**, 045 (2008)
41. S. Nojiri, S.D. Odintsov, Phys. Lett. B **686**, 44 (2010)
42. S. Nojiri, S.D. Odintsov, Phys. Rep. **505**, 59 (2011)
43. J. Hanc, S. Tuleja, M. Hancova, Am. J. Phys. **72**, 428 (2004)
44. J. Barrow, Class. Quant. Grav. **21**, L79 (2004)
45. R. Rakhi, K. Indulekha, arXiv:0910.5406

Annals of Physics 389 (2018) 283–305

Contents lists available at ScienceDirect

Annals of Physics

journal homepage: www.elsevier.com/locate/aop

Wormhole geometry and Noether symmetry in $f(R)$ gravity

M. Sharif [*,1], Iqra Nawazish

Department of Mathematics, University of the Punjab, Quaid-e-Azam Campus, Lahore-54590, Pakistan

ARTICLE INFO

Article history:
Received 11 October 2017
Accepted 25 December 2017
Available online 4 January 2018

Keywords:
Noether symmetry
Wormhole solution
$f(R)$ gravity

ABSTRACT

This paper investigates the geometry of static traversable wormhole through Noether symmetry approach in $f(R)$ gravity. We take perfect fluid distribution and formulate symmetry generators with associated conserved quantities corresponding to general form, power-law and exponential $f(R)$ models. In each case, we evaluate wormhole solutions using constant and variable red-shift functions. We analyze the behavior of shape function, viability of constructed $f(R)$ model and stability of wormhole solutions graphically. The physical existence of wormhole solutions can be examined through null/weak energy conditions of perfect fluid and null energy condition of the effective energy–momentum tensor. The graphical interpretation of constructed wormhole solutions ensures the existence of physically viable and traversable wormholes for all models. It is concluded that the constructed wormholes are found to be stable in most of the cases.

1. Introduction

On the landscape of theoretical and observational modern cosmology, the most revolutionizing fact is believed to be the current cosmic accelerated expansion. Recent experiments indicate that this expansion must be due to some enigmatic force with astonishing anti-gravitational effects, known as dark energy. There are many proposals to explain its ambiguous nature. The $f(R)$ gravity is one of such proposals established by replacing geometric part of the Einstein–Hilbert action with this generic

* Corresponding author.
E-mail addresses: msharif.math@pu.edu.pk (M. Sharif), iqranawazish07@gmail.com (I. Nawazish).

1 Fellow, Pakistan Academy of Sciences, 3 Constitution Avenue, G-5/2, Islamabad.

https://doi.org/10.1016/j.aop.2017.12.012

function depending on the Ricci scalar R. The fourth order non-linear field equations of this gravity keep triggering researchers to evaluate exact solution.

The study of exact solutions under assorted scenarios is extensively used to explore different cosmic aspects that unveil sophisticated picture of cosmic evolution. Sharif and Shamir [1] constructed vacuum as well as non-vacuum exact solutions of Bianchi I and V universe models in $f(R)$ gravity and also investigated physical behavior of these solutions. Gutiérrez-Piñeres and López-Monsalvo [2] evaluated exact vacuum solution for static axially symmetric spacetime in the same gravity and found that solution corresponds to naked singularity. Sharif and Zubair [3] considered interaction of matter with geometry to formulate some exact solutions of Bianchi I model. Gao and Shen [4] found a new method to formulate exact solutions of static spherically symmetric metric. They also analyzed some general properties of solutions like event horizon, singularity and deficit angle in Jordan and Einstein frames.

Noether symmetry approach is considered to be the most appreciable technique which explores not only exact solutions but also evaluates conserved quantities relative to symmetry generators associated with dynamical system. Capozziello et al. [5] formulated exact solution of static spherically symmetric metric for $f(R)$ power-law model. The same authors [6] generalized this work for non-static spherically symmetric spacetime and also discussed possible solutions for axially symmetric model. Vakili [7] studied the scalar field scenario of flat FRW model through this approach and discussed current cosmic phase via effective equation of state parameter corresponding to quintessence phase. Momeni et al. [8] investigated the existence of Noether symmetry for isotropic universe model in mimetic $f(R)$ as well as $f(R,T)$ gravity theories (T denotes trace of energy–momentum tensor). Sharif and his collaborators [9] investigated cosmic evolution as well as current cosmic expansion through Noether symmetry approach.

Our universe always bring eye opening questions for cosmologists regrading its surprising and mysterious nature. The existence of hypothetical geometries is considered as the most debatable issue which leads to wormhole geometry. A wormhole (WH) structure is defined through a hypothetical bridge or tunnel which allows a smooth connection among different regions only if there exists exotic matter (matter with negative energy density). The existence of a physically viable WH is questioned due to the presence of enough amount of exotic matter. Consequently, there is only one way to have a realistic WH model, i.e., the presence of exotic matter must be minimized. Besides the existence of such astrophysical configurations, the most crucial problem is stability analysis which defines their behavior against perturbations as well as enhances physical characterization. A singularity-free configuration identifies a stable state which successfully prevents the WH to collapse while a WH can also exist for quite a long time even if it is unstable due to very slow decay. The evolution of unstable system can lead to many phenomena of interest from structure formation to supernova explosions. To explore WH existence, different approaches have been proposed such as modified theories of gravity, non-minimal curvature–matter coupling, scalar field models etc. [10].

The study of WH solutions has been of great interest in modified theories of gravity. Lobo and Oliveira [11] considered constant shape function and different fluids to explore WH solution in $f(R)$ gravity. Jamil et al. [12] formulated viable WH solutions for $f(R)$ power-law model and also considered particular shape function in the background of non-commutative geometry. Bahamonde et al. [13] constructed cosmological WH threaded by perfect fluid approaching to FRW universe in the same gravity. Mazharimousavi and Halilsoy [14] found a near-throat WH solution of $f(R)$ model admitting polynomial expansion and also satisfying necessary WH conditions for both vacuum as well as non-vacuum cases. Sharif and Fatima [15] discussed static spherically symmetric WH in galactic halo region as well as investigated non-static conformal WH in $f(\mathcal{G})$ gravity, ($\mathcal{G}$ represents Gauss–Bonnet term). Noether symmetry approach elegantly explores the WH geometry by formulating exact solutions. Bahamonde et al. [16] obtained exact solutions of red-shift as well as shape functions through this approach and analyzed their geometric behavior graphically in scalar-tensor theory incorporating non-minimal coupling with torsion scalar.

In this paper, we study WH geometry threaded by perfect fluid via Noether symmetry approach in $f(R)$ gravity. The format of the paper is as follows. Section 2 explores basic review of $f(R)$ gravity. In Section 3, we construct point-like Lagrangian which is used in Section 4 to evaluate WH solutions for both constant as well as variable red-shift functions. Section 5 investigates stability of the constructed WH solutions. In the last section, we present final remarks.

2. Basics of $f(R)$ gravity

We consider a minimally coupled action of $f(R)$ gravity given by

$$\mathcal{I} = \int d^4x\sqrt{-g}[\frac{f(R)}{2\kappa^2} + \mathcal{L}_m], \tag{1}$$

where g identifies determinant of the metric tensor $g_{\mu\nu}$, $f(R)$ describes a coupling-free function while $\mathcal{L}_m$ denotes Lagrangian density of matter. The metric variation of action (1) leads to

$$f_R R_{\mu\nu} - \frac{1}{2}f g_{\mu\nu} - \nabla_\mu\nabla_\nu f_R + g_{\mu\nu}\Box f_R = \kappa^2 T^{(m)}_{\mu\nu}, \quad T^{(m)}_{\mu\nu} = g_{\mu\nu}\mathcal{L}_m - 2\frac{\partial\mathcal{L}_m}{\partial g^{\mu\nu}}. \tag{2}$$

Here, f_R shows the derivative of generic function f with respect to R, ∇_μ represents covariant derivative, $\Box = \nabla_\mu\nabla^\mu$ and $T^{(m)}_{\mu\nu}$ denotes energy–momentum tensor. The equivalent form of Eq. (2) is

$$G_{\mu\nu} = \frac{1}{f_R}(T^{(m)}_{\mu\nu} + T^{(c)}_{\mu\nu}) = T^{eff}_{\mu\nu}, \tag{3}$$

where $G_{\mu\nu}$, $T^{(c)}_{\mu\nu}$ and $T^{eff}_{\mu\nu}$ identify Einstein, curvature and effective energy–momentum tensors, respectively. The curvature terms relative to generic function define $T^{(c)}_{\mu\nu}$ as

$$T^{(c)}_{\mu\nu} = \frac{f - Rf_R}{2}g_{\mu\nu} + \nabla_\mu\nabla_\nu f_R - \Box f_R g_{\mu\nu}. \tag{4}$$

The energy–momentum tensor corresponding to perfect fluid is

$$T^{(m)}_{\mu\nu} = (\rho_m(r) + p_m(r))u_\mu u_\nu + p_m(r)g_{\mu\nu},$$

where ρ_m and p_m characterize energy density and pressure, respectively whereas u_μ denotes four velocity of the fluid as $u_\mu = (-e^{\frac{a(r)}{2}}, 0, 0, 0)$.

The static spherically symmetric spacetime is [17]

$$ds^2 = -e^{a(r)}dt^2 + e^{b(r)}dr^2 + M(r)(d\theta^2 + \sin^2\theta d\phi^2), \tag{5}$$

where a, b and M are arbitrary functions depending on radial coordinate r. The geodesic deviation equation determines that $M(r) = r^2$, $\sin r$, $\sinh r$ for $\mathcal{K} = 0, 1, -1$ ($\mathcal{K}$ denotes curvature parameter) under the limiting behavior $M(r) \to 0$ as $r \to 0$, respectively [18]. In case of $M(r) = r^2$, the spherical symmetry defines Morris–Thorne WH where $a(r)$ is recognized as red-shift function identifying gravitational red-shift while $e^{b(r)}$ explores the geometry of WH for $e^b = \left(1 - \frac{h(r)}{r}\right)^{-1}$, $h(r)$ is known as shape function. In order to locate throat of a WH, radial coordinate must follow non-monotonic behavior such that it decreases from maximum to minimum value r_0 identifying WH throat at $h(r_0) = r_0$ and then it starts increasing from r_0 to infinity. To have a WH solution at throat, the condition $h'(r_0) < 1$ is imposed, where prime denotes derivative with respect to r. The flaring-out condition is the fundamental property of WH which demands $\frac{h(r)-h(r)'r}{h(r)^2} > 0$. For the existence of traversable WH, the surface should be free from horizons, the red-shift function must be finite everywhere and $1 - h(r)/r > 0$. To formulate the field equations for the action (1), we choose $\mathcal{L}_m = p_m(r)$ [19] and use Eqs. (2)–(5), it follows that

$$\begin{aligned}&\frac{e^a}{4e^bM^2}(-4M''M + 2b'M'M + M'^2 + 4Me^b) = \frac{1}{f_R}\left[\frac{e^{-b}(Rf_R - f)}{2}\right.\\&\left.- f_R'\left(\frac{a'e^a}{2e^b}\right) + e^{a-b}f_R'' + e^{a-b}f_R'\left(\frac{a'-b'}{2} + \frac{M'}{M}\right) + e^a\rho_m\right],\end{aligned} \tag{6}$$

$$\begin{aligned}&-\frac{1}{4M^2}(M'^2 + 2a'M'M - 4Me^b) = \frac{1}{f_R}\left[\frac{(f - Rf_R)}{2} - \frac{b'f_R'}{2} - f_R'\right.\\&\left.\times\ e^{a-b}f_R'\left(\frac{a'-b'}{2} + \frac{M'}{M}\right)\left(\frac{a'-b'}{2} + \frac{M'}{M}\right) + e^b p_m\right],\end{aligned} \tag{7}$$

$$\frac{1}{4Me^b}(M'M(a'-b')+2M''M+M^2a'^2-M^2a'b'-M'^2+2M^2a'')$$
$$=\frac{1}{f_R}\left[Mp_m+\frac{M'f_R'}{2e^bM}+\frac{M(Rf_R-f)}{2}-\frac{f_R''}{Me^b}-\frac{f_R'}{Me^b}\left(\frac{a'-b'}{2}+\frac{M'}{M}\right)\right].$$

The energy conditions provide a significant way to analyze physical existence of some cosmological geometries. For WH geometry, the violation of these conditions ensures the existence of a realistic WH. To define energy conditions, Raychaudhari equations are considered to be the most fundamental ingredients given as

$$\frac{d\theta}{d\tau}=-\frac{1}{3}\theta^2-\sigma_{\mu\nu}\sigma^{\mu\nu}+\Theta_{\mu\nu}\Theta^{\mu\nu}-R_{\mu\nu}l^\mu l^\nu, \tag{8}$$
$$\frac{d\theta}{d\tau}=-\frac{1}{2}\theta^2-\sigma_{\mu\nu}\sigma^{\mu\nu}+\Theta_{\mu\nu}\Theta^{\mu\nu}-R_{\mu\nu}k^\mu k^\nu, \tag{9}$$

where $\theta,\ l^\mu,\ k^\mu,\ \sigma$ and Θ represent expansion scalar, timelike vector, null vector, shear and rotation tensors. The first equation is defined for timelike congruence while the second is for null congruence. The positivity of the last term of both equations demands attractive gravity. For the Einstein–Hilbert action, these conditions split into null (NEC) ($\rho_m+p_m\geq 0$), weak (WEC) ($\rho_m\geq 0,\ \rho_m+p_m\geq 0$), strong (SEC) ($\rho_m+p_m\geq 0,\ \rho_m+3p_m\geq 0$) and dominant (DEC) ($\rho_m\geq 0,\ \rho_m\pm p_m\geq 0$) energy conditions [20]. As the Raychaudhari equations are found to be purely geometric implying that $T^{(m)}_{\mu\nu}k^\mu k^\nu\geq 0$ can be replaced with $T^{eff}_{\mu\nu}k^\mu k^\nu\geq 0$. Thus, the energy conditions in $f(R)$ gravity turn out to be [21]

$$\begin{aligned}
\textbf{NEC}: &\quad \rho_{eff}+p_{eff}\geq 0,\\
\textbf{WEC}: &\quad \rho_{eff}\geq 0,\quad \rho_{eff}+p_{eff}\geq 0,\\
\textbf{SEC}: &\quad \rho_{eff}+p_{eff}\geq 0,\quad \rho_{eff}+3p_{eff}\geq 0,\\
\textbf{DEC}: &\quad \rho_{eff}\geq 0,\quad \rho_{eff}\pm p_{eff}\geq 0.
\end{aligned}$$

Solving Eqs. (6) and (7), we obtain

$$p_m=-\frac{f}{2}+e^{-b}f_R'\left(\frac{a'}{2}+\frac{M'}{M}\right)-\frac{f_R}{4e^bM^2}\left(2M'^2-4M''M-a'^2M^2\right.$$
$$\left.+\ a'b'M^2+2b'M'M-2M^2a''\right), \tag{10}$$
$$\rho_m=\frac{f_R}{4e^bM^2}\left(M^2a'^2-M^2a'b'+2a'M'M+2M^2a''\right)+e^{-b}f_R''+e^{-b}f_R'$$
$$\times\left(\frac{-b'}{2}+\frac{M'}{M}\right)+\frac{f}{2}. \tag{11}$$

In $f(R)$ gravity, NEC relative to the effective energy–momentum tensor for (5) yields

$$\rho_{eff}+p_{eff}=\frac{1}{2e^b}\left(\frac{M'^2}{M^2}+\frac{a'M'}{M}+\frac{b'M'}{M}-\frac{2M''}{M}\right). \tag{12}$$

3. Point-like Lagrangian

In this section, we construct point-like Lagrangian corresponding to the action (1) via Lagrange multiplier approach. In this regard, we consider following form of gravitational action [22]

$$\mathcal{I}=\int\sqrt{-g}[f(R)-\lambda(R-\bar{R})]dr, \tag{13}$$

where

$$\sqrt{-g}=e^{\frac{a}{2}}e^{\frac{b}{2}}M,\quad \lambda=f_R, \tag{14}$$
$$\bar{R}=\frac{1}{e^b}\left(-\frac{a'^2}{2}+\frac{a'b'}{2}-\frac{a'M'}{M}-\frac{2M''}{M}+\frac{b'M'}{M}+\frac{M'^2}{2M^2}-a''+\frac{2e^b}{M}\right).$$

The dynamical constraint λ is obtained by varying the action (13) with respect to R. In order to determine p_m, we consider Bianchi identity ($\nabla_\mu T^{\mu\nu}$) whose radial component gives

$$\frac{dp_m}{dr}+\frac{a'(r)}{2}(p_m+\rho_m)=0. \tag{15}$$

Solving this differential equation with $p_m=\omega\rho_m$, it follows that

$$\rho_m=\rho_0 a^{-\frac{(1+\omega)}{2\omega}},\quad p_m=\omega\rho_m=\omega\rho_0 a^{-\frac{(1+\omega)}{2\omega}}, \tag{16}$$

where ω represents equation of state parameter. Inserting Eqs. (14) and (16) in (13), we obtain

$$\begin{aligned}\mathcal{I}=\int e^{\frac{a-b}{2}}M\Big[f(R)-Rf_R+\frac{f_R}{e^b}\Big(-\frac{a'^2}{2}+\frac{a'b'}{2}-\frac{a'M'}{M}-\frac{2M''}{M}+\frac{b'M'}{M}\\+\frac{M'^2}{2M^2}-a''+\frac{2e^b}{M}\Big)+\omega\rho_0 a^{-\frac{(1+\omega)}{2\omega}}\Big]dr.\end{aligned} \tag{17}$$

Eliminating second order derivatives via integration by parts from the above action and following Lagrangian density definition, we obtain point-like Lagrangian as

$$\begin{aligned}\mathcal{L}(r,a,b,M,R,a',b',M',R')=e^{\frac{a}{2}}e^{\frac{b}{2}}M\left(f-Rf_R+\omega\rho_0 a^{-\frac{(1+\omega)}{2\omega}}+\frac{2f_R}{M}\right)\\+\frac{e^{\frac{a}{2}}M}{e^{\frac{b}{2}}}\left\{f_R\left(\frac{M'^2}{2M^2}+\frac{a'M'}{M}\right)+f_{RR}\left(a'R'+\frac{2M'R'}{M}\right)\right\}.\end{aligned} \tag{18}$$

For static spherically symmetric spacetime, the Euler–Lagrange equation and Hamiltonian of the dynamical system or energy function associated with point-like Lagrangian are defined as

$$\frac{\partial\mathcal{L}}{\partial q^i}-\frac{dp_i}{dr}=0,\quad \mathcal{H}=\sum_i q'^i p_i-\mathcal{L},$$

where q^i are generalized coordinates and $p_i=\frac{\partial\mathcal{L}}{\partial q'^i}$ represents conjugate momenta. The variation of Lagrangian with respect to configuration space leads to

$$\begin{aligned}&e^b\left(f-Rf_R+\omega\rho_0 a^{-\frac{(1+\omega)}{2\omega}}-(1+\omega)\rho_0 a^{-\frac{(1+3\omega)}{2\omega}}+\frac{2f_R}{M}\right)+\left(\frac{M'^2}{2M^2}+\frac{b'M'}{M}\right.\\&\left.-\frac{2M''}{M}\right)f_R+f_{RR}\left(b'R'-2R''-\frac{2M'R'}{M}\right)-2R'^2f_{RRR}=0,\\&e^b\left(f-Rf_R+\omega\rho_0 a^{-\frac{(1+\omega)}{2\omega}}+\frac{2f_R}{M}\right)-f_R\left(\frac{M'^2}{2M^2}+\frac{a'M'}{M}\right)-f_{RR}\left(a'R'\right.\\&\left.+\frac{2M'R'}{M}\right)=0,\\&e^b\left(f-Rf_R+\omega\rho_0 a^{-\frac{(1+\omega)}{2\omega}}+\frac{2f_R}{M}\right)+f_R\left(-\frac{a'^2}{2}+\frac{a'b'}{2}-\frac{a'M'}{2M}-\frac{M''}{M}-a''\right.\\&\left.+\frac{b'M'}{2M}+\frac{M'^2}{2M^2}\right)+f_{RR}\left(b'R'-a'R'-2R''-\frac{M'R'}{M}\right)-2R'^2f_{RRR}=0,\\&\left[e^b\left(\frac{2}{M}-R\right)-\frac{a'^2}{2}+\frac{a'b'}{2}-\frac{a'M'}{M}-\frac{2M''}{M}+\frac{b'M'}{M}+\frac{M'^2}{2M^2}-a''\right]f_{RR}=0.\end{aligned}$$

The energy function and variation of Lagrangian relative to shape function yield

$$e^b=\frac{\frac{f_RM'}{M}\left(\frac{M'}{2M^2}+a'M'\right)+R'f_{RR}(a'M+2M')}{f-Rf_R+\omega\rho_0 a^{-\frac{(1+\omega)}{2\omega}}+\frac{2f_R}{M}}. \tag{19}$$

4. Noether symmetry approach

The physical characteristics of a dynamical system can be identified by constructing the associated Lagrangian which successfully describes energy content and the existence of possible symmetries of the system. In this regard, Noether symmetry approach provides an interesting way to construct new cosmological models and geometries in modified theories of gravity. According to well-known Noether theorem, group generator yields associated conserved quantity if point-like Lagrangian remains invariant under a continuous group. In order to investigate the presence of Noether symmetry and relative conserved quantity of static spherically symmetric metric, we consider a vector field [23]

$$K=\tau(r,q^i)\frac{\partial}{\partial r}+\zeta^i(r,q^i)\frac{\partial}{\partial q^i}, \tag{20}$$

where r behaves as an affine parameter while τ and ζ^i are unknown coefficients of the vector field K.

The presence of Noether symmetry is assured only if point-like Lagrangian satisfies the invariance condition and the vector field is found to be unique on tangent space. Consequently, the vector field acts as a symmetry generator generating associated conserved quantity. In this case, the invariance condition is defined as

$$K^{[1]}\mathcal{L}+(D\tau)\mathcal{L}=DB(r,q^i), \tag{21}$$

where B denotes boundary term of the extended symmetry, $K^{[1]}$ describes first order prolongation and D represents total derivative given by

$$K^{[1]}=K+(D\zeta^i-q'^iD\tau)\frac{\partial}{\partial q'^i},\quad D=\frac{\partial}{\partial r}+q'^i\frac{\partial}{\partial q^i}. \tag{22}$$

Noether symmetries coming from invariance condition (21) lead to identify associated conserved quantities through first integral. If the Lagrangian remains invariant under translation in time and position, then the first integral identifies energy and linear momentum conservation while rotationally symmetric Lagrangian yields conservation of angular momentum [24]. For invariance condition (21), the first integral is defined as

$$\Sigma=B-\tau\mathcal{L}-(\zeta^i-q'^i\tau)\frac{\partial\mathcal{L}}{\partial q'^i}. \tag{23}$$

For configuration space $Q=\{a,b,M,R\}$, the vector field K and first order prolongation $K^{[1]}$ take the following form

$$K=\tau\frac{\partial}{\partial r}+\alpha\frac{\partial}{\partial a}+\beta\frac{\partial}{\partial b}+\gamma\frac{\partial}{\partial M}+\delta\frac{\partial}{\partial R},\quad K^{[1]}=\tau\frac{\partial}{\partial r}+\alpha\frac{\partial}{\partial a}+\beta\frac{\partial}{\partial b}$$
$$+\gamma\frac{\partial}{\partial M}+\delta\frac{\partial}{\partial R}+\alpha'\frac{\partial}{\partial a'}+\beta'\frac{\partial}{\partial b'}+\gamma'\frac{\partial}{\partial M'}+\delta'\frac{\partial}{\partial R'}, \tag{24}$$

where the radial derivative of unknown coefficients of vector field are defined as

$$\sigma'_j=D\sigma_j-q'^iD\tau,\quad j=1,\ldots,4. \tag{25}$$

Here $\sigma_1,\ \sigma_2,\ \sigma_3$ and σ_4 correspond to $\alpha,\ \beta,\ \gamma$ and δ, respectively. Inserting Eqs. (18), (24) and (25) in (21) and comparing the coefficients of $a'^2,\ a'b'M',\ a'M'^2$ and $a'R'^2$, we obtain

$$\tau_{,a}f_R=0,\quad \tau_{,b}f_R=0,\quad \tau_{,M}f_R=0,\quad \tau_{,R}f_{RR}=0. \tag{26}$$

This equation implies that either $f_R=0$ or vice verse. The first choice leads to trivial solution. Therefore, we consider $f_R\neq 0$ and compare the remaining coefficients which yield the following system of equations

$$B_{,b}=0,\quad \tau_{,a}=0,\quad \tau_{,b}=0,\quad \tau_{,M}=0,\quad \tau_{,R}=0, \tag{27}$$

$$e^{\frac{a}{2}}(\gamma_{,r}f_R+M\delta_{,r}f_{RR})=e^{\frac{b}{2}}B_{,a}, \tag{28}$$

$$e^{\frac{a}{2}}(\alpha,_r M+2\gamma,_r)f_{RR}=e^{\frac{b}{2}}B,_R, \tag{29}$$

$$e^{\frac{a}{2}}(\alpha,_r f_R+\gamma,_r M^{-1}f_R+2\delta,_r f_{RR})=e^{\frac{b}{2}}B,_M, \tag{30}$$

$$\gamma,_a f_R+M\delta,_a f_{RR}=0, \tag{31}$$

$$\gamma,_a f_R+M\delta,_a f_{RR}=0, \tag{32}$$

$$\alpha,_b f_R+\gamma,_b M^{-1}f_R+2\delta,_b f_{RR}=0, \tag{33}$$

$$M\alpha,_b f_{RR}+2\gamma,_b f_{RR}=0, \tag{34}$$

$$M\alpha,_R f_{RR}+2\gamma,_R f_{RR}=0, \tag{35}$$

$$f_R(\alpha-\beta-2\gamma M^{-1}+4M\alpha,_M+4\gamma,_M-2\tau,_r)+f_{RR}(2\delta+8M\delta,_M)=0, \tag{36}$$

$$f_R(\alpha-\beta+2\alpha,_a-2\tau,_r+2\gamma,_M+2\gamma,_a)+f_{RR}(2\delta+2M\delta,_M+4\delta,_a)=0, \tag{37}$$

$$f_R(\alpha,_R+\gamma,_R M^{-1})+f_{RR}(\alpha-\beta+M\alpha,_M+2\gamma,_M-2\tau,_r+2\delta,_R)+2\delta \times f_{RRR}=0, \tag{38}$$

$$2\gamma,_R f_R+f_{RR}(M\alpha-M\beta+2\gamma+2M\alpha,_a-2M\tau,_r+4\gamma,_a+2M\delta,_R)+2M \times\delta f_{RRR}=0, \tag{39}$$

$$e^{\frac{a}{2}}e^{\frac{b}{2}}M\{\frac{1}{2}(f-Rf_R+\omega\rho_0 a^{-\frac{(1+\omega)}{2\omega}}+\frac{2f_R}{M})(\alpha+\beta+\tau,_r)-\frac{1}{2}\alpha(1+\omega)\rho_0 \times a^{-\frac{(1+3\omega)}{2\omega}}+\delta M(2M^{-1}-R)f_{RR}\}+e^{\frac{a}{2}}e^{-\frac{b}{2}}\gamma(f-Rf_R+\omega\rho_0 a^{-\frac{(1+\omega)}{2\omega}}) =B,_r. \tag{40}$$

In order to solve this system, we consider $M(r)=r^2$ and taking $B,_a,\ B,_M,\ B,_R=0$, Eqs. (27)–(35) give

$$\alpha=Y_2(a,r),\quad \gamma=Y_1(r),\quad \delta=Y_3(r,R).$$

Inserting these values in Eqs. (36)–(39), we obtain

$$Y_1(r)=0,\quad Y_2(a,r)=c_2,\quad Y_3(r,R)=\frac{c_1f_R}{f_{RR}},\quad \beta=2c_1+c_2-2\tau,_r,$$

where c_1 and c_2 are arbitrary constants. For these solutions, the coefficients of symmetry generator turn out to be

$$\alpha=c_2,\quad \beta=2c_1+c_2,\quad \gamma=0,\quad \delta=\frac{c_1f_R}{f_{RR}},\quad \tau=c_0. \tag{41}$$

Substituting these coefficients in Eq. (40), we formulate boundary term and explicit form of $f(R)$ as follows

$$f(R)=-\frac{1}{2(c_1+c_2)}\Big[-(1+\omega)\rho_0 a^{-\frac{(1+3\omega)}{2\omega}}+2\omega(c_1+c_2)\rho_0 a^{-\frac{(1+\omega)}{2\omega}} - 6c_4e^{\frac{-a-b}{2}}\Big],\quad B=c_3+c_4r^3.$$

The coefficients of symmetry generator, boundary term and solution of $f(R)$ satisfy the system of Eqs. (27)–(39) for $c_1=0$. Thus, the symmetry generator and the corresponding first integral take the form

$$K=c_0\frac{\partial}{\partial r}+c_2\frac{\partial}{\partial a}+c_2\frac{\partial}{\partial b},$$

$$\Sigma=c_3+c_4r^3-c_0\Big[e^{\frac{a}{2}}e^{\frac{b}{2}}r^2(f-Rf_R+\omega\rho_0 a^{-\frac{(1+\omega)}{2\omega}}+2f_Rr^{-2})$$

$$+ \frac{e^{\frac{a}{2}}r^2}{e^{\frac{b}{2}}}\{f_R(2r^{-2}+2a'r^{-1})+f_{RR}(a'R'+4R'r^{-1})\}\Bigg] - c_2e^{\frac{a-b}{2}}(R'r^2f_{RR}+2rf_R).$$

The verification of Eq. (40) yields

$$b(r)=\int\frac{8c_6r^2+a''r^2+4a'r'+a'^2r^2-4c_7}{r(4+a'r)}dr+c_5, \tag{42}$$

where c_i's ($i = 3, \ldots, 8$) are arbitrary constants and this solution satisfies Eq. (40) for $\omega = 1, 1/3, -1/3, -1$. To discuss physical features and geometry of WH via shape function, we take red-shift function, $a(r)=k$ and $a(r)=-\frac{k}{r},\ k>0$, where k denotes constant [25]. In the following, we solve integral for both choices of red-shift function.

Case I: $a(r)=k$

We first consider red-shift function to be constant and evaluate $b(r)$ such as

$$b(r)=c_6r^2-c_7\ln r+c_5. \tag{43}$$

Consequently, the shape function turns out to be

$$h(r)=r(1-e^{-b(r)})=r(1-c_7re^{-c_6r^2-c_5}). \tag{44}$$

In this case, the explicit form of $f(R)$ reduces to

$$f(R)=-\frac{1}{2c_2}\left[-(1+\omega)\rho_0k^{-\frac{(1+3\omega)}{2\omega}}+2\omega c_2\rho_0k^{-\frac{(1+\omega)}{2\omega}}-6c_4\sqrt{c_7r}e^{\frac{-c_6r^2-c_5-k}{2}}\right]. \tag{45}$$

The $f(R)$ theory of gravity is one of the competitive candidates in modified theories of gravity as it naturally unifies two expansion phases of the universe, i.e., inflation at early times and cosmic acceleration at current epoch. The higher derivative of curvature terms with positive power are dominant at the early universe leading to the inflationary stage. The terms with negative power of the curvature serve as gravitational alternative for the dark energy that acts as a possible source to speed-up cosmic expansion [26]. Despite the fact that the ghost-free $f(R)$ theory is very interesting and useful as it passes solar system tests, it also suffers from instabilities. For instance, the theory with $\frac{1}{R}$ may develop the instability [27] whereas by adding a term of R^2 to this specific form of $f(R)$ model, one can easily eliminate this instability [28]. Therefore, the viable $f(R)$ models require to satisfy the following stability constraints $f_R(R)>0,\ f_{RR}(R)>0,\ R>R_0$ where R_0 is the current Ricci scalar [29].

In Fig. 1, both plots indicate that the constructed $f(R)$ model (45) preserves the stability conditions. Fig. 2 shows the graphical analysis of shape function. The upper left plot represents positive behavior of $h(r)$ while the upper right indicates that the shape function admits asymptotic behavior. The lower left plot locates the WH throat at $r_0 = 4.4$ and the corresponding right plot identifies that $\frac{dh(r_0)}{dr}=0.9427<1$. To discuss physical existence of WH, we insert constant red-shift function and Eq. (43) in (12) yielding

$$\rho_{eff}+p_{eff}=\frac{rh'(r)-h(r)}{r^3}<0,$$

which satisfies the flaring-out condition. Consequently, NEC violates in this case, $\rho_{eff}+p_{eff}<0$ and assures the presence of repulsive gravity leading to traversable WH. In order to study the realistic existence of traversable WH, we analyze the behavior of NEC and WEC in Fig. 3. Both plots indicate that energy density and pressure recover energy bounds as $\rho_m\geq 0$ and $\rho_m+p_m\geq 0$ implying physically acceptable traversable WH.

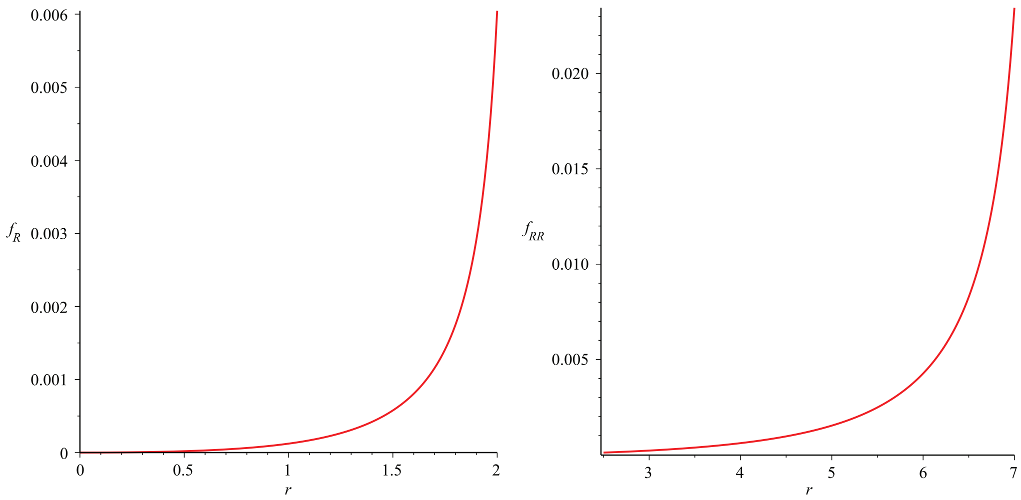

Fig. 1. Plots of stability conditions of $f(R)$ model versus r for $c_2 = 5$, $c_4 = 0.01$, $c_5 = -0.35$, $c_6 = 0.1$, $c_7 = -0.25$, $\rho_0 = 1$ and $k = 0.5$.

Case II: $a(r) = -k/r$

In this case, we choose red-shift function in terms of r leading to

$$a(r) = -\frac{k}{r}, \quad b(r) = \frac{1}{8r}(4c_6 r^2(2r-k) - 32c_8 r \ln r + (32r - 8c_7 r + c_6 k r^2) \times \ln(4r+k) - 8k/c_8) + c_5, \quad k > 0. \tag{46}$$

For this solution of $a(r)$ and $b(r)$, the generic function takes the form

$$f(R) = -\frac{1}{2c_2}\left[-(1+\omega)\rho_0\left(-\frac{k}{r}\right)^{-\frac{(1+3\omega)}{2\omega}} + 2\omega c_2 \rho_0 \left(-\frac{k}{r}\right)^{-\frac{(1+\omega)}{2\omega}} - 6c_4 \times \sqrt{c_8 r^4 (4r+k)^{-4+c_7-\frac{k^2 c_6}{8}}}\, e^{\frac{-(c_6 r^2 - \frac{c_6 k r}{2} - \frac{k}{c_8 r}) - c_5 + k}{2}}\right]. \tag{47}$$

The corresponding shape function becomes

$$h(r) = r(1 - c_8 r^4 (4r+k)^{-4+c_7-\frac{k^2 c_6}{8}} e^{-(c_6 r^2 - \frac{c_6 k r}{2} - \frac{k}{c_8 r}) - c_5}). \tag{48}$$

Fig. 4 shows that the model (47) follows the stability condition for $0 < \omega < -0.08$ whereas Fig. 5 represents the graphical behavior of the shape function. In upper face, the left plot preserves the positivity of $h(r)$ while the right plot ensures asymptotic flat geometry of WH. In lower face, the left plot detects WH throat at $r_0 = 5.878$ whereas the right plot indicates that $\frac{dh(r_0)}{dr} = 0.1673 < 1$. For Eqs. (12) and (46), we obtain

$$\rho_{eff} + p_{eff} = \frac{k}{r^2(r - h(r))} + \frac{rh'(r) - h(r)}{r^3}.$$

To investigate the presence of realistic traversable WH, we establish the graphical behavior of NEC and WEC corresponding to perfect fluid as well as NEC relative to effective energy–momentum tensor. Fig. 6 indicates that $\rho_m + p_m \geq 0$, $\rho_m \geq 0$ and $\rho_{eff} + p_{eff} < 0$ for $1 < \omega < -1$. Thus, the physical existence of WH is assured in this case.

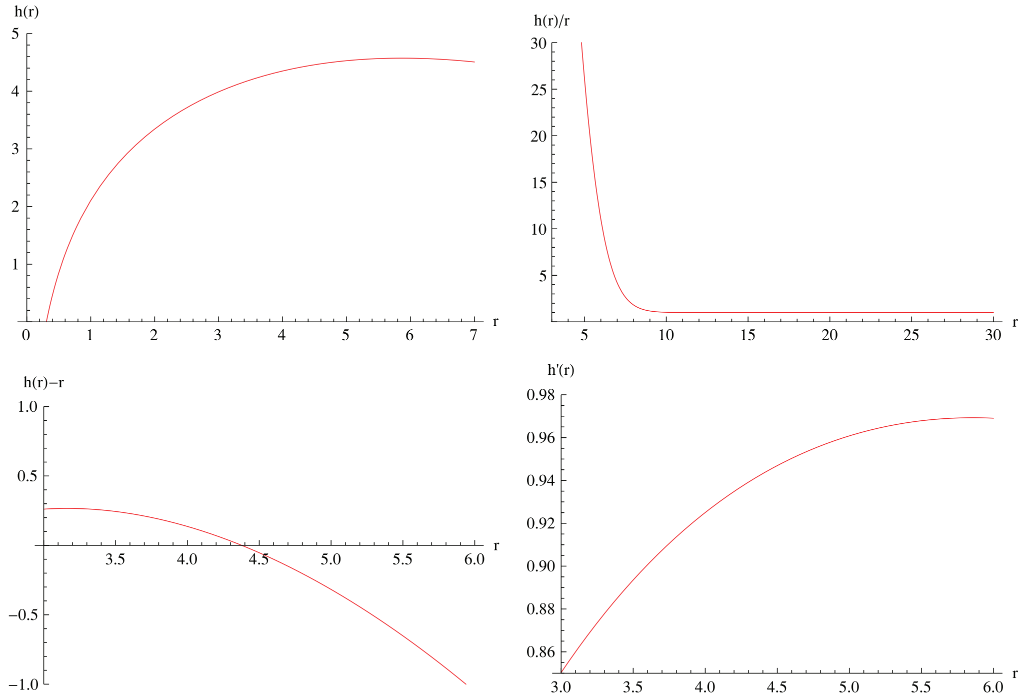

Fig. 2. Plots of $h(r)$, $\frac{h(r)}{r}$, $h(r)-r$ and $\frac{dh(r)}{dr}$ versus r for $c_5=-0.35$, $c_6=0.1$ and $c_7=-0.25$.

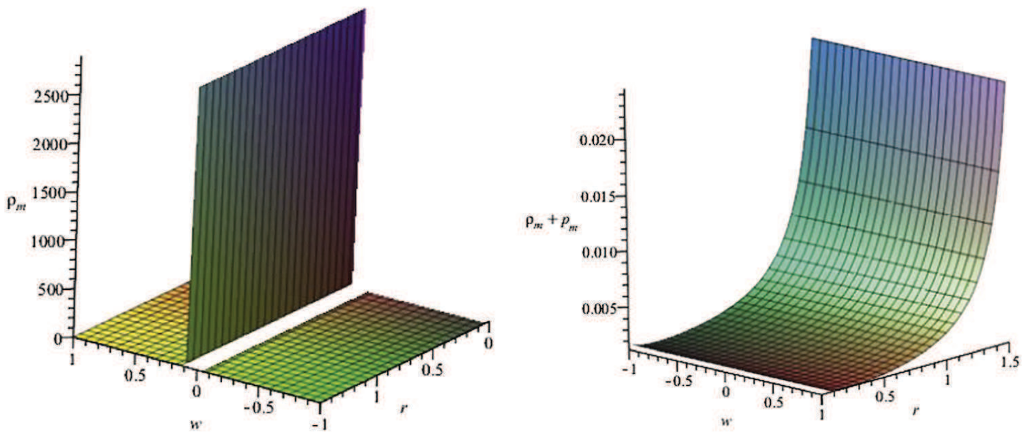

Fig. 3. Plots of ρ_m and ρ_m+p_m versus r.

4.1. Power-law $f(R)$ model

Here, we construct a WH solution with symmetry generator and corresponding conserved quantity for $f(R)$ power-law model, i.e., $f(R)=f_0R^n,\ n\neq 0,\ 1$. For this purpose, we solve Eqs. (27)–(35) leading to

$$\alpha=Y_3(a,r),\quad \gamma=Y_1(r),\quad \delta=Y_2(r,R).$$

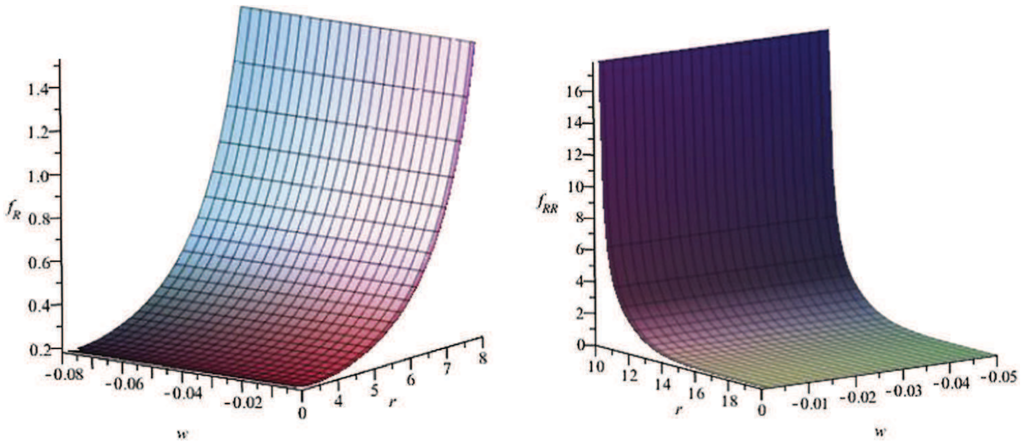

Fig. 4. Stability conditions of $f(R)$ versus r for $c_2 = 5, c_4 = 0.01, c_5 = -0.35, c_6 = 0.1, c_7 = -0.25$ and $k = 0.5$.

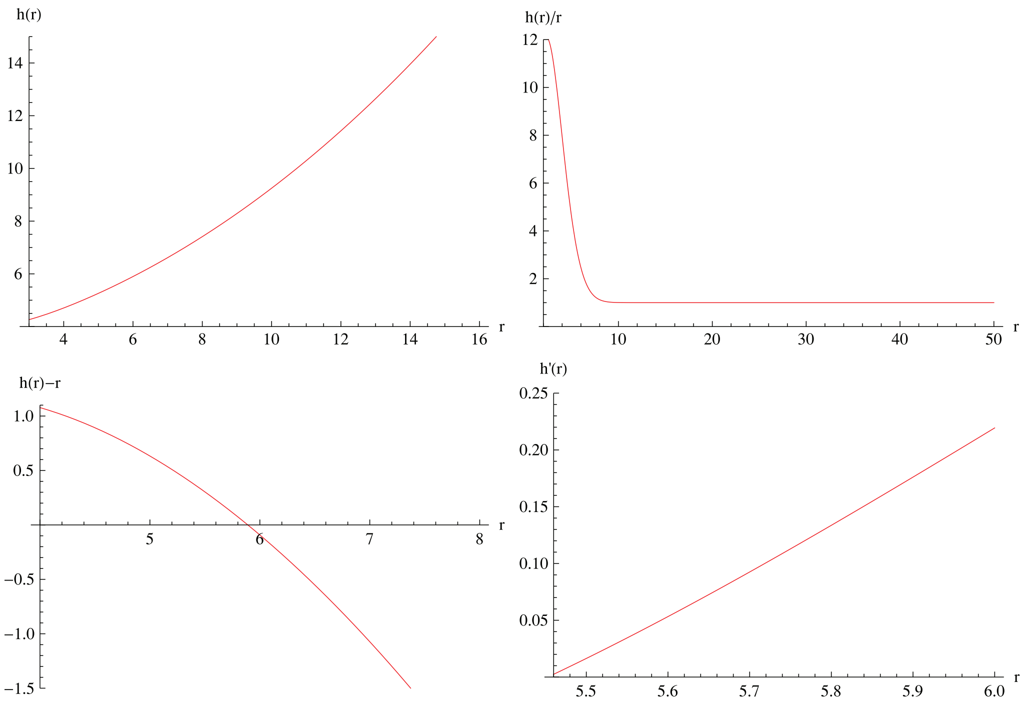

Fig. 5. Plots of $h(r)$, $\frac{h(r)}{r}$, $h(r) - r$ and $\frac{dh(r)}{dr}$ versus r for $c_5 = -4, c_6 = 0.1, c_8 = -1$ and $k = 0.25$.

Inserting this solution into Eqs. (36)–(39), we obtain

$$Y_1(r) = 0, \quad Y_3(a, r) = d_2, \quad Y_2(r, R) = d_1 R, \quad \beta = 2(n-1)d_1 + d_2 - 2\tau,_r,$$

where d_1 and d_2 represent arbitrary constants. For these values, the coefficients of symmetry generator turn out to be

$$\alpha = d_2, \quad \beta = 2(n-1)d_1 + d_2 - 2\tau,_r, \quad \gamma = 0, \quad \delta = d_1 R. \tag{49}$$

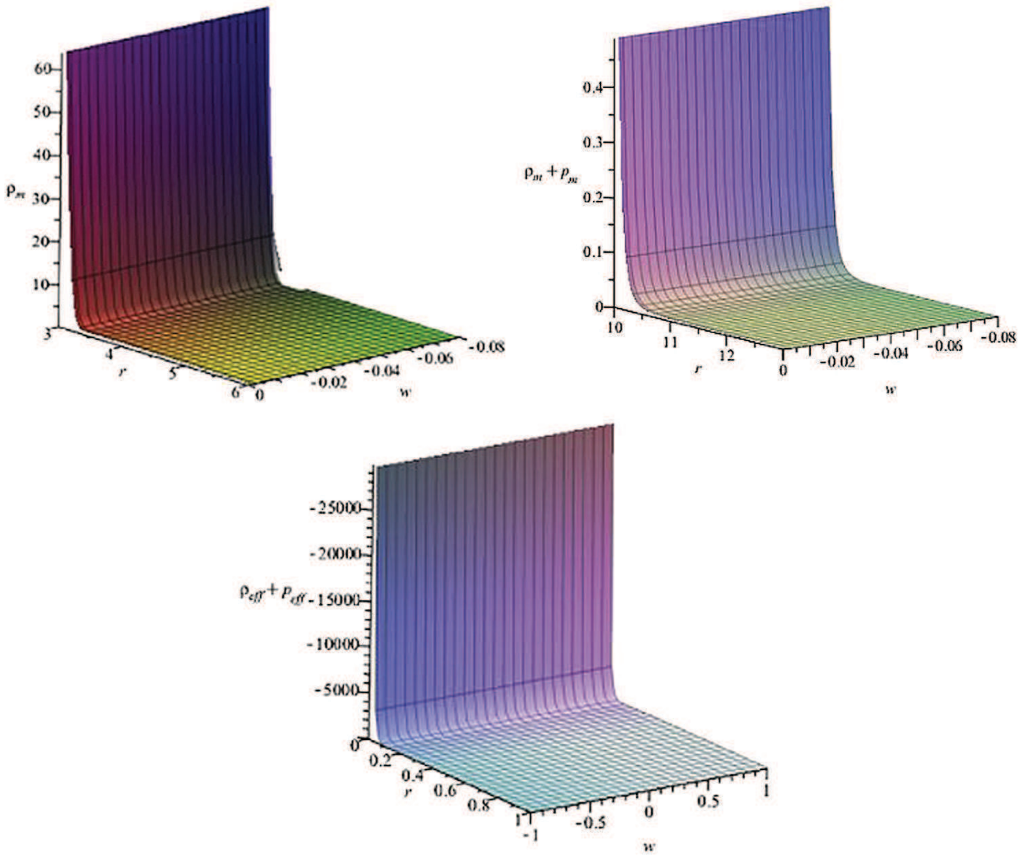

Fig. 6. Plots of ρ_m, $\rho_m + p_m$ and $\rho_{eff} + p_{eff}$ versus r.

Substituting these coefficients in Eq. (40) and assuming $B = d_0$ and $\tau = \tau_0$, it follows that

$$\begin{aligned} b(r) =& \int \frac{8d_3r^2 + 2a''r^2 + 4a'r' + a'^2r^2 - 4d_4}{r(4+a'r)} dr \\ &- \ln\left[-d_1 + 4\int \frac{e^{\int \frac{8r^2+2a''r^2+4a'r'+a'^2r^2-4}{r(4+a'r)}dr}}{r(4+a'r)} dr\right]. \end{aligned} \tag{50}$$

The resulting coefficients of symmetry generator verify the system (27)–(39) for $d_2 = -2(n-1)d_1$. Under this condition, the symmetry generator and associated first integral take the form

$$\begin{aligned} K =& \tau_0\frac{\partial}{\partial r} - 2(n-1)d_1\frac{\partial}{\partial a} + d_1\frac{\partial}{\partial R}, \\ \Sigma =& d_0 - \tau_0\left[e^{\frac{a}{2}}e^{\frac{b}{2}}r^2(f - Rf_R + \omega\rho_0 a^{-\frac{(1+\omega)}{2\omega}} + 2f_R r^{-2}) + \frac{e^{\frac{a}{2}}r^2}{e^{\frac{b}{2}}}\right. \\ &\left.\times\ \{f_R(2r^{-2} + 2a'r^{-1}) + f_{RR}(a'R' + 4R'r^{-1})\}\right] - 2d_1(1-n)e^{\frac{a-b}{2}}(R'r^2 \\ &\times\ f_{RR} + 2rf_R) - d_1Rf_{RR}e^{\frac{a-b}{2}}(a'r^2 + 4r). \end{aligned}$$

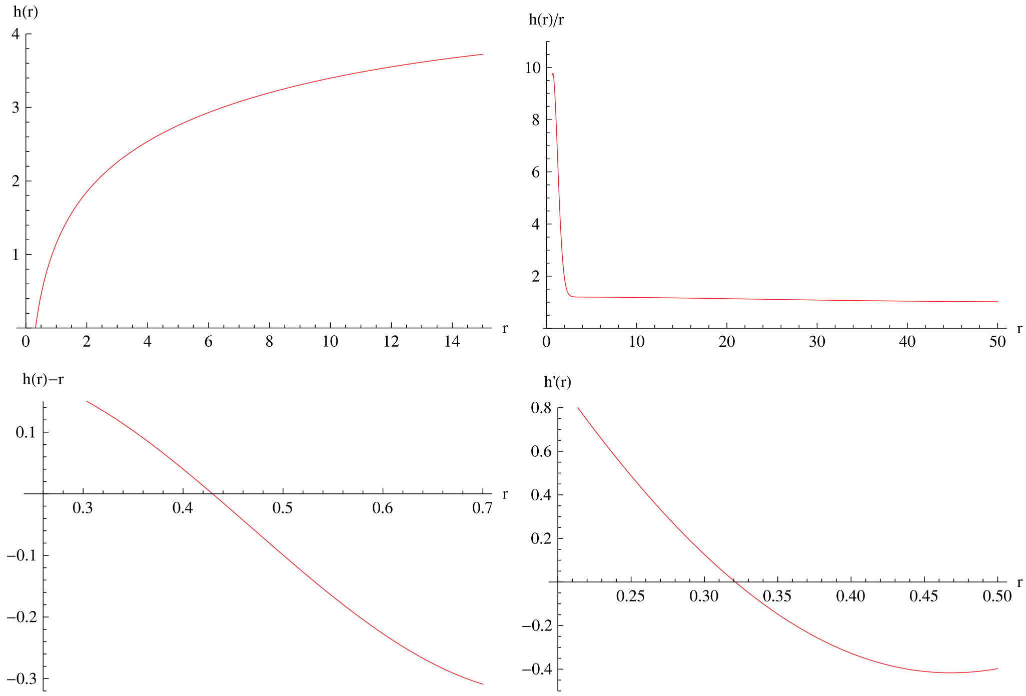

Fig. 7. Plots of $h(r)$, $\frac{h(r)}{r}$, $h(r)-r$ and $\frac{dh(r)}{dr}$ versus r for $d_2 = 16$, $d_3 = 1.001$, $d_4 = -0.2$ and $n = \frac{1}{2}$.

Now, we solve the integral (50) for constant and variable forms of red-shift function and study WH geometry via shape function.

Case I: $a(r) = k$

For constant red-shift function, the integral (50) reduces to

$$b(r) = d_3 r^2 - d_4 \ln r - \ln\left(\frac{-d_1 r + e^{r^2}}{r}\right). \tag{51}$$

This satisfies Eq. (40) for $\omega = 1, \frac{1}{3}, -\frac{1}{3}, -1$ and

$$\rho_0 = -\frac{f_o e^{\frac{3\omega \ln d_1 + 4n\omega \ln 2 + \ln d_1}{2\omega}}}{\omega d_1 - (1+\omega)}, \quad \omega \neq 0. \tag{52}$$

In this case, the shape function yields

$$h(r) = r\left[1 - d_4 r\left(\frac{-d_1 r + e^{r^2}}{r}\right) e^{-d_3 r^2}\right]. \tag{53}$$

We analyze WH geometry via shape function for $n = \frac{1}{2}$, 2 and $n = 4$. In upper face, the left and right plots of Fig. 7 show that $h(r)$ remains positive and asymptotic flat for $n = \frac{1}{2}$. The lower left plot identifies WH throat at $r_0 = 5.101$ and right plot satisfies the condition, i.e., $h'(r_0) = 0.17 < 1$. In Figs. 8 and 9, the shape function preserves its positivity condition and also admits asymptotic flat geometry for both $n = 2$ and $n = 4$. The WH throat is located at $r_0 = 0.23$ and $r_0 = 2.052$ for $n = 2$ and $n = 4$, respectively. The derivative condition is also satisfied at throat, i.e., $h'(r_0) = 0.89 < 1$ and $h'(r_0) = -0.49 < 1$. The NEC relative to effective energy–momentum tensor verifies $\rho_{eff} + p_{eff} < 0$

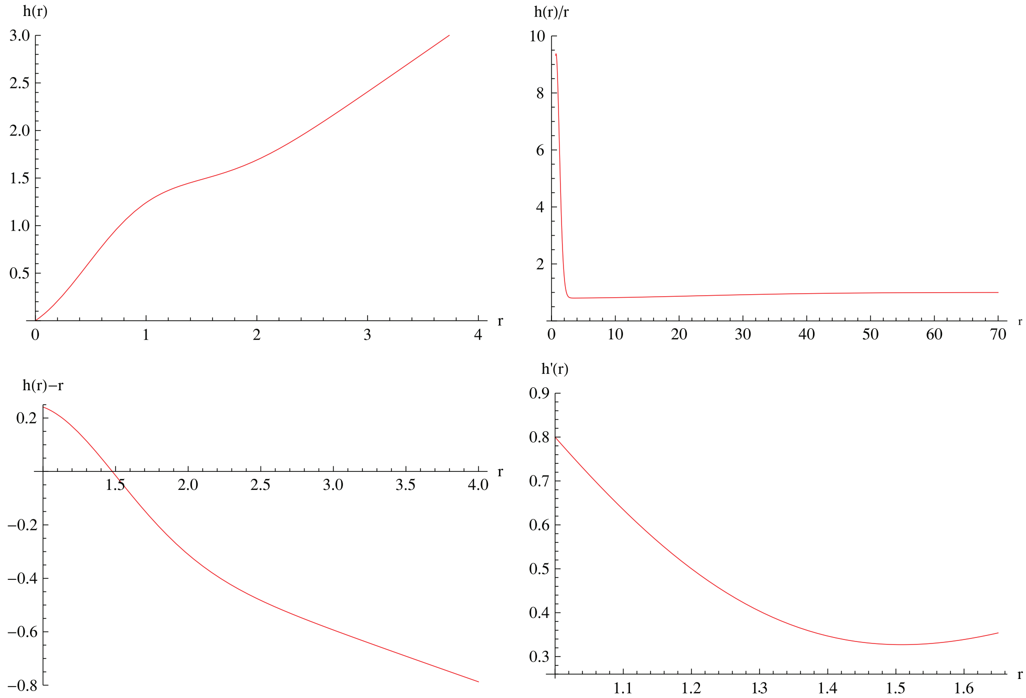

Fig. 8. Plots of $h(r)$, $\frac{h(r)}{r}$, $h(r) - r$ and $\frac{dh(r)}{dr}$ versus r for $d_2 = -200$, $d_3 = 1.001$, $d_4 = 0.2$ and $n = 2$.

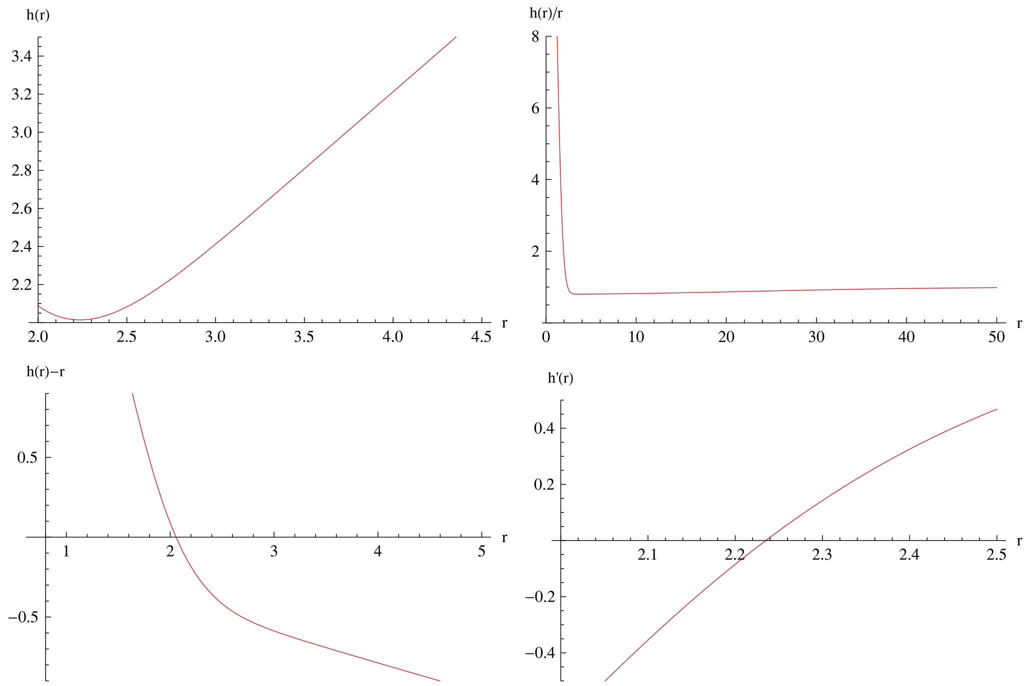

Fig. 9. Plots of $h(r)$, $\frac{h(r)}{r}$, $h(r) - r$ and $\frac{dh(r)}{dr}$ versus r for $d_2 = -200$, $d_3 = 1.001$, $d_4 = 0.2$ and $n = 4$.

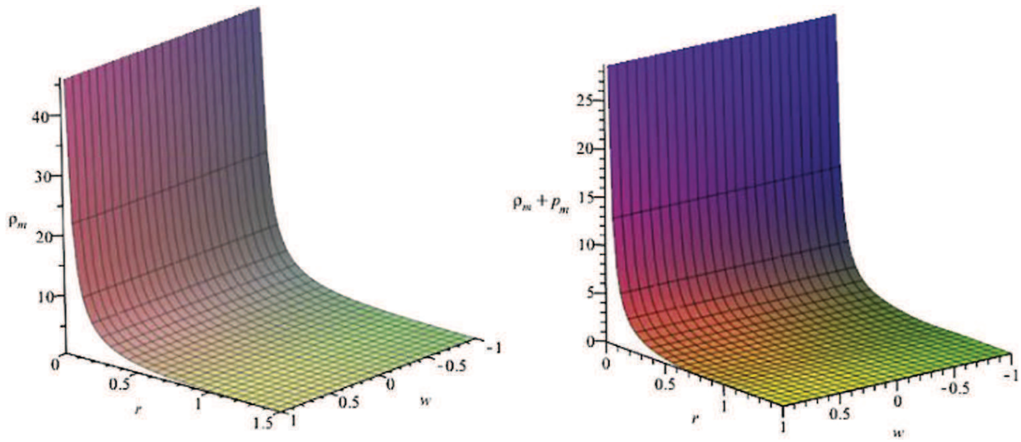

Fig. 10. Plots of ρ_m and $\rho_m + p_m$ versus r for $n = 0.5$.

while Fig. 10 identifies $\rho_m \geq 0$ and $\rho_m + p_m \geq 0$ for $n = 0.5$. In case of $n = 2$ and $n = 4$, the energy density and pressure corresponding to perfect fluid evolve in the same way.

Case II: $a(r) = -k/r$

Here we consider red-shift function to be r-dependent and solve the integral (50) implying that

$$\begin{aligned} b(r) &= r^2 - \frac{rd_1(1-n)}{2} + \frac{d_1^2(1-n)^2 \ln(d_1(1-n)+4r)}{8} + (d_1(1-n))^2 \\ &\times \left\{ -\frac{1}{rd_1(1-n)} + \frac{4\ln(d_1(1-n)+4r)}{(d_1(1-n))^2} - \frac{4\ln r}{(d_1(1-n))^2} \right\} - \ln((1-n) \\ &\times d_1 + 4r) - \ln\left[4\int \frac{1}{4r + d_1(1-n)} \left(r^{-4}(d_1(1-n)+4r)^{3+\frac{d_1^2(1-n)^2}{8}} \right.\right. \\ &\times \left.\left. e^{r^2 - \frac{rd_1(1-n)}{2} + \frac{d_1(1-n)}{r}} \right) dr - d_1 \right]. \end{aligned}$$

This solution satisfies Eq. (40) for $\omega = -1$. The shape function of WH takes the form

$$\begin{aligned} \frac{h(r)}{r} &= \left(1 - r^4(d_1(1-n)+4r)^{-3-\frac{d_1^2(1-n)^2}{8}} e^{-r^2 + \frac{rd_1(1-n)}{2} - \frac{d_1(1-n)}{r}} \right. \\ &\times \left. \left[\int \{4r + d_1(1-n)\}^{-1} \left(r^{-4}(d_1(1-n)+4r)^{3+\frac{d_1^2(1-n)^2}{8}} e^{r^2 - \frac{rd_1(1-n)}{2} + \frac{d_1(1-n)}{r}} \right) dr - d_1 \right] \right). \end{aligned}$$

When red-shift function is not constant ($a'(r) \neq 0$), then the geometry of WH cannot be analyzed for $f(R)$ power-law model due to the complicated forms of $b(r)$ and $h(r)$.

4.2. Exponential model

In this section, we consider another example of viable $f(R)$ model, i.e., exponential model to realize the existence of realistic traversable WH. The simplest version of this model is proposed as [30]

$$f(R) = R - 2\Lambda(1 - e^{-\frac{R}{R_0}}), \tag{54}$$

where Λ denotes cosmological constant while R_0 defines curvature parameter. If $R \gg R_0$, then the corresponding model recovers standard cosmological constant cold dark matter model. To formulate

WH solution, we first solve the system of Eqs. (27)–(40) for the model (54) which leads to the following coefficients of symmetry generator and boundary term

$$\alpha = 0, \quad \beta = \frac{4\Lambda\chi_1}{R_0}, \quad \gamma = 0, \quad \delta = \chi_1(R_0 e^{\frac{R}{R_0}} - 2\Lambda), \quad \tau = \tau_0,$$
$$B = \frac{2e^{\frac{a+b}{2}}\Lambda\chi_1}{R_0^2}\left[-\frac{2r^3R_0\Lambda}{3}\left(1 - e^{-\frac{R}{R_0}} - \frac{2R}{R_0}\right) + \frac{r^3R_0(1-RR_0)}{3} + 4r \times (R_0 - 2\Lambda e^{-\frac{R}{R_0}})\right] + \chi_2,$$

where χ_1 and χ_2 represent arbitrary constants. These solutions satisfy the system for $\omega = \rho_0 = -1$ and the following constraint

$$e^{\frac{R}{R_0}} r^2 R_0^2 - 2r^2R_0\Lambda + 4r^2R\Lambda - 24\Lambda = 0. \tag{55}$$

Now we determine the coefficient of radial component of the metric (5) using this constraint with Eq. (19) for both constant as well as variable forms of red-shift function and study WH geometry via shape function.

Case I: $a(r) = k$

In this case, we obtain

$$\begin{aligned} e^{b(r)} &= -(4(-2R_0r^2 + (R_0r^2 + 12r^4)\exp((1/2)(12 + R_0r^2)/(R_0r^2)) \\ &- 48r^4\chi_4 + 24(1-\chi_4)))\{(r^2((5r^4R_0^2 - 2r^4R_0 - 4R_0r^2) \\ &\times \exp((1/2)(12 + R_0r^2)(R_0r^2)^{-1}) - 6r^4R_0^2 + 48r^2\chi_4 - 48r^2 \\ &- 120R_0r^2\chi_4 + 104R_0r^2 - 96 + 96\chi_4))\}^{-1}. \end{aligned} \tag{56}$$

From this expression, we formulate shape function through $h(r) = r[1 - e^{-b(r)}]$ and analyze the WH geometry graphically. In Fig. 11, the upper face indicates that the shape function is positively increasing while the corresponding geometry is found to be asymptotically flat as $h(r)/r \to 0$ when $r \to \infty$. In the lower face, the left plot indicates that the WH throat exists at $r_0 = 0.05$ and also preserves the condition, i.e., $h(0.05) = 0.05$ while the right plot shows that $h'(r_0) = -0.007 < 1$. Since the red-shift function is constant therefore, the traversable nature of the constructed WH solution is preserved by the violation of effective NEC, i.e., $p_{eff} + \rho_{eff} < 0$. Fig. 12 evaluates the criteria for physically viable WH as $\rho_m > 0$ and $p_m + \rho_m > 0$.

Case II: $a(r) = -k/r$

Using Eqs. (19) and (55), it follows that

$$\begin{aligned} e^{b(r)} &= -(4(24 + 48kr^2 - 2R_0r^2 - 4kr^4R_0 - 12(r+4)kr^2\chi_4 \\ &- 24\chi_4(1 + 2r^4)) + (2kr^4R_0 + 3r^3k + R_0r^2 + 12r^4) \\ &\times \exp((1/2)(12 + R_0r^2)/(R_0r^2)))\{r^2(-2r^4R_0 + 5r^4R_0^2 - 4R_0r^2) \\ &\times \exp((1/2)(12 + R_0r^2)/(R_0r^2)) - (6r^2R_0 + 104)R_0r^2 - 48(r^2 + 2) \\ &- (120R_0r^2 - 48r^2 + 96)\chi_4\}^{-1}. \end{aligned}$$

Inserting the above expression in $h(r) = r[1 - e^{-b(r)}]$, we construct WH solution relative to variable but finite red-shift function whose graphical interpretation is given in Fig. 13. Both plots of the upper and lower panels indicate that the constructed WH follows asymptotic flat geometry whose throat is located at $r_0 = 0.01$ and $h'(0.01) = -0.001 < 1$. In order to analyze the presence of repulsive gravitational effects at throat, we study the behavior of effective NEC in Fig. 14 which ensures that the sum of p_{eff} and ρ_{eff} remains negative. Thus, the constructed WH is found to be traversable. Both plots of Fig. 15 shows that the WH is physically viable as NEC and WEC corresponding to ordinary matter are preserved.

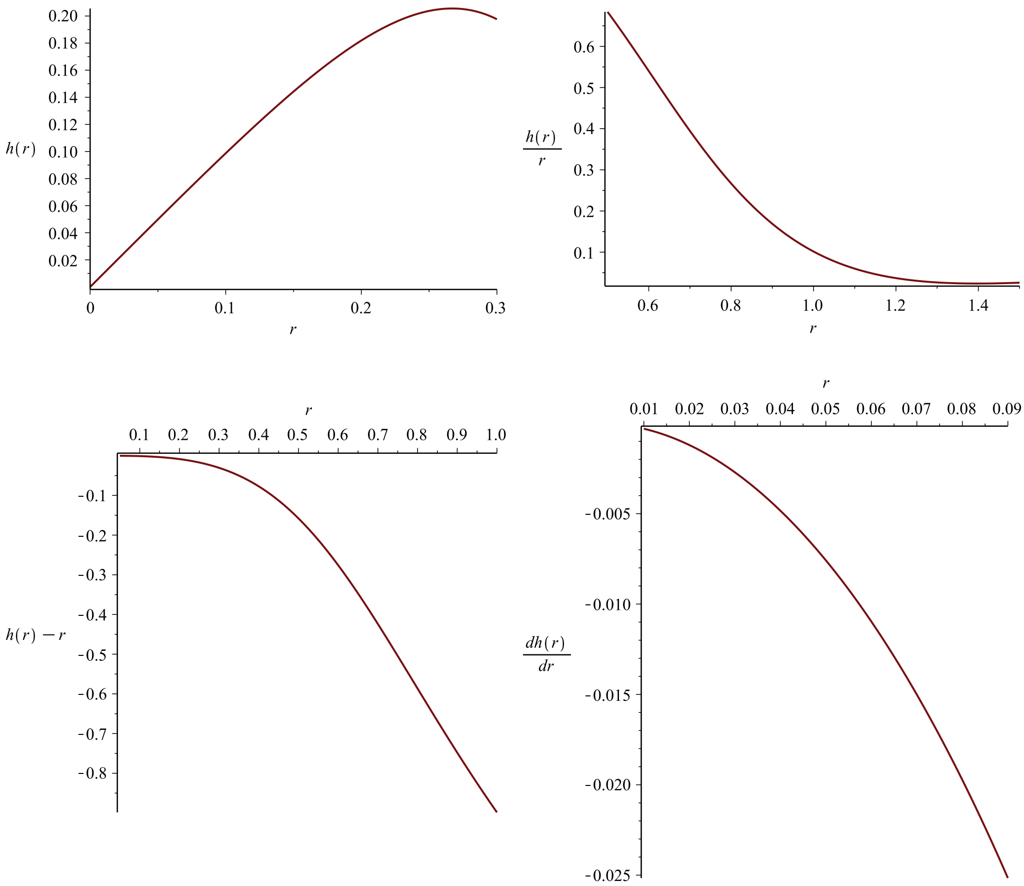

Fig. 11. Plots of $h(r)$, $\frac{h(r)}{r}$, $h(r)-r$ and $\frac{dh(r)}{dr}$ versus r for $\chi_4=-200$, $R_0=-0.95=\Lambda$ and $k=0.005$.

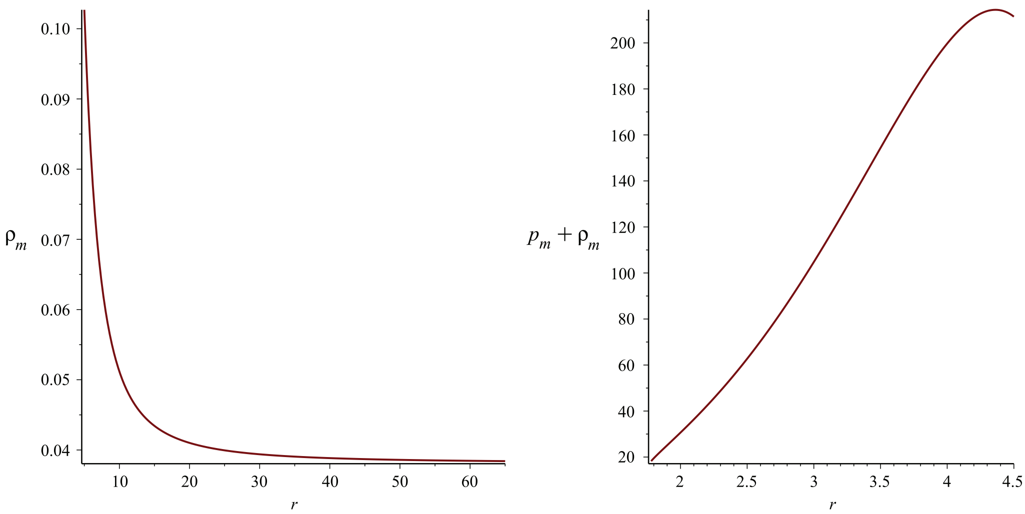

Fig. 12. Plots of ρ_m and ρ_m+p_m versus r.

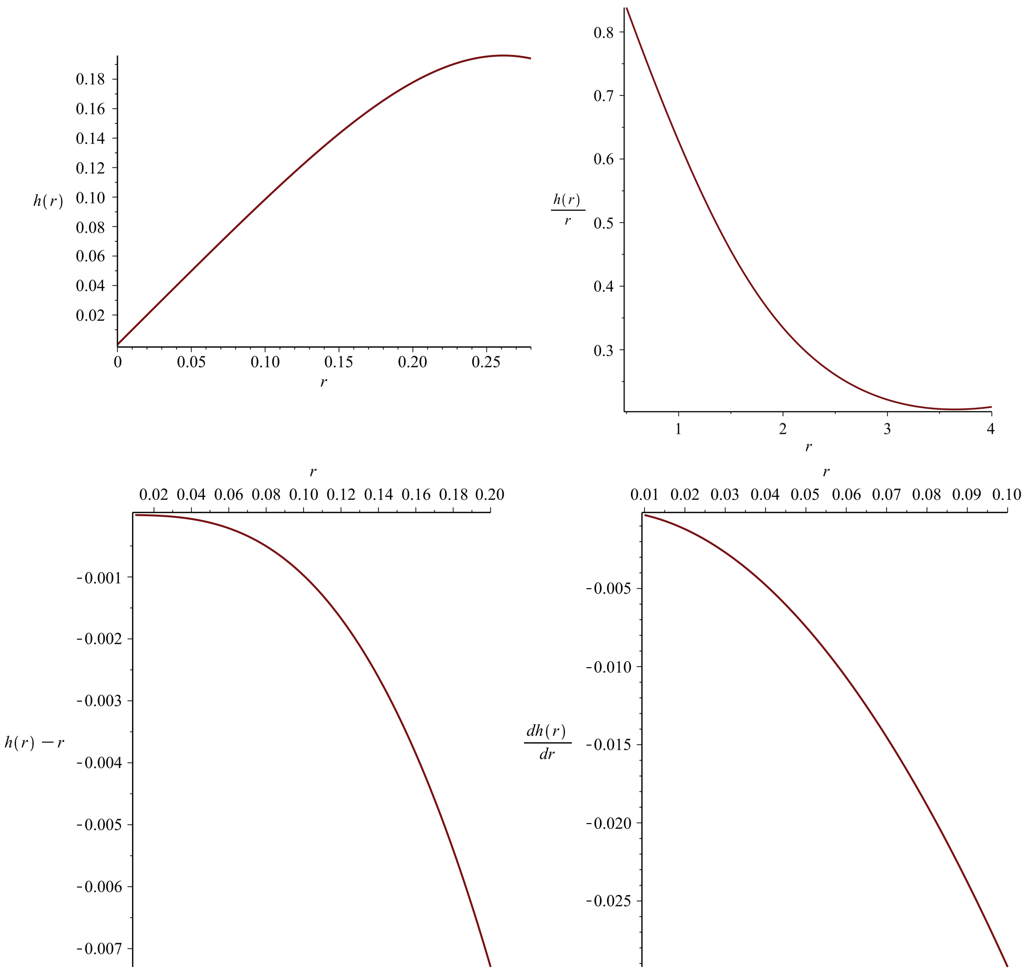

Fig. 13. Plots of $h(r)$, $\frac{h(r)}{r}$, $h(r)-r$ and $\frac{dh(r)}{dr}$ versus r for $\chi_4=-0.20$, $R_0=-0.95=\Lambda$ and $k=2$.

5. Stability analysis

Here we discuss the stability of WH solutions relative to both constant as well as variable red-shift function via Tolman–Oppenheimer–Volkov (TOV) equation. For isotropic fluid distribution, the radial component of Bianchi identity ($\nabla_\mu T^{\mu\nu}=0$) defines TOV equation as

$$\frac{dp_m}{dr}+\frac{a'(r)}{2}(p_m+\rho_m)=0. \tag{57}$$

The conservation of energy–momentum tensor relative to high order curvature terms leads to

$$T_{11}^{\prime(c)}+\frac{a'}{2}\left(T_{00}^{(c)}+T_{11}^{(c)}\right)-\frac{M'}{M}\left(f_R''-\frac{f_R'}{e^{b(r)}}\left\{\frac{b'}{2}+\frac{M'}{2M}\right\}\right)=0. \tag{58}$$

Combining Eqs. (57) and (58), it follows that

$$p'_{(eff)}+\frac{a'(r)}{2}\left(p_{eff}+\rho_{eff}\right)-\frac{M'}{M}\left(f_R''-\frac{f_R'}{e^{b(r)}}\left\{\frac{b'}{2}+\frac{M'}{2M}\right\}\right)=0, \tag{59}$$

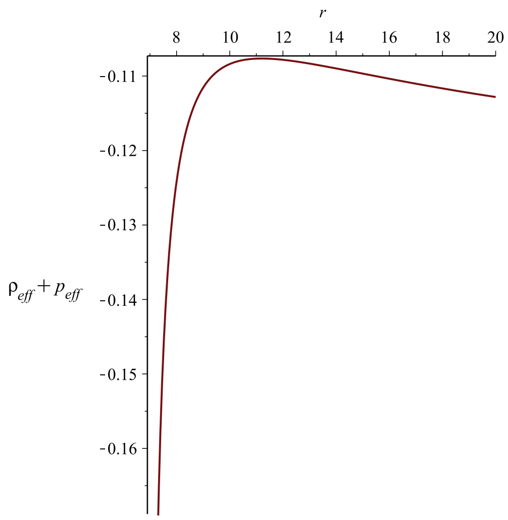

Fig. 14. Evolution of $\rho_{eff} + p_{eff}$ versus r.

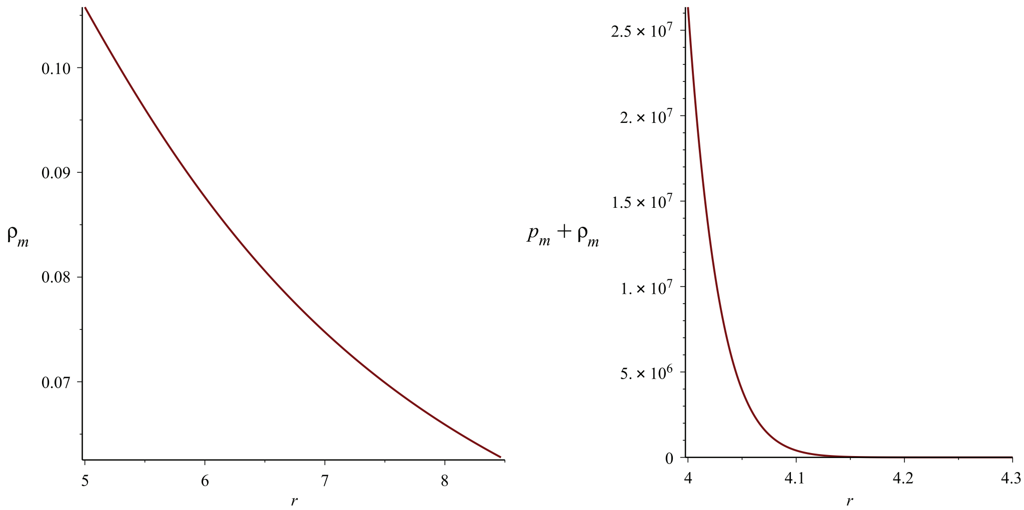

Fig. 15. Plots of ρ_m and $\rho_m + p_m$ versus r.

where $p_{eff} = p_m + T^{(c)}_{11}$ and $\rho_{eff} = \rho_m + T^{(c)}_{00}$. This equation determines the fate of the WH as it can be expressed as a combination of hydrostatic $\mathcal{F}_h$ and gravitational force $\mathcal{F}_g$. Using Eq. (59), these forces take the following form

$$\mathcal{F}_h = p'_{(eff)} = \frac{d}{dr}(p_m + T^{(c)}_{11}),$$

$$\mathcal{F}_g = \frac{\mathcal{M}_{eff} e^{\frac{a-b}{2}}}{r^2}\left(p_{eff} + \rho_{eff}\right) - \frac{M'}{M}\left(f''_R - \frac{f'_R}{e^{b(r)}}\left\{\frac{b'}{2} + \frac{M'}{2M}\right\}\right),$$

where $\mathcal{M}_{eff} = \frac{a' r^2 e^{\frac{b-a}{2}}}{2}$ denotes effective gravitational mass. The null effect ($\mathcal{F}_h + \mathcal{F}_g = 0$) of these dynamical forces leads to stable state of a WH.

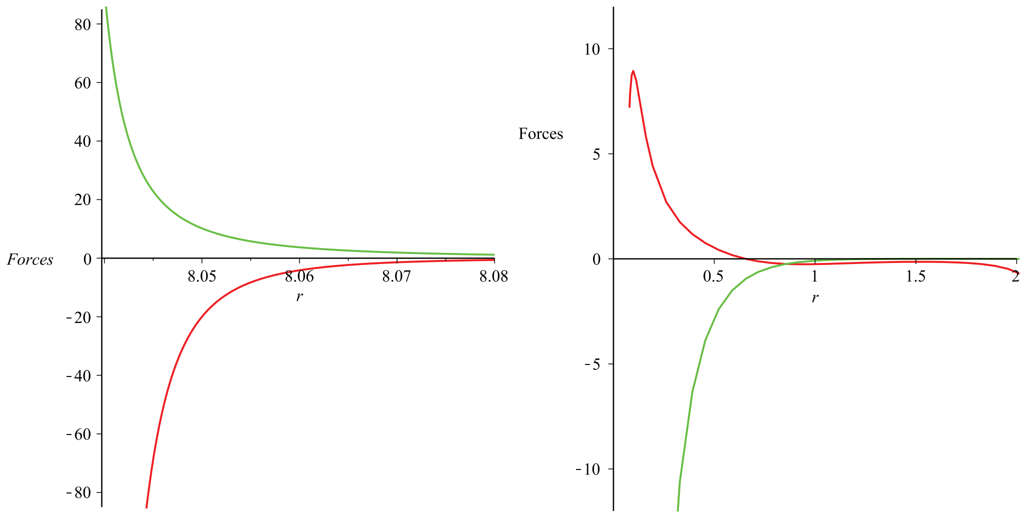

Fig. 16. Plots of $\mathcal{F}_g$ (green) and $\mathcal{F}_h$ (red) versus r for $a(r) = k$ (left) and $a(r) = -k/r$ (right) for $c_2 = 5$, $c_4 = 0.01$, $c_5 = -0.35$, $c_6 = 0.1$, $c_7 = -0.25$, $\rho_0 = -0.01$ and $k = 0.5$. (For interpretation of the references to color in this figure legend, the reader is referred to the web version of this article.)

In Figs. 16–18, we analyze the stability of WH solutions constructed with the help of a new $f(R)$ model as well as power-law and exponential forms of generic function $f(R)$. In Fig. 16, the left plot represents the stability of WH solution (44) relative to constant red-shift function and $f(R)$ model (45). The effect of gravitational and hydrostatic forces appear to be the same but in opposite directions canceling each other effect. Thus, the considered WH is found to be stable due to null effect of these forces. For variable red-shift function, the equilibrium state of WH solution (48) is analyzed in the right plot of Fig. 16. Initially, the WH geometry seems to be unstable but gradually it attains an equilibrium state due to equal but opposite effect of hydrostatic and gravitational forces. Fig. 17 determines the existence of stable WH for $n = 0.5$, $n = 2$ and $n = 4$ with constant red-shift function. For $n = 0.5$ and $n = 0.4$, the system remains unstable as $\mathcal{F}_g + \mathcal{F}_h \neq 0$ whereas the constructed WH attains a stable state for $n = 2$. In Fig. 18, the WH solutions gradually attain equilibrium state corresponding to both forms of red-shift function.

6. Final remarks

In general relativity, the physical existence of a static traversable WH demands the violation of NEC by the energy–momentum tensor. This violation confirms the presence of exotic matter which would be minimized to have a physically viable WH. In case of $f(R)$ gravity, the energy–momentum tensor threading WH satisfies NEC and WEC whereas the existence of exotic matter is assured by the effective energy–momentum tensor which violates NEC. In this paper, we have discussed the presence of static traversable WH via Noether symmetry approach in $f(R)$ gravity. For this purpose, we have considered perfect fluid distribution and studied possible existence of realistic WH solutions for generic as well as $f(R)$ power-law model. We have solved over-determined system by invariance condition and found symmetry generator, associated conserved quantity, exact solution of $f(R)$ and $b(r)$ for static spherically symmetric metric. For these solutions, we have studied WH geometry and also investigated stable state of WH solutions via modified TOV equation for the red-shift function when $a(r) = k, \ -k/r$.

In case of constant red-shift function, we have obtained viable $f(R)$ model and the shape function satisfies all the properties, i.e., $h(r) > 0$, WH geometry is found to be asymptotic flat and $\frac{dh(r)}{dr} < 1$ at $r = r_0$. The violation of NEC (using effective energy–momentum tensor) assures the presence of repulsive nature of gravity while existence of ordinary matter is supported by verification of NEC

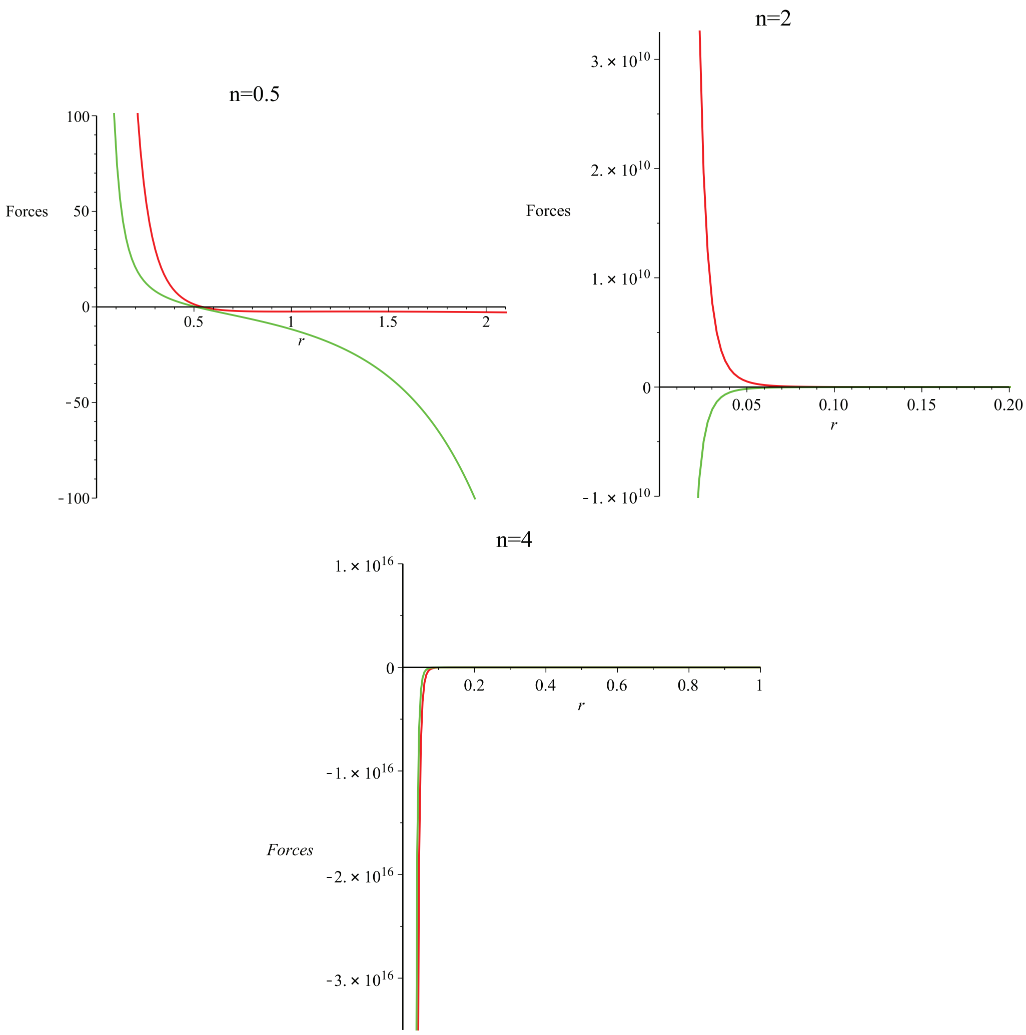

Fig. 17. Plots of $\mathcal{F}_g$ (green) and $\mathcal{F}_h$ (red) versus r for $a(r) = k, d_2 = -2.2, d_3 = 1.001, d_4 = 0.05, f_0 = 1$ and $\mathcal{M}_{eff} = 2$. (For interpretation of the references to color in this figure legend, the reader is referred to the web version of this article.)

and WEC relative to perfect fluid. When $a' \neq 0$, the $f(R)$ model preserves stability conditions for $0 < \omega < -0.08$ and the shape function has preserved all conditions of traversable WH while $\rho_{eff} + p_{eff} < 0$, $\rho_m + p_m \geq 0$ and $\rho_m \geq 0$ minimizing the presence of exotic matter due to the presence of repulsive gravity. These energy bounds confirm the presence of a realistic WH solution threaded by $T^{(m)}_{\mu\nu}$. Consequently, we have found a physically viable WH solution for $a' \neq 0$. For both forms of red-shift function, the constructed WH solutions attain an equilibrium state as $\mathcal{F}_g + \mathcal{F}_h = 0$.

We have also formulated symmetry generator, corresponding first integral and WH solutions for $f(R)$ power-law model. When $a'(r) = 0$, we have established graphical analysis of traversable WH conditions for $n = 1/2$, $n = 2$ and $n = 4$. In this case, the shape function is found to preserve all conditions and $\rho_{eff} + p_{eff} < 0$ assures the violation of NEC identifying the existence of exotic matter at throat. The consistent behavior of $\rho_m \geq 0$ and $\rho_m + p_m \geq$ indicate that the constructed traversable WH is supported by ordinary matter. The stability analysis of these realistic traversable WHs identifies that the WH geometry would be stable only for $n = 2$. For $a' \neq 0$, we have found a complicated form of the shape function. For exponential $f(R)$ model, the WH geometry is discussed near the throat.

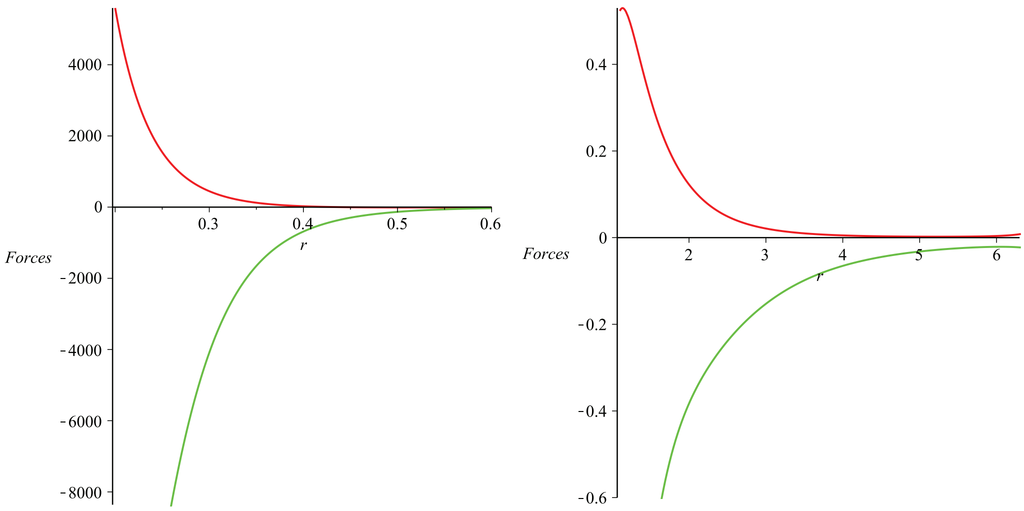

Fig. 18. Plots of $\mathcal{F}_g$ (green) and $\mathcal{F}_h$ (red) versus r for $a(r) = k$ (left), $k = 0.005$, $\mathcal{M}_{eff} = -2$ and $a(r) = -k/r$ (right), $\chi_4 = -0.2$, $R_0 = -0.95$, $k = 2$ and $\mathcal{M}_{eff} = 2$. (For interpretation of the references to color in this figure legend, the reader is referred to the web version of this article.)

The shape of WH is found to be asymptotically flat for both constant as well as variable forms of the red-shift function. The violation of effective NEC and verification of NEC as well as WEC of ordinary matter assure the presence of realistic traversable WH solutions. The total effect of gravitational and hydrostatic forces identifies equilibrium state of WHs in both cases.

The WH solutions are found in $f(R)$ gravity which is equivalent to Brans–Dicke theory under a particular conformal transformation. Coule [31] established static unrealistic WH solutions in Einstein frame of $f(R)$ theory. Nandi et al. [32] examined the possibility of static WH solutions in the background of both Jordan and Einstein frames of Brans–Dicke theory. They found that the non-traversable WH exists in the former frame whereas in the latter frame, WH solutions do not exist at all unless energy conditions are violated by hand. Furey and DeBenedictis [33] discussed geometry of the WH solutions near the throat while Bronnikov and Starobinsky [34] claimed that the existence of throat can be preserved under a conformal transformation. In general, the back transformation from Jordan to Einstein frames does not assure to get physical solutions. It has been even widely demonstrated that passing from one frame to the other can completely change the physical meaning as well as the stability of the solutions [35]. Bahamonde et al. [36] observed the presence of big-rip (type I) singularity in the Einstein frame of $f(R)$ gravity while along back mapping, the universe evolution is found to be singularity free.

In this paper, we have explored the existence of realistic and stable traversable WH solutions in the Jordan frame representation of $f(R)$ theory. It is worth mentioning here that the WH geometry is discussed at the throat in case of standard power-law and constructed $f(R)$ models whereas in case of exponential model, we have analyzed the WH geometry near the throat. The presence of repulsive gravity due to higher order curvature terms leads to traversable WHs while the existence of ordinary matter confirms the realistic nature of these traversable WH solutions in each case. For $f(R)$ power-law model, the WH solutions are stable only for $n = 2$ while stability is preserved for both exponential as well as constructed $f(R)$ models. It would be interesting to analyze the presence of these configurations in the Einstein frame where contribution of scalar field may enhance the traversable nature as it introduces anti-gravitational effects. On the other hand, the back mapping of these frames may or may not ensure the presence of stable as well as realistic traversable wormholes.

Acknowledgment

This work has been supported by the *Pakistan Academy of Sciences Project*.

References

[1] M. Sharif, M.F. Shamir, Classical Quantum Gravity 26 (2009) 235020; Gen. Relativity Gravitation 42 (2010) 2643.
[2] A.C. Gutiérrez-Piñeres, C.S. López-Monsalvo, Phys. Lett. B 718 (2013) 1493.
[3] M. Sharif, M. Zubair, Astrophys. Space Sci. 349 (2014) 457.
[4] C. Gao, Y.G. Shen, Gen. Relativity Gravitation 48 (2016) 131.
[5] S. Capozziello, A. Stabile, A. Troisi, Classical Quantum Gravity 24 (2007) 2153.
[6] S. Capozziello, A. Stabile, A. Troisi, Classical Quantum Gravity 25 (2008) 085004;
S. Capozziello, A. Stabile, A. Troisi, Classical Quantum Gravity 27 (2010) 165008.
[7] B. Vakili, Phys. Lett. B 16 (2008) 664.
[8] D. Momeni, R. Myrzakulov, E. Güdekli, Int. J. Geom. Methods Mod. Phys. 12 (2015) 1550101.
[9] M. Sharif, I. Nawazish, J. Exp. Theor. Phys. 120 (2014) 49;
M. Sharif, I. Shafique, Phys. Rev. D 90 (2014) 084033;
M. Sharif, H.I. Fatima, J. Exp. Theor. Phys. 122 (2016) 104;
M. Sharif, I. Nawazish, Gen. Relativity Gravitation 49 (2017) 76; Eur. Phys. J. C 77 (2017) 198; Modern Phys. Lett. A32 (2017)1750136.
[10] P.E. Kashargin, S.V. Sushkov, Gravit. Cosmol. 14 (2008) 80;
E.F. Eiroa, C. Simeone, Phys. Rev. D 82 (2010) 084039.
[11] F.S.N. Lobo, M.A. Oliveira, Phys. Rev. D 80 (2009) 104012.
[12] M. Jamil, et al., J. Korean Phys. Soc. 65 (2014) 917.
[13] S. Bahamonde, et al., Phys. Rev. D 94 (2016) 044041.
[14] S.H. Mazharimousavi, M. Halilsoy, Modern Phys. Lett. A 31 (2016) 1650203.
[15] M. Sharif, H.I. Fatima, Gen. Relativity Gravitation 48 (2016) 148; Astrophys. Space Sci. 361 (2016) 127.
[16] S. Bahamonde, et al., Phys. Rev. D 94 (2016) 084042.
[17] M.S. Morris, K.S. Thorne, Amer. J. Phys. 56 (1988) 395.
[18] G.F.R. Ellis, R. Maartens, M.A.H. MacCallum, Relativistic Cosmology, Cambridge University Press, 2012.
[19] B.F. Schutz Jr., Phys. Rev. D 2 (1970) 2762.
[20] S.M. Carroll, Spacetime and Geometry: An Introduction To General Relativity, Addison Wesley, 2004.
[21] J. Santos, et al., Phys. Rev. D 76 (2007) 083513.
[22] S. Capozziello, et al., Phys. Lett. B 693 (2010) 198.
[23] S. Capozziello, M. De Laurentis, S.D. Odintsov, Eur. Phys. J. C 72 (2012) 2068.
[24] J. Hanc, S. Tuleja, M. Hancova, Amer. J. Phys. 72 (2004) 428.
[25] S. Kar, D. Sahdev, Phys. Rev. D 52 (1995) 2030.
[26] S. Capozziello, Internat. J. Modern Phys. D 11 (2002) 483;
S. Nojiri, S.D. Odintsov, arXiv:hep-th/0308176.
[27] A.D. Dolgov, M. Kawasaki, Phys. Lett. B 573 (2003) 1.
[28] S. Nojiri, S.D. Odintsov, arXiv:hep-th/0307288.
[29] V. Faraoni, Phys. Rev. D 74 (2006) 104017.
[30] G. Cognola, et al., Phys. Rev. D 77 (2008) 046009.
[31] D.H. Coule, Classical Quantum Gravity 10 (1993) L25.
[32] K.K. Nandi, et al., Phys. Rev. D 57 (1998) 823.
[33] N. Furey, A. DeBenedictis, Classical Quantum Gravity 22 (2006) 313.
[34] K.A. Bronnikov, A.A. Starobinsky, J. Exp. Theor. Phys. Lett. 85 (2007) 1.
[35] V. Gorini, et al., Phys. Rev. D 72 (2005) 103518.
[36] Bahamonde, et al., Ann. Phys. 373 (2016) 96.

Viable Wormhole Solutions and Noether Symmetry in $f(R,T)$ Gravity

M. Sharif *and Iqra Nawazish †
Department of Mathematics, University of the Punjab,
Quaid-e-Azam Campus, Lahore-54590, Pakistan.

Abstract

This paper investigates wormhole solutions of spherically symmetric spacetime via Noether symmetry approach in $f(R,T)$ gravity. For this purpose, we choose $f(R,T)$ models appreciating indirect curvature-matter coupling and examine symmetry generators with associated conserved quantities. We determine possible existence of realistic traversable wormhole solutions for both dust as well as non-dust distributions and also study stable behavior of these solutions. For both models, we use constant as well as variable forms of red-shift function. To analyze physical existence of wormhole solutions, we study the behavior of null/weak energy conditions with respect to ordinary as well as effective energy-momentum tensor. It is concluded that there exist physically viable traversable as well as stable wormhole solutions in most of the cases.

Keywords: Noether symmetry; Wormhole solution; $f(R,T)$ gravity.
PACS: 04.20.Jb; 04.50.Kd; 95.36.+x.

1 Introduction

The concept of non-minimal coupling introduces one of the fascinating approaches to study current cosmic expansion. This revolutionary idea is extensively applied to different cosmological scenarios that suggests new and

*msharif.math@pu.edu.pk
†iqranawazish07@gmail.com

intriguing phenomenology. Bertolami et al. [1] emerged non-minimal coupling between curvature and matter parts such that generic function of R (R is the Ricci scalar) admits non-minimal coupling with Lagrangian density of matter ($\mathcal{L}_m$). Harko et al. [2] deduced a generalization of $f(R)$ gravity whose generic function includes both curvature as well as matter called $f(R,T)$ gravity (T is the trace of energy-momentum tensor). This non-minimally coupled theory successfully explores dark matter in galaxies or clusters of galaxies, natural preheating conditions relative to inflationary models and presence of traversable wormhole (WH) in the absence of exotic matter [3].

The analysis of exact solutions under some assorted scenarios leads to study different cosmic aspects that unveil sophisticated picture of cosmic evolution. Gutiérrez-Piñeres and López-Monsalvo [4] evaluated static axially symmetric vacuum solution which corresponds to naked singularity for minimally coupled curvature and matter contents. Sharif and Zubair [5] used power-law and exponential expansions to formulate exact solutions and associated kinematical quantities of anisotropic universe model in $f(R,T)$ gravity. Harko and Lake [6] obtained exact cylindrical solutions for non-minimal coupling of R with $\mathcal{L}_m$. Shamir [7] formulated exact anisotropic solutions and also determined their physical behavior via cosmological parameters in $f(R,T)$ gravity. Gao and Shen [8] established a new method to find exact static spherically symmetric solutions in the absence of non-minimal curvature-matter coupling.

Noether symmetry technique is considered to be the most applicable approach that establishes not only exact solutions but also proposes association between symmetry generators and conserved quantities relative to dynamical system. Capozziello et al. [9] found exact static spherically symmetric solution for $f(R)$ power-law model. The same authors [10] extended this work to evaluate non-static spherically symmetric solutions and also explored possible solutions for axially symmetric model. Momeni et al. [11] discussed the presence of Noether symmetry for flat isotropic model in $f(R)$ and $f(R,T)$ theories. Sharif and his collaborators [12] studied cosmic evolution as well as late-time cosmic expansion using this approach. We have constructed exact solution of $f(R,T)$ model admitting indirect curvature-matter coupling and also analyzed corresponding behavior via cosmological parameters [13]. We have also found exact solutions of some anisotropic universe models by taking generalized scalar field model [14].

A wormhole (WH) is a hypothetical bridge or tunnel that allows a smooth passing through different regions of spacetime. If hypothetical tunnel connects two regions of the same spacetime then intra-universe WH is established whereas inter-universe WH appears for two distinct spacetimes. The existence of exotic matter (matter with negative energy density) encourages observer to move smoothly through tunnel but its sufficient amount leads to controversial existence of a realistic WH. Consequently, the only way to have a physically viable WH model is to minimize the usage of exotic matter in the tunnel. Morris and Thorne [15] established traversable WH that allows an observer to possess traverse motion. Different proposals have been introduced to analyze the existence of traversable as well as realistic WH such as modified theories, non-minimal coupling between curvature and matter, scalar field models etc [16].

There is a growing interest about the existence of WH solutions in modified theories. Lobo and Oliveira [17] formulated WH solution for constant shape function and different fluids in $f(R)$ gravity. Jamil et al. [18] considered particular form of shape function in the background of non-commutative geometry and found physically viable WH solutions for $f(R)$ power-law model. Bahamonde et al. [19] established cosmological WH supported by perfect fluid in the same gravity. Mazharimousavi and Halilsoy [20] discussed $f(R)$ model appreciating polynomial expansion and constructed a near-throat WH solution satisfying necessary conditions of WH for both vacuum as well as non-vacuum cases. Sharif and Fatima [21] analyzed static WH solution in galactic halo region as well as non-static conformal WH in modified Gauss-Bonnet gravity. Zubair et al. [22] explored static WH solution and analyzed physical existence for anisotropic, barotropic and isotropic fluids in $f(R,T)$ gravity. Bahamonde et al. [23] used Noether symmetry approach to evaluate exact solutions of red-shift as well as shape functions. They also studied geometric behavior of WH solutions in scalar-tensor theory admitting non-minimal coupling with torsion scalar.

In this paper, we explore static wormhole solutions and analyze their physical existence via Noether symmetry approach in $f(R,T)$ gravity. The format of the paper is as follows. In section **2**, we review Lagrangian formulation and energy bounds of $f(R,T)$ gravity. Section **3** explores Noether symmetry approach to construct WH solutions for two $f(R,T)$ models and investigate physical existence via energy bounds graphically. In section **4**, we study the stable behavior of WH solution through TOV equation. In the last section, we present final remarks.

2 Basic Formalism of $f(R,T)$ Gravity

For the non-minimal coupling of curvature and matter, the Einstein-Hilbert action is modified as [2]

$$\mathcal{I}=\int d^4x\sqrt{-g}[\frac{f(R,T)}{2\kappa^2}+\mathcal{L}_m], \tag{1}$$

where g is the determinant of the metric tensor, f is the generic function which appreciates non-minimal curvature-matter coupling. The field equations are obtained through metric variation of the action (1) as

$$R_{\mu\nu}f_R(R,T)-\frac{1}{2}g_{\mu\nu}f(R,T)+(g_{\mu\nu}\nabla^\mu\nabla_\mu-\nabla_\mu\nabla_\nu)f_R(R,T)+f_T(R,T)$$
$$\times T_{\mu\nu}+\Theta_{\mu\nu}f_T(R,T)=\kappa^2T_{\mu\nu}^{(m)}. \tag{2}$$

Here subscripts of f defines corresponding partial derivatives, ∇_μ is the covariant derivative whereas the energy-momentum tensor ($T_{\mu\nu}$) and $\Theta_{\mu\nu}$ are defined as

$$T_{\mu\nu}^{(m)}=g_{\mu\nu}\mathcal{L}_m-2\frac{\partial\mathcal{L}_m}{\partial g^{\mu\nu}},\quad \Theta_{\mu\nu}=\frac{g^{\mu\nu}\delta T_{\mu\nu}^{(m)}}{\delta g^{\mu\nu}}=g_{\mu\nu}\mathcal{L}_m-2T_{\mu\nu}^{(m)}-2g^{\mu\nu}\frac{\partial^2\mathcal{L}_m}{\partial g^{\mu\nu}\partial g^{\mu\nu}}.$$

An alternative form of the field equations relating the Einstein tensor ($G_{\mu\nu}$) with matter and curvature energy-momentum tensors is given as

$$G_{\mu\nu}=\frac{1}{f_R}(T_{\mu\nu}^{(c)}+T_{\mu\nu}^{(m)})=T_{\mu\nu}^{eff}, \tag{3}$$

where $T_{\mu\nu}^{(c)}$ and $T_{\mu\nu}^{eff}$ identify curvature and effective energy-momentum tensors, respectively. For the action (1), the curvature terms are defined $T_{\mu\nu}^{(c)}$ as

$$T_{\mu\nu}^{(c)}=f_TT_{\mu\nu}^{(m)}-f_Tg_{\mu\nu}\mathcal{L}_m+\frac{1}{2}g_{\mu\nu}(f-Rf_R)+(\nabla_\mu\nabla_\nu-\nabla^\mu\nabla_\mu g_{\mu\nu})f_R. \tag{4}$$

In non-minimally coupled $f(R,T)$ gravity, the covariant derivative of energy-momentum tensor yields an extra force which behaves as a source of deviation for massive test particles given by

$$\nabla^\mu T_{\mu\nu}^{(m)}=\frac{f_T}{\kappa^2-f_T}\left[(T_{\mu\nu}^{(m)}+\Theta_{\mu\nu})\nabla^\mu\ln f_T+\nabla^\mu\Theta_{\mu\nu}-\frac{g_{\mu\nu}\nabla^\mu T}{2}\right]. \tag{5}$$

For perfect fluid distribution, the energy-momentum is defined as

$$T^{(m)}_{\mu\nu}=u_\mu u_\nu(\rho_m+p_m)+p_m g_{\mu\nu},$$

where u_μ characterizes four velocity defined as $u_\mu=(-e^{\frac{a(r)}{2}},0,0,0)$ whereas p_m and ρ_m represent pressure and energy density of perfect fluid, respectively.

A static spherically symmetric spacetime is [15]

$$ds^2=-e^{a(r)}dt^2+e^{b(r)}dr^2+M(r)(d\theta^2+\sin^2\theta d\phi^2), \tag{6}$$

where $a,\ b$ and M are radial functions. The geodesic deviation equation deduces $M(r)=r^2,\ \ \sin r,\ \ \sinh r$ for $\mathcal{K}=0,1,-1$ ($\mathcal{K}$ is curvature parameter) in the limit $M(r)\rightarrow 0$ as $r\rightarrow 0$, respectively [24]. To study WH geometry, we consider $M(r)=r^2$ and $e^{b(r)}=\left(1-\frac{h(r)}{r}\right)^{-1}$, where $h(r)$ is the shape function and $a(r)$ is referred as red-shift function determining gravitational red-shift. In order to identify a WH throat, the radial coordinate admits non-monotonic behavior such that it starts from infinity, decreases upto a minimum value r_0 locating WH throat at $h(r_0)=r_0$ and then starts increasing from minimum value to infinity providing $r>r_0$. At throat, the derivative condition $h'(r_0)<1$ is introduced, where prime denotes radial derivative. The throat is considered to be the minimum radius of WH geometry leading to the flaring-out condition, i.e., $\frac{h(r)-h(r)'r}{h(r)^2}>0$. Apart from throat, the shape of WH depends on asymptotically flat space implying $\frac{h(r)}{r}\rightarrow 0$. If a WH is independent of horizon and red-shift function is finite everywhere then there exists a traversable WH.

In order to formulate Lagrangian corresponding to the action (1), we choose $\mathcal{L}_m=p_m(a,b,M)$ [25] and use Lagrange multiplier approach

$$\mathcal{I}=\int\sqrt{-g}[f(R,T)-\lambda(R-\bar{R})-\chi(T-\bar{T})+p_m(a,b,M)]dr. \tag{7}$$

Here

$$\begin{aligned}\sqrt{-g}&=&e^{\frac{a}{2}}e^{\frac{b}{2}}M,\quad\lambda=f_R,\quad\chi=f_T,\quad\bar{T}=3p_m-\rho_m,\\ \bar{R}&=&\frac{1}{e^b}\left(-\frac{a'^2}{2}+\frac{a'b'}{2}-\frac{a'M'}{M}-\frac{2M''}{M}+\frac{b'M'}{M}+\frac{M'^2}{2M^2}-a''+\frac{2e^b}{M}\right).\end{aligned} \tag{8}$$

Using these values in Eq.(7) and eliminating second order derivative trough integration by parts, it follows that

$$\mathcal{L}(a,b,M,R,T,a',M',R',T') = e^{\frac{a}{2}}e^{\frac{b}{2}}M\left(f - Rf_R - Tf_T(R,T)\right.$$
$$\left.+ f_T(R,T)(3p_m - \rho_m) + p_m + \frac{2f_R}{M}\right) + \frac{e^{\frac{a}{2}}M}{e^{\frac{b}{2}}}\left\{f_R\left(\frac{M'^2}{2M^2} + \frac{a'M'}{M}\right)\right.$$
$$\left.+ f_{RR}\left(a'R' + \frac{2M'R'}{M}\right) + f_{RT}\left(a'T' + \frac{2M'T'}{M}\right)\right\}. \tag{9}$$

The corresponding Euler-Lagrange equation and energy function/Hamiltonian of the dynamical system are

$$\frac{\partial\mathcal{L}}{\partial q^i} - \frac{dp_i}{dr} = 0, \quad \mathcal{H} = \sum_i q'^i p_i - \mathcal{L},$$

where q^i represents n generalized coordinates and $p_i = \frac{\partial\mathcal{L}}{\partial q'^i}$ is the conjugate momenta. Varying the Lagrangian with respect to configuration space $Q = \{a,b,M,R,T\}$, we obtain

$$f - Rf_R - Tf_T + f_T(3p_m - \rho_m) + p_m + 2\{f_T(3p_{m},_a - \rho_{m},_a) + p_{m},_a\}$$
$$+\frac{1}{e^b}\left\{f_{RR}\left(b'R' - 2R'' - \frac{2M'R'}{M}\right) + f_{RT}\left(b'T' - \frac{2M'T'}{M}\right) - 2R'^2 f_{RRR}\right.$$
$$\left. - 4R'T'f_{RRT} - 2T'^2 f_{RTT}\right\} = \frac{f_R}{e^b}\left(\frac{M'^2}{2M^2} + \frac{b'M'}{M} - \frac{2M''}{M} + \frac{2e^b}{M}\right), \tag{10}$$

$$f - Rf_R - Tf_T + f_T(3p_m - \rho_m) + p_m + 2\{f_T(3p_{m},_b - \rho_{m},_b) + p_{m},_b\}$$
$$-\frac{1}{e^b}\left\{f_{RR}\left(a'R' + \frac{2M'R'}{M}\right) - f_{RT}\left(a'T' + \frac{2M'T'}{M}\right)\right\} = \frac{f_R}{e^b}\left(\frac{M'^2}{2M^2}\right.$$
$$\left.+ \frac{a'M'}{M} - \frac{2e^b}{M}\right), \tag{11}$$

$$f - Rf_R - Tf_T + f_T(3p_m - \rho_m) + p_m + 2\{f_T(3p_{m},_M - \rho_{m},_M) + p_{m},_M\}$$
$$+\frac{1}{e^b}\left\{f_{RR}\left(b'R' - a'R' - 2R'' - \frac{M'R'}{M}\right) - 4R'T'f_{RRT} - 2T'^2 f_{RTT} - 2R'^2\right.$$
$$\left.\times f_{RRR} + f_{RT}\left(b'T' - a'T' - 2T'' - \frac{M'T'}{M}\right)\right\} = -\frac{f_R}{e^b}\left(-a'' + \frac{M'^2}{2M^2} - \frac{a'^2}{2}\right.$$
$$\left. - \frac{a'M'}{2M} + \frac{a'b'}{2} + \frac{b'M'}{2M} - \frac{M''}{M}\right),$$

$$e^b(f_{RT}(3p_m-\rho_m-T)+f_{RR}(2M^{-1}R-R))+f_{RR}\left(-a''+\frac{M'^2}{2M^2}-\frac{a'^2}{2}\right.$$
$$\left.-\frac{a'M'}{2M}+\frac{a'b'}{2}+\frac{b'M'}{2M}-\frac{M''}{M}\right)=0,$$
$$e^b(f_{TT}(3p_m-\rho_m-T)+f_{RT}(2M^{-1}R-R))+f_{RT}\left(-a''+\frac{M'^2}{2M^2}-\frac{a'^2}{2}\right.$$
$$\left.-\frac{a'M'}{2M}+\frac{a'b'}{2}+\frac{b'M'}{2M}-\frac{M''}{M}\right)=0.$$

For Lagrangian (9), the variation of the energy function leads to

$$\begin{aligned}\mathcal{H} &= (f-Rf_R-Tf_T+f_T(3p_m-\rho_m)+p_m+2M^{-1}f_R)e^{b(r)}-f_R\\ &\times \left(\frac{M'^2}{2M^2}+\frac{a'M'}{M}\right)-(R'f_{RR}+T'f_{RT})\left(a'+\frac{2M'}{M}\right).\end{aligned}$$

For $\mathcal{H}=0$, the above equation yields

$$e^{b(r)}=\left(1-\frac{h(r)}{r}\right)^{-1}=\frac{f_R\left(\frac{M'^2}{2M^2}+\frac{a'M'}{M}\right)+(R'f_{RR}+T'f_{RT})\left(a'+\frac{2M'}{M}\right)}{f-Rf_R-Tf_T+f_T(3p_m-\rho_m)+p_m+2M^{-1}f_R}. \tag{12}$$

For WH geometry, the presence of physically acceptable traversable WH is possible if the energy conditions are violated. In order to specify energy conditions, we write down Raychaudhari equations as

$$\frac{d\theta}{d\tau}+\frac{1}{3}\theta^2-w_{\mu\nu}w^{\mu\nu}+\sigma_{\mu\nu}\sigma^{\mu\nu}+R_{\mu\nu}l^\mu l^\nu=0, \tag{13}$$
$$\frac{d\theta}{d\tau}+\frac{1}{2}\theta^2-w_{\mu\nu}w^{\mu\nu}+\sigma_{\mu\nu}\sigma^{\mu\nu}+R_{\mu\nu}k^\mu k^\nu=0, \tag{14}$$

where θ, l^μ, k^μ, $\sigma_{\mu\nu}$ and $w_{\mu\nu}$ represent expansion scalar, timelike and null vectors, shear and rotation tensors. These equations are determined for timelike and null congruences. In both equations, the positive behavior of last term requires attractive nature of gravity. In general relativity, these conditions are categorized as null (NEC) ($\rho_m+p_m\geq 0$), weak (WEC) ($\rho_m+p_m\geq 0,\ \rho_m\geq 0$), strong (SEC) ($\rho_m+3p_m\geq 0$) and dominant (DEC) ($\rho_m\pm p_m\geq 0$) energy conditions [26]. For non-geodesic (null or timelike) congruences, an acceleration term due to contribution of non-gravitational force evolves in the Raychaudhari equation as follows

$$\frac{d\theta}{d\tau}+\frac{1}{3}\theta^2-w_{\mu\nu}w^{\mu\nu}+\sigma_{\mu\nu}\sigma^{\mu\nu}+R_{\mu\nu}l^\mu l^\nu-\mathcal{A}=0,$$

where $\mathcal{A}=\nabla_\nu(u^\mu\nabla_\mu u^\nu)$. The purely geometric nature of Raychaudhari equations implies that $T^{(m)}_{\mu\nu}k^\mu k^\nu-\mathcal{A}\geq 0$ which can be replaced by $T^{eff}_{\mu\nu}k^\mu k^\nu-\mathcal{A}\geq 0$. Consequently, the energy conditions following non-geodesic congruences in $f(R,T)$ gravity are defined as [27]

$$\begin{aligned}
\textbf{NEC}: &\quad \rho_{eff}+p_{eff}-\mathcal{A}\geq 0,\\
\textbf{WEC}: &\quad \rho_{eff}-\mathcal{A}\geq 0,\quad \rho_{eff}+p_{eff}-\mathcal{A}\geq 0,\\
\textbf{SEC}: &\quad \rho_{eff}+p_{eff}-\mathcal{A}\geq 0,\quad \rho_{eff}+3p_{eff}-\mathcal{A}\geq 0,\\
\textbf{DEC}: &\quad \rho_{eff}-\mathcal{A}\geq 0,\quad \rho_{eff}\pm p_{eff}-\mathcal{A}\geq 0.
\end{aligned}$$

In modified theories, static WH demands the violation of NEC on effective energy-momentum tensor for the existence of physically viable WH. In $f(R,T)$ gravity, Eqs.(10) and (11) lead to a standard relation between ρ_{eff} and p_{eff} as follows

$$\rho_{eff}+p_{eff}-\mathcal{A}=\frac{1}{2e^b}\left(\frac{M'^2}{M^2}+\frac{a'M'}{M}+\frac{b'M'}{M}-\frac{2M''}{M}\right), \tag{15}$$

where acceleration term $\mathcal{A}$ is given by

$$\left(1-\frac{h(r)}{r}\right)\left[\frac{a''}{2}+\frac{a'^2}{4}+\frac{a'}{r}\right]-\frac{a'(rh'(r)-h(r))}{4r^2}. \tag{16}$$

3 Noether Symmetry Approach

Noether symmetry introduces an interesting way to establish new cosmological models and corresponding geometries in modified theories. To analyze the existence of Noether symmetry with associated conserved quantity of static spherically symmetric spacetime, we consider

$$K = \tau(r,q^i)\frac{\partial}{\partial r}+\xi^i(r,q^i)\frac{\partial}{\partial q^i}, \tag{17}$$

where r is referred as an affine parameter whereas τ and ξ^i represent unknown coefficients of the vector field K. To ensure the presence of Noether symmetries, the Lagrangian must satisfy invariance condition for unique vector field K on tangent space. In this case, the vector field behaves as a symmetry generator leading to formulate conserved quantity. The invariance condition is

$$K^{[1]}\mathcal{L}+(D\tau)\mathcal{L}=DB(r,q^i). \tag{18}$$

Here B is the boundary term, $K^{[1]}$ denotes first order prolongation and D describes total derivative defined as

$$K^{[1]} = K + (D\xi^i - q'^i D\tau)\frac{\partial}{\partial q'^i}, \quad D = \frac{\partial}{\partial r} + q'^i \frac{\partial}{\partial q^i}. \tag{19}$$

When a Lagrangian follows the invariance condition, the first integral is used to evaluate conserved quantity of the system. If the Lagrangian is translational invariant in time and position, then the first integral determines conservation of energy and linear momentum whereas if Lagrangian remains invariant under rotation, it yields conservation of angular momentum [28]. The first integral for invariance condition (18) is defined as

$$\Sigma = B - \tau\mathcal{L} - (\xi^i - q'^i\tau)\frac{\partial \mathcal{L}}{\partial q'^i}. \tag{20}$$

For configuration space $Q = \{a, b, M, R, T\}$, the vector field and corresponding first order prolongation turn out to be

$$\begin{aligned} K &= \tau\frac{\partial}{\partial r} + \alpha\frac{\partial}{\partial a} + \beta\frac{\partial}{\partial b} + \gamma\frac{\partial}{\partial M} + \delta\frac{\partial}{\partial R} + \eta\frac{\partial}{\partial T}, \\ K^{[1]} &= \tau\frac{\partial}{\partial r} + \alpha\frac{\partial}{\partial a} + \beta\frac{\partial}{\partial b} + \gamma\frac{\partial}{\partial M} + \delta\frac{\partial}{\partial R} + \eta\frac{\partial}{\partial T} + \alpha'\frac{\partial}{\partial a'} + \beta'\frac{\partial}{\partial b'} \\ &+ \gamma'\frac{\partial}{\partial M'} + \delta'\frac{\partial}{\partial R'} + \eta'\frac{\partial}{\partial T'}. \end{aligned} \tag{21}$$

The derivative of unknown coefficients of vector field with respect to r are defined as

$$\zeta'_j = D\zeta_j - q'^i D\tau, \quad j = 1...5, \tag{22}$$

where $\zeta_1,\ \zeta_2,\ \zeta_3,\ \zeta_4$ and ζ_5 correspond to $\alpha,\ \beta,\ \gamma,\ \delta$ and η, respectively. Inserting Eqs.(9), (21) and (22) in (18) and comparing the coefficients of $a'^2M',\ a'b'M',\ a'M'^2,\ a'R'^2$ and $a'T'^2$, we obtain

$$\tau_{,a} f_R = 0, \quad \tau_{,b} f_R = 0, \quad \tau_{,M} f_R = 0, \quad \tau_{,R} f_{RR} = 0, \quad \tau_{,T} f_{RT} = 0. \tag{23}$$

This implies that either $f_R,\ f_{RR},\ f_{RT} = 0$ or vice verse. The first choice yields trivial solution. Thus, we choose $f_R \neq 0$ and equate the remaining coefficients yielding

$$B_{,b} = 0, \quad \tau_{,a} = 0, \quad \tau_{,b} = 0, \quad \tau_{,M} = 0, \quad \tau_{,R} \quad \tau_{,T} = 0, \tag{24}$$

$$e^{\frac{a}{2}}(\gamma,_r f_R+M\delta,_r f_{RR}+M\eta,_r f_{RT})=e^{\frac{b}{2}}B,_a\,, \tag{25}$$
$$e^{\frac{a}{2}}(\alpha,_r M+2\gamma,_r)f_{RR}=e^{\frac{b}{2}}B,_R\,, \tag{26}$$
$$e^{\frac{a}{2}}(\alpha,_r M+2\gamma,_r)f_{RT}=e^{\frac{b}{2}}B,_T\,, \tag{27}$$
$$e^{\frac{a}{2}}(\alpha,_r f_R+\gamma,_r M^{-1}f_R+2\delta,_r f_{RR}+2\eta,_r f_{RT})=e^{\frac{b}{2}}B,_M\,, \tag{28}$$
$$\gamma,_a f_R+M\delta,_a f_{RR}+M\eta,_a f_{RT}=0, \tag{29}$$
$$\gamma,_b f_R+M\delta,_b f_{RR}+M\eta,_b f_{RT}=0, \tag{30}$$
$$\alpha,_b f_R+\gamma,_b M^{-1}f_R+2\delta,_b f_{RR}+2\eta,_b f_{RT}=0, \tag{31}$$
$$M\alpha,_b f_{RR}+2\gamma,_b f_{RR}=0, \tag{32}$$
$$M\alpha,_b f_{RT}+2\gamma,_b f_{RT}=0, \tag{33}$$
$$M\alpha,_R f_{RR}+2\gamma,_R f_{RR}=0, \tag{34}$$
$$M\alpha,_T f_{RT}+2\gamma,_T f_{RT}=0, \tag{35}$$
$$M\alpha,_T f_{RR}+2\gamma,_T f_{RR}+M\alpha,_R f_{RT}+2\gamma,_R f_{RT}=0, \tag{36}$$
$$\begin{aligned}&f_R(\alpha-\beta-2\gamma M^{-1}+4M\alpha,_M+4\gamma,_M-2\tau,_r)+f_{RR}(2\delta+8M\delta,_M)\\&+f_{RT}(2\eta+8M\eta,_M)=0,\end{aligned} \tag{37}$$
$$\begin{aligned}&f_R(\alpha-\beta+2\alpha,_a-2\tau,_r+2\gamma,_M+2\gamma,_a M^{-1})+f_{RR}(2\delta+2M\delta,_M+4\delta,_a)\\&+f_{RT}(2\eta+2M\eta,_M+4\eta,_a)=0,\end{aligned} \tag{38}$$
$$\begin{aligned}&f_R(\alpha,_R+\gamma,_R M^{-1})+f_{RR}(\alpha-\beta+M\alpha,_M+2\gamma,_M-2\tau,_r+2\delta,_R)+2\delta\\&\times f_{RRR}+2\eta f_{RRT}+2eta,_R f_{RT}=0,\end{aligned} \tag{39}$$
$$\begin{aligned}&f_R(\alpha,_T+\gamma,_T M^{-1})+f_{RT}(\alpha-\beta+M\alpha,_M+2\gamma,_M-2\tau,_r+2\eta,_T)+2\delta\\&\times f_{RRT}+2\eta f_{RTT}+2delta,_T f_{RR}=0,\end{aligned} \tag{40}$$
$$\begin{aligned}&2\gamma,_R f_R+f_{RR}(M\alpha-M\beta+2\gamma+2M\alpha,_a-2M\tau,_r+4\gamma,_a+2M\delta,_R)\\&+2M\delta f_{RRR}+2M\eta f_{RRT}+2M\eta,_R f_{RT}=0,\end{aligned} \tag{41}$$
$$\begin{aligned}&2\gamma,_T f_R+f_{RT}(M\alpha-M\beta+2\gamma+2M\alpha,_a-2M\tau,_r+4\gamma,_a+2M\delta,_R)\\&+2M\delta f_{RRT}+2M\eta f_{RTT}+2M\delta,_T f_{RR}=0,\end{aligned} \tag{42}$$
$$\begin{aligned}&e^{\frac{a}{2}}e^{\frac{b}{2}}M\Bigg[(f-Rf_R+f_T(3p_m-\rho_m-T)+2f_RM^{-1}+p_m)\left(\frac{\alpha+\beta}{2}+\tau,_r\right)\\&+\alpha\{f_T(3p_m,_a-\rho_m,_a)+p_m,_a\}+\beta\{f_T(3p_m,_b-\rho_m,_b)+p_m,_b\}+\gamma\{f_T\\&\times(3p_m,_M-\rho_m,_M)+p_m,_M\}+\frac{\gamma}{M}(f-Rf_R+f_T(3p_m-\rho_m-T)+p_m)\\&+\delta\{f_{RR}(-R+2M^{-1})+f_{RT}(3p_m-\rho_m-T)\}+\eta\{f_{RT}(-R+2M^{-1})\\&+f_{TT}(3p_m-\rho_m-T)\}\Bigg]=B,_r\,.\end{aligned} \tag{43}$$

Noether symmetry technique refers as the most admirable approach as it reduces the complexity associated with matter contents and helps to evaluate exact solutions. Thus, the study of traversable and realistic WH solutions using Noether symmetry approach and non-minimal curvature-matter coupling would be more interesting. We study possible existence of symmetry generators, associated conserved quantities and analyze WH geometry for two models. We also construct corresponding exact solutions to explore cosmological picture of these models. The models are given as [2]

- $f(R,T)$=$R+2g(T)$,
- $f(R,T)$=$F(R)+G(T)$.

3.1 $f(R,T)=R+2g(T)$

We consider a correspondence of this model with standard cosmological constant cold dark matter model by taking into account a trace dependent cosmological constant defined as

$$f(R,T)=R+2\Lambda(T)+g(T). \tag{44}$$

We formulate symmetry generators and conserved quantities by solving the system (24)-(42) which yields

$$\alpha = 0, \quad \beta=-\frac{2c_2B,_r}{r^2}, \quad \gamma=0, \quad \delta=0, \quad \eta=0, \quad \tau=c_1+\int\frac{c_2B,_r}{r^2}dr, \tag{45}$$

where c_1 and c_2 denote arbitrary constants. In gravitational theories of gravity, the study of perfect fluids is of great interest. Such matter distribution describes quite accurately matter content of several astrophysical objects such as stars, galaxies and even the universe at scales larger than 100 Mpc. The matter distribution of the universe can also be described by dust fluid only if there exist a negligible amount of radiations. The dust particles interacting with radiations are responsible for the formation of massive stars. In following, we explore the existence of realistic and traversable WH at large scales and find exact solution of $f(R,T)$ model as well as matter components for dust as well as non-dust distribution of perfect fluid.

Dust Case

For dust distribution, the energy-momentum tensor (2) reduces to

$$T_{\mu\nu}^{(m)}=\rho_m(r)u_\mu u_\nu.$$

Using Eq.(45), we solve (43) leading to

$$\rho_m=-\frac{e^{\frac{-a-b}{2}}}{2c_2c_3},\quad \Lambda(T)=-\frac{g(T)}{2}+c_3T+c_4, \tag{46}$$

where c_3 and c_4 represent arbitrary constants. Assuming $B,_r=c_5$, the non-zero coefficients of symmetry generator and $f(R,T)$ model take the form

$$B=c_5r,\quad \tau=c_1-\frac{c_2c_5}{r},\quad \beta=-\frac{2c_2c_5}{r^2},\quad f(R,T)=R+2c_3T+c_4.$$

The symmetry generators and the corresponding first integral become

$$\begin{aligned}
K_1 &= \frac{\partial}{\partial r},\quad K_2=-\frac{c_2}{r}\frac{\partial}{\partial r}-\frac{2c_2}{r^2}\frac{\partial}{\partial b},\\
\Sigma_1 &= -e^{\frac{a-b}{2}}r^2\left[e^b\left(2c_4+\frac{2}{r^2}+\frac{e^{\frac{-a-b}{2}}}{c_2}\right)+\frac{2+2a'r}{r^2}\right],\\
\Sigma_2 &= r+c_2e^{\frac{a-b}{2}}r\left[e^b\left(2c_4+\frac{2}{r^2}+\frac{e^{\frac{-a-b}{2}}}{c_2}\right)+\frac{2+2a'r}{r^2}\right].
\end{aligned}$$

Inserting Eq.(46) in (12), we obtain

$$e^{b(r)}=\frac{\frac{2}{r^2}+\frac{2a'}{r}}{2c_4+\frac{2}{r^2}+\frac{e^{\frac{-a-b}{2}}}{c_2}}. \tag{47}$$

In order to study geometry as well as realistic existence of WH via shape function and energy bounds, we consider red-shift function both constant as well as variable $a(r)=k$ and $a(r)=-\frac{k}{r}$, $k>0$, where k denotes constant [29]. In the following, we solve Eq.(47) for both choices of red-shift function.

Case I: $a(r)=k$

In this case, Eq.(47) yields

$$b(r)=2\ln\left[-\frac{e^{-\frac{k}{2}}r^2+\sqrt{e^{-k}r^4+16c_4r^2c_2^2+16c_2^2}}{4c_2(c_4r^2+1)}\right], \tag{48}$$

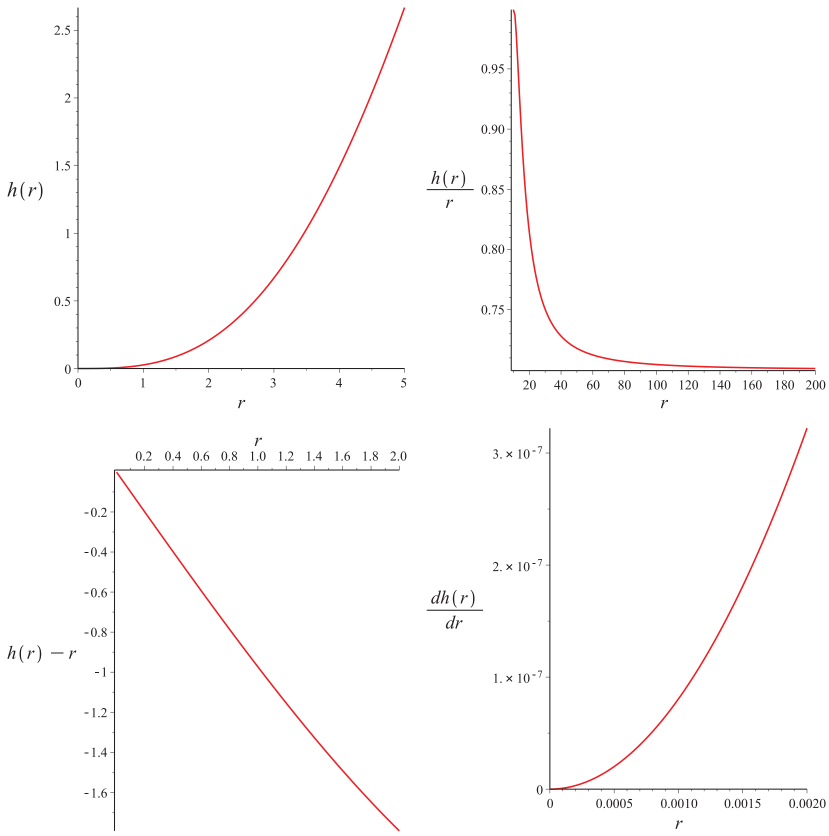

Figure 1: Plots of $h(r)$, $\frac{h(r)}{r}$, $h(r)-r$ and $\frac{dh(r)}{dr}$ versus r for $c_2 = 30$, $c_3 = -0.5$, $c_4 = -0.0095$ and $k = -0.08$.

which leads to shape function as

$$\begin{aligned} h(r) &= [2r^3(e^{-k}r^2 + ((e^{-\frac{k}{2}}\sqrt{e^{-k}r^4 + 16c_4r^2c_2^2 + 16c_2^2} - 8c_2^2c_4) - 8c_2^2c_4^2r^2))] \\ &\times \{(e^{-\frac{k}{2}}r^2 + \sqrt{e^{-k}r^4 + 16c_4r^2c_2^2 + 16c_2^2})^2\}^{-1}. \end{aligned}$$

The energy density of dust fluid becomes

$$\rho_m = -\frac{e^{-\frac{k}{2}-\ln\left[\frac{-e^{-\frac{k}{2}}r^2+\sqrt{\left(e^{-\frac{k}{2}}\right)^2 r^4+16r^2c_2^2c_4+16c_2^2}}{4(c_2(c_4r^2+1))}\right]}}{2c_2c_3}.$$

Figure **1** shows graphical behavior of the shape function. In upper panel, the left plot shows positively increasing shape function satisfying $h(r) < r_0$

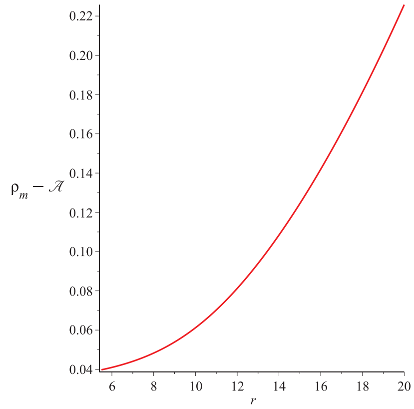

Figure 2: Evolution of $\rho_m - \mathcal{A}$ versus r.

while the right plot represents asymptotic flat behavior as $\frac{h(r)}{r} \rightarrow 0$ with $r \rightarrow \infty$. In the lower face, the left plot identifies WH throat at $r_0 = 0.001$ and the right plot yields $\frac{dh(r_0)}{dr} < 1$. Figure **2** exhibits energy density as positively increasing. For the existence of realistic WH, we substitute constant red-shift function and $b(r)$ from Eq.(48) in (15), it follows that

$$\rho_{eff} + p_{eff} = \frac{rh'(r) - h(r)}{r^3}.$$

Using flaring-out condition in non-geodesic background, this implies that $\rho_{eff} + p_{eff} - \mathcal{A} < 0$, i.e., NEC is violated for effective stress-energy tensor. This indicates the presence of repulsive gravity and consequently, assures the existence of physically viable traversable WH.

Case II: $a(r) = -k/r$

Here, Eq.(47) gives

$$\begin{aligned} b(r) &= 2\ln[(e^{\frac{k}{2r}}r^3 + \{e^{\frac{k}{r}}r^6 + 16r^4c_4c_2^2 + 16r^3c_4c_2^2k + 16c_2^2r^2 + 16c_2^2rk\}^{\frac{1}{2}}) \\ &\times (4\left(c_2r\left(c_4r^2 + 1\right)\right))^{-1}]. \end{aligned} \tag{49}$$

The corresponding shape function turns out to be

$$\begin{aligned} h(r) &= (2r^2(e^{k/r}r^5 + (e^{\frac{k}{2r}}r^2\{r(e^{k/r}r^5 + 16c_4c_2^2r^3 + 16c_4c_2^2kr^2 + 16c_2^2r \\ &+ 16kc_2^2)\}^{\frac{1}{2}} - 8c_4c_2^2r^3) + 8c_4c_2^2kr^2 + (8kc_2^2 - 8c_2^2r^5c_4^2)))/(e^{\frac{k}{2r}}r^3 \\ &+ \sqrt{r(e^{k/r}r^5 + 16c_4c_2^2r^3 + 16c_4c_2^2kr^2 + 16c_2^2r + 16kc_2^2)})^2. \end{aligned}$$

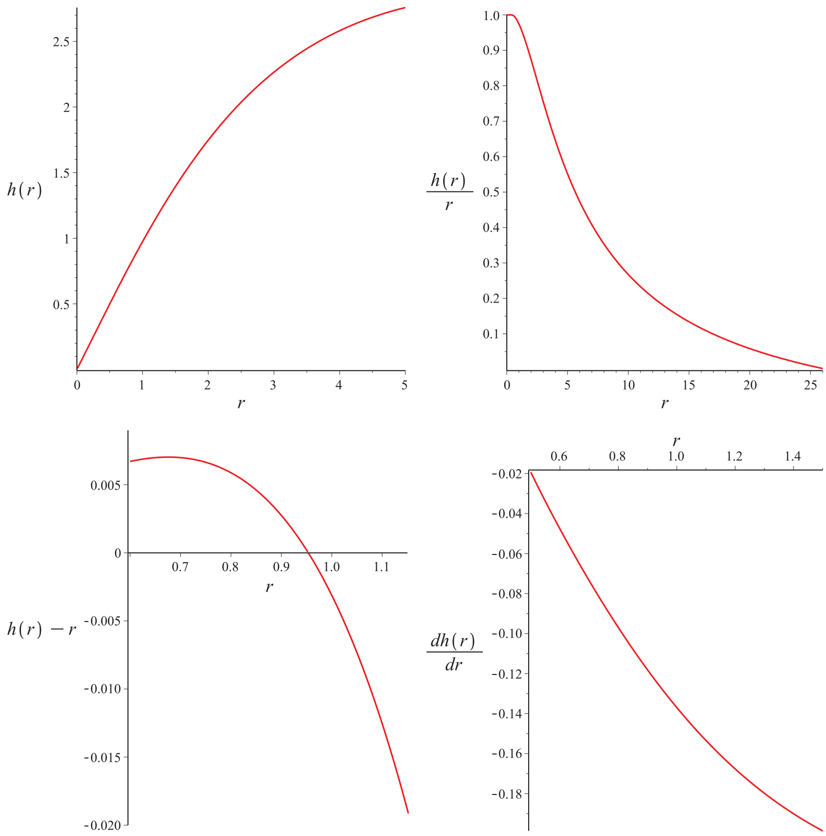

Figure 3: Plots of $h(r)$, $\frac{h(r)}{r}$, $h(r)-r$ and $\frac{dh(r)}{dr}$ versus r for $c_2 = 0.5$, $c_3 = 0.5$, $c_4 = 1.1$ and $k = 5$.

Figure **3** implies that $h(r)$ preserves its positivity with $h(r) < r$ while far from throat, the shape of WH is found to be asymptotic flat in the upper face. The left plot of the lower face locates WH throat at $r_0 = 0.95$ and the corresponding right plot indicates that $\frac{dh(r_0)}{dr} < 1$. To investigate the presence of traversable WH, we insert Eq.(49) in (15) yielding

$$\begin{aligned}
\rho_{eff} + p_{eff} &= (64(((e^{\frac{k}{2r}} r^{\frac{7}{2}} (e^{k/r} r^5 + 16c_4 c_2^2 r^3 + 16c_4 c_2^2 k r^2 + 16c_2^2 r + 16k c_2^2)^{\frac{1}{2}} \\
&- 8c_4^2 c_2^2 r^6) - 8c_4 c_2^2 r^3 k) + 4c_4^2 k^2 r^4 c_2^2 + (8c_4 k^2 r^2 c_2^2 - 8c_4^2 c_2^2 k r^5) \\
&+ (e^{k/r} r^6 - 8r^4 c_4 c_2^2) + 4k^2 c_2^2)(c_4 r^2 + 1) c_2^2)/((e^{\frac{k}{2r}} r^3 + (r(e^{k/r} r^5 \\
&+ 16c_4 c_2^2 r^3 + 16c_4 c_2^2 k r^2 + 16c_2^2 r + 16k c_2^2)^{\frac{1}{2}}))^3 (r(e^{k/r} r^5 + 16c_4 c_2^2 \\
&\times r^3 + 16c_4 c_2^2 k r^2 + 16c_2^2 r + 16k c_2^2))^{\frac{1}{2}}).
\end{aligned}$$

Figure **4** shows that density is positively decreasing while the effective energy density and pressure are negatively increasing such that $\rho_m - \mathcal{A} \geq 0$ and

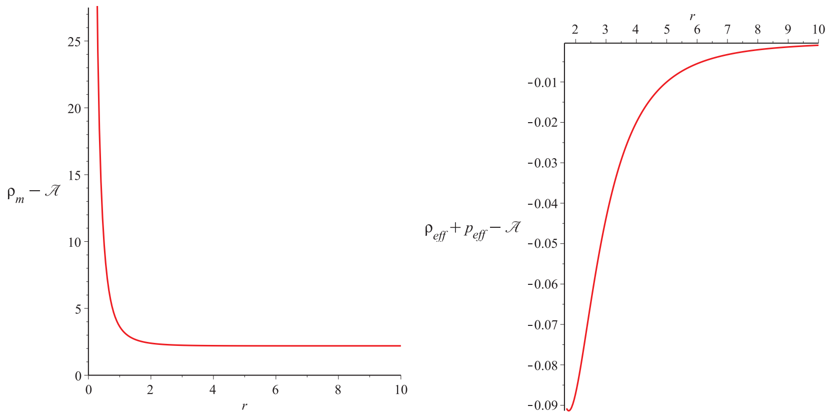

Figure 4: Plots of $\rho_m - \mathcal{A}$ and $\rho_{eff} + p_{eff} - \mathcal{A}$ versus r.

$\rho_{eff} + p_{eff} - \mathcal{A} \leq 0$. This indicates the violation of NEC by effective energy-momentum tensor leading to realistic traversable WH.

Non-Dust Case

At large scales, the non-dust distribution successfully illustrates matter distribution of the universe in the presence of radiations. In this case, we consider a particular relation between density and pressure such that $p_m(a,b,M) = \omega\rho_m(a,b,M)$ (ω denotes equation of state parameter) and solve Eq.(43) which yields

$$\rho_m = -\frac{e^{\frac{-a-b}{2}}}{2c_2(6\omega c_6 + \omega - 2c_6))}, \quad \Lambda(T) = -\frac{g(T)}{2} + c_3 T + c_4, \tag{50}$$

where c_6 denotes arbitrary constant. Here, symmetry generators remain the same as for dust case but the corresponding conserved integral gives

$$\begin{aligned} \Sigma_1 &= -e^{\frac{a-b}{2}} r^2 \left[e^b \left(2c_4 + \frac{2}{r^2} + \frac{e^{\frac{-a-b}{2}}(2c_3(3\omega - 1) + 1)}{2c_2(6\omega c_6 + \omega - 2c_6)} \right) + \frac{2 + 2a'r}{r^2} \right], \\ \Sigma_2 &= r + c_2 e^{\frac{a-b}{2}} r \left[e^b \left(2c_4 + \frac{2}{r^2} + \frac{e^{\frac{-a-b}{2}}(2c_3(3\omega - 1) + 1)}{2c_2(6\omega c_6 + \omega - 2c_6)} \right) + \frac{2 + 2a'r}{r^2} \right]. \end{aligned}$$

Inserting Eq.(50) in (12), we obtain

$$e^{b(r)} = \frac{2(1 + a'r)c_2}{2c_4 r^2 c_2 + 2c_2 + e^{-\frac{a(r)}{2} - \frac{b(r)}{2}} r^2}. \tag{51}$$

Case I: $a(r)=k$

For this case, Eq.(51) yields

$$b(r)=2\ln\left[\frac{-e^{-\frac{k}{2}}r^2+\sqrt{e^{-k}r^4+16c_4r^2c_2^2+16c_2^2}}{4c_2(c_4r^2+1)}\right]. \tag{52}$$

The associated shape function takes the form

$$\begin{aligned} h(r) &= -[2r^3(-e^{-k}r^2+e^{-\frac{k}{2}}\sqrt{e^{-k}r^4+16c_4r^2c_2^2+16c_2^2}+8c_2^2c_4+8c_2^2c_4^2r^2)] \\ &\times (e^{-\frac{k}{2}}r^2-\sqrt{e^{-k}r^4+16c_4r^2c_2^2+16c_2^2})^{-2}. \end{aligned}$$

Inserting Eq.(52) in (50), we obtain

$$\rho_m=\frac{e^{-\frac{k}{2}-\ln\left[\frac{-e^{-\frac{k}{2}}r^2+\sqrt{e^{-k}r^4+16c_4r^2c_2^2+16c_2^2}}{4c_2(c_4r^2+1)}\right]}}{c_2(6\omega c_6+\omega-2c_6)}. \tag{53}$$

The upper plane of Figure **5** indicates that $h(r)$ remains positive but it does not preserve asymptotic flat shape. In lower face, the left plot identifies WH throat at $r_0\approx 0.001$ and the right plot satisfies $h'(r_0)<1$. Figure **6** shows that $\rho_m-\mathcal{A}$ and $\rho_m+p_m-\mathcal{A}$ are positively increasing for $1\leq\omega\leq 0.3$ while $\rho_{eff}+p_{eff}-\mathcal{A}<0$ in this case. Therefore, a realistic traversable WH solution exists.

Case II: $a(r)=-k/r$

For variable red-shift function, Eq.(51) leads to

$$\begin{aligned} b(r) &= \ln[(e^{k/r}r^5+8c_2^2k+8c_2^2r^3c_4+e^{\frac{k}{2r}}r^{5/2}(e^{k/r}r^5+16kc_2^2+16c_2^2r \\ &+ 16c_2^2kr^2c_4+16c_2^2r^3c_4)^{\frac{1}{2}})\{8rc_2^2(1+2r^2c_4+r^4r^2c_4+r^4c_4^2)\}^{-1}]. \end{aligned} \tag{54}$$

The corresponding shape function is

$$\begin{aligned} h(r) &= [(e^{k/r}r^5+8c_2^2k+(8c_2^2kr^2c_4-8c_2^2r^3c_4)+(e^{\frac{k}{2r}}r^{5/2}\{e^{k/r}r^5+16c_2^2k \\ &+ 16c_2^2r+16c_2^2kr^2c_4+16c_2^2r^3c_4\}^{\frac{1}{2}}-8c_2^2r^5c_4^2))r]/(e^{k/r}r^5+8c_2^2k+8c_2^2r \end{aligned}$$

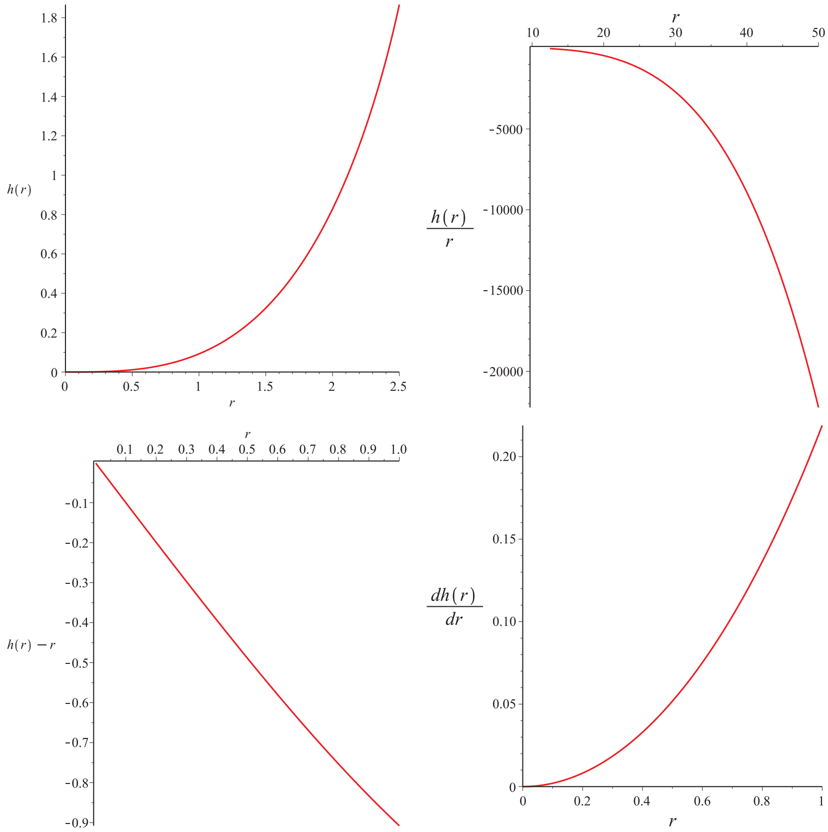

Figure 5: Plots of $h(r)$, $\frac{h(r)}{r}$, $h(r)-r$ and $\frac{dh(r)}{dr}$ versus r for $c_2 = 5$, $c_4 = -0.15$, $c_6 = 0.5$ and $k = 1$.

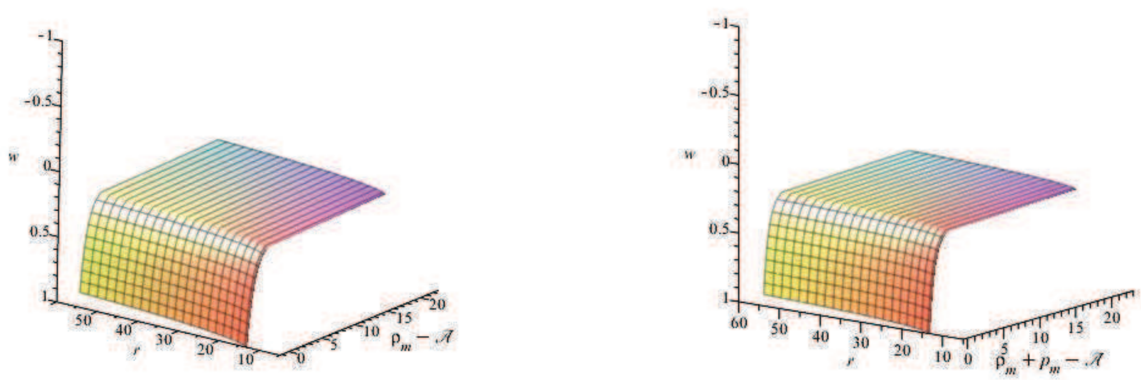

Figure 6: Plots of $\rho_m - \mathcal{A}$ and $\rho_m + p_m - \mathcal{A}$ versus r.

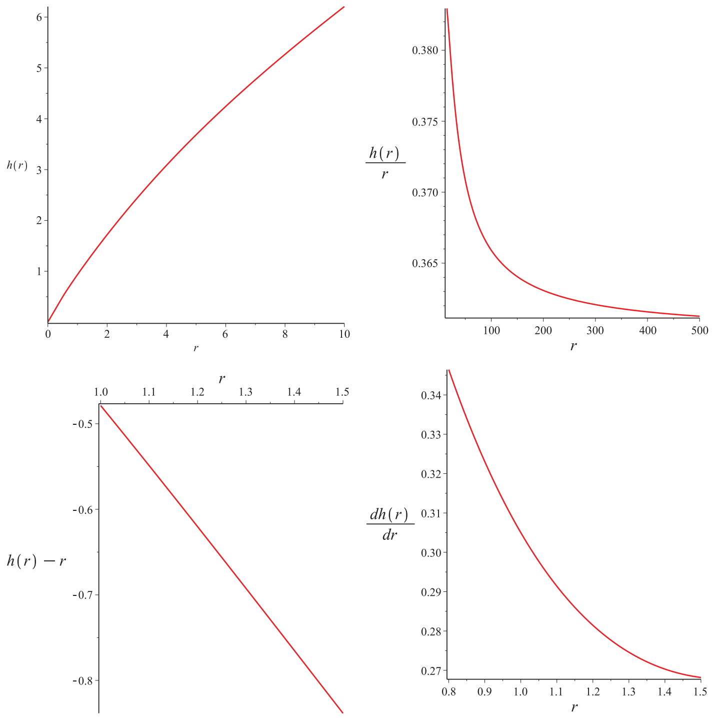

Figure 7: Plots of $h(r)$, $\frac{h(r)}{r}$, $h(r)-r$ and $\frac{dh(r)}{dr}$ versus r for $c_2=4$, $c_4=0.1$, $c_6=0.5$, and $k=1$.

$$+\quad 8c_2^2kr^2c_4+8c_2^2r^3c_4+e^{\frac{k}{2r}}r^{5/2}\{e^{k/r}r^5+16c_2^2k+16c_2^2r+16c_2^2kr^2c_4$$
$$+\quad 16c_2^2r^3c_4\}^{\frac{1}{2}}).$$

Figure **7** indicates that $h(r)<r$, $\frac{h(r)}{r}\rightarrow 0$ as $r\rightarrow\infty$, the minimum radius of throat is located at $r_0=1$ with $h'(r_0)<1$. We insert Eq.(54) in (15) and (50) which leads to establish graphical interpretation of energy density and pressure with respect to perfect fluid and effective energy-momentum tensor. Figure **8** shows that $\rho_m-\mathcal{A}\geq 0$ and $\rho_m+p_m-\mathcal{A}\geq$ for $1\leq\omega\leq 0.3$ while $\rho_{eff}+p_{eff}-\mathcal{A}<0$ for $1\leq\omega\leq -1$. Thus, a realistic traversable WH exists for variable red-shift function in non-dust distribution.

3.2 $f(R,T)=F(R)+h(T)$

Now we consider a general $f(R,T)$ model appreciating indirect non-minimal curvature-matter coupling. We specify $F(R)$ as follows [30]

$$f(R,T)=R+\mu R^2+\nu R^n+G(T),\quad n\geq 3,\tag{55}$$

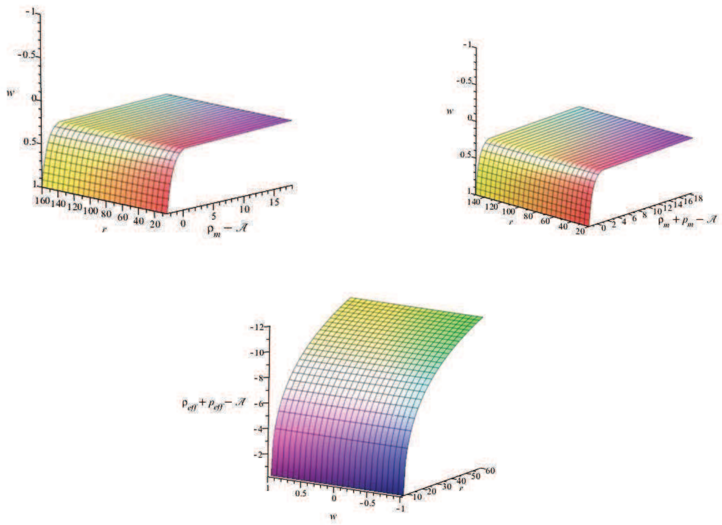

Figure 8: Plots of $\rho_m - \mathcal{A}$, $\rho_m + p_m - \mathcal{A}$ and $\rho_{eff} + p_{eff} - \mathcal{A}$ versus r for $c_2 = 4$, $c_4 = 0.1$, $c_6 = 0.5$ and $k = 1$.

where μ and ν are arbitrary constants. We solve the system (24)-(42) for both dust as well as non-dust distributions and discuss WH geometry for constant and variable red-shift function.

Dust Case

In this case, we solve the system (24)-(43) and obtain

$$
\begin{aligned}
\alpha &= d_1, \quad \beta = d_1 - 2d_4, \quad \gamma = 0, \quad \delta = 0, \quad \eta = 0, \quad \tau = d_4 r, \quad B = d_5,\\
\rho_m &= e^{-a} r^2 - \frac{1}{d_2 r^2}[-\nu R^n r^2 + \nu R^n n r^2 - 2\nu R^{(} - 1 + n)n + \mu r^2 R^2 - 4\mu R\\
&- 2 - r^2 d_3], \quad G(T) = d_2 T + d_3, \qquad (56)
\end{aligned}
$$

where d_j represents arbitrary constants. For these coefficients of K, the symmetry generators and corresponding first integrals are found to be

$$
\begin{aligned}
K_1 &= \frac{\partial}{\partial a} + \frac{\partial}{\partial b}, \quad K_2 = r\frac{\partial}{\partial r} - 2\frac{\partial}{\partial b},\\
\Sigma_1 &= -e^{\frac{a-b}{2}} r[2(1 + \mu R + n\nu R^{n-1}) + rR'(2\mu + n(n-1)\nu R^{n-2})],\\
\Sigma_2 &= -e^{\frac{a-b}{2}} r[2e^b(n-1)\nu R^{n-1} + 2(1 + \mu R + n\nu R^{n-1}) + 4rR'(2\mu + n\nu\\
&\times (n-1)R^{n-2})].
\end{aligned}
$$

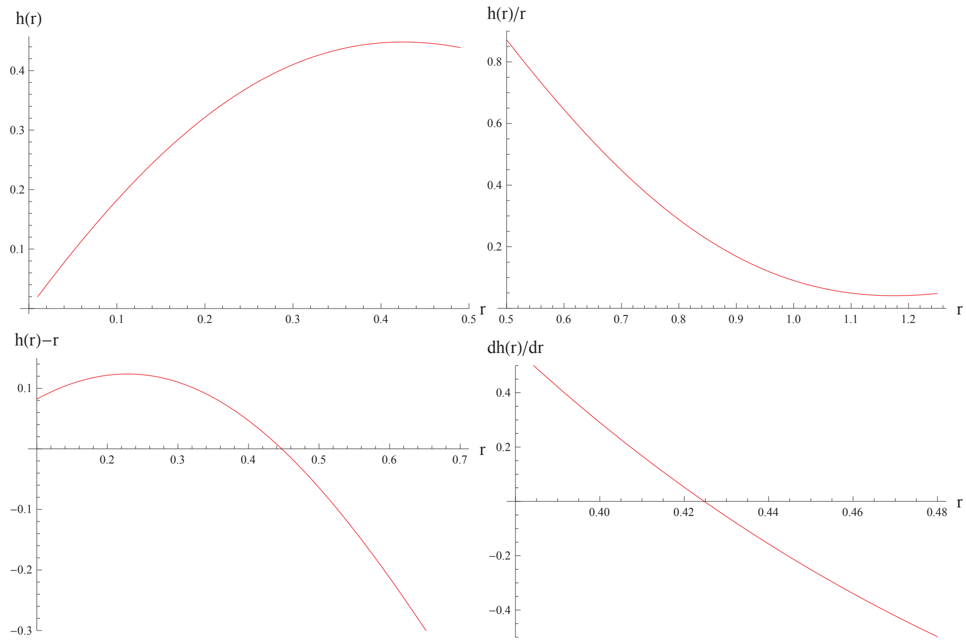

Figure 9: Plots of $h(r)$, $\frac{h(r)}{r}$, $h(r)-r$ and $\frac{dh(r)}{dr}$ versus r for $d_2 = 0.0001$, $d_3 = 1$, $\mu = 0.5$, $\nu = 0.1$ and $k = -0.15$.

For $b(r) = \ln\left(\frac{-r}{-r+h(r)}\right)$, Eq.(12) reduces to

$$-\frac{r}{(-r+h(r))} + \frac{(2(1+2\mu R))(1+a'r)e^{a}}{r^4 d_2} = 0. \tag{57}$$

We solve this equation numerically for both $a(r) = k$ and $a(r) = -\frac{k}{r}$.

Case I: $a(r) = k$

For constant red-shift function, we analyze the geometry of WH for both $n = 0$ as well as $n \neq 0$. Inserting Eq.(8) in (57) for $n = 0$, it follows that

$$\frac{r}{h(r)-r} - \frac{2e^k}{d_2 r^4}\left[2\mu\left(\left(\frac{2(h(r)-r)^2\left(\frac{r(h'(r)-1)}{(h(r)-r)^2} - \frac{1}{h(r)-r}\right)}{r^3} - \frac{2(h(r)-r)}{r^3}\right) + \frac{4(h(r)-r)}{r} + \frac{2}{r^2}\right) + 1\right] = 0. \tag{58}$$

We solve this equation for $h(r)$ and establish graphical analysis to study its geometrical properties. Figure **9** identifies that all WH conditions are

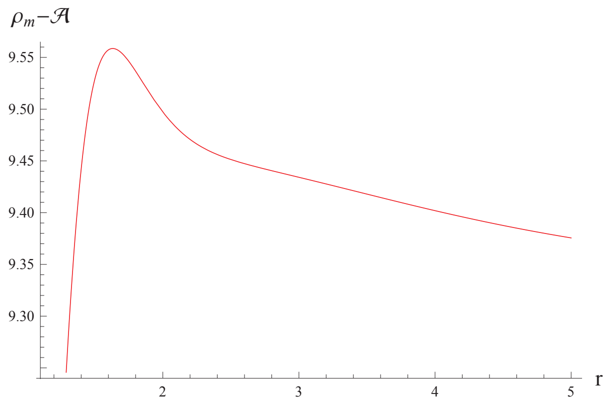

Figure 10: Evolution of $\rho_m - \mathcal{A}$ versus r.

satisfied as $h(r) < r$, $\frac{h(r)}{r} \to 0$, the minimum radius is $r_0 = 0.45$ with $h'(r_0) < 1$. Hence, $\rho_{eff} + p_{eff} - \mathcal{A} < 0$ holds trivially while Figure **10** indicates that energy density remains positive.

For $n \neq 0$, Eq.(57) reduces to

$$\frac{r}{-r+h(r)} - \frac{2e^k}{r^4 d_2}\left(2\mu\left(\frac{4(-r+h(r))}{r} + \left(\frac{2(-r+h(r))^2}{r^3}\left(-\frac{1}{-r+h(r)} + \frac{r(-1+h'(r))}{(-r+h(r))^2}\right) - 2(-r+h(r))\right) + \frac{2}{r^2}\right) + n\nu\left(\frac{4(-r+h(r))}{r} + \frac{2}{r^2} + \left(\frac{2\left(-\frac{1}{-r+h(r)} + \frac{r(-1+h'(r))}{(-r+h(r))^2}\right)(-r+h(r))^2}{r^3} - \frac{2(-r+h(r))}{r^3}\right)\right)^{-1+n}\right) - \frac{2e^k}{r^4 d_2} = 0. \quad (59)$$

The numerical solution of $h(r)$ provides two roots for $n = 3$ as shown in Figure **11**. The left plot of upper face represents that both roots remain positive with $h(r) < r$ while the right plot identifies asymptotic flat shape of WH. The lower plot locates the corresponding throat at $r_0 = 0.424$ (red) and $r_0 = 0.36$ (blue).

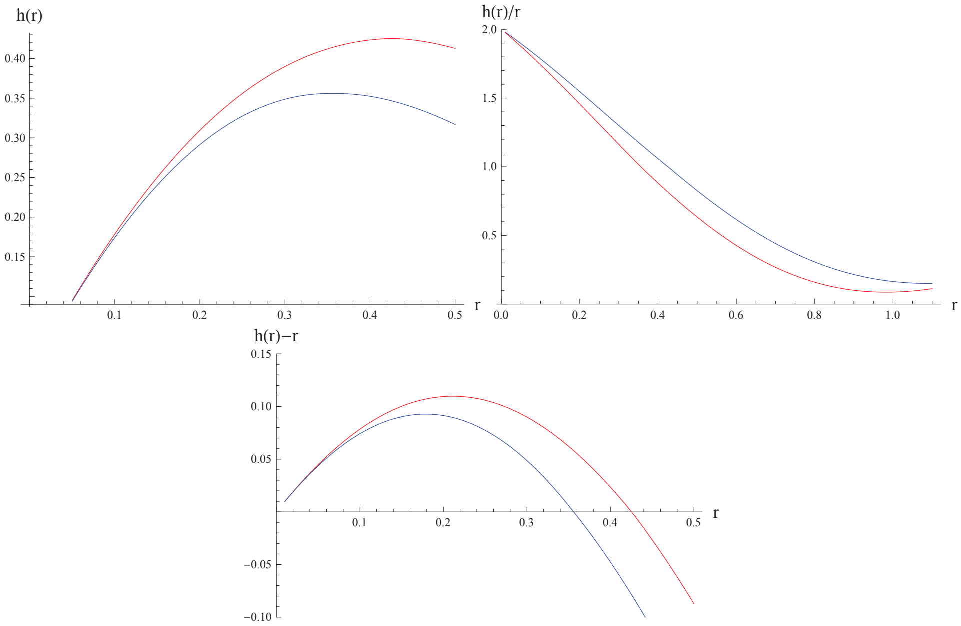

Figure 11: Plots of $h(r)$, $\frac{h(r)}{r}$ and $h(r) - r$ versus r for $d_2 = -0.0001$, $d_3 = 1$, $\mu = 0.08$, $\nu = -3.5$, $k = 0.5$ and $n = 3$.

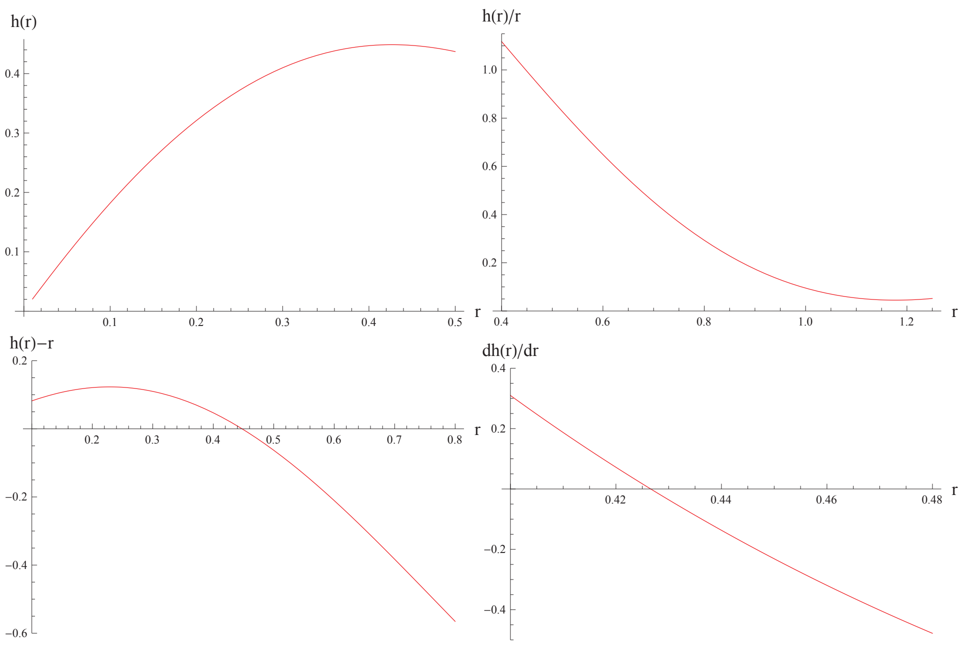

Figure 12: Plots of $h(r)$, $\frac{h(r)}{r}$, $h(r) - r$ and $\frac{dh(r)}{dr}$ versus r for $d_2 = 0.0001$, $d_3 = 1$, $\mu = 0.5$, $\nu = 0.1$ and $k = 0.01$.

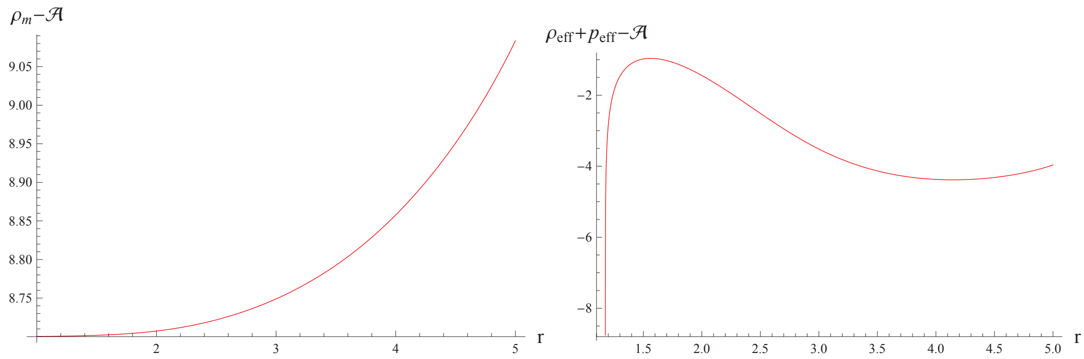

Figure 13: Evolution of $\rho_m - \mathcal{A}$ and $\rho_{eff} + p_{eff} - \mathcal{A}$ versus r.

Case II: $a(r) = -k/r$

For $n = 0$, Eq.(57) gives

$$\frac{r}{h(r)-r} + \frac{(r+k)e^{-\frac{k}{r}}}{r^5 d_2}\Bigg(1+2\mu\Bigg(\frac{k^2(-r+h(r))}{2r^5} + \frac{4(-r+h(r))}{r} + \frac{2}{r^2}$$
$$+ \frac{k\left(-\frac{1}{-r+h(r)} + \frac{r(-1+h'(r))}{(-r+h(r))^2}\right)(-r+h(r))^2}{2r^4} + \frac{2}{r^3}\Bigg(\Bigg(-\frac{1}{-r+h(r)}$$
$$+ \frac{r(-1+h'(r))}{(-r+h(r))^2}\Bigg)(-r+h(r))^2 - (-r+h(r))\Bigg)\Bigg)\Bigg) = 0. \tag{60}$$

The numerical solution of this equation is shown in Figure **12** which shows that all geometrical conditions of WH are preserved as $h(r) < r$, $\frac{h(r)}{r} \to 0$, WH throat is located at $r_0 = 0.45$ with $h'(r_0) < 1$. Figure **13** shows that $\rho_m - \mathcal{A} > 0$ and $\rho_{eff} + p_{eff} - \mathcal{A} < 0$ ensuring the violation of NEC for effective energy-momentum tensor yielding physically acceptable traversable WH.

When $n \neq 0$, Eq.(57) takes the following form

$$\frac{r}{-r+h(r)} - \frac{2(r+k)e^{-\frac{k}{r}}}{r^5 d_2}\Bigg(1+2\mu\Bigg(\frac{k^2(-r+h(r))}{2r^5} + \frac{4(-r+h(r))}{r} + \frac{2}{r^2}$$
$$+ \frac{k\left(-\frac{1}{-r+h(r)} + \frac{r(-1+h'(r))}{(-r+h(r))^2}\right)(-r+h(r))^2}{2r^4} + \frac{2(-r+h(r))}{r^3}((-r+h(r))$$
$$\times\left(-\frac{1}{-r+h(r)} + \frac{r(-1+h'(r))}{(-r+h(r))^2}\right) - 1\Bigg)\Bigg) + n\nu\Bigg(\frac{k^2(-r+h(r))}{2r^5} + \frac{2}{r^2}$$

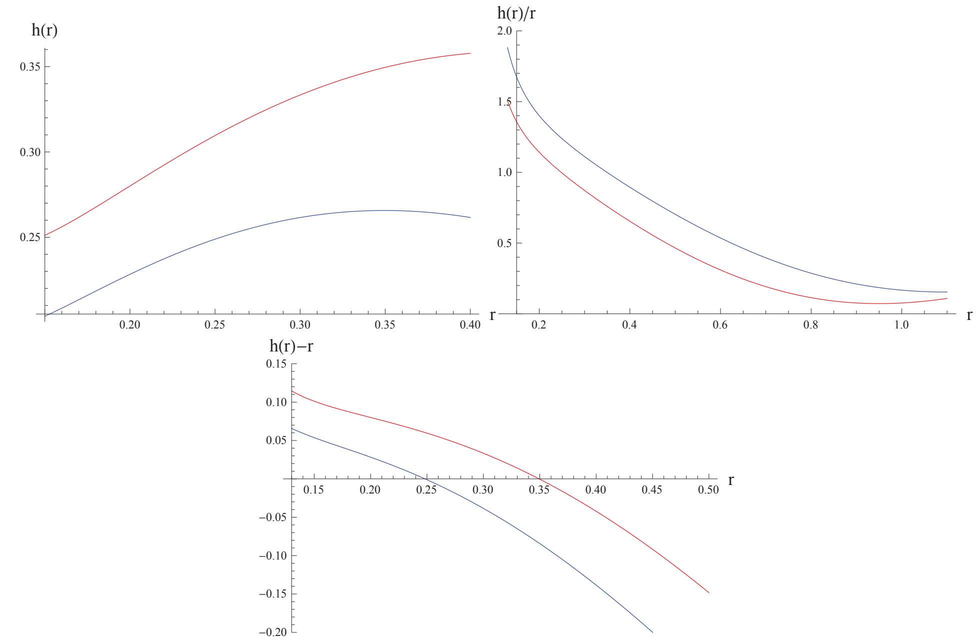

Figure 14: Plots of $h(r)$, $\frac{h(r)}{r}$ and $h(r)-r$ versus r for $d_2=-0.0001$, $d_3=1$, $\mu=0.08$, $\nu=-2$, $k=0.5$ and $n=3$.

$$+\frac{k\left(-\frac{1}{-r+h(r)}+\frac{r(-1+h'(r))}{(-r+h(r))^2}\right)(-r+h(r))^2}{2r^4}+\frac{4(-r+h(r))}{r}+\frac{2(-r+h(r))}{r^3}$$
$$\times\left(\left(\left(-\frac{1}{-r+h(r)}+\frac{r(-1+h'(r))}{(-r+h(r))^2}\right)(-r+h(r))-1\right)\right)^{-1+n}\Bigg)=0.$$

This yields two solutions of the shape function whose graphical analysis is established for $n=3$. In Figure **14**, the upper left plot shows that both solutions of $h(r)$ preserve positive behavior with $h(r)<r$ while the corresponding right plot determines asymptotic flat shape of WH. The lower plot identifies minimum radius of WH at $r_0=0.35$ (red) and $r_0=0.25$ (blue).

Non-Dust Case

For perfect fluid, we consider $p_m=\omega\rho_m$ to evaluate symmetry generators and associated conserved quantities. Solving Eqs.(24)-(43), we obtain

$$\begin{aligned}\tau &= d_4, \quad B=d_5 r, \quad \rho_m=\frac{1}{R((3d_2\omega-d_2)+\omega)r^2d_1}\left[d_5e^{-\frac{a(r)}{2}-\frac{b(r)}{2}}a(r)R\right.\\ &+ \left.\left(\left(\left(\left(R^3\mu r^2d_1-R\nu r^2d_1\right)-d_3(Rr)^2d_1\right)-2Rd_1\right)-4\mu R^2d_1\right)\right]. \qquad (61)\end{aligned}$$

These coefficients lead to the following symmetry generators and conserved integral

$$
\begin{aligned}
K_1 &= \frac{\partial}{\partial a}+\frac{\partial}{\partial b}, \quad K_2=\frac{\partial}{\partial r}-2\frac{\partial}{\partial b},\\
\Sigma_1 &= -e^{\frac{a-b}{2}}r[2(1+\mu R+n\nu R^{n-1})+rR'(2\mu+n(n-1)\nu R^{n-2})],\\
\Sigma_2 &= -e^{\frac{a-b}{2}}r^2[R+\mu R^2+\nu R^n+d_3+(2/r^2-R)(1+2\mu R+n\nu R^{n-1})\\
&- \frac{d_2}{R((3d_2\omega-d_2)+\omega)r^2d_1}\Big[\{(3\omega-1)+\omega\}(d_5e^{-\frac{a(r)}{2}-\frac{b(r)}{2}}a(r)R\\
&+ (((R^3\mu r^2d_1-R\nu r^2d_1)-d_3(Rr)^2d_1)-2Rd_1)-4\mu R^2d_1)\Big]+2\\
&\times (1+\mu R+n\nu R^{n-1})+4rR'(2\mu+n\nu(n-1)R^{n-2})].
\end{aligned}
$$

Substituting $b(r)=\ln\left(\frac{-r}{-r+h(r)}\right)$ in Eqs.(12) and (57), it follows that

$$
\begin{aligned}
&\frac{1}{(-r+h(r))r^3ad_5}\Bigg(-8\sqrt{-\frac{r}{-r+h(r)}}e^{\frac{a}{2}}d_6a'r^4h(r)\mu a''+4e^{\frac{a}{2}}d_6a'r^3\\
&\times h(r)^2\mu a''\sqrt{-\frac{r}{-r+h(r)}}-4\sqrt{-\frac{r}{-r+h(r)}}e^{\frac{a}{2}}d_6a'^3r^4\mu h(r)-18e^{\frac{a}{2}}\\
&\times d_6a'^2r^3\mu h(r)\sqrt{-\frac{r}{-r+h(r)}}-2\sqrt{-\frac{r}{-r+h(r)}}e^{\frac{a}{2}}d_6a'^2r^4\mu h'(r)+2e^{\frac{a}{2}}d_6\\
&\times a'^3r^3h(r)^2\mu\sqrt{-\frac{r}{-r+h(r)}}+8\sqrt{-\frac{r}{-r+h(r)}}e^{\frac{a}{2}}d_6a'^2r^2h(r)^2\mu-32e^{\frac{a}{2}}\\
&\times d_6a'r^4h(r)\mu\sqrt{-\frac{r}{-r+h(r)}}+16\sqrt{-\frac{r}{-r+h(r)}}e^{\frac{a}{2}}d_6a'r^3h(r)^2\mu-10e^{\frac{a}{2}}\\
&\times d_6a'rh(r)^2\mu\sqrt{-\frac{r}{-r+h(r)}}+18\sqrt{-\frac{r}{-r+h(r)}}e^{\frac{a}{2}}d_6a'r^2h(r)\mu-10e^{\frac{a}{2}}\\
&\times d_6a'r^3h'(r)\mu\sqrt{-\frac{r}{-r+h(r)}}+8\sqrt{-\frac{r}{-r+h(r)}}e^{\frac{a}{2}}d_6h(r)\mu rh'(r)+4e^{\frac{a}{2}}\\
&\times \sqrt{-\frac{r}{-r+h(r)}}d_6\mu a''r^4+r^4ad_6-16\sqrt{-\frac{r}{-r+h(r)}}e^{\frac{a}{2}}d_6\mu r^2+16e^{\frac{a}{2}}d_6r^4\\
&\times \sqrt{-\frac{r}{-r+h(r)}}\mu-16\sqrt{-\frac{r}{-r+h(r)}}e^{\frac{a}{2}}d_6\mu h(r)^2-2\sqrt{-\frac{r}{-r+h(r)}}e^{\frac{a}{2}}d_6\\
&\times a'r^5+2\sqrt{-\frac{r}{-r+h(r)}}e^{\frac{a}{2}}d_6r^3h(r)-2\sqrt{-\frac{r}{-r+h(r)}}e^{\frac{a}{2}}d_6r^4+10e^{\frac{a}{2}}d_6
\end{aligned}
$$

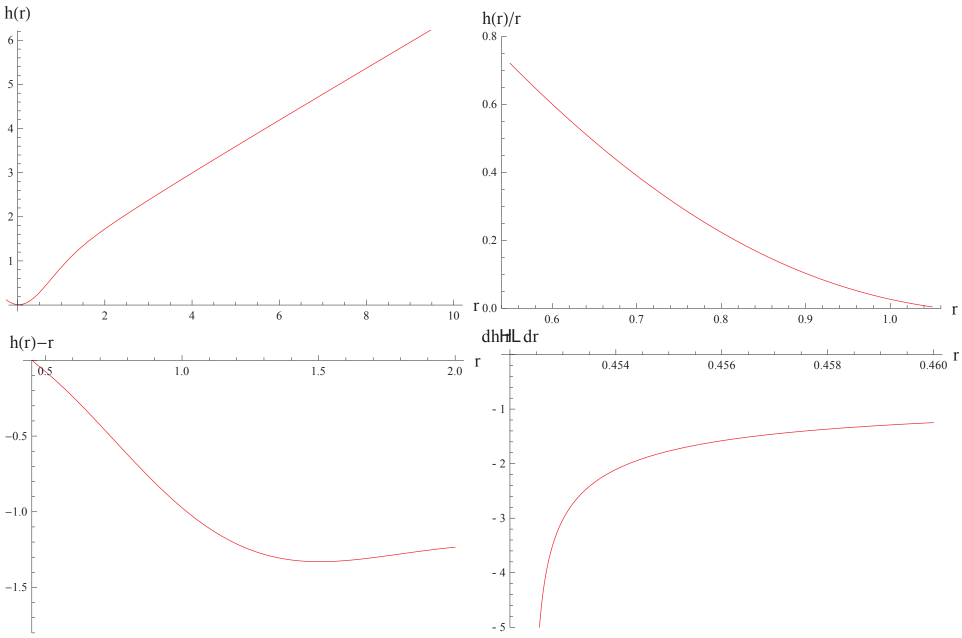

Figure 15: Plots of $h(r)$, $\frac{h(r)}{r}$, $h(r)-r$ and $\frac{dh(r)}{dr}$ versus r for $d_2=-1.5$, $d_3=1$, $d_5=-0.84$, $\mu=2.5$, $\nu=-1.1$, $k=0.01$ and $n=0$.

$$
\begin{aligned}
&\times\, a'r^2\sqrt{-\frac{r}{-r+h(r)}}h(r)\mu h'(r)+2\sqrt{-\frac{r}{-r+h(r)}}e^{\frac{a}{2}}d_6a'^2r^3h(r)\mu h'(r)\\
&+2\sqrt{-\frac{r}{-r+h(r)}}e^{\frac{a}{2}}d_6a'^3r^5\mu+10\sqrt{-\frac{r}{-r+h(r)}}e^{\frac{a}{2}}d_6a'^2r^4\mu+16e^{\frac{a}{2}}d_6\\
&\times\, a'r^5\mu\sqrt{-\frac{r}{-r+h(r)}}-8\sqrt{-\frac{r}{-r+h(r)}}e^{\frac{a}{2}}d_6a'r^3\mu-32\sqrt{-\frac{r}{-r+h(r)}}\\
&\times\, e^{\frac{a}{2}}d_6r^3\mu h(r)+16\sqrt{-\frac{r}{-r+h(r)}}e^{\frac{a}{2}}d_6r^2h(r)^2\mu+32\sqrt{-\frac{r}{-r+h(r)}}e^{\frac{a}{2}}h(r)\\
&\times\, d_6\mu r-8\sqrt{-\frac{r}{-r+h(r)}}e^{\frac{a}{2}}d_6r^2h'(r)\mu+2\sqrt{-\frac{r}{-r+h(r)}}e^{\frac{a}{2}}d_6a'r^4h(r)+4e^{\frac{a}{2}}\\
&\times\, d_6a'r^5\mu\sqrt{-\frac{r}{-r+h(r)}}a''-8\sqrt{-\frac{r}{-r+h(r)}}e^{\frac{a}{2}}d_6h(r)\mu a''r^3+4e^{\frac{a}{2}}d_6\mu\\
&\times\, \sqrt{-\frac{r}{-r+h(r)}}a''r^2h(r)^2\Bigg)=0. \qquad (62)
\end{aligned}
$$

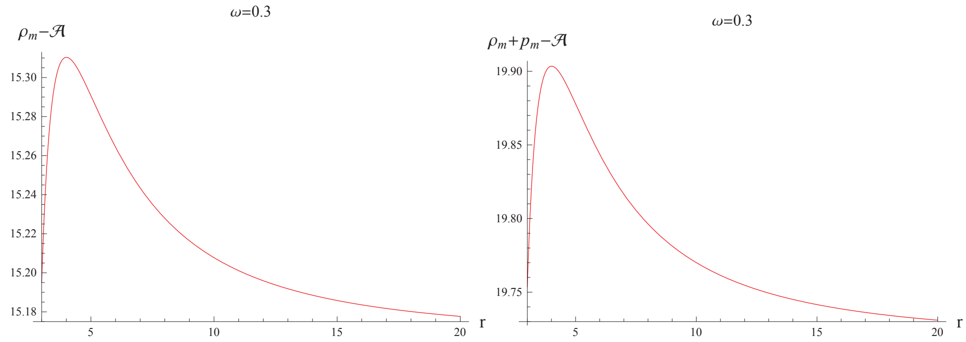

Figure 16: Plots of $\rho_m - \mathcal{A}$ and $\rho_m + p_m - \mathcal{A}$ versus r.

Case I: $a(r) = k$

We numerically solve Eq.(62) for $n = 0$ which leads to analyze WH conditions graphically. In Figure **15**, the upper left plot shows that $h(r)$ is positively increasing with $h(r) < r$ while the right plot assures asymptotic flat shape of WH. The lower left plot determines throat at the minimum radius, i.e., $r_0 = 0.456$ whereas the right plot preserves the derivative condition at throat as $h'(r_0) < 1$. We examine the behavior of energy density and pressure of perfect fluid for $\omega = -0.3$ in Figure **16**. Both plots indicate that NEC and WEC are preserved while NEC is trivially violated for the effective energy-momentum tensor. Consequently, there exists a realistic traversable WH for non-dust distribution.

Case II: $a(r) = -k/r$

In Figure **17**, the left plot of upper panel represent positively increasing behavior of $h(r)$. The upper right plot indicates that WH appreciates asymptotic flat shape. The lower left plot identifies the minimum radius at WH throat, i.e., $r_0 = 0.35$ while the right plot shows that derivative condition is satisfied at throat $h'(r_0) < 1$. Both upper plots of Figure **18** represent that NEC and WEC are recovered. For variable red-shift function, the violation of NEC relative to effective energy-momentum tensor is analyzed in lower plot. Thus, the existence of a realistic traversable WH is possible for non-dust distribution with $n = 0$.

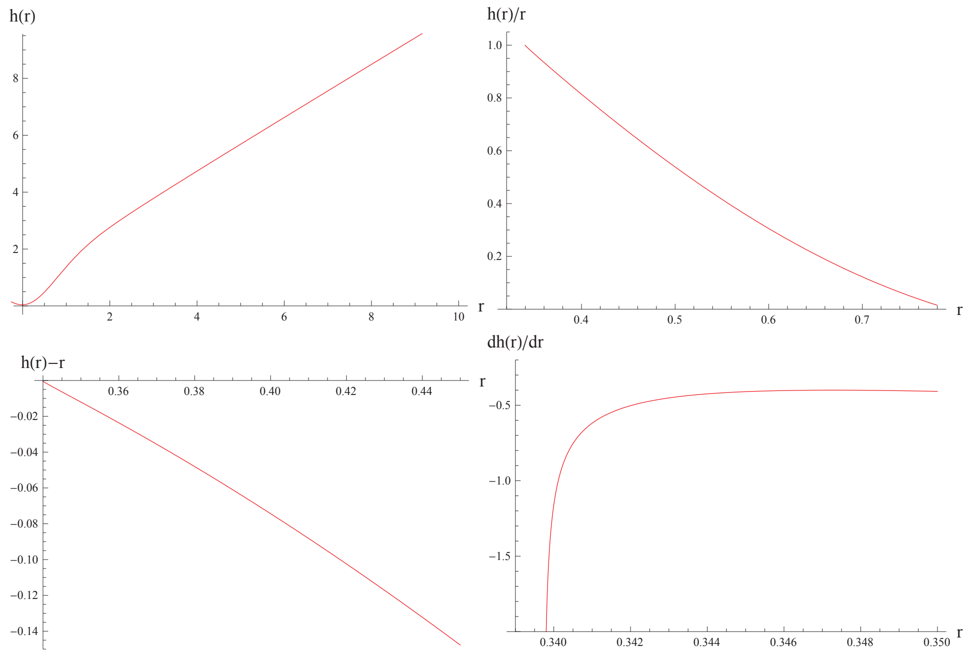

Figure 17: Plots of $h(r)$, $\frac{h(r)}{r}$, $h(r)-r$ and $\frac{dh(r)}{dr}$ versus r for $d_2=-1.5$, $d_3=1$, $d_5=-0.84$, $d_6=-0.01$, $\mu=2.5$, $\nu=-1.1$, $k=0.01$ and $n=0$.

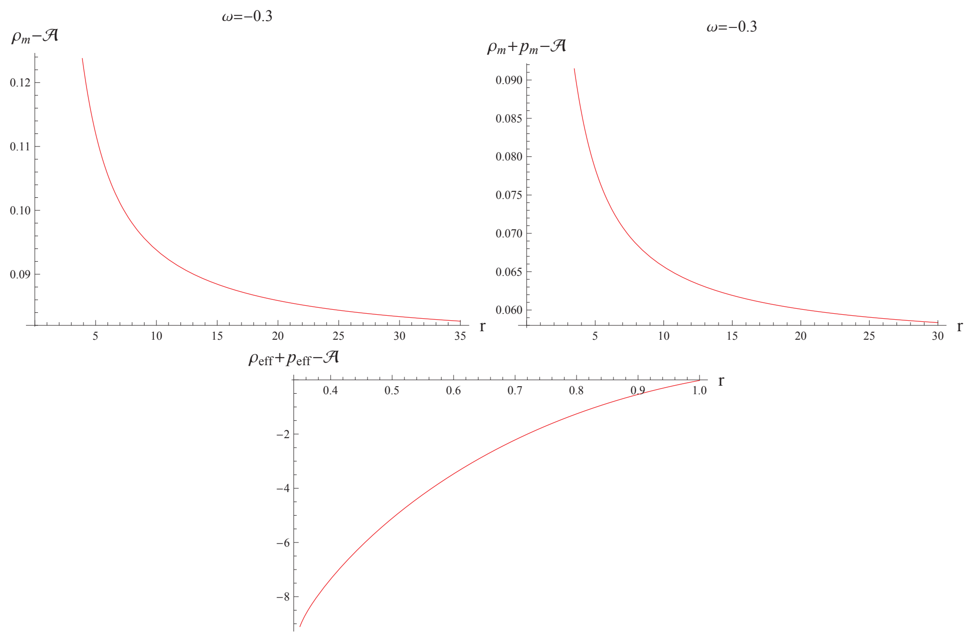

Figure 18: Evolution of $\rho_m-\mathcal{A}$, $\rho_m+p_m-\mathcal{A}$ and $\rho_{eff}+p_{eff}-\mathcal{A}$ versus r.

4 Stability Analysis

In this section, we analyze the stability of realistic and traversable WH solutions via Tolman-Oppenheimer-Volkov (TOV) equation corresponding to both minimally coupled $f(R,T)$ models and constant as well as variable red-shift function. For this purpose, we consider non-conserved energy-momentum tensor and determine TOV equation for isotropic fluid distribution. The radial component of Eq.(5) yields

$$\left\{\frac{dp_m}{dr}+\frac{a'(r)}{2}\left(p_m+\rho_m\right)\right\}\left(1+\frac{2f_T}{1-f_T}\right)+\frac{f_T(p'_m-\rho'_m)}{2(1-f_T)}=0. \tag{63}$$

This equation describes the equilibrium state of WH due to combination of hydrostatic force $\mathcal{F}_h$ and gravitational force $\mathcal{F}_g$. In view of Eq.(63), these dynamical forces can be split into following form

$$\begin{aligned}\mathcal{F}_h &= p'_m\left[\left(1+\frac{2f_T}{1-f_T}\right)+\frac{f_T}{2(1-f_T)}\right],\\ \mathcal{F}_g &= \frac{a'(r)}{2}\left(p_m+\rho_m\right)\left(1+\frac{2f_T}{1-f_T}\right)-\frac{f_T\rho'_m}{2(1-f_T)}.\end{aligned}$$

The existence of stable realistic traversable WH is possible only if the total effect of these dynamical forces is zero, i.e., $\mathcal{F}_h+\mathcal{F}_g=0$.

In Figure **19**, we study the stable/unstable behavior of physically acceptable traversable WH at different evolutionary stages, i.e., decelerating and accelerating cosmos through Eqs.(50), (52) and (53). In upper plane, both plots indicate that the hydrostatic and gravitational forces counterbalance each other effect due to same magnitude but in opposite direction for $\omega=1$ and $\omega=0.3$. The null effect of these forces defines stable state of WH at the time when universe was filled with stiff matter and this stability is maintained till radiation dominated era. In lower plane, the trajectories of gravitational and hydrostatic forces appear in the same direction and consequently, violate equilibrium condition for both $\omega=-0.3$ and $\omega=-1$. This analysis specifies the existence of stable and physically acceptable traversable WH with constant gravitational red-shift in decelerating phase of the universe whereas this stability is disturbed as the universe experiences strong anti-gravitational effects leading to an era of accelerated expansion.

In case of variable red-shift function, the shape function (54) and TOV equation (63) explores the stability of WH in the presence of stiff fluid, radiation dominated phase and DE era. The upper and lower panels of Figure

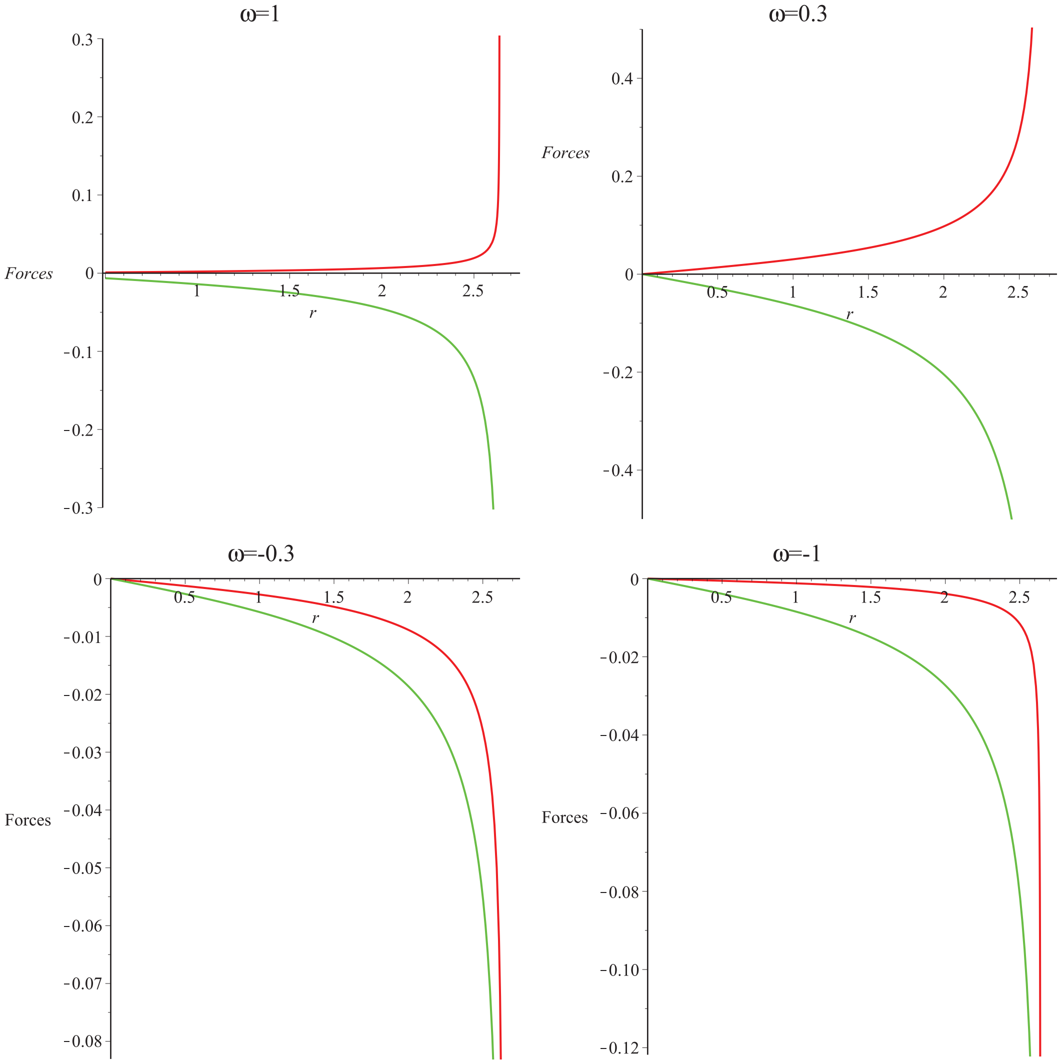

Figure 19: Plots of $\mathcal{F}_g$ (red) and $\mathcal{F}_h$ (green) versus r for $c_2 = 5$, $c_4 = -0.15$, $c_3 = c_6 = 0.5$, $a(r) = k$ and $k = 1$.

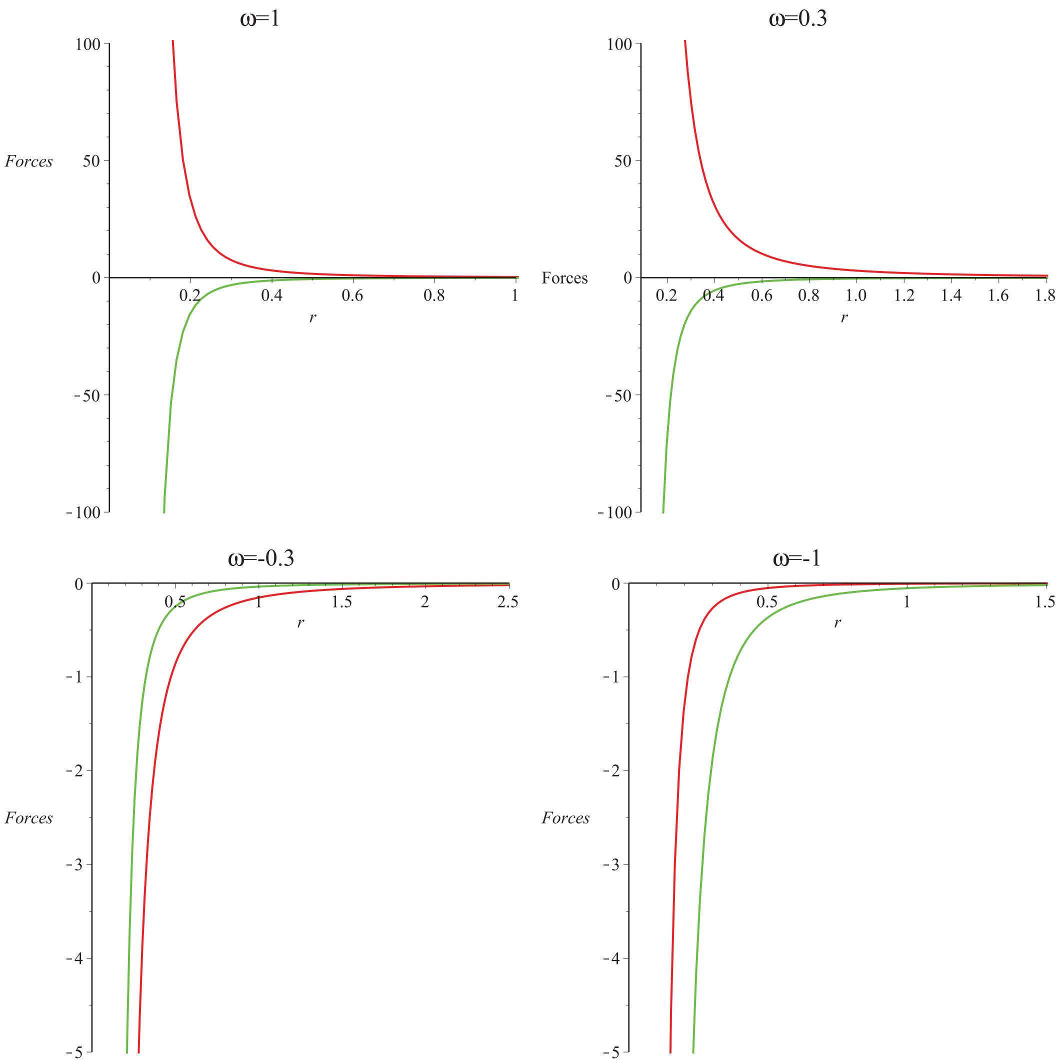

Figure 20: Plots of $\mathcal{F}_g$ (red) and $\mathcal{F}_h$ (green) versus r for $c_2 = 4$, $c_4 = 0.1$, $c_3 = c_6 = 0.5$, $a(r) = -k/r$ and $k = 1$.

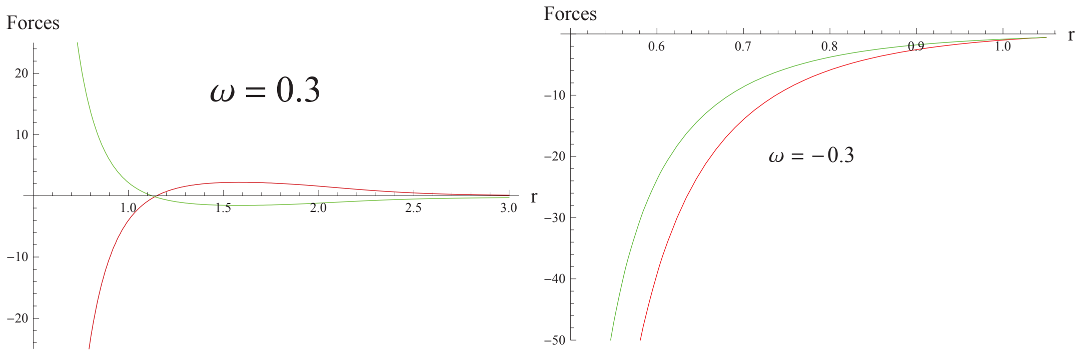

Figure 21: Plots of $\mathcal{F}_g$ (red) and $\mathcal{F}_h$ (green) versus r for $d_2 = -1$, $d_3 = 1$, $d_5 = -0.84$, $\mu = 2.5$, $\nu = -1.1$, $k = 0.01$ and $n = 0$.

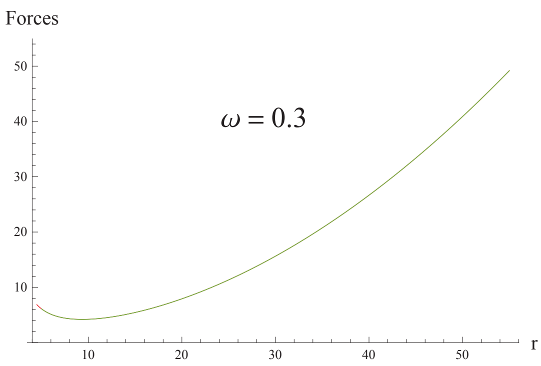

Figure 22: Plots of $\mathcal{F}_g$ (green) and $\mathcal{F}_h$ (red) versus r for $d_2 = -0.5$, $d_3 = 1$, $d_5 = -0.84$, $d_6 = -0.01$, $\mu = 2.5$, $\nu = -1.1$, $k = 0.01$ and $n = 0$.

20 determine the fate of traversable WH as it attains stable state when universe is decelerating whereas gets unstable in DE era. The stability analysis of traversable WHs (62) corresponding to second $f(R,T)$ model is shown in Figures **21** and **22**. For constant red-shift function, both plots of Figure **21** represent that the stability of WH solution is preserved only in radiation dominating phase while repulsive effects of DE destroy this equilibrium state. In case of variable red-shift function, the WH solution remains unstable during decelerating as well as accelerating cosmic expansion.

5 Final Remarks

In this paper, we have investigated the presence of physically viable WHs through Noether symmetry approach and also checked whether normal matter supports WHs or not in $f(R,T)$ gravity. For this purpose, we have considered two $f(R,T)$ models appreciating indirect curvature-matter coupling and analyzed possible existence of realistic WH solutions for both dust as well as non-dust distributions. We have also analyzed the stability of these WH solutions via TOV equation. For both models, we have solved over-determined system via Noether symmetry approach and evaluated symmetry generators as well as associated conserved quantities with explicit forms of density, $f(R,T)$ models and shape function.

For the first $f(R,T)$ model (admitting a correspondence with ΛCDM model) with constant red-shift function, WH solution satisfies all geometric conditions for dust distribution whereas in non-dust case, WH does not appreciate asymptotic flatness condition. The energy density corresponding to ordinary matter remains positive for both cases while the violation of NEC on effective energy-momentum tensor trivially holds. Thus, the repulsive gravitational effects appear at throat describe traversable nature of WH while the presence of ordinary matter leads to physically viable WH. For variable red-shift function, we have considered $p_m=\omega\rho_m$ in non-dust case and all WH conditions hold for both fluid distributions. In dust case, we have $\rho_m-\mathcal{A}\geq 0$ while $\rho_m-\mathcal{A},\ \rho_m+p_m-\mathcal{A}\geq 0$ for non-dust case whereas $\rho_{eff}+p_{eff}-\mathcal{A}\leq 0$ for both fluid distributions. These inequalities indicate that the WH is found to be traversable and physically acceptable. In case of both constant as well as variable red-shift function, the $f(R,T)$ model admitting minimal coupling between linear curvature and matter parts identifies stable state of WH against stiff fluid as well as in radiation dominated era. The realistic and stable traversable WHs lost their stability as universe crosses dust dominated era and smoothly entered into DE era.

For the second $f(R,T)$ model, we have considered $F(R) = r + \mu R^2 + \nu R^n$ and discussed WH solutions for $n = 0$ and $n = 3$. When $a(r) = k$ and $n = 0$, we have found that WH conditions are recovered for both cases. The validity of NEC and WEC by ordinary matter indicates that WH is supported by normal matter. For $a(r) = -k/r$, we have found viable WH solutions for both dust as well as non-dust cases. The physical existence of WH is verified as $\rho_m - \mathcal{A} \geq 0$ with $\rho_{eff} + p_{eff} - \mathcal{A} \leq 0$ for dust distribution. For non-dust case, we have $\rho_m - \mathcal{A}$, $\rho_m + p_m - \mathcal{A} \geq 0$ and $\rho_{eff} + p_{eff} - \mathcal{A} \leq 0$ except for $\omega = 1$. When $n \neq 0$ (dust fluid), we have found two solutions of shape function which admit $h(r) < r$, $h(r)/r \to 0$ and $h(r_0) = r_0$ for both constant as well as variable red-shift function. For constant red-shift function $(n = 0)$, we have analyzed that the WH solution preserves its stability only in radiation dominated phase while in case of variable red-shift function, the WH solution remains unstable through cosmic evolution. The summary for viable WH solutions are given in Table **1**.

Table 1: Viable WH solutions in $f(R,T)$ gravity.

Red-Shift Function	**Model I**	**Model II**
$a(r) = k$	Dust	Dust & Non-dust, $n = 0$
$a(r) = -k/r$	Dust & Non-dust	Dust & Non-dust, $n = 0$

Table **1** indicates that Noether symmetry approach leads to viable wormhole solutions in most of the cases. Zubair et al. [22] found static WH solutions with anisotropic, isotropic, and barotropic matter contents without using Noether symmetry technique in $f(R,T)$ gravity. For this purpose, they have considered a generalization of Starobinsky $f(R)$ model with linear form of $f(T)$ and tackled the complexity of field equations via numerical approach. To analyze physical viability of WHs, they constructed graphical analysis of energy bounds for all considered fluids and found that WH solutions can be constructed without evolving exotic matter in certain regions of spacetime. They concluded that WH solutions are realistic and stable only for anisotropic matter in $f(R,T)$ gravity. In the present paper, we have found realistic and stable traversable WH solutions in most of the cases for isotropic fluid via Noether symmetry approach in the same gravity.

References

[1] Bertolami, O., Böhmer, C.G., Harko, T. and Lobo, F.S.N.: Phys. Rev. D **75**(2007)104016.

[2] Harko,T., Lobo, F.S.N., Nojiri, S. and Odintsov, S.D.: Phys. Rev. D **84**(2011)024020.

[3] Bertolami, O. and Sequeira, M.C.: Phys. Rev. D **79**(2009)104010; Bertolami, O. and Páramos, J.: J. Cosmol. Astropart. Phys. **03**(2010)009; Bertolami, O., Frazão, P. and Páramos, J.: Phys. Rev. D **81**(2010)104046; Bertolami, O., Frazão, P. and Páramos, J.: Phys. Rev. D **83**(2011)044010.

[4] Gutiérrez-Piñeres, A.C., and López-Monsalvo., C.S.: Phys. Lett. B **718**(2013)1493.

[5] Sharif, M. and Zubair, M.: Astrophys. Space Sci. **349**(2014)457.

[6] Harko, T. and Lake, M.J.: Eur. Phys. J. C **75**(2015)60.

[7] Shamir, M.F.: Eur. Phys. J. C **75**(2015)354.

[8] Gao, C. and Shen, Y.: Gen. Relativ. Gravit. **48**(2016)131.

[9] Capozziello, S., Stabile, A. and Troisi, A.: Class. Quantum Grav. **24**(2007)2153.

[10] Capozziello, S., Stabile, A. and Troisi, A.: Class. Quantum Grav. **25**(2008)085004; ibid. **27**(2010)165008.

[11] Momeni, D., Myrzakulov, R. and Güdekli, E.: Int. J. Geom. Methods Mod. Phys. **12**(2015)1550101.

[12] Sharif, M. and Nawazish, I.: J. Exp. Theor. Phys. **120**(2014)49; Sharif, M. and Shafique, I.: Phys. Rev. D **90**(2014)084033; Sharif, M. and Fatima, I.: J. Exp. Theor. Phys. **122**(2016)104.

[13] Sharif, M. and Nawazish, I.: Gen. Relativ. Gravit. **49**(2017)76.

[14] Sharif, M., and Nawazish, I.: Eur. Phys. J. C **77**(2017)198.

[15] Morris, M. and Thorne, A.: Am. J. Phys. **56**(1988)395.

[16] Kashargin P.E. and Sushkov S.V.: Gravitation and Cosmology **14**(2008)80; Eiroa E.F. and Simeone C.: Phys. Rev. D **82**(2010)084039.

[17] Lobo F.S. and Oliveira M.A.: Phys. Rev. D **80**(2009)104012.

[18] Jamil, M. et al.: J. Kor. Phys. Soc. **65**(2014)917.

[19] Bahamonde, S., Jamil, M., Pavlovic, P. and Sossich, M.: Phys. Rev. D **94**(2016)044041.

[20] Mazharimousavi, S.H. and Halilsoy, M.: Mod. Phys. Lett. A **31**(2016)1650203.

[21] Sharif, M. and Fatima, I.: Gen. Relativ. Gravit. **48**(2016)148; Astrophys. Space Sci. **361**(2016)127.

[22] Zubair, M., Waheed, S. and Ahmed, Y.: Eur. Phys. J. C **76**(2016)444.

[23] Bahamonde, S., Camci, U., Capozziello, S. and Jamil, M.: Phys. Rev. D **94**(2016)084042.

[24] Ellis, G.F.R., Maartens, R. and MacCallum, M.A.H.: *Relativistic Cosmology* (Cambridge University Press, 2012).

[25] Schutz, B.F.: Phys. Rev. D **2**(1970)2762.

[26] Carroll, S.: *Spacetime and Geomety: An Introduction to General Relativity* (Addison Wesley, 2004).

[27] Santos, J., Alcaniz, J.S., Reboucas, M.J. and Carvalho, F.C.: Phys.Rev. D **76**(2007)083513; Dadhich, N.: arXiv: gr-qc/0511123v2; Kar, S. and Sengupta, S.: Pramana J. Phys. **69**(2007)49.

[28] Hanc, J., Tuleja, S. and Hancova, M.: Am. J. Phys. **72**(2004)428.

[29] Kar, S. and Sahdev, D.: Phys. Rev. D **52**(1995)2030.

[30] Ozkan, M. and Pang, Y.: Class. Quantum Grav. **31**(2014)205004.